Metalodendrímeros y Materiales Nanoestructurados que Incorporan Clústeres de Boro.

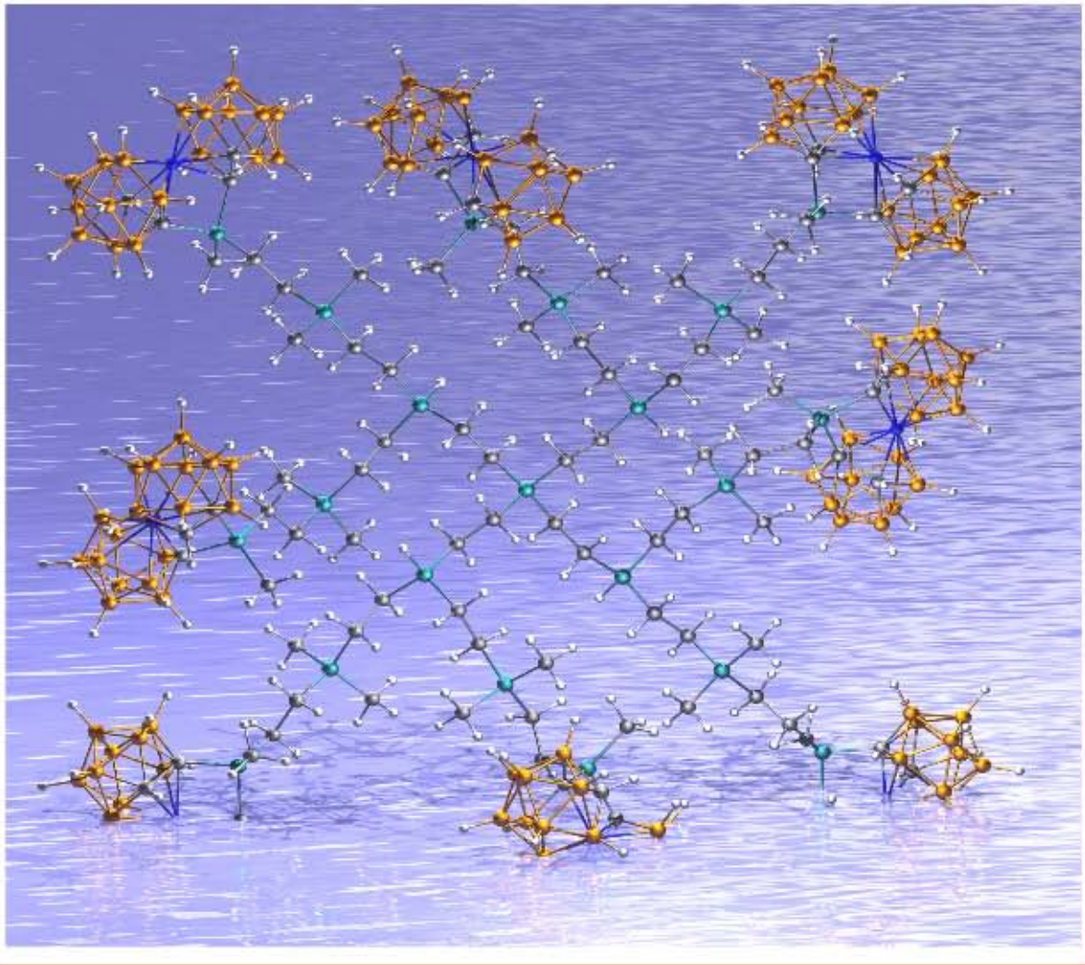

Tesis Doctoral

Emilio José Juárez Pérez

2009

Metalodendrímeros y Materiales Nanoestructurados que Incorporan Clústeres de Boro

Tesis Doctoral
Emilio José Juárez Pérez
2009

Universitat Autònoma de Barcelona

Tesis Doctoral

Metalodendrímeros y Materiales Nanoestructurados que Incorporan Clústeres de Boro.

Autor:

Emilio José Juárez Pérez

Directora:

Dra. M^a Rosario Núñez Aguilera

Programa de Doctorado en Química

Dept. Química. Facultat de Ciencies

2009

ICMAB

CSIC

Memòria presentada per aspirar al Grau de Doctor per l'Emilio José Juárez Pérez

Vist i plau Dra. M^a Rosario Núñez Aguilera

Bellaterra 29-04-2009

Consejo Superior de Investigaciones Científicas
INTITUT DE CIÈNCIA DE MATERIALS DE BARCELONA
Campus de la UAB. E-08193-Bellaterra. España
Tel. +34 93 580 18 53 Fax +34 93 580 57 29

La Dra. M^a Rosario Núñez Aguilera, Científica Titular del Consejo Superior de Investigaciones Científicas en el Instituto de Ciencia de Materiales de Barcelona

Certifica

Que Emilio José Juárez Pérez, licenciado en Ingeniería Química, ha realizado bajo su dirección la tesis doctoral titulada "Metalodendrímeros y Materiales Nanoestructurados que Incorporan Clústeres de Boro." y que se recoge en esta memoria para optar al grado de Doctor en Química.

Y para que así conste y tenga los efectos oportunos, firmo este certificado en Bellaterra, a 30 de abril de 2009.

Dra. Rosario Núñez Aguilera

Este trabajo de investigación está financiado por la Comisión Interministerial de Ciencia y Tecnología, CICYT, mediante los proyectos MAT2004-01108 y MAT2006-05339; por la Generalitat de Catalunya mediante el proyecto 2005/SGR/00709; y por la European Comission, mediante el proyecto FP6-508854; y se ha podido realizar gracias a una beca de postgrado del Programa Nacional para la Formación de Profesorado Universitario, concedida por el Ministerio de Educación y Ciencia.

Agradecimientos

Agradezco a la Dra. Rosario Núñez la dirección de esta Tesis Doctoral pues sin sus consejos y recomendaciones no se hubiera podido realizar.

Agradezco a los Profesores Francesc Teixidor y Clara Viñas el acogerme en su grupo de investigación y estar disponibles para ayudarme siempre que lo necesité.

Agradezco al Dr. José Giner-Planas todos sus consejos y los artículos tan interesantes que me prestó.

Agradezco al Prof. Carles Miratvilles, ex-Director del Institut de Ciència de Materials de Barcelona del CSIC y al actual Director, Prof. Xavier Obradors la acogida en el centro.

Agradezco al Dr. Lluis Escriche el haber aceptado la tutoría de este trabajo en el Pla de Doctorat de Químiques de la Universitat Autónoma de Barcelona.

Agradezco al Prof. Raikko Kivekäs (Universidad de Helsinki, Finlandia) y al Dr. Reijo Sillanpää (Universidad de Jyväskyla, Finlandia) la resolución de las estructuras cristalinas presentadas en este trabajo.

Agradezco al Dr. Norberto Farfán de la Universidad Nacional Autónoma de México, a la Dra. Rosa Santillan, Dr. Arturo Abreu y Rebeca Yepes, del Centro de Investigación y de Estudios Avanzados del Instituto Politécnico Nacional de México, la cesión de algunos de los dendrímeros precursores como compuestos de partida en este trabajo.

Agradezco al Dr. Hubert Mutin y al Dr. Michel Granier, del Laboratoire de Chimie Moléculaire et Organisation du Solide, su acogida para realizar la estancia en la Universidad de Montpellier y su ayuda para realizar parte del trabajo que se presenta en esta Tesis.

Agradezco a Jordi Cortés su ayuda y disponibilidad en el laboratorio y a Anna Fernández por la resolución de los espectros de RMN y MALDI-TOF.

A mis compañeros de laboratorio estos años: Dra. Arantzázu González-Campo, Dr. Albert Vaca, Dra. Eulalia Crespo, Dr. Fréderic Lerouge, Dr. Antonio Sousa, Mila, Ari,

Patri, Pau, Albert Ferrer, David, Radu y Ana, a todos gracias.

A mis amigos de siempre Carmen y Ángel.

A mis padres, hermanos, primos y tios.

A Nadine.

Organización de la Tesis

De acuerdo con la normativa vigente, esta Tesis Doctoral se presenta como un compendio de artículos. No obstante, además de incluir los artículos publicados y presentados a la comisión de Doctorado de la UAB en abril de 2009 (Capítulo 5), con la idea de presentar una Memoria lo más completa posible, también se han incluido los trabajos realizados en el marco de esta Tesis Doctoral y que están enviados o en proceso de elaboración (Anexo).

Los trabajos incluidos en esta Memoria son:

Capítulo 5: Artículos publicados y presentados a la Comisión de Doctorado de la UAB en Abril de 2009:

a) Controlled Direct Synthesis of C-Mono- and C-Disubstituted Derivatives of [3,3'-Co(1,2-$C_2B_9H_{11})_2$]$^-$with Organosilane Groups: Theoretical Calculations Compared with Experimental Results. Emilio José Juárez-Pérez, Clara Viñas, Arántzazu González-Campo, Francesc Teixidor, Reijo Sillanpää, Raikko Kivekäs, Rosario Núñez. *Chem. Eur. J.* **2008**, *14*, 4924-4938.

b) Carboranyl Substituted Siloxanes and Octasilsesquioxanes: Synthesis, Characterization and Reactivity. Arántzazu González-Campo, Emilio José Juárez-Pérez, Clara Viñas, Bruno Boury, Reijo Sillanpää, Raikko Kivekäs, Rosario Núñez. *Macromolecules* **2008**, *41*, 8458-8466.

c) First example of the formation of a Si−C bond from an intramolecular Si−H$\cdots$H−C diyhydrogen interaction in a metallacarborane:

A theoretical study. Emilio José Juárez-Pérez, Clara Viñas, Francesc Teixidor, Rosario Núñez. *J. Organomet. Chem.* **2009**, *694*, 1764-1770.

Anexo: Artículos enviados o pendientes de publicación posteriores a la Comisión de Doctorado de la UAB en Abril de 2009:

a) Polyanionic Carbosilane And Carbosiloxane Metallodendrimers Based On Cobaltabisdicarbollide Derivatives. Emilio José Juárez-Pérez, Clara Viñas, Francesc Teixidor, Rosario Núñez. *Organometallics* **2009**, *submitted.*

b) Polyanionic Aryl-Ether Metallodendrimers Based On Cobaltabisdicarbollide Derivatives. Photoluminescent Properties. Emilio José Juárez-Pérez, Clara Viñas, Francesc Teixidor, Rosa Santillan, Norberto Farfán, Arturo Abreu, Rebeca Yépez, Rosario Núñez. *In preparation.*

c) Decorating Poly(Alkyl Aryl-Ether) Dendrimers With Metallacarboranes. Rosario Núñez, Emilio José Juárez-Pérez, Francesc Teixidor, Rosa Santillan, Norberto Farfán, Arturo Abreu, Rebeca Yépez, Clara Viñas. *In preparation.*

d) Anchoring Phosphorous-containing Cobaltabisdicarbollide Derivatives on Titania Particles. Emilio José Juárez-Pérez, Hubert Mutin, Michel Granier, Francesc Teixidor, Rosario Núñez. *In preparation.*

e) Approaches For Anchoring Cobaltabisdicarbollide Anions Onto Oxidized Silicon Wafers. Emilio José Juárez-Pérez, Michel Granier, Hubert Mutin, Clara Viñas, Rosario Núñez. *In preparation.*

f) Thumb Rules to Establish the Rotamer Configuration in Metallacarborane Sandwiches. The relevance of the $C_C-H\cdots H-B$ Self Interactions. Emilio J. Juárez-Pérez, Rosario Núñez, Clara Viñas, Reijo Sillanpää, Francesc Teixidor. *Inorg. Chem.* **2009**, *submitted.*

Figuras

Cobaltacarboranos

C-derivados:

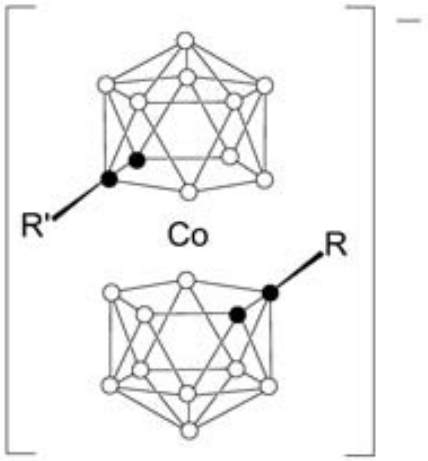

compuesto	R	R'
[1]⁻	H	H
[3]⁻	$SiH(CH_3)_2$	H
[4]⁻	μ-$Si(CH_3)_2$	
[5]⁻	μ-$SiH(CH_3)$	
[6]⁻	$Si(CH_3)_3$	H
[7]⁻	$Si(CH_3)_3$	$Si(CH_3)_3$

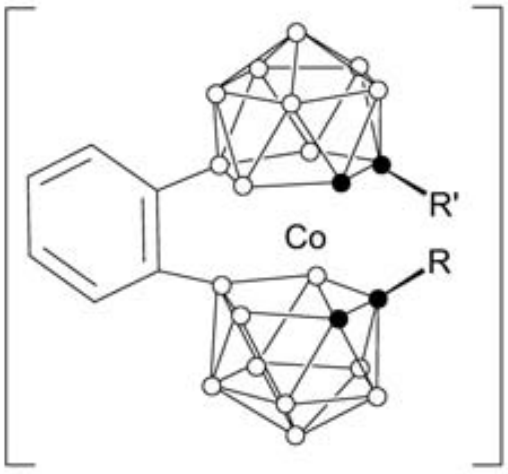

compuesto	R	R'
[2]⁻	H	H
[8]⁻	μ-$Si(CH_3)_2$	
[9]⁻	μ-$SiH(CH_3)$	
[10]⁻	$Si(CH_3)_3$	H

Nota: los vertices de los clústeres representan: ● C_c-H y ○ B-H si no van enlazados a un grupo expresamente.

Dendrímeros de partida

carbosilano:

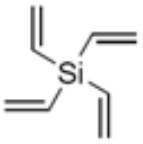

TViS

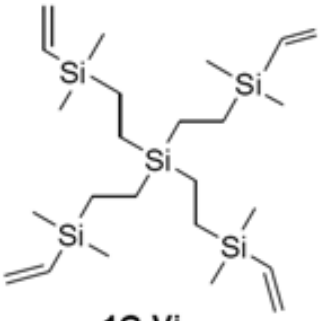

1G-Vi$_4$

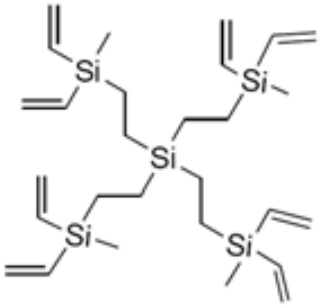

1G-Vi$_8$

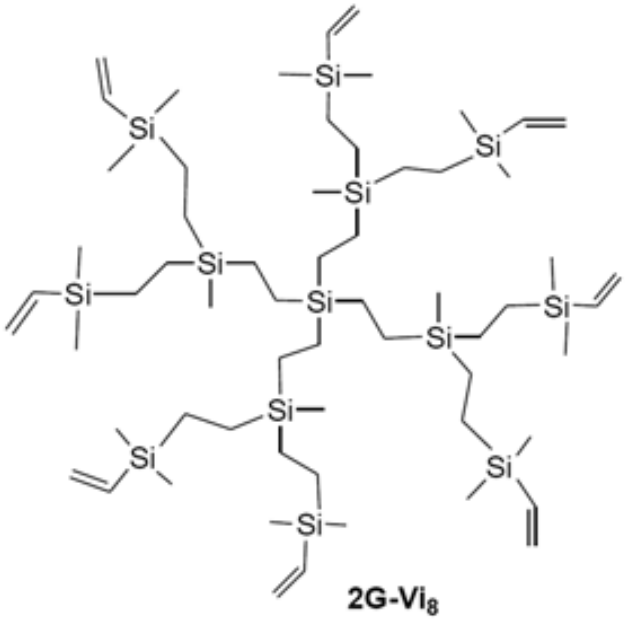

2G-Vi$_8$

carbosiloxano:

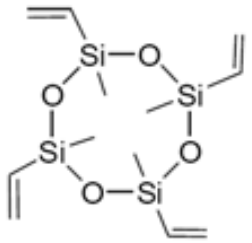

TMViCTS

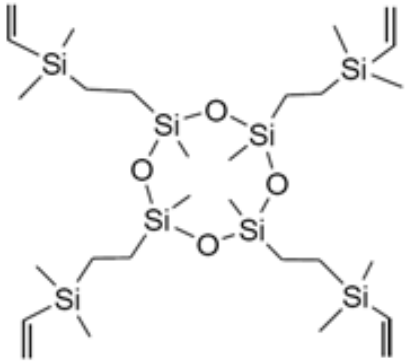

1G-TMViCTS(SiVi)$_4$

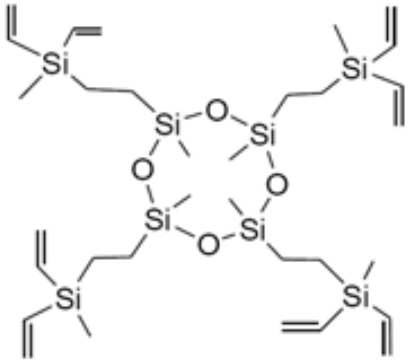

1G-TMViCTS(SiVi)$_8$

Aril - Éter (TFB):

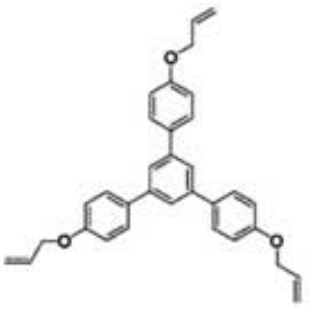

0G-TFB(Alil)$_3$

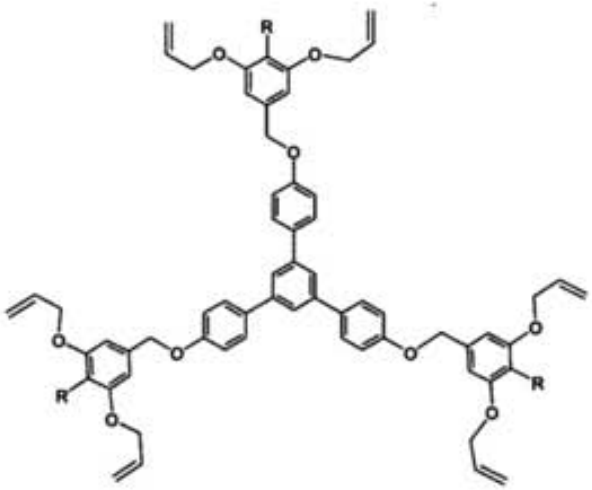

R = H **1G-TFB(Alil)$_6$**

R =  **1G-TFB(Alil)$_9$**

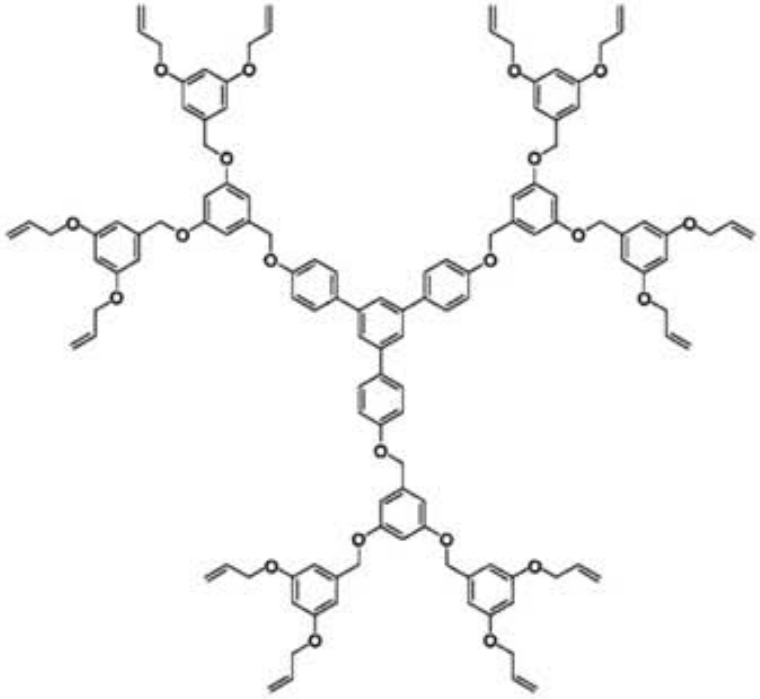

2G-TFB(Alil)$_{12}$

Aril - Éter (XBO):

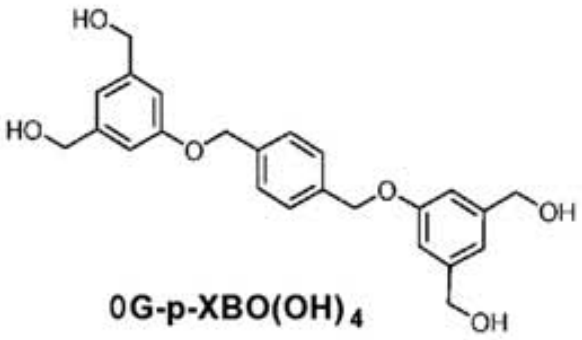

0G-p-XBO(OH)$_4$

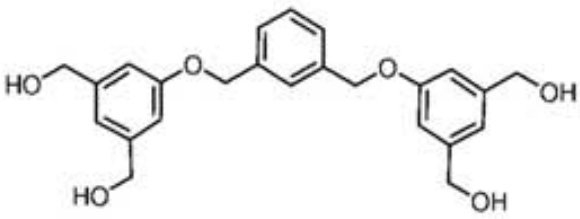

0G-m-XBO(OH)$_4$

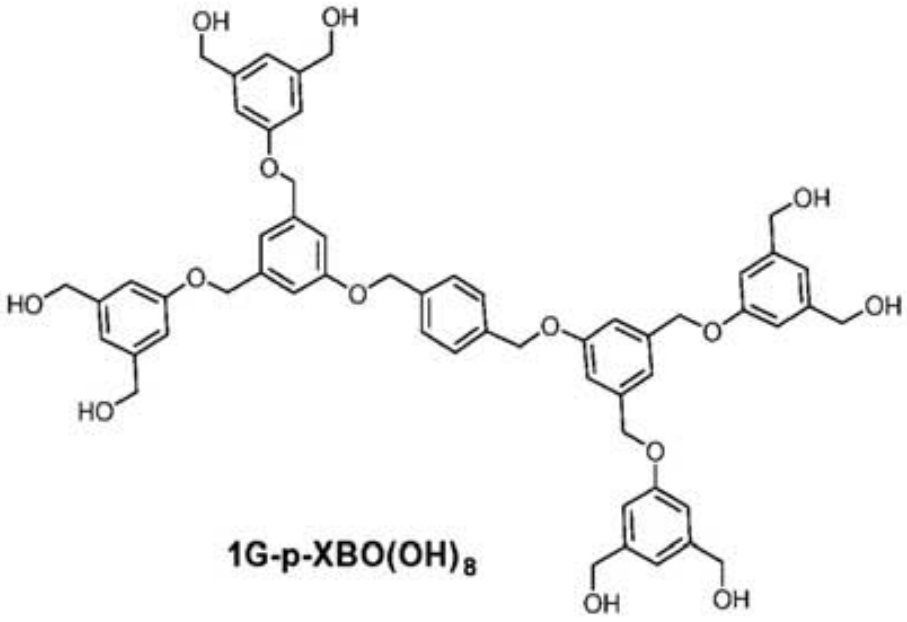

1G-p-XBO(OH)$_8$

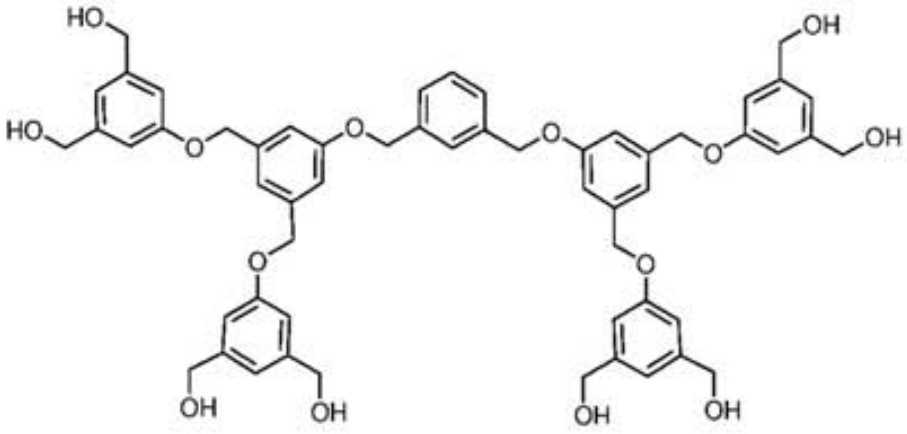

1G-m-XBO(OH)$_8$

Metalodendrímeros

carbosilano:

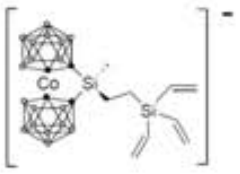

[11]$^{-}$

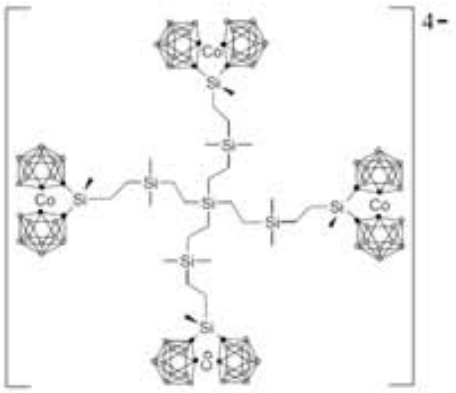

[12]$^{4-}$

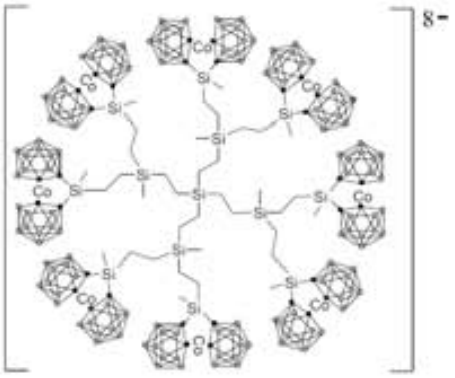

[13]$^{8-}$

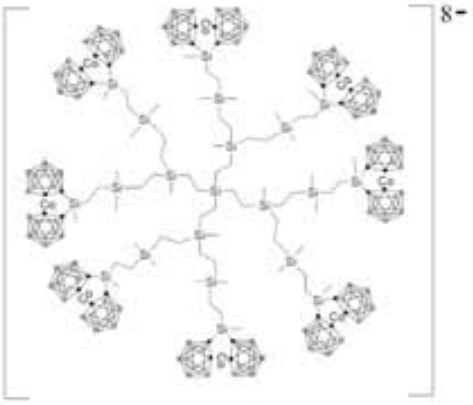

[14]$^{8-}$

carbosiloxano:

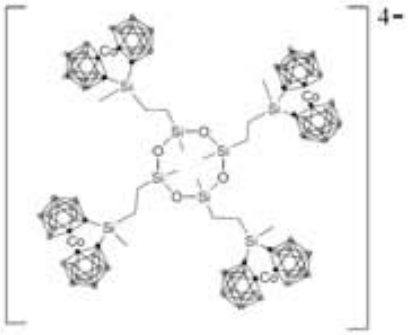

[15]$^{4-}$

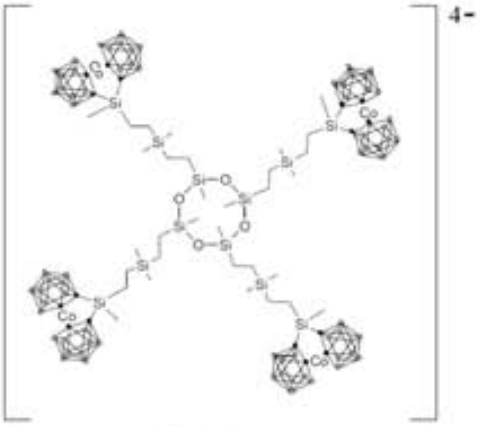

[16]$^{4-}$

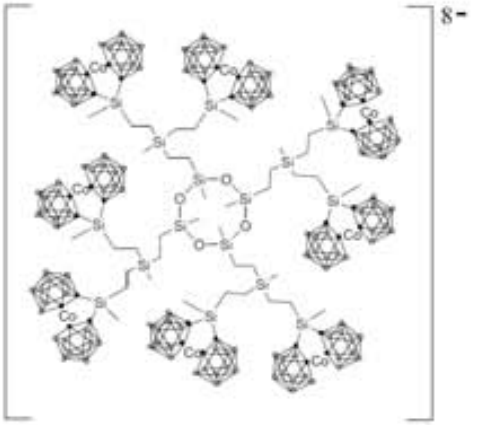

[17]$^{8-}$

Aril - Éter (TFB):

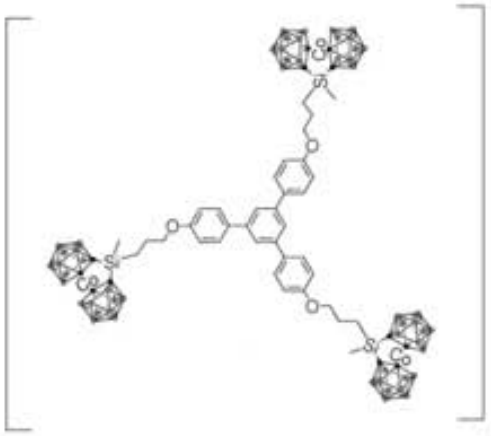

3-

$[18]^{3-}$

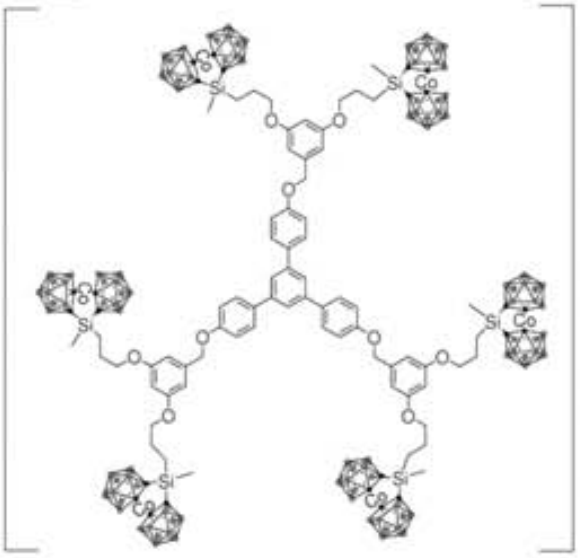

6-

$[19]^{6-}$

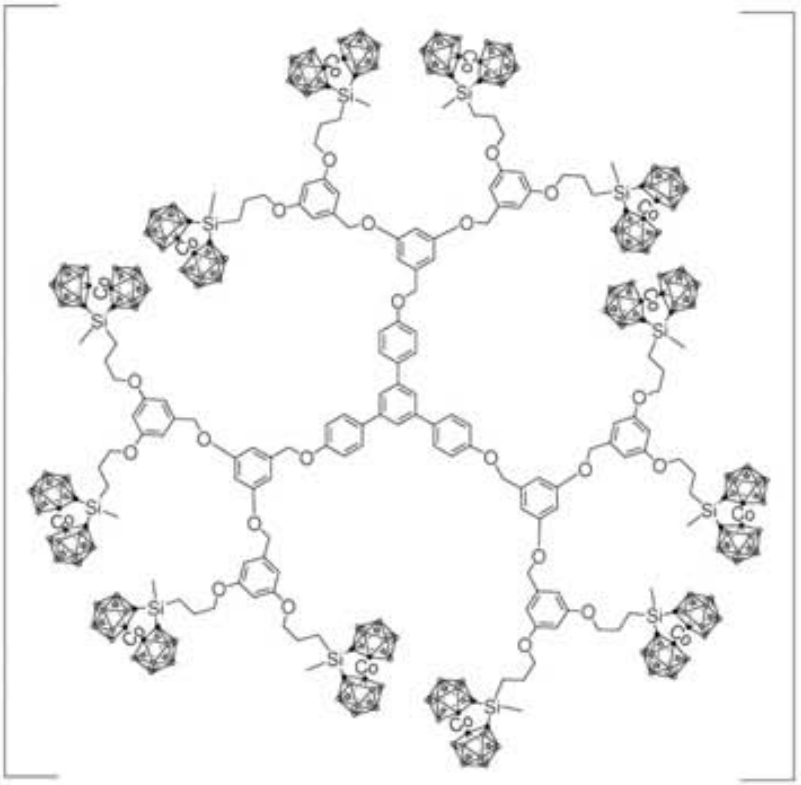

12-

$[20]^{12-}$

Aril - Éter (XBO):

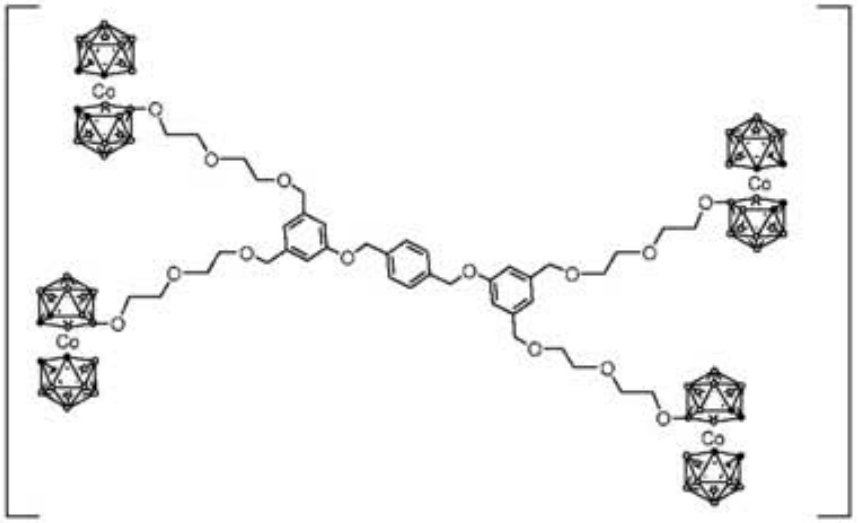

[21]$^{4-}$

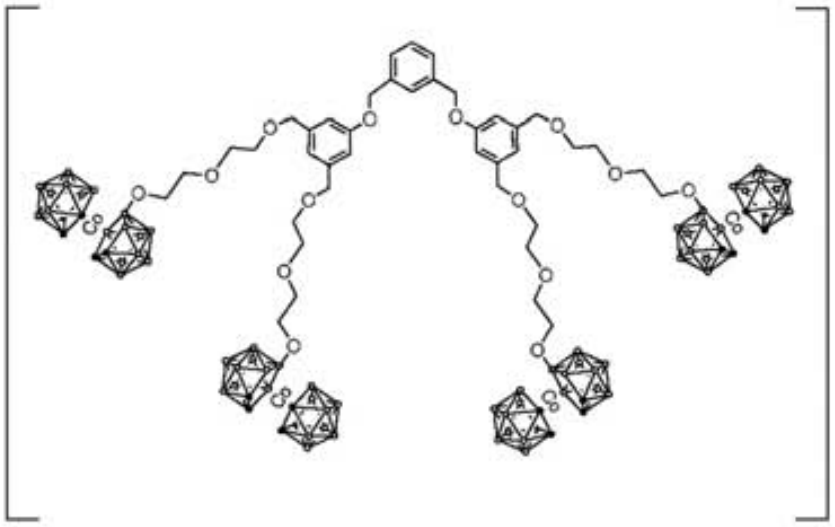

[22]$^{4-}$

Aril - Éter (XBO):

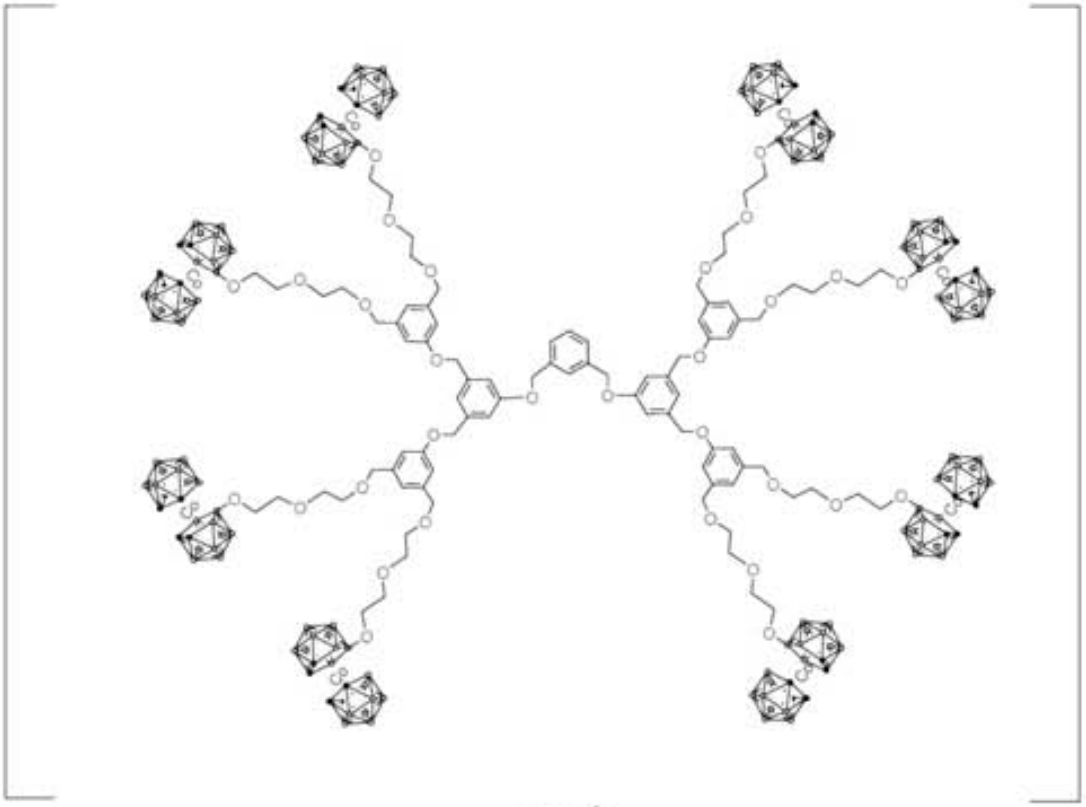

8-

[23]$^{8-}$

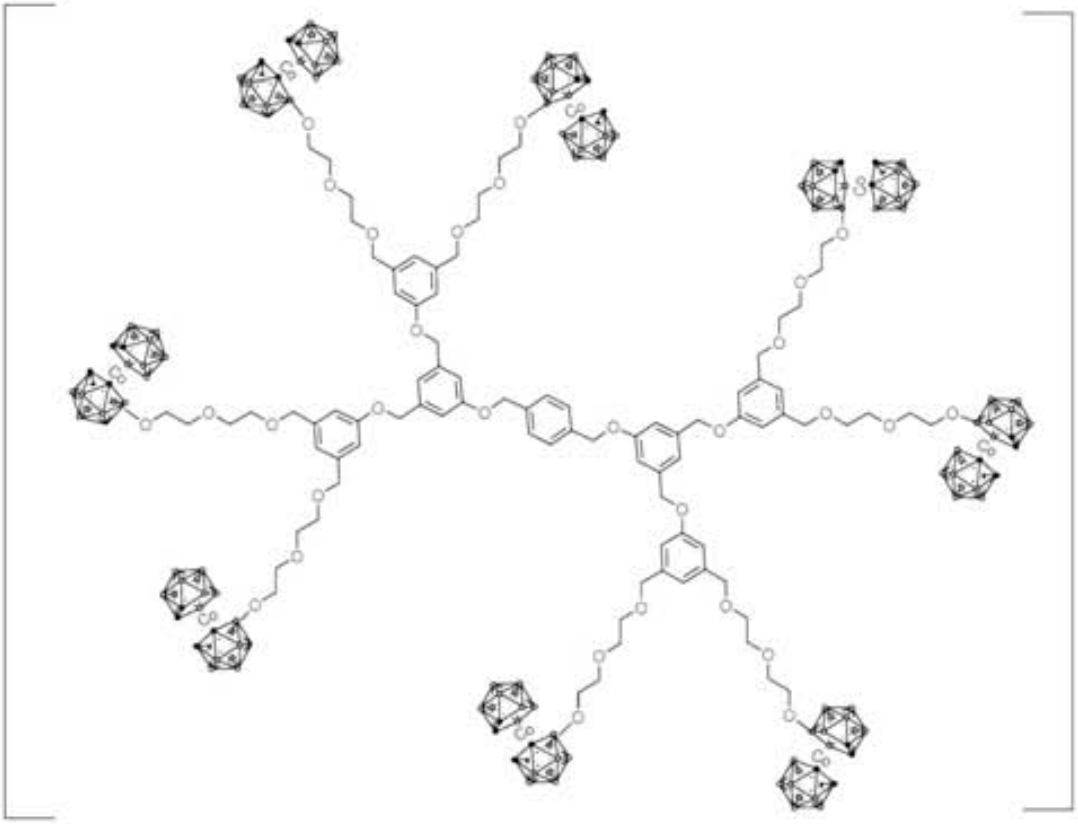

8-

[24]$^{8-}$

Silanos, Siloxanos y Silsesquioxanos:

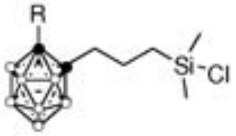

R = Me, **25**
R = Ph, **26**

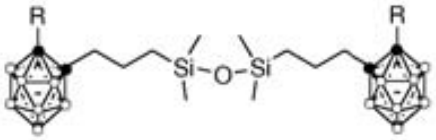

R = Me, **27**
R = Ph, **28**

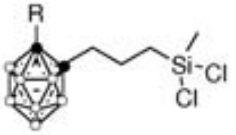

R = Me, **29**
R = Ph, **30**

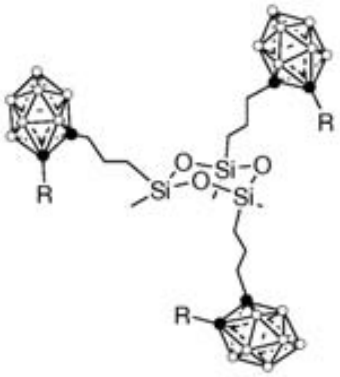

R = Me, **31**
R = Ph, **32**

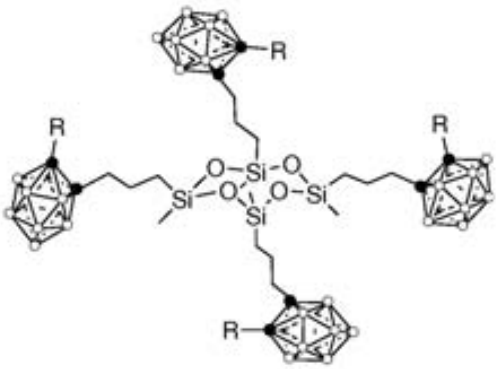

R = Me, **33**
R = Ph, **34**

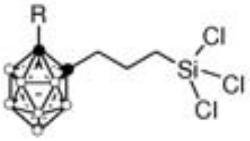

R = Me, **35**
R = Ph, **36**

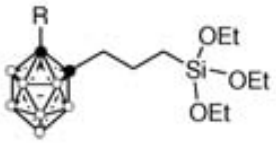

R = Me, **37**
R = Ph, **38**

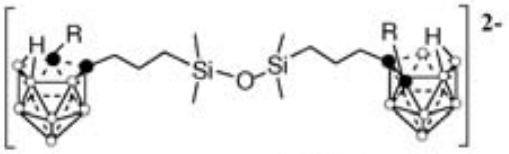

R = Me, **[41]** $^{2-}$
R = Ph, **[42]** $^{2-}$

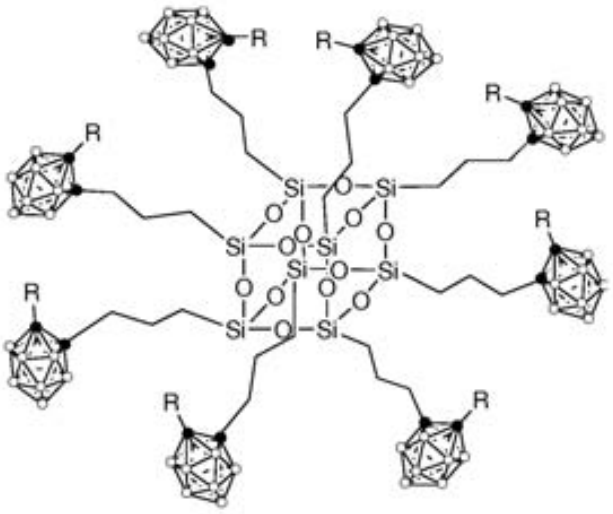

R = Me, **39**
R = Ph, **40**

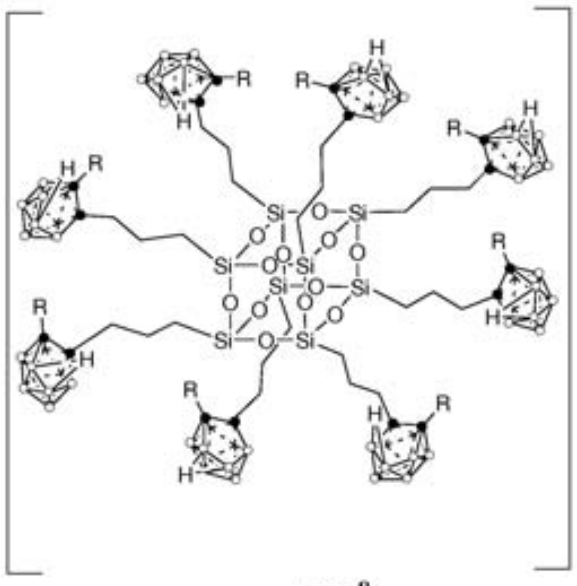

R = Me, **[43]** $^{8-}$

Cobaltacarboranos:

Funcionalización de nanopartículas de TiO_2

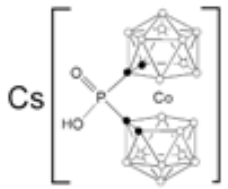

Cs**[44]**

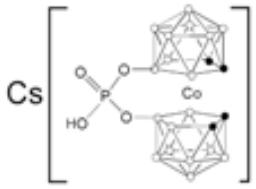

Cs**[45]**

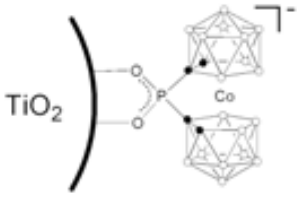

44@TiO_2

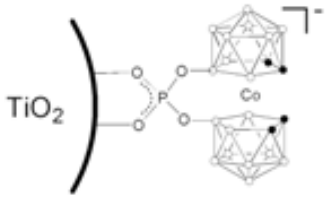

45@TiO_2

Funcionalización de *wafers* de Si oxidado

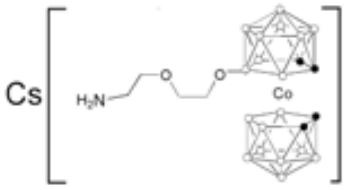

Cs**[47]**

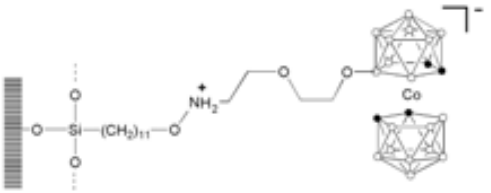

46@SiO_2

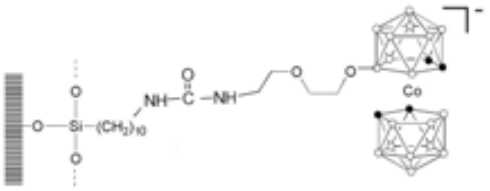

47@SiO_2

Abreviaturas

$B(n)$	átomo de boro situado en el vértice n del clúster
C_c	átomo de carbono del clúster de carborano o del ligando dicarballuro
CSD	*Cambridge Structural Database*
n-BuLi	n-butillitio
t-BuOK	*tert*-butóxido potásico
Me	metil
DMSO	dimetilsulfóxido
DME	$1\,,2-$dimetoxietano
THF	tetrahidrofurano
TMEDA	$N, N, N', N'-$Tetrametiletilenediamina
TBAF	Fluoruro de tetrabutilamonio
TFB-	1,3,5-TriFenilBenceno (núcleo de dendrímero)
XBO-	XililBenzÓxi- (núcleo de dendrímero)
Et_2O	éter dietílico
EtOH	etanol
MeOH	metanol
AcOEt	acetato de etilo
TCE	tricloroetileno
cat	catalizador
liq	fase líquida
exc	exceso
eq	equivalente-mol
IR	Infrarrojo (espectroscopía de)
RMN	Resonancia magnética nuclear (espectroscopía de)
CP-MAS	*Cross Polarization-Magic Angle Spinning*
COSY	Resonancia magnética nuclear bidimensional (*COrrelation SpectroscopY*)
EM	espectrometría de masas
MALDI-TOF	*Matrix Assisted Laser Desorption/Ionisation-Time of Flight*
ESI	*Electrospray Ionisation*
UV-Vis	Ultravioleta - Visible (espectroscopía de)
AFM	*Atomic Force Microscopy*
XPS	*X-ray Photoelectron Spectroscopy*

XRD	*X-Ray Difraction*
DFT	*Density Functional Theory*
QTAIM	*Quantum Theory of Atoms In Molecules*
En espectros de IR	
ATR	*Attenuated Total Reflectance*
I	Intensa
mI	muy Intensa
pI	poco Intensa
ν	vibración de tensión
δ	deformación
γ	vibración esqueletal
En espectros de RMN	
δ (ppm)	desplazamiento químico en ppm
I	spin
s	singulete
d	doblete
t	triplete
m	multiplete
sept	septuplete
a	amplio
$^{n}J(A, B)$	constante de acoplamiento entre los átomos A y B a n enlaces
TMS	TetraMetilSilano

Abstract

This work has open new strategies in the synthesis of large molecules, such as dendrimers and metallodendrimers, and other nanostructured materials, in the boron chemistry field.

The main aim of this work was the preparation of polyanionic boron-rich metallodendrimers containing cobaltabisdicarbollide derivaties at the periphery, with potential applications in biomedicine. For this purpose a set of novel C_c-mono- and C_c-disubstituted cobaltabisdicarbollide derivatives with silyl functions, $[\mathbf{3}]^-$–$[\mathbf{10}]^-$, have been prepared by the reaction of lithium salts of [3,3'-Co(1,2-$C_2B_9H_{11})_2]^-$, $[\mathbf{1}]^-$, and [8,8'-μ-C_6H_4-3,3'-Co(1,2-$C_2B_9H_{10})_2]^-$, $[\mathbf{2}]^-$, with different chlorosilanes. DFT theoretical studies at the B3LYP/6-311G(d,p) level of theory were applied to optimise the geometries of these compounds and calculate their relative energies, showing a good concordance between theoretical and experimental results. The unexpected formation of a bridge -$\mu-SiMe_2-$ between both dicarbollide clusters, through the C_c atoms, after the reaction of the monolithium salt of cobaltabisdicarbollide with $HSiMe_2Cl$, suggested an intramolecular reaction, in which the acidic C_c-H proton reacts with the hydridic Si−H, with subsequent loss of H_2. Some aspects of this reaction have been studied by using DFT and QTAIM calculations.

From all the previous compounds, the anion [1,1'-μ-SiMeH-3,3'-Co(1,2-$C_2B_9H_{10})_2]^-$, $[\mathbf{5}]^-$, was chosen as hydrosilylating agent for the preparation of different types of metallodendrimers. Thus, different generations of polyanionic metallacarborane-containing metallodendrimers were constructed via hydrosilylation of various generation of carbosilane and cyclic carbosiloxane dendrimers containing terminal vinyl functions with $[\mathbf{5}]^-$, to achieve the corresponding metallodendrimers with four and eight peripheral cobaltacarboranes. For metallodendrimers with high molecular weights, the UV-Vis spectroscopy was used for corroborating the full functionalization and consequently the unified charac-

ter of dendrimers. The solubility of these dendrimers is very interesting from the point of view of potential applications, i.e. in medicine or BNCT. For that reason, some solubility studies have been carried out by using UV-Vis measurements in water/DMSO solutions of these metallodendrimers.

Following the same strategy, poly(aryl-ether) type dendrimers with a fluorescente core and peripheral allyl functions have also been hydrosilylated using the anion $[\mathbf{5}]^-$, to obtain metallodendrimers with three, six and twelve cobaltacarborane moieties. It is important to emphasize that photoluminescent measured on these compounds, showed that after functionalization, the presence of metallacarboranes at the periphery causes a quenching of the fluorescence previously exhibited by the starting dendrimers. Nowadays, we have not the explication to this phenomenon that is still under study.

Other type of polyanionic poly-(alkyl aryl-ether) metallodendrimers have also been prepared by using the ring opening reaction of the 8–dioxanate in [3,3'-Co(8-$C_4H_8O_2$-1,2-$C_2B_9H_{10}$)(1',2'-$C_2B_9H_{11}$)], by the nucleophilic attack to the oxygen with the alcoholate functions obtained by deprotonation of the alcohol groups (−OH) located at the starting dendrimers periphery.

Carborane-containing siloxane and octasilsesquioxane derivatives have been prepared following a hydrolitic approach by hydrolisis-polycondensation of carboranylchlorosilane or carboranylethoxysilane. A second approach was a non hydrolytic route using carboranylchlorosilane and DMSO as oxygen source.

In parallel, we have also worked on the anchoring of cobaltabisdicarbollide derivatives on the surface of TiO_2 nanoparticles and oxidized silicon wafers. Thus, adequate organophosphorous derivatives of [3,3'-Co(1,2-$C_2B_9H_{11}$)$_2$]$^-$ have been prepared to be used as coupling molecules for the modification of titanium dioxide surfaces. The functionalization of the surface results from the formation of Ti−O−P bridges by condensation of P−OH groups with surface hydroxyl groups and coordination of the phosphoryl groups to surface Lewis acidic sites. Besides, for anchoring cobaltabisdicarbollide derivatives on the surface of an oxidized silicon wafer, two different approaches were used, both based on the ring-opening reaction of the 8–dioxanate [3,3'-Co(8-$C_4H_8O_2$-1,2-$C_2B_9H_{10}$)(1',2'-$C_2B_9H_{11}$)] with amines or isocyanate functions previously anchored to the surfaces.

Thus, cobaltabisdicarbollide derivatives have demostrated to be suitable groups for functionalization of dendrimers and other nanostructures such as nanoparticles and wafers providing a large number of materials with interesting potential applications.

Índice general

1

Introducción

1.1. El Boro, una perspectiva histórica

El Boro es el único elemento del grupo 13 de carácter semi-metálico (o *metaloide*) y al igual que los elementos carbono y silicio es capaz de enlazarse consigo mismo y formar estructuras estables de tipo clúster mediante enlaces covalentes. En la Naturaleza se encuentran dos isótopos de boro estables, ^{11}B (80,1 %) y ^{10}B (19,9 %), y no es posible encontrarlo en su forma elemental, sino enlazado a oxígeno formando boratos de sodio o calcio en minerales como $Na_2B_4O_7 \cdot 10\,H_2O$ (bórax) o $Ca_2B_6O_{11} \cdot 5\,H_2O$ (colemanita). El empleo de bórax está documentado desde hace miles de años en diversas civilizaciones y la primera mención a estos boratos la realizó el alquimista Rhazes (865 - 925 d.C).

En 1808 los químicos franceses Gay-Lussac y L. J. Thenard, e independientemente el inglés Humphry Davy, obtuvieron boro elemental. Davy ya dominaba la producción de los metales alcalinos más reactivos,[1] el paso previo para aislar B elemental. Ninguno de ellos reconoció la sustancia como un nuevo elemento, algo que haría Jöns Jacob Berzelius en 1824. En el año 1912, Alfred Stock sintetiza los primeros boranos,[2] compuestos basados exclusivamente de hidrógeno y boro. El carbono y el boro resultan ser los únicos elementos capaces de formar una serie compleja y extendida de hidruros, con la diferencia que los hidrocarburos se encuentran en la Naturaleza y el origen de los boranos es puramente sintético. Las formas estructurales que adoptan los boranos son tridimensionales, esqueletos de boro poliédricos o clústeres de boro, cerrados o abiertos en sus caras. Los boranos serían el nexo de unión entre las estructuras condensadas basadas en fragmentos de redes metálicas y las estructuras habituales de tipo lineal y anillos que se dan en las estructuras químicas orgánicas e inorgánicas con elementos del bloque p (Figura 1.1).

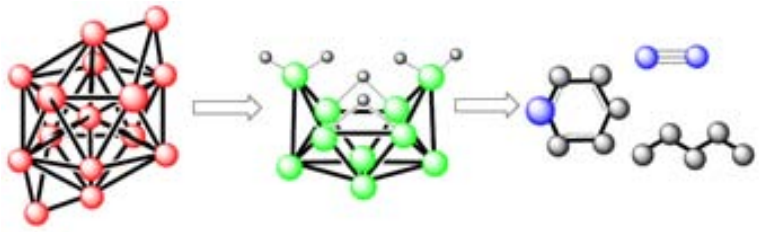

Figura 1.1: El continuo estructural; desde clústeres metálicos (izquierda) a cadenas y anillos (derecha) pasando por los clústeres de borano (centro).

Hasta 1948 ningún borano, a excepción del diborano (B_2H_6), se encontraba caracteri-

zado estructuralmente. H.C. Longuet-Higgins había introducido recientemente el concepto de enlace *tres-centros dos-electrones.*[3] Este tipo de enlace explica la alta conectividad en los boranos a pesar del bajo número de electrones que disponen para hacerlo. Los boranos representaban en aquella época ser una mera curiosidad académica, pero en los primeros años de la Guerra Fría, debido a la posibilidad de usar los hidruros de boro B_5H_9 y $B_{10}H_{14}$ como combustibles para cohetes, asentó los cimientos de la investigación de estos hidruros de boro.[4] Posteriormente, un nuevo avance en la química de los boranos lo dió H.C. Brown elaborando los compuestos denominados organoboranos, derivados orgánicos de BH_3 que son uno de los reactivos más importantes en síntesis orgánica.[5] También los estudios que realizó W.N. Lipscomb sobre la estructura tridimensional de los clústeres de borano representan otro hito en el estudio de estos compuestos.[6]

Pero a pesar de la gran cantidad de información y estudios llevados a cabo durante el siglo pasado, la química de los clústeres de boro no está tan desarrollada como la química orgánica. La predicción exitosa del comportamiento químico de estos compuestos ocurre en contadas ocasiones, ya que, el conocimiento de estos compuestos denominados *deficientes en electrones* es aún insuficiente.

1.2. Boranos, Carboranos y Metalacarboranos

Los boranos son compuestos moleculares diamagnéticos, incoloros, blancos o amarillo pálido que pueden ser neutros o aniónicos y que forman clústeres poliédricos de caras triangulares cuyos vértices están formados por la unidad B−H. Los clústeres de menor número de vértices son gases a temperatura ambiente, pero a medida que aumenta su peso molecular son líquidos volátiles o sólidos. Los boranos de bajo peso molecular son muy reactivos, llegando algunos a producir combustión espontánea en aire, y sin embargo, en el otro extremo tenemos especies como el *closo* $[B_{12}H_{12}]^{2-}$ de una estabilidad térmica excepcional. Estos últimos además poseen una reactividad química y unas propiedades magnéticas tales que a menudo se habla de que poseen aromaticidad tridimensional.[7]

1.2.1. Carboranos

La sustitución de uno o más vértices de boro por algún heteroátomo genera los denominados heteroboranos y entre éstos, los más estudiados son los carboranos en los

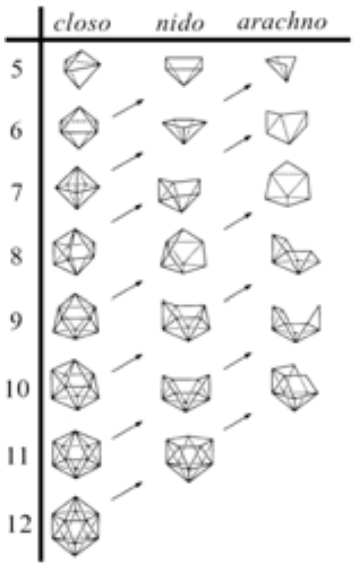

Figura 1.2: Principales redes de boranos o heteroboranos.

cuales uno o más átomos de boro han sido substituidos por carbono.[8] La fórmula empírica de estos compuestos es:

$$[C_pB_qH_{p+q+r}]=[(CH)_p(BH)_qH_r]^{x-}$$

donde p es el número de átomos de carbono en los vértices del clúster, q es el número de átomos de boro y r es el número de átomos de hidrógeno pontal.

Las reglas que gobiernan la estructura, el enlace y el contaje de electrones en los boranos y heteroboranos fueron estudiadas por Wade, Rudolph, Mingos y Willians, y son conocidos como *Las reglas de Wade*.[9] Los términos *closo*, *nido* y *arachno* (Figura 1.2) se usan para clasificar los clústeres poliédricos y tienen un papel doble. Por un lado describen el tipo de clúster, si es cerrado se denomina *closo*, si es abierto debido a la eliminación de uno de los vértices se denomina *nido*, si se han eliminado dos vértices se denomina *arachno*. Por otro lado, indican cuantos electrones se deslocalizan en el clúster, si el clúster tiene $n+1$ pares de electrones es *closo*, $n+2$ *nido* y si tiene $n+3$ pares de electrones es *arachno*, donde n es el número de vértices del clúster. Conocido el número de vértices y el número de pares de electrones que proporcionan cada uno de ellos se puede determinar la estructura tridimensional del borano. Por ejemplo, el clúster

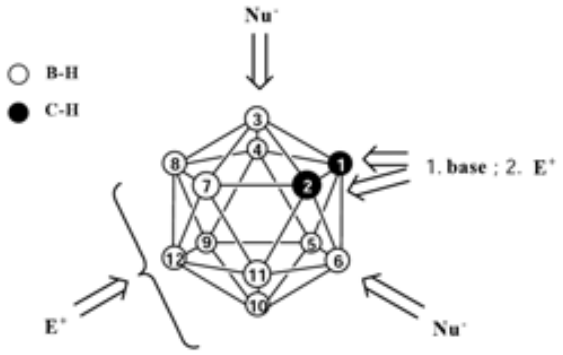

Figura 1.3: Enumeración y reactividad de los diferentes vértices del 1,2-*o*-$C_2B_{10}H_{12}$ frente a bases fuertes, nucleófilos (Nu^-) y electrófilos (E^+).

de carborano tiene la fórmula empírica $C_2B_{10}H_{12}$, 12 vértices de los cuales 10 son B−H y aportan dos electrones al clúster cada uno y dos vértices C−H que aportan 3 electrones cada uno. Siguiendo el esquema de *las reglas de Wade*, esta red tendría 13 pares de electrones, como la molécula es neutra y tiene 12 vértices ($n = 12$) el compuesto es un clúster de tipo *closo* pues la igualdad ocurre para $n + 1 = 13$.

El carborano se descubrió en 1950[4,10] aunque su síntesis no fue publicada hasta 1963.[11] El clúster de *o*-carborano, también conocido como dicarba-*closo*-dodecaborano, 1,2-*o*-$C_2B_{10}H_{12}$ (Figura 1.3), es relativamente estable termodinámica y químicamente, y esta estabilidad está relacionada con la deslocalización electrónica en el clúster.

La introducción de sustituyentes en el clúster.

La diferente reactividad de los vértices de B−H frente a los de C_c−H da lugar a una química especialmente versátil en la síntesis de compuestos derivados del 1,2-*o*-$C_2B_{10}H_{12}$ con características muy diferentes entre sí.[12] A su vez, los vértices de B−H del clúster presentan diferente reactividad dependiendo de la posición relativa respecto a los C_c−H. En la Figura 1.3 se esquematiza de forma general las distintas posibilidades que posee el cluster de *o*-carborano para ser funcionalizado.

Debido a la mayor electronegatividad de los átomos de C frente a los de B (2.5 frente a 2 en la escala de Pauling), el carácter relativamente ácido de los protones unidos a C_c permite substituirlos por metales alcalinos utilizando bases como el n-BuLi, Figura

1.4. Posteriormente, se hacen reaccionar estas sales de litio del carborano con derivados halogenados o el elemento en estado puro (S, Se) y se obtienen los correspondientes derivados con enlace C_c-R.

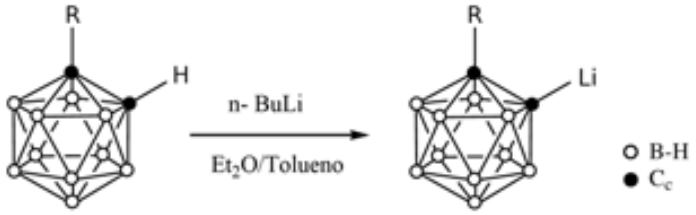

Figura 1.4: Reacción de sustitución de los hidrógenos unidos a los carbonos del clúster.

En una búsqueda en la base de datos cristalográfica de Cambridge (CSD),[13] podemos encontrar derivados del 1,2-*o*-$C_2B_{10}H_{12}$ con un C_c enlazado a una gran variedad de elementos de los grupos principales como: B, C, N, O, Mg, Si, P, S, Ga, Ge, As, Se, Br, I, Sn y Te; metales de transición: Ti, Mn, Co, Ni, Cu, Y, Zr, Ru, Rh, Hf, Pt, Au y Hg; e incluso metales del bloque f: Nd, Sm, Er y Yb. En este punto cabe resaltar la versatilidad del 1,2-*o*-$C_2B_{10}H_{12}$ para actuar de ligando en complejos organometálicos, como por ejemplo de Au o Ag, en los cuales los carboranos C_c-substituidos (S, P, N) actuan como ligandos complejando estos metales via estos átomos dadores e incluso directamente con enlaces C_c-σ hacia el metal.[14] En nuestro grupo se han sintetizado derivados del 1,2-*o*-carborano (con estructuras cristalina publicada) con C_c enlazado a: silicio,[15] fósforo,[16] azufre,[17] y selenio.[18]

La densidad de carga sobre los átomos de B más alejados de los C_c es mucho mayor que la de los B conectados simultáneamente a los C_c. La reactividad de los primeros favorece las sustituciones electrofílicas, de donde las posiciones $B(9)$ y $B(12)$ seguidas de las $B(8)$ y $B(10)$ son las más susceptibles de ser atacadas electrofílicamente (Figura 1.3).[8,19–21] La halogenación y en concreto la creación de enlaces B−I es importante en la síntesis de derivados del *o*-carborano, ya que permite mediante reacciones de acoplamiento cruzado, en presencia de catalizadores de Pd(II) y el reactivo de Grignard apropiado, sintetizar *orto*-carboranos B-organo substituidos, siendo esta técnica como la más factible para crear enlaces B−C en el clúster.[21]

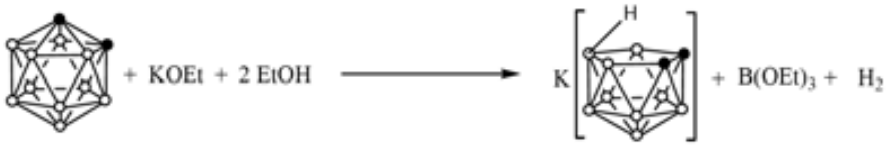

Figura 1.5: Reacción de degradación parcial del *o*-carborano.

Degradación parcial del clúster por eliminación de un vértice.

Otra de las modificaciones importantes que se pueden realizar sobre el clúster de 1,2-*o*-$C_2B_{10}H_{12}$ y que da lugar a una química bastante rica es la decapitación o degradación parcial del mismo, que consiste básicamente en la eliminación de un vértice B−H del clúster. Esta reacción data de 1964 cuando Wiesboeck y Hawthorne aislaron en alto rendimiento el 7,8-*nido*-$[C_2B_9H_{12}]^-$, utilizando reactivos nucleofílicos,[22] véase Figura 1.5. El mayor carácter electronegativo de los C_c, respeto a los átomos de B, provoca una polarización de los enlaces C_c−B, dejando una mayor densidad de carga positiva sobre los dos núcleos de B unidos simultáneamente a los dos C_c (posiciones 3 y 6 en la Figura 1.3), haciendo que sean los más susceptibles de ser atacados por un nucleófilo. En el 1,2-*o*-$C_2B_{10}H_{12}$, la eliminación de uno de estos átomos de boro (formalmente un B^+) deja el clúster con una cara pentagonal abierta, C_2B_3, donde se sitúa un átomo de hidrógeno y el clúster *nido* resultante es monoaniónico (Figura 1.5). El átomo de hidrógeno situado en la cara abierta del clúster *nido*, denominado hidrógeno puente o pontal, es ácido[23] y se puede eliminar en medio acuoso fuertemente básico o en medio anhidro con *n*-BuLi, NaH o *t*-BuOK.[24] Una vez eliminado este hidrógeno pontal se obtiene un clúster nido dianiónico, con fórmula empírica $[C_2B_9H_{11}]^{2-}$, que se denomina dicarballuro. Se considera que este dianión tiene una hibridación de tipo sp^3 en los átomos de la cara pentagonal abierta que apuntan a la posición vacante dejada por el B^+. Nótese la similitud con el anión ciclopentadienuro, $[C_5H_5]^-$, Figura 1.6.

1.2.2. Metalacarboranos

La semejanza estructural y electrónica del dianión dicarballuro con el ciclopentadienuro llevó a pensar que el primero debería tener orbitales con una simetría y energía apropiada para complejar metales de transición. Los primeros metalacarboranos se pre-

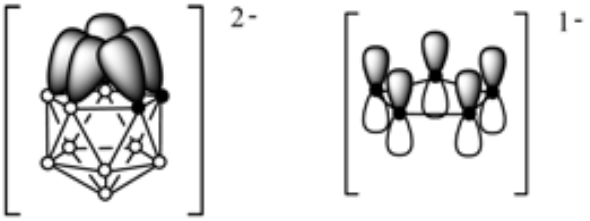

Figura 1.6: Representaciones esquemáticas del anión dicarballuro (izq.) y el anión ciclopentadienuro (dcha).

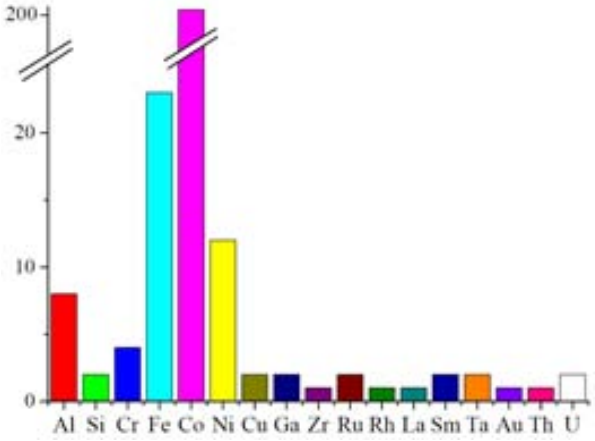

Figura 1.7: Número de casos encontrados en la CSD de estructuras cristalinas con determinado elemento central en un complejo tipo sándwich con dos ligados dicarballuro.

pararon en el año 1965 cuando Hawthorne y su grupo obtuvieron el primer clúster de boro y carbono en el cual dos ligandos dicarballuro complejaban en forma sándwich un átomo de Fe, [3,3'-Fe(1,2-$C_2B_9H_{11})_2]^-$,[25] y pocos meses después se publicó la síntesis del cobaltabisdicarballuro, [3,3'-Co(1,2-$C_2B_9H_{11})_2]^-$, también llamado *cosane* o *cosan.*[26] Dos años después este grupo reporta los complejos tipo sandwich con Ni[27] y poco después los de Cr,[28] y los de Cu, Au y Pd en 1968.[29] Una búsqueda de estructuras cristalográficas en CSD de este tipo de compuestos permite un ejemplo gráfico de los compuestos sintetizados hasta la fecha,[30] véase Figura 1.7. Estos metalacarboranos presentan unas diferencias significativas con los metalocenos, ya que los primeros son mucho más estables química y térmicamente y el par de ligandos dicarballuro permite estabilizar estados

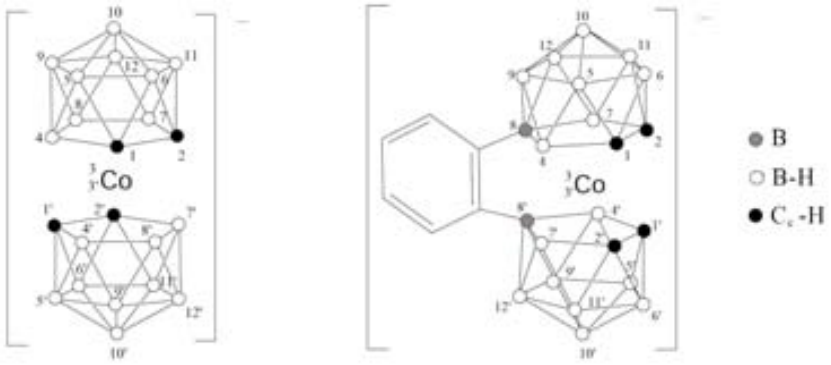

Figura 1.8: Anión de cobaltabisdicarballuro, [3,3'-Co(1,2-$C_2B_9H_{11})_2]^-$ (izq.) y anión pinzado en los $B(8)$ y $B(8')$ por puente fenilo, [8,8'-μ-C_6H_4-3,3'-Co(1,2-$C_2B_9H_{10})_2]^-$(dcha.) con numeración en los vértices.

de oxidación más altos en el metal que con el análogo con ciclopentadienuro. Como un ejemplo se puede poner el caso del metaloceno de Cu(II), el cual es aún desconocido y del correspondiente con dicarballuro, [3,3'-Cu(1,2-$C_2B_9H_{11})_2]^{2-}$, existe estructura cristalina.[31]

Reacciones sobre el cobaltabisdicarballuro [3,3'-Co(1,2-$C_2B_9H_{11})_2]^-$.

El metalacarborano en el que se centra este trabajo, el anión [3,3'-Co(1,2-$C_2B_9H_{11})_2]^-$, es el más estudiado (Figura 1.7) y consiste en un átomo de cobalto central en estado de oxidación +3 coordinado mediante enlaces π (y cierta componente σ) a dos ligandos dicarballuro. Cada dicarballuro tiene dos cargas negativas y por tanto la especie global es monoaniónica. La carga negativa se deslocaliza por todo el gran volumen de la molécula, por esto se dice que es un anión de baja densidad de carga. En la Figura 1.8 (izq.) se representa este anión con la numeración indicada en los vértices.

Este anión presenta dos puntos diferentes de reactividad, los vértices C_c−H y los B−H. Las sustituciones directas en los átomos de boro[32] han sido mucho más estudiadas que las sustituciones en los átomos de carbono, y existe relativa facilidad para la formación de derivados que tienen conectados los átomos de boro $B(8)$ y $B(8')$,[33] como el derivado con un puente fenilo uniendo los dos clústers (Figura 1.8 (dcha.)).[34] Otra vía para derivatizar el complejo [3,3'-Co(1,2-$C_2B_9H_{11})_2]^-$ en los vértices B−H es la Sustitución Nucleofílica Inducida Electrofílicamente (SNIE), que aprovecha que en el vértice

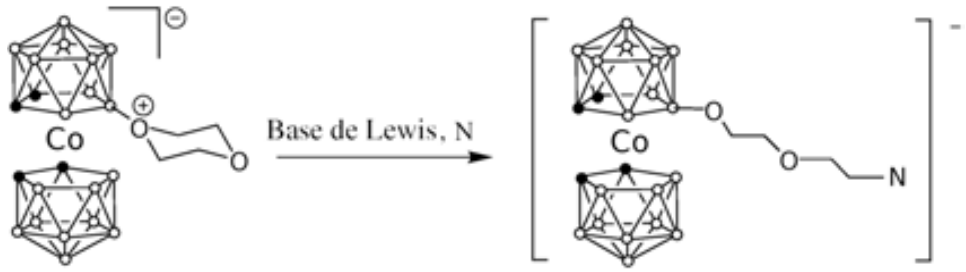

Figura 1.9: Esquema de síntesis de la apertura del anillo de dioxano por una base de Lewis (N).

$B(8)$ está el hidrógeno más hidruro o rico en electrones y éste reacciona con ácidos fuertes produciéndose su eliminación y posteriormente la posición vacante la ocupa el nucleófilo. De esta forma se sintetiza el zwitterion formado por este complejo y una molécula de dioxano, [3,3'-Co(8-$C_4H_8O_2$-1,2-$C_2B_9H_{10}$)(1',2'-$C_2B_9H_{11}$)].[35,36] que a su vez puede reaccionar con bases de Lewis que producen la apertura del anillo de dioxano (Figura 1.9).[37] Los nucleófilos que se han usado para esta reacción reportados en bibliografía son de lo más variado, como por ejemplo: pirrolil,[38] imidas, cianuro o aminas,[39] fenolato, fosfito,[40] N-alquilcarbamoyldifenilfosfinas,[41] alcóxidos,[36,42] nucleosidos,[43] y recientemente en nuestro grupo por ácidos carboxílicos, reactivos de Grignard y tiocarboranos.[44]

Hasta hace relativamente poco tiempo, la principal vía de síntesis de C-derivados del [3,3'-Co(1,2-$C_2B_9H_{11}$)$_2$]$^-$ discurría de forma paralela a la propia síntesis del complejo sin derivatizar, esto es, se preparaba el *o*-carborano substituido en los átomos de C_c por alguno de los métodos descritos en el apartado 1.2.1, a continuación se degradaba para obtener la especie monoaniónica [7-R-7,8-$C_2B_9H_{11}$]$^-$, seguido de la desprotonación del hidrógeno pontal para dar el dianión dicarballuro, el cual finalmente se hacía reaccionar con $CoCl_2$, véase Figura 1.10. Este método de síntesis requiere muchos pasos, cada uno de los cuales necesita un balón de reacción diferente e implica al menos cuatro purificaciones, lo que conduce a rendimientos bajos y sólo permite substituyentes idénticos en los ligandos dicarballuro. El mayor inconveniente, además, es que no permite introducir grupos funcionales que no soporten las condiciones alcalinas empleadas durante la preparación del anión dicarballuro. Por todo esto, recientemente se está desarrollando una nueva metodología para simplificar la síntesis de C-derivados del [3,3'-Co(1,2-$C_2B_9H_{11}$)$_2$]$^-$. El método emplea el propio cobaltabisdicarballuro como producto de partida y consiste en

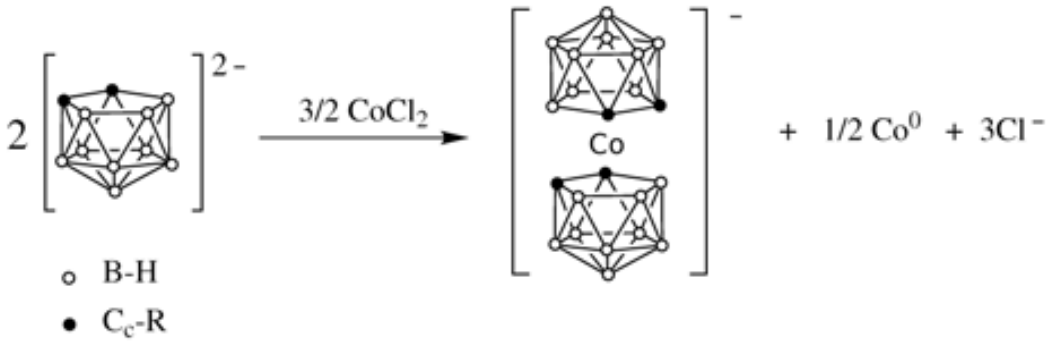

Figura 1.10: Esquema de síntesis de un cobaltabisdicarballuro substituido en los C_c.

adicionar n-BuLi para formar las correspondientes sales litiadas del cobaltabisdicarballuro por desprotonación de los C_c-H, para después éstas hacerlas reaccionar con derivados halogenados.[45–47]

Aplicaciones de los Metalacarboranos.

El campo de aplicación de los metalacarboranos ha crecido en las últimas decadas en direcciones muy diferentes como son la catálisis homogénea, ciencia de materiales, medioambiente y medicina.[48] A continuación se hace un resumen de las más importantes relacionadas con $[3,3'\text{-}Co(1,2\text{-}C_2B_9H_{11})_2]^-$ y derivados.

Una de las principales aplicaciones del anión cobaltabisdicarballuro, y específicamente su B-hexacloro derivado, es la extracción de radionúclidos.[37,49,50] Debido a la gran solubilidad de estas sales en disolventes orgánicos, propiedad que los hace fácilmente extraíbles desde fases acuosas, y su gran estabilidad química, térmica y resistencia a la radiación, el anión cobaltabisdicarballuro es uno de los compuestos químicos más idóneos como agente extractante de iones metálicos procedentes de aguas residuales de centrales nucleares.[51] El desarrollo de esta tecnología con el anión cobaltabisdicarballuro tuvo su *milestone* con la puesta en marcha en 1996 en Rusia de una planta de fraccionamiento de deshechos altamente radioactivos para la separación de ^{137}Cs y ^{90}Sr.[52]

Otras aplicaciones relevantes para los cobaltocarboranos han sido la introducción de estos como aniones dopantes en polímeros conductores[53] y para la construcción de electrodos selectivos de iones.[54]

$$^{10}B + n_{th}\ (0.025\,eV) \rightarrow [^{11}B]^{*} \rightarrow \quad ^{4}He + {}^{7}Li + 2.31\ MeV\ (94\%)$$

Figura 1.11: Esquema de la reacción de fisión nuclear que da lugar a que el isótopo ^{10}B irradiado con neutrones de baja energía produzca partículas α de alta energía (^{4}He) y ^{7}Li.

En medicina y farmacología, los cobaltocarboranos encuentran aplicaciones debido a la anteriormente mencionada estabilidad y a su naturaleza *artificial* que los hace invisibles al metabolismo de los seres vivos, y por tanto presentan baja toxicidad. Una de las aplicaciones más prometedoras es el uso del [3,3'-Co(1,2-$C_2B_9H_{11})_2$]$^-$ como plataforma para funcionalizar con otros grupos que presenten actividad biológica. En una reciente investigación se ha encontrado que unos derivados del cobaltabisdicarballuro actúan como un potente y específico inhibidor de la proteasa HIV-1.[55] En esta línea ya se conoce que ciertas sales de ferroceno tienen propiedades antitumorales,[56] debido a la similitud del ligando ciclopentadienuro con algunos carboranos, se sintetizaron unos complejos semi-sandwich de Fe análogos usando el ligando [Me$C_3B_7H_9$]$^-$ y éste también presentó propiedades citotóxicas contra algunas variedades de células tumorales.[57] En las ramas de radioinmunoterapia/radioinmunodiagnosis, los metalacarboranos con puentes intramoleculares entre las dos cajas de dicarballuro funcionan como reactivos *Venus Flytrap* (VFT) y pueden complejar irreversiblemente radionúclidos como el ^{57}Co, ^{99}Tc o ^{186}Re, dando lugar a radiofármacos.[58] Se están investigando los clústeres yodados de metalacarboranos o carboranos como agentes de contraste en técnicas de rayos X, debido a la opacidad de los átomos de yodo a este tipo de radiación.[59]

La terapia de captura de neutrones por boro (Boron Neutron Capture Therapy, BNCT) es un tratamiento contra el cáncer basado en la reacción de fisión nuclear de captura de neutrones. Cuando un átomo de ^{10}B es irradiado con neutrones de baja energía se producen partículas α de alta energía (^{4}He) y ^{7}Li que destruyen las células (Figura 1.11).[60] Uno de los mayores retos en esta terapia es lograr la correcta distribución y la cantidad necesaria de ^{10}B en las células implicadas. Derivados del cobaltabisdicarballuro han sido considerado como unos compuestos prometedores portadores de boro para BNCT.[61–65] Estos compuestos de B pueden ser suministrados en células tumorales usando estrategias como sintetizar biomoléculas que contienen funciones cobaltabisdicar-

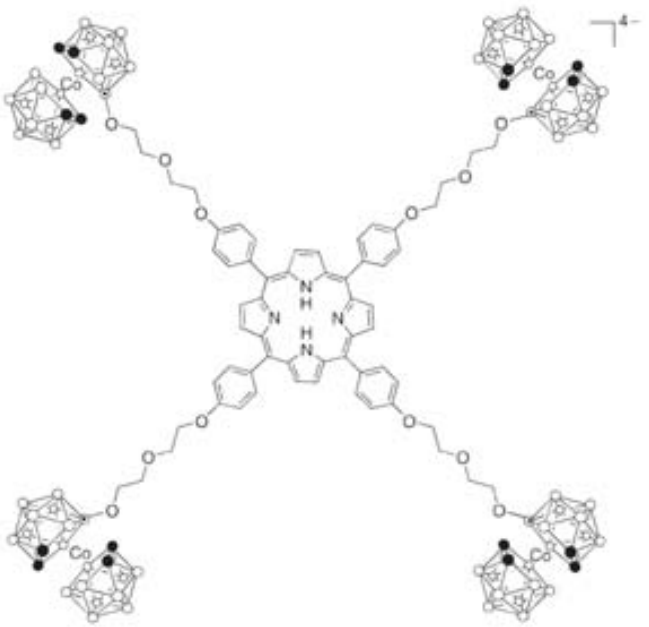

Figura 1.12: Conjugado de porfirina y cobaltacarborano.[66]

balluro como por ejemplo nucleósidos[43] y porfirinas (Figura 1.12).[61,66,67]

La sal de Li^+ del $[3,3'\text{-}Co(1,2\text{-}C_2B_9H_{11})_2]^-$ ha sido reportada como un ácido de Lewis, en el cual el ión de litio débilmente coordinado al anión $[3,3'\text{-}Co(1,2\text{-}C_2B_9H_{11})_2]^-$ cataliza la reacción de adición de acetales silil-cetenes sobre compuestos insaturados carbonílicos.[68]

1.3. Dendrímeros y Metalodendrímeros

1.3.1. Antecedentes históricos

Los dendrímeros son macromoléculas tridimensionales de medida controlada, idealmente monodispersos y con una estructura ramificada bien definida.[69] Los dendrímeros son sintetizados en una secuencia iterativa de reacciones creándose nuevas capas que aumentan el tamaño de la molécula de forma controlada y precisa. La primera síntesis se remonta a 1978 cuando Vötgle y colaboradores describen una síntesis de forma controlada de un polímero de poliamina ramificada acíclica.[70] En 1981, Denkewalter patenta

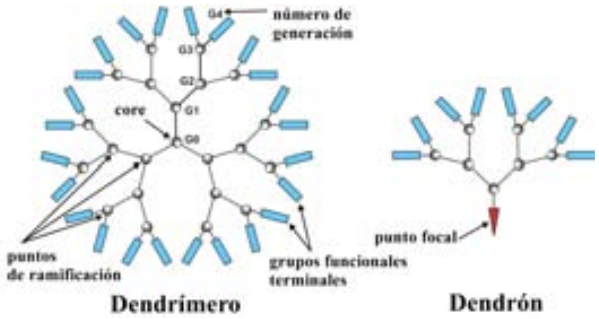

Figura 1.13: Representación esquemática de un dendrímero y un dendrón.

la síntesis de derivados de polilisina ramificados.[71] Y en 1984, Tomalia acuña el termino *dendrímero*[72] para su polímero de poli(amidoamina) (PAMAM),[73] coincidiendo con la comunicación de la síntesis de micelas unimoleculares de Newkome.[74] Desde entonces el campo de los dendrímeros ha suscitado un gran interés en el mundo científico y ha permitido la construcció sistemática de nanoestructuras a un nivel de control atómico nunca antes conocido.[75–78]Algunas referencias seleccionadas de los últimos tres años muestra los principales campos donde se está investigando con dendrímeros en la actualidad, donde destaca sobre todo las aplicaciones farmacológicas,[79] catálisis[80–82] y diseño de dispositivos electrónicos.[83]

1.3.2. Generelidades sobre la Estructura y Métodos de Síntesis de Dendrímeros

La estructura de un dendrímero puede ser dividida en tres regiones: a) core o núcleo, donde nacen las diferentes ramas; b) ramas y puntos de ramificación que se repiten dando lugar a las generaciones del dendrímero; y c) periferia, donde se encuentran los grupos funcionales, que serán los responsables de propiedades como la solubilidad, viscosidad, comportamiento térmico y químico (Figura 1.13). Un dendrón o arborol es un dendrímero que posee un punto focal o grupo funcional desde donde se prolongan las ramas y por tanto tiene menos forma esférica.

Los dendrímeros se organizan por capas o generaciones. Al núcleo central se le considera la generación cero (G0) y así se van enumerando las sucesivas generaciones hasta la periferia. En la Figura 1.13, el dendrímero representado llega hasta una generación

G4 y el punto focal del dendrón está adornado con una rama de generación G3. Conforme el dendrímero va creciendo en número de generaciones, el impedimento estérico que provoca cada rama, hace que la macromolécula vaya adoptando una conformación globular.[76] El crecimiento no puede ser ilimitado y llegado un momento el dendrímero no puede crecer de forma monodispersa, a este fenómeno se le conoce con el nombre de *de Gennes dense-packing phenomenon.*[84]

Métodos de Síntesis

Las estratégias sintéticas principales que se usan para la construcción de la estructura dendrimérica son dos, el método convergente y el divergente (Figura 1.14), aunque pueden mezclarse ambos métodos a tal de conseguir una determinada estructura.

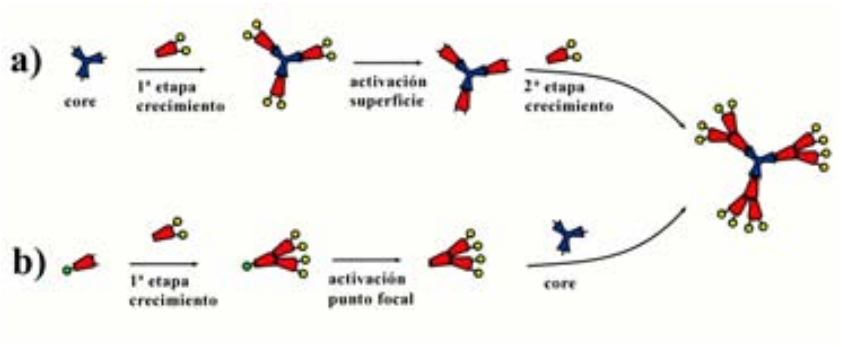

Figura 1.14: Métodos de síntesis de dendrímeros: a) divergente, b) convergente.

Método Divergente

La síntesis comienza sobre una molécula polifuncional que desempeña el papel de *core* en el dendrímero. Los grupos funcionales de esta molécula se hacen crecer mediante una determinada reacción y cuando todas las ramas del *core* han sido funcionalizadas el proceso se detiene. En este momento, la periferia del dendrímero no tiene grupos funcionales para proseguir y se da por concluida la primera etapa de crecimiento. La siguiente etapa en el proceso de construcción del dendrímero es la activación de estos grupos funcionales de la periferia para después seguir con una nueva etapa de crecimiento y así sucesivamente hasta alcanzar la generación deseada, la Figura 1.14.a esquematiza este método.

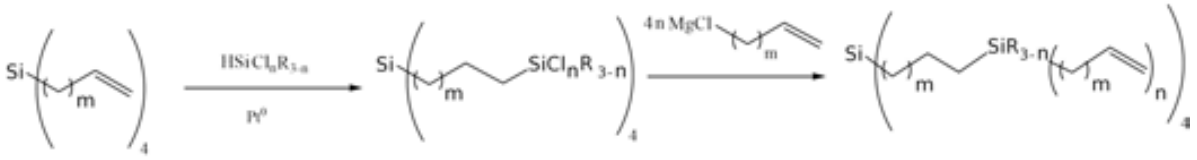

Figura 1.15: Síntesis divergente de dendrímeros de tipo carbosilano.

Método Convergente

Este método se publicó por primera vez en 1990 por Fréchet.[85] Consiste en sintetizar primero las ramas del dendrímero (dendrones) y hacerlas reaccionar con una molécula que actuará de core del dendrímero, véase Figura 1.14.b. La síntesis de las ramas se realiza en dos etapas, crecimiento y activación, como en el caso del método divergente pero como diferencia, en este caso la activación del grupo funcional se realiza en la posición focal y no en la superficie. La síntesis via método convergente finaliza cuando los dendrones sintetizados se hacen reaccionar con una molécula multifuncional, que es el *core*.

1.3.3. Tipología de sistemas dendriméricos

Los sistemas dendriméricos más ampliamente usados son aquellos que poseen un esqueleto orgánico y sus conectividades están basadas en los grupos amida, éster y éter, debido a la simplicidad sintética de introducir bloques ramificados con la formación de estos enlaces. Si bien la mayoría de los dendrímeros reportados son de base orgánica, también han sido sintetizados una variedad de dendrímeros conteniendo heteroátomos en su esqueleto (Si, P, B, Ge, Bi).[86]

A continuación se detallan generalidades de los tipos de estructuras dendriméricas que se usan en este trabajo.

Dendrímeros de tipo Carbosilano y Carbosiloxano.

Las estructuras dendriméricas cuyo esqueleto está constituido por átomos de C y Si, son los dendrímeros llamados de tipo carbosilano.[87] Estos dendrímeros presentan la

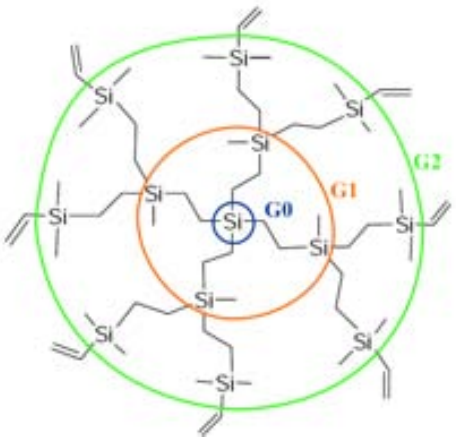

Figura 1.16: Dendrímero de tipo carbosilano 2G-Vi_8.

Figura 1.17: Esquema de reacción genérico de un silano halogenado con un silanol.

principal ventaja de una síntesis sencilla por el método divergente y una amplia versatilidad a la hora de construir diferentes variantes, siguiendo una misma estrategia de síntesis y cambiando simplemente el tipo de reactivos empleados (Figura 1.15).[88] Las etapas de crecimiento y activación son la alquenización con un reactivo de Grignard para hacer crecer las ramas y la reacción catalizada de hidrosililación de alquenos (adición anti-Markovnikov de una función Si−H a un alqueno) utilizando clorosilanos, respectivamente.[89] Alternando sucesivamente este par de reacciones se formarían las diferentes generaciones de este dendrímero de tipo carbosilano, como por ejemplo el representado en la Figura 1.16. Debido a una alta energía de disociación del enlace Si-C y una baja polaridad del mismo, estos dendrímeros son bastante estables termodinámicamente. Las moléculas más usadas como *core* en este tipo de dendrímeros son el tetravinilsilano[90] y el tetraalilsilano,[91] aunque se han usado otras moléculas.[92]

Los dendrímeros de tipo carbosiloxano son preparados por hidrosililación de dobles enlaces con clorosilanos para formar enlaces Si-Cl en la estructura dendrimérica. En uno de los pasos de crecimiento, estos enlaces reaccionaran fácilmente con los silanoles (Figura 1.17). Las estructuras dendriméricas así sintetizadas además de tener enlaces de tipo Si-O-Si tendrán también de tipo $-(CH_2)_n-$ en el esqueleto dendrimérico.[89,92]

Figura 1.18: Síntesis de un dendrón de tipo Fréchet

Dendrímeros de tipo poli(aril-éter) o tipo Fréchet

El procedimiento general de síntesis consiste en la alquilación selectiva de alcoholes fenólicos con un bromuro de alquilo o bencilo en presencia de un exceso de carbonato potásico y del éter 18-corona-6. La segunda etapa consiste en la activación de un alcohol bencílico focal mediante la bromación con tetrabromuro de carbono en presencia de trifenilfosfina, tal como queda esquematizado en la Figura 1.18.

Estas estructuras dendriméricas de tipo oligoéter, descritas originariamente por Fréchet y Hawker,[85] son unas de las más utilizadas y que presentan mayores aplicaciones debido a la estabilidad del enlace tipo éter y su obtención en altos rendimientos.[75,93] En la Figura 1.18 se esquematiza el procedimiento de síntesis de un dendrón.

1.3.4. Dendrímeros que incorporan clústeres de Carborano

El primer dendrímero funcionalizado con un derivado con clúster de borano fue diseñado con el objetivo de ser usado en BNCT y lo reportó Newkome en 1994.[94] En este contexto, y para aumentar la solubilidad de estos dendrímeros,[95] también han sido sintetizados dendrímeros que incorporan *p*-carborano en el interior de la estructura dendrimérica permitiendo que la periferia fuese funcionalizada con grupos hidrófilos.[96] Recientemente, nuestro grupo se ha interesado en la preparación de dendrímeros ricos en boro, para lo cual ha sintetizado dendrímeros con carboranos (*closo* y *nido*) situados en la periferia de dendrímeros de tipo carbosilano,[15,97] (Figura 1.19) y en dendrímeros de tipo Fréchet.[98] Es importante destacar que los dendrímeros aniónicos con *nido*-carboranos presentan cierta solubilidad en agua, en función del tipo de catión que posean.[98]

Según nuestro conocimiento, existen muy pocos ejemplos de metalodendrímeros que

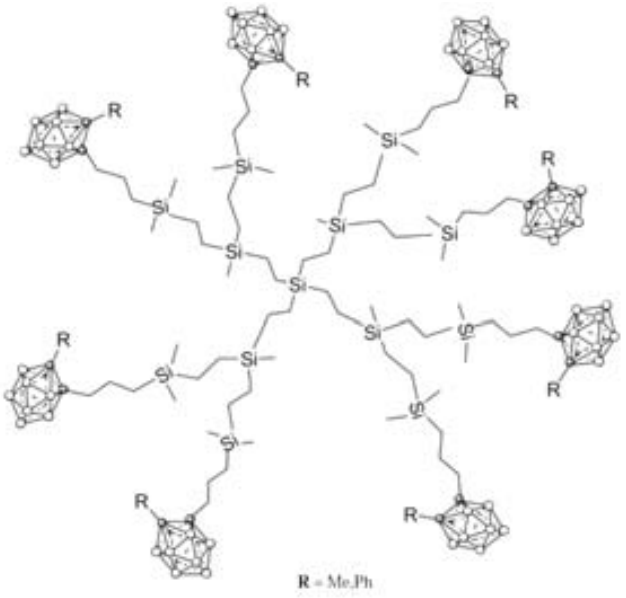

Figura 1.19: Dendrímero de carbosilano funcionalizado con ocho carboranos.[97]

incorporen boranos, así se ha descrito un ejemplo de un metalodendrímero sintetizado por Grimes, funcionalizado en la periferia con complejos de Co tipo *sandwich*.[99]

1.3.5. Metalodendrímeros

La introducción de atómos metálicos (metales de transición) en la estructura de los dendrímeros da pie a la generación de los denominados metalodendrímeros. El primer metalodendrímero se sintetizó en 1992,[100] y desde entonces este campo ha estado en continua expansión. La combinación de los dendrímeros con su naturaleza monodispersa con compuestos organometálicos permite la síntesis de unas macromoléculas cuya características estarán muy influenciadas por tal funcionalización y dotarán de nuevas propiedades de interés para los dendrímeros. Los *reviews* sobre este tema son muchos pero destacamos el de Newkome en 1999,[101] y el de otros autores en el campo de los *Metallodendrimers* como Gorman,[102] Cuadrado[103] y Majoral.[104]

La incorporación de metales de transición en un dendrímero puede realizarse de forma muy específica: en el core (Figura 1.20d);[105] formando parte de la unidad repetitivas de las ramas (Figura 1.20c);[106] también pueden estar ocluidos en sitios específicos dentro

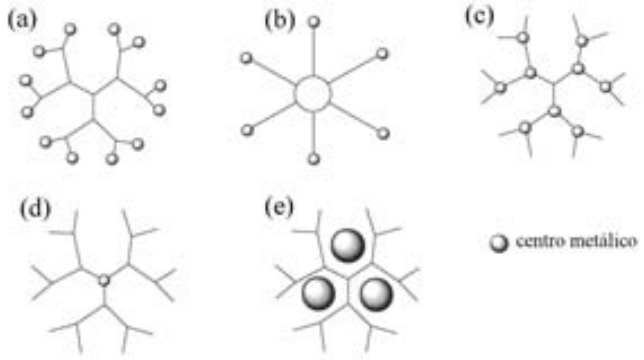

Figura 1.20: Diferentes posiciones que puede ocupar un metal en un dendrímero.

del dendrímero (Figura 1.20e)[107] y en la superficie como grupo terminal (Figura 1.20a-b)).[90] Esta última es la opción más habitual pues es la superficie del dendrímero (en este caso metalodendrímero (a) o metaloestrella (b)) donde las propiedades físico-químicas del compuesto se muestran con mayor protagonismo pero ante todo, la elección de uno u otro lugar depende de las propiedades buscadas.

1.3.6. Aplicaciones de los Dendrímeros y de los Metalodendrímeros en general.

La razón de incorporar especies metálicas en las estructuras dendriméricas es debida a que las propiedades magnéticas, electrónicas, ópticas y químicas de los complejos metálicos se transfieren y se añaden a las ventajas que ofrecen los dendrímeros. Por ello, los metalodendrímeros tienen un amplio campo de aplicaciones, que abarcan disciplinas tan dispares como catálisis, nanoelectrónica, detección molecular, nuevos materiales y medicina.

Catálisis

Las propiedades catalíticas de unos complejos metálicos unidos a la periferia de un dendrímero, situaría estos centros catalíticos en la interfase entre la catálisis homogénea y la heterogénea. En un metalodendrímero, la actividad de los centros catalíticos periféricos es similar a la encontrada en los complejos monometálicos usados en catálisis homogénea, pero la estructura dendrítica sobre la que van soportados (de escala nanométrica), podría permitir una separación y recuperación sencilla del catalizador por filtración.[90a] Varios

reviews abordando este tema han sido publicados.[81,82,108]

Reconocimiento Molecular

El proceso de reconocimiento molecular puede ocurrir tanto en el interior como en la superficie del dendrímero si se situan ciertos grupos específicos en el *core*/ramas o en la periferia, respectivamente.[109] Por ejemplo el reconocimiento de *guest* aniónicos por receptores neutros o cargados que selectivamente emiten una respuesta redox distinta cuando se produce la interacción *host-guest* han sido ampliamente estudiados como sensores,[103] y también se ha revelado que la topología del dendrímero en la función del reconocimiento es muy importante.[82a]

Cristales Líquidos

La versátil construcción de los dendrímeros, junto a la posibilidad de una alta funcionalización y diversidad de los grupos funcionales, permite un control de las propiedades mesomórficas muy interesante que hace a estas macromoléculas aptas para el desarrollo de cristales líquidos.[110–112]

Nanoelectrónica y Foto-óptica

Una de las aplicaciones más interesantes en los metalodendrímeros es preparar compuestos luminiscentes o que sean activos a procesos redox. Los dendrímeros funcionalizados con metales o compuestos organometálicos suelen retener sus propiedades (aunque modificadas por la estructura dendrimérica), como son la capacidad de absorber y emitir luz visible o experimentar procesos redox multielectrónicos. Estas capacidades tienen aplicaciones potenciales en dispositivos moleculares fotoquímicos o electrónicos,[83,108,113] y otras aplicaciones como antenas artificiales para la trasformación de energía lumínica,[83b,83c,83g,83h] o material emisor de luz en OLEDs.[83e,83f]

Medicina

Una de las aplicaciones terapéuticas que actualmente están en desarrollo relacionadas con dendrímeros es su uso como dosificadores de fármacos o sistemas para *drug delivery*. El alto nivel de control en la síntesis de un dendrímero, así como el hecho de poder modular la superficie de éste con el número y tipo de cargas apropiado, los convierte en un portador de fármacos óptimo (Figura 1.21).[79,114,115] Las técnicas de dosificación usando nanoestructuras como los dendrímeros presentan mucho interés debido a monodispersidad y su habilidad para penetrar membranas.[114]

En este punto es importante resaltar, que existen relativamente pocos dendrímeros polianiónicos descritos en literatura en contraste con los policatiónicos. Recientemente,

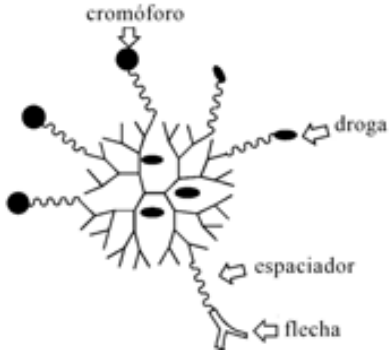

Figura 1.21: Esquema ideal de un dendrímero multifuncionalizado y cargado de fármaco.

se reportó uno basado en grupos benzoato periféricos con la habilidad de transportar cationes de intéres biomédico como la acetilcolina.[116]

Otra aplicación de los dendrímeros bajo investigación es su uso como portadores de agentes de contraste. La resonancia magnética de imagen usa complejos de Gd^{III} para modificar el tiempo de relajación de los protones del H_2O.[117,118]

Respecto a aplicaciones en BNCT, un estudio sobre un conjugado entre PAMAN G5 y un clúster de borano portando en total 1100 átomos de boro en la superficie y con un anticuerpo específico para un receptor en la membrana celular de la célula cancerosa mostró que el conjugado se concentraba preferentemente en estas células respecto a las sanas.[119,120]

A modo de conclusión, se postula que la sinergia entre estos dos tipos de compuestos, dendrímeros y metalacarboranos, generaría un gran abanico de posibles aplicaciones, ya que combinarán las propiedades que ellos presentan separadamente.[48]

1.4. Materiales Nanoestructurados basados en TiO_2 y SiO_2.

La preparación de monocapas auto-organizadas (*self-assembly monolayers*, SAMs) en sustratos sólidos es importante tecnológicamente. En la naturaleza, el proceso de auto-ensamblaje (*self-assembly*) da como resultado la formación de sistemas complejos supermoleculares. Las SAMs son estructuras altamente ordenadas en dos dimensiones

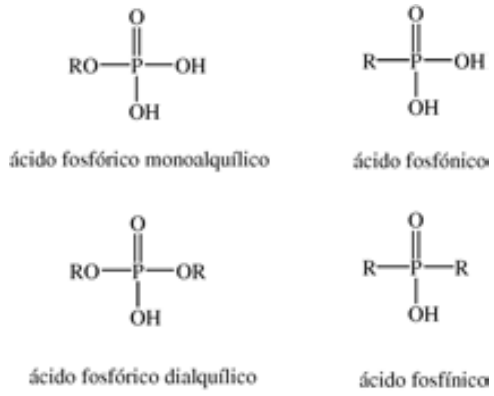

Figura 1.22: Distintos derivados ácidos de derivados organofosforados usados para el acoplamiento con sustratos inorgánicos.

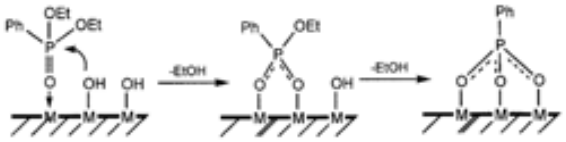

Figura 1.23: Representación esquemática de la reacción de $PhPO_3Et_2$ en una superficie de óxido metálico para formar la especie tridentada $PhP(O_3Ti)_3$.

que ofrecen una oportunidad única como modelo de estudio para aumentar la comprensión fundamental de esta auto-organización, así como el estudio de las relaciones entre estructura, propiedades y fenómenos interfaciales.[121]

1.4.1. Modificación de Superficies de TiO_2.

Los ácidos derivados de compuestos organofosforados (Figura 1.22) presentan gran afinidad hacia óxidos metálicos como el TiO_2 y al igual que los organoclorosilanos sirven para el diseño de materiales híbridos de clase II.[122,123]

En la modificación de la superficie de nanopartículas de TiO_2 se crean enlaces de tipo Ti−O−P (Figura 1.23) por la condensación hidrolítica del grupo P−OH y una ventaja que presentan estos compuestos es que la homocondensación de los grupos P−OH no está tan favorecida como en el caso de los Si−OH.

El uso de organofosforados para la funcionalización de superficies está menos ex-

tendido que el de clorosilanos pero esta técnica está encontrando aplicación en campos como la separación,[124] catálisis,[125] células solares[126] o la funcionalización de implantes de titanio.[127]

1.4.2. Modificación de Superficies de SiO_2.

La fijación convalente de moléculas a sustratos de silicio u oxido de silicio ha recibido mucha atención durante la pasada década.[128] Hay ejemplos en la literatura de moléculas soportadas en estas superficies como pueden ser fullerenos, cromóforos, fluoróforos o biomoléculas, como péptidos o ADN. Los organosilanos de fórmula general $RSiX_3$ (donde R es un grupo funcional orgánico y X es un alcóxido o haluro) forman fácilmente SAMs por quimisorción.[129] La auto-organización espontánea de estas especies al fijarse al sustrato es la formación de una monocapa bastante homogénea y las propiedades físicas de éstas pueden ser fácilmente controladas por la elección apropiada de R. La formación de SAMs es explicada por dos tipos de mecanismos de crecimiento, dependiendo de las condiciones empleadas. Uno es el modelo de crecimiento de tipo "isla", y el otro es el modelo homogéneo del crecimiento dándose este último mecanismo cuando las condiciones en la condensación son de muy bajo contenido en agua.[130]

Las potenciales aplicaciones de estas nanoestructuras son su uso como sensores,[131] inmobilización de biomoleculas,[132,133] *patterning*,[134] OLEDs,[135] puentes dieléctricos para transistores de tipo orgánico en capa fina,[136] óptica no lineal,[137] o modificación de superficies para la formación de cristales líquidos.[138]

2

Objetivos

La preparación y caracterización de nuevos materiales tienen gran interés científico debido al gran abanico de posibles aplicaciones. La creación de nuevas vías para la modificación química de la periferia de dendrímeros, recubrimientos de superficies y funcionalización de nanopartículas, abre la puerta a nuevas posibilidades de aplicación o modificación de las propiedades que presentan estos materiales.

En los últimos años, nuestro grupo se ha interesado en la preparación de compuestos ricos en boro que muestran una cierta tendencia a ser solubles en agua y potenciales aplicaciones en medicina. El objetivo general de este trabajo es desarrollar estrategias para la incorporación de derivados de carborano, y en particular del cobaltacarborano [3,3'-Co(1,2-$C_2B_9H_{11}$)$_2$]$^-$ a diferentes plataformas con el fin de preparar, por un lado, compuestos aniónicos ricos en boro, y por otro lado, estudiar las propiedades que estos clústeres les puedan transmitir. Para ello se han establecido los siguientes objetivos concretos:

1. Sintetizar y caracterizar derivados del [3,3'-Co(1,2-$C_2B_9H_{11}$)$_2$]$^-$ con funciones Si−H apropiadas para hacer hidrosililación sobre dobles enlaces en la periferia de un dendrímero.

2. Sintetizar estructuras dendriméricas de tipo carbosilano y ciclocarbosiloxano de diferentes generaciones con grupos vinilo terminales, para después funcionalizarlas mediante hidrosililación con un derivado del [3,3'-Co(1,2-$C_2B_9H_{11}$)$_2$]$^-$ que contenga un grupo Si−H.

3. Funcionalizar estructuras dendriméricas de tipo poli(aril-éter) (dendrímeros tipo Fréchet) de distinta generación que presentan grupos alilo terminales, mediante reacciones de hidrosililación con derivados del cobaltacarborano.

4. Funcionalizar estructuras dendriméricas de tipo poli(aril-éter) que posean grupos -OH en la periferia, mediante la apertura de anillo dioxano del derivado de cobaltacarborano, [3,3'-Co(8-$C_4H_8O_2$-1,2-$C_2B_9H_{10}$)(1',2'-$C_2B_9H_{11}$)].

5. Obtención de siloxanos, ciclosiloxanos y octasilsesquioxanos que contengan clústeres de carborano, a partir de carboranilclorosilanos y carboraniletoxisilanos.

6. Preparación de derivados fosforados del [3,3'-Co(1,2-$C_2B_9H_{11}$)$_2$]$^-$ adecuados para funcionalizar la superficie de nanopartículas de TiO_2.

7. Preparación de derivados de [3,3'-Co(1,2-$C_2B_9H_{11})_2$]$^-$ adecuados para ensamblar a superficies de *wafers* de silicio oxidado.

3

Resultados y Discusión

3.1. C_c-derivados del $[3,3'\text{-}Co(1,2\text{-}C_2B_9H_{11})_2]^-$ con grupos silano.

3.1.1. Síntesis.

En este apartado se describe la síntesis y caracterización de unos nuevos derivados de cobaltacarborano, que contienen grupos silano enlazados exo-clúster a los carbonos de los ligandos $[C_2B_9H_{11}]^{2-}$, utilizando como productos de partida $Cs[3,3'\text{-}Co(1,2\text{-}C_2B_9H_{11})_2]$, Cs[**1**] y $Cs[8,8'\text{-}\mu\text{-}C_6H_4\text{-}3,3'\text{-}Co(1,2\text{-}C_2B_9H_{10})_2]$, Cs[**2**]. El principal objetivo es la preparación de derivados que contengan una función Si−H en el clúster.[47]

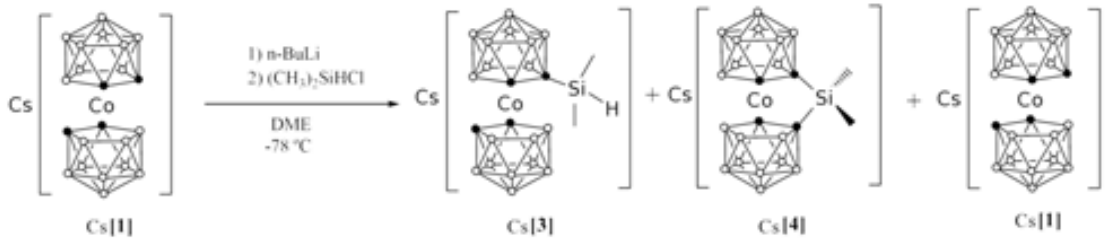

Figura 3.1: Síntesis de cobaltacarboranos Cs[**3**] y Cs[**4**] .

Como se ha comentado en la Introducción, una de las formas de funcionalizar los átomos de carbono del compuesto $Cs[3,3'\text{-}Co(1,2\text{-}C_2B_9H_{11})_2]$es haciendo reaccionar la sal litiada del mismo con derivados halogenados.[45,46] En nuestro caso, con el objetivo de obtener un derivado de $[3,3'\text{-}Co(1,2\text{-}C_2B_9H_{11})_2]^-$ monosubstituido, se hizo reaccionar una disolución de Cs[**1**] en DME con 1 equivalente de *n*-BuLi a -78 ºC. Después, las sales litiadas reaccionaron con 1 equivalente de dimetilclorosilano también a -78 ºC, Figura 3.1. El resultado de la reacción es una mezcla de producto monosubstituido $[\mathbf{3}]^-$ y un producto no esperado $[\mathbf{4}]^-$, además de una considerable cantidad de producto de partida $[\mathbf{1}]^-$. Estos compuestos se precipitan con CsCl, para dar lugar a las correspondientes sales: Cs[**3**], Cs[**4**] y Cs[**1**]. La única manera de aislar Cs[**3**] fue tratando primero la mezcla con Et_2O, donde la especie Cs[**4**] es más insoluble, y posteriormente, separar Cs[**3**] de Cs[**1**], mediante extracciones con CH_2Cl_2, donde Cs[**1**] es ligeramente más insoluble. Finalmente, Cs[**3**] se obtiene con un rendimiento del 4 %, mientras que utilizando $[N(CH_3)_4]^+$ como contraión, se obtiene $[N(CH_3)_4][\mathbf{3}]$ en un 11 %. La razón de emplear dichas condiciones

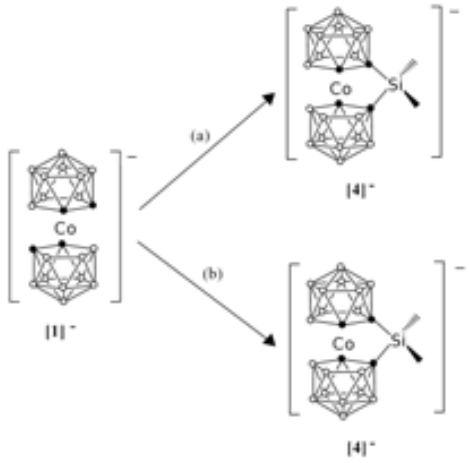

Figura 3.2: Dos rutas de síntesis para obtener $[\mathbf{4}]^-$: a) -40 ºC, DME, 1 eq. *n*-BuLi, $(CH_3)_2SiHCl$ exc. b) -78 ºC, DME, 2 eq. *n*-BuLi, $(CH_3)_2SiCl_2$ exc.

de reacción era forzar la formación del cobaltacarborano monosubstituido con un grupo $-Si(CH_3)_2H$, $[\mathbf{3}]^-$, ya que la utilización de temperaturas más altas (-40 o 0 ºC),[17c] el empleo de THF, o la adición de cantidades estequiométricas de TMEDA,[139] no conducen a una mejora en el rendimiento de obtención del mismo.

La obtención de la especie aniónica $[\mathbf{4}]^-$ de forma inesperada nos llevó a profundizar más en la preparación y estudio de la misma y para ello se desarrollaron dos rutas alternativas con rendimientos relativamente altos, Figura 3.2. En la primera de las rutas que vemos en la Figura 3.2a se lleva a cabo la litiación del compuesto $[\mathbf{1}]^-$, usando 1 equivalente de *n*-BuLi a -40 ºC en DME, y a continuación se hace reaccionar la sal litiada con un exceso de $(CH_3)_2SiHCl$ a la misma temperatura. El anión $[\mathbf{4}]^-$ se puede aislar como sal de cesio, Cs[**4**], rendimiento del 75 %, o como $[N(CH_3)_4][\mathbf{4}]$ si se hace precipitar con $[N(CH_3)_4]Cl$. La segunda de las rutas busca exclusivamente la obtención de la sal dilitiada de $[\mathbf{1}]^-$, usando dos equivalentes de *n*-BuLi, a -78 ºC en DME. Posteriormente, se hace reaccionar esta sal con $(CH_3)_2SiCl_2$, a la misma temperatura, obteniéndose finalmente el compuesto Cs[**4**] con un rendimiento del 95 %.

En el primer intento para obtener el compuesto monosubstituido con la función Si−H, Cs[**3**], el rendimiento fue muy bajo, por eso se decide cambiar de estrategia para derivar los compuestos de cobaltabisdicarballuro con una función Si−H. El proceso seguido se esquematiza en la Figura 3.3. Para sintetizar el compuesto Cs[**5**] se lleva a cabo la

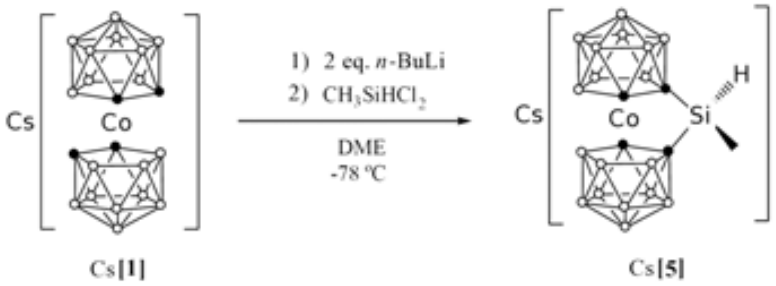

Figura 3.3: Procedimientos para la síntesis del derivado $[\mathbf{5}]^-$

.

dilitiación de $[\mathbf{1}]^-$, usando dos equivalentes de *n*-BuLi a -78 ºC en DME. A continuación, se hace reaccionar la sal dilitiada con un exceso de CH_3SiHCl_2, en las mismas condiciones de reacción. La especie aniónica $[\mathbf{5}]^-$ se aisla como sal de cesio en un alto rendimiento, 92 %. La temperatura juega un papel importante en esta síntesis, ya que, de hacerla a temperatura mayor de -78 ºC nos aparecen una mezcla de isómeros estructurales y producto de partida $[\mathbf{1}]^-$.

Para tener más amplio conocimiento de los diferentes isómeros rotacionales posibles en este tipo de compuestos, además de aportarnos información sobre datos espectroscópicos de los grupos silano enlazados a los átomos de C_c, se ha estudiado la reactividad de la sal monolitiada de $[\mathbf{1}]^-$ frente al $(CH_3)_3SiCl$ obteniéndose el derivado monosubstituido Cs[1-$SiMe_3$-3,3'-$Co(1,2\text{-}C_2B_9H_{10})(1',2'\text{-}C_2B_9H_{11})$], Cs[**6**], en un 33 %. Cuando se hace reaccionar la sal dilitiada con el mismo clorosilano se obtiene el compuesto con dos grupos $-Si(CH_3)_3$ exo-clúster, el compuesto Cs[1,1'-$(SiMe_3)_2$-3,3'-$Co(1,2\text{-}C_2B_9H_{10})_2$], Cs[**7**].

De la misma forma que con los compuestos anteriores, se han sintetizado C-derivados del $[8,8'\text{-}\mu\text{-}C_6H_4\text{-}3,3'\text{-}Co(1,2\text{-}C_2B_9H_{10})_2]^-$, $[\mathbf{2}]^-$, como reactivo de partida. Una de las características más diferenciadora respecto a $[\mathbf{1}]^-$ es que posee la rotación de los ligandos sobre el centro metálico impedida por un grupo fenilo.

Para tratar de obtener el compuesto monosubstituido, se lleva a cabo la reacción de Cs[**2**] con 1 equivalente de *n*-BuLi a -78 ºC en DME, y a continuación se hace reaccionar la sal litiada con el clorodimetilsilano, $(CH_3)_2SiHCl$. Sin embargo, pese a los intentos realizados fue imposible obtener el compuesto monosubstituido derivado de Cs[**2**] con una función Si−H. Al igual que con Cs[**1**], bajo estas conciones de reacción se obtuvo el compuesto pinzado Cs[**8**], tal como se muestra en la Figura 3.4. La sal de cesio del

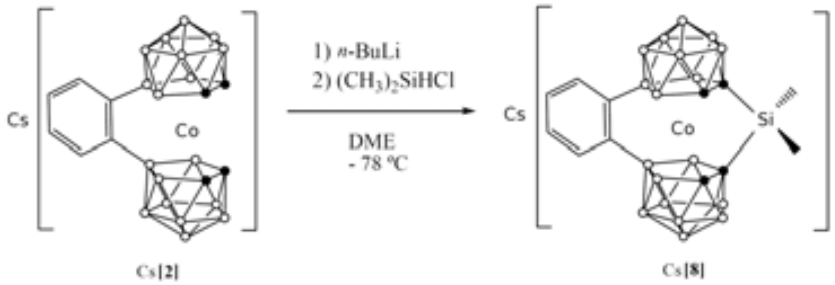

Figura 3.4: Procedimiento para la síntesis del derivado $[\mathbf{8}]^-$

.

anión $[\mathbf{8}]^-$ se aisló con un rendimiento del 85 % y puso en evidencia que el anión $[\mathbf{2}]^-$ reaccionaba de una manera muy similar a su homólogo $[\mathbf{1}]^-$ frente a $(CH_3)_2SiHCl$, dando lugar de nuevo a un compuesto disubstituido y pinzado en los átomos de C_c de dos dicarballuros diferentes.

Por tanto, con el objetivo de funcionalizar $[\mathbf{2}]^-$ con un grupo Si−H exo-clúster, se decide utilizar la misma estrategia que se utilizó para obtener $[\mathbf{5}]^-$. Se lleva a cabo la dilitiación de $[\mathbf{2}]^-$ usando 2 equivalentes de *n*-BuLi a -78 ºC en DME. A continuación, se hace reaccionar la sal dilitiada con un exceso de diclorometilsilano, CH_3SiHCl_2, en las mismas condiciones de reacción. Los dos grupos Si−Cl de este silano reaccionan con la sal dilitiada pinzando los dos clústeres y manteniendo la función Si−H. El compuesto Cs[8,8'-μ-(C_6H_4)-1,1'-μ-SiMeH-3,3'-Co(1,2-$C_2B_9H_9)_2$], Cs[**9**], se obtiene con un rendimiento del 65 %.

Es destacable el hecho de que a partir de Cs[**2**], si intentamos sintetizar el homólogo a Cs[**7**], obtenemos como producto mayoritario el compuesto monosubstituido Cs[8,8'-μ-(C_6H_4)-1-$SiMe_3$-3,3'-Co(1,2-$C_2B_9H_9$)(1',2'-$C_2B_9H_{10}$)], Cs[**10**]. Seguramente el impedimento estérico del primer $-Si(CH_3)_3$ y la imposibilidad de rotación de los ligandos, impediría substituir el segundo C_c para obtener la especie disubstituida.

3.1.2. Caracterización.

Los compuestos han sido caracterizados por IR, RMN de ^1H, ^{11}B, ^{13}C y ^{29}Si, en algunos casos COSY $^{11}B\{^1H\}$-$^{11}B\{^1H\}$-RMN, espectrometría de masas, analisis elemental y los compuestos $[N(CH_3)_4][\mathbf{3}]$, $[N(CH_3)_4][\mathbf{4}]$ y $[N(CH_3)_4][\mathbf{7}]$ por difracción de rayos X.

Espectroscopía de Infrarrojo (IR)

La frecuencia de vibración de los enlaces C_c−H aparece como absorciones finas y poco intensas, entre 3090 y 3034 cm^{-1}. Entre 2584 y 2554 cm^{-1} aparece una absorción muy intensa correspondiente a ν(B−H); la zona donde aparece esta absorción es la característica para los carboranos tipo *nido*. Una señal característica de los compuestos $[\mathbf{3}]^-$, $[\mathbf{5}]^-$ y $[\mathbf{9}]^-$ es la correspondiente a la frecuencia de vibración del enlace Si−H, que aparece entorno a 2160 cm^{-1} y que nos confirma la presencia de la función Si-H. Otra banda común a todos los compuestos es la correspondiente a ν(Si−CH_3), que aparece entre 1250 y 1257 cm^{-1}.

^{1}H-RMN

Los espectros de ^{1}H-RMN se han realizado en acetona deuterada y los desplazamientos químicos están referidos a TMS. En la Tabla 3.1 se recogen los desplazamientos químicos de protón. A efectos comparativos se han incluido los productos de partida $[\mathbf{1}]^-$ y $[\mathbf{2}]^-$ en la tabla.

compuesto	Si−H	C_c−H	Si−CH_3	B−$H_{terminal}$
$[\mathbf{1}]^-$	-	3.94	-	3.37-1.57
$[\mathbf{3}]^-$	4.31	3.85, 3.69	0.29	3.61-1.60
$[\mathbf{4}]^-$	-	4.5	0.31	3.38-1.43
$[\mathbf{5}]^-$	5.06	4.59	0.44	3.40-1.44
$[\mathbf{6}]^-$	-	4.02, 3.83, 3.72	0.28	3.57-1.50
$[\mathbf{7}]^-$	-	4.19, 3.77	0.33, 0.30	3.98-1.58
$[\mathbf{2}]^-$	-	3.58	-	3.76-1.49
$[\mathbf{8}]^-$	-	3.48	0.39, 0.25	4.00-1.43
$[\mathbf{9}]^-$	5.25, 4.97	3.61	0.48, 0.38	4.11-1.43
$[\mathbf{10}]^-$	-	3.52, 3.45	0.28	3.99-1.51

Tabla 3.1: Desplazamientos químicos de los protones (ppm) en el espectro de ^{1}H-{^{11}B}-RMN.

En los compuestos $[\mathbf{3}]^-$ y $[\mathbf{5}]^-$ se observa una única señal a 4.31 y 5.06 ppm, respec-

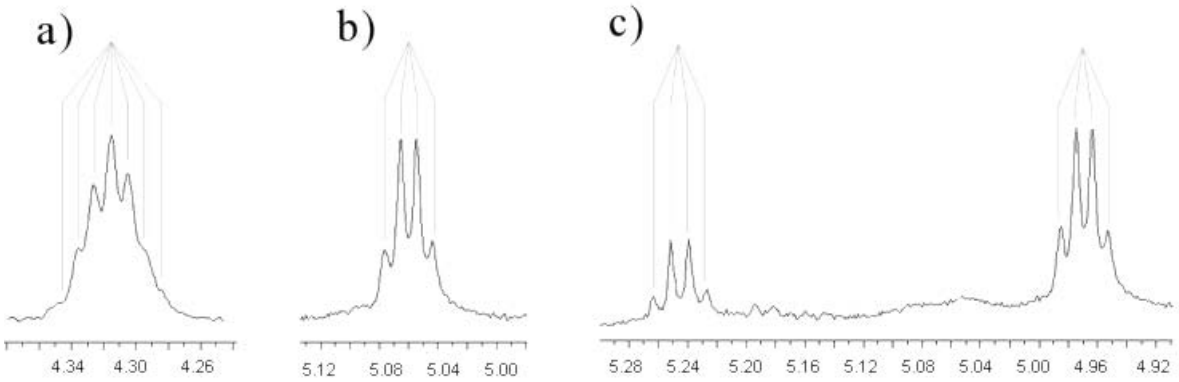

Figura 3.5: Espectro de ^{1}H-RMN correspondiente a la zona de desplazamiento químico de los protones Si−H: a) $[\mathbf{3}]^-$, b) $[\mathbf{5}]^-$ y c) $[\mathbf{9}]^-$ mostrando proporción relativa de los dos isómeros 24 y 76 %.

tivamente, atribuible al protón del grupo Si−H. Sin embargo, en el compuesto $[\mathbf{9}]^-$ se observan dos desplazamientos químicos atribuibles a este protón, a 5.25 y 4.97 ppm, lo cual nos indica la presencia de isómeros estructurales. El Si−H de los compuestos $[\mathbf{3}]^-$, $[\mathbf{5}]^-$ y $[\mathbf{9}]^-$ se acopla a los protones del grupo metilo, con una constante de ^{3}J=3.4 Hz, dando un sistema septuplete o cuadruplete segun corresponda, Figura 3.5.

Todos los compuestos disubstituidos y pinzados presentan una sola señal amplia correspondiente a los C_c−H, debido a su simetría. Contrariamente, el disubstituido no pinzado en los carbonos $[\mathbf{7}]^-$ presenta dos señales en distinta proporción, que indican la presencia de dos isómeros posicionales. El espectro de ^{1}H-RMN del monosubstituido $[\mathbf{3}]^-$ muestra dos señales para los C_c−H: la primera a 3.85 ppm que integra por un protón y la segunda a 3.69 ppm, que integra por dos protones. Sin embargo, en el caso del compuesto monosubstituido $[\mathbf{6}]^-$ aparecen 3 señales integrando por un protón. Los protones metílicos del grupo Si−CH_3 aparecen entre 0.29 y 0.48 ppm. En los compuestos $[\mathbf{3}]^-$, $[\mathbf{5}]^-$ y $[\mathbf{9}]^-$ estos protones aparecen como dobletes, por el acoplamiento con el protón del Si−H. En el compuesto $[\mathbf{4}]^-$ los protones metílicos dan un único singulete, sin embargo, en su homólogo $[\mathbf{8}]^-$ se observan dos singuletes debido a la presencia de isómeros estructurales.

Respecto a los protones unidos a boro, aparecen en el intervalo comprendido entre 1.43 y 4.11 ppm, Tabla 3.1.

^{13}C-RMN

En general las señales correspondientes a los C_c, se observan con menor intensidad si las comparamos con las señales de los carbonos de los metilos unidos a silicio. Además, de todas las señales asignadas a C_c, aquellas desplazadas a campo más alto se pueden asignar a los C_c-Si, ya que, la naturaleza más electropositiva del silicio hace que los átomos unidos a él aparezcan más apantallados. Los desplazamientos químicos de los C_c-H aparecen en el intervalo amplio de 42.11 a 59.04 ppm y tienden a tener la señal desplazada a campo bajo respecto a los productos de partida, $[\mathbf{1}]^-$ y $[\mathbf{2}]^-$. Los átomos de carbono correspondientes a los metilos enlazados a Si están muy apantallados y aparecen siempre a campo más alto en todos los casos, en un intervalo que va desde 3.20 a -6.87 ppm.

^{11}B-RMN

Los dieciocho átomos de boro de los compuestos $[\mathbf{3}]^-$ – $[\mathbf{7}]^-$ presentan bandas en los espectros de $^{11}B\{^1H\}$-RMN, en el rango comprendido entre +9.10 y -22.26 ppm. En cambio, los átomos de boro de los compuestos $[\mathbf{8}]^-$ – $[\mathbf{10}]^-$ aparecen en el intervalo de +27.47 a -24.51 ppm. En el espectro de ^{11}B-RMN, todos los desplazamientos químicos de los átomos de boro aparecen como un doblete, por acoplamiento de los átomos de boro con el protón al que van enlazados. En los compuestos $[\mathbf{8}]^-$-$[\mathbf{10}]^-$, la resonancia a campo más bajo (+ 27 ppm) no se desdobla en el espectro de ^{11}B-RMN, debido a que esta señal se atribuye a los átomos de boro que van enlazados a los carbonos del fenilo.

Si los compuestos funcionalizados con grupos silano se comparan con su precursor $[\mathbf{1}]^-$, se observa una similitud en el rango donde aparecen los desplazamientos químicos de los átomos de boro. En general, la presencia del substituyente en los carbonos del clúster produce un ligero desplazamiento a campo bajo de todas las señales respecto a las de sus precursores, y el aumento del número de resonancias en los espectros de $^{11}B\{^1H\}$-RMN de los C-substituidos. En estos compuestos se produce un desdoblamiento de las señales atribuidas a los $B(4,7,9,12)$ y $B(5,11)$, debido a que las dos caras C_2B_3 del cobaltacarborano dejan de ser totalmente paralelas, y por tanto la estructura pierde simetría. Este hecho no sucede en los derivados de $[\mathbf{2}]^-$, debido a la mayor rigidez que le confiere el grupo fenilo que pinza los átomos $B(8)$ y $B(8')$.[47]

El espectro de $^{11}B\{^1H\}$-RMN del compuesto monosubstituido, $[\mathbf{3}]^-$, presenta un

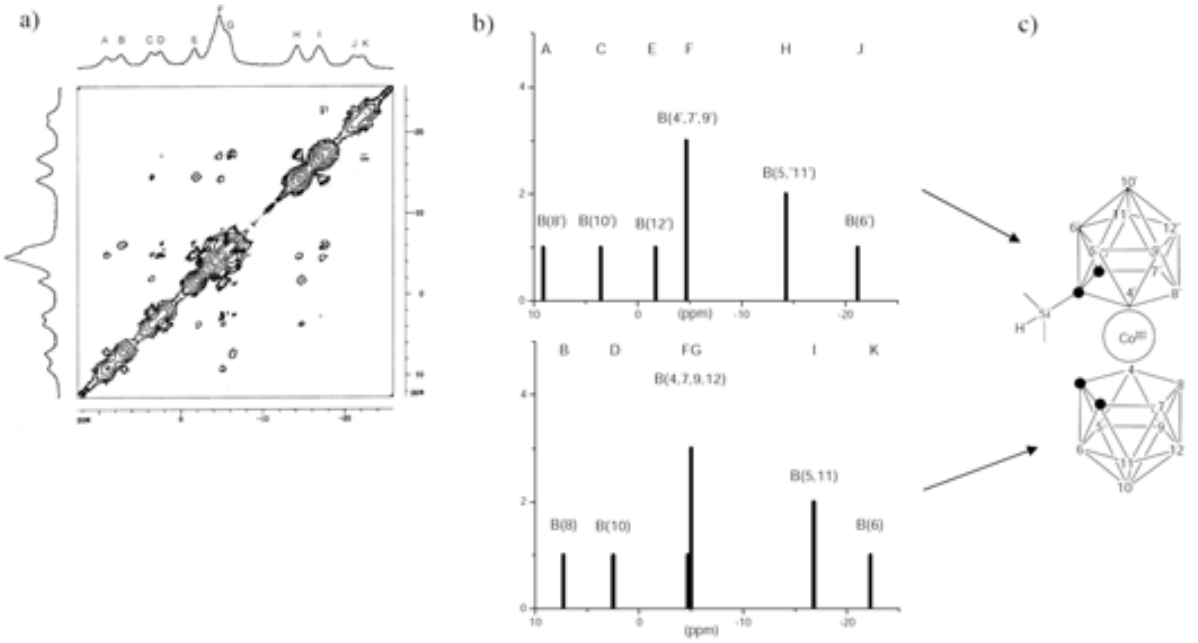

Figura 3.6: a) Espectro bidimensional COSY $^{11}B\{^1H\}$ - $^{11}B\{^1H\}$-RMN. b) Desglose de señales del espectro COSY para cada ligando. c) Esquema con boros numerados del compuesto $[\mathbf{3}]^-$.

patrón de intensidades 1:1:1:1:1:3:4:2:2:1:1, muy distinto a los observados en los compuestos que tienen disubstitución y pinzamiento. Con un mayor número de señales debido a su mayor asimetría, nos ha permitido realizar un espectro bidimensional COSY $^{11}B\{^1H\}$-$^{11}B\{^1H\}$-RMN (Figura 3.6a), a través del cual se han podido asignar todas las resonancias de este espectro a los átomo de boro.[47,140]

El compuesto $[\mathbf{7}]^-$ está disubstituido pero no pinzado, por lo que no tiene impedida la rotación a través del eje que atraviesa el centro metálico. El espectro de $^{11}B\{^1H\}$-RMN de este compuesto presenta 9 señales en el intervalo de +8.25 a -19.99 ppm, con un patrón de intensidades de 2:2:4:2:2:1:2:1:2, el cual nos sugiere la presencia de varios isómeros rotacionales.

^{29}Si-RMN

Los desplazamientos químicos de los átomos de Si en los espectros de ^{29}Si-RMN para los compuestos sintetizados en este trabajo se muestran en la Tabla 3.2.

compuesto	Si
$[\mathbf{3}]^-$	-8.28
$[\mathbf{4}]^-$	13.98
$[\mathbf{5}]^-$	2.94
$[\mathbf{6}]^-$	10.74
$[\mathbf{7}]^-$	10.75
$[\mathbf{8}]^-$	11.74
$[\mathbf{9}]^-$	2.69
$[\mathbf{10}]^-$	8.63

Tabla 3.2: Desplazamientos químicos de los átomos de Si (ppm) en los espectros de ^{29}Si-RMN.

Se aprecia que el desplazamiento químico del átomo de silicio en estos compuestos está bastante afectado por sus substituyentes. El átomo de Si del grupo -$SiH(CH_3)_2$ en el compuesto $[\mathbf{3}]^-$ aparece a campo muy alto (-8.28 ppm), mientras que en los compuestos pinzados $[\mathbf{5}]^-$ y $[\mathbf{9}]^-$, el grupo -μ-$SiH(CH_3)$ aparece alrededor de 2.8 ppm. El átomo de Si perteneciente a un grupo -μ-$Si(CH_3)_2$ o -$Si(CH_3)_3$ aparece a campo más bajo, en el rango de 8.63 a 13.98 ppm.

Ultravioleta-Visible.

Los espectros UV-Vis de los compuestos sintetizados $[\mathbf{3}]^-$ - $[\mathbf{10}]^-$ fueron medidos en acetonitrilo. Un ajuste por gausianas[141] fue aplicado para su mejor comparación con otros espectros UV-Vis de compuestos similares. Como ejemplo se muestra el espectro de $[\mathbf{4}]^-$ en la Figura 3.7

Los aniones presentan tres absorciones comunes alrededor de 280, 340, y 450 nm, que pueden atribuirse al anión [3,3'-Co(1,2-$C_2B_9H_{11})_2]^-$ como ya ha sido descrito.[141] La absorción cerca de 450 nm se asigna a la transición d-d del Co en el complejo. En el compuesto $[\mathbf{7}]^-$ muestra un desplazamiento batocrómico con respecto a $[\mathbf{1}]^-$ de alrededor de 40 nm y las disoluciones de este compuesto son de un tono más rojo oscuro en comparación con $[\mathbf{1}]^-$ y $[\mathbf{3}]^-$ - $[\mathbf{6}]^-$, que presentan un color más anaranjado. Es importante enfatizar que cuando los ligandos están pinzados por un grupo silano se muestra una

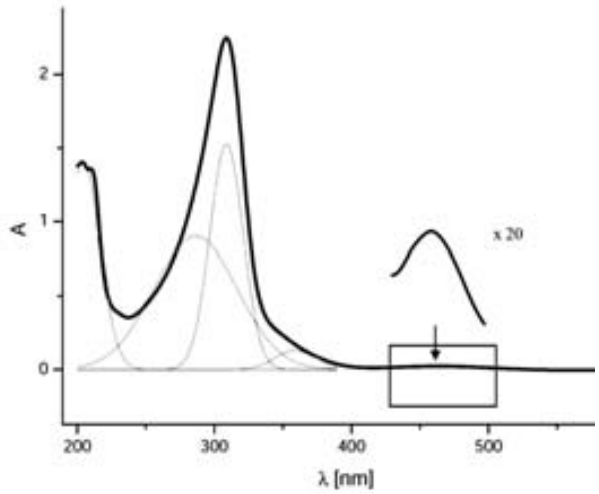

Figura 3.7: Espectro UV-Vis de $[\mathbf{4}]^-$ (linea negra) y ajuste con curvas gaussianas (lineas color gris). La sección expandida muestra una absorción cerca de 445 nm y está ampliada x20.

absorción adicional entorno a 310 nm. Los compuestos preparados a partir de $[\mathbf{2}]^-$ exhiben un máximo alrededor de 230 nm atribuido al grupo fenilo.[142] La principal diferencia entre el precursor y sus derivados obtenidos en este trabajo $[\mathbf{8}]^-$ - $[\mathbf{10}]^-$ es una señal entorno a 270 nm y un desplazamiento batocrómico de 10 nm en el segundo máximo entorno a 320 nm.

Estructuras Cristalinas.

Las estructuras cristalinas de los compuestos $[N(CH_3)_4][\mathbf{3}]$, $[N(CH_3)_4][\mathbf{4}]$ y $[N(CH_3)_4][\mathbf{7}]$ fueron resueltas por difracción de rayos X. Las tres sales cristalizaron en una disolución de acetona y con contraión $[N(CH_3)_4]^+$. En las Figura 3.8 se muestra las representaciones ORTEP de estas tres sales.

Un hecho relevante, común a las tres estructuras cristalinas, es que la presencia del catión $[N(CH_3)_4]^+$ ayuda a cristalizar los compuestos. Nunca fueron obtenidos cristales aptos para resolución por difracción de rayos X con otro catión. El anión $[\mathbf{3}]^-$ tiene simetría C_1, la conformación de los clústeres es *cisoide* y el grupo $-SiH(CH_3)_2$ está proyectado entre los dos C_c del clúster vecino (Figura 3.8 izq.). El anión $[\mathbf{4}]^-$ tiene simetría σ con el Co, Si y C metílicos en el mismo plano (Figura 3.8 centro). El grupo $\mu-Si(CH_3)_2$

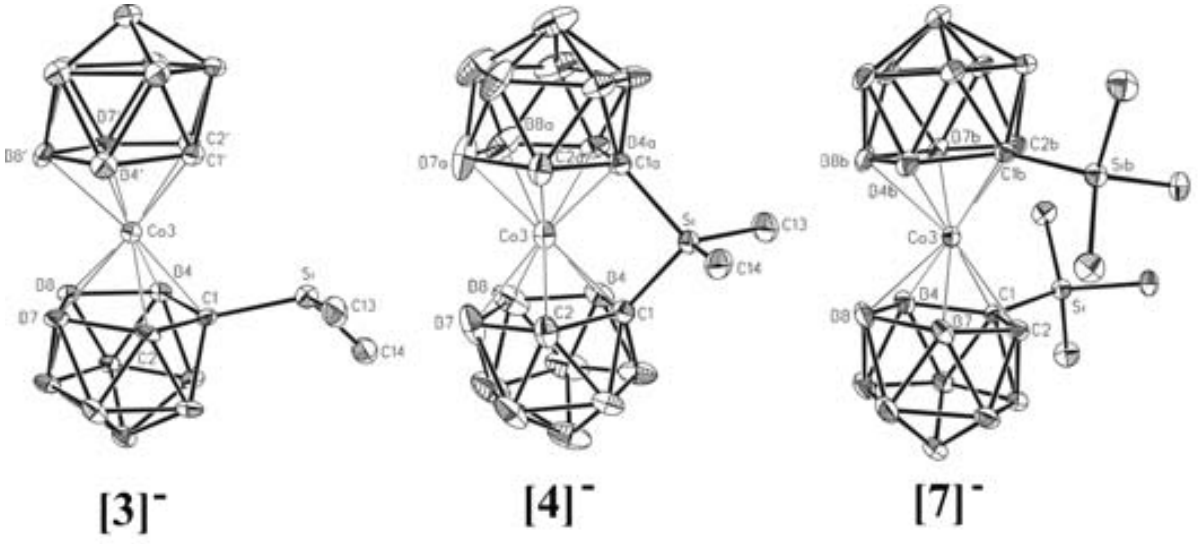

Figura 3.8: Representación ORTEP para las estructuras de los aniones de $[N(CH_3)_4]$[**3**], $[N(CH_3)_4]$[**4**] y $[N(CH_3)_4]$[**7**] con los elipsoides de desplazamiento térmico al 30 %.

está enlazado a ambos clústeres por los C_c, lo que hace que los carbonos y boros del anillo C_2B_3 estén eclipsados en los ligandos. El anión $[\mathbf{7}]^-$ tiene simetría C_2 con el metal situado en el eje principal y la disposición de los ligandos es *cisoide* como se puede apreciar en la Figura 3.8.

Estas tres estructuras cristalinas representan los tres primeros ejemplos de C-substituidos del [3,3'-Co(1,2-$C_2B_9H_{11})_2]^-$ con grupos silano. Además, la estructura del compuesto monosubstituido $[N(CH_3)_4]$[**3**] es el primer ejemplo de monosubstitución en los C_c para el [3,3'-Co(1,2-$C_2B_9H_{11})_2]^-$.

3.1.3. Cálculos DFT en los C_c-substituidos de [3,3'-Co(1,2-$C_2B_9H_{11})_2]^-$.

En este apartado estudiamos ciertos aspectos de la formación y caracterización de los aniones descritos en el apartado anterior mediante teoría del funcional de la densidad (DFT, *density functional theory*).[143] La optimización de las geometrías de los aniones $[\mathbf{1}]^-$ - $[\mathbf{10}]^-$ se realizó con el funcional híbrido B3LYP[144] con la base 6-311G(d,p). También se ha llevado a cabo el cálculo de los desplazamientos químicos teóricos en los

espectros de $^{11}B\{^1H\}$-RMN para las estructuras optimizadas y así comparar espectros experimentales en disolución y teóricos en fase gas.[47]

Isomeros rotacionales de los compuestos $[\mathbf{3}]^-$, $[\mathbf{6}]^-$ y $[\mathbf{7}]^-$.

Experimentalmente se conocen tres rotámeros para el anión $[\mathbf{1}]^-$: *cisoide* (C_{2v}), *gauche* y *transoide* (C_{2h}).[145] Teóricamente, en fase gas y en ausencia de contraiones, la conformación *transoide* es 12.8 kJ/mol más estable que la conformación *cisoide*, siendo la intermedia la *gauche*. Las barreras energéticas de rotación se sitúan entorno a los 35 kJ/mol.[146] En este trabajo se han calculado las energías de los isómeros rotacionales de los compuestos $[\mathbf{3}]^-$, $[\mathbf{6}]^-$ y $[\mathbf{7}]^-$. En este caso, los C-substituidos tienen 5 posibles isómeros rotacionales. Dos *cisoide*, dos *gauche* y una *transoide*. En el caso del anión $[\mathbf{3}]^-$, el confórmero *gauche*-1 is más estable que *cisoide*-1 por 2.8 kJ/mol (Figura 3.9a). Esta conformación *cisoide*-1 es el rotámero experimental obtenido en la estructura cristalina (Figura 3.8).

Es interesante notar que el hidrógeno en Si−H está interaccionando con un C_c−H. Si las estructura *cisoide*-1 de $[\mathbf{3}]^-$ es optimizada evitando tal interacción, la conformación *cisoide*-1 es incluso más inestable que la *gauche*-1. Por tanto tal interacción tiene cierta importancia a nivel teórico y a nivel experimental, como veremos más adelante.

Para el caso del anión monosubstituido, $[\mathbf{6}]^-$, de nuevo una conformación *gauche* es la más estable (Figura 3.9a). Para el anión C_c-disubstituido $[\mathbf{7}]^-$, se optimizaron sólo los rotámeros *cisoide*-2, *gauche*-2 y *transoide*, pues la optimización de los rotámeros *cisoide*-1 y *gauche*-1 nunca convergió debido a su gran impedimento estérico. El rotámero más estable en este caso es el *cisoide*-2 que además coincide con el determinado en la estructura cristalina (3.8).

Isómeros estructurales de los compuestos $[\mathbf{4}]^-$, $[\mathbf{5}]^-$ y $[\mathbf{9}]^-$.

Los compuestos pinzados $[\mathbf{4}]^-$, $[\mathbf{5}]^-$ y $[\mathbf{9}]^-$ no tienen isómeros rotacionales pero pueden formar isómeros estructurales que serán estables en un rango amplio de temperatura, al estar unidos los dos ligandos dicarballuro por el puente de Si.

El anión $[\mathbf{4}]^-$ tiene la posibilidad de configurar tres isómeros estructurales, una pareja de enantiómeros y un diastereoisómero, cuyas formas estructurales serían la mezcla racémica, denominada forma $[\mathbf{4}]^-$-*rac*, y la forma $[\mathbf{4}]^-$-*meso*. En la Figura 3.10 se en-

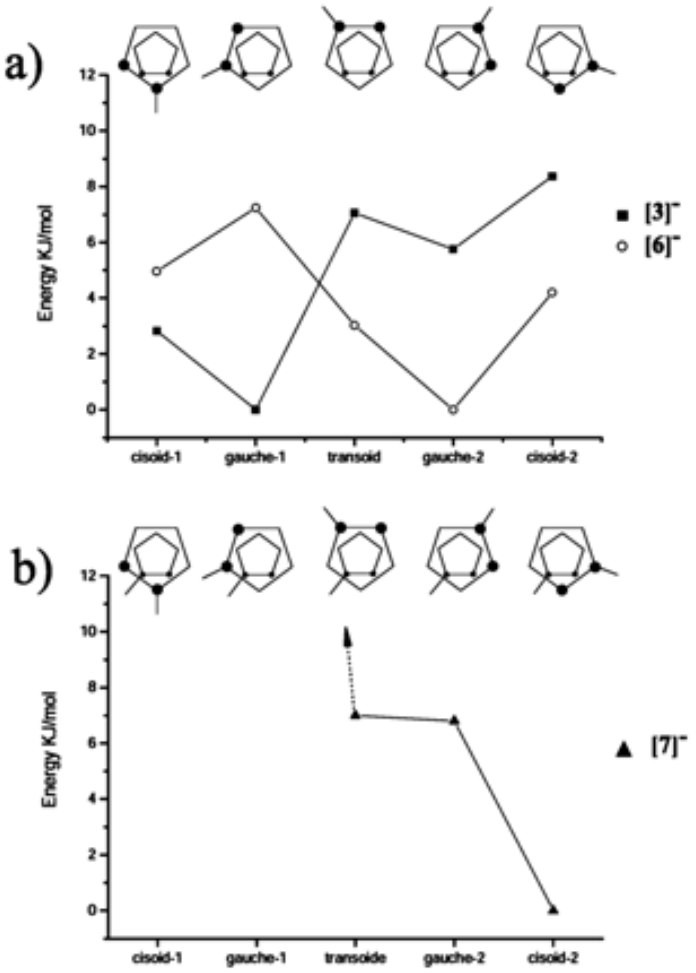

Figura 3.9: Energías relativas calculadas para las estructuras optimizadas de a) [**3**]$^-$, [**6**]$^-$ y b) [**7**]$^-$.

cuentran representados estos isómeros. Se puede apreciar que los metilos unidos a silicio en las formas *l* y *d* de [**4**]$^-$-*rac* son magnética y químicamente equivalentes. Sin embargo, en la forma [**4**]$^-$-*meso*, con los cuatro átomos de carbono del clúster eclipsados, los metilos no son equivalentes porque uno de los metilos se pueda proyectar sobre los C_c de los ligandos, y el otro lo hace sobre los boros. Según los cálculos teóricos, la forma [**4**]$^-$-*rac* es 12.7 kJ/mol más estable que la [**4**]$^-$-*meso*. En las condiciones de síntesis óptimas (-78ºC) se obtiene principalmente la forma [**4**]$^-$-*rac*, y en proporciones minoritarias una

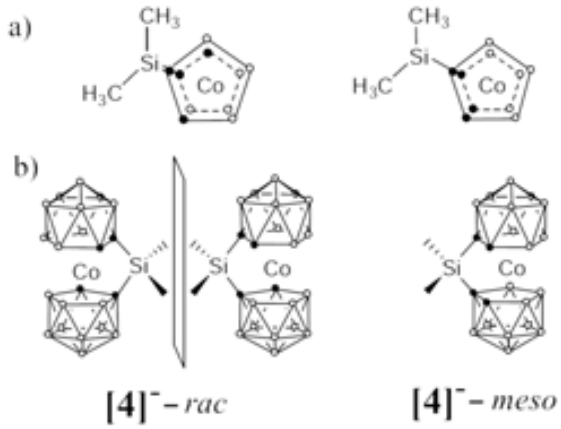

Figura 3.10: Isómeros estructurales del anion $[\mathbf{4}]^-$. a) Proyección en el plano C_2B_3, b) Vista frontal.

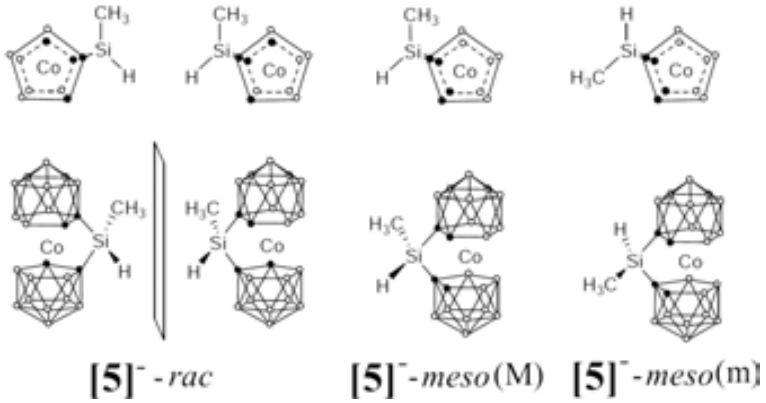

Figura 3.11: Isómeros estructurales del anion$[\mathbf{5}]^-$.

cierta cantidad de $[\mathbf{4}]^-$-*meso*. La estructura cristalina para $[\mathbf{4}]^-$ es la forma -*meso* y fue obtenida de una reacción a - 40 °C.

El anión $[\mathbf{5}]^-$ puede configurar cuatro isómeros estructurales: una pareja de enantiómeros y dos diastereoisómeros, que corresponderían a la mezcla racémica o formas *rac* y a dos formas *meso*, respectivamente. En la Figura 3.11 se esquematizan los cuatro isómeros estructurales. La forma $[\mathbf{5}]^-$-*meso*(M) y la forma $[\mathbf{5}]^-$-*meso*(m) tienen en común que los cuatro átomos de carbono del clúster están eclipsados dos a dos, pero en la primera el metilo unido a silicio se proyecta sobre los B−H del clúster y en la segunda el

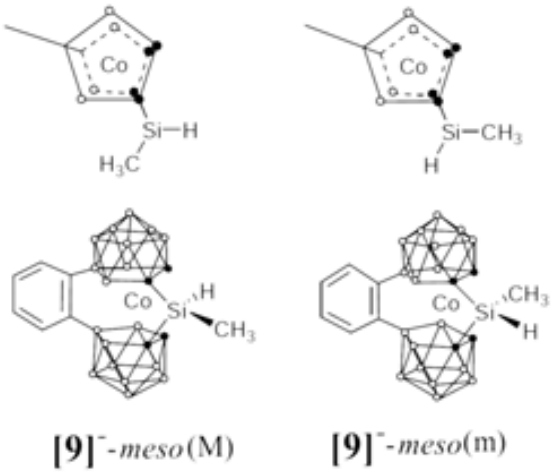

Figura 3.12: Isómeros estructurales del anion [**9**]$^-$.

metilo se proyecta sobre los C_c—H. Según los cálculos teóricos, la forma [**5**]$^-$-*rac* es 10.5 kJ/mol más estable que la forma [**5**]$^-$-*meso*(M) y 15.4 kJ/mol más estable que la forma [**5**]$^-$-*meso*(m). Si se lleva a cabo la síntesis de [**5**]$^-$ a -78 ºC, en el espectro de ^{1}H-RMN se observa una única señal debida al protón Si—H, que correspondería a [**5**]$^-$-*rac*. Si la síntesis se realiza a más de -40 ºC, en el espectro de ^{1}H-RMN aparecen tres resonancias debidas a protones Si—H que pertenecerían a las formas [**5**]$^-$-*rac*, [**5**]$^-$-*meso*(M) y ([**5**]$^-$-*meso*(m), con unas proporciones relativas de 65, 22, y 13 %, respectivamente. La asignación a las formas [**5**]$^-$-*meso*(M) y ([**5**]$^-$-*meso*(m) se hace en base a las energías relativas calculadas.

El anión [**9**]$^-$ tiene la posibilidad de configurar dos isómeros estructurales que son diastereoisómeros, cuyas formas estructurales se denominarían [**9**]$^-$-*meso*(M) y [**9**]$^-$-*meso*(m), Figura 3.12. Al tener los ligandos fijados con la rotación impedida, la forma -*rac* de este compuesto no se obtiene en ningún caso. En la síntesis de este compuesto a -78 ºC se obtiene una mezcla de dos isómeros en una proporción de 76 % y 24 %, que se podrían asignar a las formas [**9**]$^-$-*meso*(M) y [**9**]$^-$-*meso*(m), respectivamente. Proporción que se mantiene incluso realizando la síntesis a 0 ºC. Los cálculos teóricos indican que la forma [**9**]$^-$-*meso*(M) es 5.70 kJ/mol más estable que la y [**9**]$^-$-*meso*(m).

Podemos concluir este apartado de isómeros estructurales afirmando que, de forma general, siempre que sea posible formar la mezcla racémica, ésta será la estructura mayo-

ritaria, seguida de aquella forma *meso*, que tenga los metilos proyectados sobre los B−H del clúster, es decir, la denominada forma -*meso*(M).

Comparación de espectros teóricos y experimentales de $^{11}B\{^1H\}$-RMN para los aniones $[\mathbf{4}]^-$ y $[\mathbf{5}]^-$.

Este apartado tiene una importancia fundamental en relación con los apartados siguiente relacionados con la funcionalización de dendrímeros.

A continuación se presentan los espectros reales de $^{11}B\{^1H\}$-RMN de los compuestos $[\mathbf{4}]^-$ y $[\mathbf{5}]^-$ junto a los espectros teóricos de los mismos. Pese a la similitud, se aprecian diferencias entre ambos espectros de $[\mathbf{4}]^-$ y de $[\mathbf{5}]^-$, una bastante importante es la resonancias correspondientes a los boros $B(6)$ y $B(6')$. Mientras que $[\mathbf{4}]^-$ no distingue estos boros, el compuesto $[\mathbf{5}]^-$ si lo hace. Este hecho se debe (dado que ambos compuestos están en su forma -*rac* mayoritariamente) a que el compuesto $[\mathbf{5}]^-$ tendrá los boros $B(6)$ y $B(6')$ en entornos diferentes, según estén próximos al hidrógeno del puente $\mu-\mathrm{SiH}$ o sobre el metilo del $\mu-\mathrm{SiCH_3}$. En cambio, en la estructura de $[\mathbf{4}]^-$ se espera un único tipo de $B(6)$. A la vez que los $B(6)$ están afectados, los $B(5)$ y $B(11)$ por cercanía, también podrían estarlo cómo se aprecia en la Figura 3.13a.

Para corroborar este efecto sobre los átomos de boro que tienen los substituyentes del silicio a una distancia de tres enlaces, se llevaron a cabo los cálculos de los desplazamientos químicos teóricos por el método GIAO, que se muestran como barras en la Figura 3.13b. Se puede apreciar que esta distinción entre átomos de boro $B(6)$ también queda reflejada teóricamente.

Este hecho nos ayudará en el futuro en las reacciones de hidrosililacion de dobles enlaces en la periferia de dendrímeros con el compuesto $[\mathbf{5}]^-$. El anión $[\mathbf{5}]^-$ con puente $\mu-\mathrm{Si(CH_3)H}$ tras hidrosililar el doble enlace pasará a ser un puente $\mu-\mathrm{Si(CH_3)CH_2}-$, de mayor similitud con el grupo puente $\mu-\mathrm{Si(CH_3)_2}$ de $[\mathbf{4}]^-$. Por tanto, se espera que la resonancia diferenciada de $B(6)$ y $B(6')$ en $[\mathbf{5}]^-$ desaparezca y se unifique en una sola señal similar a la que presenta $[\mathbf{4}]^-$, tal como se muestra en los espectros de la Figura 3.13. Este hecho será una prueba más de que $[\mathbf{5}]^-$ ha hidrosililado un doble enlace y ya no tiene la función Si−H.

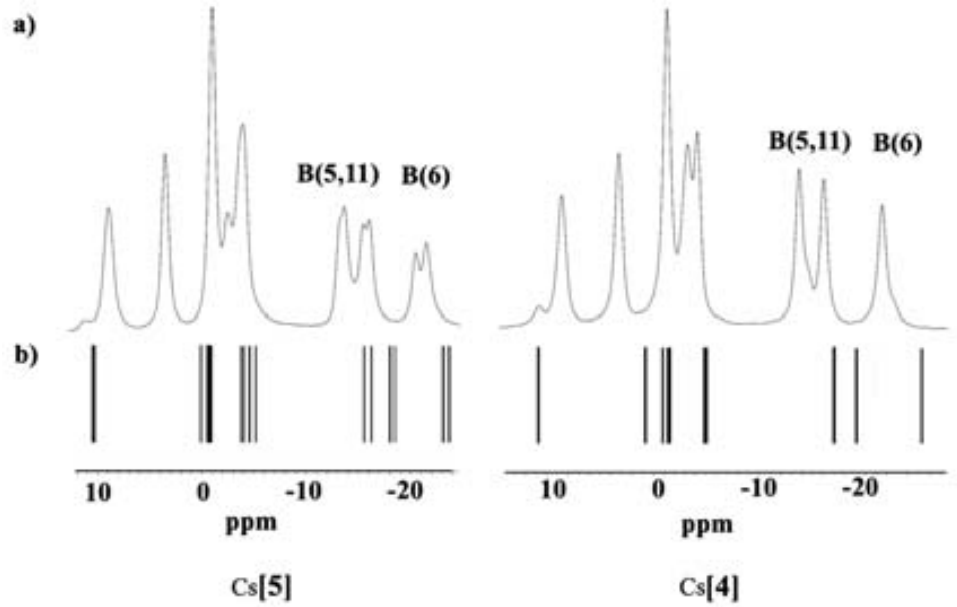

Figura 3.13: Espectros de $[\mathbf{5}]^-$ y $[\mathbf{4}]^-$ a) $^{11}B\{^1H\}$-RMN experimental b) Simulación de $^{11}B\{^1H\}$-RMN por método teórico GIAO.

Estudio teórico de los mecanismos para la formación de los compuestos $[\mathbf{4}]^-$ y $[\mathbf{8}]^-$.

Una pregunta que intentamos responder en este apartado es: ¿por qué formamos el silano monosubstituido, $[\mathbf{3}]^-$, cuando utilizamos $[\mathbf{1}]^-$ como producto de partida y nunca lo detectamos cuando usamos $[\mathbf{2}]^-$ como precursor? Por otro lado, en la reacción de la síntesis del compuesto monosubstituido $[\mathbf{3}]^-$, se nos forma también el anión $[\mathbf{4}]^-$. Sin embargo, a partir de $[\mathbf{2}]^-$ obtenemos siempre exclusivamente el pinzado $[\mathbf{8}]^-$. Por tanto, nos pareció de gran interés estudiar la formación de los compuestos $[\mathbf{4}]^-$ y $[\mathbf{8}]^-$, ya que, no esperábamos en un principio que se produjera la reacción del grupo Si−H con el grupo C_c−H, para dar lugar al pinzamiento. Nuestra hipótesis es que ocurre una reacción intramolecular que da como resultado el pinzamiento de los clústeres y para explicarla se ha propuesto un mecanismo de reacción, Figura 3.14.

El mecanismo propuesto consiste en la formación del compuesto monosubstituido con un grupo $-SiH(CH_3)_2$ y posterior reacción del protón ácido de un carbono del clúster con el hidrógeno de carácter hidruro Si−H, Figura 3.14. Se han realizado una serie

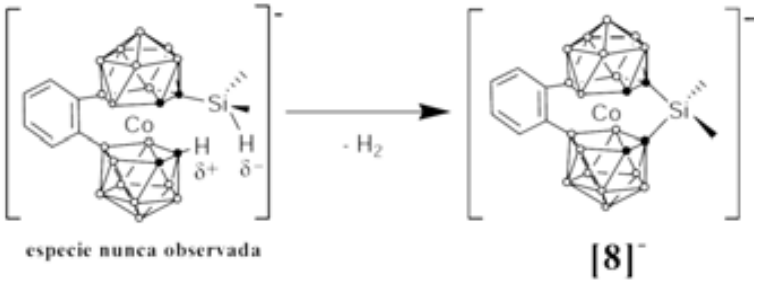

Figura 3.14: Posible mecanismo para la reacción de pinzamiento de los clústeres para formar el compuesto $[\mathbf{8}]^-$.

de cálculos teóricos para corroborar el mecanismo para la formación de $[\mathbf{8}]^-$ a partir del supuesto anión monosubstituido. Con el método de *Natural Population of Charges* (NPA) hemos constatado que el hidruro de la función $-\mathrm{SiH(CH_3)_2}$ tiene una densidad de carga de -0.195 y la densidad de carga del protón ácido del $\mathrm{C_c}-\mathrm{H}$ más cercano es de +0.282, lo que favorece la interacción entre ambas funciones, como hemos supuesto. También se ha encontrado un estado de transición para la reacción de la formación de $[\mathbf{8}]^-$ usando el método *Synchronous Transit-Guided quasi-Newton* (STQN), véase la Figura 3.15. El mínimo correspondiente al estado de transición tiene una frecuencia imaginaria correspondiente al modo vibracional de elongación de enlace de la molécula de $\mathrm{H_2}$ involucrada en la reacción.

También se ha calculado la entalpía de esta reacción intramolecular que ha resultado ser endotérmica a -78 ºC, $\Delta_r \mathrm{H}_{195} = +37.2$ kJ/mol y no espontánea, $\Delta_r \mathrm{G}_{195} = +13.8$ kJ/mol. Siguiendo la evolución de la temperatura hasta un valor ambiental, a medida que aumenta la temperatura de la reacción, alrededor de 32 ºC, Δ_rG comienza a tener valores negativos.[47]

Los cálculos se hicieron sin considerar el efecto del disolvente. Aún así, se puede apreciar una evolución hacía energías libres de Gibbs negativas, debido a que el término entrópico de la ecuación de estado se hace más negativo a medida que aumenta la temperatura. Se concluye entonces que, debido a que la conformación *cisoide* y *eclipsada* en los derivados de $[\mathbf{2}]^-$ es estable en las temperaturas de reacción investigadas, la reacción intramolecular para la formación de $[\mathbf{8}]^-$ está muy favorecida, y por eso nunca se ha detectado la presencia de monosubstituido en estos derivados de $[\mathbf{2}]^-$, porque siempre se

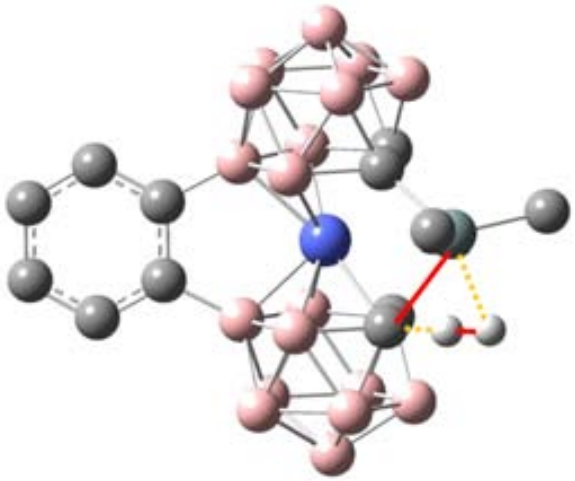

Figura 3.15: Estado de transición encontrado para la reacción intramolecular de obtención de **[8]**$^-$ a partir del monosubstituido correspondiente. Lineas punteadas representan enlaces rotos y líneas sólidas nuevos enlaces creados.

produciría el pinzamiento. Contrariamente, dada la posibilidad de rotación que tienen los ligandos en el compuesto **[3]**$^-$, se debe de establecer un equilibrio entre las 5 conformaciones rotacionales *alternadas* posibles: *transoide*, *gauche*-1, *cisoide*-1, *cisoide*-2 y *gauche*-2. Además de requerirse una energía "extra" necesaria para pasar entre conformaciones *alternadas* a *eclipsar* los ligandos. Sólo dos conformaciones *eclipsadas* de **[3]**$^-$ permitirían la reacción intramolecular. Por todo ello, es posible encontrar cierta cantidad de este compuesto monosubstituido **[3]**$^-$ sin haber reaccionado intramolecularmente y por esto mismo, es imposible encontrar compuesto monosubstituido derivado de **[2]**$^-$ sin que haya reaccionado.

Estudio de las interacciones intramoleculares de dihidrógeno Si−H···H−C_c del anión [3]$^-$.

Las distancias atómicas son el principal indicador para probar la existencia de un enlace o una interacción. Esto también es válido para un enlace de hidrógeno. La estructura cristalina del derivado C_c-monosubstituido **[3]**$^-$ (Figura 3.8) presenta tres contactos intramoleculares entre hidrógenos a distancias de 2.409, 2.212 y 2.059 Å. Distancias más cortas de 2.4 Å para dos átomos de H (dos veces el radio atómico de Van der Waals del

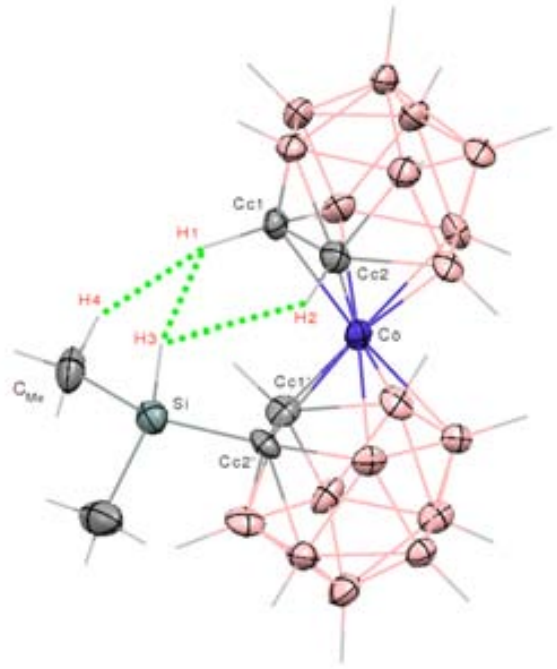

Figura 3.16: Disposición espacial de las tres distancias cortas presentes en la estructura cristalina del anión $[\mathbf{3}]^-$.

H) indican que tales átomos están interaccionando. En la Figura 3.16 se representa la disposición espacial de estas tres distancias cortas en la estructura cristalina.

Además de la estructura cristalina, se observó una notable diferencia en los espectros ^{1}H-RMN de los aniones monosubstituidos $[\mathbf{3}]^-$ y $[\mathbf{6}]^-$. Mientras el primeros presentaba solo dos señales correspondientes al protón C_c-H, el segundo tenía tres señales.[147] Por ello, en este apartado se estudiará la naturaleza de estas interacciones intramoleculares que el grupo protón aceptor Si−H establece con los dos enlaces C_c-H (protón donador) del ligando dicarballuro vecino y también la interacción $C_{Me}-H\cdots H-C_c$ que se observa en la estructura del anión $[\mathbf{3}]^-$.

El enlace de dihidrógeno (*dihydrogen bond*, DHB) es un tipo de enlace poco convencional de hidrógeno en el que una función protón donadora D−H interactúa con un protón aceptor A−H, ver Figura 3.17. Estos enlaces muestran características muy similares a los enlaces de hidrógeno convencionales.[148]

Una de las herramientas utilizadas más a menudo para estudiar un posible DHB es la

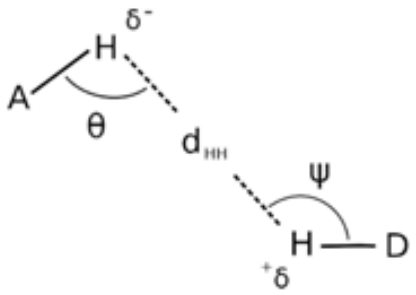

Figura 3.17: Representación geométrica de los parámetros que caracterizan un DHB.

Quantum Theory of Atoms in Molecules (QTAIM) de Bader.[149] Para hacer este estudio se necesita la densidad electrónica de la molécula y ésta se puede obtener por medios experimentales[150] o se puede calcular teóricamente. En este estudio hemos usado la densidad electrónica teórica a dos niveles diferentes de DFT. En el primero aprovechamos las optimizaciones B3LYP/6-311(d,p) del apartado anterior y añadimos otra optimización de la geometría del anión mediante el funcional BP86[144,151] con unas bases TZ2P.[152]

Primero compararemos la estructura experimental con las dos optimizaciones. La Tabla 3.3 muestra los parámetros más importantes de las tres interacciones y las distancias de los enlaces involucrados para la estructura cristalina (nivel 0), la estructura optimizada con B3LYP/6-311(d,p) (nivel 1) y la optimizada con BP86/TZ2P(+) (nivel 2).

	Estructura Cristalina			B3LYP /6-311(d,p)			BP86 /TZ2P(+)		
interacción (Å,º]									
	d_{HH}	θ	ψ	d_{HH}	θ	ψ	d_{HH}	θ	ψ
H1···H3	2.409	83.1	108.7	2.440	87.7	112.9	2.413	86.1	112.7
H2···H3	2.212	111.4	115.2	2.167	119.1	122.8	2.154	117.7	122.0
H1···H4	2.059	119.5	155.7	2.224	113.0	150.0	2.157	112.1	148.8
enlaces (Å]									
		d			d			d	
C_c–H1		1.121			1.079			1.086	
C_c–H2		1.121			1.080			1.086	
Si–H3		1.541			1.488			1.498	
C_{Me}–H4		0.980			1.092			1.099	

Tabla 3.3: Parámetros geométricos de las distancias cortas H$\cdots$H y distancia de los enlaces involucrados.

Vemos en la Tabla 3.3 que una de las distancias más cortas en la estructura cristalina

corresponde a $C_{Me}-H4\cdots H1-C_c$. Esto es sorprendente debido a la similar naturaleza de estos hidrógenos. En las otras dos interacciones, $Si-H3\cdots H1-C_c$ y $Si-H3\cdots H2-C_c$, Figura 3.16, la diferencia de electronegatividad entre Si y C, (1.90 vs. 2.55) sugiere que podría formarse un DHB, pero el *cutoff* marcado por las distancias Van der Waals descartaría el DHB que mantiene una distancia de 2.409 Å entre sus hidrógenos. La Tabla 3.3 muestra las distancias $H\cdots H$ calculadas a nivel 1 y 2. La distancia $C_{Me}-H4\cdots H1-C_c$ y $Si-H3\cdots H2-C_c$ se mantiene por debajo de los 2.4 Å y la $Si-H3\cdots H1-C_c$ por encima de 2.4 Å, como en el nivel 0 o experimental. Un estudio en la base de datos de estructuras cristalinas de Cambridge (CSD) sobre DHB basados en $B-H\cdots H-N$ encontró que el rango experimental para el ángulo $A-H\cdots H$, el ángulo θ, está en el rango de 95 - 120º mientras que el ángulo ψ es más abierto: 150 - 170º.[153] Es más característico de un DHB tener un ángulo más cerrado para θ que mantener un arreglo lineal entre los cuatro centros. El rango de los DHB de este estudio se mantiene en el rango normal en todos los niveles (0, 1 y 2) con un ángulo ψ más cerrado, pero seguramente debido a la disposición geométrica del conjunto.

Un dato a tener en cuenta en estas interacciones es calcular las cargas atómicas de los hidrógenos involucrados. En este trabajo hemos determinado estas cargas por dos métodos diferentes: primero con *Natural Population Analysis* (NPA) en la estructura optimizada con B3LYP/6-311(d,p) y *Voronoi Deformation Density methods* (VDD) en la optimizada con BP86/TZ2P(+) (Tabla 3.4).

	NPA			VDD		
	H hidruro	H protón	diferencia	H hidruro	H protón	diferencia
$H3\cdots H1$	-0.195	+0.267	0.462	-0.085	+0.130	0.215
$H3\cdots H2$	-0.195	+0.282	0.477	-0.085	+0.122	0.207
$H4\cdots H1$	+0.224	+0.267	0.043	+0.025	+0.130	0.105

Tabla 3.4: Cargas atómicas (au) de los hidrógenos involucrados en interacciones $H\cdots H$.

El método NPA da un carácter más iónico a los átomos de hidrógeno que el método VDD. Es interesante notar la similitud de la carga de H1 y H4 en el método NPA, mientras que en VDD, el H4 es un hidrógeno bastante neutral. De acuerdo con las cargas atribuidas por ambos métodos, sólo $Si-H3\cdots H1-C_c$ y $Si-H3\cdots H2-C_c$ encajan en la definición de DHB de ser una interacción puramente electrostática.

Analizando la densidad electrónica obtenida para las estructuras optimizadas a nivel

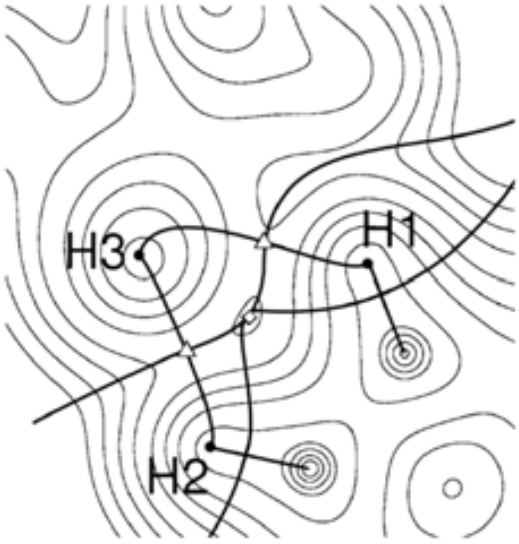

Figura 3.18: Líneas de contorno de la densidad electrónica (linea fina), *bond paths* conectando los núcleos y las *zero flux surfaces* (linea gruesa) para el plano H1-H2-H3 en el nivel de teoría 2. Los dos BCPs (△) y el RCP (⋄) estan proyectados sobre el plano.

1 y 2, las interacciones $Si{-}H3\cdots H1{-}C_c$ y $Si{-}H3\cdots H2{-}C_c$ tienen un punto crítico de enlace (*bond critical point*, BCP) entre los dos hidrógenos. De acuerdo con la QTAIM, la existencia de tal punto es la condición necesaria y universal para la existencia de enlace o interacción entre dos átomos. En la Figura 3.18 se muestra la densidad electrónica en el plano de los hidrógenos H1, H2 y H3 con la situación del BCP y *bond paths*.

Sin embargo, la interacción $C_{Me}{-}H4\cdots H1{-}C_c$ sólo presenta BCP en la densidad electrónica del nivel 1, y además este BCP está justo en el límite de considerarse BCP por el criterio de $\bigtriangledown^2\rho_{cp}$. En la densidad electrónica del nivel 2, ese BCP no se encuentra. En la Tabla 3.5 se presentan los datos topológicos que caracterizan los BCP's en el nivel 2 de teoría. Además, se ha incluido una estimación de la energía de enlace de los dos DHB's detectados según la ecuación empírica de Espinosa.[154]

Por lo tanto, usando QTAIM junto a la determinación de la carga en los hidrógenos, se puede concluir que:[147]

1. La distancia corta $C_{Me}{-}H4\cdots H1{-}C_c$ no es un DHB y que a lo sumo podría ser una débil *H-H bonding interaction* según el nivel de teoría 1.

2. La interacción $Si{-}H3\cdots H2{-}C_c$, que sobrepasa el límite establecido de 2.4 Å tanto

	$\triangle_{H\cdots H}-$VdW (Å)	ρ_{cp} (au)	$\bigtriangledown^2\rho_{cp}$ (au)	E_{DHB} (kcal/mol)
H3$\cdots$H1	+0.013	0.098	0.0302	-1.6
H3$\cdots$H2	-0.246	0.0106	0.0316	-1.7
H4$\cdots$H1	-0.243	-	-	-

Tabla 3.5: Parámetros topológicos para los DHB's detectados para el nivel 2.

experimentalmente como en los dos niveles de teoría, según QTAIM es un DHB.

3. La interacción Si$-$H3$\cdots$H1$-$C$_c$ es claramente un DHB y junto con la interacción Si$-$H3$\cdots$H2$-$C$_c$ forman un DHB bifurcado (ver Figura 3.16).

4. La presencia del DHB formado por Si$-$H3$\cdots$H1$-$C$_c$ corrobora que en condiciones óptimas el protón ácido reaccione con el Si$-$H hidruro para formar la especie $[\mathbf{4}]^-$, como se estimó en el apartado anterior.

3.2. Síntesis y funcionalización de metalodendrímeros con [3,3'-Co(1,2-$C_2B_9H_{11})_2]^-$

3.2.1. Síntesis de dendrímeros polianiónicos de tipo carbosilano y carbosiloxano.

Se han sintetizado metalodendrímeros de tipo carbosilano y carbosiloxano que contienen 4 y 8 unidades de [3,3'-Co(1,2-$C_2B_9H_{11})_2]^-$ en la periferia, mediante una reacción de hidrosililación con el compuesto $[\mathbf{5}]^-$, descrito en el apartado anterior,[47] sobre los vinilos terminales de diversos esqueletos dendriméricos de distinta generación.[155] Los *cores* utilizados para funcionalizar son: el tetravinilsilano (**TViS**) y el 1,3,5,7-tetrametilvinilciclotetrasiloxano (**TMViCTS**), los cuales son comerciales y a su vez han servido como *core* para hacer crecer las distintas generaciones de dendrímeros de tipo carbosilano: $\mathbf{1\,G{-}Vi_4}$, $\mathbf{1\,G{-}Vi_8}$ y $\mathbf{2\,G{-}Vi_8}$; y de tipo ciclocarbosiloxano: $\mathbf{1\,G{-}TMViCTS(SiVi)_4}$ y $\mathbf{1\,G{-}TMViCTS(SiVi)_8}$, respectivamente (Figuras 3.19 y 3.20). La metodología usada para obtener estos últimos es la divergente con las etapas de alquenización e hidrosililación ya mencionadas en la Introducción (apartado 1.3.3).

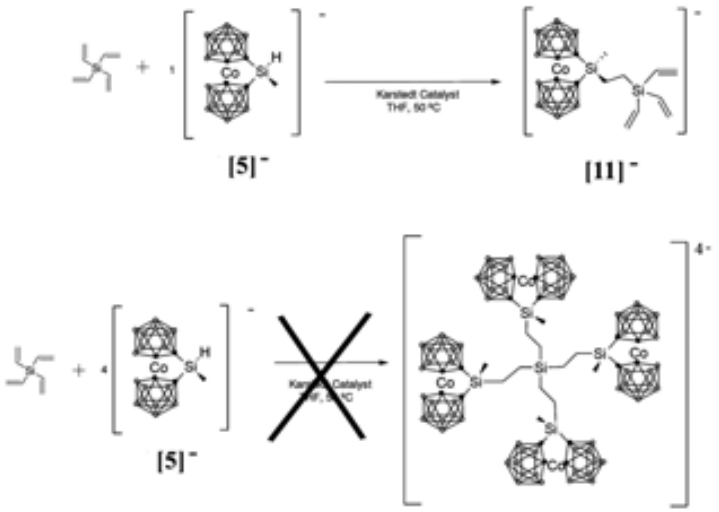

Figura 3.19: Preparación del dendrón $[\mathbf{11}]^-$.

Síntesis

La reacción de un equivalente del compuesto $[\mathbf{5}]^-$ con un equivalente de tetravinilsilano (**TViS**), en presencia de catalizador de Karstedt, THF como disolvente y 50 ºC de temperatura, lleva a la síntesis del compuesto monoaniónico $[\mathbf{11}]^-$ en un 77 % de rendimiento (Figura 3.19). Sin embargo, si usamos 4 equivalentes de $[\mathbf{5}]^-$ con un equivalente de **TViS** bajo condiciones similares o incluso aumentando la temperatura y el disolvente, no se consigue la completa funcionalización de éste. Probablemente, el impedimento estérico debido al volumen del [3,3'-Co(1,2-$C_2B_9H_{11})_2]^-$ sea el responsable de no obtener la tetrafuncionalización y en cambio se obtenga una mezcla de productos, mono-, di- y trifuncionalizados muy difícil de separar y aislar (Figura 3.19). Es destacable el hecho de que si en lugar de **TViS** se utiliza tetraalilsilano como *core*, las evidencias experimentales muestran que no ocurre ningún tipo de hidrosililación sobre doble enlaces de tipo alilo conectados a silicio. Este hecho contrasta con el hecho de que la hidrosililación sobre alilos ha sido ampliamente reportada, pero parece que ciertos complejos organometálicos funcionalizados con Si−H, como por ejemplo el ferroceno o en nuestro caso el anión $[\mathbf{5}]^-$, tienen completamente inhibida tal hidrosililación sobre el tetraalilsilano.[156,157]

Por el contrario, la reacción de cuatro equivalente de $[\mathbf{5}]^-$ con un equivalente de

una primera generación de dendrímero carbosilano, $\mathbf{1\,G{-}Vi_4}$, en las mismas condiciones anteriores, lleva a la obtención del correspondiente metalodendrímero, $[\mathbf{12}]^{4-}$, esta vez completamente funcionalizado y que se aisla como sal de Cs con un rendimiento del 51 %, Figura 3.20.

De igual forma y en similares condiciones, utilizando reacciones estequiométricas, se obtuvieron los metalodendrímeros con estructura dendrimérica basadas en carbosilano $[\mathbf{13}]^{8-}$ y $[\mathbf{14}]^{8-}$, y los basados en ciclosiloxano $[\mathbf{15}]^{4-}$, $[\mathbf{16}]^{4-}$ y $[\mathbf{17}]^{8-}$ (Figura 3.20). En todos los casos los metalodendrímeros se aislan como sales de Cs. En todos los casos, las reacciones de hidrosililación fueron monitorizadas por espectroscopía de IR siguiendo la desaparición de la señal de Si−H, y por RMN de ^{1}H siguiendo la desaparición completa de las señales de los vinilos que se encuentran en la periferia del dendrímero de partida.[155]

Caracterización.

El compuesto monoaniónico $[\mathbf{11}]^{-}$ y las estructuras dendriméricas, $[\mathbf{12}]^{4-}$ – $[\mathbf{17}]^{8-}$, fueron caracterizadas en base a espectroscopia de FT-IR, UV-Vis, RMN de ^{1}H, ^{11}B, ^{13}C y ^{29}Si; análisis elemental y espectrometría de masas (MALDI-TOF y ESI).

El espectro de IR muestra en todos los casos la típica banda correspondiente a ν(B−H) alrededor de 2550 cm^{-1} y una banda intensa en 1257 cm^{-1} correspondiente a δ(Si−CH_3). Además, para los dendrímeros de ciclosiloxano se observa una banda intensa a 1090 cm^{-1} correspondiente a δ(Si−O).

El espectro de ^{1}H-{^{11}B}-RMN para $[\mathbf{11}]^{-}$ muestra los desplazamientos típicos a 6.12 y 5.82 ppm, para los protones vinílicos que integran por 6 protones indicando que solo una rama del **TViS** fue hidrosililada. Para todos los compuestos se observa en torno a 4.50 ppm una señal correspondiente a C_c−H. El desplazamiento químico de los protones del grupo Si−CH_3 está alrededor de 0.30 ppm para el metilo enlazado al silicio unido al cobaltacarborano, y en el rango de 0.10-0.00 ppm para los Si−CH_3 de las ramas de los dendrímeros. Los metilenos de las ramas muestran multipletes complejos situados entre 0.50 y 0.85 ppm. Los espectros de ^{13}C-RMN muestran los desplazamientos químicos de los C_c−H y C_c−Si entorno a 56.16 y 40.99 ppm, respectivamente. Los carbonos del grupo Si−CH_3 aparecen todos a campo alto, en la región comprendida entre -7.0 y -0.6 ppm, mientras que los −CH_2− aparecen en el rango 2.4 - 8.9 ppm. El espectro de ^{11}B-RMN muestra un patrón muy similar para todas las estructuras dendriméricas reportadas

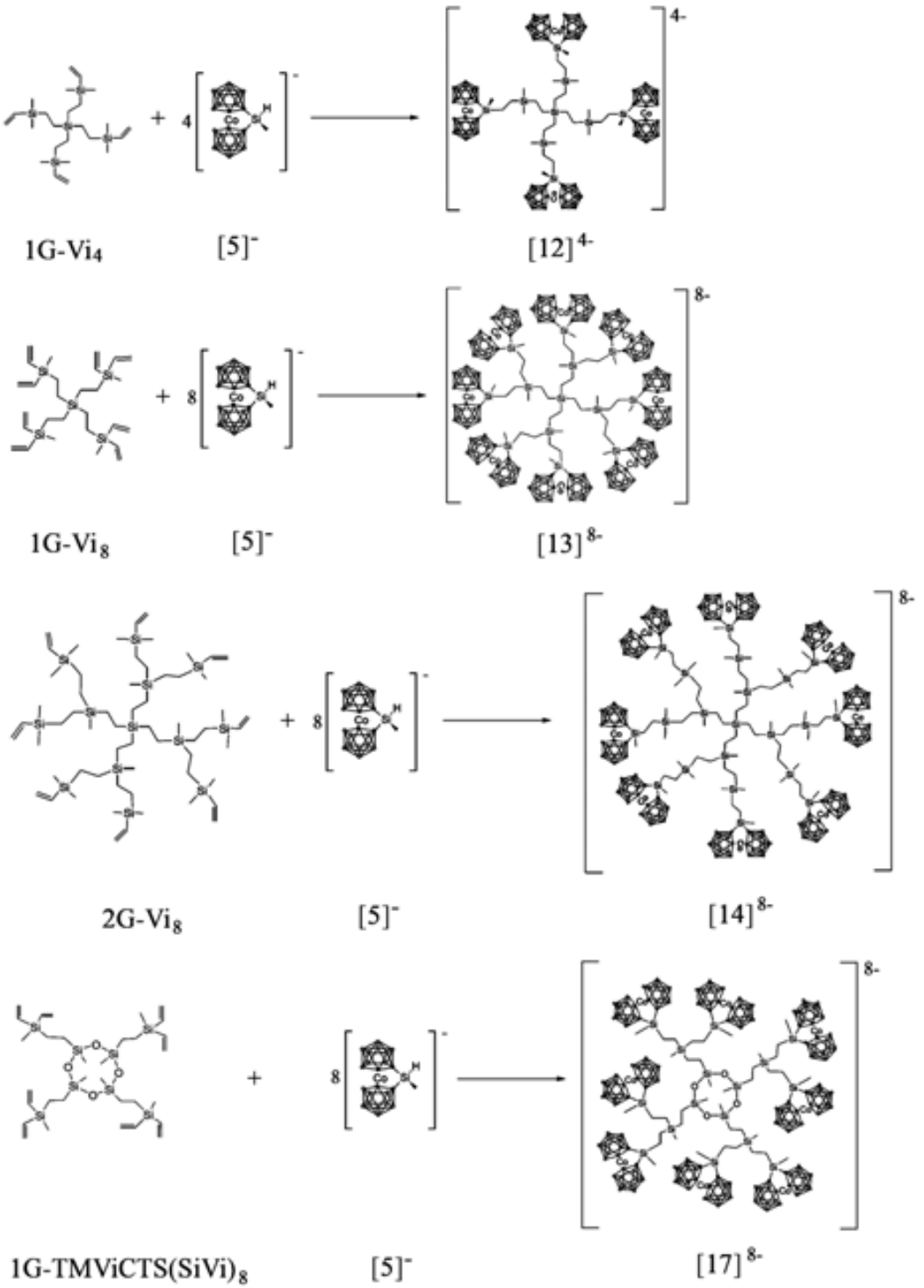

Figura 3.20: Preparación de los dendrímeros $[\mathbf{12}]^{4-}$, $[\mathbf{13}]^{8-}$, $[\mathbf{14}]^{8-}$ y $[\mathbf{17}]^{8-}$. En todos los casos la reacción se lleva a cabo a 50 ºC en THF y usando catalizador de Karstedt.

(2:2:4:4:2:2:2). El rango típico va desde +8.3 a -22.0 ppm. En la Figura 3.21 se muestran los espectros de varias de las estructuras dendriméricas descritas, así como el compuesto de partida $[\mathbf{5}]^-$y uno de los compuestos que nos ha servido como modelo para comparar, el compuesto $[\mathbf{4}]^-$. Se observa una gran similitud de éste último con el de las estructuras

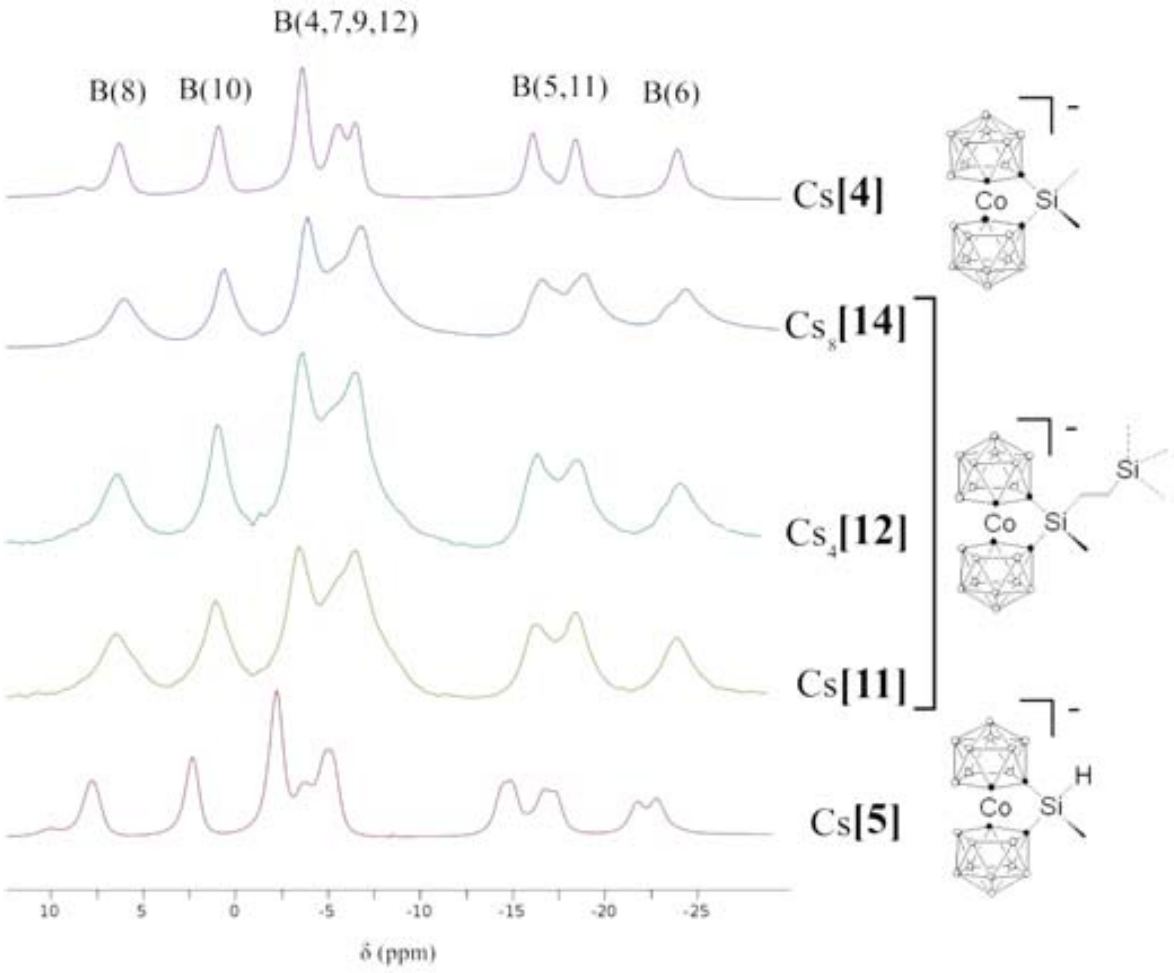

Figura 3.21: Espectros de ^{11}B-RMN para el reactivo de partida, Cs([**5**]), estructuras dendriméricas Cs[**11**], Cs_4[**12**] y Cs_8[**14**]; y para el compuesto modelo Cs[**4**].

dendriméricas, sobre todo, en el desplazamiento químico del boro B(6), en su unificación a una sola señal respecto al compuesto $[\mathbf{5}]^-$. Este hecho reflejado en ^{11}B-RMN, también se detecta en los espectros de ^{1}H-RMN para los desplazamientos químicos de protón del grupo $C_c-Si-CH_3$ y C_c-H.

La asignación en los espectros de ^{29}Si-RMN fue realizada en base a la intensidad de las señales y en la Tabla 3.6 se muestran los desplazamientos químicos. De forma

Compuesto	Si_{core}	Si_{rama}	$Si-C_c$
Cs[**11**]	11.8		12.15
Cs_4[**12**]	5.88	6.65	11.98
Cs_8[**13**]	8.28	9.78	11.73
Cs_8[**14**]		6.32, 8.03	11.52
Cs_4[**15**]	-20.53		11.85
Cs_4[**16**]	-19.88	7.63	11.15
Cs_8[**17**]	-19.94	8.88	11.74

Tabla 3.6: Desplazamientos químicos de los átomos de Si (ppm) en los espectros de ^{29}Si-RMN.

similar que con los anteriores núcleos, en los espectros de ^{29}Si-RMN de estas estructuras dendriméricas, el desplazamiento del silicio pontal ($C_c-\mu-Si$) es más similar al del compuesto modelo [**4**]$^-$ (13.98 ppm), que al desplazamiento de ese silicio en el compuesto [**5**]$^-$ (2.94 ppm).[47]

Se llevaron a cabo los análisis elementales de C y H para varios de los metalodendrímeros. Los resultados se encuentran en el anexo en el artículo correspondiente.[155] Como se ha podido observar en otras ocasiones,[158,159] la reproducibilidad y correcta composición de los análisis elementales para compuestos con un elevado porcentaje de boros es difícil y los márgenes de error son más amplios que en compuestos orgánicos clásicos.

Dos técnicas diferentes de espectrometría de masas han sido usadas para la caracterización de los dendrímeros: MALDI-TOF y ESI. La masa molecular del monoanión [**11**]$^-$ ha sido bien establecida usando la primera técnica, obteniéndose un pico molecular m/z = 502.2 con una concordancia perfecta para el patrón isotópico calculado. La espectrometría de masas del dendrímero [**12**]$^{4-}$ fue realizada en una disolución $CHCl_3/CH_3OH$ y mostró una señal a m/z = 2490.2, que corresponde a $[(M-H)^+H_2O]^-$. Sin embargo, la determinación del resto de estructuras dendriméricas polianiónicas por MALDI-TOF ha demostrado gran dificultad debido a la gran fragmentación existente, y por tanto, no se ha detectado el pico correspondiente al peso molecular. En este aspecto la técnica no ha servido para confirmar completamente la formación de los dendrímeros.[155]

Los espectros de UV-Vis se midieron en acetonitrilo y muestran una banda de absorción a 310 nm, que es característica para derivados de cobaltabisdicarballuro que contienen un puente de silicio.[47,155] La técnica de UV-Vis se mostrará muy útil en la caracterización global de las estructuras dendriméricas como se verá en el apartado siguiente 3.2.1.

Método para la identificación indirecta de funcionalización completa con cobaltacarboranos basado en medidas de UV-Vis.

Como se ha mencionado antes, sólo el compuesto $[\mathbf{11}]^-$ y el dendrímero de tipo carbosilano $[\mathbf{12}]^{4-}$ han sido caracterizados exitosamente por espectrometría de masas. La dificultad de analizar estructuras dendriméricas con un número elevado de cargas ha sido constatado anteriormente. De hecho, bajo nuestro conocimiento, sólo una vez y muy recientemente se ha reportado en bibliografía un espectro MALDI-TOF de una estructura dendrimérica que no fuera neutra.[160] Un método alternativo, aplicado por Kim *et. al.*,[161] utiliza la relación lineal que se establece entre una determinda estructura con un número de unidades de un grupo que absorbe en UV-Visible y su absortividad molar. En nuestro caso, hemos escogido la banda de absorción en el visible entorno a 460 nm y se han calculado las absortividades molares (ε) de todos los dendrímeros a esa longitud de onda. En la Figura 3.22 se muestra la relación lineal entre la absortividad molar y el número de [3,3'-Co(1,2-$C_2B_9H_{11})_2]^-$ en la periferia de cada una de las estructuras dendriméricas. Se observa que ε es proporcional al número de [3,3'-Co(1,2-$C_2B_9H_{11})_2]^-$ que contiene cada una de ellas. Y por tanto, apoyándonos en el resto de datos experimentales de caracterización (IR, RMN y MALDI-TOF en algunos casos) esta técnica nos corrobora que las estructuras dendriméricas supuestas, correlacionan con unas estructuras completamente funcionalizadas y unificadas.

Solubilidad de las sales de cesio de las estructuras dendriméricas funcionalizadas con [3,3'-Co(1,2-$C_2B_9H_{11})_2]^-$.

Una de las propiedades más interesantes para estos dendrímeros, y sus potenciales aplicaciones, es la solubilidad en agua. Aunque este catión no destaca especialmente por favorecer la solubilidad del anión [3,3'-Co(1,2-$C_2B_9H_{11})_2]^-$ en agua, como otros cationes tal como sodio o potasio, se ha llevado a cabo un estudio de solubilidad a T ambiente,

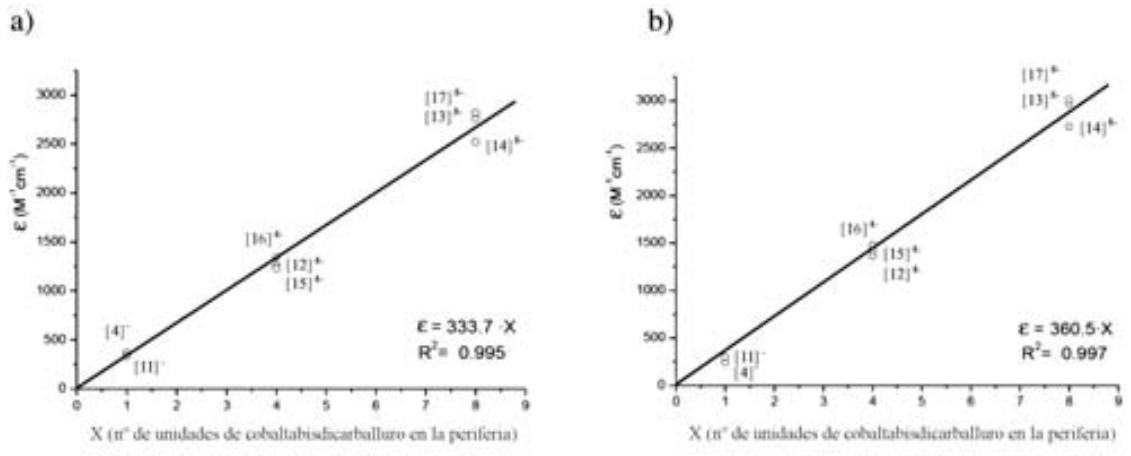

Figura 3.22: Representación de la absortividad molar a $\lambda = 462$ nm *versus* el número de [3,3'-Co(1,2-$C_2B_9H_{11})_2$]$^-$ en la periferia de cada metalodendrímero: a) DMSO, b) acetonitrilo.

mediante medidas de UV-Vis. De esta manera, crearemos un referente experimental constrastable en el futuro con posibles experimentos con cationes biocompatibles.

Para realizar los experimentos, se ha procedido a solubilizar las sales de cesio en un disolvente orgánico (y ampliamente usado como excipiente) como es el DMSO.[162] Posteriormente, se lleva a cabo una dilución en agua de manera que no se observe precipitado o suspensión alguna. La correspondiente disolución se mide espectrofotométricamente y se obtiene qué cantidad de [3,3'-Co(1,2-$C_2B_9H_{11})_2$]$^-$ se ha solubilizado en estas disoluciones con un alto porcentaje en agua ($\geq 98\,\%$). En la Figura 3.23 se muestra un gráfico de la absorbancia (A) vs. la concentración para las distintas disoluciones de estas sales. Como referencia patrón se construye una recta de calibrado utilizando diferentes concentraciones del compuesto Cs[**4**]. En la gráfica se aprecia que pese a estar el [3,3'-Co(1,2-$C_2B_9H_{11})_2$]$^-$ unido a un esqueleto dendrimérico altamente insoluble en agua como es el de carbosilano/carbosiloxano, la solubilidad de este no ha cambiado apreciablemente respecto al compuesto libre Cs[**4**], mostrando todos los metalodendrímeros un comportamiento similar. Este estudio, además de darnos información sobre la solubilidad en agua de estos metalodendrímeros, nos indica que ellos son estables en dichas disoluciones.

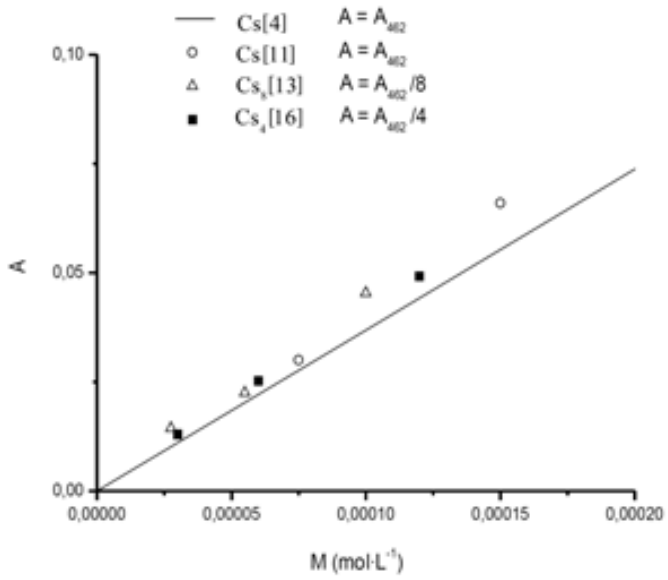

Figura 3.23: Medidas de solubilidad para las sales de Cs de los metalodendrímeros polianiónicos.

3.2.2. Funcionalización de dendrímeros de tipo poli(aril-éter) con derivados de $[3,3'\text{-}Co(1,2\text{-}C_2B_9H_{11})_2]^-$.

Este apartado se ha llevado a cabo en colaboración con los grupos del Dr. Norberto Farfán de la Universidad Nacional Autónoma de México y la Dra. Rosa Santillan, del Centro de Investigación y Estudios Avanzados del Instituto Politécnico Nacional de México. Ellos han preparado las estructuras dendriméricas de tipo aril-éter que contienen en la periferia grupos alilo y que serán funcionalizadas con derivados de $[3,3'\text{-}Co(1,2\text{-}C_2B_9H_{11})_2]^-$ para obtener los correspondientes metalodendrímeros polianiónicos.[163]

Síntesis

En esta sección se resume la síntesis y caracterización de una nueva familia de moléculas *star-shaped* y dendrímeros polianiónicos siguiendo el procedimiento de hidrosililación de alquenos terminales con el anión $[1,1'\text{-}\mu\text{-}SiMeH\text{-}3,3'\text{-}Co(1,2\text{-}C_2B_9H_{10})_2]^-$, $[\mathbf{5}]^-$. Las estructuras dendriméricas utilizadas para funcionalizar se preparan a partir de un núcleo fluorescente que actua como *core*, 1,3,5-trifenilbenceno (TFB), y el crecimiento de las

generaciones se realiza utilizando el método de Fréchet, dando lugar a ramas de tipo aril-éter para acabar la periferia con tres, seis, nueve y doce grupos alilo: **0G-TFB(Alil)**$_3$, **1G-TFB(Alil)**$_6$, **1G-TFB(Alil)**$_9$ y **2G-TFB(Alil)**$_{12}$ (ver estructuras en el apartado Figuras, al principio del manuscrito).

El núcleo se prepara por ciclocondensación de acetofenonas substituidas.[164] En la Figura 3.24 se muestra la triple condensación del reactivo de partida para dar **0G-TFB(Alil)**$_3$.[163]

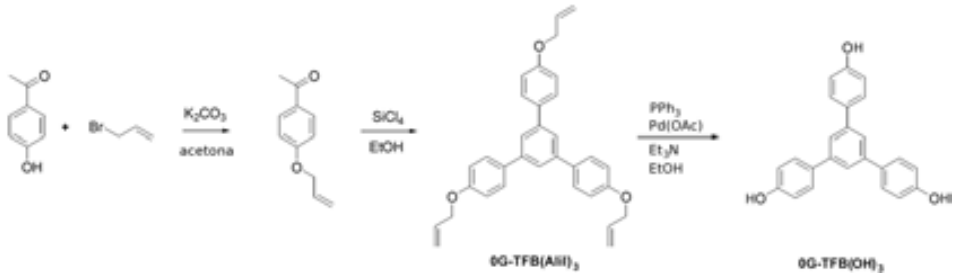

Figura 3.24: Síntesis de **0G-TFB(Alil)**$_3$.

Para hacer crecer el dendrímero de generación 0 **0G-TFB(Alil)**$_3$ a la siguiente generación, los grupos alilo de éste son eliminados para dar **0G-TFB(OH)**$_3$ y éste se hace reaccionar en acetonitrilo en presencia de K_2CO_3 y cantidades catalíticas del éter corona 18-C-6, con el reactivo apropiado para dar **1G-TFB(Alil)**$_6$ o **1G-TFB(Alil)**$_9$ (Figura 3.25). Estos dendrímeros pueden seguir creciendo mediante etapas de alquilación una vez sustituidos los alilos terminales por el grupo −OH y así dar **2G-TFB(Alil)**$_{12}$.[163]

El procedimento para la funcionalización de la periferia de estos dendrímeros consiste en la reacción de hidrosililación de los dobles enlaces con [1,1'-μ-SiMeH-3,3'-Co(1,2-$C_2B_9H_{10})_2]^-$en THF, a 50 ºC, en presencia de catalizador de Karstedt. La reacción de tres equivalentes de $[\mathbf{5}]^-$ con un equivalente de **0G-TFB(Alil)**$_3$ da lugar al metalodendrímero $[\mathbf{18}]^{3-}$ que se aisla como sal de Cs, con un rendimiento del 54 %. Una relación 6:1 de $[\mathbf{5}]^-$/**1G-TFB(Alil)**$_6$ y 12:1 para $[\mathbf{5}]^-$/**2G-TFB(Alil)**$_{12}$ bajo las mismas condiciones da lugar a los metalodendrímeros $[\mathbf{19}]^{6-}$ y $[\mathbf{20}]^{12-}$] (Figura 3.26) que se aislan como sales de Cs en un 63 % y 51 % de rendimiento, respectivamente. Los tiempos de reacción han variado en función del número de grupos alilo a funcionalizar. En todos los casos, las reacciones fueron monitorizadas por IR (desaparición banda Si−H) y por ^{1}H-RMN la desaparición de los protones del grupo alilo.

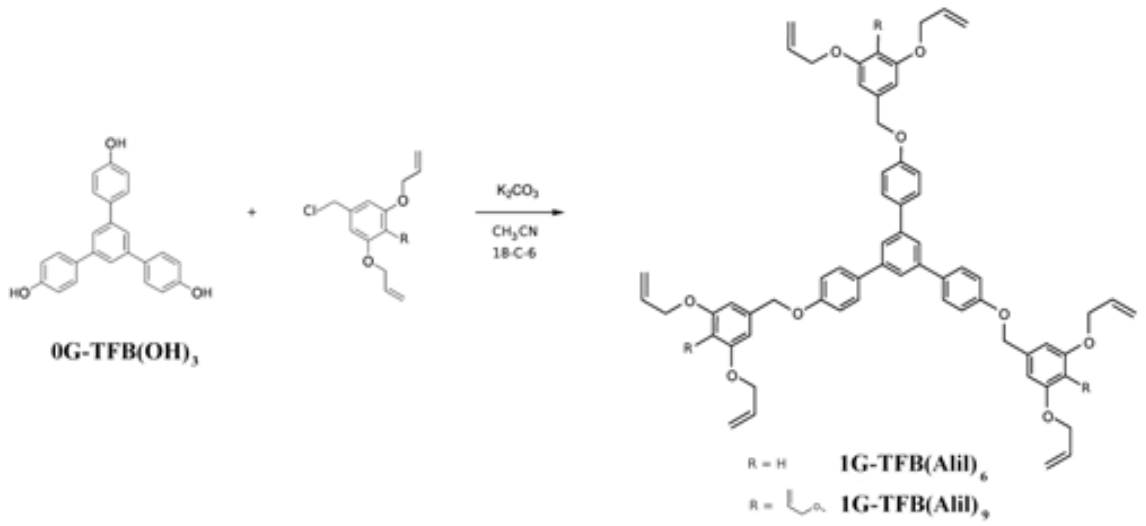

Figura 3.25: Síntesis de dendrímeros **1G-TFB(Alil)**$_6$ y **1G-TFB(Alil)**$_9$.

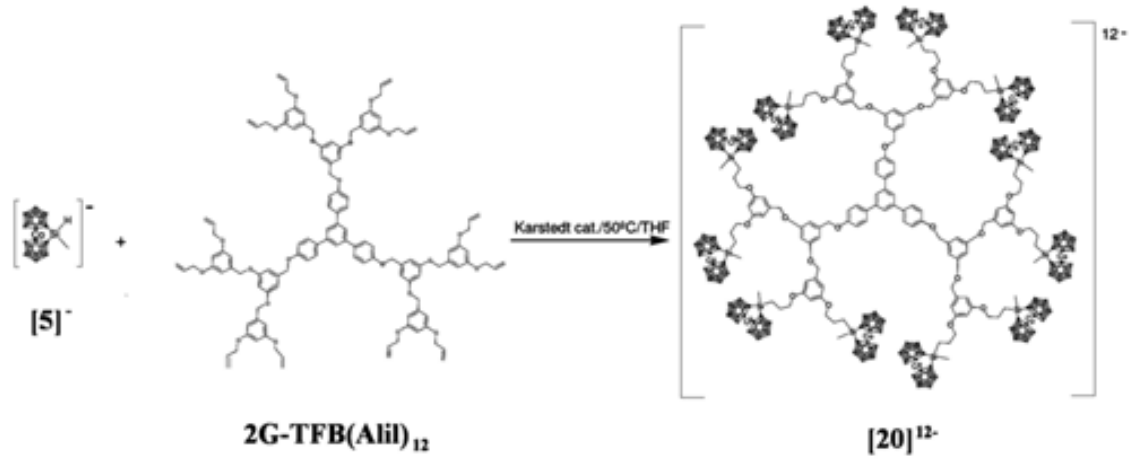

Figura 3.26: Síntesis del metalodendrímero $[\mathbf{20}]^{12-}$ a partir de $[\mathbf{5}]^{-}$ y **2G-TFB(Alil)**$_{12}$.

Sin embargo, los intentos de hidrosililación completa para **1G-TFB(Alil)$_9$** fueron infructuosos debido, seguramente, al impedimento estérico por el volumen del anión [3,3'-Co(1,2-$C_2B_9H_{11})_2]^-$. Este hecho ya fue observado y comentado para la reacción de **TVSi** con $[\mathbf{5}]^-$ del apartado anterior.[155]

Caracterización

Las estructuras dendriméricas de $[\mathbf{18}]^{3-}$, $[\mathbf{19}]^{6-}$ y $[\mathbf{20}]^{12-}$ fueron caracterizadas en base a FT-IR, UV-Vis, RMN de ^{1}H, ^{11}B, ^{13}C y ^{29}Si, y espectrometría de masas. La caracterización de los precursores terminados con grupo alilo no se ha incluido en este apartado, pero se encuentra anexada en el artículo.[163]

El espectro de IR muestra en todos los casos la típica banda correspondiente a ν(B−H) alrededor de 2550 cm^{-1} y una banda intensa en 1257 cm^{-1} correspondiente a δ(Si−CH_3).

Los espectros de ^{1}H-RMN muestran los desplazamientos típicos para los protones aromáticos entre 7.80 y 7.00 ppm. Las señales de los protones atribuidos a la función alilo en **0G-TFB(Alil)$_3$**, **1G-TFB(Alil)$_6$** y **2G-TFB(Alil)$_{12}$** han desaparecido indicando una completa funcionalización y han aparecido las resonancias de los protones −OCH_2− (4.00 ppm), −CH_2− (1.85 ppm) y −$SiCH_2$− (1.00 ppm), que confirman la completa hidrosililación de los grupos alilo. Se observa una resonancia ancha en torno a 4.50 ppm, correspondiente a C_c−H del cobaltacarborano. El desplazamiento químico de los protones del grupo Si−CH_3 se observa alrededor de 0.30 ppm. El espectro de ^{13}C-RMN muestra los desplazamientos químicos de los carbonos aromáticos en la region de 160.5 a 100.5 ppm y de los grupos −OCH_2− en el rango comprendido entre 65.0 y 79.0 ppm. Las resonancias de C_c−H y C_c−Si aparecen alrededor de 55.25 y 40.50 ppm, respectivamente. Los carbonos del grupo Si−CH_3 aparecen entorno a -6.5 ppm. El espectro de ^{11}B-RMN de todas las estructuras dendriméricas muestra el típico patrón de ligandos dicarballuro pinzados por átomo de Si (2:2:4:4:2:2:2) y en el rango típico de +8.3 a -22.0 ppm. Los tres metalodendrímeros muestran una resonancia alrededor de 12 ppm en el espectro de ^{29}Si-RMN, correspondiente a C_c−Si. Este desplazamiento es muy cercano al del compuesto modelo $[\mathbf{4}]^-$ (13.98 ppm).[47]

Se han usado dos técnicas diferentes de espectrometría de masas para la caracterización de los metalodendrímeros: MALDI-TOF y ESI. La masa molecular de Cs_3[**18**] ha

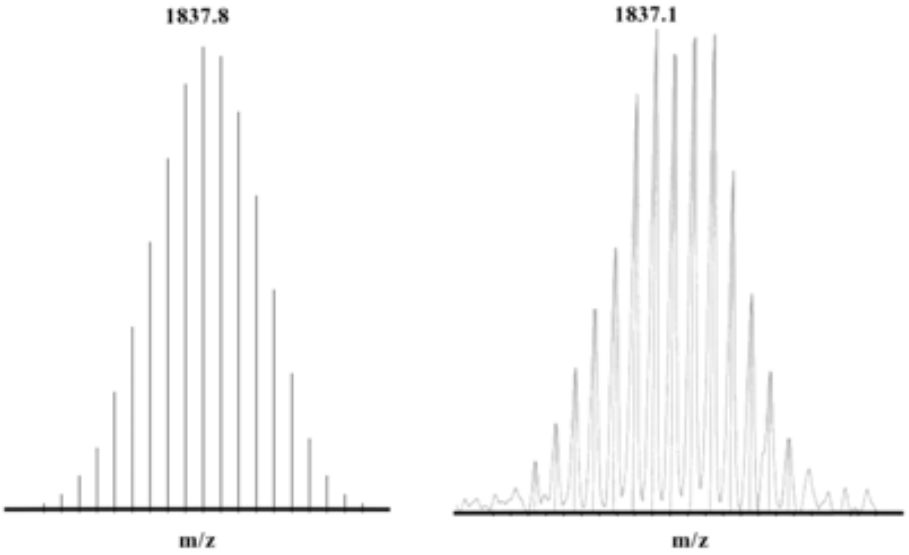

Figura 3.27: Espectro ESI para $[M-Cs]^-$ donde M= Cs_3[**18**]. Izquierda: simulación. Derecha: Experimental.

sido bien establecida por ESI dando un pico molecular a m/z = 1837.1, que corresponde a $[M-Cs]^-$ (Figura 3.27). Sin embargo, la determinación del resto de estructuras dendriméricas polianiónicas por MALDI-TOF ha mostrado gran dificultad, debido a la gran fragmentación existente como en el caso de los dendrímeros de carbosilano del apartado anterior.[155] Esta técnica solamente nos ha ayudado a determinar ciertos fragmentos del dendrímero, pero nunca se observó el correspondiente pico molecular.

Medidas de UV-Vis y Fluorescencia

Las medidas de absorción de UV-Vis para los precursores **0G-TFB(Alil)**$_3$, **1G-TFB(Alil)**$_6$, **1G-TFB(Alil)**$_9$ y **2G-TFB(Alil)**$_{12}$; y los metalodendrímeros polianiónicos $[\mathbf{18}]^{3-}$, $[\mathbf{19}]^{6-}$ y $[\mathbf{20}]^{12-}$ fueron realizadas en acetonitrilo. La Tabla 3.7 muestra los datos correspondientes a las medidas de estos compuestos y los espectros se muestran en las Figuras 3.28 y 3.29.

Los dendrímeros de partida muestran un máximo de absorción en la region 269-272 nm que corresponde a la transiciones π - π^* del core aromático como ocurre en compuestos de 1,3,5-trifenilbenceno substituidos similares.[165] Para los compuestos **1G-TFB(Alil)**$_6$, **1G-TFB(Alil)**$_9$ y **2G-TFB(Alil)**$_{12}$ existen absorciones por debajo de 240 que no se

	Absorción $\lambda_{max}(\varepsilon, 10^3)$	
0G-TFB(Alil)$_3$	269 (127)	
1G-TFB(Alil)$_6$	270 (66)	
1G-TFB(Alil)$_9$	270 (65)	
2G-TFB(Alil)$_{12}$	272 (78)	
Cs_3[**18**]	271 (86)	310 (52)
Cs_6[**19**]	276 (175)	309 (109)
Cs_{12}[**20**]	272(141)	307(171)

Tabla 3.7: Absorciones máximas (λ_{max}, nm) para cada compuesto en el espectro de UV-Vis. El coeficiente de extinción molar (ε, $dm^3mol^{-1}cm^{-1}$) figura entre paréntesis.

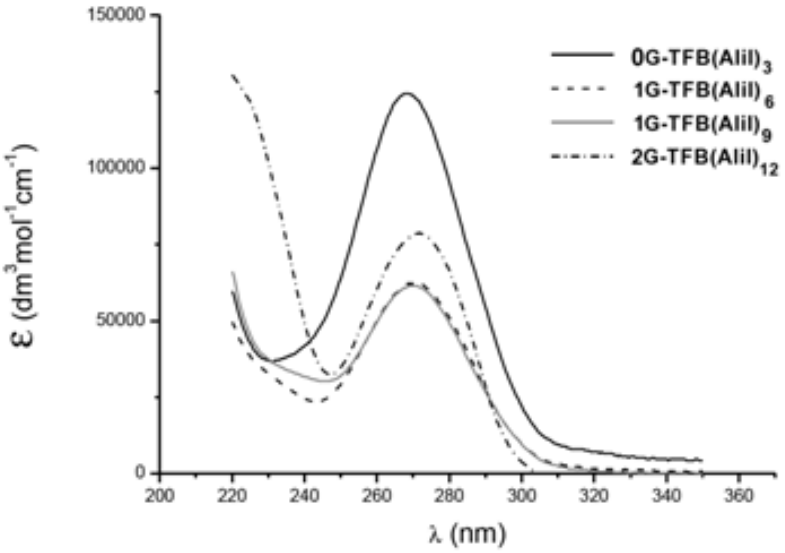

Figura 3.28: Espectro UV-Vis para los dendrímeros precursores.

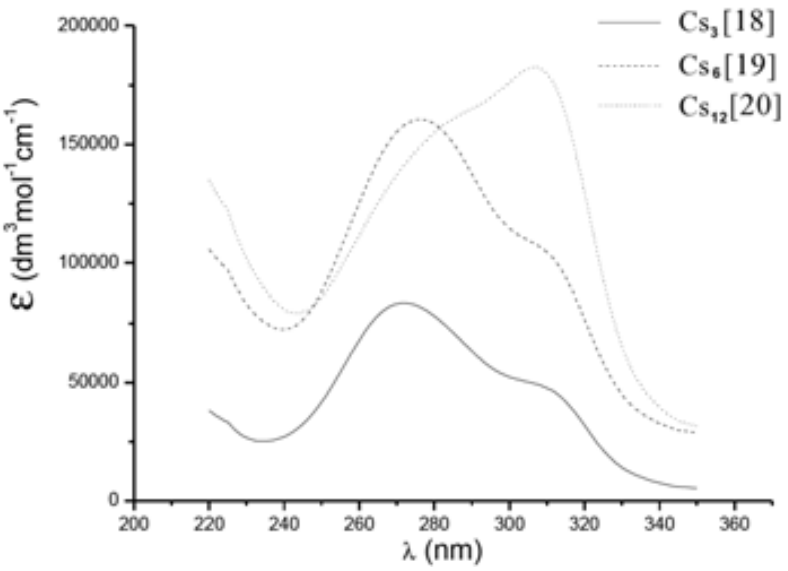

Figura 3.29: Espectro UV-Vis para los metalodendrímeros conteniendo [3,3'-Co(1,2-$C_2B_9H_{11})_2]^-$.

pueden asignar debido a que solapan con el disolvente (ver Figura 3.28). Los metalodendrímeros por su parte presentan dos absorciones claramente definidas en el espectro de UV-Vis. Una correspondería al *core* aromático, como en los compuestos de partida, que aparece entre 271 y 276 nm, y la situada entorno a 310 nm corresponde al fragmento [1,1'-μ-Si(CH_2-)(CH_3)-3,3'-Co(1,2-$C_2B_9H_{10})_2]^-$. Esta última señal es característica para los derivados del cobaltabisdicarballuro que poseen un puente de silicio.[47,155,163] Al igual que ocurría con los metalodendrímeros de carbosilano y carbosiloxano, para estos metalodendrímeros se puede apreciar una correlación lineal entre el numero de unidades de cobaltabisdicarballuro localizadas en la periferia y el coeficiente de extinción molar correspondiente a su señal (véase Figura 3.30). De nuevo la técnica de UV-Vis nos ha servido para corroborar el carácter unificado de los metalodendrímeros.

Respecto a los estudios de fluorescencia, los espectros de emisión se midieron en acetonitrilo y los dendrímeros precursores exhibieron emisión en el azul, alrededor de 364 nm, tras ser excitados a 270 nm. Sin embargo, los dendrímeros funcionalizados con cobaltabisdicarballuro no muestran una emisión apreciable. La Tabla 3.8 muestra los valores de longitud de onda de la emisión, rendimiento cuántico y tiempo de vida medio para los dendrímeros precursores.[163]

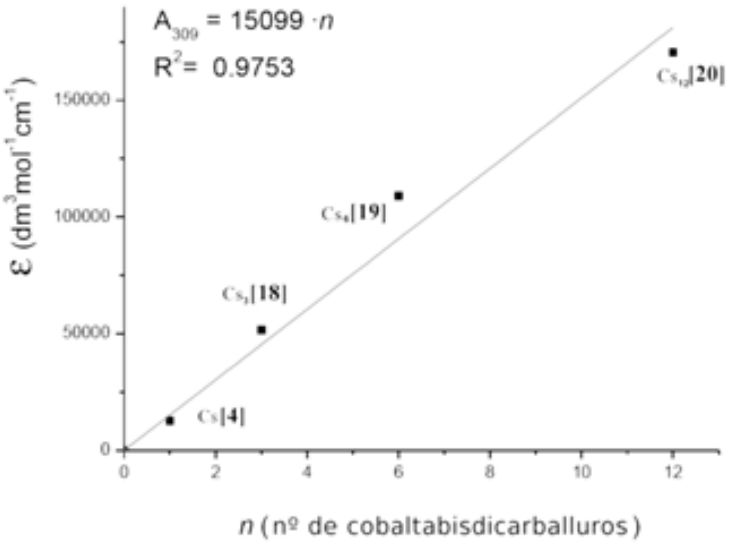

Figura 3.30: Correlación lineal entre el número de unidades de cobaltabisdicarballuro y la absortividad a $\lambda_{max} = 309$ nm.

	Emisión		
Compuesto	λ_{max}(nm)	ϕ(%)	μ(ns)
0G-TFB(Alil)$_3$	364	20	9.3
1G-TFB(Alil)$_6$	364	21	9.5
1G-TFB(Alil)$_9$	364	21	9.5
2G-TFB(Alil)$_{12}$	363	22	9.5

Tabla 3.8: Datos de emisión para los dendrímeros precursores.

El hecho de que los metalodendrímeros no posean en principio propiedades luminiscentes, nos lleva a pensar en la posibilidad de que al funcionalizar el dendrímero de partida, la fluorescencia sufra un *quenching* por algún determinado mecanismo. Uno de los experimentos realizados para comprobar esta drástica variación de las propiedades fluorescentes fue disolver en una proporción 1:3 el dendrímero precursor **0G-TFB(Alil)$_3$** y Cs[**5**] en acetonitrilo, para comprobar si colisiones (*quenching* dinámico) entre el cobaltabisdicarballuro y el fluoróforo o la formación de un complejo fluoróforo-cobaltabisdicarballuro (*quenching* estático) eran las responsables de este *quenching*. Ni

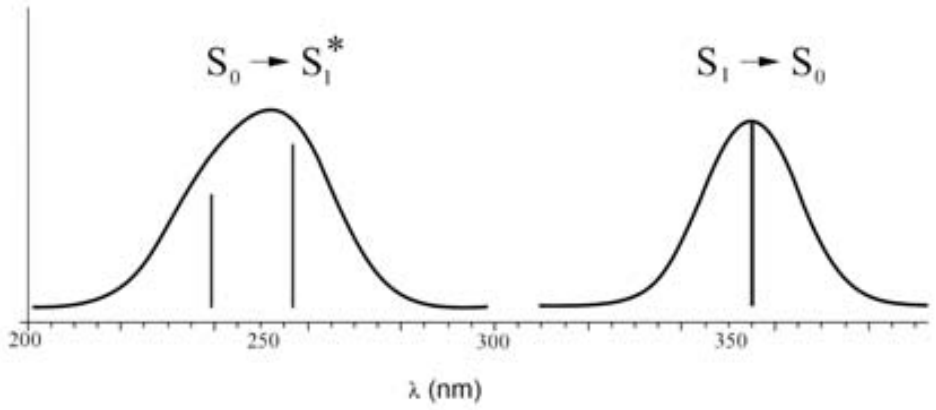

Figura 3.31: Espectros calculados para la absorción y emisión de **0G-TFB(Alil)$_3$**.

el espectro de emisión de **0G-TFB(Alil)$_3$** ni su rendimiento cuántico varió significativamente en el experimento. Otra posibilidad es que no exista emisión porque se produce una transferencia de energía por un camino no radiativo para volver al estado S_0. El mecanismo de este *quenching* de la fluorescencia en los metalodendrímeros sigue bajo estudio.

Simulación de espectros UV-Vis y de Fluorescencia por métodos semiempíricos.

Utilizando el método semiempírico PM6 implementado en MOPAC se calcularon diferentes estados excitados de **0G-TFB(Alil)$_3$** y así se simuló su espectro de absorción.[163] Con un tiempo de vida suficiente, como es el caso, el sistema en estado excitado S_1 (primer estado excitado singlete) de la molécula vuelve al estado base S_0 con la emisión de un fotón. El método semiempírico PM6 permite la optimización de estados excitados con lo cual el espectro de fluorescencia también puede ser simulado. En la Figura 3.31 se representan los espectros calculados. Las longitudes de onda calculadas presentan una buena concordancia con las experimentales. Las longitudes de onda de la absorción (257 nm) y la emisión (355 nm) calculadas están en buen acuerdo con las experimentales. La diferencia de energía de la molécula en estado S_0 y S_1 es de 4.29 eV, mientras que el desplazamiento de Stokes calculado es aproximadamente 1.34 eV. Por tanto, el rendimiento cuántico calculado estaría entorno al 30 % que es un valor bastante cercano al

experimental (20 %). En resumen, el grado de concordancia entre los parámetros determinados experimentalmente y calculados es bastante bueno, sin embargo, la imposibilidad de hacer optimizaciones geométricas de compuestos como el [3,3'-Co(1,2-$C_2B_9H_{11})_2]^-$ a nivel semiempírico nos impide profundizar en el mecanismo del *quenching* de los metalodendrímeros.

Cuantificación del impedimento estérico en la periferia del dendrímero por el método de Monte Carlo.

Como se ha visto en los apartados anteriores, la funcionalización completa por hidrosililación de los dobles enlaces de tetravinilsilano y el **1G-TFB(Alil)**$_9$ no pudo realizarse. En nuestra opinión, la razón de tal hecho es debida fundamentalmente al gran impedimento estérico existente en la periferia, que impide tal funcionalización completa. En este apartado se muestra un procedimiento teórico para cuantificar tal impedimento estérico en todos los dendrímeros estudiados y que es soportado por los datos experimentales. De esta manera, se podría conocer *a priori* qué dendrímeros con dobles enlaces terminales pueden ser completamente funcionalizados con [1,1'-μ-SiMeH-3,3'-Co(1,2-$C_2B_9H_{10})_2]^-$, y cuales no.

Las simulaciones de dinámica molecular por el método de Monte Carlo son utilizadas para conocer propiedades termodinámicas y estructurales de una molécula a una determinada temperatura.[166] El método de Monte Carlo ha sido aplicado aquí para la generación de un amplio número de conformaciones estructurales de un dendrímero completo o una rama. Para simplificar y reducir el tiempo de cálculo, el fragmento [1,1'-μ-Si(CH_2-)(CH_3)-3,3'-Co(1,2-$C_2B_9H_{10})_2]^-$ ha sido substituido por Si(CH_2-)($CH_3)_3$. Se ha definido un parámetro teniendo en cuenta los átomos de Si más externos de las ramas y mediando todas las distancias que se establecen entre ellos en una determinada estructura dendrimérica. Este parámetro (η, Å) es un valor representativo de cómo de alejados están estos Si terminales entre sí e indirectamente da información del impedimento estérico existente en la periferia de la estructura estudiada, valores bajos de η indican un gran impedimento estérico y altos lo contrario.[155,163] En la Figura 3.32 se representan los valores calculados de η (Å) para los distintos tipos de dendrímeros.

Se puede observar que los compuestos **TViS** y **1G-TFB(Alil)**$_9$ hidrosililados *in silico* con HSi($CH_3)_3$, y que dan lugar a TViS0s4 y 1TFB0s9 tienen ambos un valor de η

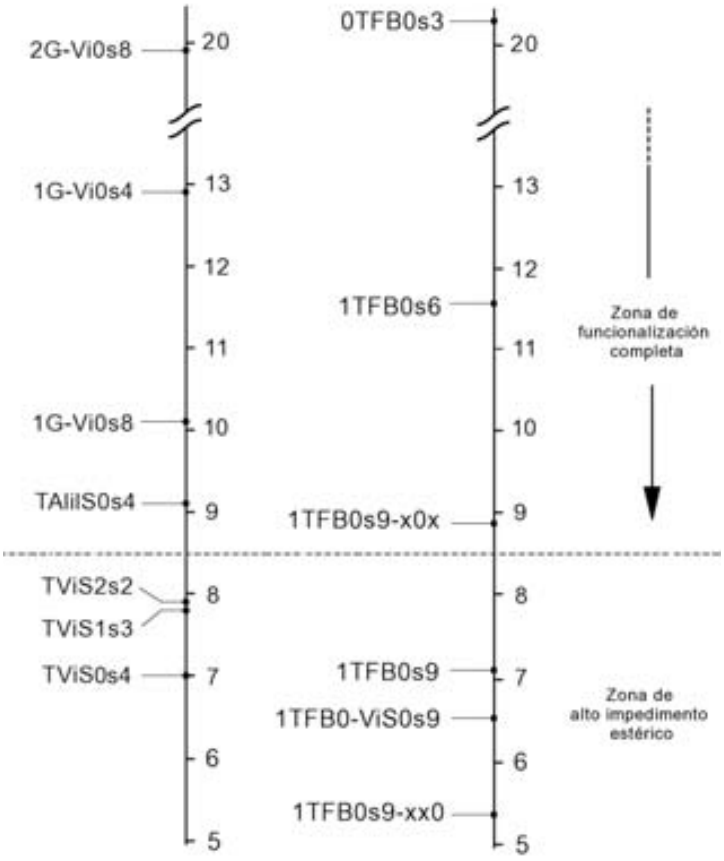

Figura 3.32: Valores del parámetro η (Å) calculados para los dendrímeros de tipo carbosilano (izq.) y los de tipo aril - éter de este apartado (dcha.) (Ver texto para más detalles).

entorno a 7 Å. La hidrosililación parcial de **TViS** aumenta el valor de η a valores cerca de 8 Å, sin embargo, la hidrosililación parcial de **1G-TFB(Alil)**$_9$ en alilos adyacentes 1TFB0s9-xx0 disminuye su valor (5.4 Å) y en vinilos separados (1TFB0s9-x0x) lo aumenta hasta cerca de 9 Å. Los dendrímeros que experimentalmente no presentaron ningún problema en la hidrosililación tienen todos en la simulación un valor de η a partir de 10 Å hacia arriba. Tentativamente y acorde con los resultados experimentales obtenidos en la preparación de metalodendrímeros con $[\mathbf{5}]^-$, podríamos situar un valor frontera entorno a 8.5 Å a partir del cual no tendrían lugar problemas de impedimento estérico para la funcionalización completa. Es interesante notar, por tanto, que la elongación de las

ramas de **1G-TFB(Alil)**$_9$ con Si$-CH_2-CH_2$, 1TFB0-ViS0s9, no produce un aumento del valor de η y que la falta de funcionalización del tetraalilsilano no es debida a razones de impedimento estérico.

3.2.3. Apertura de anillo de dioxano como mecanismo para la funcionalización de estructuras dendriméricas con [3,3'-Co(1,2-$C_2B_9H_{11})_2]^-$.

Las estructuras dendriméricas usadas en este apartado han sido preparadas por el grupo del Dr. Norberto Farfán,[167] utilizando unas condiciones similares a las síntesis de dendrones de tipo Fréchet.[168] La reacción del $\alpha,\alpha'-$dibromo$-p-$xileno y el $5-$hidroxi$-$(dimetil)benzoato a reflujo de acetonitrilo, en presencia de K_2CO_3, da un tetraéster que después es reducido para dar un tetraalcohol (Figura 3.33). Este tetraalcohol es considerado en este trabajo el dendrímero de generación cero o *core* y ha sido obtenido en sus formas *para*, **0G-p-XBO(OH)**$_4$ y *meta*, **0G-m-XBO(OH)**$_4$. Con una metodología divergente se puede seguir creciendo estos núcleos; en una etapa de activación se produce la bromación de los cuatro alcoholes bencílicos terminales y se sigue con la secuencia i) y ii) de la Figura 3.33. Se obtienen de esta manera los dendrímeros con 8 alcoholes terminales **1G-p-XBO(OH)**$_8$ y **1G-p-XBO(OH)**$_8$, respectivamente.

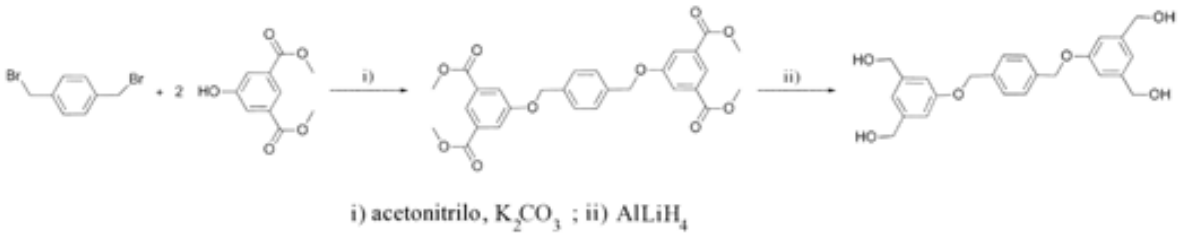

Figura 3.33: Síntesis de estructuras dendriméricas de tipo Fréchet. En la figura, secuencia para la obtención de **0G-p-XBO(OH)**$_4$.

Síntesis

Para la funcionalización de la periferia de estos dendrímeros con [3,3'-Co(1,2-$C_2B_9H_{11})_2]^-$ se utiliza el zwitterión [3,3'-Co(8-$C_4H_8O_2$-1,2-$C_2B_9H_{10})$(1',2'-$C_2B_9H_{11})$] que

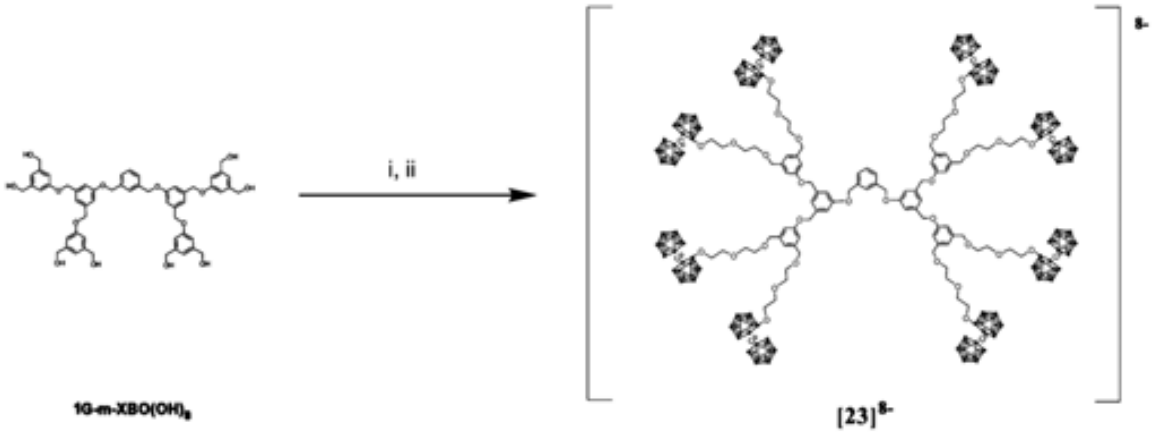

Figura 3.34: Síntesis del metalodendrímero $[\mathbf{23}]^{8-}$: i) DMSO, *t*-BuOK; ii) exc. [3,3'-Co(8-$C_4H_8O_2$-1,2-$C_2B_9H_{10}$)(1',2'-$C_2B_9H_{11}$)]. Los metalondendrímeros $[\mathbf{21}]^{4-}$, $[\mathbf{22}]^{4-}$ y $[\mathbf{24}]^{8-}$ se obtendrían de forma similar.

contiene un anillo de dioxano en el $B(8)$ (Figura 1.9 de la Introducción). Para la apertura del dioxano, los nucleófilos que se utilizaron fueron los grupo alcoholato formados al desprotonar los alcoholes benzílicos situados en la periferia de los dendrímeros de partida, Figura 3.34.

La reacción de **0G-p-XBO(OH)$_4$** con *t*-BuOK en DMSO da lugar al correspondiente tetraalcóxido, que reacciona con más de cuatro equivalentes de [3,3'-Co(8-$C_4H_8O_2$-1,2-$C_2B_9H_{10}$)(1',2'-$C_2B_9H_{11}$)] para dar $[\mathbf{21}]^{4-}$, con un rendimiento del 51 %. De forma similar se obtiene $[\mathbf{22}]^{4-}$ a partir de **0G-m-XBO(OH)$_4$** con un rendimiento del 62 %. Empleando más de ocho equivalentes de [3,3'-Co(8-$C_4H_8O_2$-1,2-$C_2B_9H_{10}$)(1',2'-$C_2B_9H_{11}$)] y tras la desprotonación de **1G-p-XBO(OH)$_8$** y **1G-m-XBO(OH)$_8$** se obtienen $[\mathbf{23}]^{8-}$ y $[\mathbf{24}]^{8-}$ con un rendimiento del 41 % y 47 %, respectivamente. La reacción puede ser monitorizada por capa fina hasta la desaparición total del reactivo [3,3'-Co(8-$C_4H_8O_2$-1,2-$C_2B_9H_{10}$)(1',2'-$C_2B_9H_{11}$)]. Tras el proceso de purificación, la funcionalización completa de estos metalodendrímeros es fácilmente verificable mediante ^{1}H-RMN y el desplazamiento del pico asignado al metileno de los alcoholes bencílicos. En el del producto de partida, este metileno es un doblete centrado a 4.60, y en el metalodendrímero es un singulete a 4.55 ppm.

En este punto, cabe recalcar que la dificultad de las síntesis de estos compuestos no reside en la funcionalización del dendrímero con el cobaltocarborano, sino en la ob-

tención del nucleófilo que va a realizar el ataque al dioxano de [3,3'-Co(8-$C_4H_8O_2$-1,2-$C_2B_9H_{10}$)(1',2'-$C_2B_9H_{11}$)]. La solubilidad de los dendrímeros **0G-p-XBO(OH)**$_4$, **0G-m-XBO(OH)**$_4$, **1G-p-XBO(OH)**$_8$ y **1G-m-XBO(OH)**$_8$ en disolventes apróticos es ya de por sí muy reducida y la forma salina de estos lo es aún más. Además, la solubilidad de los cobaltocarboranos queda acotada básicamente al empleo de disolventes polares. Con todas estas variables tenidas en cuenta, los únicos disolventes factibles para realizar la reacción de la Figura 3.34 son DMSO o DMF. En nuestro caso escogimos DMSO por la relativa facilidad para secarlo sin que ocurra descomposición. Es de vital importancia que el único nucleófilo presente en el medio de reacción sea la correspondiente sal de los dendrímeros, debido a que la presencia de agua y el medio básico para desprotonar aumenta la concentración de aniones OH^- y estos aniones rápidamente abren el anillo de dioxano del derivado [3,3'-Co(8-$C_4H_8O_2$-1,2-$C_2B_9H_{10}$)(1',2'-$C_2B_9H_{11}$)], quedando éste inservible para la funcionalización del dendrímero. Otro punto importante en la obtención de los derivados dendriméricos desprotonados es la base a utilizar. Se realizaron varias pruebas empleando n-BuLi, NaH y finalmente se escogió *t*-BuOK por ser más fácilmente manipulable y tener el pK_a más apropiado. Excesos en la cantidad de base introducirían nucleófilos indeseados en el medio de reacción que atacarían al derivado [3,3'-Co(8-$C_4H_8O_2$-1,2-$C_2B_9H_{10}$)(1',2'-$C_2B_9H_{11}$)], por lo que es importante trabajar en condiciones estequiométricas.[169] En este punto es importante destacar que una vez funcionalizados los dendrímeros con [3,3'-Co(1,2-$C_2B_9H_{11})_2]^-$, la solubilidad de éstos aumenta considerablemente hasta asemejarse a la de este complejo aislado.

Caracterización

Las estructuras dendriméricas funcionalizadas con [3,3'-Co(1,2-$C_2B_9H_{11})_2]^-$, $[\mathbf{21}]^{4-}$, $[\mathbf{22}]^{4-}$, $[\mathbf{23}]^{8-}$ y $[\mathbf{24}]^{8-}$ fueron caracterizadas en base a espectroscopía de FT-IR, UV-Vis, RMN de ^{1}H, ^{11}B y ^{13}C; espectrometría de masas MALDI-TOF y HPLC. La caracterización de los precursores dendriméricos terminados con grupo −OH, no se ha incluido aquí, pero se encuentra en el Anexo de esta tesis.[169]

El espectro de IR muestra en todos los casos la típica banda intensa correspondiente a ν(B−H) alrededor de 2550 cm^{-1} y bandas correspondientes a $\nu(C_{alquil}-H)$ entorno a 2950, 2920, 2870 cm^{-1}.

Los espectros de ^{1}H-RMN muestran los desplazamientos típicos para los protones

aromáticos entre 7.62 y 6.93 ppm. La señal de los protones del metileno que conecta el anillo benzenico con el grupo −OH tras funcionalizar pasa de doblete centrado en 4.60 a un singulete a 4.55 ppm. El desplazamiento de los C_c−H es indicativo de que el anillo de dioxano está abierto[44] y han aparecido dos resonancias en forma de multiplete debidas a los protones $-OCH_2-$ entorno a 3.65 y 3.55 ppm. El espectro de ^{13}C-RMN muestra los desplazamientos químicos de los carbonos aromáticos en la region de 160.5 a 100.5 ppm y los del grupo $-OCH_2-$ sobre 70 ppm. Las resonancias debidas a C_c−H aparecen como dos singuletes sobre 53 y 46 ppm en todos los casos, indicativo esto también de que el anillo de dioxano está abierto para todas las estructuras dendriméricas reportadas. El espectro de ^{11}B-RMN muestra un patrón típico de un derivado de cobaltabisdicarballuro con el anillo de dioxano abierto en el rango de +25 a -20 ppm, siendo la señal entorno a +25 ppm la única que no se desdobla por acoplamiento con el H en el ^{11}B-RMN y que corresponde a $B(8)$.

El MALDI-TOF ha sido empleado para la caracterización de los metalodendrímeros. Excepto para $[\mathbf{23}]^{8-}$, que se detecta el pico m/z con z=8, el resto de metalodendrímeros se caracterizan por haber sufrido intercambio de cesios por protones y quedar registrados con un valor de z variable. Algo típico de esta técnica de MALDI-TOF que ocurre con moléculas policargadas. En este caso, como en anteriores, las pruebas dan soporte a la síntesis pero no establecen claramente el peso molecular completo del metalodendrímero debido a la gran fragmentación existente, como en el caso de los dendrímeros de carbosilano del apartado anterior.[155]

Para este tipo de metalodendrímeros conectados a la estructura dendrimérica por el $B(8)$ del cobaltabisdicarballuro se han realizado unas medidas de tiempo de retención en HPLC que nos ha servido para corroborar el carácter unificado de los diferentes dendrímeros. El eluyente empleado ha sido metanol y la columna es de fase reversa de tipo C18. El detector acoplado a la columna está fijado para señalar compuestos que absorban a la longitud de onda de 310 nm (la máxima señal en estos dendrímeros). Los tiempos de retención son significativamente diferentes dependiendo de si el metalodendrímero es de generación cero o primera, mostrándo mayores tiempos de retención los dendrímeros con 4 cobaltacarboranos, véase Tabla 3.9.

La explicación es sencilla ya que los dendrímeros de mayor generación, $[\mathbf{23}]^{8-}$ y $[\mathbf{24}]^{8-}$, con 8 cobaltacarboranos en la periferia, camuflarían mejor el esqueleto aromático apolar del dendrímero, mientras que los de menor generación, al estar este esqueleto

Compuesto	t_r(min)
ref.	1.31
[21]$^{4-}$	1.38
[22]$^{4-}$	1.39
[23]$^{8-}$	1.32
[24]$^{8-}$	1.31

Tabla 3.9: Tiempos de retención para los metalodendrímeros **[21]**$^{4-}$-**[24]**$^{8-}$ y el compuesto referencia [3,3'-Co(8-O-CH_2-CH_2-O-CH_2-CH_2-O-CH_3-1,2-$C_2B_9H_{11}$)(1',2'-$C_2B_9H_{11}$)]$^-$.

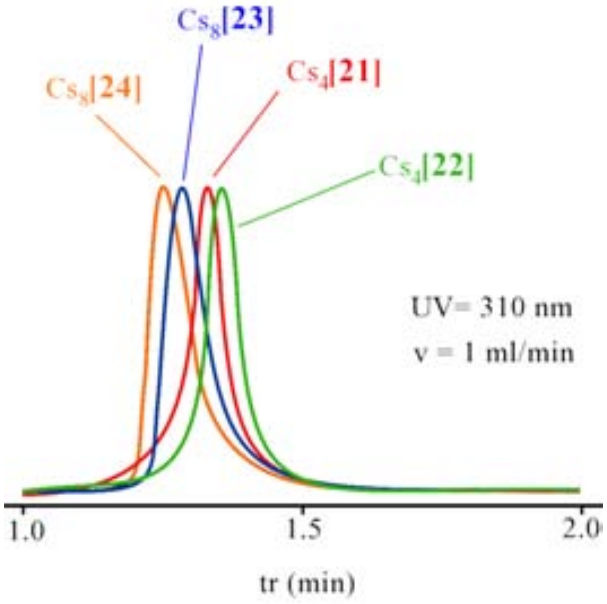

Figura 3.35: Tiempos de retención en columna de HPLC para los metalondendrímeros **[21]**$^{4-}$, **[22]**$^{4-}$, **[23]**$^{8-}$ y **[24]**$^{8-}$.

más expuesto tendrían más afinidad por permanecer en la fase reversa de la columna y por tanto mostrar mayores tiempos de retención. Además, los tiempos de retención de los dendrímeros con más funcionalización son muy similares al del compuesto usado como referencia. En la Figura 3.35 se muestran los gráficos obtenidos con los dendrímeros estudiados.

Actualmente investigamos la manera de perfeccionar este método usando mezclas

compuesto	λ_{max} (ε)		
$[\mathbf{21}]^{4-}$	268 (69697)	310 (110909)	372 (16364)
$[\mathbf{22}]^{4-}$	273 (56364)	312 (117576)	371 (18788)
$[\mathbf{23}]^{8-}$	274 (99394)	312 (216970)	370 (35758)
$[\mathbf{24}]^{8-}$	273 (109697)	311 (220000)	369 (35152)

Tabla 3.10: Absorciones máximas (nm) para cada compuesto en el espectro de UV-Vis. El coeficiente de extinción molar (ε, $10^3 dm^3 mol^{-1} cm^{-1}$) figura entre paréntesis al lado de la señal correspondiente.

de disolventes que maximicen esta diferencia en los tiempos de retención. El HPLC por tanto, y seguramente otras técnicas relacionadas como la electroforesis capilar, se convierte en una prometedora herramienta para caracterizar estos metalodendrímeros polianiónicos, frente al bajo exito de las técnicas de espectrometría de masas o el analisis elemental en este tipo de compuestos.[158,159]

Medidas de UV-Vis

Los espectros de UV-Vis de los compuestos $[\mathbf{21}]^{4-}$, $[\mathbf{22}]^{4-}$, $[\mathbf{23}]^{8-}$ y $[\mathbf{24}]^{8-}$ disueltos en etanol muestran 3 señales entorno a 270, 310 y 370 nm, véase la Tabla 3.10 y la Figura 3.36. Como en los casos anteriores, para estos metalodendrímeros se puede apreciar una correlación lineal entre el número de unidades de cobaltabisdicarballuro localizadas en la periferia y el coeficiente de extinción molar correspondiente a su longitud de onda máxima como ocurría en los apartados anteriores. En la Figura 3.37 se muestra el ajuste lineal para este tipo de metalodendrímeros disueltos en etanol.

3.2.4. Siloxanos y Octasilsesquioxanos funcionalizados con derivados de *o*-carborano.

Disiloxanos, ciclosiloxanos y octasilsesquioxanos funcionalizados con derivados del *o*-carborano (metil-*o*-carborano y fenil-*o*-carborano) han sido preparados mediante el proceso de hidrólisis-condensación de los correspondientes carboranilclorosilanos o carboraniletoxisilanos, siguiendo la vía hidrolítica y también por un proceso no hidrolítico usando DMSO como fuente de oxígeno.[97]

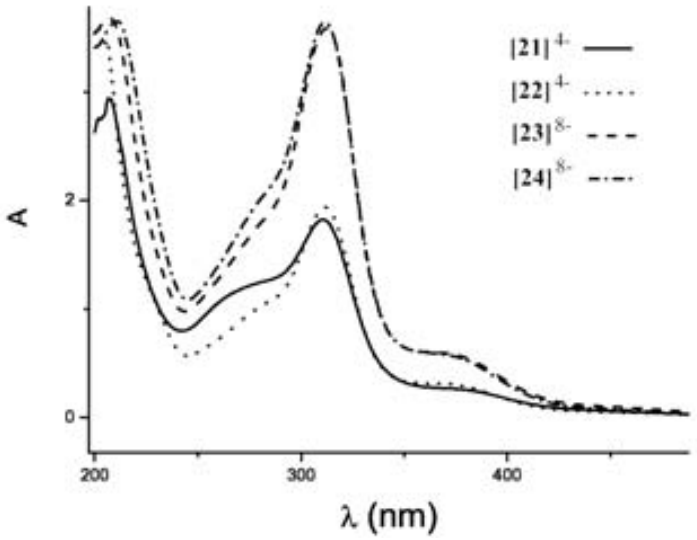

Figura 3.36: Espectros de Absorción UV-Vis para los metalodendrímeros $[\mathbf{21}]^{4-}$, $[\mathbf{22}]^{4-}$, $[\mathbf{23}]^{8-}$ y $[\mathbf{24}]^{8-}$.

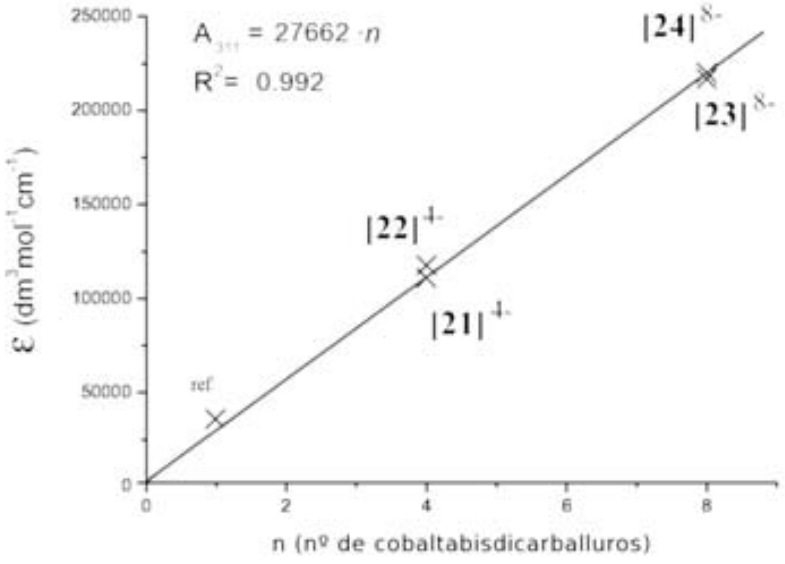

Figura 3.37: Correlación lineal entre el número de unidades de cobaltabisdicarballuro y la absortividad a $\lambda_{max} = 311$ nm. También se incluye el punto correspondiente a [3,3'-Co(8-O-CH_2-CH_2-O-CH_2-CH_2-O-CH_3-1,2-$C_2B_9H_{11}$)(1',2'-$C_2B_9H_{11}$)]$^-$ (referencia).

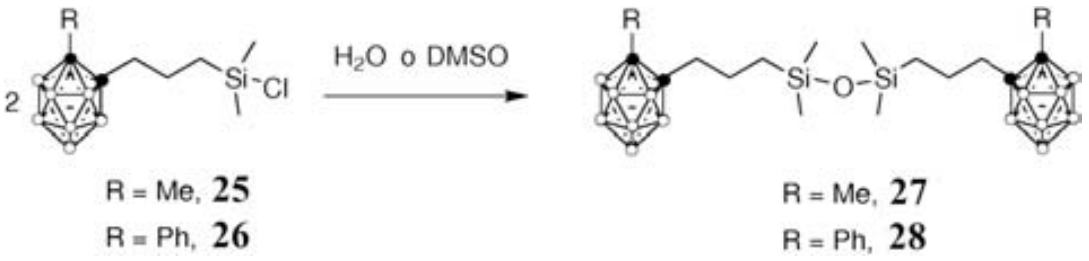

Figura 3.38: Preparación de los dímeros de carboranildisiloxano **27** y **28** usando la ruta acuosa y la no acuosa con DMSO.

Síntesis

Para la síntesis de los disiloxanos **27** y **28** se prepararon los carbonilclorosilanos **25** y **26** correspondientes[97b] y se realizó la hidrólisis-condensación en presencia de agua, lo que dio lugar a la obtención de los disiloxanos en un alto rendimiento (72-81 %). En cambio, la vía no acuosa usando DMSO[170] necesitó más tiempo para completarse y sin embargo el rendimiento no mejoró (40 %).

La síntesis de los ciclosiloxanos se llevo a cabo de manera similar usando los carboranildiclorosilanos **29** y **30** (véase Figura 3.39). Ambos métodos conducen a la formación de una mezcla de ciclotrisiloxano (D_3), ciclotetrasiloxano (D_4) y un porcentaje variable de oligómeros lineales (L), siendo la principal diferencia entre ambos métodos que por la vía no acuosa la cantidad de oligómeros lineales es significativamente menor que empleando el método acuoso. La mezcla de ciclos y oligómeros lineales, tras purificación en columna de sílica, queda como un aceite incoloro.

La síntesis de octasilsesquioxanos T_8 se realizó utilizando dos vías diferentes, a partir de los precursores triclorosilano **35** y **36** en condiciones no acuosas utilizando DMSO en $CHCl_3$ (Figura 3.40), y con los precursores trietoxisilano **37** y **38** en THF, con la cantidad estequiométrica de H_2O y catalizador (TBAF o NaOH). En todo caso, por el método no hidrolítico se obtuvo el T_8 y no se detectó la formación del T_6 por ^{29}Si-RMN . El método acuoso con TBAF y en tiempos de reacción de 130 días resulto el mejor método con rendimientos rondando el 70 %.

Degradaciones parciales sobre los carboranos de los compuestos **27**, **28** y **39** nos han permitido obtener los derivados polianiónicos $[\mathbf{41}]^{2-}$, $[\mathbf{42}]^{2-}$ y $[\mathbf{43}]^{8-}$, funcionalizados con las especies *nido* en la periferia. Para el caso de los dímeros la degradación se hizo

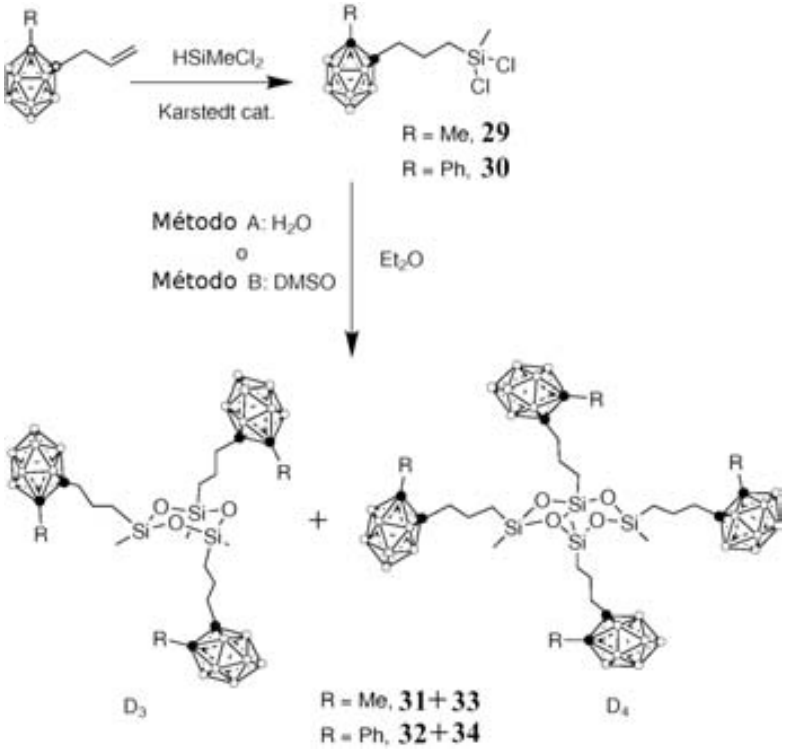

Figura 3.39: Preparación de los ciclocarboranildisiloxanos usando la ruta acuosa y la no acuosa con DMSO.

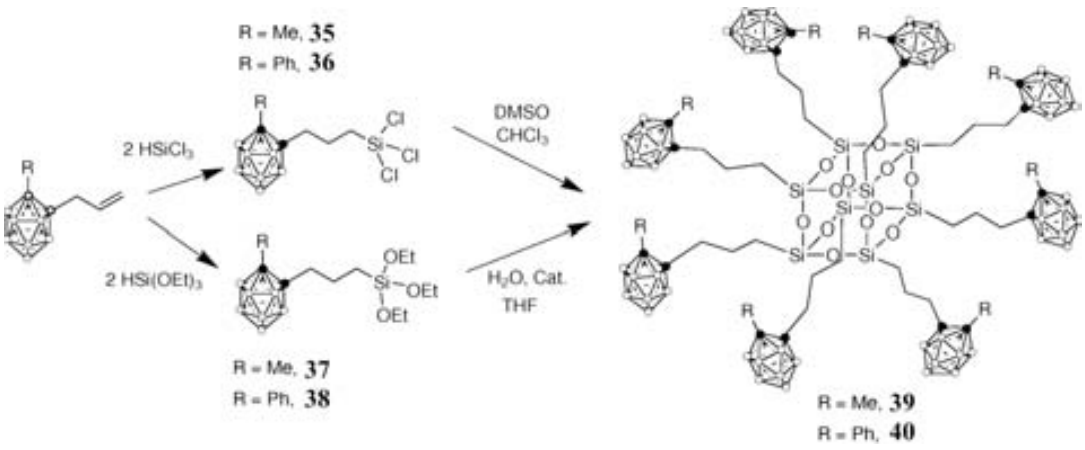

Figura 3.40: Preparación de los octasilsesquioxano, T_8, **39** y **40**.

utilizando dos métodos: piperidina en EtOH y KOH en EtOH. En ambos casos se produce la degradación del clúster *closo* sin afectar al enlace Si−O−Si. En el caso del T_8 las degradación se realiza en KOH/EtOH.

Caracterización

Las estructuras de los compuestos **27**-$\mathbf{(43)}^{8-}$ fueron caracterizadas en base a FT-IR, RMN de ^{1}H, ^{11}B, ^{13}C y ^{29}Si; y espectrometría de masas ESI y MALDI-TOF. La estructura cristalina de **27** también pudo ser determinada por difracción de rayos X (3.41).

El espectro de IR de los compuestos con carborano *closo* muestra una banda correspondiente a ν(B−H) alrededor de 2584 cm^{-1} y para los clústeres *nido* una banda intensa a 2515 cm^{-1}.

Los espectros de ^{1}H-RMN muestran resonancias entre 7.68 y 7.36 ppm para los protones aromáticos de los compuestos con fenil-*o*-carborano, mientras que una resonancia entorno a 2.02 ppm corresponde al metilo en los derivados con metil-*o*-carborano. Las resonancias de los protones de las cadenas propílicas se situan en el rango 2.23-0.24 ppm. Las señales de los protones atribuidos a los metilos del grupo Si−CH_3 aparecen entorno a 0.07 y -0.18 ppm. La resonancia amplia, entre -2.60 y -2.19 ppm, en los compuestos con *nido*-carborano corresponde al hidrógeno pontal. El espectro de ^{13}C-RMN muestra los desplazamientos químicos de los carbonos aromáticos en la region de 131 a 127 ppm para fenil-*o*-carborano y entorno a 22 ppm para el metilo en compuestos con metil-*o*-carborano. Los Si−CH_3 aparecen alrededor de 0.4 ppm y los átomos de C_c aparecen entorno a 78 ppm. El espectro de ^{11}B-RMN para los compuestos con *closo*-carborano tiene un rango típico de señales que abarca desde -2.6 a -10.0 ppm y cuando el carborano es de tipo *nido* las resonancias aparecen entre -5.9 y -36.9 ppm. Los espectros de ^{29}Si-RMN en los disiloxanos **27** y el **28** muestran un desplazamiento a 6.7 ppm y los T_8 muestran una única resonancia en el ^{29}Si CP-MAS a -66.6 ppm.

La mezcla de estructuras de ciclosiloxanos D_3 y D_4 fue confirmada por MALDI-TOF, que junto con las integrales de los desplazamientos de los protones del grupo Si−CH_3 en el ^{1}H-RMN nos permite tentativamente dar los porcentajes relativos de cada especie, D_3, D_4 y L, en cada método (hidrolítico o no hidrolítico) y para cada derivado de carborano (metil- o fenil-*o*-carborano). El dímero con *nido*-carborano $\mathbf{(41)}^{2-}$ y el T_8 **39** fueron

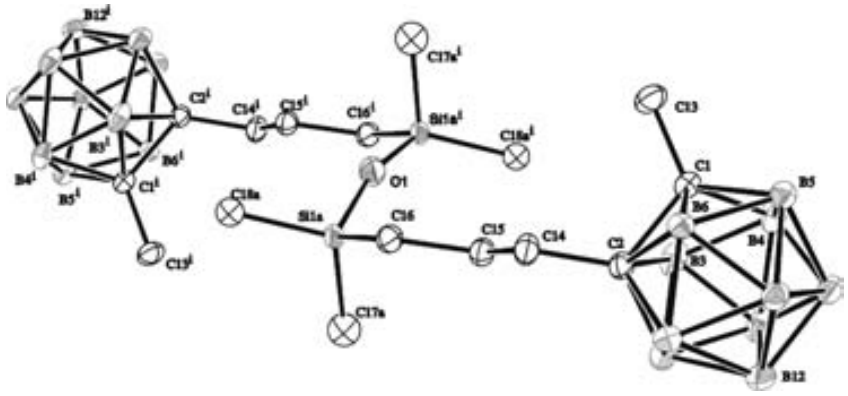

Figura 3.41: Estructura molecular del compuesto **27**.

también caracterizados por ESI-MS. Estos datos se encuentran ampliados en el Capítulo 5 de esta tesis en el artículo correspondiente.[97]

97

3.3. Funcionalización de Superficies.

3.3.1. Nanopartículas de TiO_2 funcionalizadas con derivados de $[3,3'\text{-}Co(1,2\text{-}C_2B_9H_{11})_2]^-$.

Dos derivados fosforados del anión $[3,3'\text{-}Co(1,2\text{-}C_2B_9H_{11})_2]^-$, $[1,1'\text{-}\mu\text{-}(HO)(O)P\text{-}3,3'\text{-}Co(1,2\text{-}C_2B_9H_{10})_2]^-$, [**44**]$^-$, y $[8,8'\text{-}\mu\text{-}(OH)(O)\text{-}P(O)_2\text{-}C_2B_9H_{10})_2\text{-}3,3'\text{-}Co]^-$, [**45**]$^-$, han sido usados para funcionalizar la superfice de nanopartículas de TiO_2 siguiendo un procedimiento previamente descrito con otros derivados de fósforo.[122]

Síntesis de precursores.

El derivado de fosfinato, [**44**]$^-$, ha sido preparado por metalación del anión $[3,3'\text{-}Co(1,2\text{-}C_2B_9H_{11})_2]^-$ con 2 eq. de n-BuLi seguido de la reacción con $Cl_3P(O)$ en DME. Después de un tratamiento con NaOH y la correspondiente purificación, se ha obtenido Cs[**44**] como un sólido rojo con un rendimiento del 82 %. Los espectros de RMN de ^1H, ^{11}B, ^{13}C y ^{31}P respaldan la estructura propuesta.[171]

El derivado fosfato, [**45**]$^-$, ha sido preparado de acuerdo con la bibliografía.[172]

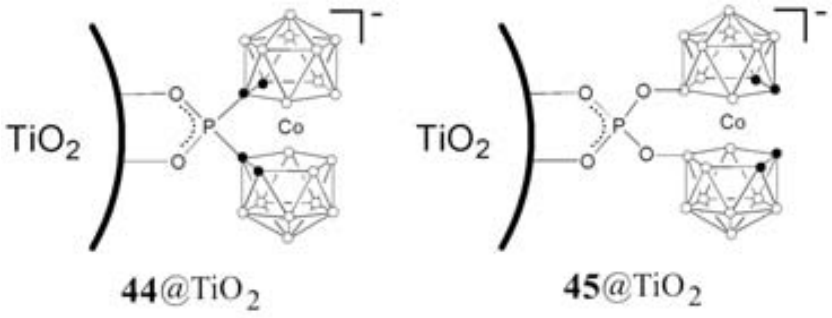

Figura 3.42: Nanopartículas de TiO_2 funcionalizadas con derivados fosforados del [3,3'-$Co(1,2\text{-}C_2B_9H_{11})_2]^-$.

Procedimiento para la funcionalización de la superficie.

La superfice de las nanopartículas de TiO_2 fue modificada haciendo reaccionar una suspensión de las nanopartículas con una disolución $EtOH/H_2O$ (3:1) de cada uno de los derivados, Cs[**44**] y Cs[**45**], durante 5 días. Tras filtrar la suspensión y lavar abundantemente el sólido con EtOH, acetona y H_2O, para eliminar todas aquellas moléculas fisisorbidas, el óxido de titanio funcionalizado se seca a vacío durante 5 horas a 110º. La simple inspección visual muestra que las nanopartículas han pasado de tener color blanco a ser rosa-marrón en el caso del **44**@TiO_2 y amarillo-naranja para **45**@TiO_2.

El material obtenido, **44**@TiO_2 y **45**@TiO_2, respectivamente (Figura 3.42) es caracterizado por IR, ^{31}P y ^{11}B CP-MAS RMN.

Los espectros de IR de las nanopartículas muestran una señal ancha entorno a 2550 cm^{-1} correspondiente a $\nu(B-H)$, lo que indica que los derivados de cobaltabisdicarballuro han quedado anclados en la superficie. La región de la frecuencia de vibración de P-O se muestra muy diferente si se comparan los espectros de los precursores con los del derivado anclado en el TiO_2, Figura 3.43, lo cual es indicativo del acoplamiento en la superficie de las partículas.[171]

El espectro de ^{11}B CP-MAS-RMN en estado sólido de las nanopartículas modificadas revela que los desplazamientos químicos aparecen en los mismos lugares que los precursores, Figura 3.44, lo que confirma la presencia de estos derivados. Aunque las señales son bastante anchas debido a acoplamientos cuadrupolares.[173] Es importante destacar, sin embargo, que en la muestra **45**@TiO_2 es bastante distinguible la señal correspondiente

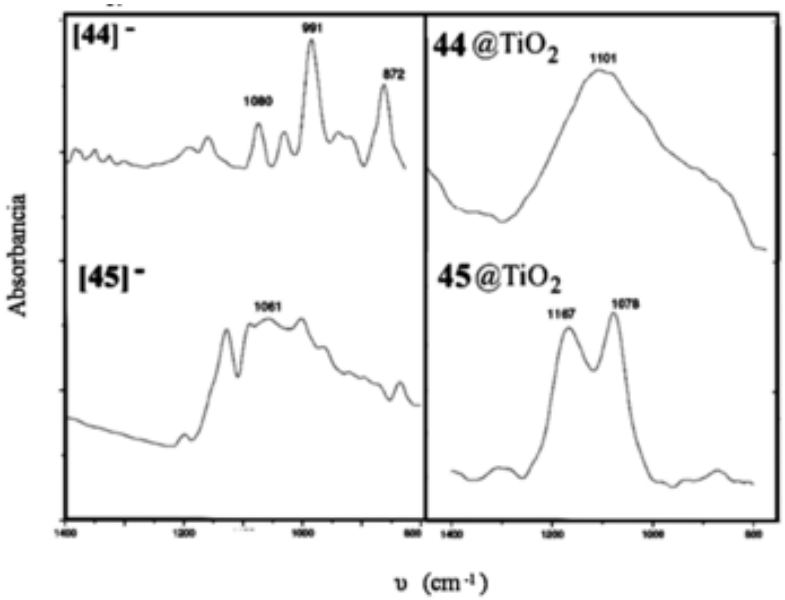

Figura 3.43: Espectros de IR para los compuesto $[\mathbf{44}]^-$ y $[\mathbf{45}]^-$ (izda.) y para $\mathbf{44}$@TiO_2 y $\mathbf{45}$@TiO_2 (dcha.).

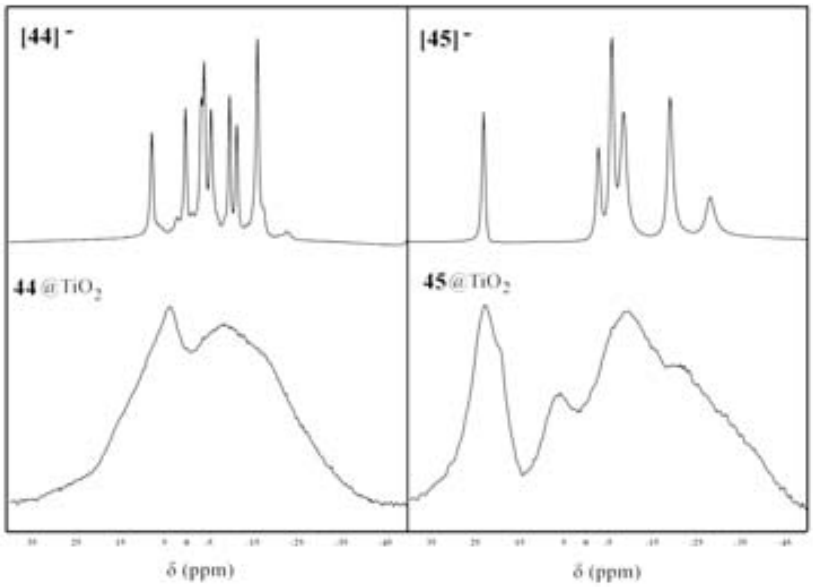

Figura 3.44: Espectro de ^{11}B-{^{1}H}-RMN en disolución para los compuestos $[\mathbf{44}]^-$ y $[\mathbf{45}]^-$ (arriba) y espectros de ^{11}B CP-MAS-RMN para $\mathbf{44}$@TiO_2 y $\mathbf{45}$@TiO_2 (abajo).

a $B(8)$-O centrada a 25 ppm en el espectro.

Los espectros de ^{31}P CP-MAS-RMN de las nanopartículas **44**@TiO_2 y **45**@TiO_2 son indicativos de que este fósforo esta anclado en la superficie del material.[171] Así, el espectro de ^{31}P-CP-MAS RMN de **44**@TiO_2 muestra una resonancia a 21.0 ppm que ha sido desplazada respecto al precursor, Cs[**44**] (47.5 ppm). Por el contrario, para el caso de **45**@TiO_2, la resonancia está a -11.5 ppm y en el precursor (Cs[**45**]) aparecía a -5.3 ppm. En este último caso, los desplazamientos químicos del átomo de P son más parecidos, ya que el entorno de éste átomo es muy parecido en el precursor y en el producto final.

Teniendo en cuenta los datos expuestos arriba, nos atrevemos a confirmar que los derivados de fósforo de [3,3'-Co(1,2-$C_2B_9H_{11})_2]^-$ se han acoplado a la superficie de las nanopartículas de TiO_2, a través de los grupos fosfato y fosfinato dando lugar a una superficie de cargas negativas las cuales se espera prometedoras aplicaciones como por ejemplo en células de Grätzel.

3.3.2. Funcionalización de *wafers* de Si oxidado con derivados de [3,3'-Co(1,2-$C_2B_9H_{11})_2]^-$.

Dos aproximaciones han sido utilizadas para funcionalizar superficies de Si oxidado con derivados de [3,3'-Co(1,2-$C_2B_9H_{11})_2]^-$, que se exponen a continuación.

Preparación y funcionalización de las superficies.

El primer método consiste en la apertura *in situ* del anillo de dioxano del derivado zwitterión [3,3'-Co(8-$C_4H_8O_2$-1,2-$C_2B_9H_{10}$)(1',2'-$C_2B_9H_{11}$)](Figura 1.9), por ataque nucleofílico de una amina terminal que previamente ha sido anclada en el *wafer* de Si oxidado.[174]

La preparación de la superficie de silicio oxidado (100) se realizó eliminando la capa nativa de óxido por inmersión del *wafer* en un baño de una disolución acuosa de HF (40 %), después tras un lavado con agua de calidad HPLC, los substratos son expuestos a una corriente de ozono durante 30 minutos para obtener de nuevo una superficie lisa de sílice libre de contaminación orgánica. Tras este tratamiento, la superficie de sílice hidrofílica presenta ángulos de contacto de 10º y el expesor de esta capa de SiO_2 sobre el *wafer* de Si medido por elipsometría está entorno a 1.8-2.0 nm. La rugosidad medida por AFM (en modo *tapping*) es de 0.15 nm.

Una vez prepara la superficie, el wafer se hace reaccionar con una disolución de (11-aminooxi)undeciltrimetoxisilano en TCE seco en un Schlenk bajo atmósfera de nitrógeno durante 24 horas (0º) y sin agitación. A continuación, se retira esta disolución y se añade otra con [3,3'-Co(8-$C_4H_8O_2$-1,2-$C_2B_9H_{10}$)(1',2'-$C_2B_9H_{11}$)](50 veces en exceso sobre la primera). Tras 48 h. el *wafer* es lavado intensivamente con TCE, THF y $CHCl_3$ bajo sonicación para dar lugar al *wafer* funcionalizado **46**@SiO_2 (Figura 3.45).

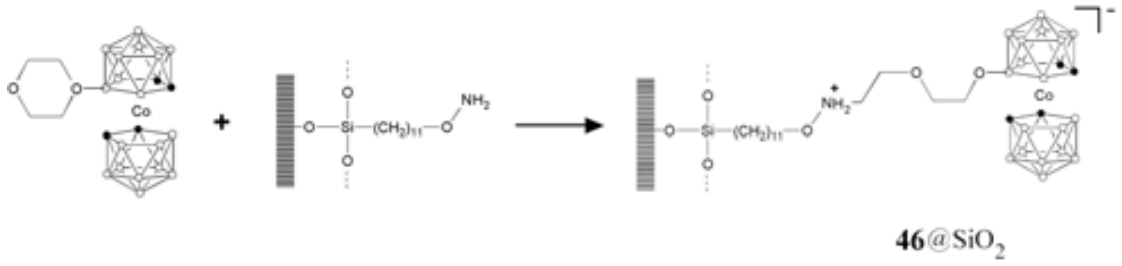

Figura 3.45: Procedimiento para el *grafting* de [3,3'-Co(8-$C_4H_8O_2$-1,2-$C_2B_9H_{10}$)(1',2'-$C_2B_9H_{11}$)]en un *wafer* de silicio oxidado para dar **46**@SiO_2.

En el segundo método empleado en este trabajo,[174] se prepara la superficie de silicio oxidado (100) como anteriormente y ésta se hace reaccionar con 10-isocianatodeciltriclorosilano a 0º durante 45 minutos, bajo atmósfera de nitrógeno y sin agitación.[175] Después el *wafer* funcionalizado con el isocianato terminal se hace reaccionar con una disolución de un derivado del cobaltabisdicarballuro con amina terminal, Cs[3,3'-Co(8-NH_2-$C_4H_8O_2$-1,2-$C_2B_9H_{10}$)(1',2'-$C_2B_9H_{11}$)], preparado siguiendo un procedimientod descrito en bibliografía,[39] en TCE por dos horas a 0º de temperatura. Finalmente el wafer se lava como en el primer método y se obtiene **47**@SiO_2 (Figura 3.46).

Caracterización de las superficies.

Las superficies de los *wafers* funcionalizados **46**@SiO_2 y **47**@SiO_2 han sido caracterizadas por medidas de ángulo de contacto, FTIR-ATR, AFM, elipsometría y XPS.

Los ángulos de contacto para una gota de agua (calidad HPLC) en las superficies funcionalizadas **46**@SiO_2 y Cs**47**@SiO_2 son 81.8 ± 2.3 y 75.2 ± 2.0 respectivamente. El aumento del ángulo de contacto corrobora la funcionalización de la superficie con la especie hidrofóbica [3,3'-Co(1,2-$C_2B_9H_{11}$)$_2$]$^-$.

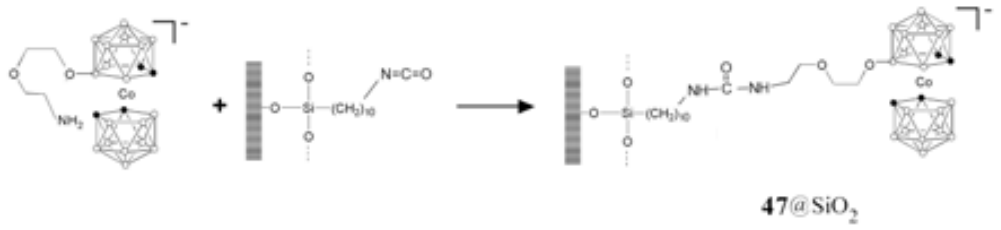

Figura 3.46: Procedimiento para el *grafting* de [3,3'-Co(8-NH_2-$C_4H_8O_2$-1,2-$C_2B_9H_{10}$)(1',2'-$C_2B_9H_{11}$)]$^-$ en un *wafer* de silicio oxidado para dar **47**@SiO_2.

El anclado de los derivados de [3,3'-Co(1,2-$C_2B_9H_{11}$)$_2$]$^-$ sobre las superficies funcionalizadas fue estudiado *in situ* por ATR-FTIR. En la Figura 3.47 se representan los espectros del *wafer* de partida, NH_2-O-$(CH_2)_{11}$@SiO_2, y el preparado en este trabajo, **46**@SiO_2. En ambos espectros se observan las bandas $\nu_{as}(CH_2)$ y $\nu_s(CH_2)$ a 2924 y 2853

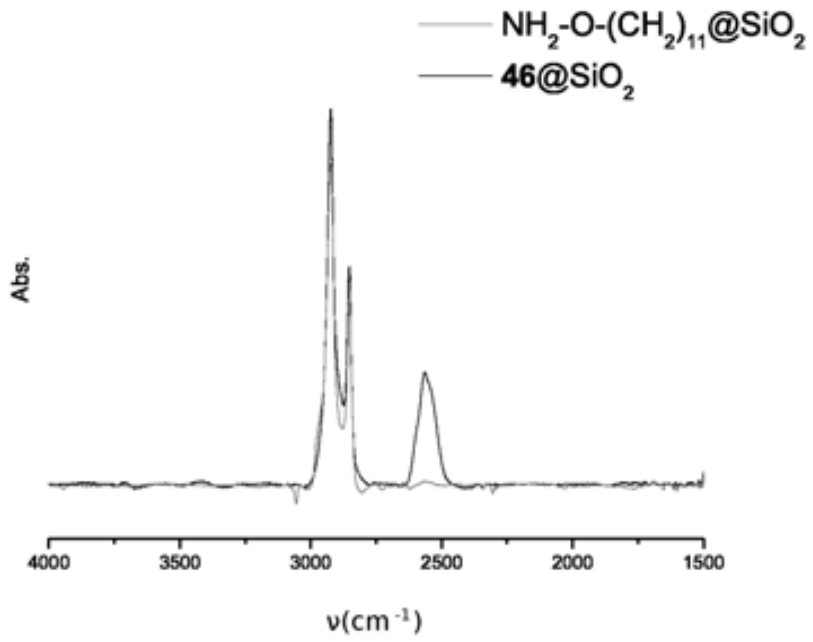

Figura 3.47: Espectros FTIR-ATR de las superficies antes y despues de ser funcionalizados con [3,3'-Co(8-$C_4H_8O_2$-1,2-$C_2B_9H_{10}$)(1',2'-$C_2B_9H_{11}$)]para dar **46**@SiO_2.

cm^{-1} indicativas de la organización de las cadenas alifáticas. En **46**@SiO_2, tras funcionalizar, aparece una absorción a 2565 cm^{-1} correspondiente a la frecuencia de vibración de los B−H. En ninguno de los casos se observa la señal de N−H debido a que el espectro ha sido restado con el espectro del *wafer* sin funcionalizar, que contiene la banda de los silanoles que solaparía con la primera.

Para el caso de Cs**47**@SiO_2, la Figura 3.48 presenta los espectros antes y despues de su funcionalización con el derivado de [3,3'-Co(1,2-$C_2B_9H_{11}$)$_2$]$^-$.

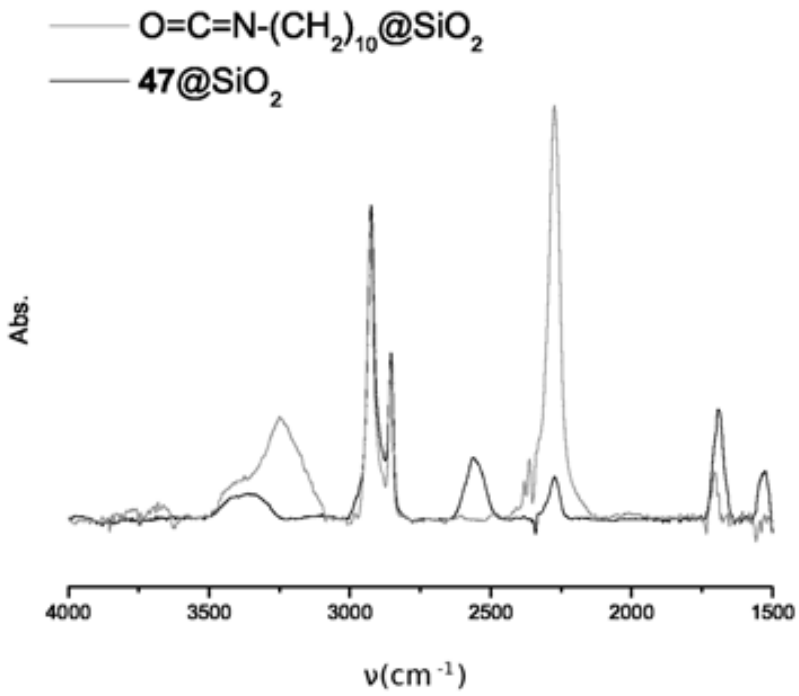

Figura 3.48: Espectros FTIR-ATR de las superficies antes y despues de ser funcionalizados con Cs[3,3'-Co(8-NH_2-$C_4H_8O_2$-1,2-$C_2B_9H_{10}$)(1',2'-$C_2B_9H_{11}$)] para dar Cs**47**@SiO_2.

En estos espectros también se pueden apreciar las bandas correspondientes a $\nu_{as}(CH_2)$ y $\nu_s(CH_2)$ a 2925 y 2854 cm^{-1} indicativas de la organización de las cadenas alifáticas. A 2563 cm^{-1} aparece una absorción correspondiente a la frecuencia de vibración de los B−H y también se puede apreciar que la banda de la función isocianato (2274 cm^{-1}) no ha desaparecido completamente pero a disminuido bastante su intensidad. Aparecen

nuevas bandas a 1687 y 1528 cm^{-1} correspondientes al grupo urea.

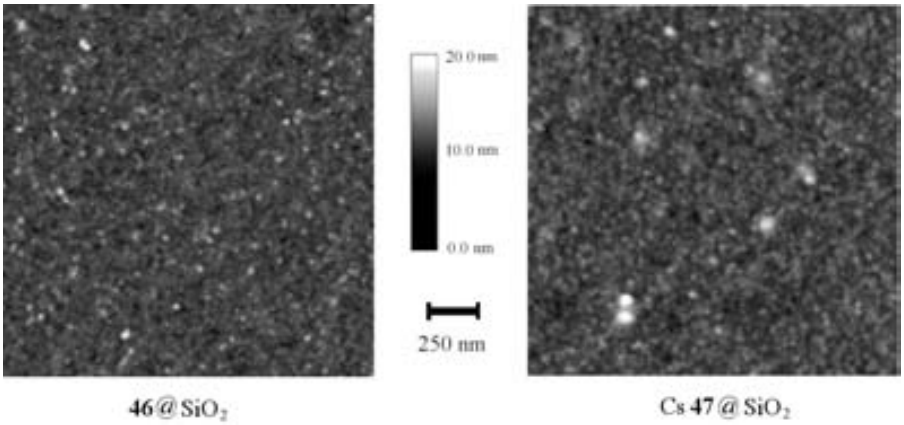

Figura 3.49: AFM en modo *tapping* para los wafers funcionalizados.

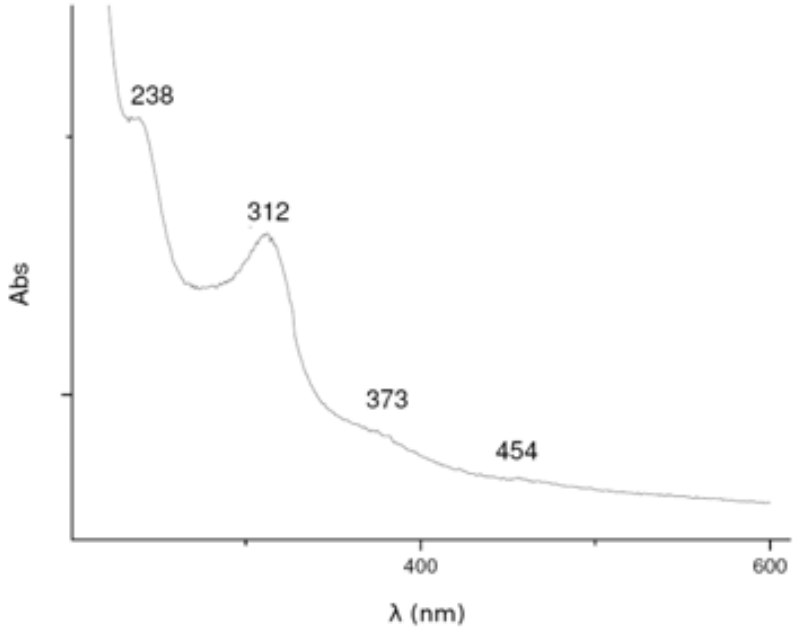

Figura 3.50: Espectro UV-vis de **46**@cuarzo.

Las elipsometría da una distancia experimental para las cadenas $Si{-}(CH_2)_{11}{-}O{-}NH_2$ y $Si{-}(CH_2)_{10}{-}N{=}C{=}O$ de 1.7 y 1.6 nm, respectivamente.[133,175]

Para los *wafers* preparados en este trabajo, **46**@SiO_2 y Cs**47**@SiO_2 se obtuvieron unos valores de 2.0 y 2.2 nm, respectivamente. Esto nos indica que las ramas no están completamente desplegadas, en cuyo caso los valores de espesor rondarían los 3.0 nm.

Las medidas de rugosidad media realizadas por AFM dan valores para **46**@SiO_2 y Cs**47**@SiO_2 de 0.6 nm y 1.0 nm, respectivamente. En la Figura 3.49 se muestra la superficie de los *wafers* medida por AFM.

Para el caso de **46**@SiO_2 se pudo hacer una funcionalización sobre un *wafer* de cuarzo y hacer una medida del espectro UV-vis, en la Figura 3.50 se representa el espectro, y en él se puede observar la banda típica en los derivados de [3,3'-Co(8-R-$C_4H_8O_2$-1,2-$C_2B_9H_{10}$)(1',2'-$C_2B_9H_{11}$)]$^-$ entorno a 312 nm.

Respecto a las medidads de XPS sobre las muestras en el caso de Cs**47**@SiO_2 se detectan todos los picos correspondientes a C, N, B, O, Co y Cs, y en el caso de **46**@SiO_2 la señal correspondiente a B se detecta pero no es tan intensa como en el Cs**47**@SiO_2.

Según todos estos datos podemos concluir que ambos métodos son efectivos para poder llevar a cabo la funcionalización de los *wafers* de Si mediante la apertura del anillo de dioxano del [3,3'-Co(8-$C_4H_8O_2$-1,2-$C_2B_9H_{10}$)(1',2'-$C_2B_9H_{11}$)]. Actualmente, se está tratando de estudiar las posibles aplicaciones de estos *wafers*, principalmente el estudio de las interacciones de estos metalacarboranos con biomoléculas.

4

Conclusiones

1. The first C_c-mono and C_c-disubstituted cobaltabisdicarbollide derivatives containing different organosilane functions have been successfully prepared by the direct reaction of the mono or dilithium salts of starting anions, $[\mathbf{1}]^-$ and $[\mathbf{2}]^-$, with the appropriate chlorosilanes and under careful control of the temperature. The reaction temperature was a key factor, because at very low temperatures (78 ^{o}C) C_c-monosubstituted species and high isomeric purity were obtained, whereas increasing the temperature led to C_c-disubstituted anions and structural isomers mixtures.

2. Density functional theory (DFT) at the B3LYP/6-311G (d,p) level was applied to optimise the geometries of the prepared silyl-containing cobaltabisdicarbollide derivatives, $[\mathbf{3}]^-$–$[\mathbf{10}]^-$, and calculate their relative energies. The theoretical studies perfectly agree with the experimental results, indicating that racemic mixtures (*rac* isomers) are more stable than *meso* isomers.

3. The anion [1-$SiMe_2$H-3,3'-Co(1,2-$C_2B_9H_{10}$)(1',2'-$C_2B_9H_{11}$)]$^-$, $[\mathbf{3}]^-$, represents the first example of a C_c-monosubstituted cobaltabisdicarbollide fully characterised by X-ray diffraction. The crystal structure shows three H$\cdots$H short contacts: two Si$-$H$\cdots$H$-C_c$ and one Si$-CH_2-$H$\cdots$H$-C_c$ contact. The shortest one corresponds to Si$-CH_2-$H$\cdots$H$-C_c$ with a H$\cdots$H distance of 2.059 Å, whereas the two longest correspond to Si$-$H$\cdots$H$-C_c$ with 2.212 and 2.409 Å, respectively. However, by using QTAIM and Charge Analyses Population on the hydrogen atoms, it has been conclude that the C$-$H$\cdots$H$-C_c$, is not a dihydrogen bond (DHB) or it is a weak H$-$H interaction. On the contrary, both Si$-$H$\cdots$H$-C_c$ interactions are DHB and can be considered part of an asymmetric bifurcated DHB.

4. Compounds [1,1'-μ-$SiMe_2$-3,3'-Co(1,2-$C_2B_9H_{10}$)$_2$]$^-$, $[\mathbf{4}]^-$ and [1,1'-μ-$SiMe_2$-8,8'-μ-C_6H_4-3,3'-Co(1,2-$C_2B_9H_{10}$)$_2$]$^-$, $[\mathbf{8}]^-$, that contain a bridge (-$\mu-SiMe_2-$) between both dicarbollide ligands, were obtained unexpectedly from the reaction of the respective monolithium salt of $[\mathbf{1}]^-$ and $[\mathbf{2}]^-$ with Me_2SiHCl at low temperatures. A hypothetical mechanism has been proposed to explain the formation of these compounds through an intramolecular reaction, that implies the reaction of an acidic C_c-H with the Si$-$H hydride, and the loss of hydrogen. This has been supported by theoretical studies, that are related to the crystal structure of anion

$[\mathbf{3}]^-$.

5. A trifunctional molecule containing a cobaltacarborane and three vinylsilane functions, $[\mathbf{11}]^-$; as well as, two families of polyanionic carbosilane and cyclic carbosiloxane metallodendrimers peripherally decorated with four or eight cobaltabisdicarbollide moieties, $[\mathbf{12}]^{4-}$–$[\mathbf{17}]^{8-}$, have been prepared by hydrosilylation of the suitable dendritic molecules containing terminal C=C functionalities by using the anion [1,1'-μ-SiMeH-3,3'-Co(1,2-$C_2B_9H_{10})_2]^-$, $[\mathbf{5}]^-$, in the presence of Karstedt catalyst and optimized reaction conditions. The reaction were monitored by ^{1}H-NMR spectroscopy by the desappearance of vinyl-functions.

6. Polyanionic boron-rich metallodendrimers based on poly (aryl-eter) dendrimers with the fluorescence triphenilbenzene (TFB) core, and allyl-terminated functions at the surface, have been functionalizated with $[\mathbf{5}]^-$ to achieve the metallodendrimers $[\mathbf{18}]^{3-}$, $[\mathbf{19}]^{6-}$ and $[\mathbf{20}]^{12-}$ that contain three, six and twelve cobaltacarboranes at the periphery. To our knowledge, the last represents the high metallacarborane containing molecule describe in the literature.

7. Poly(alkyl aryl-ether) type star-shape molecules and dendrimers were decorated by metallacarboranes by using the ring-opening reaction of 8–dioxanate [3,3'-Co(8-$C_4H_8O_2$-1,2-$C_2B_9H_{10}$)(1',2'-$C_2B_9H_{11}$)], by the nucleophilic attack with the alcoholate functions, obtained by deprotonation of alcohol groups (−OH) located at the starting dendrimers periphery, to give polyanionic species $[\mathbf{21}]^{4-}$–$[\mathbf{24}]^{8-}$ with high-boron-content.

8. All metallodendrimers have been characterized by FT-IR, ^{1}H, ^{11}B, ^{13}C and ^{29}Si NMR and UV-Vis spectroscopy, and in some cases elemental analysis and mass spectrometry (MALDI-TOF or ESI). However, for dendrimers with the highest molecular weights it was not possible to obtain the mass spectra, due to the great fragmentation.

9. The UV-Vis spectroscopy have shown a linear relationship between the absortivity and the numbers of cobaltabisdicarbollides located at the periphery. Thus, this technique was used as an undirected method to corroborate the full functionalization of dendrimers with cobaltabisdicarbollide moieties, and subsequently confirm the unified character of the dendritic macromolecules.

10. The UV-Vis spectroscopy has also been a good tool for the study of the carbosilane and cyclic carbosiloxane metallodendrimers solubility in water/DMSO solutions, by measuring the absorptivities of different metallodendrimer solutions.

11. Carboranyl-containing disiloxanes, cyclic-siloxane and cage-like silsesquioxane have been prepared in high yields. Two routes are compared for their preparation: a classical hydrolytic process based on hydrolysis and condensation of the adequated carboranylchlorosilane and carboranylethoxysilane precursors and a non-hydrolytic route based on the specific reactivity of chorosilane toward DMSO, that is the oxygen source. Based on the typical reactivity of the carboranyl group toward nucleophiles, dianionic disiloxanes ($[\mathbf{41}]^{2-}$ and $[\mathbf{42}]^{2-}$) and octaanionic silsesquioxanes ($[\mathbf{43}]^{8-}$) were obtained without modification of the siloxane bond. The present results have pointed out the efficiency of the non-hydrolytic route with DMSO, that is particularly attractive for limiting the formation of linear oligopolysiloxane. Products are fully characterized by FTIR, NMR and MALDI-TOF methods.

12. Two phosphorus-containing cobaltabisdicarbollide derivatives, $[\mathbf{44}]^{-}$ and $[\mathbf{45}]^{-}$, have been prepared to modify the surface of titanium dioxide particle, following an experimental procedure previously described. The TiO_2 particles were reacted with a solution of the phosphate or phosphinate coupling molecules in a 5-fold excess relative to the amount needed for a full surface coverage on the particles, to obtain **44**@TiO_2 and **45**@TiO_2, respectively. These surfaces are fully characterized by FTIR and ^{31}P and ^{11}B CP-MAS-NMR.

13. Anchoring cobaltabisdicarbollide derivatives on the SiO_2 surface of Si wafers has been achieved by using two approaches. The first approach is a "in situ" ring-opening reaction of 8–dioxanate [3,3'-Co(8-$C_4H_8O_2$-1,2-$C_2B_9H_{10}$)(1',2'-$C_2B_9H_{11}$)] by nucleophilic attack of previously anchorated amines in the SiO_2 surface. The second approach is the reaction of the amine-terminated cobaltabisdicarbollide Cs[**47**] with an isocyanate group previously anchoraded in the SiO_2 surface to give an urea connection. Both surfaces, **46**@SiO_2 and Cs**47**@SiO_2 have been characterized by FTIR-ATR, contact angle, AFM, UV-Vis, ellipsometry and XPS.

5

Artículos publicados. Comisión de Doctorado de Abril de 2009.

Artículos publicados y presentados a la Comisión de Doctorado de la UAB en Abril de 2009:

a) Controlled Direct Synthesis of C-Mono- and C-Disubstituted Derivatives of [3,3'-Co(1,2-$C_2B_9H_{11}$)$_2$]$^-$ with Organosilane Groups: Theoretical Calculations Compared with Experimental Results. Emilio José Juárez-Pérez, Clara Viñas, Arántzazu González-Campo, Francesc Teixidor, Reijo Sillanpää, Raikko Kivekäs, Rosario Núñez. *Chem. Eur. J.* **2008**, *14*, 4924-4938.

b) Carboranyl Substituted Siloxanes and Octasilsesquioxanes: Synthesis, Characterization and Reactivity. Arántzazu González-Campo, Emilio José Juárez-Pérez, Clara Viñas, Bruno Boury, Reijo Sillanpää, Raikko Kivekäs, Rosario Núñez. *Macromolecules* **2008**, *41*, 8458-8466.

c) First example of the formation of a Si−C bond from an intramolecular Si−H$\cdots$H−C diyhydrogen interaction in a metallacarborane: A theoretical study. Emilio José Juárez-Pérez, Clara Viñas, Francesc Teixidor, Rosario Núñez. *J. Organomet. Chem.* **2009**, *694*, 1764-1770.

5.a) Controlled Direct Synthesis of C-Mono- and C-Disubstituted Derivatives of [3,3'-Co(1,2-$C_2B_9H_{11}$)$_2$]$^-$with Organosilane Groups: Theoretical Calculations Compared with Experimental Results.

CHEMISTRY
A EUROPEAN JOURNAL

DOI: 10.1002/chem.200702013

Controlled Direct Synthesis of C-Mono- and C-Disubstituted Derivatives of $[3,3'\text{-}Co(1,2\text{-}C_2B_9H_{11})_2]^-$ with Organosilane Groups: Theoretical Calculations Compared with Experimental Results

Emilio José Juárez-Pérez,[a] Clara Viñas,[a] Arántzazu González-Campo,[a] Francesc Teixidor,[a] Reijo Sillanpää,[b] Raikko Kivekäs,[c] and Rosario Núñez*[a]

Abstract: Mono- and dilithium salts of $[3,3'\text{-}Co(1,2\text{-}C_2B_9H_{11})_2]^-$, (**1**$^-$), react with different chlorosilanes (Me_2SiHCl, Me_2SiCl_2, Me_3SiCl and $MeSiHCl_2$) with an accurate control of the temperature to give a set of novel C_c-mono- ($C_c = C_{cluster}$) and C_c-disubstituted cobaltabis(dicarbollide) derivatives with silyl functions: $[1\text{-}SiMe_2H\text{-}3,3'\text{-}Co(1,2\text{-}C_2B_9H_{10})(1',2'\text{-}C_2B_9H_{11})]^-$ (**3**$^-$); $[1,1'\text{-}\mu\text{-}SiMe_2\text{-}3,3'\text{-}Co(1,2\text{-}C_2B_9H_{10})_2]^-$ (**4**$^-$); $[1,1'\text{-}\mu\text{-}SiMeH\text{-}3,3'\text{-}Co(1,2\text{-}C_2B_9H_{10})_2]^-$ (**5**$^-$); $[1\text{-}SiMe_3\text{-}3,3'\text{-}Co(1,2\text{-}C_2B_9H_{10})\text{-}(1',2'\text{-}C_2B_9H_{11})]^-$ (**6**$^-$) and $[1,1'\text{-}(SiMe_3)_2\text{-}3,3'\text{-}Co(1,2\text{-}C_2B_9H_{10})_2]^-$ (**7**$^-$). In a similar way, the $[8,8'\text{-}\mu\text{-}(1'',2''\text{-}C_6H_4)\text{-}1,1'\text{-}\mu\text{-}SiMe_2\text{-}3,3'\text{-}Co(1,2\text{-}C_2B_9H_9)_2]^-$ (**8**$^-$); $[8,8'\text{-}\mu\text{-}(1'',2''\text{-}C_6H_4)\text{-}1,1'\text{-}\mu\text{-}SiMeH\text{-}3,3'\text{-}Co(1,2\text{-}C_2B_9H_9)_2]^-$ (**9**$^-$) and $[8,8'\text{-}\mu\text{-}(1'',2''\text{-}C_6H_4)\text{-}1\text{-}SiMe_3\text{-}3,3'\text{-}Co(1,2\text{-}C_2B_9H_9)(1',2'\text{-}C_2B_9H_{10})]^-$ (**10**$^-$) ions have been prepared from $[8,8'\text{-}\mu\text{-}(1'',2''\text{-}C_6H_4)\text{-}3,3'\text{-}Co(1,2\text{-}C_2B_9H_{10})_2]^-$ (**2**$^-$). Thus, depending on the chlorosilane, the temperature and the stoichiometry of *n*BuLi used, it has been possible to control the number of substituents on the C_c atoms and the nature of the attached silyl function. All compounds were characterised by NMR and UV/Vis spectroscopy and MALDI-TOF mass spectrometry; $[NMe_4]$-**3**, $[NMe_4]$-**4** and $[NMe_4]$-**7** were successfully isolated in crystalline forms suitable for X-ray diffraction analyses. The **4**$^-$ and **8**$^-$ ions, which contain one bridging -μ-$SiMe_2$ group between each of the dicarbollide clusters, were unexpectedly obtained from the reaction of the monolithium salts of **1**$^-$ and **2**$^-$, respectively, with Me_2SiHCl at −78 °C in 1,2-dimethoxyethane. This suggests that an intramolecular reaction has taken place, in which the acidic C_c–H proton reacts with the hydridic Si–H, with subsequent loss of H_2. Some aspects of this reaction have been studied by using DFT calculations and have been compared with experimental results. In addition, DFT theoretical studies at the B3LYP/6-311G(d,p) level of theory were applied to optimise the geometries of ions **1**$^-$–**10**$^-$ and calculate their relative energies. Results indicate that the racemic mixtures, *rac* form, are more stable than the *meso* isomers. A good concordance between theoretical studies and experimental results has been achieved.

Keywords: carboranes · cluster compounds · density functional calculations · sandwich complexes · silanes

Introduction

In the last four decades, interest in the functionalisation and application of the cobaltabis(dicarbollide) ion **1**$^-$ and its derivatives has grown due to their extraordinary chemical, thermal and radiation stability, and their similar properties to the inorganic superacids.[1] In addition, these compounds are hydrophobic[2,3] and weakly coordinating anions,[4] which have made them appropriate to be used as solid electrolytes,[3] strong non-oxidizing acids,[3] doping agents in conducting polymers[5] and extractants of radionuclides.[6] Cobaltabis(dicarbollide) derivative have also been used in diverse applications such as medical imaging and radiothera-

[a] E. J. Juárez-Pérez,[+] Prof. C. Viñas, Dr. A. González-Campo, Prof. F. Teixidor, Dr. R. Núñez
Institut de Ciència de Materials de Barcelona
CSIC, Campus U.A.B., 08193 Bellaterra (Spain)
Fax (+34) 935-805-729
E-mail: rosario@icmab.es

[b] Dr. R. Sillanpää
Department of Chemistry, University of Jyväskylä
40351, Jyväskylä (Finland)

[c] Prof. R. Kivekäs
Department of Chemistry, P.O. Box 55
University of Helsinki, 00014 (Finland)

[+] Emilio José Juárez-Pérez is enrolled in the Ph.D. program of the U.A.B.

py as boron-rich carriers for boron neutron capture therapy (BNCT).[7]

Many cobaltabis(dicarbollide) derivatives with substituents bonded to the cluster, preferably on the boron atoms, have been described.[8,9] However, there are few examples of C_c-substituted (C_c = cluster carbon atom) derivatives of $\mathbf{1}^-$ obtained directly from the deprotonation of C_c–H and subsequent attack by an electrophile. In 1997, Chamberlin et al. published a new synthetic method to bind methyl groups to the C_c atoms obtaining mono- and di-C_c-substituted cobaltabis(dicarbollide) derivatives.[10] More recently, we have reported the preparation of C_c-substituted cobaltabis(dicarbollide) derivatives with phosphine groups analogous to 2,2′-bis(diphenylphosphino)-1,1′-binaphthyl (BINAP) by the reaction of the dilithium salts of $\mathbf{1}^-$ with chlorodiarylphosphine in 1,2-dimethoxyethane (DME).[11]

Our interest in the synthesis and functionalisation of boron-rich dendrimeric structures containing carboranyl derivatives required us to develop new carboranylsilane compounds to use as molecular precursors and building blocks for the desired dendrimers, peripherally attached to carborane moieties.[12] Additionally, these carboranylsilane systems have been useful in the study of the reactivity of carborane derivatives towards different organosilanes and in testing them as hydrosilylating agents.[12a,b] In this work, we have extended our study to the cobaltabis(dicarbollide) anion due to its attractive properties and possible applications.[1–7] Special emphasis has been placed on bonding organosilane functions to the C atoms of the cluster to obtain previously unknown C_c-mono- and C_c-disubstituted cobaltabis(dicarbollide) derivatives with silyl groups. For this purpose, compounds have been prepared by the direct reaction of the lithium salts of $[3,3'\text{-}Co(1,2\text{-}C_2B_9H_{11})_2]^-$ ($\mathbf{1}^-$), and $[8,8'\text{-}\mu\text{-}(1'',2''\text{-}C_6H_4)\text{-}3,3'\text{-}Co(1,2\text{-}C_2B_9H_{10})_2]^-$ ($\mathbf{2}^-$), with different chlorosilanes. Some of these compounds have been proven to be active as hydrosilylating agents and can be used to functionalise different generations of dendrimers. Additionally, a theoretical study, using B3LYP density functional methods at the 6-311G(d,p) basis has provided remarkable data on conformational habits and relative energies of the metallacarborane reported here. The discussion is completed with the X-ray crystal structures of $[NMe_4][1\text{-}SiMe_2H\text{-}3,3'\text{-}Co(1,2\text{-}C_2B_9H_{10})(1',2'\text{-}C_2B_9H_{11})]$, $[NMe_4][1,1'\text{-}\mu\text{-}SiMe_2\text{-}3,3'\text{-}Co(1,2\text{-}C_2B_9H_{10})_2]$ and $[NMe_4][1,1'\text{-}(SiMe_3)_2\text{-}3,3'\text{-}Co(1,2\text{-}C_2B_9H_{10})_2]$.

Results and Discussion

Synthesis of C_c-substituted cobaltabis(dicarbollide) derivatives with silyl groups: With the goal of preparing a C_c-monosubstituted cobaltabis(dicarbollide) derivatives functionalised with the silyl group $-SiMe_2H$, the metallation of Cs-$[3,3'\text{-}Co(1,2\text{-}C_2B_9H_{11})_2]$ (Cs-**1**), with one equivalent of *n*-butyllitium (*n*BuLi) followed by the reaction with Me_2SiHCl (Me = methyl) in 1,2-dimethoxyethane at −78 °C for 1 h was performed. The resulting orange residue was dissolved in MeOH to yield, after precipitation with an aqueous solution of $[NMe_4]Cl$, a mixture of salts, which according to the ^1H and ^{11}B NMR spectra correspond to unreacted starting material $\mathbf{1}^-$ together with the monosubstituted $[1\text{-}SiMe_2H\text{-}3,3'\text{-}Co(1,2\text{-}C_2B_9H_{10})(1',2'\text{-}C_2B_9H_{11})]^-$ ($\mathbf{3}^-$), and $[1,1'\text{-}\mu\text{-}SiMe_2\text{-}3,3'\text{-}Co(1,2\text{-}C_2B_9H_{10})_2]^-$, ($\mathbf{4}^-$), obtained in 51 and 18%, respectively (Scheme 1). Attempts to separate these compounds by silica or alumina column chromatography were unsuccessful and led to $\mathbf{1}^-$ in all cases. The compound $[NMe_4]$-**3** was isolated in 11% yield after recrystallisation from CH_2Cl_2. The $\mathbf{3}^-$ ion was uniquely obtained when the reaction was carried out at −78 °C. At higher temperatures (e.g. −40 or 0 °C) or by using other solvents, such as THF, $\mathbf{3}^-$ was not formed. Crystals of $[NMe_4]$-**3** were obtained by slow evaporation of the compound in a mixture of acetone and water. The anion $\mathbf{3}^-$ represents the first example of a C_c-monosubstituted cobalta(bisdicarbollide) derivative that has been fully characterised by X-ray diffraction.

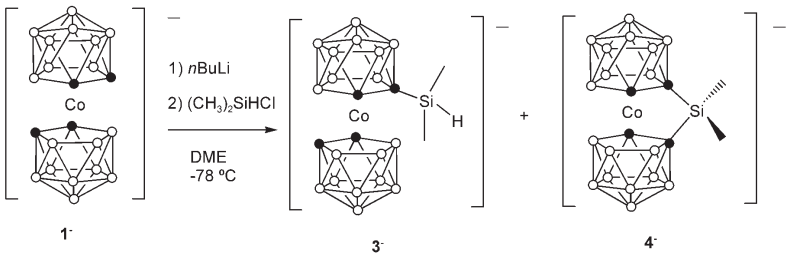

Scheme 1. Synthesis of ions $\mathbf{3}^-$ and $\mathbf{4}^-$.

The unexpected synthesis of $\mathbf{4}^-$ motivated us to study its synthesis in more detail. Two different strategies were used (Scheme 2): 1) the reaction of Cs-**1** with one equivalent of *n*BuLi at −40 °C in DME, followed by the reaction with an excess of Me_2SiHCl gave, after 3 h at room temperature, $[Li(dme)_2]$-**4**, according to the ^1H NMR spectrum; and 2) the reaction of Cs-**1** with 2 equivalents of *n*BuLi at −78 °C in DME, followed by the reaction with Me_2SiCl_2, gave the same species $[Li(dme)_2]$-**4**. The $\mathbf{4}^-$ ion could be isolated by using cations such as $[NMe_4]^+$, Cs^+ and $[PMe(Ph)_3]^+$ (Ph = phenyl) by dissolving $[Li(dme)_2]$-**4** in MeOH and adding aqueous solutions of $[NMe_4]Cl$, CsCl or a methanolic solution of $[PMe(Ph)_3]Br$ to yield the corresponding salts of $\mathbf{4}^-$ in 45, 62, and 70% yield, respectively. When $\mathbf{4}^-$ was synthesised at −40 °C, a mixture of structural isomers (as will be described in depth in a later section) was obtained as shown by the $^{11}B\{^1H\}$ NMR spectrum. However, at −78 °C mainly one isomer was formed. Monocrystals of $[NMe_4]$-**4** were ob-

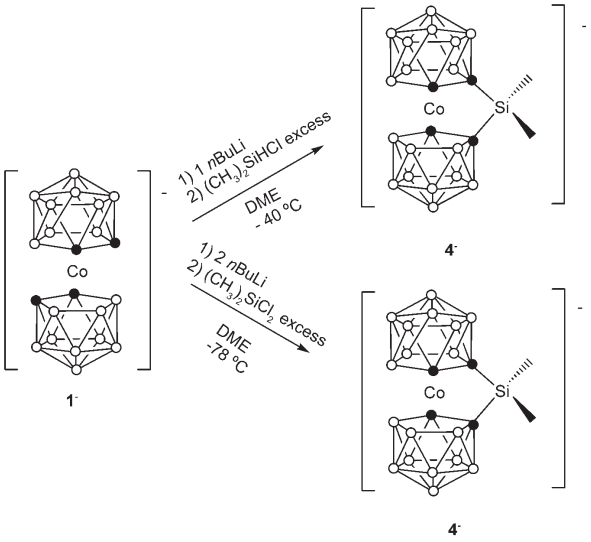

Scheme 2. Synthesis of ion $\mathbf{4}^-$ using two different approaches.

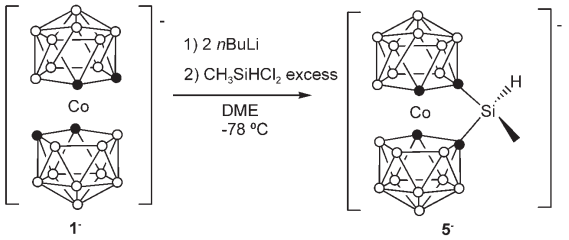

Scheme 3. Synthesis of the ion $\mathbf{5}^-$.

tained by slow evaporation of a solution of the compound synthesised at −40 °C in acetone.

As already mentioned, an attempt to get C_c-monosubstitution on cobaltabis(dicarbollide) with a group containing the −SiH function with $SiMe_2HCl$ led to $\mathbf{3}^-$ in low yield. As we were interested in the reactivity of a Si−H-containing cobaltabis(dicarbollide) derivative, we used $MeSiHCl_2$ as a chlorosilane source (Scheme 3). Cs-**1** was treated with two equivalents of *n*BuLi at −78 °C in DME followed by an excess of $MeSiHCl_2$ at the same temperature. Then, after stirring for 6 h at room temperature, the solution was evaporated and the residue treated with MeOH. The anion $\mathbf{5}^-$ was isolated as the Cs salt in 76% yield by precipitation with an aqueous solution of CsCl. The temperature of −78 °C used in this reaction was a key factor to produce $\mathbf{5}^-$ in 95% isomeric purity, according to the NMR spectra. The use of higher temperatures caused the formation of a mixture of structural isomers (see later section) along with unreacted starting material $\mathbf{1}^-$.

To learn about the reactivity of $\mathbf{1}^-$ towards chlorosilanes, its mono- and dilithium salts were treated with an excess of Me_3SiCl at −78 °C in DME. The monolithium salt of $\mathbf{1}^-$ led to a mixture of products, from which the C_c-monosubstituted [NMe_4]-**6** was isolated in 33% yield. Conversely, the dilithium salt gave the C_c-disubstituted $\mathbf{7}^-$, which was isolated as the [NMe_4]-**7** and Cs-**7** salts in 91 and 90% yield, respectively. Red crystals of [NMe_4]-**7** were successfully obtained from acetone. Metallacarboranes $\mathbf{6}^-$ and $\mathbf{7}^-$ were very convenient to interpret spectroscopic data and to get information about the possible rotational isomers in related compounds.

Silyl-functionalised derivatives of the rigid Cs[8,8′-μ-(1″,2″-C_6H_4)-3,3′-Co(1,2-$C_2B_9H_{10})_2$] compound (Cs-**2**) with chlorosilanes were also studied. The reaction of Cs-**2** with one equivalent of *n*BuLi at −78 °C in DME, followed by the reaction with chlorodimethylsilane (Me_2SiHCl), led uniquely to [8,8′-μ-(1″,2″-C_6H_4)-1,1′-μ-$SiMe_2$-3,3′-Co(1,2-$C_2B_9H_9)_2$]$^-$ ($\mathbf{8}^-$; Scheme 4), which was isolated as a red solid in 77% yield by precipitation with an aqueous solution of [NMe_4]Cl. The spectroscopic study of [NMe_4]-**8**, which will be discussed later, indicated that $\mathbf{2}^-$ behaves similarly to homologous $\mathbf{1}^-$ with Me_2SiHCl. However, the formation of a C_c-monosubstituted species analogous to $\mathbf{3}^-$ was never observed, even at very low temperatures. Likewise, Cs-**2** was treated with two equivalents of *n*BuLi at −78 °C in DME and subsequently with an excess of $MeSiHCl_2$ to give $\mathbf{9}^-$ (Scheme 4). After

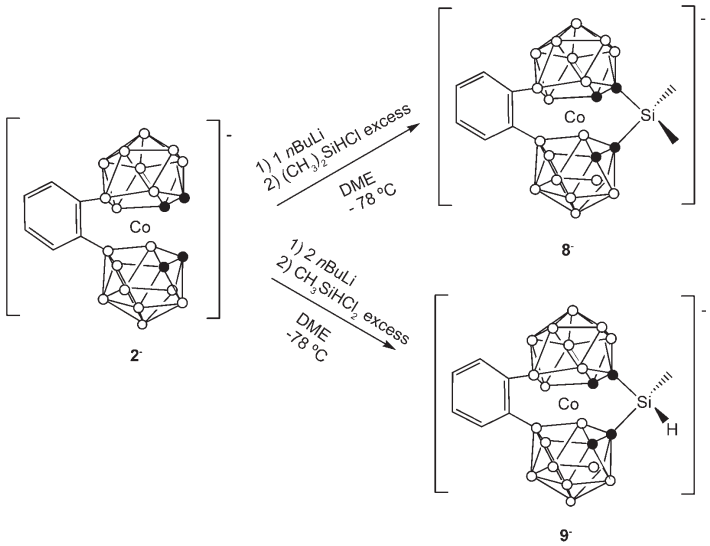

Scheme 4. Synthesis of cobaltabis(dicarbollide) ions $\mathbf{8}^-$ and $\mathbf{9}^-$.

their workup, the compounds [NMe_4]-**9** and Cs-**9** were isolated in 60 and 65% yield, respectively, by precipitation with aqueous solutions of [NMe_4]Cl and CsCl, respectively (Scheme 4).

Similarly, Cs-**2** was treated with two equivalents of *n*BuLi at −78°C in DME followed by an excess of Me_3SiCl under the same conditions to give mainly the monosubstituted compound [NMe_4]-**10** in 69% yield by precipitation with an aqueous solution of [NMe_4]Cl.

These results show that C_c-silyl derivatives of cobaltabis(dicarbollide) can be produced in good yields. The metallacarboranes containing the Si–H function are potential hydrosilylation agents and can be used to functionalise dendrimeric structures.

Characterisation of functionalised cobaltabis(dicarbollide) derivatives with silyl groups: All of the compounds described above were characterised by elemental analysis; UV/Vis, FTIR, and ^1H, ^{13}C, ^{11}B, and ^{29}Si NMR spectroscopy and matrix-assisted laser desorption ionisation time of flight (MALDI-TOF) mass spectrometry. In addition the compounds [NMe_4]-**3**, [NMe_4]-**4** and [NMe_4]-**7** were unequivocally confirmed by X-ray diffraction analysis.

Spectroscopic data: The ^1H, ^{11}B, ^{13}C and ^{29}Si NMR spectra of the products reported here agree with the structures proposed in the schemes. The IR spectra of all compounds present typical ν(B–H) strong bands for *closo*-clusters between 2554 and 2577 cm^{-1} and, additionally, intense bands in the region of 1250–1257 cm^{-1} corresponding to δ(Si–CH_3). Complexes **3**$^-$, **5**$^-$ and **9**$^-$ show a characteristic band near 2160 cm^{-1} attributed to ν(Si–H). The $^1H\{^{11}B\}$ NMR spectra of compounds **3**$^-$ and **5**$^-$ exhibit resonances at 4.31 and 5.06 ppm, respectively, which can be assigned to the Si–H function (Figure 1, Table 1). However, **9**$^-$ shows two resonances at 4.97 and 5.25 ppm with different areas. Both peaks can be attributed to the Si–H proton, indicating the presence of structural isomers in the solution, (see later). Moreover, **3**$^-$, **5**$^-$ and **9**$^-$ have a ^3J(H,H) = 3.4 Hz due to Si–H coupling with the protons on CH_3 and giving a quartet for **5**$^-$ and **9**$^-$ and a septet for **3**$^-$ (Figure 1). The corresponding

Table 1. Chemical shift values [ppm] of the selected protons in the ^1H NMR spectra of C_c-substituted derivatives **3**$^-$–**10**$^-$ and the starting ions **1**$^-$ and **2**$^-$.

	δ ^1H NMR			
	Si–H	C_c–H	Si–CH_3	B–H
1$^-$	–	3.94	–	3.37–1.57
3$^-$	4.31	3.85, 3.69	0.29	3.61–1.60
4$^-$	–	4.50	0.31	3.38–1.43
5$^-$	5.06	4.59	0.44	3.40–1.44
6$^-$	–	4.02, 3.83, 3.72	0.28	3.57–1.50
7$^-$	–	4.19, 3.77	0.33, 0.30	3.98–1.58
2$^-$	–	3.58	-	3.76–1.49
8$^-$	–	3.48	0.39, 0.25	4.00–1.43
9$^-$	5.25, 4.97	3.61	0.48, 0.38	4.11–1.43
10$^-$	–	3.52, 3.45	0.28	3.99–1.51

Si–CH_3 protons are exhibited at a higher field in the region 0.25–0.48 ppm (Table 1). These resonances appear as a doublet for **3**$^-$, **5**$^-$ and **9**$^-$, a singlet for **4**$^-$ (Figure 2) and two different singlets for its homologous **8**$^-$ due to the presence of structural isomers. Due to their symmetry, compounds **4**$^-$, **5**$^-$, **8**$^-$ and **9**$^-$ have only one resonance attributed to the C_c–H protons, while **7**$^-$ shows two signals in different ratios, indicating the presence of geometrical isomers. The C_c-monosubstituted **3**$^-$, **6**$^-$ and **10**$^-$ exhibit two resonances for C_c–H

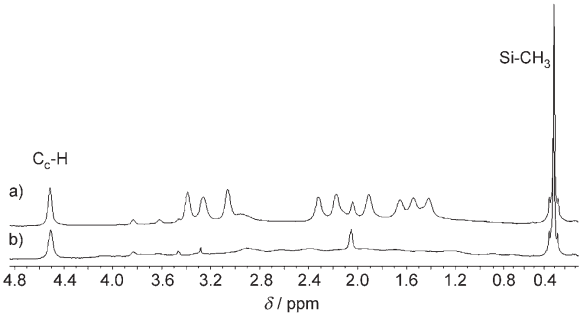

Figure 2. a) $^1H\{^{11}B\}$-NMR spectrum of Cs-**4** and b) ^1H NMR spectrum of Cs-**4**.

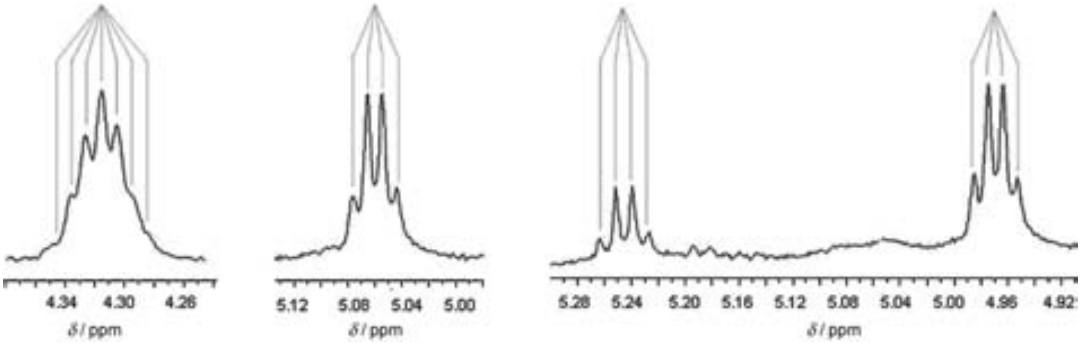

Figure 1. A portion of the ^1H NMR spectra corresponding to the Si–H protons chemical shifts in compounds: **3**$^-$ (left), **5**$^-$ (middle) and **9**$^-$ (right) with relative composition of 24 and 76% for the two structural isomers.

protons, one assigned to the substituted cluster and the second from the unsubstituted cluster (Table 1). The cluster B–H protons appear in the region ranging from 1.43–4.11 ppm (Table 1). In the $^{1}H\{^{11}B\}$ NMR spectrum of $\mathbf{4}^{-}$, nine resonances attributed to the nine B–H protons of each cluster are clearly observed (Figure 2a). The $^{13}C\{^{1}H\}$ NMR spectra show low intensity peaks in a wide region between 31.88 and 55.86 ppm. These high field C_c atoms can be assigned to the C_c–Si atoms. Resonances for the carbon atoms in the Si–CH_3 groups are high field, from 3.20 to −6.87 ppm. The $^{11}B\{^{1}H\}$ NMR spectra of ions $\mathbf{3}^{-}$–$\mathbf{7}^{-}$ display bands in a typical range from +9.1 to −22.3 ppm, indicative of *closo* species with all boron atoms in non-equivalent vertices. However, the resonances for boron atoms in $\mathbf{8}^{-}$, $\mathbf{9}^{-}$ and $\mathbf{10}^{-}$ appear between +27.5 and −24.5 ppm with a 2:6:4:4:2 pattern. In this case, the low-field resonance does not split in the ^{11}B NMR spectrum, which is attributed to the B8 atoms bonded to the phenyl group. Figure 3 shows a schematic representation of the $^{11}B\{^{1}H\}$ NMR spectra for $\mathbf{4}^{-}$ and $\mathbf{5}^{-}$ along with their precursor $\mathbf{1}^{-}$. Bands assignment has been done using a bidimensional COSY $^{11}B\{^{1}H\}/^{11}B\{^{1}H\}$ spectrum. In general, the presence of the silyl substituent at the C_c atoms shifts the ^{11}B resonances downfield with respect to the precursor. For $\mathbf{4}^{-}$, the resonances due to B4, 4′, 7, 7′, 9, 9′, 12, 12′ and B5, 5′, 11, 11′, which appear as two resonances of intensity 8 and 4 in $\mathbf{1}^{-}$, have evolved to three resonances of intensity 4, 2 and 2 and two resonances of intensity 2 due to the lost of symmetry. For $\mathbf{5}^{-}$, the presence of two different groups on the Si atom (CH_3 and H) causes higher asymmetry in the molecule, and this is reflected in the ^{11}B NMR spectrum. In addition, the $^{11}B\{^{1}H\}$ NMR spectrum of $\mathbf{3}^{-}$ shows a 1:1:1:1:1:4:3:2:2:1:1 pattern in the range from +9.10 to −22.26 ppm, while $\mathbf{6}^{-}$ exhibits a 1:1:1:1:1:1:2:2:2:1:1:1:1:1:1 pattern in the region of +8.20 to −23.00 ppm. Both spectra show a large number of resonances due to the loss of any symmetry operation besides E. Figure 4a displays the bidimensional $^{11}B\{^{1}H\}/^{11}B\{^{1}H\}$2D

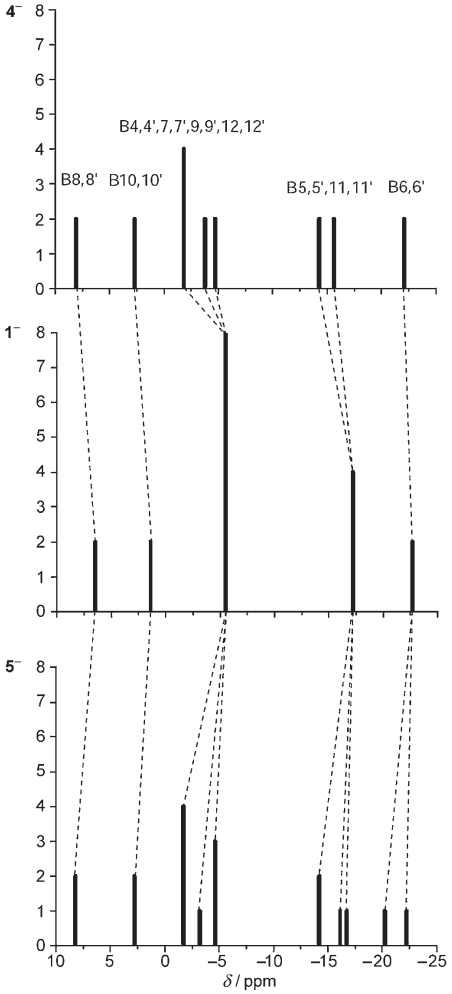

Figure 3. Stick representation of the chemical shifts and relative intensities in the $^{11}B\{^{1}H\}$ NMR spectra of some selected compounds.

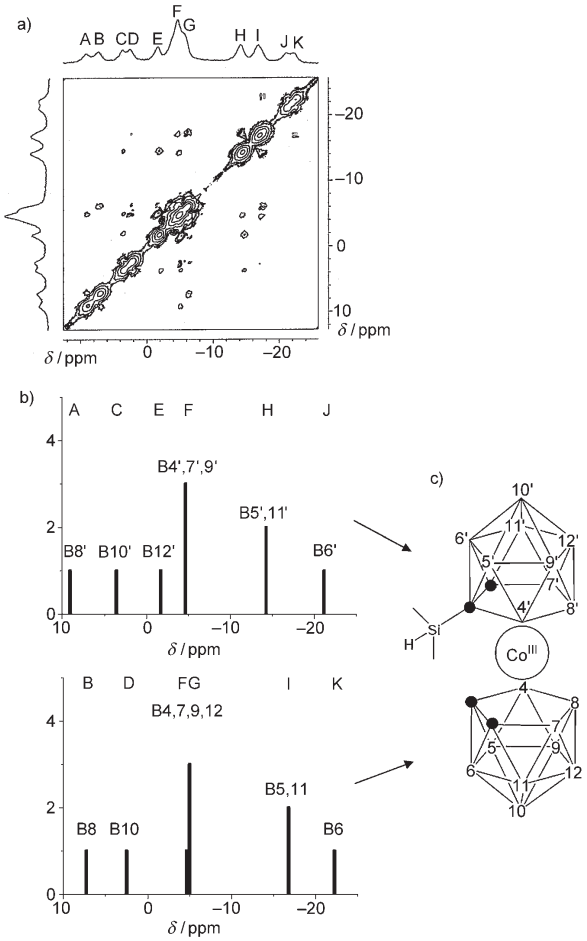

Figure 4. a) $^{11}B\{^{1}H\}$-$^{11}B\{^{1}H\}$2D COSY NMR spectrum of $\mathbf{3}^{-}$. b) Stick representation of the $^{11}B\{^{1}H\}$ NMR spectra of each dicarbollide ligand in $\mathbf{3}^{-}$. c) Schematic representation of the anion $\mathbf{3}^{-}$.

COSY NMR spectrum of $\mathbf{3}^-$ in which the resonances have been assigned to the corresponding boron atoms.[13] The spectrum has been assigned on the basis that each dicarbollide moiety behaves independently of the second.[14] These independent spectra are represented as stick diagrams in Figure 4b with the non-substituted ligand (lower diagram) and the substituted ligand (upper diagram). The combination of both produces a realistic image of the experimental spectrum. The ^{29}Si NMR spectra exhibit peaks in the range of 13.98 to −8.28 ppm (Table 2). The ^{29}Si chemical shifts are dependent on the substituents at the Si atom. The high-field (−8.28 ppm) signal is due to the $-SiMe_2H$ group in $\mathbf{3}^-$, and the corresponding resonances in $\mathbf{5}^-$ and $\mathbf{9}^-$ appear at 2.94 and 2.69 ppm, respectively. The Si atoms of the $-SiMe_3$ and bridging $-SiMe_2$ groups appear at a low field, between 10.75 and 13.98 ppm. Formulas of all the compounds were established by using MALDI-TOF mass spectrometry in the negative-ion mode without a matrix. Figure 5a displays the MALDI-TOF mass spectrum of the [1,1′-μ-SiMeH-3,3′-Co(1,2-$C_2B_9H_{10})_2$]$^-$ ion ($\mathbf{5}^-$) in which the molecular ion peak appears at $m/z = 366.2$ with a perfect concordance with the calculated pattern (Figure 5b). For all anions, a full agreement between the experimental and calculated patterns was also obtained for the molecular ion peaks. Thus, for $\mathbf{3}^-$, $\mathbf{6}^-$ and $\mathbf{10}^-$, this technique shows the corresponding molecular ion peaks at $m/z = 382.2$, 396.3 and 369.2, respectively, which agrees with the proposed structures.

Table 2. Chemical shift values [ppm] of the silicon nuclei in the ^{29}Si NMR spectrum of C_c-substituted cobaltabis(dicarbollides).

Compound	δ ^{29}Si	Compound	δ ^{29}Si
$\mathbf{3}^-$	−8.28	$\mathbf{7}^-$	10.75
$\mathbf{4}^-$	13.98	$\mathbf{8}^-$	11.74
$\mathbf{5}^-$	2.94	$\mathbf{9}^-$	2.69
$\mathbf{6}^-$	10.74	$\mathbf{10}^-$	8.63

UV/Vis spectra: The UV/Vis spectra of $\mathbf{1}^-$ and several *exo*-skeletal derivatives in different solvents such as methanol, but mostly in acetonitrile have been reported in different publications.[9j,15] There are some differences in the positions and absorption coefficients of the maxima, indicating that these values are dependent on the solvent. In this work, the UV/Vis spectra of the studied compounds were measured in acetonitrile. In order to perform an adequate comparison of the parameters of the different UV/Vis spectra, a line-fitting analysis with Gausssians was performed in a similar manner to that reported earlier by us.[9j] The results obtained are shown in Table 3, and the spectrum of $\mathbf{4}^-$ is shown in Figure 6. Ions $\mathbf{1}^-$ and $\mathbf{3}^-$ give spectra consisting of four absorptions near 210, 280, 340, and 450 nm; the first maximum is one order of magnitude lower than the second. It can be observed that absorptions near 280, 340 and 450 nm are

Table 3. UV/Vis spectra for $\mathbf{1}^-$–$\mathbf{10}^-$ in acetonitrile. λ positions [nm] and ε values [L cm^{-1} mol^{-1}] are reported and were calculated following line-fitting analysis.

	λ (ε)					
$\mathbf{1}^-$	207 (14502)		280 (25943)		340 (2199)	449 (300)
$\mathbf{3}^-$	209 (15028)		283 (24531)		342 (2269)	461 (436)
$\mathbf{4}^-$	222 (3752)		286 (9941)	309 (12687)	360 (1241)	464 (239)
$\mathbf{5}^-$	213 (12343)		282 (10376)	310 (26940)	353 (2553)	465 (340)
$\mathbf{6}^-$			281 (22916)		342 (2528)	460 (560)
$\mathbf{7}^-$			293 (16583)		363 (2178)	492 (504)
$\mathbf{2}^-$	234 (15694)		280 (18672)	314 (5061)	398 (777)	516 (280)
$\mathbf{8}^-$	236 (9911)	270 (5595)	289 (9983)	316 (4779)	376 (930)	500 (290)
$\mathbf{9}^-$	235 (6489)	272 (2415)	291 (6068)	307 (3626)		518 (190)
$\mathbf{10}^-$	234 (12363)	272 (3662)	290 (10887)	324 (4150)	398 (729)	548 (310)

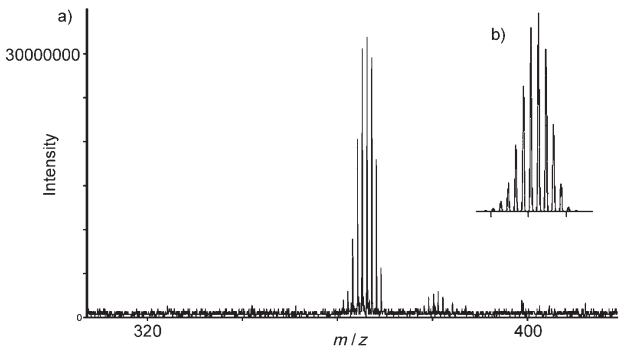

Figure 5. a) Experimental MALDI-TOF mass spectrum obtained for the anion $\mathbf{5}^-$. b) Calculated MALDI-TOF spectrum for $\mathbf{5}^-$.

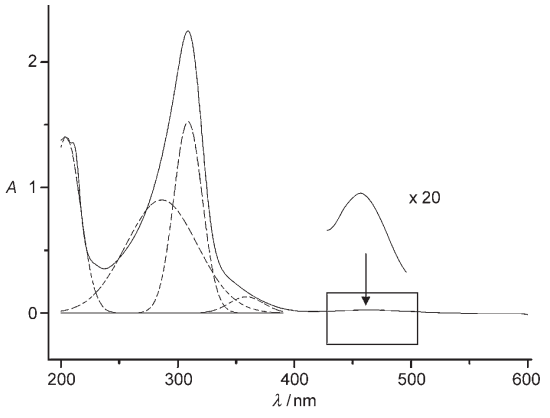

Figure 6. UV/Vis spectrum (solid line) of $\mathbf{4}^-$ and the result of line fitting with Gaussians (dash lines). The expanded section on the right shows the absorption near 445 nm amplified 20 times.

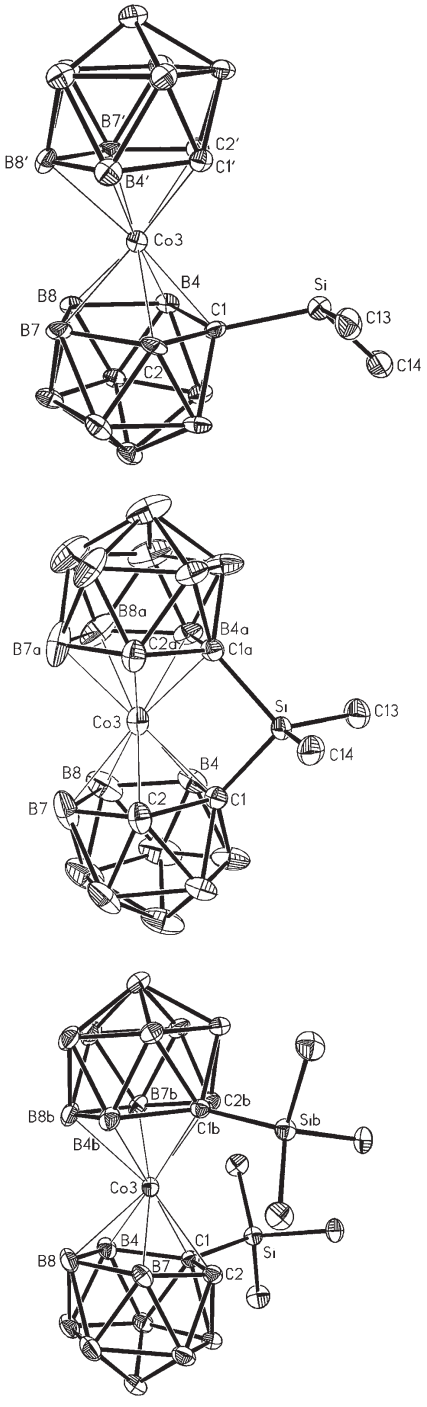

Figure 7. Top: Drawing of the anion of $[NMe_4]$-**3** with 30% thermal displacement ellipsoids. Middle: Drawing of the anion of $[NMe_4]$-**4** with 30% thermal displacement ellipsoids. The "a" refers equivalent position $x, -y+1/2, z$. Bottom: Drawing of the anion of $[NMe_4]$-**7** with 30% thermal displacement ellipsoids. The "b" refers equivalent position $-x+2, y, -z+1/2$. In all cases the hydrogen atoms have been omitted for clarity.

present in all compounds and are attributed to the anion $[3,3\text{-}Co(1,2\text{-}C_2B_9H_{11})_2]^-$, as has already been reported.[9j] The absorption with longest wavelength, near 450 nm, shows a bathochromic shift with respect to $\mathbf{1}^-$ that is larger (about 40 nm) for $\mathbf{7}^-$. This represents a dark red colour in solution or in the solid state. In contrast, the metallacarboranes $\mathbf{1}^-$, $\mathbf{3}^-$, $\mathbf{4}^-$, $\mathbf{5}^-$ and $\mathbf{6}^-$ are orange. It is important to emphasise that the $\mathbf{4}^-$ and $\mathbf{5}^-$ ions show an additional absorbance around 310 nm (Table 3), which could be attributed to the presence of a silyl bridge between the ligands. Compounds prepared from $\mathbf{2}^-$ exhibit a maximum around 230 nm attributed to the benzene moiety.[15c] However, the main differences in the UV/Vis spectra between the precursor and compounds $\mathbf{8}^-$, $\mathbf{9}^-$ and $\mathbf{10}^-$ are due to the presence of an extra signal around 270 nm and a bathochromic shift of 10 nm in the second maximum around 320 nm (Table 3).

X-ray crystallography: Single-crystal X-ray analyses of $[NMe_4]$-**3**, $[NMe_4]$-**4** and $[NMe_4]$-**7** confirmed the expected sandwich structures for the three cobaltabis(dicarbollide) anions. The $\mathbf{3}^-$ ion contains one non-bridging $SiMe_2H$ group, whereas $\mathbf{4}^-$ has a bridging $SiMe_2$ group between the dicarbollide clusters. In $\mathbf{7}^-$, one non-bridging $SiMe_3$ group is bonded to each dicarbollide moiety through the C_c atoms. The structures of $\mathbf{3}^-$, $\mathbf{4}^-$ and $\mathbf{7}^-$ are presented in Figure 7 and selected bond parameters are listed in Tables 4 and 5. It is important to note that for each cobaltabis(dicarbollide) cluster, the presence of the $[NMe_4]^+$ ion is necessary for crystal-

Table 4. Selected bond lengths [Å] and angles [°] for $[NMe_4]$-**3**.

Co3−C1	2.104(6)	Co3−C1′	2.058(6)
Co3−C2	2.056(6)	Co3−C2′	2.048(6)
Co3−B8	2.110(7)	Co3−B8′	2.127(7)
Si−C1	1.907(6)	C1′−C2′	1.608(9
C1−C2	1.627(8)		
Co3-C1-Si	116.8(3)	C1-Co3-C1′	101.2(2)
C1-Co3-C2′	103.6(2)		

Table 5. Selected bond lengths [Å] and angles [°] for $[NMe_4]$-**4**[a] and $[NMe_4]$-**7**[b].

	$[NMe_4]$-**4**	$[NMe_4]$-**7**
Co3−C1	2.0387(16)	2.139(3)
Co3−C2	2.058(2)	2.085(3)
Co3−B4	2.067(2)	2.084(3)
Co3−B7	2.112(3)	2.108(3)
Co3−B8	2.108(3)	2.117(4)
Si−C1	1.8838(16)	1.944(3)
C1−C2	1.668(2)	1.649(4)
Co3-C1-Si	90.47(7)	122.33(15)
C1-Co3-C1a	85.04(9)	
C1-Co3-C1b	132.01(16)	
B8-Co3-B8a	93.71(15)	
B8-Co3-B8b	84.5(2)	

[a] Equivalent positions: a: $x, -y+1/2, z$; [b] Equivalent positions: b: $-x+2, y, -z+1/2$.

lisation of the compounds, since no crystals were obtained with other cations.

The cobaltabis(dicarbollide) anion $\mathbf{3}^-$ has crystallographic C_1 symmetry. The conformation of the dicarbollide clusters is *cisoid*, and the $SiMe_2H$ group is projected between the cluster carbons of the neighbouring $C_2B_9H_{11}^-$ moiety. The conformation can be seen in Figure 7 (top) and by the C1-c-c′-C1′ and C1-c-c′-C2′ torsion angle values of 28.2(4) and −41.3(4)° (c and c′ refer to centres of pentagons C1,C2,B4,B7,B8 and C1′,C2′,B4′,B7′,B8′, respectively). The cobaltabis(dicarbollide) anion of $[NMe_4]$-**4** assumes σ symmetry with metal and silicon atoms as well as with the methyl carbons lying in the mirror plane (Figure 7, middle). The $SiMe_2$ group is bonded to both clusters through carbon atoms and thus bridge the dicarbollide groups. Owing to the symmetry, the configuration of the dicarbollide ligands is *meso* (the boron cages are in an eclipsed conformation). The anion of $[NMe_4]$-**7** assumes a two-fold symmetry with the metal lying at the symmetry axis. One $SiMe_3$ group is bonded to a carbon atom of each cage and the groups are oriented so that their disposition in $\mathbf{7}^-$ is *cisoid*, as can be seen in Figure 7 (bottom) and from the C1-c-c[b]-C1[b] dihedral angle of −97.6° (c refers to centre of pentagon C1,C2,B4,B7,B8 and the superscripted b refers equivalent position $-x+2$, y, $-z+1/2$) and the C1-c-c[b]-C2[b] dihedral angle of −26.9°.

A comparison of the structures of $\mathbf{3}^-$, $\mathbf{4}^-$ and $\mathbf{7}^-$ reveals marked differences because of the different silyl groups and bonding modes. Comparing the conformation of $\mathbf{4}^-$ with the ideal cobaltabis(dicarbollide) moiety with parallel coordinating C_2B_3 pentagons, in $\mathbf{4}^-$ the cages are twisted so that the cluster carbons C1 and C1[a] are closer to each other (C1···C1a = 2.755(9) Å, a = x, $-y+1/2$, z). On the opposite side of the coordinating pentagon the distance between the B7 and B7a atoms is increased to 3.10(2) Å. The closing angle on the silicon's side between the two pentagons is 6.91(10)°. In the structures of $\mathbf{3}^-$ and $\mathbf{7}^-$, the influence of the bulky $SiMe_2H$ and $SiMe_3$ groups on the orientation of the coordinating C_2B_3 pentagons is the opposite. The silyl groups repulse the neighbouring pentagons away from each other so that the opening dihedral angle on the silicon atoms' side between the two pentagons are 6.6(2) and 11.16(10)° for $\mathbf{3}^-$ and $\mathbf{7}^-$, respectively.

Theoretical studies related to the formation and conformational structures of compounds: In this section, some aspects related to the formation and characterisation of the anions described above are studied using density functional theory (DFT) calculations.[16] Studies leading to geometric optimisation for ions $\mathbf{1}^-$–$\mathbf{10}^-$ and relative energy calculations were conducted at the B3LYP/6-311G(d,p) level of theory.

Rotational isomers for the metallacarboranes $\mathbf{3}^-$, $\mathbf{6}^-$ and $\mathbf{7}^-$: Three broad conformations for metallacarborane sandwiches exist: *cisoid* (C_{2v}), *gauche* and *transoid* (C_{2h}).[17,18] When relative energy calculations are applied to $\mathbf{1}^-$, it has been reported that the *transoid* conformation is 12.8 kJ mol^{-1} more stable than the *cisoid*.[19] Nevertheless, for the $\mathbf{3}^-$, $\mathbf{6}^-$ and $\mathbf{7}^-$ ions five different conformations are available due to the substitution on the $C_{cluster}$ atoms: two *cisoid*, two *gauche* and one *transoid* rotamers (Figure 8). For $\mathbf{3}^-$, the *gauche* conformation (*gauche*-1) is the more stable than the *cisoid* rotamer (*cisoid*-1) by 2.83 kJ mol^{-1} (Figure 8). In both conformations the Si–H is in proximity to C_c–H, facilitating a dihydrogen interaction. In fact, the *cisoid*-1 corresponds to the rotamer found in the crystal structure. However, in the C_c-monosubstituted $\mathbf{6}^-$ ion, the *gauche* conformation (*gauche*-2) is the more stable, being 3.03 and 4.20 kJ mol^{-1} more stable than the *transoid* and *cisoid*-2 rotamers, respectively (Figure 8). The difference on the relative energies between rotamers of $\mathbf{3}^-$ and $\mathbf{6}^-$ is most probably due to the dihydrogen interactions in the case of $\mathbf{3}^-$. In addition, $\mathbf{7}^-$, like other C_c-disubstituted derivatives of cobaltabis(dicarbollide),[11] revealed that the synthesised geometrical isomer shows racemic substitution according to the X-ray diffraction study, and the dicarbollide ligands are rotated with respect to each other along the axis passing through B10 and B10′. Using the B8-Co3-B10-B8 dihedral angle "q"[19] as a parameter for the dicarbollide ligands rotation, a rotational energy path profile was calculated by using optimised structures of $\mathbf{7}^-$. Three minima for $q = 38.1°$ (*cisoid*-2), 122.3° (*gauche*-2) and 197.4°

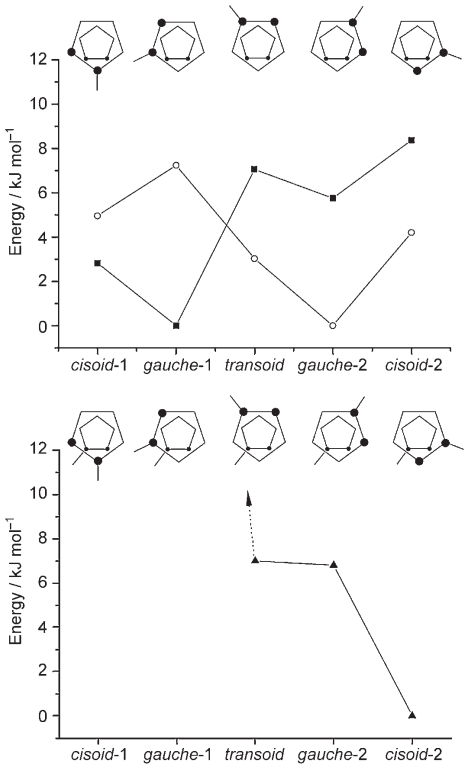

Figure 8. Calculated relative energies and conformational isomers for compounds $\mathbf{3}^-$ (■), $\mathbf{6}^-$ (○) and $\mathbf{7}^-$ (▲).

(*transoid*) were obtained with relative energies 0, 6.8 and 7.0 kJ mol^{-1}, respectively (Figure 8). The minimum energy conformer found with $q = 38.1°$ corresponds to the *cisoid* rotamer and agrees well with what was found in the crystal structure. However, for **7**$^-$, the relative energies of *cisoid*-1 and *gauche*-1 were not possible to calculate due to the steric hindrance.

Proposed mechanism for the formation of compounds **4**$^-$ *and* **8**$^-$*—comparison of the theoretical and experimental results*: In the course of this research two questions have arisen: 1) why is it possible to get the C_c-monosubstitution on **1**$^-$ by using one equivalent of *n*BuLi and Me_2SiHCl to give **3**$^-$, whereas its homologous derivative from **2**$^-$ was never detected; and 2) why is compound **4**$^-$ obtained as a byproduct in the synthesis of **3**$^-$, while its homologue **8**$^-$ is the main product in a similar reaction from **2**$^-$?. These questions may both be answered taking into account an "intramolecular reaction" that leads to the formation of the bridging μ-$SiMe_2$ group. A possible pathway that explains this intramolecular reaction is shown in Scheme 5. After the formation of the monolithium salt of **1**$^-$ or **2**$^-$, a C_c-monosubstituted compound with a $-SiMe_2H$ group is generated. The geometrical disposition of one acidic C_c–H proton and the hydride of the Si–H function favours the elimination of H_2 with the formation of the second C_c–Si bond. Theoretical calculations were carried out to corroborate this mechanism in the case of **8**$^-$ from **2**$^-$. In the latter, the rotation around the metallic centre is hindered by the presence of the phenyl group bonded both to B8 and B8′, which provides a stable eclipsed *cisoid* configuration (Scheme 5). Thus, the geometry of a hypothetical C_c-monosubstituted intermediate derivative of **2**$^-$ with a $SiMe_2H$ group, which has never been isolated (Scheme 5), was optimised. A natural population analysis (NPA) was carried out to determine the charges of the hydrogen atoms that may be involved in the intramolecular reaction. The charge on Si–H is −0.194 (more negative that the Si–H in $SiMe_2HCl$, which is −0.185), and the charge of the hydrogen in C_c–H is +0.306 (more acidic than **2**$^-$, which is +0.265). The opposite charges should then favour the interaction between both hydrogen atoms to give the C_c-disubstituted ion **8**$^-$ (Scheme 5). Additionally, a transition state for the formation of **8**$^-$ was found by using the synchronous transit-guided quasi-newton (STQN) method. Figure 9 shows the optimised structure of this transition state. In addition, using the equation $\Delta G(T) = \Delta H(T) - T\Delta S(T)$, the enthalpy for the intramolecular reaction proposed in this mechanism has also been calculated and is endothermic at −78 °C (195 K), ($\Delta_r H^{195} = +37.2$ kJ mol^{-1}) and not spontaneous ($\Delta_r G^{195} = +13.8$ kJ mol^{-1}). Plotting $\Delta_r G$ versus the temperature (T), it is observed that at $T = 32$ °C (305 K) the Gibbs free energy becomes negative as is shown in Figure 10. The evolution of $\Delta_r G$ to negative values is a consequence of the entropic terminus in the state equation. It may be concluded that due to the required *cisoid* conformation for this reaction to occur, in the case of **2**$^-$, the intramolecular reaction leading to **8**$^-$ is favoured; in contrast, the corresponding monosubstituted compound from **2**$^-$, equivalent to **3**$^-$, is never observed.

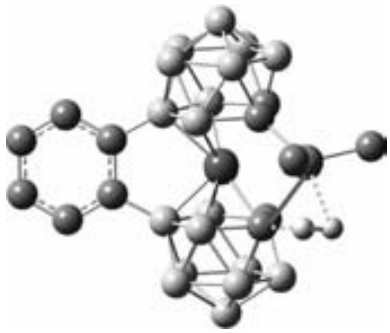

Figure 9. The transition state found for the intramolecular reaction to obtain **8**$^-$. This minimum has a single imaginary frequency corresponding to the vibrational modes of the hydrogen involved in the reaction. Dash lines represent the cleaved bonds and solid lines represent the new bonds.

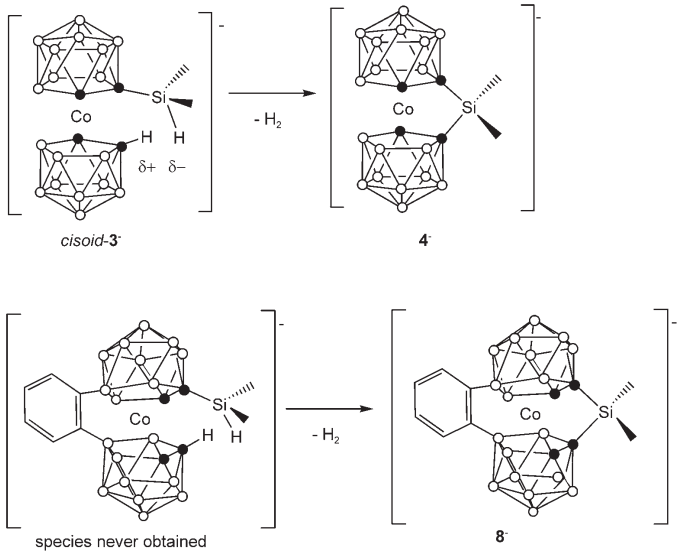

Scheme 5. Suggested pathway for the intramolecular reaction that causes a bridge between both dicarbollide clusters in ions **4**$^-$ and **8**$^-$.

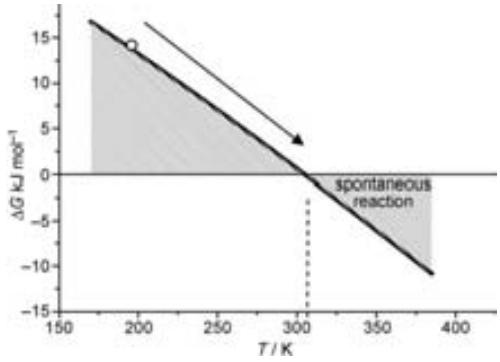

Figure 10. Gibbs free-energy temperature dependence calculated for the intramolecular reaction: $\Delta G(T) = \Delta H(T) - T\Delta S(T)$.

Theoretical calculations of the relative energy for the optimised conformation in $\mathbf{3}^-$ indicated that the *cisoid*-1 conformation observed in the crystal structure, in which the Si–H group is closest to the C_c–H, is 10.96 kJ mol^{-1} more stable than the same rotamer, but with the Si–H rotated and farthest from the C_c–H. The stability of this structure is then attributed to the existence of two intramolecular dihydrogen interactions, C_c–H···H–Si, 2.44 and 2.16 Å, according to the DFT calculations. These match well with those found in the crystal structure, 2.409 and 2.212 Å. This provides an explanation to the first question about the formation of $\mathbf{3}^-$. In addition, experimental results have shown that the temperature is critical in the reaction leading to $\mathbf{3}^-$ and $\mathbf{4}^-$. By keeping the reagents and solvents at −40 °C or higher, only $\mathbf{4}^-$ was formed, whereas at −78 °C a mixture of $\mathbf{3}^-$ and $\mathbf{4}^-$ is obtained (see Scheme 1). Therefore, we hypothesise that the formation of $\mathbf{4}^-$ is clearly dependent on the temperature, and the activation barrier of this process is favoured at higher temperatures. Increasing the reaction temperature favours the intramolecular dihydrogen contacts (Scheme 5), which is assumed to precede the formation of H_2 from the reaction of one positive and one negative hydrogen atom, corroborating the mechanism proposed to explain the intramolecular process.[20] Consequently, $\mathbf{3}^-$ may be obtained only if very low reaction temperatures are used.

Geometrical isomers for compounds $\mathbf{4}^-$, $\mathbf{5}^-$ *and* $\mathbf{9}^-$: The ions $\mathbf{4}^-$, $\mathbf{5}^-$ and $\mathbf{9}^-$ may form structural isomers, which are dependent on the reaction temperature. Complex $\mathbf{4}^-$ has three geometrical isomers, two enantiomers and one diastereomer, the structures of which are the racemic mixture *rac*-$\mathbf{4}^-$ and the meso isomer *meso*-$\mathbf{4}^-$, respectively (Figure 11). In the *rac*-$\mathbf{4}^-$ isomers, both methyl groups bonded to the Si atom are equivalent. However, the *meso*-$\mathbf{4}^-$ isomer has eclipsed C_c atoms and non-equivalent methyl groups because one CH_3 faces the two non-substituted cluster carbon atoms, whereas the other does not. Theoretical calculations have shown that the *rac*-$\mathbf{4}^-$ form is 12.7 kJ mol^{-1} more stable than *meso*-$\mathbf{4}^-$. Therefore, and if only thermodynamic conditions are taken into account, it could be hypothesised that when

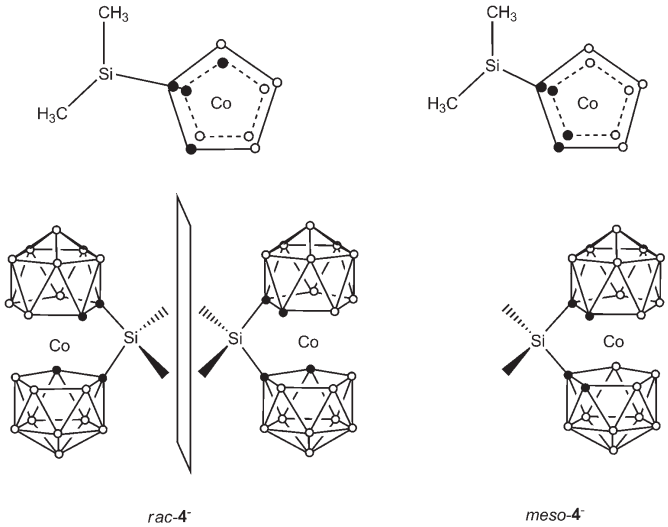

Figure 11. Geometrical isomers of compound $\mathbf{4}^-$. Top: Plane projections of the pentagonal faces. Bottom: *rac*-$\mathbf{4}^-$ sketching of *d* and *l* enantiomers and isomer *meso*-$\mathbf{4}^-$.

$\mathbf{4}^-$ was prepared at −78 °C, the resonances observed in the $^{11}B\{^1H\}$ NMR spectrum were mostly due to the *rac*-$\mathbf{4}^-$, and other signals of lower intensity were assigned to the less stable isomer, *meso*-$\mathbf{4}^-$ (Figure 12 top). This was confirmed when $\mathbf{4}^-$ was synthesised at 0 °C and −40 °C, at which temperatures the *meso*-$\mathbf{4}^-$ isomer is more abundant according to the ^{11}B NMR spectrum (Figure 12 bottom). To corroborate

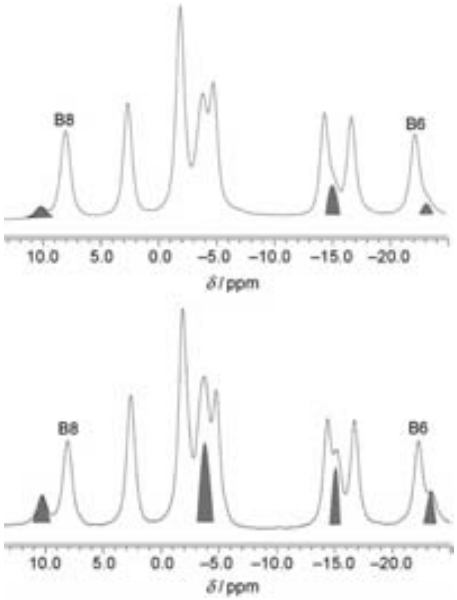

Figure 12. $^{11}B\{^1H\}$ NMR spectra of the anion $\mathbf{4}^-$. The shaded areas are attributed to the boron atoms of *meso*-$\mathbf{4}^-$. Top: $\mathbf{4}^-$ synthesised at −78 °C. Bottom: $\mathbf{4}^-$ synthesised at $T > -40$ °C.

this interpretation, the $^{11}B\{^1H\}$ NMR absolute shielding of *meso*-**4**$^-$and *rac*-**4**$^-$ were calculated at the GIAO/B3LYP/6-31++G(d) level of theory.[21] The $^{11}B\{^1H\}$ NMR theoretical chemical shifts for **4**$^-$ exhibit a resonance assigned to B8 atoms and shifted 4.5 ppm to lower field in *meso*-**4**$^-$ than in the *rac*-**4**$^-$. In addition, calculations indicate that B6 atoms in the *meso*-**4**$^-$ form are shifted 2 ppm to higher field than the isomer *rac*-**4**$^-$. The experimental values for B8 and B6 for *meso*-**4**$^-$ are 10.34 and −23.36 ppm, and for *rac*-**4**$^-$ they are 8.07 and −22.11 ppm, respectively. Although the theoretical values do not fit exactly with the experimental values, they are indicative of the patterns' tendency. This confirms that at −78 °C the *rac*-**4**$^-$ enantiomers are mostly obtained, whereas at higher temperatures the *meso*-**4**$^-$ can be also isolated. Specifically, the crystal structure of [NMe_4]-**4** (Figure 7, middle) corresponds to the *meso*-**4**$^-$ isomer and was obtained from the crystallisation of a reaction carried out at −40 °C.

Four different geometrical isomers could be expected for **5**$^-$: a pair of enantiomers and two diastereomers, which should correspond to the racemic mixture (or *rac* isomers) and two *meso* isomers. For the latter, we have used the notation M and m to identify the major and minor diastereomers, respectively (Figure 13). Theoretical calculations indicate that the *rac*-**5**$^-$ form is 10.5 and 15.4 kJ mol^{-1} more stable than isomers *meso*(M)-**5**$^-$ and *meso*(m)-**5**$^-$, respectively. The stability of *meso*(M)-**5**$^-$ over *meso*(m)-**5**$^-$ could be anticipated by considering the possible coulombic interactions shown in the plane projection (Figure 13). When **5**$^-$ was prepared at −78 °C, the ^1H NMR spectrum shows only one resonance due to the Si–H proton and attributed to the racemic mixture or *rac*-**5**$^-$ (Figure 14a). Nevertheless, when **5**$^-$ was prepared at higher temperatures (−40 °C), a mixture of three compounds appeared in the ^1H NMR spectrum and were assigned to the Si–H and SiMe protons. Resonances

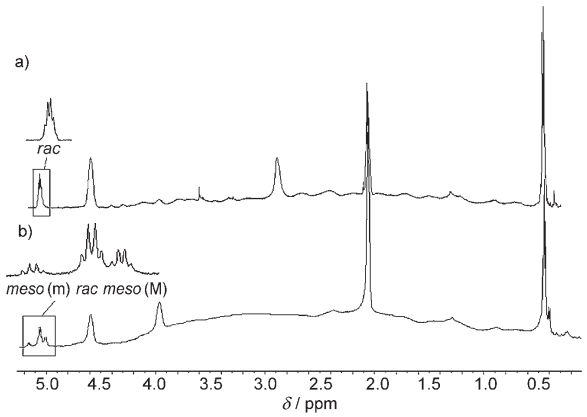

Figure 14. ^1H NMR spectra of Cs-**5** synthesised at different temperatures: a) −78 °C and b) > −40 °C.

were assigned according to the relative energies calculated for isomers, and an integration of signals indicated the formation of *rac*-**5**$^-$, *meso*(M)-**5**$^-$ and *meso*(m)-**5**$^-$ in the percentage of 65, 22 and 13, respectively (Figure 14b).

Finally, compound **9**$^-$ may form two different diastereomers or *meso* isomers, denoted as *meso*(M)-**9**$^-$ and *meso*(m)**9**$^-$ (Figure 15), because the impossibility of rotating the ligands prevents the formation of the *rac* isomer. Theoretical calculations indicate again that *meso*(M)-**9**$^-$ is just 5.70 kJ mol^{-1} more stable than isomer *meso*(m)**9**$^-$. Consequently, when **9**$^-$ was prepared, even at very low temperatures (−78 °C), a mixture of both isomers was observed according to the ^1H NMR spectrum (see Experimental Section).

Therefore, we can confirm that for these metallacarboranes, the racemic mixture (or *rac* form) is the most stable

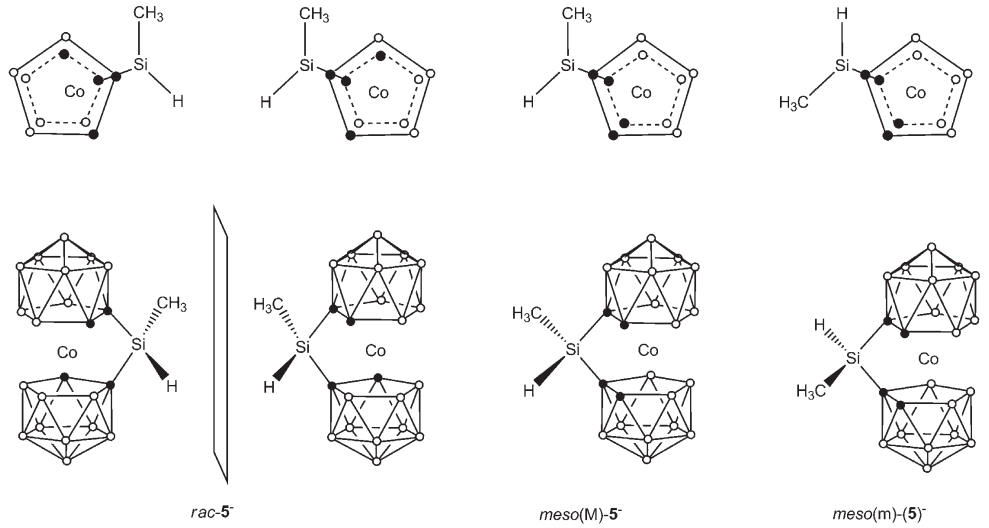

Figure 13. The *rac*-**5**$^-$ and *meso*-**5**$^-$ structures for **5**$^-$.

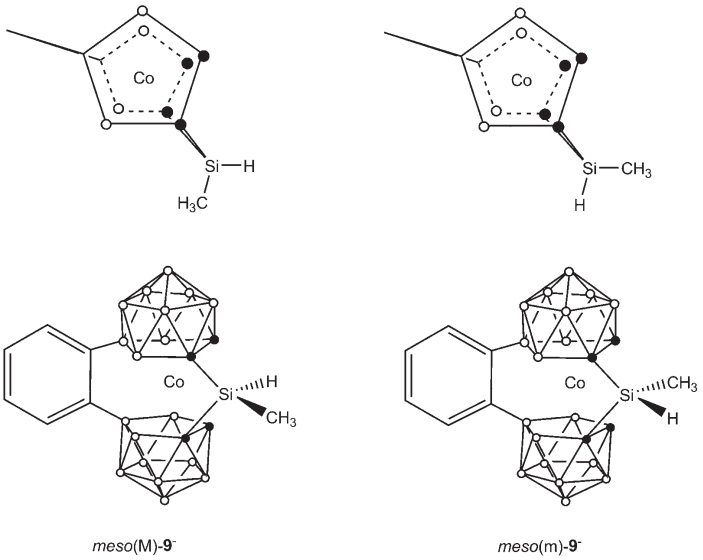

meso(M)-**9**$^-$ *meso*(m)-**9**$^-$

Figure 15. The *meso* isomers for anion **9**$^-$.

and the main reaction product, followed by the *meso* isomer with the CH_3 groups projected on the clusters B–H, *meso*(M). Finally the least stable would be the *meso* isomer with the $-CH_3$ group projected on the C_c–H, *meso*(m).

Conclusion

The first C_c-mono and C_c-disubstituted cobaltabis(dicarbollide) derivatives containing different organosilane functions have been successfully prepared by the direct reaction of the mono or dilithium salts of starting anions **1**$^-$ and **2**$^-$ with the appropriate chlorosilanes and under careful monitoring of the temperature. The reaction temperature was a key factor in the direct reaction to major isomers, since at very low temperatures (−78 °C) C_c-monosubstituted species and high isomeric purity were obtained, whereas increasing the temperature (−40 °C or 0 °C) led to C_c-disubstituted anions and structural isomeric mixtures. The ion **3**$^-$ represents the first example of a C_c-monosubstituted cobaltabis(dicarbollide) derivative that has been fully characterised by X-ray diffraction analysis. Compounds **4**$^-$ and **8**$^-$, containing a bridging (-μ-$SiMe_2$) between both dicarbollide ligands, were obtained unexpectedly from the reaction of the respective monolithium salt of **1**$^-$ or **2**$^-$ with Me_2SiHCl at low temperatures. A hypothetical mechanism has been proposed to explain the formation of these compounds through an intramolecular interaction and has been supported by theoretical calculations compared with experimental results. Density functional theory (DFT) at the B3LYP/6-311G(d,p) level was applied to optimise the geometries of ions **1**$^-$–**10**$^-$ and calculate their relative energies. The theoretical studies perfectly agree with the experimental results, indicating that *rac* isomers are more stable than *meso* isomers. Some of the metallacarboranes **3**$^-$, **5**$^-$ and **9**$^-$ functionalised with –SiH have actually been used as hydrosilylating agents to be attached to the periphery of dendrimeric structures by the hydrosilylation of alkenes.

Experimental Section

General considerations: Elemental analyses were performed by using a Carlo Erba EA1108 microanalyser. FTIR spectra were recorded with KBr pellets on a Shimadzu FTIR-8300 spectrophotometer. UV/Vis spectroscopy was carried out with a Shimadzu UV/Vis 1700 spectrophotometer with 1 cm cuvettes. The concentration of the complexes was 1×10^{-4} M. UV/Vis spectra were measured using the following procedure: stock solutions of the compounds were prepared by making a solution of several milligrams of the solid compound in 5 mL of acetonitrile (HPLC grade, Sigma-Aldrich). After this, a sample of this stock solution was diluted to a concentration of 10^{-4} M. The matrix-assisted laser desorption ionisation time-of-flight mass spectra (MALDI-TOF-MS) were recorded in the negative ion mode with a Bruker Biflex MALDI-TOF instrument (N_2 laser; λ_{exc} 337 nm (0.5 ns pulses); voltage ion source 20.00 kV (Uis1) and 17.50 kV (Uis2)). ^{1}H and ^{1}H{^{11}B} NMR (300.13 MHz), ^{13}C{^{1}H} NMR (75.47 MHz), ^{11}B and ^{11}B{^{1}H} NMR (96.29 MHz), and ^{29}Si{^{1}H} (59.62 MHz) spectra were recorded at room temperature on a Bruker ARX 300 instrument equipped with the appropriate decoupling accessories. All NMR measurements were performed in [D_6]acetone at 22 °C. Chemical shift data for ^{1}H, ^{1}H{^{11}B}, ^{13}C{^{1}H}and ^{29}Si{^{1}H} NMR spectra are referenced to $SiMe_4$; those for ^{11}B{^{1}H} and ^{11}B NMR spectra are referenced to external $BF_3{\cdot}OEt_2$. Chemical shifts are reported in ppm, followed by a description of the multiplet (e.g. d = doublet), its relative intensity and observed coupling constants (in Hz). Unless otherwise noted, all manipulations were carried out in a nitrogen atmosphere using standard vacuum line techniques. Solvents were purified by distillation from appropriate drying agents before use. 1,2-Dimethoxyethane (DME) was distilled from sodium/benzophenone prior to use. The metallacarboranes Cs[3,3′-Co(1,2-$C_2B_9H_{11})_2$] (Cs-**1**) and Cs[8,8′-μ-(1″,2″-C_6H_4)-3,3′-Co(1,2-$C_2B_9H_{10})_2$], (Cs-**2**) were commercially obtained from KATCHEM. *n*-Butyllitium (1.6 M in hexane) was purchased from Alfa Aesar; $MeSiHCl_2$ and Me_2SiHCl were obtained from Aldrich; Me_2SiCl_2 and Me_3SiCl were purchased from FluoroChem, and were used as received. The [NMe_4]Cl was purchased from Panreac, and CsCl and [PMe(Ph)$_3$]Br were received from Fluka.

Synthesis of [NMe_4][1-$SiMe_2$H-3,3′-Co(1,2-$C_2B_9H_{10}$)(1′,2′-$C_2B_9H_{11}$)] ([NMe_4]-3): *n*BuLi (0.50 mL, 0.79 mmol) was added dropwise to a Schlenk flask containing a stirred solution of Cs-**1** (360 mg, 0.79 mmol) in DME (12 mL) at −78 °C. The low-temperature bath was removed and the purple suspension was stirred for 45 min. The suspension was then cooled to −78 °C and Me_2SiHCl (0.10 mL, 0.88 mmol) was added dropwise. The suspension was stirred at room temperature for 1 h to give an orange solution and a white solid. The solid was filtered off and the solution evaporated to dryness. The residue was dissolved in MeOH (0.5 mL) and an aqueous solution of [NMe_4]Cl (50 mg, 7 mL) was added dropwise to give an orange solid. The solid was washed with H_2O (2×15 mL) and hexane (2×15 mL). The resultant solid was purified from a solution of CH_2Cl_2 to afford [NMe_4]-**3** (yield: 40 mg, 11 %). Alternatively, the addi-

tion of an aqueous solution of CsCl to the residue dissolved in MeOH (0.5 mL) gave an orange solid. The solid was washed with H_2O (2× 15 mL) and hexane (2×15 mL) and subsequently purified several times using a mixture of Et_2O/CH_2Cl_2 (1:1) to afford Cs-**3** (yield: 16 mg, 4%). $^1H\{^{11}B\}$ NMR: $\delta=4.31$ (sept, $^3J(H,H)=3.4$, 1H; Si-*H*), 3.85 (brs, 1H; $C_{cluster}$-*H*), 3.69 (brs, 2H; $C_{cluster}$-*H*), 3.45 (s, 12H; N-CH_3), 0.29 ppm (d, $^3J(H,H)=3.4$, 6H; Si-CH_3); $^{13}C\{^1H\}$ NMR: $\delta=57.00$ (N-CH_3), 55.57 (C_c-H), 51.65 (C_c-H), 49.26 (C_c-Si), −1.34 ppm (Si-CH_3); ^{11}B NMR: $\delta=9.10$ (d, $^1J(H,B)=163$, 1B; B8′), 7.29 (d, $^1J(H,B)=146$, 1B; B8), 3.56 (d, $^1J(H,B)=121$, 1B; B10′), 2.50 (d, $^1J(H,B)=123$, 1B; B10), −1.70 (d, $^1J(H,B)=143$, 1B; B12′), −4.65 (d, 4B; B4,4′,7′,9′), −5.00 (d, 3B; B4,7,9,12), −14.25 (d, $^1J(H,B)=159$, 2B; B5′,11′), −16.79 (d, $^1J(H,B)=156$, 2B; B5,11), −21.15 (d, $^1J(H,B)=106$, 1B; B6′), −22.26 ppm (d, $^1J(H,B)=111$, 1B; B6); $^{29}Si\{^1H\}$ NMR: $\delta=-8.28$ ppm; IR: $\tilde{\nu}=3040$ (C_c–H), 2557 (B–H), 2160 (Si–H), 1481 (C–N), 1254 cm^{-1} (Si–CH_3); MALDI-TOF-MS: *m/z* calcd for $[M-NMe_4]^-$: 382.3; found: 382.2; elemental analysis calcd (%) for $C_{10}H_{40}B_{18}CoNSi$: C 26.34, H 8.84, N 3.07; found: C 26.55, H 8.85, N 3.12.

Synthesis of Cs[1,1′-μ-SiMe$_2$-3,3′-Co(1,2-C$_2$B$_9$H$_{10}$)$_2$] (Cs-4)

Method A: The procedure was similar to that used to prepare Cs-**3**, with Cs-**1** (105 mg, 0.23 mmol) in DME (10 mL) at −40 °C, *n*BuLi (0.15 mL, 0.24 mmol) and Me_2SiHCl (35 μL, 0.31 mmol). After addition of Me_2SiHCl, the suspension was stirred at room temperature for 3 h. The suspension was filtered and the solution evaporated to dryness giving a brown-orange residue of [Li(dme)$_2$]-**4**, according to the ^1H NMR spectrum. At this point, different cations were used to isolate the **4**$^-$ ion. [Li(dme)$_2$]-**4** (100 mg, 0.18 mmol) was dissolved in MeOH (0.3 mL) and an aqueous solution of CsCl was added dropwise to give an orange solid. The solid was washed with H_2O (2×15 mL) and hexane (2×15 mL) to obtain Cs-**4** (yield: 73 mg, 62%). Alternatively, the addition of an aqueous solution of $[NMe_4]Cl$ to the orange residue of [Li(dme)$_2$]-**4** (100 mg, 0.18 mmol) dissolved in MeOH led to[NMe$_4$]-**4** (yield: 47 mg, 45%). Orange crystals suitable for an X-ray diffraction study were grown by slow evaporation of a solution of [NMe$_4$]-**4** in acetoneat room temperature. Furthermore, [PMe(Ph)$_3$]-**4** (yield: 83 mg, 70%) was also isolated from the addition of a methanolic solution of [PMe(Ph)$_3$]Br to the orange residue of [Li(dme)$_2$]-**4** dissolved in MeOH.

Method B: The procedure was similar to that used to prepare Cs-**3**, with Cs-**1** (360 mg, 0.79 mmol) in DME (12 mL) at −78 °C, *n*BuLi (1 mL, 1.60 mmol) and Me_2SiCl_2 (0.20 mL, 1.66 mmol). After addition of Me_2SiCl_2, the suspension was stirred at room temperature for 3 h. Then, the suspension was filtered and the solution evaporated to dryness giving a brown-orange residue of [Li(dme)$_2$]-**4** (426 mg). [Li(dme)$_2$]-**4** (100 mg, 0.18 mmol) was dissolved in MeOH (0.6 mL) and the dropwise addition of an aqueous solution of CsCl gave an orange solid. The solid was washed with H_2O (2×15 mL) and hexane (2×15 mL) to afford Cs-**4** (yield: 69 mg, 71%). ^1H NMR: $\delta=4.50$ (brs, 2H; C_c-*H*), 0.31 ppm (s, 6H, Si-CH_3); $^{13}C\{^1H\}$ NMR: $\delta=55.59$ (C_c-H), 41.68 (C_c-Si), −4.12 ppm (Si-CH_3); ^{11}B NMR: $\delta=8.07$ (d, $^1J(H,B)=142$ Hz; 2B), 2.70 (d, $^1J(H,B)=141$ Hz; 2B), −1.83 (d, $^1J(H,B)=150$ Hz; 4B), −3.78 (d, $^1J(H,B)=138$ Hz; 2B), −4.70 (d, $^1J(H,B)=128$ Hz, 2B), −14.29 (d, $^1J(H,B)=160$ Hz, 2B), −15.61 (d, $^1J(H,B)=157$ Hz, 2B), −22.11 ppm (d, $^1J(H,B)=165$ Hz, 2B); $^{29}Si\{^1H\}$ NMR: $\delta=13.98$ ppm; IR: $\tilde{\nu}=3070$ (C_c–H), 2554 (B–H), 1256 cm^{-1} (Si–CH_3); MALDI-TOF-MS: *m/z* calcd for $[M-Cs]^-$: 380.33; found: 380.34; elemental analysis calcd (%) for $C_6H_{26}B_{18}CoCsSi$: C 14.05, H 5.11; found: C 13.75, H 4.84.

Synthesis of Cs[1,1′-μ-SiMeH-3,3′-Co(1,2-C$_2$B$_9$H$_{10}$)$_2$] (Cs-5): The procedure was similar to that used to prepare Cs-**4**, with Cs-**1** (500 mg, 1.10 mmol) in DME (14 mL) at −78 °C, *n*BuLi (1.40 mL, 2.24 mmol) and $MeSiHCl_2$ (0.30 mL, 2.82 mmol). After addition of $MeSiHCl_2$, the suspension was stirred at room temperature for 6 h. The suspension was filtered and the solution evaporated to dryness. The residue was dissolved in MeOH (0.30 mL) and a solution of CsCl in water was added dropwise to give an orange solid. The solid was washed with H_2O (2×15 mL) and hexane (2×15 mL) to afford of Cs-**5** (yield: 417 mg, 76%). ^1H NMR: $\delta=5.06$ (q, $^3J(H,H)=3.4$ Hz, 1H; Si-*H*), 4.59 (brs, 2H; C_c-*H*), 0.44 ppm (d, $^3J(H,H)=3.4$ Hz, 3H,; Si-CH_3); $^{13}C\{^1H\}$ NMR: $\delta=55.86$ (C_c-H), 53.89 (C_c-H), 36.67 (C_c-Si), −6.76 ppm (Si-CH_3); ^{11}B NMR: $\delta=8.20$ (d, $^1J(H,B)=140$ Hz, 2B), 2.80 (d, $^1J(H,B)=141$ Hz, 2B), −1.72 (d, $^1J(H,B)=143$ Hz, 4B), −3.20 (d, $^1J(H,B)=131$ Hz, 1B), −4.63 (d, $^1J(H,B)=131$ Hz, 3B), −13.95 (d, $^1J(H,B)=162$ Hz, 1B), −14.37 (d, $^1J(H,B)=162$ Hz, 1B), −16.13 (d, $^1J(H,B)=162$ Hz, 1B), −16.74 (d, $^1J(H,B)=162$ Hz, 1B), −20.23 (d, $^1J(H,B)=108$–, 1B), −22.24 ppm (d, $^1J(H,B)=105$ Hz, 1B); $^{29}Si\{^1H\}$ NMR: $\delta=2.94$ ppm; IR: $\tilde{\nu}=3063$ (C_c–H), 2554 (B–H), 2160 (Si–H), 1257 cm^{-1} (Si–CH_3); MALDI-TOF-MS: *m/z* calcd for $[M-Cs]^-$: 366.33; found: 366.2; elemental analysis calcd (%) for $C_5H_{24}B_{18}CoCsSi$: C 12.04, H 4.85; found: C 12.62, H 4.95.

Synthesis of Cs[1-SiMe$_3$-3,3′-Co(1,2-C$_2$B$_9$H$_{10}$)(1′,2′-C$_2$B$_9$H$_{11}$)] (Cs-6): The procedure was similar to that used to prepare Cs-**3**, with Cs-**1** (205 mg, 0.45 mmol) in DME (8 mL) at −78 °C, *n*BuLi (0.30 mL, 0.48 mmol) and Me_3SiCl (0.10 mL, 0.77 mmol). After addition of Me_3SiCl, the suspension was stirred at room temperature for 5 h to give a red solution and a white solid. The solid was filtered off and the solution evaporated to dryness. The residue was dissolved in MeOH (0.20 mL) and a solution of $[NMe_4]Cl$ (50 mg) in water (7 mL) was added dropwise to give a red solid. The solid was washed with H_2O (2×10 mL) and hexane (2× 10 mL). The resultant solid was purified from CH_2Cl_2 to afford [NMe$_4$]-**6** (yield: 70 mg, 33%). Alternatively, the addition of an aqueous solution of CsCl to the residue dissolved in MeOH (0.5 mL) gave an orange solid. The solid was washed with H_2O (2×15 mL) and hexane (2×15 mL) and subsequently purified several times using a mixture of Et_2O/CH_2Cl_2 (1:1) to afford Cs-**6** (yield: 36 mg, 15%). $^1H\{^{11}B\}$ NMR: $\delta=4.02$ (brs, 1H; C_c-*H*), 3.83 (brs, 1H; C_c-*H*), 3.72 (brs, 1H; C_c-*H*), 0.28 ppm (s, 9H; Si-CH_3); $^{13}C\{^1H\}$ NMR: $\delta=59.04$ (C_c-H), 52.84 (C_c-H), 50.54 (C_c-H), 48.66 (C_c-Si), 3.08 ppm (Si-CH_3); ^{11}B NMR: $\delta=8.20$ (d, $^1J(H,B)=181$ Hz, 1B), 6.10 (d, $^1J(H,B)=180$ Hz, 1B), 3.53 (d, $^1J(H,B)=155$ Hz, 1B), 1.19 (d, $^1J(H,B)=143$ Hz, 1B), −1.95 (d, $^1J(H,B)=142$ Hz, 1B), −4.04 (1B), −5.60 (2B), −6.32 (2B), −7.32 (2B), −14.26 (d, $^1J(H,B)=143$ Hz, 1B), −15.15 (d, $^1J(H,B)=154$ Hz, 1B), −17.58 (d, $^1J(H,B)=154$ Hz, 1B), −18.40 (d, $^1J(H,B)=144$ Hz, 1B), −21.40 (d, $^1J(H,B)=165$ Hz, 1B), −23.06 ppm (d, $^1J(H,B)=161$ Hz, 1B); $^{29}Si\{^1H\}$ NMR: $\delta=10.74$ ppm; IR: $\tilde{\nu}=3090$ (C_c–H), 3038 (C_c–H), 2562 (B–H), 1259 cm^{-1} (Si–CH_3); MALDI-TOF-MS: *m/z* calcd for $[M-Cs]^-$: 396.37; found: $[M\text{-}Cs]^-$ 396.3; elemental analysis calcd (%) for $C_7H_{30}B_{18}CoCsSi$: C 15.89, H 5.72; found: C 15.47, H 5.69.

Synthesis of Cs[1,1′-(SiMe$_3$)$_2$-3,3′-Co(1,2-C$_2$B$_9$H$_{10}$)$_2$] (Cs-7): *n*BuLi (0.60 mL, 0.96 mmol) was added dropwise to a Schlenk flask containing a stirred solution of Cs-**1** (214 mg, 0.47 mmol) in DME (10 mL) at −78 °C. The low-temperature bath was removed and the suspension was stirred at room temperature for 45 min. Then, Me_3SiCl (0.20 mL, 1.55 mmol) was added at −78 °C. After addition of Me_3SiCl, the suspension was stirred at room temperature for 3 h and filtered and the solution evaporated to dryness. The residue was dissolved in MeOH (0.5 mL) and an aqueous solution of CsCl (200 mg, 20 mL) was added dropwise to give a red solid. The solid was washed with H_2O (2×15 mL) and hexane (2× 15 mL) to afford Cs-**7** (yield: 254 mg, 90%). Alternatively, [NMe$_4$]-**7** can be isolated in 95% yield, by the addition of an aqueous solution of $[NMe_4]Cl$. Red crystals suitable for an X-ray diffraction study were grown by slow evaporation of a solution of [NMe$_4$]-**7** in acetone at room temperature. ^1H NMR: $\delta=4.19$ (brs, 0.66H; C_c-*H*), 3.77 (brs, 1.33H; C_c-*H*), 0.33 (s, 6H; Si-CH_3), 0.30 ppm (s, 12H; Si-CH_3); $^{13}C\{^1H\}$ NMR: $\delta=55.84$ (C_c-H), 54.56 (C_c-H), 51.96 (C_c-H), 46.85 (C_c-Si), 3.20 ppm (Si-CH_3); ^{11}B NMR: $\delta=8.25$ (d, $^1J(H,B)=140$ Hz, 2B), 3.71 (d, $^1J(H,B)=141$ Hz, 2B), −2.45 (d, $^1J(H,B)=126$ Hz, 4B), −5.44 (d, $^1J(H,B)=119$ Hz, 2B), −6.52 (d, $^1J(H,B)=123$ Hz, 2B), −11.59 (d, $^1J(H,B)=172$ Hz, 1B), −13.42 (d, $^1J(H,B)=158$ Hz, 2B), −15.09 (d, $^1J(H,B)=156$ Hz, 1B), −19.66 ppm (d, $^1J(H,B)=177$ Hz, 2B); $^{29}Si\{^1H\}$ NMR: $\delta=10.75$ ppm; IR: $\tilde{\nu}=3055$ (C_c–H), 2561 (B–H), 1250 cm^{-1} (Si–CH_3); MALDI-TOF-MS: *m/z* calcd for $[M-Cs]^-$: 468.42; found: 467.3; elemental analysis calcd (%) for $C_{10}H_{38}B_{18}CoCsSi_2$ (601): C 19.98, H 6.37; found: C 20.49, H 6.48.

Synthesis of [NMe$_4$][8,8′-μ-(1″,2″-C$_6$H$_4$)-1,1′-μ-SiMe$_2$-3,3′-Co(1,2-C$_2$B$_9$H$_9$)$_2$] ([NMe$_4$]-8): The procedure was similar to that used to prepare Cs-**4**, with Cs-**2** (95 mg, 0.18 mmol) in DME (5 mL)at −78 °C, *n*BuLi (0.12 mL, 0.19 mmol) and Me_2SiHCl (40 μL, 0.35 mmol). After addition of Me_2SiHCl, the suspension was stirred at room temperature for 3 h, and subsequently filtered and evaporated to dryness. The residue was dis-

solved in MeOH (0.1 mL) and an aqueous solution of $[NMe_4]Cl$ (25 mg, 5 mL) was added dropwise to give a red solid. The solid was washed with H_2O (2×10 mL) and hexane (2×10 mL). The resultant solid was purified from a solution of CH_2Cl_2 to afford $[NMe_4]$-**8** (yield: 92 mg, 77%). ^{1}H NMR: δ=6.78 (s, 4H; C_6H_4), 3.48 (br s, 2H; C_c-*H*), 3.35 (s, 12H, N-CH_3), 0.39 (s, 3H, Si-CH_3), 0.25 ppm (s, 3H, Si-CH_3); ^{13}C{^{1}H} NMR: δ=128.98 (C_6H_4), 124.83 (C_6H_4), 55.11 (N-CH_3), 49.67 (C_c-H), 36.73 (C_c-Si), −4.46 (Si-CH_3), −5.84 ppm (Si-CH_3); ^{11}B NMR: δ=25.93 (s, 2B), 2.41 (d, ^1J(H,B)=131 Hz, 3B), 1.69 (d, ^1J(H,B)=75 Hz, 3B), −2.98 (d, ^1J(H,B)=131 Hz, 4B), −11.76 (d, ^1J(H,B)=147 Hz, 4B), −24.51 ppm (d, ^1J(H,B)=161 Hz, 2B); ^{29}Si{^{1}H} NMR: δ=11.74 ppm; IR: $\tilde{\nu}$=3034 (C_c–H), 2975 (C_{aryl}–H), 2954, 2923, 2561 (B–H), 1481 (C–N), 1254 cm^{-1} (Si–CH_3); MALDI-TOF-MS: *m/z* calcd for $[M-NMe_4]^-$: 454.3; found: 454.3; elemental analysis calcd (%) for $C_{16}H_{40}B_{18}CoNSi$: C 30.97, H 6.35 N 2.01; found: C 29.76, H 6.48, N 1.99.

Synthesis of Cs[8,8′-μ-(1″,2″-C_6H_4)-1,1′-μ-SiMeH-3,3′-Co(1,2-$C_2B_9H_9$)$_2$] (Cs-9): The procedure was similar to that used to prepare Cs-**5**, with Cs-**2** (373 mg, 0.70 mmol) in DME (9 mL) at −78°C, *n*BuLi (0.90 mL, 1.44 mmol) and CH_3SiHCl_2 (0.15 mL, 1.42 mmol). After addition of CH_3SiHCl_2, the suspension was stirred at room temperature for 3 h and subsequently filtered and the solution evaporated to dryness. The resultant residue was dissolved in MeOH, and an aqueous solution of $[NMe_4]Cl$ was added to give $[NMe_4]$-**9** (yield 60%). Furthermore, Cs-**9** can be isolated from the addition of an aqueous solution of CsCl in a 65% yield. ^{1}H NMR: δ=6.76 (s, 4H; C_6H_4), 5.25 (q, ^3J(H,H)=3.4 Hz, 0.24H; Si-H), 4.97 (q, ^3J(H,H)=3.4 Hz, 0.76H; Si-H), 3.61 (br s, 2H; C_c-*H*), 0.48 (d, ^3J(H,H)=3.4 Hz, 2.28H,; Si-CH_3), 0.38 ppm (d, ^3J(H,H)=3.4 Hz, 0.72H; Si-CH_3); ^{13}C{^{1}H} NMR: δ=128.96, 124.84 (C_6H_4), 50.84 (C_c-H), 48.56 (C_c-H), 32.30 (C_c-Si), 31.88 (C_c-Si),-6.32 (Si-CH_3), −6.87 ppm (Si-CH_3); ^{11}B NMR: δ=27.47 (s, 2B), 2.56 (d, ^1J(H,B)=131 Hz; 6B), −2.73 (d, ^1J(H,B)=122 Hz; 4B), −11.55 (d, ^1J(H,B)=132 Hz; 4B), −24.04 ppm (d, ^1J(H,B)=144 Hz, 2B); ^{29}Si{^{1}H} NMR: δ=2.69 ppm; IR: $\tilde{\nu}$=3036 (C_c–H), 2970 (C_{aryl}–H), 2577 (B–H), 2162 (Si–H), 1257 cm^{-1} (Si–CH_3); MALDI-TOF-MS: *m/z* calcd for $[M-Cs]^-$: 440.3; found: 440.2; elemental analysis calcd (%) for $C_{11}H_{26}B_{18}CoSiCs$ (572.8): C 23.06, H 4.57; found: C 22.96, H 5.00.

Synthesis of $[NMe_4]$[8,8′-μ-(1″,2″-C_6H_4)-1-$SiMe_3$-3,3′-Co(1,2-$C_2B_9H_9$)-(1′,2′-$C_2B_9H_{10}$)] ($[NMe_4]$-10): The procedure was similar to that used to prepare Cs-**7**, with Cs-**2** (100 mg, 0.19 mmol) in DME (5 mL) at −78°C, *n*BuLi (0.25 mL, 0.40 mmol) and Me_3SiCl (0.10 mL, 0.77 mmol). After addition of Me_3SiCl, the suspension was stirred at room temperature for 3 h. The suspension was filtered and the solution evaporated to dryness. The residue was dissolved in MeOH (0.1 mL) and a solution of $[NMe_4]Cl$ (25 mg, 5 mL) in water was added dropwise to give a red solid. The solid was washed with H_2O (2×10 mL) and hexane (2×10 mL) and recrystallised from acetone to afford $[NMe_4]$-**10** (yield: 72 mg, 69%). ^{1}H NMR: δ=6.78 (s, 4H; C_6H_4), 3.52 (br s, 2H; C_c-*H*), 3.45 (br s, 1H; C_c-*H*), 3.28 (s, 12H; N-CH_3), 0.28 ppm (s, 9H; Si-CH_3); ^{13}C{^{1}H} NMR: δ=128.86, 128.56, 125.16 (C_6H_4), 55.12 (N-CH_3), 50.12 (C_c-H), 49.84 (C_c-H), 42.11 (C_c-H), 41.06 (C_c-Si), 0.10 ppm (Si-CH_3); ^{11}B NMR: δ=26.50 (s, 1B), 24.50 (s, 1B), 1.06 (2B), −1.46 (2B), −2.58 (2B), −4.64 (2B), −5.67 (2B), −10.80 (1B), −11.96 (1B), −13.67 (2B), −23.64 (d, ^1J(H,B)=155 Hz; 1B), −25.00 ppm (d, ^1J(H,B)=155 Hz; 1B); ^{29}Si{^{1}H} NMR: δ=8.63 ppm; IR: $\tilde{\nu}$=3036 (C_c–H), 2954 (C_{aryl}–H), 2584 (B–H), 1481 (C–N), 1253 cm^{-1} (Si–CH_3); MALDI-TOF-MS: *m/z* calcd for $[M-NMe_4]^-$: 470.39; found: 469.17; elemental analysis calcd (%) for $C_{17}H_{44}B_{18}CoNSi\cdot Me_2CO$: C 39.88, H 8.37, N 2.33; found: C 39.64, H 8.28, N 2.32.

Table 6. Crystallographic data for $[NMe_4]$-**3**, $[NMe_4]$-**4** and $[NMe_4]$-**7** at −100°C.

	$[NMe_4]$-**3**	$[NMe_4]$-**4**	$[NMe_4]$-**7**
empirical formula	$C_{10}H_{40}B_{18}CoNSi$	$C_{10}H_{38}B_{18}CoNSi$	$C_{14}H_{50}B_{18}CoNSi_2$
M_r	456.03	0454.01	542.24
crystal system	monoclinic	monoclinic	monoclinic
crystal shape/colour	plate/yellow	plate/red	plate/red
space group	$P2_1/c$ (no. 14)	$P2_1/m$ (no. 11)	$C2/c$ (no. 15)
a [Å]	7.1294(5)	7.3092(3)	15.9542(6)
b [Å]	30.456(2)	13.7910(11)	14.6275(6)
c [Å]	11.5788(7)	13.6504(8)	13.1513(4)
β [°]	91.206(4)	104.204(3)	98.714(2)
V [Å^3]	2513.6(3)	1237.19(14)	3033.69(19)
Z	4	2	4
ρ [g cm^{-3}]	1.205	1.219	1.187
μ [cm^{-1}]	7.32	7.43	6.54
goodness-of-fit[a]	1.084	1.042	1.029
R[b] [$I>2\sigma(I)$]	0.0949	0.0733	0.0524
R_w[c] [$I>2\sigma(I)$]	0.1646	0.1591	0.1042

[a] $S=[\Sigma(w(F_o^2-F_c^2)]/(n-p)^{1/2}$. [b] $R=\Sigma||F_o|-|F_c||/\Sigma|F_o|$. [c] $R_w=[\Sigma w(|F_o^2|-|F_c^2|)^2/\Sigma w|F_o^2|^2]^{1/2}$.

X-ray diffraction studies—structure determinations of $[NMe_4]$-3, $[NMe_4]$-4 and $[NMe_4]$-7: Single-crystal data collections for $[NMe_4]$-**3**, $[NMe_4]$-**4** and $[NMe_4]$-**7** were performed at −100°C on an Enraf Nonius KappaCCD diffractometer with graphite monochromatised $Mo_{K\alpha}$ radiation (λ=0.71073 Å). A total of 4538, 2499 and 2976 unique reflections were collected for $[NMe_4]$-**3**, $[NMe_4]$-**4** and $[NMe_4]$-**7**, respectively. Crystallographic data are presented in Table 6. The structures were solved by direct methods and refined on F^2 by the SHELX-97 program.[22] For each structure, the carbon and boron atoms could be reliably distinguished.

For $[NMe_4]$-**3**, non-hydrogen atoms were refined with anisotropic thermal displacement parameters and hydrogen atoms were treated as riding atoms using the SHELX-97 default parameters. *R* values were fairly high because of the high mosaicity of the crystals.

For $[NMe_4]$-**4**, the cobaltabis(dicarbollide) anion had a crystallographic mirror symmetry with the cobalt, silicon and methyl carbon atoms lying at the symmetry element. The $[NMe_4]^+$ ion was disordered in two orientations with the partially occupied nitrogen atom and the two partially occupied methyl carbon atoms of each orientation lying in the mirror plane. The cation was refined as a rigid group, but as refinement of the site occupation parameters did not converge well, the parameters were fixed to 0.6 and 0.4. Non-hydrogen atoms of the anion were refined with anisotropic thermal displacement parameters, but those of the disordered cation were refined with isotropic displacement parameters. All hydrogen atoms were treated as riding atoms using the SHELX-97 default parameters.

For $[NMe_4]$-**7**, the cobaltabis(dicarbollide) anion had a crystallographic twofold symmetry with the cobalt atom lying at the symmetry element. The $[NMe_4]^+$ ion was disordered in two orientations with the partially occupied nitrogen atom lying at the vicinity of the twofold axis. The cation was refined as a rigid group. All non-hydrogen atoms were refined with anisotropic thermal displacement parameters and the hydrogen atoms were treated as riding atoms using the SHELX-97 default parameters.

CCDC-659301 ($[NMe_4]$-**3**), 652272 ($[NMe_4]$-**4**) and 652273 ($[NMe_4]$-**7**) contain the supplementary crystallographic data for this paper. These data can be obtained free of charge from The Cambridge Crystallographic Data Centre via www.ccdc.cam.ac.uk/data_request/cif.

Calculation details: Geometries of the compounds were optimised with the B3LYP hybrid functional[23] and the 6-311G(d,p) basis for all elements. Unless otherwise noted, energies are reported at this level. Natural population analysis was performed at the same level. Transition states were found at the B3LYP/6-31G level, characterised by a single imaginary frequency, and visualisation of the corresponding vibrational modes ensured that the desired minima are connected. Magnetic shieldings were computed for optimised geometries by employing gauge-including atomic orbitals (GIAOs)[21] with the B3LYP hybrid functional together with the

basis 6-31++G(d). The ^{11}B chemical shifts were calculated relative to B_2H_6 and converted to the usual $BF_3{\cdot}OEt_2$. These combinations of functional and basis set gave good results, for more exhaustive calculations on cobaltacarboranes see Bühl et al.[19] All computations were performed with the Gaussian 03 program.[24]

Acknowledgements

This work has been supported by MEC, MAT 2006—05339 and Generalitat de Catalunya, 2005/SGR/00709. E.J.J.-P. thanks MEC for a FPU grant.

[1] I. B. Sivaev, V. I. Bregadze, *Collect. Czech. Chem. Commun.* **1999**, *64*, 783.
[2] a) L. Ma, J. Hamdi, M. F. Hawthorne, *Inorg. Chem.* **2005**, *44*, 7249; b) P. Matejicek, P. Cigler, K. Procházka, V. Kral, *Langmuir* **2006**, *22*, 575; c) G. Chevrot, R. Schurhammer, G. Wipff, *J. Phys. Chem. B* **2006**, *110*, 9488.
[3] J. Plesek, *Chem. Rev.* **1992**, *92*, 269.
[4] a) S. H. Strauss, *Chem. Rev.* **1993**, *93*, 927; b) C. A. Reed, *Acc. Chem. Res.* **1998**, *31*, 133.
[5] a) C. Masalles, S. Borrós, C. Viñas, F. Teixidor, *Adv. Mater.* **2000**, *12*, 1199; b) C. Masalles, J. Llop, C. Viñas, F. Teixidor, *Adv. Mater.* **2002**, *14*, 826; c) S. Gentil, E. Crespo, I. Rojo, A. Friang, C. Viñas, F. Teixidor, B. Grüner, D. Gabel, *Polymer* **2005**, *46*, 12218.
[6] a) C. Viñas, S. Gómez, J. Bertran, F. Teixidor, J.-F. Dozol, H. Rouquette, *Chem. Commun.* **1998**, 191; b) C. Viñas, S. Gómez, J. Bertran, F. Teixidor, J.-F. Dozol, H. Rouquette, *Inorg. Chem.* **1998**, *37*, 3640; c) B. Grüner, J. Plesek, J. Baca, I. Cisarova, J.-F. Dozol, H. Rouquette, C. Viñas, P. Selucky, J. Rais, *New J. Chem.* **2002**, *26*, 1519.
[7] M. F. Hawthorne, A. Maderna, *Chem. Rev.* **1999**, *99*, 3421.
[8] a) J. N. Francis, M. F. Hawthorne, *Inorg. Chem.* **1971**, *10*, 594; b) J. Plesek, S. Hermanek, K. Base, L. J. Todd, W. F. Wright, *Collect. Czech. Chem. Commun.* **1976**, *41*, 3509; c) Z. Janousek, J. Plesek, S. Hermanek, K. Base, L. J. Todd, W. F. Wright, *Collect. Czech. Chem. Commun.* **1981**, *46*, 2818; d) L. Matel, F. Mascasek, P. Rajec, S. Hermanek, J. Plesek, *Polyhedron*, **1982**, *1*, 511.
[9] a) P. Selucky, J. Plesek, J. Rais, M. Kyrs, L. Kadlecova, *J. Radioanal. Nucl. Chem.* **1991**, *149*, 131; b) J. Plesek, S. Hermanek, *Collect. Czech. Chem. Commun.* **1995**, *60*, 1297; c) P. K. Hurlburt, R. L. Miller, K. D. Abney, T. M. Foreman, R. J. Butcher, S. A. Kinkead, *Inorg. Chem.* **1995**, *34*, 5215; d) J. C. Fanning, L. A. Huff, W. A. Smith, A. S. Terell, L. Yasinsac, L. J. Todd, S. A. Jasper, D. J. McCabe, *Polyhedron* **1995**, *14*, 2893; e) M. D. Mortimer, C. B. Knoble, M. F. Hawthorne, *Inorg. Chem.* **1996**, *35*, 5750; f) A. Franken, J. Plesek, C. Nachtigal, *Collect. Czech. Chem. Commun.* **1997**, *62*, 746; g) J. Plesek, S. Hermanek, A. Franken, I. Cisarova, C. Nachtigal, *Collect. Czech. Chem. Commun.* **1997**, *62*, 47; h) J. Plesek, B. Grüner, J. Báca, J. Fusek, I. Cisarová, *J. Organomet. Chem.* **2002**, *649*, 181; i) J. Plesek, B. Grüner, I. Cisarová, J. Báca P. Selucky, J. Rais, *J. Organomet. Chem.* **2002**, *657*, 59; j) I. Rojo, F. Teixidor, C. Viñas, R. Kivekäs, R. Sillanpää, *Chem. Eur. J.* **2003**, *9*, 4311; k) I. Rojo, F. Teixidor, R. Kivekäs, R. Sillanpää, C. Viñas, *J. Am. Chem. Soc.* **2003**, *125*, 14720; l) F. Teixidor, J. Pedrajas, I. Rojo, C. Viñas, R. Kivekäs, R. Sillanpää, I. Sivaev, V. Bregadze, S. Sjöberg, *Organometallics* **2003**, *22*, 3414; m) B. Grüner, L. Mikulasek, J. Báca, I. Cisarova, V. Bohmer, C. Danila, M. M. Reinoso-Garcia, W. Verboom, D. N. Reinhoudt, A. Casnati, R. Ungaro. *Eur. J. Org. Chem.* **2005**, 2022.
[10] a) R. M. Chamberlin, B. L. Scott, M. M. Melo, K. D. Abney, *Inorg. Chem.* **1997**, *36*, 809; b) S. A. Fino, K. A. Benwitz, K. M. Sullivan, D. L. LaMar, K. M. Stroup, S. M. Giles, G. J. Balaich, R. M. Chamberlin, K. D. Abney, *Inorg. Chem.* **1997**, *36*, 4604.
[11] I. Rojo, F. Teixidor, C. Viñas, R. Kivekäs, R. Sillanpää, *Chem. Eur. J.* **2004**, *10*, 5376.
[12] a) R. Núñez, A. González, C. Viñas, F. Teixidor, R. Sillanpää, R. Kivekäs, *Org. Lett.* **2005**, *7*, 231; b) R. Núñez, A. González-Campo, C. Viñas, F. Teixidor, R. Sillanpää, R. Kivekäs, *Organometallics* **2005**, *24*, 6351; c) R. Núñez, A. González-Campo, A. Laromaine, F. Teixidor, R. Sillanpää, R. Kivekäs, C. Viñas, *Org. Lett.* **2006**, *8*, 4549; d) A. González-Campo, R. Núñez, F. Teixidor, C. Viñas, R. Sillanpää, R. Kivekäs, *Macromolecules* **2007**, *40*, 5644.
[13] T. Venable, W. Hutton, R. Grimes, *J. Am. Chem. Soc.* **1984**, *106*, 29.
[14] I. Rojo, F. Teixidor, R. Kivekäs, R. Sillanpää, C. Viñas, *Organometallics* **2003**, *22*, 4642.
[15] a) M. F. Hawthorne, D. C. Young, T. D. Andrews, D. V. Howe, R. L. Pilling, A. D. Pitts, M. Reintjes, L. F. Warren, Jr., Patrick, A. Wegner, *J. Am. Chem. Soc.* **1968**, *90*, 879; b) L. Matel, F. Macasek, P. Rajec, S. Hermanek, J. Plesek, *Polyhedron* **1982**, *1*, 511; c) H. Horáková, R. Vespalec, *Spectrochim. Acta Part A* **2006**, *65*, 378.
[16] a) R. Bauernschmitt, R. Ahlrichs, *Chem. Phys. Lett.* **1996**, *256*, 454; b) R. E. Stratmann, G. E. Scuseria, M. J. Frisch, *J. Chem. Phys.* **1998**, *109*, 8218.
[17] M. F. Hawtorne, J. I. Zink, J. M. Skelton, M. J. Bayer, C. Liu, E. Livshits, R. Baer, D. Neuhauser, *Science* **2004**, *303*, 1849.
[18] a) J. Llop, C. Viñas, F. Teixidor, L. Victori, R. Kivekäs, R. sillanpää, *Organometallics* **2002**, *21*, 355; b) R. Núñez, O. Tutusaus, F. Teixidor, C. Viñas, R. Sillanpää, R. Kivekäs, *Chem. Eur. J.* **2005**, *11*, 5637.
[19] M. Bühl, D. Hnyk, J. Machácek, *Chem. Eur. J.* **2005**, *11*, 4109.
[20] R. Custelcean, J. E. Jackson, *Chem. Rev.* **2001**, *101*, 1963.
[21] a) R. Ditchfield, *Mol. Phys.* **1974**, *27*, 789; b) K. Wolinski, J. F. Hinton, P. Pulay, *J. Am. Chem. Soc.* **1990**, *112*, 8251; c) GIAO-DFT implementation: J. R. Cheeseman, G. W. Trucks, T. A. Keith, M. J. Frisch, *J. Chem. Phys.* **1996**, *104*, 5497.
[22] G. M. Sheldrick, SHELX-97, University of Göttingen, Germany, **1997**.
[23] a) A. D. Becke *J. Chem. Phys.* **1993**, *98*, 5648; b) C. Lee, W. Yang, R. G. Parr, *Phys. Rev. B* **1988**, *37*, 785.
[24] Gaussian 03 (Revision BO.1), M. J. Frisch, G. W. Trucks, H. B. Schlegel, G. E. Scuseria, M. A. Robb, J. R. Cheeseman, J. A. Montgomery, Jr., T. Vreven, K. N. Kudin, J. C. Burant, J. M. Millam, S. S. Iyengar, J. Tomasi, V. Barone, B. Mennucci, M. Cossi, G. Scalmani, N. Rega, G. A. Petersson, H. Nakatsuji, M. Hada, M. Ehara, K. Toyota, R. Fukuda, J. Hasegawa, M. Ishida, T. Nakajima, Y. Honda, O. Kitao, H. Nakai, M. Klene, X. Li, J. E. Knox, H. P. Hratchian, J. B. Cross, C. Adamo, J. Jaramillo, R. Gomperts, R. E. Stratmann, O. Yazyev, A. J. Austin, R. Cammi, C. Pomelli, J. W. Ochterski, P. Y. Ayala, K. Morokuma, G. A. Voth, P. Salvador, J. J. Dannenberg, V. G. Zakrzewski, S. Dapprich, A. D. Daniels, M. C. Strain, O. Farkas, D. K. Malick, A. D. Rabuck, K. Raghavachari, J. B. Foresman, J. V. Ortiz, Q. Cui, A. G. Baboul, S. Clifford, J. Cioslowski, B. B. Stefanov, G. Liu, A. Liashenko, P. Piskorz, I. Komaromi, R. L. Martin, D. J. Fox, T. Keith, M. A. Al-Laham, C. Y. Peng, A. Nanayakkara, M. Challacombe, P. M. W. Gill, B. Johnson, W. Chen, M. W. Wong, C. Gonzalez, J. A. Pople, Gaussian, Inc., Pittsburgh PA, **2004**.

Received: December 20, 2007
Published online: April 11, 2008

5.b) Carboranyl Substituted Siloxanes and Octasilsesquioxanes: Synthesis, Characterization and Reactivity.

8458 *Macromolecules* **2008**, *41*, 8458−8466

Carboranyl Substituted Siloxanes and Octasilsesquioxanes: Synthesis, Characterization, and Reactivity

Arántzazu González-Campo,[†] Emilio José Juárez-Pérez,[†,‡] Clara Viñas,[†] Bruno Boury,[§] Reijo Sillanpää,[||] Raikko Kivekäs,[⊥] and Rosario Núñez*,[†]

Department of Chemistry, Institut de Ciència de Materials de Barcelona (CSIC), Campus de la U.A.B, 08193 Bellaterra, Spain, Institut Charles Gerhardt Montpellier - UMR 5253 - CNRS-UM2-ENSCM-UM1, CMOS - Place E. Bataillon, 34095 Montpellier, France, Department of Chemistry, University of Jyväskylä, FIN-40351, Jyväskylä, Finland, and Department of Chemistry, University of Helsinki, Post Office Box 55, FIN-00014, Finland

Received July 3, 2008; Revised Manuscript Received September 7, 2008

ABSTRACT: Carboranyl-containing disiloxane, cyclic-siloxane and cage-like silsesquioxane have been prepared in high yields. Two routes are compared for their preparation, a classical hydrolytic process based on hydrolysis and condensation of the freshly prepared carboranylalkylchlorosilane and ethoxysilane precursors and a nonhydrolytic route based on the specific reactivity of chorosilane toward DMSO. Based on the typical reactivity of the carboranyl group toward nucleophiles, dianionic disiloxanes and octaanionic silsesquioxanes were obtained without modification of the siloxane bond. Products are fully characterized by FTIR, NMR and MALDI-TOF methods.

Introduction

The 1,2-dicarba-*closo*-dodecaborane and derivatives present exceptional characteristics,[1,2] such as low nucleophilicity, chemical inertness, thermal stability,[3] electron-withdrawing properties,[4] and stability and low toxicity in biological systems,[5] which have stimulated the development of a wide range of potential applications based on a molecular approach of the synthesis of material.[6,7] Moreover, the rigid geometry and the relative easiness of derivatization of the carborane allows the preparation of a wide number of compounds in view of the preparation of precursors of materials.[8] Indeed, we have reported the synthesis of carboranyl-containing star-shaped molecules and dendrimers in which carbosilane cores are used as scaffold.[9] Due to the specificity and the versatility of carboranes to be chemically modified,[10] they have been an ideal stable and suitable group whose partial degradation allows a unique route to very large carboranyl-containing polyanionic dendrimers.[9c] On the other hand, as a part of our ongoing studies, hybrid organic−inorganic silicon-based material have been prepared by Sol−Gel chemistry.[11] The resulting insoluble organo-carboranyl bridged polysilsesquioxanes have been prepared and have shown to be a versatile class of materials in which the presence of carborane units provides mesostructuration and a high thermal and chemical stability.[3b,11]

Following with our interest on the functionalization of carborane clusters-containing dendrimers and macromolecules, we thought that the preparation of a new family of siloxane compounds was an important field to explore. In this paper, we report on the association of the cage structure of carborane with siloxane and silsesquioxane cage-like structure. Such polyhedral oligomeric silsesquioxanes [POSS; $(RSiO_{1.5})_n$; $n = 8$] are nanosized building blocks for organic/inorganic hybrid materials; their high potential for applications is based on the possibility to control and balance the inorganic and organic moieties in their architecture.[12] Therefore, they can be tuned for very different applications in accordance with the nature of the organic functionality, as demonstrated by some recent examples: in biomaterial systems, POSS have been used for preparing a new generation of silica nanocomposites with particular use in cardiovascular interventional devices,[13] and in material chemistry, they are used as coupling agents of metal oxide nanoparticles,[14] cross-linking agents into organic polymers,[15] and as octa-arms dendrimers-core.[12f,16,17]

Our aim is to obtain new carboranyl-containing molecules and macromolecules in which the clusters are attached to linear, cyclic, or cage structures like in siloxanes and silsesquioxanes as cores, respectively. Such silicon-containing structures are usually prepared by hydrolysis and condensation of alkylchlorosilanes but this approach is limited due to the formation of linear siloxanes or resins and a large variety of cages as byproduct. Nevertheless, their formation can be controlled using a water-free approach such as employing DMSO as oxygen source[18] or the condensation between Si−H and Si−OMe.[19] This former method has recently been used to prepare hexasilsesquioxanes (T_6),[18a] silicones,[18b] cyclodisiloxanes,[18c,d] and silsesquioxanes particles,[18e] providing a well controlled way to obtain Si−O bonds using soft conditions.

The controlled chemical modification of the carborane moieties in such siloxane structure is, *a priori*, achievable according to the known literature procedure, by elimination of one vertex BH from the *closo* clusters using nucleophiles, such as alkoxides,[20] amines,[21] fluorides,[22] or phosphanes.[23] One important point was to clarify if this chemical modification of the carborane part could be compatible with the siloxane linkage in the present compounds. It is well-known that the Si−O−Si bond presents a great thermal, hydrolytic, and photostability; however, at high temperatures and in the presence of acids or bases, the Si−O bond in silicones can undergo hydrolytic scission.[24]

Although the disiloxyl link is formally analogous to an ether link, it is considerably more polar so that it is both more hydrophilic and more susceptible to hydrolysis.

* To whom correspondence should be addressed. Tel.: +34 93 580 1853. Fax: +34 93 580 5729. E-mail: rosario@icmab.es.
[†] Institut de Ciència de Materials de Barcelona (CSIC).
[‡] Enrolled in the UAB Ph.D. program.
[§] Institut Charles Gerhardt Montpellier.
[||] University of Jyväskylä.
[⊥] University of Helsinki.

10.1021/ma801483c CCC: $40.75
Published on Web 10/25/2008

Scheme 1. Preparation of Carboranyldisiloxane Dimers 3 and 4 Using Either Water or Dimethylsulfoxyde as an Oxygen Donor

Scheme 2. Preparation of 7 and 8 as a Mixture of D_3 and D_4 Cyclosiloxanes via the Hydrolysis of Dichlorosilanes 5 and 6

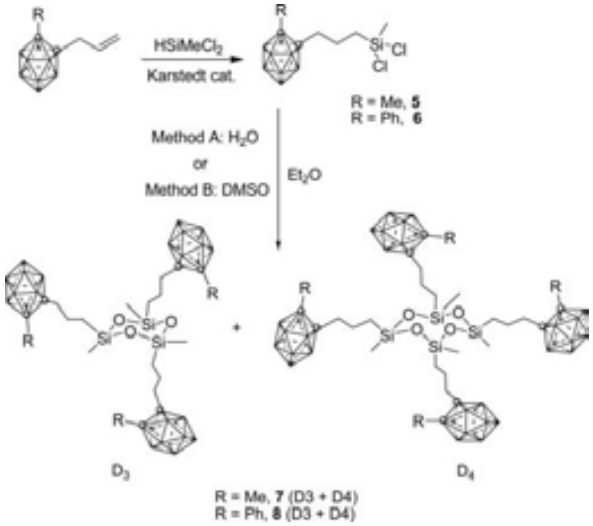

Results and Discussion

Preparation of Disiloxanes, Cyclosiloxanes, and Octasilsesquioxanes. Recently, we have reported the synthesis of 1-CH_3-2-[$CH_2CH_2CH_2(CH_3)_2SiCl$]-1,2-*closo*-$C_2B_{10}H_{10}$ (**1**) and 1-C_6H_5-2-[$CH_2CH_2CH_2(CH_3)_2SiCl$]-1,2-*closo*-$C_2B_{10}H_{10}$ (**2**) by hydrosilylation of the corresponding allylic precursor.[9c]

Here, monomers **1** and **2** displayed the typical reactivity of silylchloride in the presence of water leading, respectively, to the disiloxane [1-CH_3-2-$CH_2CH_2CH_2(CH_3)_2$Si-1,2-*closo*-$C_2B_{10}H_{10}]_2O$, (**3**) and [1-C_6H_5-2-$CH_2CH_2CH_2(C_6H_5)_2$Si-1,2-*closo*-$C_2B_{10}H_{10}]_2O$ (**4**; Scheme 1), without any other byproduct and in high yield. The HCl released by the hydrolysis of the Si−Cl bond acts as a catalyst for the condensation of the silanol without hydrolysis of the Si−O bonds that is sometime observed.[24]

Likewise, a "non-aqueous" approach using DMSO as oxygen source[18b] has also been used to form the carboranyl-containing disiloxanes **3** and **4**. The reaction of **1** and **2** with DMSO in $CHCl_3$ at room temperature overnight led to the formation of the corresponding siloxane, although the yield is lower than that of the hydrolytic route.

Following the same general approaches, we intended the preparation of cyclic siloxanes from dichlorosilanes via hydrolytic or DMSO route. In a first step, compounds 1-CH_3-2-[$CH_2CH_2CH_2(CH_3)SiCl_2$]-1,2-*closo*-$C_2B_{10}H_{10}$ (**5**) and 1-C_6H_5-2-[$CH_2CH_2CH_2(CH_3)SiCl_2$]-1,2-*closo*-$C_2B_{10}H_{10}$ (**6**) were prepared by hydrosilylation of the corresponding allylic compound with $H(CH_3)SiCl_2$ in the presence of Karstedt catalyst (Scheme 2). Reaction of compounds **5** and **6** in Et_2O with the stoichiometric amount of DMSO for 30 min at room temperature (Method B) or an excess of H_2O (Method A) for 2 h give compounds **7** and **8**, respectively (Scheme 2). According to the NMR and the MALDI-TOF data (see results below) **7** and **8** are a mixture of cyclic siloxanes: D_3 (cyclotrisiloxane), D_4 (cyclotetrasiloxane), along with different quantities of linear polysiloxanes (L). After chromatography of the crude over a silica column (hexane/Et_2O (1:1)) the following mixture was identified: the DMSO method leads to mostly a D_3/D_4/L (50:50:0) mixture for **7**, and a D_3/D_4/L (50:44:6) mixture for **8**; whereas, the hydrolytic approach leads to a D_3/D_4/L (33:40:27) mixture for **7** and a D_3/D_4/L (22:12:66) mixture for **8**. As previously reported,[18c] when DMSO was used as oxygen source, the percentage of D_3 was slightly higher compared to D_4. In addition, minor amounts of linear siloxanes were produced by this route, whereas in the hydrolytic method an elevated concentration of linear polysiloxane was obtained.

The next step was to prepare the T_8 structures[12b] either by the "anhydrous" DMSO methods or the hydrolytic one. The required precursors were prepared by hydrosilylation of 1-CH_3-2-$CH_2CH{=}CH_2$-1,2-$C_2B_{10}H_{10}$ and 1-C_6H_5-2-$CH_2CH{=}CH_2$-1,2-$C_2B_{10}H_{10}$ with $HSiCl_3$ and $HSi(OCH_2CH_3)_3$, respectively. Compounds **9**−**12** were obtained quantitatively, and remarkably, only the α adduct is formed (Scheme 3). Preparation of POSS by the nonhydrolytic method from trichlorosilanes **9** and **10** was carried out in DMSO/$CHCl_3$ mixture (2:1) or (3:1) at room temperature leading to T_8 cages **13** and **14** in 23 and 21% yields, respectively (Scheme 3). Remarkably, only one signal at −66 ppm was observed by ^{29}Si NMR spectroscopy. This is in accordance with the chemical shifts for Si atoms in T_8 cages (from −65 to −67 ppm),[25] and this is clearly different from the chemical shifts measured for T_6 cage (usually between −54 to −57 ppm) reported by Taylor and Bassindale who prepared them by the DMSO route.[18a] POSS **13** and **14** were also obtained by the hydrolysis of **11** and **12**, respectively, using different reaction conditions for each case. POSS **13** was obtained in 70% yield by adding the stoichiometric amount of water to a solution of **11** in THF using TBAF as catalyst at room temperature for a long reaction time (133 days). When the NaOH was used as catalyst, a longer reaction time was necessary (180 days), however, a lower yield was obtained (55%). On the other hand, POSS **14** was also obtained in only 28% yield by addition of water to a solution of **12** in $CHCl_3$ using TBAF at room temperature for 24 h. The TBAF was a better catalyst, however, attempts to decrease the reaction time led to lower yields and increasing the amounts of TBAF or NaOH were unsuccessful because they gave rise to the *closo* cluster degradation and formation of *nido* compounds.

Controlled Chemical Transformation of Disiloxanes and Octasilsesquioxanes. Partial degradation of the carborane moiety in **3** and **4** was achieved in a first approach by the deboronation reaction using soft conditions such as piperidine in ethanol at reflux with a carborane/piperidine ratio of 1:5.[26] This method was developed by our group to avoid the $C_{cluster}$−P (C_c-P) cleavage by the nucleophilic attack in the degradation of *closo*-carboranylphosphines and have been recently used for the degradation of *closo*-carboranyldisulfides.[27] In this method, the nucleophile, the ion EtO^-, is smoothly generated by reaction of the ethanol with piperidine. In the present work, the dianionic disiloxanes {[1-CH_3-2-$CH_2CH_2CH_2(CH_3)_2$Si-1,2-*nido*-$C_2B_9H_{10}]_2O\}^{2-}$, $[\mathbf{15}]^{2-}$, and {[1-C_6H_5-2-$CH_2CH_2CH_2(CH_3)_2$Si-1,2-*nido*-$C_2B_9H_{10}]_2O\}^{2-}$, $[\mathbf{16}]^{2-}$ were isolated in high yield (Scheme 4). The modification of the carboranyldisiloxanes **3** and **4** was also performed by the classical reaction of KOH in ethanol at reflux, with a carborane/KOH ratio of 1:5, leading again to the formation of the dianionic compounds $[\mathbf{15}]^{2-}$ and $[\mathbf{16}]^{2-}$. Contrarily, to the *closo*-carboranyldisulfides, (1-*S*-2-*R*-1,2-*closo*-$C_2B_{10}H_{10})_2$,[27] in which the disulfide bridge S−S was split to give the anionic thiolate fragment [1-*S*-2-*R*-1,2-*closo*-$C_2B_{10}H_{10}]^-$, in our case, the EtO^- act as nucleophile, removing the B(3) or B(6) from the *closo* cluster and keeping the Si−O−Si bond unaltered. In addition, both clusters were

Scheme 3. Preparation of Precursors 9−12 by Hydrosilylation of 1-*R*-$CH_2CH{=}CH_2$-1,2-*closo*-$C_2B_{10}H_{10}$ and the Preparation of Carboranyl-Containing Silsesquioxanes 13 and 14 by the Hydrolytic and the Nonhydrolytic Methods

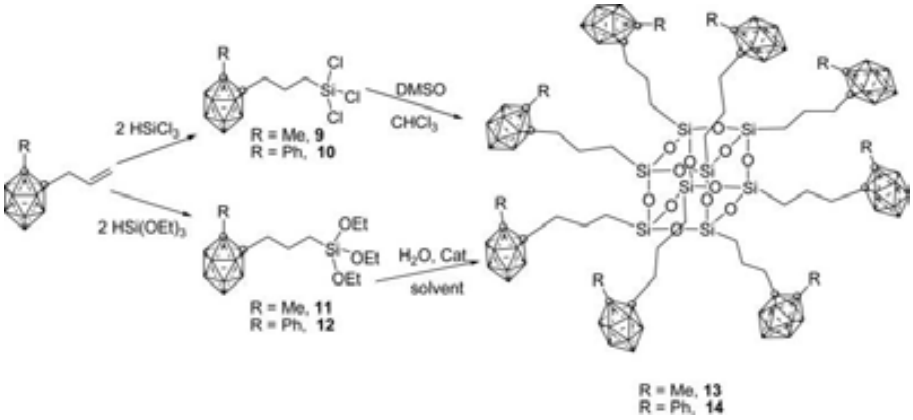

Scheme 4. Chemical Transformation of Carboranyldisiloxanes 3 and 4 Leading to Dianionic Species $[15]^{2-}$ and $[16]^{2-}$

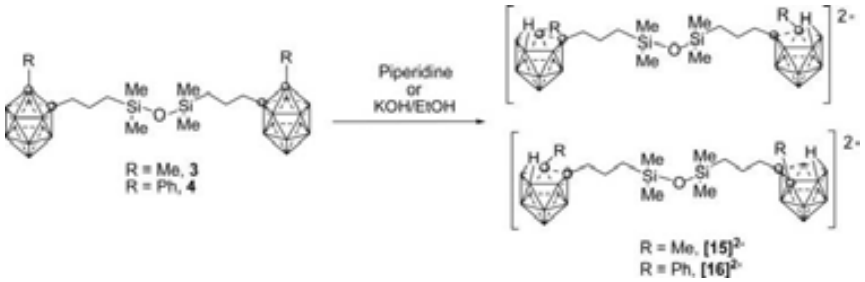

Scheme 5. Chemical Transformation of *closo*-Carboranylsilsesquioxane 13 Leading to the Octaanionic Species $[17]^{8-}$

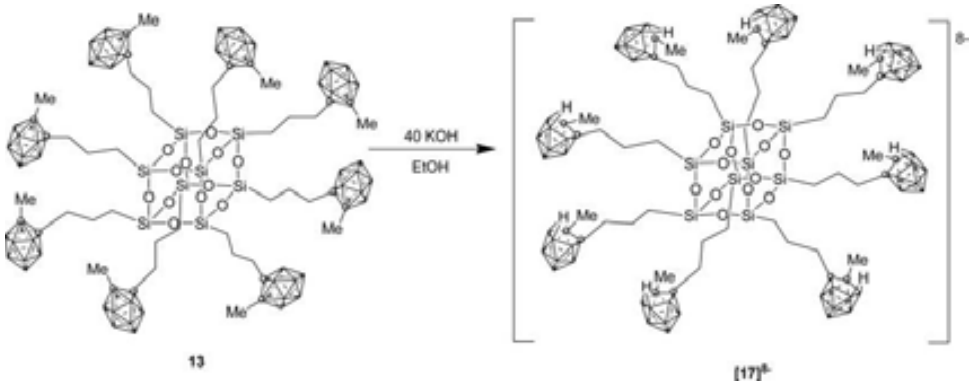

deboronated to obtain the dianionic species, quite the opposite than for dicarboranylthioether (2-CH_3-1,2-*closo*-$C_2B_{10}H_{10})_2S$ in which the monoanionic sulfur bridge anion [(2-CH_3-1,2-*closo*-$C_2B_{10}H_{10})S$(8-CH_3-7,8-*nido*-$C_2B_9H_{10})]^-$ was formed. Dianions $[\mathbf{15}]^{2-}$ and $[\mathbf{16}]^{2-}$ were isolated as $[N(CH_3)_4]^+$ salts by precipitation with a solution of $[N(CH_3)_4]Cl$.

Likewise, the chemical modification of T_8 cage **13**, using EtO^- as nucleophile, was also achieved using KOH with the same carboranyl/KOH ratio as used for the carboranyldisiloxanes, getting the octaanionic species $[\mathbf{17}]^{8-}$ (Scheme 5).

Characterization of Compounds. The structures of compounds **3**−$[\mathbf{17}]^{8-}$ were established on the basis of FT-IR, ^1H, ^{11}B, ^{13}C, and ^{29}Si NMR spectroscopy, MALDI-TOF and ESI mass spectrometry in some cases and the structure of **3** was also confirmed by X-ray diffraction analysis. The IR spectra of compounds containing *closo* clusters present the typical υ(B−H) strong bands around 2584 cm^{-1}, whereas for anionic species the υ(B−H) appears at 2515 cm^{-1}, due to the presence of *nido* clusters. In compounds **3**, **4**, **7**, and **8**, bands near 1256 cm^{-1} corresponding to $\delta(Si{-}CH_3)$ and characteristic bands between 1065 and 1072 cm^{-1} due to the vibration frequency of the Si−O bond are presented. In octasilsesquioxanes **13** and **14**, the absorption on this vibration is shifted to 1103−1119 cm^{-1}. The ^1H NMR spectra of the methyl-carborane exhibit resonances around 2.02 ppm attributed to the C_c-CH_3 protons, whereas the phenyl-carborane derivatives show signals in the 7.68−7.36 ppm due to phenyl protons. Resonances for protons of the propyl chain -$(CH_2)_3$-, in the region 2.23−0.24 ppm, have been unambiguously assigned in most cases. As can be appreciated, in the phenyl-carborane derivatives, -$(CH_2)_3$- proton resonances are shifted to a higher field with respect to methyl-carborane derivatives, probably due to the electronic ring effect caused

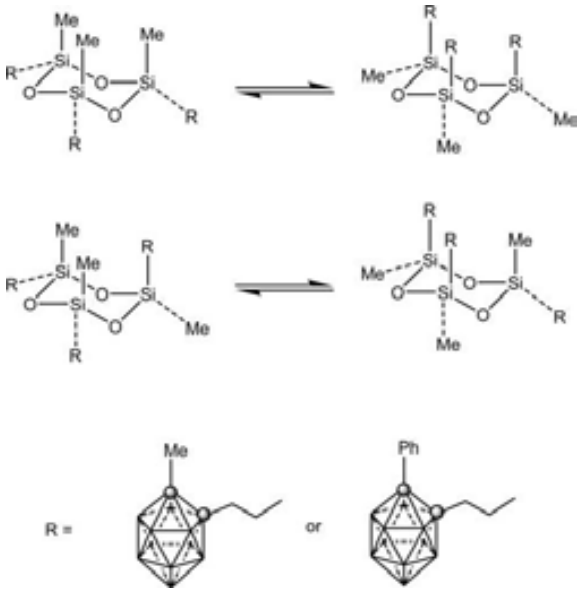

Figure 1. Different isomers for cyclotrisiloxanes D3.

by the phenyl group.[28] It has been reported that in carboranyl derivatives, when hydrogen atoms are placed on the top of the phenyl ring, a displacement to a high field is observed in the ^{1}H NMR spectrum.[9a,28b] The same effect was observed in anionic species, in which methylene protons appear in the region 1.68 to 0.46 ppm for [**15**]$^{2-}$ and [**17**]$^{8-}$, whereas [**16**]$^{2-}$ appears between 1.24 and −0.04 ppm. Another important point of the ^{1}H NMR spectra of compounds **3**−**8** is the resonances for Si−C*H*$_3$ protons from 0.07 to −0.18 ppm. For the mixture, the signals are difficult to assign due to the presence of chains and isomers of cycles D_3 and D_4, in which the methyl groups can be distributed in axial or equatorial positions, such as shown in Figure 1 for D_3. Indeed, for D_3 and D_4, the Si−CH$_3$ signals in the ^{1}H NMR appear as a set of three resonances. A tentative attribution is given in the experimental part and is based on the ^{1}H NMR integration supported by the MALDI-TOF data. For anionic compounds, the signal of the B−H−B bridge was unambiguously characterized by ^{1}H{^{11}B} NMR spectra, which appears between −2.60 and −2.19 ppm. The ^{13}C{^{1}H} NMR spectra for phenyl-*o*-carborane derivatives show resonances around 83.0 and 81.1 ppm attributed to the C_c atoms and additional resonances between 131 and 127 ppm due to phenyl carbon atoms. For methyl-*o*-carborane derivatives, the resonances attributed to the C_c atoms appear at higher fields, between 78.7 and 74.6 ppm, and CH$_3$ groups bonded to the cluster at 22−23 ppm. The Si-*C*H$_3$ carbon resonances appear at 0.4 and 0.2 ppm in the ^{13}C{^{1}H} NMR spectra. The ^{11}B{^{1}H} NMR resonances for **3**, **4**, **7**, **8**, **9**, and **10** appear in the *closo* region,[29] from δ −2.6 to −9.9 ppm, signals appearing in these cases with the following patterns 1:1:8 and 2:8, in general. Conversely, the ^{11}B resonances of anionic compounds appear between −5.9 and −36.3 ppm due to the presence of *nido*-carboranes with patterns 1:2:4:1:1 or 1:1:1:2:1:1:1 (see Figure 2).

The ^{29}Si{^{1}H} NMR spectra of both disiloxanes **3** and **4** exhibit a single signal around 6.7 ppm. In agreement with the previous literature, the trichlorosilanes precursors **9** and **10** show resonances at 11.5 and 11.3 ppm, respectively, whereas the triethoxysilanes precursors **11** and **12** show resonances at higher fields, around −46.5 ppm. The ^{29}Si CP MAS spectrum for **13** and **14** show a resonance at −66.0 ppm, which confirmed the formation of T_8 cages. The presence of *nido* carborane clusters in compounds [**15**]$^{2-}$, [**16**]$^{2-}$, and [**17**]$^{8-}$ did not affect the ^{29}Si

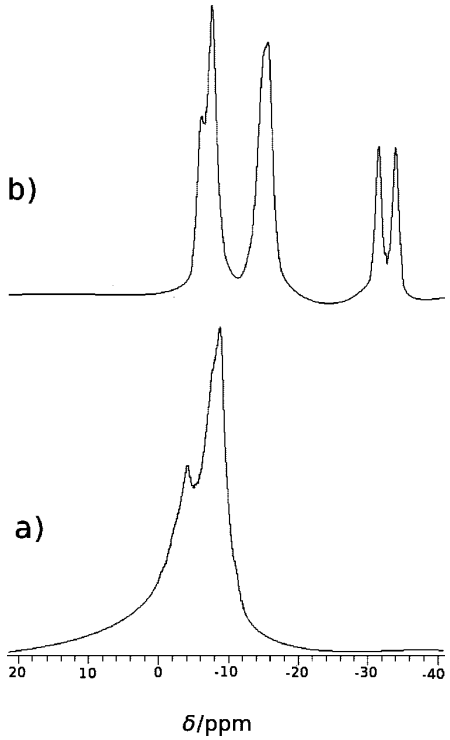

Figure 2. ^{11}B NMR spectra for (a) **13** and (b) [**17**]$^{8-}$.

NMR chemical shifts with respect to their respective precursors **3**, **4**, and **13**. No influence on the ^{29}Si{^{1}H} NMR chemical shifts for related *closo* and *nido* compounds (**3** and [**15**]$^{2-}$; **4** and [**16**]$^{2-}$; **13** and [**17**$^{8-}$) was observed. Finally, as was remarked previously, for T_8 cages, only one signal was observed at −66 ppm, in agreement with the range for common octasilsesquioxanes.[25]

The molecular formula of disiloxanes and cyclosiloxanes was confirmed by using the MALDI-TOF mass spectrometry in the negative-ion mode without matrix. For all cases, a full agreement between the experimental and calculated patterns was also obtained for the molecular ion peaks. The MALDI-TOF mass spectrum of **3** indicated that the molecular ion peak appears at m/z = 529.68, with a perfect concordance with the calculated pattern. For **7**, two molecular ion peaks at m/z = 776.34 and 1034.81, corresponding to the respective D_3 and D_4, indicated the presence of both cyclosiloxanes in the solid. In addition, an elevated number of molecular peaks corresponding to different fragments were also found, which was higher when the hydrolytic process was used.

Crystal Structure of 3. The molecular structure of **3** is shown in Figure 3. Molecule **3** is located around a crystallographic inversion center, which means that the oxygen atom (O1) is disordered in two positions in the vicinity of the inversion center, and also, each Si, C17, and C18 atom occupies two neighboring positions (a and b) leading to nonlinear Si−O−Si angles of about 166° (see Figure 3, only the a form is shown). If the structure was more ordered, the central oxygen atom would occupy the center of inversion thus leading to a linear Si−O−Si angle.

The Si−O−Si angle of 166° that is measured here is in the range of that recently reported for 40 acyclic disiloxanes varying from 140 to 180°, with no clear reason for this variation.[30]

The quality of the crystal and the structural disorder that results does not allow for deeper discussion of the bonding

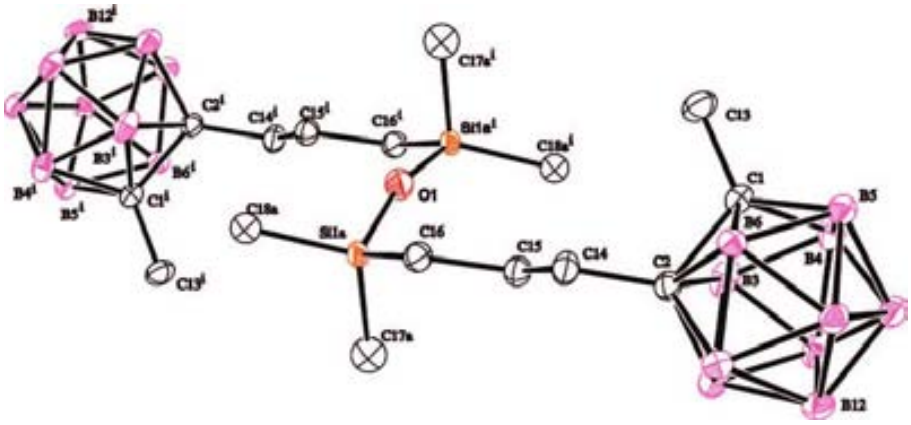

Figure 3. Molecular structure of [1-CH_3-2-$CH_2CH_2CH_2(CH_3)_2$Si-1,2-*closo*-$C_2B_{10}H_{10}]_2O$ (**3**).

parameters. However, the bonding parameters in the boron cage are quite usual. This is exemplified by the C1−C2 bond of 1.664(7) Å, which is quite a normal C−C bond in this type of the boron cages.

Conclusions

The present results have demonstrated the possibility to combine easily in the same molecule a carboranyl substructure with the Si−O−Si linkage of either a cyclic siloxane or a cage-like structure of polysilsesquioxane. Moreover, we point out the efficiency of the nonhydrolytic route with DMSO, which is particularly attractive for limiting the formation of linear oligo-polysiloxane. Finally, in all the cases, the Si−O−Si bond is chemically stable enough to allow the specific and clean partial degradation of the carboranyl group. The polyanionic species that results from this transformation could be further tested for silicon or ionic liquid applications.

Experimental Section

Instrumentation. Microanalyses were performed in the analytical laboratory using a Carlo Erba EA1108 microanalyser. IR spectra were recorded with KBr pellets or NaCl on a Shimadzu FTIR-8300 spectrophotometer. The electrospray-ionization mass spectra (ESI-MS) were recorded on a Bruker Esquire 3000 spectrometer using a source of ionization and an ions trap analyzer. The MALDI-TOF-MS mass spectra were recorded in the negative ion mode using a Bruker Biflex MALDI-TOF [N_2 laser; λ_{exc} 337 nm (0.5 ns pulses); voltage ion source 20.00 kV (Uis1) and 17.50 kV (Uis2)]. The ^{1}H,^{1}H{^{11}B} NMR (300.13 MHz), ^{11}B, ^{11}B{^{1}H} NMR (96.29 MHz), ^{13}C{^{1}H} NMR (75.47 MHz), and ^{29}Si NMR (59.62 MHz) spectra were recorded on a Bruker ARX 300 spectrometer equipped with the appropriate decoupling accessories at room temperature. ^{29}Si CP MAS NMR (at 79.49 MHz) spectra were obtained on a Bruker Advance ASX400 using a CP MAS sequence. All NMR spectra were recorded in $CDCl_3$ or CD_3COCD_3 solutions at 22 °C. Chemical shift values for ^{11}B NMR spectra were referenced to external $BF_3 \cdot OEt_2$, and those for ^{1}H, ^{1}H{^{11}B}, ^{13}C{^{1}H}NMR and ^{29}Si NMR spectra were referenced to $SiMe_4$. Chemical shifts are reported in units of parts per million downfield from reference, and all coupling constants are reported in Hertz.

Materials. All manipulations were carried out under a dinitrogen atmosphere using standard Schlenck techniques at room temperature otherwise it is mentioned. Solvents were reagent grade and were purified by distillation from appropriate drying agents before using. 1-CH_3-1,2-*closo*-$C_2B_{10}H_{11}$ and 1-C_6H_5-1,2-*closo*-$C_2B_{10}H_{11}$ were supplied by Katchem Ltd. (Prague) and used as received. Karstedt's catalyst (platinum−divinyltetramethyldisiloxane complex, 2.1−2.4% platinum in vinyl-terminated polydimethylsiloxane in xylene solution), $HSiCl_3$, and $HSi(OCH_2CH_3)_3$ were purchased from ABCR and used as received. Compound [$Si(CH{=}CH_2)_4$] was purchased from Acros. The *n*-BuLi solution (1.6 M in hexanes) and $H(CH_3)SiCl_2$ were purchased from Aldrich. The TBAF solution (1 M in THF) and NaOH were purchased from Aldrich and used as received. 1-(C_6H_5)-2-$CH_2CH{=}CH_2$-1,2-*closo*-$C_2B_{10}H_{10}$, 1-(CH_3)-2-$CH_2CH{=}CH_2$-1,2-*closo*-$C_2B_{10}H_{10}$, 1-(C_6H_5)-2-[$CH_2CH_2CH_2(CH_3)_2$SiCl]-1,2-*closo*-$C_2B_{10}H_{10}$ and 1-(CH_3)-2-[$CH_2CH_2CH_2Si(CH_3)_2$Cl]-1,2-*closo*-$C_2B_{10}H_{10}$ were prepared according to the literature.[9c] Silica SDS 60 with 35−70 μm and 550 m^2g^{-1} was used for column chromatography.

Preparation of [1-CH_3-2-$CH_2CH_2CH_2(CH_3)_2$Si-1,2-*closo*-$C_2B_{10}H_{10}]_2O$ (3). *Method A.* To a round-bottom flask containing 1-(CH_3)-2-$CH_2CH_2CH_2(CH_3)_2$SiCl-1,2-*closo*-$C_2B_{10}H_{10}$ (0.28 g, 0.95 mmol), 0.05 mL (2.7 mmol) of H_2O, and 5 mL of dried Et_2O were added. The mixture was stirred over a period of 10 min, transferred to a separatory funnel, and extracted. The organic layer was dried over $MgSO_4$ and concentrated in vacuum to obtain **3** as a white waxy solid. Yield: 0.18 g, 72%.

Method B. In a Schlenk flask, 1-(CH_3)-2-$CH_2CH_2CH_2((CH_3))_2$SiCl-1,2-*closo*-$C_2B_{10}H_{10}$ (0.28 g, 0.95 mmol), $(CH_3)_2SO$ (0.3 mL, 4.22 mmol), and 4 mL of $CHCl_3$ were mixed and stirred overnight. The mixture was then quenched with 8 mL of H_2O and transferred to a separatory funnel. The organic layer was washed with water (2 × 8 mL), dried over $MgSO_4$, and concentrated in vacuum to obtain **3** as a white waxy solid. Yield: 0.10 g, 40%. Hexane vapor diffusion into $CHCl_3$ solution of **3** gave single crystals for X-ray analysis. ^{1}H NMR δ 2.20 (t, $^3J_{(H,H)}$ = 8.5, 4H, C_c-CH_2), 2.02 (s, 6H, C_c-CH_3), 1.59 (m. 4H, $CH_2CH_2CH_2$), 0.54 (t, $^3J_{(H,H)}$ = 8.5, 4H, CH_2-Si), 0.10 (s, 12H, Si−CH_3). ^{1}H{^{11}B} NMR δ 2.20 (t, $^3J_{(H,H)}$ = 8.5, 4H, C_c-CH_2), 2.25, 2.21, 2.15, 2.11 (br s, B-*H*), 2.02 (s, 6H, C_c-CH_3), 1.59 (m, 4H, $CH_2CH_2CH_2$), 0.54 (t, $^3J_{(H,H)}$ = 8.5, 4H, CH_2-Si), 0.10 (s, 12H, Si−CH_3). ^{11}B NMR δ −3.9 (d, $^1J_{(B,H)}$ = 123, 2B), −5.0 (d, $^1J_{(B,H)}$ = 141, 2B), −9.9 (d, $^1J_{(B,H)}$ = 132, 16B). ^{13}C{^{1}H} NMR δ 78.0 (C_c), 74.6 (C_c), 38.7 (CH_2), 23.7 CH_2 or C_c-CH_3), 23.1 (CH_2 or C_c-CH_3), 18.2 (Si-CH_2), 0.4 (Si-CH_3). ^{29}Si{^{1}H} NMR δ 6.9. FTIR (KBr), cm^{-1}: 2954−2878 (ν (C_{alkyl}-H)), 2584 (ν (B−H)), 1256 (ν (Si-CH_3)), 1076 (ν (Si−O)). Anal. Calcd for $C_{16}H_{50}B_{20}Si_2O$: C, 36.19; H, 9.49. Found: C, 36.27; H 9.58. MALDI-TOF-MS (*m*/*z*): calcd, 530.97; found, 529.68 [M − 1]$^-$.

Preparation of [1-C_6H_5-2-$CH_2CH_2CH_2(CH_3)_2$Si-1,2-*closo*-$C_2B_{10}H_{10}]_2O$ (4). To a round-bottom flask containing 1-(C_6H_5)-2-$CH_2CH_2CH_2(CH_3)_2$SiCl-1,2-*closo*-$C_2B_{10}H_{10}$ (0.28 g, 0.80 mmol), 3 mL of dried Et_2O, and 13 μL (0.81 mmol) of H_2O were added. The mixture was stirred over a period of 10 min and transferred to a separatory funnel. The organic layer was washed with H_2O (2 × 5 mL) and the aqueous layer was washed with Et_2O (3 × 5 mL). Then the organic layer was dried over $MgSO_4$ and concentrated in vacuum to obtain compound **4** as a yellowish oil. Yield: 0.21 g, 81%. ^{1}H NMR δ 7.66−7.40 (m, 10H, C_6H_5), 1.77 (t, $^3J_{(H,H)}$ = 8.1,

4H, C_c-CH_2), 1.38 (m, 4H, $CH_2CH_2CH_2$), 0.24 (t, $^3J_{(H,H)}$ = 8.5, 4H, CH_2-Si), −0.08 (s, 12H, Si−CH_3). ^{1}H{^{11}B} NMR δ 7.66−7.40 (m, 10H, C_6H_5), 2.73 (br s, 4H, B-*H*), 2.37 (br s, 12H, B-*H*), 2.27 (br s, 4H, B-*H*), 1.77 t, $^3J_{(H,H)}$ = 8.1, 4H, C_c-CH_2), 1.38 (m, 4H, $CH_2CH_2CH_2$), 0.24 (t, $^3J_{(H,H)}$ = 8.5, 4H, CH_2-Si), −0.08 (s, 12H, Si−CH_3). ^{11}B NMR δ −2.7 (d, $^1J_{(B,H)}$ = 133, 4B), −9.5 (br s, 16B). ^{13}C{^{1}H} NMR δ 131.1, 130.8, 130.6, 128.9 (C_6H_5), 83.4 (C_c), 82.3 (C_c), 38.3 (CH_2), 23.5 (CH_2), 17.9 (CH_2), 0.19 (Si-CH_3). ^{29}Si{^{1}H} NMR δ 6.6. FTIR (NaCl, cm^{-1}) 3063 (ν (C_{aryl}-H)), 2955−2893 (ν (C_{alkyl}-H)), 2584 (ν (B−H)), 1257 (δ (Si-CH_3)), 1065 (ν (Si−O)). MALDI-TOF-MS (*m*/*z*) calcd, 655.12; found, 654.42 [M − 1]$^-$.

Preparation of 1-CH_3-2-$CH_2CH_2CH_2(CH_3)SiCl_2$-1,2-*closo*-$C_2B_{10}H_{10}$ (5). In a Schlenk flask, 1-(CH_3)-2-CH_2CH=CH_2-1,2-*closo*-$C_2B_{10}H_{10}$ (0.21 g, 1.03 mmol), Karstedt catalyst (5 μL, 0.01 mmol), and H(CH_3)$SiCl_2$ (0.13 mL, 1.25 mmol) were mixed and stirred under dinitrogen for 5 h at room temperature. Evaporation of the excess of H(CH_3)$SiCl_2$ gave **5** as a yellow oil. Yield: 0.32 g, >90%. ^{1}H NMR δ 2.26 (t, $^3J_{(H,H)}$ = 8.7, 2H, C_c-CH_2), 2.02 (s, 3H, C_c-CH_3), 1.87 (m, 2H, $CH_2CH_2CH_2$), 1.39 (t, $^3J_{(H,H)}$ = 8.1, 2H, Si−CH_2), 0.81 (s, 3H, Si−CH_3). ^{1}H{^{11}B} NMR δ 2.26 (t, $^3J_{(H,H)}$ = 8.7, 2H, C_c-CH_2), 2.26, 2.18, 2.11 (br s, B-*H*), 2.02 (s, 3H, C_c-CH_3), 1.87 (m, 2H, $CH_2CH_2CH_2$), 1.39 (t, $^3J_{(H,H)}$ = 8.1, 2H, Si−CH_2), 0.81 (s, 3H, Si−CH_3). ^{11}B NMR δ −4.1 (d, $^1J_{(B,H)}$ = 140, 1B), −5.6 (d, $^1J_{(B,H)}$ = 143, 1B), −10.6 (d, $^1J_{(B,H)}$ = 135, 8B). ^{13}C{^{1}H} NMR δ 77.4 (C_c), 74.8 (C_c), 37.2 (CH_2), 23.1 (CH_2), 22.7 (C_c-CH_3), 20.9 (Si-CH_2), 5.1 (Si-CH_3). ^{29}Si{^{1}H} NMR δ 31.6.

Preparation of 1-C_6H_5-2-$CH_2CH_2CH_2(CH_3)SiCl_2$-1,2-*closo*-$C_2B_{10}H_{10}$ (6). In a Schlenk flask, 1-(C_6H_5)-2-CH_2CH=CH_2-1,2-$C_2B_{10}H_{10}$ (0.25 g, 0.95 mmol), H(CH_3)$SiCl_2$ (0.12 mL, 1.14 mmol), and Karstedt catalyst (5 μL, 0.01 mmol) were mixed and stirred under dinitrogen for 5 h at room temperature. Evaporation of the excess of H(CH_3)$SiCl_2$ gave **6** as a yellow oil. Yield: 0.34 g, >90%. ^{1}H NMR δ 7.68−7.36 (m, 5H, C_6H_5), 1.90 (t, $^3J_{(H,H)}$ = 7.2, 2H, C_c-CH_2), 1.65 (m, 2H, $CH_2CH_2CH_2$), 0.93 (t, $^3J_{(H,H)}$ = 8.1, 2H, Si−CH_2), 0.70 (s, 3H, Si−CH_3). ^{1}H{^{11}B} NMR δ 7.68−7.36 (m, 5H, C_6H_5), 2.78 (br s, 2H, B-*H*), 2.38 (br s, 6H, B-*H*), 2.32 (br s, 2H, B-*H*), 1.90 (t, $^3J_{(H,H)}$ = 7.2, 2H, C_c-CH_2), 1.65 (m, 2H, $CH_2CH_2CH_2$), 0.93 (t, $^3J_{(H,H)}$ = 8.1, 2H, Si−CH_2), 0.70 (s, 3H, Si−CH_3). ^{11}B NMR δ −3.5, (d, $^1J_{(B,H)}$ = 135, 2B), −10.3 (8B). ^{13}C{^{1}H} NMR δ 129.9, 129.0, 128.9, 127.5 (C_6H_5), 83.7 (C_c), 81.7 (C_c), 37.2 (CH_2), 22.6 (CH_2), 20.9 (Si-CH_2), 5.1 (Si-CH_3). ^{29}Si{^{1}H} NMR δ 31.4.

Preparation of [1-CH_3-2-$CH_2CH_2CH_2(CH_3)$Si-1,2-*closo*-$C_2B_{10}H_{10}$]O)$_n$ (n = 3−4) (7). *Method A.* To a round-bottom flask containing a solution of 1-(CH_3)-2-$CH_2CH_2CH_2(CH_3)SiCl_2$-1,2-*closo*-$C_2B_{10}H_{10}$ (0.32 g, 1.03 mmol) in 2.5 mL of dried Et_2O, 2.5 mL of H_2O were added dropwise with continuous vigorous stirring. After 30 min of reaction at room temperature, the mixture was transferred to a separatory funnel and the organic phase was extracted with H_2O (2 × 10 mL). The organic layer was dried over $MgSO_4$ and concentrated in vacuum to obtain a clear yellow oil. This oily residue was purified in a SiO_2 column chromatography of 15 cm length and 1.5 cm diameter. First, the oil was eluted with 250 mL of C_6H_{14} to remove Karstedt catalyst and minor impurities. After this, 250 mL of a mixture of C_6H_{14}/Et_2O (1:1) was used as eluent. The solvents were removed under reduced pressure to obtain 32 mg of **7** as a colorless oil.

Method B. To a Schlenk flask containing a vigorous stirring solution of 1-(CH_3)-2-$CH_2CH_2CH_2(CH_3)SiCl_2$-1,2-*closo*-$C_2B_{10}H_{10}$ (0.32 g, 1.03 mmol) in 2.5 mL of dried Et_2O, 0.1 mL (1.41 mmol) of dried $(CH_3)_2SO$ was added dropwise. The mixture was stirred over 2 h at room temperature. Then, the mixture was quenched with 10 mL of H_2O, transferred to a separatory funnel and the organic layer was washed with brine (2 × 10 mL). The organic phase was dried over $MgSO_4$ and concentrated in vacuum to obtain a yellow oil. After that, the purification workup was the same than in Method A to give 45 mg of **7** as a colorless oil. ^{1}H NMR (from Method A) δ 2.19 (t, $^3J_{(H,H)}$ = 8.5, 2H, C_c-CH_2), 2.01 (s, 3H, C_c-CH_3), 1.62 (m. 2H, $CH_2CH_2CH_2$), 0.60 (m, 2H, CH_2-Si), 0.21 (m, 1H, Si−CH_3, D3), 0.17 (s, 0.8H, Si−CH_3, linear siloxanes L), 0.14 (m, 1.2H, Si−CH_3, D4). ^{1}H{^{11}B} NMR (from Method A) δ 2.32, 2.25, 2.17, 2.10 (br s, B-*H*), 2.19 (t, $^3J_{(H,H)}$ = 8.5, 2H, C_c-CH_2), 2.01 (s, 3H, C_c-CH_3), 1.62 (m. 2H, $CH_2CH_2CH_2$), 0.60 (m, 2H, CH_2-Si), 0.21 (m, 1H, Si−CH_3, D3), 0.17 (s, 0.8H, Si−CH_3, linear siloxanes L), 0.14 (m, 1.2H, Si−CH_3, D4). ^{1}H NMR (from Method B) δ 2.19 (t, $^3J_{(H,H)}$ = 8.5, 2H, C_c-CH_2), 2.01 (s, 3H, C_c-CH_3), 1.63 (m. 2H, $CH_2CH_2CH_2$), 0.60 (m, 2H, CH_2-Si), 0.21 (m, 1.5H, Si−CH_3, D3), 0.14 (m, 1.5H, Si−CH_3, D4). ^{1}H{^{11}B} NMR (from Method B) δ 2.32, 2.25, 2.17, 2.10 (br s, B-*H*), 2.19 (t, $^3J_{(H,H)}$ = 8.5, 2H, C_c-CH_2), 2.01 (s, 3H, C_c-CH_3), 1.63 (m. 2H, $CH_2CH_2CH_2$), 0.60 (m, 2H, CH_2-Si), 0.21 (m, 1.5H, Si−CH_3, D3), 0.14 (m, 1.5H, Si−CH_3, D4). ^{11}B NMR δ −4.4 (d, $^1J_{(B,H)}$ = 111, 2B), −5.7 (d, $^1J_{(B,H)}$ = 145, 2B), −10.6 (d, $^1J_{(B,H)}$ = 133, 16B). ^{13}C{^{1}H} NMR δ 77.85 (C_c), 74.8 (C_c), 38.5 (CH_2), 29.65 (CH_2), 26.52 (CH_2), 23.1 (C_c-CH_3), 16.9 (Si-CH_2), −0.5 (Si-CH_3). FTIR (NaCl, cm^{-1}) 2957−2878 (ν (C_{alkyl}-H)), 2590 (ν (B−H)), 1261 (ν (Si-CH_3)), 1072 (ν (Si−O)). MALDI-TOF-MS (*m*/*z*) calcd, 775.73 [D3]; found, 776.34 [D3]$^-$; calcd [D4], 1034.01; found, 1034.81 [D4]$^-$.

Synthesis of [1-(C_6H_5)-2-$CH_2CH_2CH_2(CH_3)$Si-1,2-*closo*-$C_2B_{10}H_{10}$]O)$_n$ (n = 3−4) (8). *Method A.* To Schlenk flask containing a vigorous stirring solution of 1-(C_6H_5)-2-$CH_2CH_2CH_2(CH_3)SiCl_2$-1,2-closo-$C_2B_{10}H_{10}$ (0.31 g, 0.84 mmol) in 2.0 mL of dried diethyl ether, 2.0 mL of water was added drop by drop. The procedure was the same as for **7** using Method A to give 35 mg of **8** as a colorless oil.

Method B. To a Schlenk flask containing a vigorous stirring solution of 1-C_6H_5-2-$CH_2CH_2CH_2(CH_3)SiCl_2$-1,2-*closo*-$C_2B_{10}H_{10}$ (353 mg, 0.94 mmol) in 2.5 mL of dried diethyl ether, 0.1 mL (1.41 mmol) of dry DMSO was added dropwise. The mixture was stirred over 2 h at room temperature. The procedure was the same as for **7** using the Method B to obtain 33 mg of **8** as a colorless oil. ^{1}H NMR (from Method A) δ 7.63−7.37 (m, 5H, C_6H_5), 1.77 (t, $^3J_{(H,H)}$ = 8.4, 2H, C_c-CH_2), 1.43 (m, 2H, $CH_2CH_2CH_2$), 0.31 (t, $^3J_{(H,H)}$ = 8.4, 2H, CH_2-Si), 0.06 (m, 2H, Si−CH_3, linear siloxanes L), −0.04 (m, 0.6H, Si−CH_3, D3), −0.08 (m, 0.4H, Si−CH_3, D4). ^{1}H{^{11}B} NMR (from Method A) δ 7.63−7.37 (m, 5H, C_6H_5), 2.70, 2.37, 2.32, 2.24 (br s, B-*H*), 1.77 (t, $^3J_{(H,H)}$ = 8.4, 2H, C_c-CH_2), 1.43 (m, 2H, $CH_2CH_2CH_2$), 0.31 (t, $^3J_{(H,H)}$ = 8.4, 2H, CH_2-Si), 0.06 (m, 2H, Si−CH_3, linear siloxanes L), −0.04 (m, 0.6H, Si−CH_3, D3), −0.08 (m, 0.4H, Si−CH_3, D4). ^{1}H NMR (from Method B) δ 7.63−7.37 (m, 5H, C_6H_5), 1.77 (t, $^3J_{(H,H)}$ = 8.4, 2H, C_c-CH_2), 1.43 (m, 2H, $CH_2CH_2CH_2$), 0.31 (t, $^3J_{(H,H)}$ = 8.4, 2H, CH_2-Si), 0.06 (m, 0.2H, Si−CH_3, linear siloxanes L), −0.04 (m, 1.5H, Si−CH_3, D3), −0.08 (m, 1.3H, Si−CH_3, D4). ^{1}H{^{11}B} NMR (from Method B) δ 7.63−7.37 (m, 5H, C_6H_5), 2.70, 2.37, 2.32, 2.24 (br s, B-*H*), 1.77 (t, $^3J_{(H,H)}$ = 8.4, 2H, C_c-CH_2), 1.43 (m, 2H, $CH_2CH_2CH_2$), 0.31 (t, $^3J_{(H,H)}$ = 8.4, 2H, $CH_2CH_2CH_2$), 0.06 (m, 2H, Si−CH_3, linear siloxanes L), −0.04 (m, 0.6H, Si−CH_3, D3), −0.08 (m, 0.4H, Si−CH_3, D4). ^{11}B NMR δ −3.5 (d, $^1J_{(B,H)}$ = 138, 4B), −10.2 (d, $^1J_{(B,H)}$ = 123, 16B). ^{13}C{^{1}H} NMR δ 131.1, 130.7, 130.6, 128.9 (C_6H_5), 83.5 (C_c), 82.1 (C_c), 38.0 (CH_2), 22.8 (CH_2), 16.8 (CH_2), 14.1 (CH_2), −0.7 (Si-CH_3). FTIR (NaCl, cm^{-1}) 3067 (ν (C_{aryl}-H)), 2957−2872 (ν (C_{alkyl}-H)), 2582 (ν (B−H)), 1261 (δ (Si-CH_3)), 1080 (ν (Si−O)). MALDI-TOF-MS (*m*/*z*) calcd, 961.86 [D3]; found, 962.8 [D3]$^-$; calcd, 1282.1 [D4]; found, 1016.45 [D4-{1-C_6H_5-2-$CH_2CH_2CH_2$-1,2-*closo*-$C_2B_{10}H_{10}$}]$^-$.

Synthesis of 1-(CH_3)-2-$CH_2CH_2CH_2SiCl_3$-1,2-*closo*-$C_2B_{10}H_{10}$ (9). In a Schlenk flask, 1-(CH_3)-2-CH_2CH=CH_2-1,2-*closo*-$C_2B_{10}H_{10}$ (0.21 g, 1.05 mmol), $HSiCl_3$ (0.21 mL, 2.10 mmol), and Karstedt catalyst (5 μL, 0.01 mmol) were mixed and stirred under dinitrogen for 5 h at room temperature. Evaporation of the excess of $HSiCl_3$ gave **9** as a yellow oil. Yield: 0.42 g, >99%. ^{1}H NMR δ 2.29 (t, $^3J_{(H,H)}$ = 8.1, 2H, C_c-CH_2), 2.02 (s, 3H, C_c-CH_3), 1.88 (m, 2H, $CH_2CH_2CH_2$), 1.45 (t, $^3J_{(H,H)}$ = 8.1, 2H, Si−CH_2). ^{1}H{^{11}B} NMR δ 2.26, 2.18 (br s, B-*H*), 2.02 (s, 3H, C_c-CH_3), 1.88 (m, 2H, $CH_2CH_2CH_2$), 1.45 (t, $^3J_{(H,H)}$ = 8.1, 2H, Si−CH_2). ^{11}B NMR δ −3.2 (d, $^1J_{(B,H)}$ = 141, 1B), −4.6 (d, $^1J_{(B,H)}$ = 146, 1B), −9.0 (8B). ^{13}C{^{1}H} NMR δ 76.8 (C_c), 74.7 (C_c), 36.8 (CH_2), 23.7 (CH_2), 23.2 (C_c-CH_3), 22.6 (Si-CH_2). ^{29}Si{^{1}H} NMR δ 11.5.

Synthesis of 1-(C_6H_5)-2-$CH_2CH_2CH_2SiCl_3$-1,2-*closo*-$C_2B_{10}H_{10}$ (10). In a Schlenk flask, 1-(C_6H_5)-2-CH_2CH=CH_2-1,2-*closo*-$C_2B_{10}H_{10}$ (0.21 g, 0.81 mmol), $HSiCl_3$ (0.17 mL, 1.60 mmol), and

Karstedt catalyst (5 μL, 0.01 mmol) were mixed and stirred under dinitrogen for 5 h at room temperature. Evaporation of the excess of $HSiCl_3$ gave **10** as a yellow oil. Yield: 0.32 g, >99%. ^{1}H NMR δ 7.67−7.42 (m, 5H, C_6H_5), 1.91 (t, $^3J_{(H,H)}$ = 8.2, 2H, C_c-CH_2), 1.70 (m, 2H, $CH_2CH_2CH_2$), 1.21 (t, $^3J_{(H,H)}$ = 8.1, 2H, Si−CH_2). ^{1}H{^{11}B} NMR δ 7.67−7.42 (m, 5H, C_6H_5), 2.74 (br s, 2H, B-*H*), 2.39 (br s, 6H, B-*H*), 2.28 (br s, 2H, B-*H*), 1.91 (t, $^3J_{(H,H)}$ = 8.2, 2H, C_c-CH_2), 1.70 (m, 2H, $CH_2CH_2CH_2$), 1.21 (t, $^3J_{(H,H)}$ = 8.1, 2H, Si−CH_2). ^{11}B NMR δ −2.6, (d, $^1J_{(B,H)}$ = 145, 2B), −9.4 (8B). ^{13}C{^{1}H} NMR δ 131.1, 130.8,130.5, 129.0 (C_6H_5), 83.6 (C_c), 81.1 (C_c), 36.5 (CH_2), 23.5 (CH_2), 22.3 (Si-CH_2). ^{29}Si{^{1}H} NMR 11.3.

Synthesis of 1-(CH_3)-2-$CH_2CH_2CH_2Si(OCH_2CH_3)_3$-1,2-*closo*-$C_2B_{10}H_{10}$ (11). In a Schlenk flask, 1-(CH_3)-2-CH_2CH=CH_2-1,2-*closo*-$C_2B_{10}H_{10}$ (0.80 g, 4.0 mmol), $HSi(OCH_2CH_3)_3$ (1.53 mL, 8.04 mmol), and Karstedt catalyst (10 μL, 0.02 mmol) were mixed and stirred under dinitrogen for 5 h at room temperature. Evaporation of the excess of $HSi(OCH_2CH_3)_3$ at 50 °C gave **11** as a brown oil. Yield: 1.46 g, >99%. ^{1}H NMR δ 3.83 (q, $^3J_{(H,H)}$ = 6.9, 6H, O−CH_2), 2.20 (t, $^3J_{(H,H)}$ = 8.1, 2H, C_c-CH_2), 2.01 (s, 3H, C_c-CH_3), 1.68 (quint, $^3J_{(H,H)}$ = 8.1, 6H, $CH_2CH_2CH_2$), 1.23 (t, $^3J_{(H,H)}$ = 6.9, 9H, CH_2−CH_3), 0.63 (t, $^3J_{(H,H)}$ = 8.1, 2H, $CH_2CH_2CH_2$). ^{1}H{^{11}B} NMR δ 3.83 (q, $^3J_{(H,H)}$ = 6.9, 6H, O−CH_2), 2.26, 2.18 (br s, B-*H*), 2.01 (s, 3H, C_c-CH_3), 1.68 (quint, $^3J_{(H,H)}$ = 8.1, 6H, $CH_2CH_2CH_2$), 1.23 (t, $^3J_{(H,H)}$ = 6.9, 9H, CH_2−CH_3), 0.63 (t, $^3J_{(H,H)}$ = 8.1, 2H, $CH_2CH_2CH_2$). ^{11}B NMR δ −3.2 (d, $^1J_{(B,H)}$ = 122, 1B), −4.63 (d, $^1J_{(B,H)}$ = 141, 1B), −9.2 (d, $^1J_{(B,H)}$ = 145, 8B). ^{13}C{^{1}H} NMR δ 78.7 (C_c), 75.0 (C_c). 58.9 (O-CH_2), 38.2 (CH_2), 23.7 (CH_2), 23.5 (C_c-CH_3), 18.5 (CH_2CH_3), 10.6 (Si-CH_2). ^{29}Si{^{1}H} NMR δ −46.6.

Synthesis of 1-(C_6H_5)-2-$CH_2CH_2CH_2Si(OCH_2CH_3)_3$-1,2-$C_2B_{10}H_{10}$ (12). In a Schlenk flask, 1-(C_6H_5)-2-CH_2CH=CH_2-1,2-*closo*-$C_2B_{10}H_{10}$ (0.16 g, 0.60 mmol), $HSi(OCH_2CH_3)_3$ (0.24 mL, 1.23 mmol), and Karstedt catalyst (5 μL, 0.01 mmol) were mixed and stirred under dinitrogen for 14 h at room temperature. Evaporation of the excess of $HSi(OCH_2CH_3)_3$ at 50 °C gave **12** as a brown oil. Yield: 0.26 g, >99%. ^{1}H NMR δ 7.62−7.39 (m, 5H, C_6H_5), 3.37 (q, $^3J_{(H,H)}$ = 6.9, 6H, O−CH_2), 1.83 (t, $^3J_{(H,H)}$ = 8.1, 2H, C_c-CH_2), 1.53 (m, 2H, $CH_2CH_2CH_2$), 1.20 (t, $^3J_{(H,H)}$ = 6.9, 9H, CH_2-CH_3), 0.40 (t, $^3J_{(H,H)}$ = 8.1, 2H, Si-CH_2). ^{1}H{^{11}B} NMR δ 7.62−7.39 (m, 5H, C_6H_5), 3.37 (q, $^3J_{(H,H)}$ = 6.9, 6H, O−CH_2), 2.73 (br s, 2H, B-*H*), 2.36 (br s, 6H, B-*H*), 2.25 (br s, 2H, B-*H*), 1.83 (t, $^3J_{(H,H)}$ = 8.1, 2H, C_c-CH_2), 1.53 (m, 2H, $CH_2CH_2CH_2$), 1.20 (t, $^3J_{(H,H)}$ = 6.9, 9H, CH_2-CH_3), 0.40 (t, $^3J_{(H,H)}$ = 8.1, 2H, Si-CH_2). ^{11}B NMR δ −2.6 (d, $^1J_{(B,H)}$ = 143, 2B), −9.4 (d, $^1J_{(B,H)}$ = 134, 8B). ^{13}C{^{1}H} NMR δ 131.1, 130.8, 130.5, 128.8 (C_6H_5), 83.4 (C_c), 82.4 (C_c), 58.3 (O-CH_2), 37.8 (CH_2), 23.1 (CH_2), 18.1 (CH_2-CH_3), 10.2 (Si-CH_2). ^{29}Si{^{1}H} NMR −46.2.

Synthesis of (1-(CH_3)-2-$CH_2CH_2CH_2SiO_{1.5}$-1,2-*closo*-$C_2B_{10}H_{10})_8$ (13). *Method A.* In a Schlenk flask, **9** (0.42 g, 1.05 mmol), 0.2 mL of $CHCl_3$, and DMSO (0.23 mL, 3.24 mmols) were mixed and stirred under dinitrogen for 48 h at room temperature. Then the mixture was washed with water (3 × 10 mL) and dried with $MgSO_4$. Evaporation of the solvent under reduced pressure gave an oily product. The addition of EtOH to the residue gave **13** as a white solid. Yield: 60 mg, 23%.

Method B. In a tube, 0.72 g (1.99 mmol) of **11** was dissolved in 993 μL of dried THF. After, 993 μL of a solution containing 19 μL (19 μmol) of TBAF (1 M in THF), 54 μL (2.98 mmol) of H_2O, and 920 μL of dried THF were added. The suspension was stirred for 10 s. After 133 days at room temperature, evaporation of volatiles gave a yellowish solid. This solid was washed with ethanol to isolate **11** as a white solid. Yield: 0.35 g, 70%.

Method C. In a tube, 0.53 g (1.46 mmol) of **11** was dissolved in 731 μL of dried THF. After, 731 μL of a solution containing 0.58 mg (0.015 mmol) of NaOH, 40 μL (3.95 mmol) of H_2O, and 691 μL of dried THF were added. Then the suspension was stirred for 10 s. After 180 days, evaporation of volatiles gave a yellowish solid. This solid was washed with ethanol to isolate **13** as a white solid. Yield: 0.20 g, 55%. ^{1}H NMR δ 2.23 (br s, 16H, C_c-CH_2), 2.03 (br s, 24H, C_c-CH_3), 1.70 (br s, 16H, $CH_2CH_2CH_2$), 0.74 (br s, 16H, $CH_2CH_2CH_2$). ^{11}B NMR δ −4.2 (16B), −8.9 (64B). ^{13}C{^{1}H} NMR δ 75.1 (C_c), 37.9 (CH_2), 23.2 (CH_2, C_c-CH_3), 12.6 (Si-CH_2). ^{29}Si CP MAS NMR δ −66.1. FTIR (KBr, cm^{-1}) 2939−2893 (ν (C_{alkyl}-H)), 2592 (ν (B−H)), 1119 (ν (Si−O)). Anal. Calcd for $C_{48}H_{152}B_{80}O_{12}Si_8$: C, 28.66; H, 7.62. Found: C, 28.77; H, 7.52. ESI-MS (*m*/*z*) calcd, 2033.0 (**13**)Na^+; found, 2033.8.

Synthesis of (1-(C_6H_5)-2-$CH_2CH_2CH_2SiO_{1.5}$-1,2-*closo*-$C_2B_{10}H_{10})_8$ (14). *Method A.* The procedure was the same as for **13** using **10** (0.31 g, 0.78 mmol), 0.2 mL of $CHCl_3$, and DMSO (0.17 mL, 2.39 mmol). The mixture was stirred under dinitrogren for 48 h at room temperature, washed with water (3 × 10 mL), and dried with $MgSO_4$. Evaporation of the solvent under reduced pressure gave an oily product. The addition of EtOH to the residue gave **14** as a white solid. Yield: 51.6 mg, 21%.

Method B. To a solution of **12** (0.26 g, 0.60 mmol) in $CHCl_3$ (10 mL) was added TBAF (0.3 mL, 0.30 mmol) and the mixture was stirred for 24 h. The mixture was transferred to a separatory funnel and the organic phase was extracted with H_2O (3 × 10 mL) for three days consecutively. The organic layer was dried over $MgSO_4$ and concentrated in vacuum to obtain **14** as a white solid. Yield: 53.7 mg, 28%. ^{1}H NMR δ 7.64−7.39 (m, 40H, C_6H_5), 1.75 (br s, 16H, C_c-CH_2), 1.43 (br s, 16H, $CH_2CH_2CH_2$), 0.36 (br s, 16H, $CH_2CH_2CH_2$). ^{1}H{^{11}B} NMR δ 7.64−7.39 (m, 40H, C_6H_5), 2.40 (br s, B-*H*), 2.27 (br s, B-*H*), 1.75 (br s, 16H, C_c-CH_2), 1.43 (br s, 16H, $CH_2CH_2CH_2$), 0.36 (br s, 16H, $CH_2CH_2CH_2$). ^{11}B NMR δ −2.0 (16B), −8.6 (64B). ^{13}C{^{1}H} NMR δ 131.1, 130.8,130.5, 129.0 (C_6H_5), 82.6 (C_c), 37.5 (CH_2), 23.5 (CH_2), 12.3 (Si-CH_2). ^{29}Si CP MAS NMR δ −66.0. FTIR (KBr, cm^{-1}) 3063 (ν (C_{aryl}-H)), 2939−2893 (ν (C_{alkyl}-H)), 2584 (ν (B−H)), 1103 (ν (Si−O)). Anal. Calcd for $C_{88}H_{168}B_{80}O_{12}Si_8$: C, 42.15; H, 6.75. Found: C, 41.76; H, 7.05.

Synthesis of $[N(CH_3)_4]_2$[(7-(CH_3)-8-$CH_2CH_2CH_2(CH_3)_2$Si-7,8-*nido*-$C_2B_9H_{10})_2O]$ $[N(CH_3)_4]_2$[15]. *Method A.* To a two-necked round-bottom flask containing a solution of **3** (42.6 mg, 0.08 mmol) in deoxygenated ethanol (4 mL) was added an excess of piperidine (0.08 mL, 0.80 mmol). The mixture was stirred and refluxed during 20 h. After this time, the solvent was removed and a white solid was isolated by precipitation after addition of saturated aqueous solution of $[N(CH_3)_4]Cl$. The solid is filtered off, washed with H_2O (3 × 10 mL), and dried under vacuum to obtain **15** as a white solid. Yield: 21.0 mg, 40%.

Method B. To a two-necked round-bottom flask containing a solution of KOH (0.13 g, 1.98 mmol) in deoxygenated EtOH (5 mL) was added **3** (0.10 g, 0.19 mmol). The mixture was stirred and refluxed during 6 h. After this time, the solvent was removed and a white solid was isolated by precipitation after addition of saturated aqueous $[N(CH_3)_4]Cl$ solution. The solid is filtered off, washed with H_2O (3 × 10 mL) and dried under vacuum to obtain $[N(CH_3)_4]_2$[**15**]. Yield: 55.3 mg, 44%. ^{1}H NMR (CD_3OCD_3) δ 3.43 (s, 24H, $N(CH_3)_4$), 1.64 (m, 8H, C_c-CH_2CH_2), 1.39 (br s, 6H, C_c-CH_3), 0.46 (t, $^3J_{(H,H)}$ = 8.4, 4H, $CH_2CH_2CH_2$), 0.07 (s, 6H, Si−CH_3), 0.04 (s, 6H, Si−CH_3), −2.60 (br s, 2H, B*H*B). ^{1}H{^{11}B} NMR δ 3.43 (s, 24H, $N(CH_3)_4$), 1.64 (m, 8H, C_c-CH_2CH_2), 1.39 (br s, 6H, C_c-CH_3), 0.46 (t, $^3J_{(H,H)}$ = 8.4, 4H, $CH_2CH_2CH_2$), 0.07 (s, 6H, Si−CH_3), 0.04 (s, 6H, Si−CH_3), −2.60 (br s, 2H, B*H*B). ^{11}B NMR δ −8.2 (d, $^1J_{(B,H)}$ = 157, 2B), −10.0 ($^1J_{(B,H)}$ = 151, 4B), −17.3 ($^1J_{(B,H)}$ = 122, 8B), −33.8 (dd,$^1J_{(B,H)}$ = 126, $^1J_{(B,H)}$ = 45, 2B), −36.3 ($^1J_{(B,H)}$ = 138, 2B). ^{13}C{^{1}H} NMR δ 55.2 ($N(CH_3)_4$). 40.2, 40.0 (CH_2), 24.4 (CH_2), 21.5 (C_c-CH_3), 18.9, 18.7 (CH_2), −0.1, −0.7 (Si-CH_3). ^{29}Si{^{1}H} NMR δ 6.7. FTIR (KBr, cm^{-1}) 2932−2870 (ν (C_{alkyl}-H)), 2515 (ν (B−H)), 1481 (ν (C−N)), 1250 (δ (Si-CH_3)), 1034 (ν (Si−O)). Anal. Calcd for $C_{24}H_{74}B_{18}N_2OSi_2$: C, 43.83; H, 11.34; N, 4.26. Found: C, 44.40; H, 11.83; N, 4.27. ESI-MS (*m*/*z*) calcd, 255.2, {[15]-$[N(CH_3)_4]_2$}$^{2-}$; found, 254.5.

Synthesis of $[N(CH_3)_4]_2$[(7-(C_6H_5)-$CH_2CH_2CH_2(CH_3)_2$Si-7,8-*nido*-$C_2B_9H_{10})_2O]$ $[N(CH_3)_4]_2$[16]. To a two-necked round-bottom flask containing a solution of KOH (0.12 g, 1.78 mmol) in deoxygenated ethanol (10 mL) was added **4** (0.12 g, 0.18 mmol). The mixture was stirred and refluxed during 14 h. After this time, the solvent was evaporated and a white solid was isolated by precipitation after addition of saturated aqueous $[N(CH_3)_4]Cl$ solution. The solid is filtered off, washed with water (3 × 15 mL) and dried under vacuum to obtain $[N(CH_3)_4]_2$[**16**]. Yield: 0.55 g,

40%. ^{1}H NMR (CD_3OCD_3) δ 7.30−7.03 (m, 10H, C_6H_5), 3.38 (s, 24H, $N(CH_3)_4$), 1.24 (m, 8H, C_c-CH_2CH_2), −0.04 (m, 4H, CH_2), −0.18 (s, 12H, Si-CH_3), −2.19 (br s, 2H, B*H*B). ^{1}H{^{11}B} NMR δ 7.30−7.03 (m, 10H, C_6H_5), 3.38 (s, 24H, $N(CH_3)_4$), 1.50 (br s, B-*H*), 1.24 (m, 8H, C_c-CH_2CH_2), 0.62 (br s, B-*H*), 0.18 (br s, B-*H*), −0.04 (m, 4H, CH_2), −0.18 (s, 12H, Si-CH_3), −2.19 (br s, 2H, B*H*B). ^{11}B NMR δ −5.9 (d, $^1J_{(B,H)}$ = 145, 2B), −8.1 (d, $^1J_{(B,H)}$ = 141, 2B), −10.9 (2B), −14.0 (d, $^1J_{(B,H)}$ = 156, 2B), −15.3 (d, $^1J_{(B,H)}$ =127, 4B), −16.4 (2B), −30.8 (d, $^1J_{(B,H)}$ = 131, 2B), −33.8 (d, $^1J_{(B,H)}$ = 144, 2B). ^{29}Si{^{1}H} NMR δ 6.9. FTIR (KBr), cm^{-1} 2930−2870 (ν (C_{alkyl}-H)), 2515 (ν (B-H)), 1481 (ν (C-N)), 1250 (δ (Si-CH_3)), 1034 (ν (Si-O)).

Synthesis of $[N(CH_3)_4]_8[7\text{-}(CH_3)\text{-}CH_2CH_2CH_2SiO_{1.5}\text{-}7,8\text{-}nido\text{-}C_2B_9H_{10}]_8$ $[N(CH_3)_4]_8$[17]. To a two-necked round-bottom flask containing a solution of KOH (0.13 g, 2.00 mmol) in deoxygenated ethanol (10 mL) was added a solution of **13** (0.10 g, 0.05 mmol) in 1 mL of THF. The mixture was refluxed during 6 h. Then, the volatiles were evaporated in the vacuum and an excess of $[N(CH_3)_4]Cl$ in water was added to obtain a white solid. This was filtered off, washed with water (3 × 10 mL), and dried under vacuum to obtain $[N(CH_3)_4]_8$[**17**] as a white solid. Yield: 52.6 mg, 42%. ^{1}H NMR (CD_3OCD_3) δ 3.43 (s, 96H, $[NCH_3]_4$), 1.68 (br s, 32H, C_c-$CH_2CH_2CH_2$), 1.47 (br s, 24H, C_c-CH_3), 0.63 (br s, 16H, $CH_2CH_2CH_2$). ^{1}H{^{11}B} NMR δ 3.43 (s, 96H, $[NCH_3]_4$), 1.68 (br s, 32H, C_c-$CH_2CH_2CH_2$), 1.47 (br s, 24H, C_c-CH_3), 0.63 (br s, 16H, $CH_2CH_2CH_2$), 0.50 (br s, B-*H*), 0.05 (br s, B-*H*), −2.57 (br s, 8H, B*H*B). ^{11}B NMR δ −6.8 (8B), −8.3 (16B), −16.3 (32B), −32.2 (dd, $^1J_{(B,H)}$ = 115, $^1J_{(B,H)}$ = 43, 8B), −34.6 (d, $^1J_{(B,H)}$ = 138, 8B). ^{13}C{^{1}H} NMR δ 61.6 (C_c), 55.4 ($[NCH_3]_4$), 39.4 (CH_2), 23.8 (CH_2), 21.8 (C_c-CH_3), 13.3 (Si-CH_2). ^{29}Si CP MAS NMR δ −66.2. FTIR (KBr, cm^{-1}) 2932−2893 (ν (C_{alkyl}-H)), 2515 (ν (B−H)), 1489 (ν (C−N)), 1111 (ν (Si−O)). Anal. Calcd for $C_{80}H_{248}B_{72}N_8O_{12}Si_8$: C, 38.16; H, 9.93; N, 4.45. Found: C, 37.62; H, 9.31; N, 3.99.

X-ray Structure Determination of 3. Hexane vapor diffusion of compound **3** into $CHCl_3$ solution gave crystalline material with the specimen formed of very thin plate-like sheets connected together. Single-crystal data collection for **3** was performed at −100° with an Enraf Nonius KappaCCD diffractometer using graphite monochromatized Mo Kα radiation. The structure was solved by direct methods and refined on F^2 by the SHELXL97 program.[31] The structure was refined in centrosymmetric space group $P2_1/c$ as also calculations in lower symmetry space groups resulted partial disordering for the central oxygen atom. The oxygen atom is disordered in two positions at the vicinity of inversion center, and also Si, C17, and C18 each occupies two neighboring positions. The disordered carbon atoms were refined with isotropic thermal displacement parameters but rest of the non-hydrogen atoms with anisotropic displacement parameters. The hydrogen atoms were treated as riding atoms using the SHELX97 default parameters.

Acknowledgment. This work has been supported by the CICYT (MAT2006-05339) and the Generalitat de Catalunya, 2005/SGR/00709. E.J.J.P. thanks MEC for a FPU Grant.

Supporting Information Available: Crystallographic data (CIF) for **3**. This material is available free of charge via the Internet at http://pubs.acs.org.

References and Notes

(1) (a) Grimes, R. N. In *Carboranes*; Academic Press: New York, 1970; p 54. (b) Hawthorne, M. F. In *Advances in Boron Chemistry*; The Royal Society of Chemistry: Cornwall, U.K., 1997; p 261. (c) Teixidor, F.; Viñas, C. In *Science of Synthesis, Houben-Weyl Methods of Molecular Transformations*; Kaufmann, D. E., Matteson, D. S. Eds.; Georg Thieme Verlag: Stuttgart-New York, 2005; Vol. 6, p 1235.

(2) (a) Bregadze, V. I. *Chem. Rev.* **1992**, *92*, 209. (b) Plesek, J. *Chem. Rev.* **1992**, *269*.

(3) (a) Kolel-Veetil, M. K.; Keller, T. M. *J. Polym. Sci.* **2006**, *44A*, 147. (b) González-Campo, A.; Núñez, R.; Viñas, C.; Boury, B. *New J. Chem.* **2006**, *30*, 546.

(4) (a) Teixidor, F.; Núñez, R.; Viñas, C.; Sillanpää, R.; Kivekäs, R. *Angew. Chem., Int. Ed.* **2000**, *39*, 4290. (b) Núñez, R.; Farrás, P.; Teixidor, F.; Viñas, C.; Sillanpää., R.; Kivekäs, R. *Angew. Chem., Int. Ed.* **2006**, *45*, 1270. (c) Núñez, R.; Teixidor, F.; Kivekäs, R.; Sillanpää, R.; Viñas, C. *Dalton Trans.* **2008**, 1471.

(5) (a) Cígler, P.; Kozísek, M.; Rezácová, P.; Brynda, J.; Otwinowski, Z.; Pokorná, J.; Plesek, J.; Grüner, B.; Doleckóvá-Maresová, L.; Mása, M. *Proc. Natl. Acad. Sci. U.S.A.* **2005**, *102*, 15394. (b) Julius, R.; Farha, O.; Chiang, J.; Perry, L.; Hawthorne, M. F. *Proc. Natl. Acad. Sci. U.S.A.* **2007**, *104*, 4808.

(6) (a) Hawthorne, M. F. In *Advances in Boron and the Boranes*; Liebman, J. F., Grenberg, A., Williams, R. S., Eds.; VCH: New York, 1988; p 225. (b) Teixidor, F.; Flores, M. A.; Viñas, C.; Kivekäs, R.; Sillanpää, R. *Angew. Chem., Int. Ed.* **1996**, *108*, 2388. (c) Felekidis, A.; Goblet-Stachow, M.; Liegeois, J. F.; Pirotte, B.; Delarge, J.; Demonceau, A.; Fontaine, M.; Nöels, A. F.; Chizvensky, I. T.; Zinevich, T. V.; Bregadze, V. I.; Dolgushin, F. M.; Yanovsky, A. I.; Struchkov, Y. T. *J. Organomet. Chem.* **1997**, *536/537*, 405. (d) Teixidor, F.; Flores, M. A.; Viñas, C.; Sillanpää, R.; Kivekäs, R. *J. Am. Chem. Soc.* **2000**, *122*, 1963. (e) Tutusaus, O.; Delfosse, S.; Demonceau, A.; Nöels, A. F.; Viñas, C.; Núñez, R.; Teixidor, F. *Tetrahedron Lett.* **2002**, *43*, 983. (f) Xie, Z. *Acc. Chem. Res.* **2003**, *36*, 1. (g) Tutusaus, O.; Viñas, C.; Núñez, R.; Teixidor, F.; Demonceau, A.; Delfosse, S.; Noels, A. F.; Mata, I.; Molins, E. *J. Am. Chem. Soc.* **2003**, *125*, 11830. (h) Lerouge, F.; Viñas, C.; Teixidor, F.; Núñez, R.; Abreu, A.; Xochitiotzi, E.; Santillán, R.; Farfán, N. *Dalton Trans.* **2007**, 1898.

(7) (a) Grüner, B.; Plesek, J.; Baca, J.; Cisarova, I.; Dozol, J.-F.; Rouquette, H.; Viñas, C.; Selucký, P.; Rais, J. *New J. Chem.* **2002**, *26*, 1519. (b) Hawthorne, M. F.; Maderna, A. *Chem. Rev.* **1999**, *99*, 3421. (c) Lu, S.-Y.; Hamerton, I. *Prog. Polym. Sci.* **2002**, *27*, 1661. (d) Masalles, C.; Borrós, S.; Viñas, C.; Teixidor, F. *Adv. Mater.* **2000**, *12*, 1199. (e) Masalles, C.; Llop, J.; Viñas, C.; Teixidor, F. *Adv. Mater.* **2002**, *14*, 826. (f) Gentil, S.; Crespo, E.; Rojo, I.; Friang, A.; Viñas, C.; Teixidor, F.; Grüner, B.; Gabel, D. *Polymer* **2005**, *46*, 12218.

(8) (a) King, R. B. *Chem. Rev.* **2001**, *101*, 1119. (b) Masalles, C.; Llop, J.; Viñs, C.; Teixidor, F.; Sillanpä, R.; Kivekäs, R. *Dalton Trans.* **2003**, 556. (c) Yao, H.; Sabat, M.; Grimes, R. N.; de Biani, F. F.; Zanello, P. *Angew. Chem., Int. Ed.* **2003**, *42*, 1002.

(9) (a) Núñez, R.; González, A.; Viñas, C.; Teixidor, F.; Sillanpää, R.; Kivekäs, R. *Org. Lett.* **2005**, *7*, 231. (b) Núñez, R.; González-Campo, A.; Viñas, C.; Teixidor, F.; Sillanpää, R.; Kivekäs, R. *Organometallics* **2005**, *24*, 6351. (c) González-Campo, A.; Viñas, C.; Teixidor, F.; Núñez, R.; Sillanpää, R.; Kivekäs, R. *Macromolecules* **2007**, *40*, 5644.

(10) Valliant, J. F.; Guenther, K. J.; King, A. S.; Morel, P.; Schaffer, P.; Sogbein, O. O.; Stephenson, K. A. *Coord. Chem. Rev.* **2002**, *232*, 173.

(11) González-Campo, A.; Núñez, R.; Teixidor, F.; Boury, B. *Chem. Mater.* **2006**, *18*, 4344.

(12) (a) Feher, F. J.; Wyndham, K. D. *Chem. Commun.* **1998**, 323. (b) Zhang, C.; Bunning, T. J.; Laine, R. M. *Chem. Mater.* **2001**, *13*, 3653. (c) Neumann, D.; Fisher, M.; Tran, M.; Matisons, J. G. *J. Am. Chem. Soc.* **2002**, *124*, 13998. (d) Constable, G. S.; Lesser, A. J.; Coughlin, B. *Macromolecules* **2004**, *37*, 1276. (e) Baker, E. S.; Gidden, J.; Anderson, S. E.; Haddad, T. S.; Bowers, M. T. *Nano Lett.* **2004**, *4*, 779. (f) Laine, R. M. *J. Mater. Chem.* **2005**, *15*, 3725. (g) Blanc, F.; Copéret, C.; Thivolle-Cazat, J.; Basset, J.-M.; Lesage, A.; Emsley, L.; Sinha, A.; Schrock, R. R. *Angew. Chem., Int. Ed.* **2006**, *45*, 1216.

(13) Kanna, R. Y.; Salacinski, H. J.; Butler, P. E.; Seifalian, A. M. *Acc. Chem. Res.* **2005**, *38*, 879.

(14) Frankamp, B. L.; Fischer, N. O.; Hong, R.; Srivastava, S.; Rotello, V. M. *Chem. Mater.* **2006**, *18*, 956.

(15) (a) Lichtenhan, J. D. In *Polymeric Materials Encyclopedia*; Salamone, J. C., Ed.; CRC Press: New York, 1996; p 7769. (b) Li, G. Z.; Pittman, C. U. In *Macromolecules Containing Metals and Metal-like Elements*; Abd El Aziz, A. S., Carraher, C. E., Pitman, C. E., Zeldin, M., Eds.; John Wiley & Sons: Hoboken, NJ, 2005; Vol. 5, Chapter 5, p 79.

(16) Dvornic, P. R.; Hartmann-Thompson, C. H.; Keinath, S. E.; Hill, E. J. *Macromolecules* **2004**, *37*, 7818.

(17) (a) Casado, C. M.; Cuadrado, I.; Morán, M.; Alonso, B.; Barranco, M.; Losada, *J. Appl. Organomet. Chem.* **1999**, *13*, 245. (b) Lang, H.; Lühmann, B. *Adv. Mater.* **2001**, *13*, 1523.

(18) (a) Bassindale, A. R.; Mackinnon, I. A.; Maesano, M. G.; Taylor, P. G. *Chem. Commun.* **2003**, 1382. (b) BrookM. A. In *Silicon in Organic, Organometallic, and Polymer Chemistry*; John Wiley & Sons, Inc.: New York, 2000; p 256. (c) Le Roux, C.; Yang, H.; Wenzel, S.; Brook, M. A. *Organometallics* **1998**, *17*, 556. (d) Lu, P.; Paulasaari, J. K.; Weber, W. P. *Organometallics* **1996**, *15*, 4649. (e) Arkhireeva, A.; Hay, J. N.; Manzano, M. *Chem. Mater.* **2005**, *17*, 875.

(19) (a) Rubinsztajn, S.; Cella, J. A. *Macromolecules* **2005**, *38*, 1061. (b) Chojnowski, J.; Rubinsztajn, S.; Cella, J. A.; Fortuniak, W.; Cypryk, M.; Kurjata, J.; Kazmierski, K. *Organometallics* **2005**, *24*, 6077. (c) Zhou, D.; Yusuke, K. *Macromolecules* **2005**, *38*, 6902. (d) Chojnowski, J.; Rubinsztajn, S. *Macromolecules* **2006**, *39*, 3802.

(20) (a) Weisboeck, R. A.; Hawthorne, M. F. *J. Am. Chem. Soc.* **1964**, *86*, 1642. (b) Garret, P. M.; Tebbe, F. N.; Hawthorne, M. F. *J. Am. Chem.*

Soc. 1964, *86*, 5016. (c) Hawthorne, M. F.; Young, D. C.; Garret, P. M.; Owen, D. A.; Schwerin, S. G.; Tebbe, F. N.; Wegner, P. M. *J. Am. Chem. Soc.* **1968**, *90*, 862. (d) Plesek, J.; Hermanek, S. Stibr, B. In *Inorganic Synthesis*; John Wiley & Sons: New York, 1983; Vol. 22, p 231.

(21) (a) Zakharkin, L. I.; Kalinin, U. N. *Tetrahedron Lett.* **1965**, 407. (b) Zakharkin, L. I.; Kirillova, V. S. *Izv. Akad. Nauk SSSR, Ser. Khim.* **1975**, 2596.

(22) (a) Fox, M. A.; Gill, W. R.; Herbertson, P. L.; MacBride, J. A. H.; Wade, K. *Polyhedron* **1996**, *16*, 565. (b) Fox, M. A.; MacBride, J. A. H.; Wade, K. *Polyhedron* **1997**, *16*, 2499. (c) Fox, M. A.; Wade, K. *Polyhedron* **1997**, *16*, 2517. (d) Yoo, J.; Hwang, J. W.; Do, Y. *Inorg. Chem.* **2001**, *40*, 568.

(23) Davidson, M. G.; Fox, M. A.; Hibbert, T. G.; Howard, J. A. K.; Mackinnon, A.; Neretin, I. S.; Wade, K. *Chem. Commun.* **1999**, 1649.

(24) Cypryk, M.; Apeloig, Y. *Organometallics* **2002**, *21*, 2165.

(25) Rikowski, E.; Marsmann, H. C. *Polyhedron* **1997**, *16*, 3357.

(26) Teixidor, F.; Viñas, C.; Abad, M. M.; Núñez, R.; Kivekäs, R.; Sillanpää, R. *J. Organomet. Chem.* **1995**, *503*, 193.

(27) (a) Laromaine, A.; Teixidor, F.; Kivekäs, R.; Sillanpää, R.; Benakki, R.; Grüner, B.; Viñas, C. *Dalton. Trans.* **2005**, 1785. (b) Laromaine, A.; Teixidor, F.; Kivekäs, R.; Sillanpää, R.; Arca, M.; Lippolis, V.; Crespo, E.; Viñas, C. *Dalton Trans.* **2006**, 5240.

(28) (a) Schleyer, P. R.; Maerker, C.; Dransfeld, A.; Jiao, H.; Hommes, N. J. R. v. E. *J. Am. Chem. Soc.* **1996**, *118*, 6317. (b) Mitchell, R. G. *Chem. Rev.* **2001**, *101*, 1301. (c) Llop, J.; Viñas, C.; Teixidor, F.; Victori, L.; Kivekäs, R.; Sillanpää, R. *Organometallics* **2002**, *21*, 355.

(29) Tood, L. J.; In *Progress in NMR Spectroscopy*; Pergamon Press Ltd: Elmsford, NY, 1979; Vol. *13*, p 87.

(30) Kropidlowska, A.; Turowska-Tyrk, I.; Becker, B. *Acta Crystallogr.* **2007**, *E63*, o855, and references therein.

(31) Sheldrick, G. M. *SHELX97*; University of Göttingen: Germany, 1997.

MA801483C

5.c) First example of the formation of a Si−C bond from an intramolecular Si−H· · ·H−C diyhydrogen interaction in a metallacarborane: A theoretical study.

Journal of Organometallic Chemistry 694 (2009) 1764–1770

Contents lists available at ScienceDirect

Journal of Organometallic Chemistry

journal homepage: www.elsevier.com/locate/jorganchem

First example of the formation of a Si–C bond from an intramolecular Si–H···H–C diyhydrogen interaction in a metallacarborane: A theoretical study

Emilio José Juárez-Pérez [1], Clara Viñas, Francesc Teixidor, Rosario Núñez *

Institut de Ciència de Materials de Barcelona, CSIC, Campus U.A.B., 08193 Bellaterra, Spain

ARTICLE INFO

Article history:
Received 14 November 2008
Received in revised form 5 December 2008
Accepted 8 December 2008
Available online 24 December 2008

Keywords:
Boron clusters
Carborane
DFT calculations
QTAIM
Dihydrogen bonds
Sandwich complexes

ABSTRACT

The recently reported crystal structure of $[NMe_4][1\text{-}SiMe_2H\text{-}3,3'\text{-}Co(1,2\text{-}C_2B_9H_{10})(1',2'\text{-}C_2B_9H_{11})]$ shows short contacts between the Si–H proton acceptor group and the C_c–H proton donor moiety in the dicarbollide ligand. These short contacts were studied within the framework of the Quantum Theory of Atoms in Molecules (QTAIM) at different levels of DFT theory (B3LYP/6-311(d,p) and BP86/TZ2P(+)) that shows the existence of a bifurcated Si–H···H–C_c dihydrogen bond. This paper presents the study of an experimental uncommon Si–H group playing as proton acceptor bond in a dihydrogen bond where hydrides like M–H (M, as metal transition), B–H or Al–H usually perform this role. Furthermore, this paper accounts with a new simple method to estimate bonding energies for closed-shell intramolecular interactions in the scheme of Voronoi charge population analysis and Coulomb's Law.

1. Introduction

In the course of our investigations to incorporate silane groups on the cluster carbon of the sandwich complex $[3,3'\text{-}Co(1,2\text{-}C_2B_9H_{11})_2]^-$ we observed an unexpected reaction [1]. By mixing 1 equiv. of Me_2SiHCl with 1 equiv. of $[1\text{-}Li\text{-}3,3'\text{-}Co(1,2\text{-}C_2B_9H_{10})(1,2\text{-}C_2B_9H_{11})]^-$, at −40 °C that expectedly should have produced $[1\text{-}Me_2SiH\text{-}3,3'\text{-}Co(1,2\text{-}C_2B_9H_{10})(1,2\text{-}C_2B_9H_{11})]^-$, it was obtained instead $[1,1'\text{-}\mu\text{-}Me_2Si\text{-}3,3'\text{-}Co(1,2\text{-}C_2B_9H_{10})_2]^-$. The reaction conditions implied that an intramolecular hydride-protonic reaction had taken place. This was unanticipated because the charges on both hydrogen atoms had to be very weak. The reaction is shown in Scheme 1. Our hypothesis was that a dihydrogen bond develops as a result of the favorable geometric characteristics of the cobaltabisdicarbollide anion, that weakens both the C_c–H and Si–H bonds producing a Si–C_c. The C_c–H stands for the hydrogen bonded to the cluster carbon. It is well established that agostic C–H interactions can significantly weaken the C–H bond, thereby rendering it susceptible to a wide range of inter- and intramolecular reactions. Likewise dihydrogen interactions may play an important role in lowering the activation energy for dihydrogen evolution and in influencing the generation of new covalent bonds. We could not find, however, any example in the literature of a Si–H and C–H interacting groups that at low temperatures evolved to a Si–C bond. Thus we wanted to confirm first, the existence of a C_c–H···H–Si dihydrogen bond in $[1\text{-}Me_2SiH\text{-}3,3'\text{-}Co(1,2\text{-}C_2B_9H_{10})(1,2\text{-}C_2B_9H_{11})]^-$and, second, its particular characteristics that made it to react so uniquely.

The dihydrogen bond (DHB) is a type of unconventional hydrogen bond in which a proton donating moiety D–H interacts with a proton acceptor A–H, see Scheme 2. They display characteristics similar to conventional hydrogen bonding [2].

The usual functional groups performing proton donating characteristics are F–H, O–H, N–H or C–H with a remarkable excess of positive charge on the hydrogen atom, and the usual proton acceptor groups contain hydridic atoms connected to Al, B, Ga, Ir, Mo, Mn, Os, Re, Ru or W atoms. Other systems have been described where two interacting hydrogen atoms do not show a clear protic and hydridic character [3]; it is the case of the H–H bonding interaction. The latter results from the close approach of two bonded hydrogen atoms bearing the same or similar net charges that estabilize the whole system. While it is also a closed shell interaction, the H–H bonding is distinct from DHB in its atomic and geometric characteristics [4]. Since the first DHB was found [5] until present, the DHB has been extensively studied in theoretical and experimental aspects [6]. The Quantum Theory of Atoms in Molecules of Bader [7] (QTAIM) is an important tool often applied to study DHB; Popelier established a sort of criteria based on the QTAIM to characterize DHB [8], and recently, Alkorta and co-workers [6b] have applied natural bond orbital methods (NBO) to determine whether intramolecular H···H interactions can be classified as DHB.

* Corresponding author.
E-mail address: rosario@icmab.es (R. Núñez).
[1] Enrolled in the UAB Ph.D. program.

0022-328X/$ - see front matter © 2008 Elsevier B.V. All rights reserved.
doi:10.1016/j.jorganchem.2008.12.022

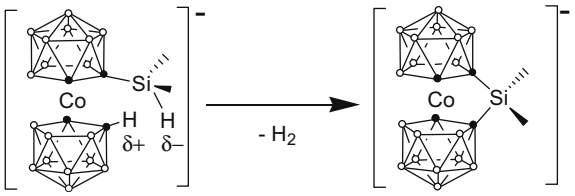

Scheme 1. Suggested pathway for the intramolecular reaction that causes the clusters' bridge in anions [1].

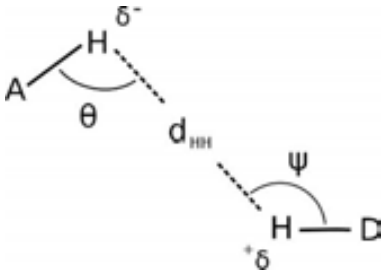

Scheme 2. Geometrical representation of the parameters of the DHB. A (Si or C_{Me}), D (C_c).

In this study, we will analyze the factors that have led to this intramolecular reaction shown in Scheme 1, by using QTAIM at different levels of DFT theory (B3LYP/6-311(d,p) and BP86/TZ2P(+)). For this purpose the H···H interactions in the crystal structure of $[NMe_4][1\text{-}SiMe_2H\text{-}3,3'\text{-}Co(1,2\text{-}C_2B_9H_{10})(1',2'\text{-}C_2B_9H_{11})]$[1] have been studied. Three intramolecular H···H interactions that might be treated as dihydrogen bonds, H–H bonding interactions or Van der Waals complexes are observed there. In addition, bonding energies for closed-shell intramolecular interactions in the scheme of Voronoi charge population analysis and Coulomb's Law have also been calculated.

2. Results and discussion

2.1. Experimental evidences for DHB in the $[NMe_4][1\text{-}SiMe_2H\text{-}3,3'\text{-}Co(1,2\text{-}C_2B_9H_{10})(1',2'\text{-}C_2B_9H_{11})]$ salt

Atomic distances are one of the main indicators for the existence of a bond. This is also valid for hydrogen and dihydrogen bonding [9]. Distances shorter than the Van der Waals radii point to a some type of interaction. Therefore distances shorter than 2.4 Å are indicative of a H···H interaction. The crystal structure of $[NMe_4][1\text{-}SiMe_2H\text{-}3,3'\text{-}Co(1,2\text{-}C_2B_9H_{10})(1',2'\text{-}C_2B_9H_{11})]$ is the first example of C_c-monosubstituted cobaltabisdicarbollide anion reported in literature [1]. This unique molecular structure presents an anion with three intramolecular short contacts with distances at 2.409, 2.212 and 2.059 Å between the H atoms. Two are clearly below the Van der Waals cut-off while one is slightly longer than 2.4 Å. First two short contacts are involving the hydridic hydrogen atom of the Si–H function and the protonic hydrogen atoms of the carbon cluster atoms (C_c–H) of the dicarbollide ligand. The third short contact (2.059 Å) is established between the hydrogen atom of a methyl moiety in the silane function (C_{Me}–H) and the hydrogen atom of one C_c–H function. Fig. 1 shows the spatial disposition of these three short contacts. Are all of them true DHBs? According to the crystal data these with 2.212 and 2.059 Å should, but what about the 2.409 Å distance?

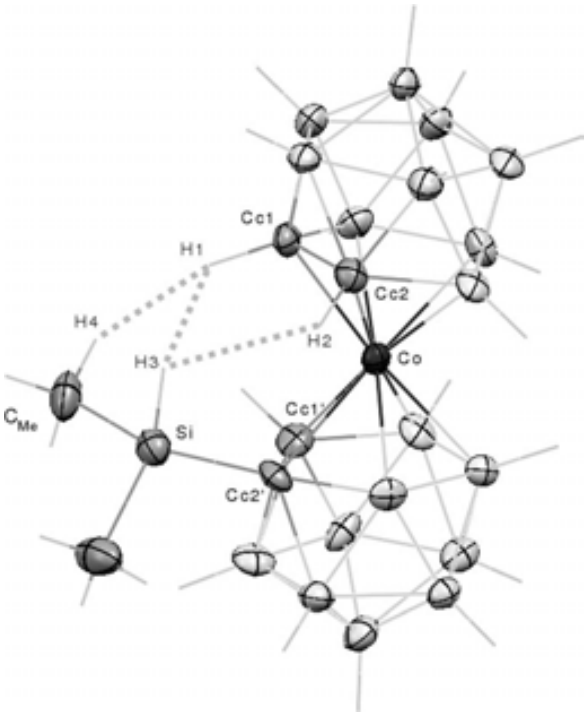

Fig. 1. XRD molecular structure of the anion $[1\text{-}SiMe_2H\text{-}3,3'\text{-}Co(1,2\text{-}C_2B_9H_{10})(1',2'\text{-}C_2B_9H_{11})]^-$ shows intramolecular short contacts Si–H3···H1–C_c, Si–H3···H2–C_c and C_{Me}–H4···H1–C_c. The non hydrogen atoms are represented at 40% probability level thermal ellipsoids.

Furthermore, the shortest contact corresponds to (Si–CH_2)H···H–C. This is surprising due to the equal nature of the donor and acceptor atoms C_{Me}—H and C_c–H. The two other interactions are Si–H···H–C_c contacts. The difference in electronegativity between Si and C, 1.90 versus 2.55 suggests that DHB could be formed. If this was the case it would imply a shift of the interacting C_c–H resonance in the ^{1}H NMR. Solution NMR data of weak intermolecular dihydrogen bonds is scarce due to the perturbing effect of the solvent, however, the intramolecular interaction reported here could afford first details on the C_c—H···H–Si interaction. Fortunately, the C_c—H chemical shift in the ^{1}H NMR can be informative because few other types of protons resonate in its region, 3.94 ppm in pristine $[3,3'\text{-}Co(1,2\text{-}C_2B_9H_{11})_2]^-$. For an adequate comparison of the chemical shifts involved, $[1\text{-}SiMe_3\text{-}3,3'\text{-}Co(1,2\text{-}C_2B_9H_{10})(1',2'\text{-}C_2B_9H_{11})]^-$ was taken as a reference. This anion has been recently described in our group [1] and its ^{1}H NMR spectrum shows three resonances at 4.02, 3.83, and 3.72 ppm due to the three C_c–H bonds. Conversely, in $[1\text{-}SiMe_2H\text{-}3,3'\text{-}Co(1,2\text{-}C_2B_9H_{10})(1',2'\text{-}C_2B_9H_{11})]^-$, only two resonances are observed at 3.85 and 3.69 ppm, with relative areas 1:2. Therefore, the resonance at 4.02 ppm in $[1\text{-}SiMe_3\text{-}3,3'\text{-}Co(1,2\text{-}C_2B_9H_{10})(1',2'\text{-}C_2B_9H_{11})]^-$ has been shifted to 3.69 ppm in $[1\text{-}SiMe_2H\text{-}3,3'\text{-}Co(1,2\text{-}C_2B_9H_{10})(1',2'\text{-}C_2B_9H_{11})]^-$, see Fig. 2. It can be interpreted as if H^+ in C_c—H has received electron density from H^- in Si–H to become more shielded, or more electron-rich. These experimental data are fully consistent with the formation of a H···H interaction, and were supportive of a more thorough investigation by using computational methods.

After a thorough search at the Cambridge Structural Database (CSD), it appears that the crystal structures of $[NMe_4][1\text{-}SiMe_2H\text{-}3,3'\text{-}Co(1,2\text{-}C_2B_9H_{10})(1',2'\text{-}C_2B_9H_{11})]$ and $[1,1'\text{-}\mu\text{-}Me_2Si\text{-}3,3'\text{-}Co(1,2\text{-}C_2B_9H_{10})_2]^-$ are the only pair of related X-ray determined com-

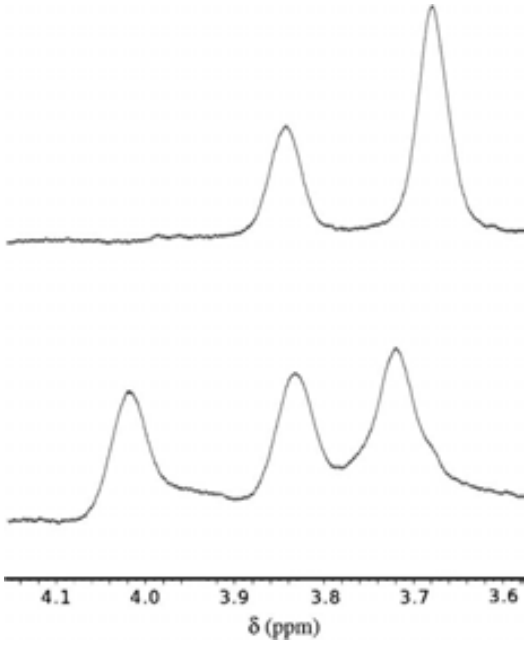

Fig. 2. ^{1}H NMR spectra of [1-SiMe$_2$H-3,3′-Co(1,2-$C_2B_9H_{10}$)(1′,2′-$C_2B_9H_{11}$)]$^-$ (up) and [1-SiMe$_3$-3,3′-Co(1,2-$C_2B_9H_{10}$)(1′,2′-$C_2B_9H_{11}$)]$^-$ (down).

pounds, one with a Si–H···H–C DHB bond and the second with a Si–C bond, all other elements being equal. In fact, few examples of crystal structures with Si–H···H–C contacts in which the Si–H has an environment comparable to carborane-Si(alkyl)$_2$-H are very scarce. For similar environment we understand aryl-Si(alkyl)$_2$-H or even alkyl-Si(alkyl)$_2$-H. In none of these cases the intramolecular reaction was ever observed [10]. This evidences the difficulty of dihydrogen evolution to generate a Si–C bond.

A possible explanation for the uniqueness of the Si–H···H–C to Si–C transformation may arise from the geometric disposition of substituents on the C_2B_3 faces. Whereas in the chemical sandwich complex ferrocene, substituents are coplanar to the C_5 framework, in [3,3′-Co(1,2-$C_2B_9H_{11}$)$_2$]$^-$ the substituents are tilted regarding the C_2B_3 plane. This is visualized in Fig. 1, in which the Si atom is closer to the C_c–H proton than would be in ferrocene. Because of the tilted disposition of the substituents in dicarbollide derivatives, the formation of the bridging silane does not distort as much the geometric characteristics of [3,3′-Co(1,2-$C_2B_9H_{11}$)$_2$]$^-$, as would have been the case in other arrangements, this perhaps facilitating the Si–H···H–C to Si–C transformation.

2.2. DFT geometry optimization of the crystal structure and charge population analysis

Two levels of theory, B3LYP/6-311(d,p) and BP86/TZ2P(+), have been used for the geometry optimization in gas phase of [1-SiMe$_2$H-3,3′-Co(1,2-$C_2B_9H_{10}$)(1′,2′-$C_2B_9H_{11}$)]$^-$. Comparison between calculated and experimental averaged bond lengths in each type of bond with their standard deviation is shown in Table 1. It can there be observed that the optimized structure of the anion at BP86/TZ2P(+) matches better the crystal structure than B3LYP/6-311(d,p).

As it is well-known X-ray diffraction methods do not reflect properly the X–H bond lengths, where X in the case studied here indicates B, C_{Me}, C_c and Si atoms. The DFT calculations are used to correct these H atom position. In Table 2 the geometrical parameters of the three intramolecular short contacts and the bond lengths of the Si–H, C_c–H and C_{Me}–H moieties at the different levels of theory and for the crystal structure are shown. An important X–H length correction can be seen, mainly with the two stronger H···H interactions.

Table 2 shows that H···H distances are below 2.4 Å for the short contacts C_{Me}–H4···H1–C_c and Si–H3···H2–C_c in all theory levels and in the crystal structure. However, the H···H distance for the Si–H3···H1–C_c short contact is in the range 2.409–2.440 Å; the closest value to 2.4 Å is found in the crystal structure whereas the farthest is in the geometry optimization at B3LYP/6-311(d,p) level. The angles θ and ψ are important geometrical parameters of a DHB. A Cambridge Structural Database (CSD) investigation [11] evidenced that the experimental range for the B–H···H angle (θ) is in a range of 95–120° and for the N–H···H angle (ψ) 150–170°. It is characteristic of DHB the strong bent in the θ angle, more than a linear arrangement that usually is a exception [2b,6e,11]. Our values for θ are in the range for normal DHBs but ψ values are smaller possibly due to the constrained geometry of the intramolecular interactions.

Atomic charges and population analysis were computed with the Natural Population Analysis (NPA) and Voronoi Deformation Density methods (VDD) at B3LYP/6-311(d,p) and BP86/TZ2P(+) level of theory, respectively (Table 3).

NPA and VDD are adequate basis set independent methods to compute atomic charges. Care should be taken, however, with this data as it is accepted that in general NPA tends to give a too ionic view of the bonds [12] and more reliable methods already have already been used to compute atomic charges in heteroboranes [6y,6z]. In this regard, the NPA charge in the hydrogen atom in the C_{Me}–H4 bond seems to be too positive (+0.224) for a methylen-

Table 1
Average bond lengths for each type of bond in the C-substituted cobaltabisdicarbollide anion (Å). In parenthesis standard deviation (Å X1000).

	Co–C_c	Co–B	C_c–C_c	C–B	B–B	Si–C_c	Si–C_{Me}
B3LYP/6-311G(d,p)							
C-substituted[a]	2.114(31)	2.120(12)	1.623(0)	1.715(13)	1.780(14)	1.914(0)	1.889(4)
Unsubstituted[b]	2.078(4)	2.129(10)	1.604(0)	1.703(17)	1.782(13)	–	–
BP86/TZ2P(+)							
C-substituted	2.081(28)	2.102(12)	1.639(0)	1.715(11)	1.783(15)	1.909(0)	1.891(4)
Unsubstituted	2.056(5)	2.112(12)	1.615(0)	1.704(14)	1.781(16)	–	–
Crystal structure							
C-substituted	2.081(25)	2.099(8)	1.627(0)	1.728(14)	1.778(16)	1.906(0)	1.864(1)
Unsubstituted	2.054(4)	2.107(15)	1.608(0)	1.707(14)	1.785(18)	–	–

[a] C-substituted dicarbollide ligand with SiMe$_2$H function.
[b] Unsubstituted dicarbollide ligand.

Table 2
Geometrical parameters of the H···H short contacts and X–H bond distances for the crystal structure and optimized geometries. Distances in Å, angles in degrees.

	Crystal structure			B3LYP/6-311G (d,p)			BP86/TZ2P (+)		
	d_{HH}	θ	ψ	d_{HH}	θ	ψ	d_{HH}	θ	ψ
Short contacts interactions [a]									
H3···H1	2.409	83.1	108.7	2.440	87.7	112.9	2.413	86.1	112.7
H3···H2	2.212	111.4	115.2	2.167	119.1	122.8	2.154	117.7	122.0
H4···H1	2.059	119.5	155.7	2.224	113.0	150.0	2.157	112.1	148.8
	d			*d*			*d*		
Bond distances[b]									
C_c–H1		1.121			1.079			1.086	
C_c–H2		1.121			1.080			1.086	
Si–H3		1.541			1.488			1.498	
C_{Me}–H4		0.980			1.092			1.099	

[a] See Fig. 1 and Scheme 1.
[b] See Fig. 1.

Table 3
Atomic charges on H atoms (au).

	NPA[a]			VDD[b]		
	Hydride	Proton	Difference	Hydride	Proton	Difference
H3···H1	−0.195	+0.267	0.462	−0.085	+0.130	0.215
H3···H2	−0.195	+0.282	0.477	−0.085	+0.122	0.207
H4···H1	+0.224	+0.267	0.043	+0.025	+0.130	0.105

[a] Optimized anion at B3LYP/6-311G(d,p).
[b] Optimized anion at BP86/TZ2P(+).

Table 4
VDD charges on hydrogen atoms (au).

	BP86/TZ2P(+)
Methane	+0.022
Ethene	+0.037
Benzene	+0.046
Ethyne	+0.098
C_c–H[a]	+0.125
SiH_4	−0.063
$SiMe_3H$[b]	−0.090

[a] Protonic hydrogen in $[3,3'\text{-}Co(C_2B_9H_{11})]^-$.
[b] Hydridic hydrogen in Si–H.

ic hydrogen atom. It is known that the acidity of the C–H bond in hydrogen bonds increases in the order C(sp3)–H < C(sp2)–H < C(sp)–H that corresponds with the strength of the C–H···Y hydrogen bonds. With the aim to compare the possibilities of C_c–H as a proton-donating bond, a VDD population analysis over methane, ethene, ethyne and benzene along with the hydridic hydrogens of two generic silanes has been calculated and compared with C_c–H in $[3,3'\text{-}Co(C_2B_9H_{11})_2]^-$. The results are shown in Table 4. It is to be noticed that the positive VDD charge of the hydrogen atom in C_c–H is even larger than C–H in ethyne. It is then clear the importance of the C_c–H moiety to generate a DHB with the appropriate H acceptor.

According to the calculated charges and the adopted geometry of the H3, H2, H1 and H4 hydrogen atoms, it can be stated that Si–H3···H1–C_c and Si–H3···H2–C_c short contacts are candidates to an asymmetric bifurcated Si–H3···(H–C_c)$_2$ DHB [6] and C_{Me}–H4···H1–C_c for H–H bonding [2b,4]. Next section offers more insight in the nature of these interactions.

3. QTAIM calculations

The above mentioned dihydrogen short contacts were analyzed in terms of their calculated electron density with DFT methods. For the two optimized geometries at different levels of theory, bond critical points (BCP) are found for Si–H3···H1–C_c and Si–H3···H2–C_c. The electron density at the BCP (ρ_{cp}) is in a range between 0.0088 and 0.0106 au, whereas for the C_{Me}–H4···H1–C_c hydrogen interaction, the BCP is found only in the optimized structure at B3LYP/6-311(d,p) level with a value of ρ_{cp} equal to 0.0077 au. We have been unable to find a BCP for C_{Me}–H4···H1–C_c at BP86/TZ2P(+) level of theory, even when the length is clearly lower than the sum of the Van der Waals radii see Table 5.

The corresponding electronic density Laplacian in the BCP ($\nabla^2\rho_{cp}$) is positive for all contacts. It indicates that all interactions are closed-shell type and their nature is mostly electrostatic [13]. The $\nabla^2\rho_{cp}$ for Si–H3···H1–C_c and Si–H3···H2–C_c are in the range 0.0316–0.0269 au for all calculation levels. For C_{Me}–H4···H1–C_c at B3LYP/6-311(d,p) level, $\nabla^2\rho_{cp}$ is 0.0242 au. According to the topological criteria for DHB given by Popelier [8], in the BCP the ρ_{cp} and $\nabla^2\rho_{cp}$ should be within the ranges 0.0020–0.0350 au, and 0.0240–0.1390 au respectively. Both Si–H3···H–C interactions are in these ranges. However, the $\nabla^2\rho_{cp}$ for C_{Me}–H4···H1–C_c at B3LYP/6-311(d,p) level is near to the minimum limit according to $\nabla^2\rho_{cp}$ criterion. The bond paths ellipticities (ε) reflect the structural instability for each interaction [14]. In Table 5 it can be seen that at B3LYP/6-311(d,p) level, the C_{Me}–H4···H1–C_c ellipticity is larger than both Si–H3···H–C_c interactions confirming that the former bond is weaker. The ε decreases in all levels from Si–H3···H1–C_c to Si–H3···H2–C_c, the last being the strongest according to the ε criterion in DHB [8]. In line with these topological parameters from QTAIM, the observed geometry and the atomic charge populations above, the Si–H3···H1–C_c and Si–H3···H2–C_c form an asymmetric bifurcated DHB whereas the C_{Me}–H4···H1–C_c would be classified as a weak H–H interaction (only found at B3LYP/6-311(d,p) level). Fig. 3 represents the contour lines for ρ in the plane of the bifurcated DHB dihydrogen bond formed by H1, H2 and H3 at BP86/TZ2P(+) level.

4. Bonding energies in the intramolecular interactions

Dihydrogen bonding has been classified as a medium-strong interaction with binding energies that generally lie between 0.5 and 7 kcal/mol [2b,6b,6q]. High-level ab initio calculations have already been performed on dihydrogen-bonded simple molecules with SiH_4 as a proton-acceptor and HF as a proton-donating molecule shows that H-bond energies for such systems are in the range 0.65–0.89 kcal/mol [6m]. Also, experimental values around 2 kcal/mol for Si–H3···H–O interactions have been found for mixtures of phenol-diethylmethylsilane [15]. In the scheme of the QTAIM theory, the strength of a DHB, as a subgroup of hydrogen bond, can be classified using the criteria of energy density at the BCP (H_{cp}) and $\nabla^2\rho_{cp}$ [6q,16]. The weak-medium strength dihydrogen bond

Table 5
Topological parameters (au) of this H-bonded system at two different levels of theory.

	Short contact	$\Delta_{H\cdots H} - VdW$[a]	ρ_{cp}[b]	$\nabla^2\rho_{cp}$[c]	ε[d]
B3LYP/6-311G(d,p)	H3···H1	0.040	0.0088	0.0269	0.534
	H3···H2	−0.233	0.0101	0.0293	0.178
	H4···H1	−0.176	0.0077	0.0242	1.322
BP86/TZ2P(+)	H3···H1	0.013	0.0098	0.0302	0.528
	H3···H2	−0.246	0.0106	0.0316	0.189
	H4···H1	−0.243	–	–	–

[a] Length$_{H\cdots H}$–VdW radii, distance H···H minus sum of Van der Waalls radii (2.4 Å).
[b] Electronic density at BCP.
[c] Laplacian of electronic density at BCP.
[d] Ellipticity.

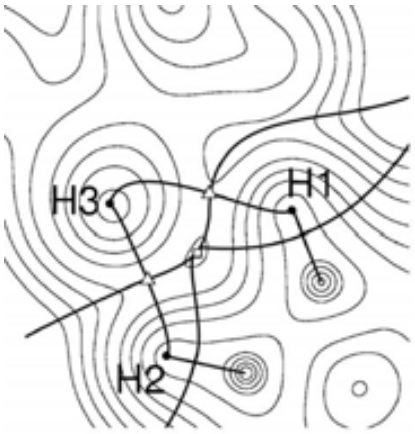

Fig. 3. Superposition of the contour lines (thin) of the electron density, bond paths connecting nuclei (bold) and interatomic zero flux surfaces (bold) for the H1–H2–H3 plane at BP86/TZ2P(+) level of theory. The two BCPs (Δ) and the RCP (□) corresponding to the bifurcated DHB are depicted as projections on the plane.

(closed shell interactions) has bonding energies of $0.5 < |E_{HB}| < 7$ kcal/mol, H···H distances in the range 1.70–2.60 Å and both parameters H_{cp} and $\nabla^2\rho_{cp}$ with positive values. Strong interaction, partially covalent has bonding energy of $7 < |E_{HB}| < 20$ kcal/mol, H···H distances in 1.20–1.70 Å, negative H_{cp} and positive $\nabla^2\rho_{cp}$, and finally, very strong interaction is a covalent hydrogen bond with $20 < |E_{HB}| < 30$ kcal/mol, H···H distances in 1.06–1.20 Å, and both H_{cp} and $\nabla^2\rho_{cp}$ are negative.

H_{cp} is defined as the sum of potential energy at BCP (V_{cp}) and kinetic energy at BCP (G_{cp}) [17]. G_{cp} can be evaluated theoretically with the wavefunction [13], and V_{cp} can be obtained with the virial theorem [7]. In Table 6, the values for G_{cp}, V_{cp}, and H_{cp} for the BCPs have been calculated at two different levels of theory. H_{cp} and $\nabla^2\rho_{cp}$ are positive values and the H···H distances are within the range 1.7–2.6 Å that indicate that the H···H interactions reported here can be classified as of weak-medium strength closed shell interactions. The H-bond energy (E_{HB}) has been estimated from the energy parameters of QTAIM according to the empirical relationship of Espinosa et al. [18] Values for E_{HB} in the range 1.24 kcal/mol for C_{Me}–H4···H1–C_c at B3LYP/6-311(d,p) level and 1.70 kcal/mol for Si–H3···H2–C_c at BP86/TZ2P(+) level have been calculated.

A second procedure to obtain an estimation of the bonding energy of these interactions is by optimizing the anion [1-$SiMe_2$H-3,3′-Co(1,2-$C_2B_9H_{10}$)(1′,2′-$C_2B_9H_{11}$)]$^-$ in such a way that the moiety –$SiMe_2$H is rotated so that it cannot generate the hydrogen interactions in the molecule. However, other effects as the steric hindrance could be present that may distort the energy difference between the two conformations [6b]. Energy difference values of 27.5 at B3LYP/6-311G(d,p) and 30.2 kcal/mol at BP86/TZ2P(+) have been found. This fact indicates a clear overestimation of the H···H interaction energy. They are exceedingly large compared to the sum of the computed H···H bonding energies both at B3LYP/6-311(d,p) level and BP86/TZ2P(+) level (Table 6), that compute 4.35 and 3.30 kcal/mol, respectively.

As there is a large discrepancy between the two previous methods, we have applied a new approach to estimate the bonding energy for each H···H interaction. For this purpose we applied the simple Coulomb's Law (Eq. (1)). The charge on each participating hydrogen atom is known either by NPA or VDD; the distance between the interacting hydrogen atoms is also known, therefore a simple application of Eq. (1) led to the Coulombic energy U (see Table 6)

$$U = k\frac{q_1 \cdot q_2}{r}. \quad (1)$$

Table 6
Topological parameters (au) of this H-bonded system at two different levels of theory.

	Short contact	G_{cp}[a]	V_{cp}[b]	H_{cp}[c]	E_{HB}[d]	U[e]
B3LYP/6-311G(d,p)	H3···H1	0.00572	−0.00471	0.00101	−1.48	−7.08
	H3···H2	0.00625	−0.00518	0.00107	−1.63	−8.42
	H4···H1	0.00498	−0.00392	0.00106	−1.24[f]	8.92
BP86/TZ2P(+)	H3···H1	0.00631	−0.00506	0.00125	−1.60	−1.52
	H3···H2	0.00665	−0.00540	0.00125	−1.70	−1.60
	H4···H1	–	–	–	–	0.50

[a] Kinetic electron energy density at BCP.
[b] Potential electron energy density at BCP.
[c] Total electron energy density at BCP.
[d] Bonding energy (kcal/mol) according to Espinosa empirical relationship.
[e] Bonding energy (kcal/mol) according to Eq. (1).
[f] The Espinosa equation is not strictly applicable in this case because according to atomic charges the two atoms are not forming a hydrogen bond (DHB).

An inspection of the results indicates that NPA charges do not produce a good matching between E_{HB} and U. However, this is reasonable when U is evaluated using VDD charges. This procedure to estimate bonding energies in this kind of intramolecular DHB, taken it with caution, could be useful as a fast estimation of the interacting energy due to the inherent difficulty to calculate bonding energies in intramolecular DHB [6b,n].

5. Conclusion

$[1,1'$-μ-$SiMe_2$-$3,3'$-$Co(1,2$-$C_2B_9H_{10})_2]^-$ was generated in very mild conditions from $[1$-$SiMe_2H$-$3,3'$-$Co(1,2$-$C_2B_9H_{10})(1',2'$-$C_2B_9H_{11})]^-$ without the aid of any additional reagent. The reaction implies a loss of dihydrogen, that presumes the existence of a DHB in $[1$-$SiMe_2H$-$3,3'$-$Co(1,2$-$C_2B_9H_{10})(1',2'$-$C_2B_9H_{11})]^-$. These two compounds represent the only examples, at least structurally characterized, of a Si–H···H–C_c to Si–C_c conversion. To get more insight into this process the crystal structure of $[NMe_4][1$-$SiMe_2H$-$3,3'$-$Co(1,2$-$C_2B_9H_{10})(1',2'$-$C_2B_9H_{11})]$ was carefully studied. Three H···H short contacts were observed, two Si–H···H-C_c and one $SiCH_2$–H···H–C_c contact. The shortest one corresponds to $SiCH_2$–H···H–C_c with the H···H distance equal to 2.059 Å, whereas the two longest correspond to Si–H···H–C_c with 2.212 and 2.409 Å, according to X-ray. From this data it could be deduced that the C–H···H–C_c and one of the Si–H···H–C_c were clear H···H interactions, while the second Si–H···H–C_c would not exist or would be very weak. However, by using QTAIM and Charge Analyses Population on the hydrogen atoms, it has been conclude that the C–H···H–C, is not a DHB or it is a weak H–H interaction. On the contrary, the Si–H···H–C_c with a 2.409 Å distance is a real DHB, as it is the second Si–H···H–C_c. Therefore the two Si–H···H–C short contacts can be considered part of an asymmetric bifurcated DHB. The preorganization of $[1$-$SiMe_2H$-$3,3'$-$Co(1,2$-$C_2B_9H_{10})(1',2'$-$C_2B_9H_{11})]^-$ generated by the Si–H···H–C_c DHB and the geometrical characteristics of $[3,3'$-$Co(1,2$-$C_2B_9H_{10})_2]^-$ may be the reason for the singular transformation from Si–H···H–C_c to Si–C_c bond.

6. Experimental

6.1. Computational details

Optimized geometries were performed using Density Functional Methods [19] of the GAUSSIAN 03 [20] sets of codes using the hybrid functional B3LYP [21] with the 6-311G(d,p) basis set for all atoms. Atomic charges and population analysis were computed within the Natural Population Analysis (NPA) [22]. Also, density functionals geometries optimizations were carried out using the Amsterdam Density Functional Package [23]. The generalized gradient approximation (GGA nonlocal) method was used, by means of Vosko, Wilk and Nusair's local exchange correlation [24] with nonlocal exchange corrections by Becke [25] and nonlocal correlation corrections by Perdew [26]. The basis set employed in the calculations for C, B and H atoms are all-electron double-zeta Slater type orbital in the core and triple-zeta in the valence shell with two polarization functions (TZ2P according to ADF nomenclature) and TZ2P+ basis set for the cobalt atom. This TZ2P+ basis set are nearly identical to TZ2P except for a better description introducing 4 d-functions instead of 3. We label in this paper the choice of basis set for each atom as TZ2P(+). Atomic charges were computed within Voronoi Deformation Density method (VDD) as implemented in ADF [12]. Topological Bader analyses [7] were performed using Xaim software [27] and AIM2000 [28]. QTAIM calculations were also carried out for the full ionic systems (cation + anion) and no significantly difference was encountered analyzing the electronic density.

Acknowledgments

This work has been supported by the CICYT (MAT2006-05339) and the Generalitat de Catalunya, 2005/SGR/00709. E.J.J.P. thanks to MEC for a FPU grant. Calculations have been carried out at the CESCA and CTI (CSIC).

References

[1] E.J. Juárez-Pérez, C. Viñas, A. González-Campo, F. Teixidor, R. Sillanpää, R. Kivekäs, R. Núñez, Chem. Eur. J. 14 (2008) 4924–4938.
[2] (a) I. Alkorta, J. Elguero, Chem. Soc. Rev. 27 (1998) 163–170;
(b) R. Custelcean, J.E. Jackson, Chem. Rev. 101 (2001) 1963–1980;
(c) G.R. Desiraju, Dalton Trans. (2000) 3745–3751;
(d) L.M. Epstein, E.S. Shubina, Coord. Chem. Rev. 231 (2002) 165–181.
[3] (a) S.J. Grabowski, A. Pritzner, M. Zabel, A.T. Dubis, M. Palusiak, J. Phys. Chem. B 108 (2004) 1831–1837;
(b) P. Lipkowski, S.J. Grabowski, T.L. Robinson, J. Leszczynski, J. Phys. Chem. A 108 (2004) 10865–10872;
(c) K.N. Robertson, O. Knop, T.S. Cameron, Can. J. Chem. 81 (2003) 727–743.
[4] C.F. Matta, J. Hernandez-Trujillo, T.H. Tang, R.F.W. Bader, Chem. Eur. J. 9 (2003) 1940–1951.
[5] (a) R.H. Crabtree, P.E.M. Siegbahn, O. Eisenstein, A.L. Rheingold, Acc. Chem. Res. 29 (1996) 348–354;
(b) J.C. Lee, E. Peris, A.L. Rheingold, R.H. Crabtree, J. Am. Chem. Soc. 116 (1994) 11014–11019.
[6] (a) Some references I. Alkorta, J. Elguero, C. Foces-Foces, Chem. Commun. (1996) 1633–1634;
(b) I. Alkorta, J. Elguero, S.J. Grabowski, J. Phys. Chem. A 112 (2008) 2721–2727;
(c) I. Alkorta, J. Elguero, O. Mo, M. Yanez, J.E. Del Bene, J. Phys. Chem. A 106 (2002) 9325–9330;
(d) I. Alkorta, K. Zborowski, J. Elguero, M. Solimannejad, J. Phys. Chem. A 110 (2006) 10279–10286;
(e) M.J. Calhorda, Chem. Commun. (2000) 801–809;
(f) H. Cybulski, M. Pecul, J. Sadlej, T. Helgaker, J. Chem. Phys. 119 (2003) 5094–5104;
(g) Y. Feng, S.W. Zhao, L. Liu, J.T. Wang, X.S. Li, Q.X. Guo, J. Phys. Org. Chem. 17 (2004) 1099–1106;
(h) F. Fuster, B. Silvi, S. Berski, Z. Latajka, J. Mol. Struct. 555 (2000) 75–84;
(i) M.M.S. de Giambiagi, P. Bultinck, J. Braz. Chem. Soc. 19 (2008) 263–267;
(j) S.J. Grabowski, J. Phys. Org. Chem. 17 (2004) 18–31;
(k) S.J. Grabowski, J. Phys. Chem. A 105 (2001) 10739–10746;
(l) S.J. Grabowski, Chem. Phys. Lett. 338 (2001) 361–366;
(m) S.J. Grabowski, J. Phys. Chem. A 104 (2000) 5551–5557;
(n) S.J. Grabowski, Chem. Phys. Lett. 327 (2000) 203–208;
(o) S.J. Grabowski, Chem. Phys. Lett. 312 (1999) 542–547;
(p) S.J. Grabowski, T.L. Robinson, J. Leszczynski, Chem. Phys. Lett. 386 (2004) 44–48;
(q) S.J. Grabowski, W.A. Sokalski, J. Leszczynski, Chem. Phys. 337 (2007) 68–76;
(r) S.J. Grabowski, W.A. Sokalski, J. Leszczynski, J. Phys. Chem. A 109 (2005) 4331–4341;
(s) W.T. Klooster, T.F. Koetzle, P.E.M. Siegbahn, T.B. Richardson, R.H. Crabtree, J. Am. Chem. Soc. 121 (1999) 6337–6343;
(t) B.G. Oliveira, R.C.M.U. Araujo, M.N. Ramos, Struct. Chem. 19 (2008) 185–189;
(u) M. Palusiak, S.J. Grabowski, J. Mol. Struct. 674 (2004) 147–152;
(v) E.S. Shubina, E.V. Bakhmutova, A.M. Filin, I.B. Sivaev, L.N. Teplitskaya, A.L. Chistyakov, I.V. Stankevich, V.I. Bakhmutov, V.I. Bregadze, L.M. Epstein, J. Organomet. Chem. 657 (2002) 155–162;
(w) S. Wojtulewski, S.J. Grabowski, J. Mol. Struct. 645 (2003) 287–294;
(x) Y. Wu, L. Feng, X.D. Zhang, J. Mol. Struct. 851 (2008) 294–298;
(y) J. Fanfrlík, D. Hnyk, M. Lepsík, P. Hobza, Phys. Chem. Chem. Phys. 9 (2007) 2085–2093;
(z) J. Fanfrlík, M. Lepsík, D. Horinek, Z. Havlas, P. Hobza, ChemPhysChem 7 (2006) 1100–1105.
[7] R.F.W. Bader, Atoms in Molecules: A Quantum Theory, Clarendon Press, Oxford; New York, 1990.
[8] P.L.A. Popelier, J. Phys. Chem. A 102 (1998) 1873–1878.
[9] W.C. Hamilton, J.A. Ibers, Hydrogen Bonding in Solids, Benjamin, New York, 1968.
[10] (a) D.H. Berry, T.S. Koloski, P.J. Carroll, Organometallics 9 (1990) 2952;
(b) R. Ruffolo, A. Decken, L. Girard, H.K. Gupta, M.A. Brook, M. McGlinchey, Organometallics 13 (1994) 4328;
(c) M. Hofmann, W. Malisch, H. Hupfer, M. Nieger, Z. Naturfrosch. B 58 (2003) 36.
[11] T. Richardson, S. de Gala, R.H. Crabtree, P.E.M. Siegbahn, J. Am. Chem. Soc. 117 (1995) 12875–12876.
[12] C.F. Guerra, J.W. Handgraaf, E.J. Baerends, F.M. Bickelhaupt, J. Comput. Chem. 25 (2004) 189–210.
[13] Cherif F. Matta, Russell J. Boyd, The Quantum Theory of Atoms in Molecules, Wiley-WCH Verlag GmbH & Co., 2007.

[14] D. Cremer, E. Kraka, T.S. Slee, R. Bader, C. Lau, T. Nguyen Dang, P. MacDougall, J. Am. Chem. Soc. 105 (1983) 5069–5075.
[15] H. Ishikawa, A. Saito, M. Sugiyama, N. Mikami, J. Chem. Phys. 123 (2005) 224309.
[16] I. Rozas, I. Alkorta, J. Elguero, J. Am. Chem. Soc. 122 (2000) 11154–11161.
[17] D. Cremer, E. Kraka, Angew. Chem., Int. Ed. 23 (1984) 627–628.
[18] E. Espinosa, E. Molins, C. Lecomte, Chem. Phys. Lett. 285 (1998) 170–173.
[19] R.G. Parr, W. Yang, Density-Functional Theory of Atoms and Molecules, Oxford University Press, New York, 1989.
[20] M.J. Frisch, G.W. Trucks, H.B. Schlegel, G.E. Scuseria, M.A. Robb, J.R. Cheeseman, J.A. Montgomery Jr., T. Vreven, K.N. Kudin, J.C. Burant, J.M. Millam, S.S. Iyengar, J. Tomasi, V. Barone, B. Mennucci, M. Cossi, G. Scalmani, N. Rega, G.A. Petersson, H. Nakatsuji, M. Hada, M. Ehara, K. Toyota, R. Fukuda, J. Hasegawa, M. Ishida, T. Nakajima, Y. Honda, O. Kitao, H. Nakai, M. Klene, X. Li, J.E. Knox, H.P. Hratchian, J.B. Cross, V. Bakken, C. Adamo, J. Jaramillo, R. Gomperts, R.E. Stratmann, O. Yazyev, A.J. Austin, R. Cammi, C. Pomelli, J.W. Ochterski, P.Y. Ayala, K. Morokuma, G.A. Voth, P. Salvador, J.J. Dannenberg, V.G. Zakrzewski, S. Dapprich, A.D. Daniels, M.C. Strain, O. Farkas, D.K. Malick, A.D. Rabuck, K. Raghavachari, J.B. Foresman, J.V. Ortiz, Q. Cui, A.G. Baboul, S. Clifford, J. Cioslowski, B.B. Stefanov, G. Liu, A. Liashenko, P. Piskorz, I. Komaromi, R.L. Martin, D.J. Fox, T. Keith, M.A. Al-Laham, C.Y. Peng, A. Nanayakkar, A.M. Challacombe, P.M.W. Gill, B. Johnson, W. Chen, M.W. Wong, C. Gonzalez, J.A. Pople, Gaussian 03, Revision E.01, Gaussian, Inc., Wallingford CT, 2004.
[21] (a) A.D. Becke, J. Chem. Phys. 98 (1993) 5648;
(b) C. Lee, W. Yang, R.G. Parr, Phys. Rev. B 37 (1988) 785.
[22] E.D. Glendening, A.E. Reed, J.E. Carpenter, F. Weinhold, NBO Version 3.1.
[23] (a) ADF2007.01, SCM, Theoretical Chemistry, Vrije Universiteit, Amsterdam, The Netherlands;
(b) G. te Velde, F.M. Bickelhaupt, E.J. Baerends, C. Fonseca Guerra, S.J.A. van Gisbergen, J.G. Snijders, T. Ziegler, J. Comput. Chem. 22 (2001) 931–967;
(c) C.F. Guerra, J.G. Snijders, G. te Velde, E.J. Baerends, Theor. Chem. Acc. 99 (1998) 391–403.
[24] S.H. Vosko, L. Wilk, M. Nusair, Can. J. Phys. 58 (1980) 1200–1211.
[25] A.D. Becke, Phys. Rev. A 38 (1988) 3098–3100.
[26] J.P. Perdew, Phys. Rev. B 33 (1986) 8822–8824.
[27] J.C. Ortiz, C. Bo, Xaim 1.0, 1998.
[28] AIM2000 designed by Friedrich Biegler-König, University of Applied Sciences, Bielefeld, Germany.

Bibliografía

[1] Davy, H. The Bakerian Lecture: On Some New Phenomena of Chemical Changes Produced by Electricity, Particularly the Decomposition of the Fixed Alkalies, and the Exhibition of the New Substances Which Constitute Their Bases; And on the General Nature of Alkaline Bodies. *Philosophical Transactions of the Royal Society of London* **1808**, *98*, 1–44.

[2] Stock, A. Hydrides of Boron and Silicon; Cornell Univ. Press, Ithaca, NY, 1933.

[3] Longuet-Higgins, H. C.; Bell, R. P. The Structure Of The Boron Hydrides. *J. Chem. Soc.* **1943**, 250–255.

[4] Wade, K. Bonding With Boron. *Nature* **2009**, *1*, 92–92.

[5] Brown, H. C.; Stehle, P. F.; Tierney, P. A. Singly-Bridged Compounds Of The Boron Halides And Boron Hydrides. *J. Am. Chem. Soc.* **1957**, *79*, 2020–2021.

[6] (a) Hoffmann, R.; Lipscomb, W. N. Theory of Polyhedral Molecules. III. Population Analyses and Reactivities for the Carboranes. *J. Chem. Phys.* **1962**, *36*, 3489–3493; (b) Lipscomb, W. N. Boron Hydrides; WA Benjamin, 1963; (c) Lipscomb, W. N. The Boranes and Their Relatives. *Science* **1977**, *196*, 1047–1055.

[7] (a) Volkov, V. V.; Ikorskii, V. N. Magnetochemistry Of Boron Hydride Structures. Empirical Aspects. *J. Struct. Chem.* **2004**, *45*, 694–705; (b) Schleyer, P. v. R.; Najafian, K. Stability and Three-Dimensional Aromaticity of closo-Monocarbaborane Anions and closo-Dicarboranes. *Inorg. Chem.* **1998**, *37*, 3454–3470.

[8] (a) Grimes, R. Carboranes; Academic Press, New York, 1970; (b) Muetterties, E., E. L. Boron Hydride Chemistry; Academic Press: New York, 1975; (c) Rudolph, R. Boranes And Heteroboranes: A Paradigm For The Electron Requirements Of Clusters. *Acc. Chem. Res.* **1976**, *9*, 446–452; (d) O'Neill, M.; Wade, K. Comprehensive Organometallic Chemistry; G. Wilkinson, F. G. A. Stone, and E. W. Abel, Pergamon Press, Oxford, 1982; Vol. 1, p 2; (e) Hosmane, N. S.; Maguire, J. A. Syntheses, Structures, Bonding, and Reactivity of Main Group Heterocarboranes. *Adv. Organomet. Chem.* **1990**, *30*, 99–242.

[9] (a) Williams, R. E. Carboranes And Boranes; Polyhedra And Polyhedral Fragments. *Inorg. Chem.* **1971**, *10*, 210–214; (b) Wade, K. Structural Significance Of Number Of Skeletal Bonding Electron-Pairs In Carboranes, Higher Boranes And Borane Anions, And Various Transition-Metal Carbonyl Cluster Compounds. *Chem. Commun.* **1971**, 792–793; (c) Mingos, D. M. P. General Theory For Cluster And Ring Compounds Of Main Group And Transition-Elements. *Nature-Physical Science* **1972**, *236*, 99.

[10] Carborane. Encyclopedia Britannica. 2008.

[11] (a) Heying, T.; Ager Jr, J.; Clark, S.; Mangold, D.; Goldstein, H.; Hillman, M.; Polak, R.; Szymanski, J. A New Series of Organoboranes. I. Carboranes from the Reaction of Decaborane with Acetylenic Compounds. *Inorg. Chem.* **1963**, *2*, 1089–1092; (b) Fein, M.; Bobinski, J.; Mayes, N.; Schwartz, N.; Cohen, M. Carboranes. I. The Preparation and Chemistry of 1-Isopropenylcarborane and its Derivatives (a New Family of Stable Clovoboranes). *Inorg. Chem.* **1963**, *2*, 1111–1115.

[12] (a) Plešek, J. Potential Applications Of The Boron Cluster Compounds. *Chem. Rev.* **1992**, *92*, 269–278; (b) Saxena, A.; Maguire, J.; Hosmane, N. Recent Advances in the Chemistry of Heterocarborane Complexes Incorporating s-and p-Block Elements. *Chem. Rev.* **1997**, *97*, 2421–2462.

[13] Cambridge Structural Database, versión 5.29, Agosto 2008.

[14] (a) Crespo, O.; Gimeno, M. C.; Laguna, A. Carboranyl C-σ-Bonded and C-functionalized Carboranes As Ligands In Gold And Silver Chemistry. *J. Organomet. Chem.* **2009**, *694*, 1588–1598; (b) Crespo, O.; Gimeno, M. C.; Jones, P. G.; Laguna, A.; Villacampa, M. D. Small gold clusters with carborane ligands: Synthesis and structural characterization of the novel compound $[Au_4\{(PPh_2)_2)C_2B_9H_{10}\}_2(AsPh_3)_2)]$. *Angew. Chem. Int. Ed.* **1997**, *36*, 993–995.

[15] (a) Núñez, R.; González, A.; Viñas, C.; Teixidor, F.; Sillanpää, R.; Kivekäs, R. Approaches To The Preparation Of Carborane-Containing Carbosilane Compounds. *Org. Lett.* **2005**, *7*, 231–233; (b) Núñez, R.; González-Campo, A.; Laromaine, A.; Teixidor, F.; Sillanpää, R.; Kivekäs, R.; Viñas, C. Synthesis Of Small Carboranylsilane Dendrons As Scaffolds For Multiple Functionalizations. *Org. Lett.* **2006**, *8*, 4549–4552; (c) Núñez, R.; González-Campo, A.; Viñas, C.; Teixidor, F.; Sillanpää, R.; Kivekäs, R. Boron-Functionalized Carbosilanes: Insertion Of Carborane Clusters Into Peripheral Silicon Atoms Of Carbosilane Compounds. *Organometallics* **2005**, *24*, 6351–6357.

[16] (a) Sundberg, M. R.; Uggla, R.; Viñas, C.; Teixidor, F.; Paavola, S.; Kivekäs, R. Nature of intramolecular interactions in hypercoordinate C-substituted 1,2-dicarba-closo-dodecaboranes with short P...P distances. *Inorg. Chem.*

Commun. **2007**, *10*, 713–716; (b) Sundberg, M. R.; Paavola, S.; Viñas, C.; Teixidor, F.; Uggla, R.; Kivekäs, R. Plasticity of the five-membered chelate ring in Palladium-Carborane Complexes. *Inorg. Chim. Acta* **2005**, *358*, 2107–2111; (c) Núñez, R.; Farràs, P.; Teixidor, F.; Viñas, C.; Sillanpää, R.; Kivekäs, R. A Discrete P...I-I...P Assembly: The Large Influence Of Weak Interactions On The P-31 NMR Spectra Of Phosphane-Diiodine Complexes. *Angew. Chem. Int. Ed.* **2006**, *45*, 1270–1272.

[17] (a) Laromaine, A.; Teixidor, F.; Kivekäs, R.; Sillanpää, R.; Benakki, R.; Grüner, B.; Viñas, C. Synthesis, reactivity and structural studies of carboranyl thioethers and disulfides. *Dalton Trans.* **2005**, 1785–1795; (b) Teixidor, F.; Viñas, C.; Benakki, R.; Kivekäs, R.; Sillanpää, R. A route to exo-heterodisubstituted and monosubstituted o-carborane derivatives. *Inorg. Chem.* **1997**, *36*, 1719–1723; (c) Viñas, C.; Benakki, R.; Teixidor, F.; Casabó, J. Dimethoxyethane As A Solvent For The Synthesis Of C-Monosubstituted O-Carborane Derivatives. *Inorg. Chem.* **1995**, *34*, 3844–3845; (d) Llop, J.; Viñas, C.; Oliva, J. M.; Teixidor, F.; Flores, M. A.; Kivekäs, R.; Sillanpää, R. Modulation of the C-C distance in disubstituted 1,2-R-2-o-carboranes. *J. Organomet. Chem.* **2002**, *657*, 232–238.

[18] Laromaine, A.; Teixidor, F.; Kivekäs, R.; Sillanpää, R.; Arca, M.; Lippolis, V.; Crespo, E.; Viñas, C. Synthesis, reactivity and structural studies of selenide bridged carboranyl compounds. *Dalton Trans.* **2006**, 5240–5247.

[19] Schroeder, H.; Heying, T. L.; Reiner, J. R. A New Series of Organoboranes. II. The Chlorination of 1,2-Dicarbaclovododecaborane(12). *Inorg. Chem.* **1963**, *2*, 1092–1096.

[20] Heřmánek, S. Boron Chemistry: Introduction. *Chem. Rev.* **1992**, *92*, 175–175.

[21] Viñas, C.; Barberà, G.; Oliva, J. M.; Teixidor, F.; Welch, A. J.; Rosair, G. M. Are halocarboranes suitable for substitution reactions? The case for 3-I-1,2-closo-$C_2B_{10}H_{11}$: Molecular orbital calculations, aryldehalogenation reactions, B-11 NMR interpretation of closo-carboranes, and molecular structures of 1-Ph-3-Br-1,2-closo-$C_2B_{10}H_{10}$ and 3-Ph-1,2-closo-$C_2B_{10}H_{11}$. *Inorg. Chem.* **2001**, *40*, 6555–6562.

[22] Wiesboeck, R.; Hawthorne, M. Dicarbaundecaborane (13) and Derivatives. *J. Am. Chem. Soc.* **1964**, *86*, 1642–1643.

[23] Farràs, P.; Teixidor, F.; Branchadell, V. Prediction of pK(a) values of nido-carboranes by density functional theory methods. *Inorg. Chem.* **2006**, *45*, 7947–7954.

[24] (a) Hawthorne, M.; Young, D.; Andrews, T.; Howe, D.; Pilling, R.; Pitts, A.; Reintjes, M.; Warren Jr, L.; Wegner, P. pi-Dicarbollyl derivatives of the transition metals. Metallocene analogs. *J. Am. Chem. Soc.* **1968**, *90*, 879–896; (b) Hawthorne, M.; Young, D.; Garrett, P.; Owen, D.; Schwerin, S.; Tebbe, F.; Wegner, P. Preparation and characterization of the (3)-1, 2-and (3)-1, 7-dicarbadodecahydroundecaborate (-1) ions. *J. Am. Chem. Soc.* **1968**, *90*, 862–868; (c) Viñas, C.; Pedrajas, J.; Bertran, J.; Teixidor, F.; Kivekäs, R.; Sillanpää, R. Synthesis of cobaltabis(dicarbollyl) complexes incorporating exocluster SR substituents and the improved synthesis of [3,3'-Co(1,2-$C_2B_9H_{11}$)$_2$]$^-$ derivatives. *Inorg. Chem.* **1997**, *36*, 2482–2486.

[25] Hawthorne, M. F.; Young, D. C.; Wegner, P. A. Carbametallic Boron Hydride Derivatives. I. Apparent Analogs of Ferrocene and Ferricinium Ion. *J. Am. Chem. Soc.* **1965**, *87*, 1818–1819.

[26] Hawthorne, M.; Andrews, T. Carborane analogues of cobalticinium ion. *Chem. Commun.* **1965**, 443–444.

[27] Warren, L. F.; Hawthorne, M. F. Dicarbollyl Complexes of Nickel(III) and Nickel(IV). *J. Am. Chem. Soc.* **1967**, *89*, 470–471.

[28] Ruhle, H.; Hawthorne, M. pi-Dicarbollyl derivatives of chromium. Metallocene analogs. *Inorg. Chem.* **1968**, *7*, 2279–2282.

[29] Warren, L. F.; Hawthorne, M. F. Metallocene analogs of copper, gold, and palladium derived from the (3)-1,2-dicarbollide ion. *J. Am. Chem. Soc.* **1968**, *90*, 4823–4828.

[30] En bibliografía existen muchos más ejemplos de los cuales no se ha conseguido estructura cristalina.

[31] Wing, R. Crystal and molecular structure of tetraethylammonium bis [(3)-1, 2-dicarbollyl] cuprate (II). *J. Am. Chem. Soc.* **1967**, *89*, 5599–5604.

[32] (a) Churchill, M. R.; Gold, K.; Francis, J. N.; Hawthorne, M. F. Preparation and crystallographic characterization of a bridged metallo-carborane complex containing a carbonium ion center. *J. Am. Chem. Soc.* **1969**, *91*, 1222–1223; (b) Plešek, J.; Heřmánek, S. The First Doubly Bridged Metallacarborane Complex. Synthesis, Properties and Structure. *Collect. Czech. Chem. Commun.* **1995**, *60*, 1297–1302; (c) Franken, A.; Plešek, J.; Nachtigal, C. Unusual Rearrangement of Naphthalene in the Synthesis of a Novel B8-B8-Bridged Derivative in the [Co-3-(1, 2-$C_2B_9H_{11}$)$_2$]$^-$ Series. *Collect. Czech. Chem. Commun.* **1997**, *62*, 746–751.

[33] Sivaev, I.; Bregadze, V. Chemistry of Cobalt Bis (dicarbollides). A Review. *Collect. Czech. Chem. Commun.* **1999**, *64*, 783–805.

[34] Francis, J.; Jones, C.; Hawthorne, M. Chemistry of bis ((π-7, 8-dicarballyl) metalates. Reaction between $[(\pi\text{-}7,8\text{-}B_9C_2H_{11})_2Co]^-$ and aryl diazonium salts. *J. Am. Chem. Soc.* **1972**, *94*, 4878–4881.

[35] Plešek, J.; Heřmánek, S.; Franken, A.; Císařová, I.; Nachtigal, C. Dimethyl Sulfate Induced Nucleophilic Substitution of the [Bis (1, 2-dicarbollido)-3-cobalt (1-)] ate Ion. Syntheses, Properties and Structures of Its 8, 8'-μ-Sulfato, 8-Phenyl and 8-Dioxane Derivatives. *Collect. Czech. Chem. Commun.* **1997**, *62*, 47–56.

[36] Teixidor, F.; Pedrajas, J.; Rojo, I.; Viñas, C.; Kivekäs, R.; Sillanpää, R.; Sivaev, I.; Bregadze, V.; Sjöberg, S. Chameleonic Capacity of $[3,3'\text{-}Co(1,2\text{-}C_2B_9H_{11})_2]^-$ in Coordination. Generation of the Highly Uncommon S (thioether)-Na Bond. *Organometallics* **2003**, *22*, 3414–3423.

[37] Grüner, B.; Plešek, J.; Báča, J.; Císařová, I.; Dozol, J.; Rouquette, H.; Viñas, C.; Selucký, P.; Rais, J. Cobalt bis (dicarbollide) ions with covalently bonded CMPO groups as selective extraction agents for lanthanide and actinide cations from highly acidic nuclear waste solutions. *New J. Chem.* **2002**, *26*, 1519–1527.

[38] Llop, J.; Masalles, C.; Viñas, C.; Teixidor, F.; Sillanpää, R.; Kivekäs, R. The cosane anion as a platform for new materials: synthesis of its functionalized monosubstituted derivatives incorporating synthons for conducting organic polymers. *Dalton Trans.* **2003**, 556–561.

[39] Sivaev, I.; Starikova, Z.; Sjöberg, S.; Bregadze, V. Synthesis of functional derivatives of the $[3,3'\text{-}Co(1,2\text{-}C_2B_9H_{11})_2]^-$ anion. *J. Organomet. Chem.* **2002**, *649*, 1–8.

[40] Plešek, J.; Grüner, B.; Heřmánek, S.; Báča, J.; Mareček, V.; Jänchenova, J.; Lhotský, A.; Holub, K.; Selucký, P.; Rais, J.; Císařová, I.; Čáslavsky, J. Synthesis of functionalized cobaltacarboranes based on the closo-$[Co\text{-}3\text{-}(1,2\text{-}C_2B_9H_{11})_2]^-$ ion bearing polydentate ligands for separation of M^{3+} cations from nuclear waste solutions. *Polyhedron* **2002**, *21*, 975–986.

[41] Viñas, C.; Bertran, J.; Gomez, S.; Teixidor, F.; Dozol, J. F.; Rouquette, H.; Kivekäs, R.; Sillanpää, R. Aromatic Substituted Metallacarboranes As Extractants Of Cs And Sr From Nuclear Wastes. *Dalton Trans.* **1998**, 2849.

[42] Grüner, B.; Mikulášek, L.; Báca, J.; Císarová, I.; Böhmer, V.; Danila, C.; Reinoso-García, M.; Verboom, W.; Reinhoudt, D.; Casnati, A.; R., U. Cobalt Bis (dicarbollides)(1–) Covalently Attached to the Calix [4] arene Platform: The First Combination of Organic Bowl-Shaped Matrices and Inorganic Metallaborane Cluster Anions. *Eur. J. Org. Chem.* **2005**, 2022–2039.

[43] (a) Olejniczak, A.; Plešek, J.; Lesnikowski, Z. Nucleoside-Metallacarborane Conjugates for Base-Specific Metal Labeling of DNA. *Chem. Eur. J.* **2007**, *13*, 311–318; (b) Matejicek, P.; Cígler, P.; Olejniczak, A. B.; Andrysiak, A.; Wojtczak, B.; Prochazka, K.; Lesnikowski, Z. J. Aggregation Behavior of Nucleoside-Boron Cluster Conjugates in Aqueous Solutions. *Langmuir* **2008**, *24*, 2625–2630.

[44] Farràs, P.; Teixidor, F.; Kivekäs, R.; Sillanpää, R.; Viñas, C.; Grüner, B.; Císařová, I. Metallacarboranes as Building Blocks for Polyanionic Polyarmed Aryl-Ether Materials. *Inorg. Chem.* **2008**, *47*, 9497–9508.

[45] Chamberlin, R.; Scott, B.; Melo, M.; Abney, K. Butyllithium Deprotonation vs Alkali Metal Reduction of Cobalt Dicarbollide: A New Synthetic Route to C-Substituted Derivatives. *Inorg. Chem.* **1997**, *36*, 809–817.

[46] Rojo, I.; Teixidor, F.; Viñas, C.; Kivekäs, R.; Sillanpää, R. Synthesis and Coordinating Ability of an Anionic Cobaltabisdicarbollide Ligand Geometrically Analogous to BINAP. *Chem. Eur. J.* **2004**, *10*, 5376–5385.

[47] Juárez-Pérez, E. J.; Viñas, C.; González-Campo, A.; Teixidor, F.; Sillanpää, R.; Kivekäs, R.; Núñez, R. Controlled Direct Synthesis of C-Mono- and C-Disubstituted Derivatives of $[3,3'\text{-}Co(1,2\text{-}C_2B_9H_{11})_2]^-$ with Organosilane Groups: Theoretical Calculations Compared with Experimental Results. *Chem. Eur. J.* **2008**, *14*, 4924–4938.

[48] Grimes, R. Metallacarboranes in the new millennium. *Coord. Chem. Rev.* **2000**, *200*, 773–811.

[49] (a) Viñas, C.; Gomez, S.; Bertran, J.; Teixidor, F.; Dozol, J.; Rouquette, H. New Polyether-Substituted Metallacarboranes as Extractants for (137) Cs and (90) Sr from Nuclear Wastes. *Inorg. Chem.* **1998**, *37*, 3640–3643; (b) Viñas, C.; Gomez, S.; Bertran, J.; Teixidor, F.; Dozol, J. F.; Rouquette, H. Cobaltabisdicarbollide derivatives as extractants for europium from nuclear wastes. *Chem. Commun.* **1998**, 191–192; (c) Viñas, C.; Gomez, S.; Bertran, J.; Barron, J.; Teixidor, F.; Dozol, J. F.; Rouquette, H.; Kivekäs, R.; Sillanpää, R. C-substituted bis(dicarbollide) metal compounds as sensors and extractants of radionuclides from nuclear wastes. *J. Organomet. Chem.* **1999**, *581*, 188–193.

[50] Mikulasek, L.; Grüner, B.; Dordea, C.; Rudzevich, V.; Bohmer, V.; Haddaoui, J.; Hubscher-Bruder, V.; Arnaud-Neu, F.; Čáslavsky, J.; Selucký, P. Tert-Butyl-calix [4] arenes Substituted at the Narrow Rim with Cobalt Bis (dicarbollide)(1-) and CMPO Groups-New and Efficient Extractants for Lanthanides and Actinides. *Eur. J. Org. Chem.* **2007**, *2007*, 4772.

[51] Marcus, Y.; Sengupra, A. Ion Exchange and Solvent Extraction; Marcel Dekker Inc, 2001.

[52] J. Rais, M. Krys, S. Heřmánek, Czech Patent Nº 153933, 1974.

[53] (a) Crespo, E.; Gentil, S.; Viñas, C.; Teixidor, F. Post-Overoxidation Self-Recovery of Polypyrrole Doped with a Metallacarborane Anion. *J. Phys. Chem. C* **2007**, *111*, 18381–18386; (b) Masalles, C.; Llop, J.; Viñas, C.; Teixidor, F. Extraordinary overoxidation resistance increase in self-doped polypyrroles by using non-conventional low charge-density anions. *Adv. Mater.* **2002**, *14*, 826–829.

[54] Stoica, A.-I.; Viñas, C.; Teixidor, F. Application of the cobaltabisdicarbollide anion to the development of ion selective PVC membrane electrodes for tuberculosis drug analysis. *Chem. Commun.* **2008**, 6492 – 6494.

[55] Cígler, P.; Kožíšek, M.; Řezáčová, P.; Brynda, J.; Otwinowski, Z.; Pokorná, J.; Plešek, J.; Grüner, B.; Doležková-Marešová, L.; Máša, M. et al. From nonpeptide toward noncarbon protease inhibitors: Metallacarboranes as specific and potent inhibitors of HIV protease. *Proc. Natl. Acad. Sci.* **2005**, *102*, 15394–15399.

[56] Köpf-Maier, P.; Köpf, H.; Neuse, E. Ferricenium complexes: A new type of water-soluble antitumor agent. *J. Cancer Res. Clin. Oncol.* **1984**, *108*, 336–340.

[57] Hall, I.; Warren, A.; Lee, C.; Wasczcak, M.; Sneddon, L. Cytotoxicity of Ferratricarbadecaboranyl Complexes in Murine and Human Tissue Cultured Cell Lines. *Anticancer Res.* **1998**, *18*, 951–962.

[58] Nabakka, J.; Harwell, D.; Knobler, C.; Hawthorne, M. Synthesis and structural characterization of a thioether-bridged commo-metallabis (dicarbollide) species: a model system for Venus flytrap cluster reagents. *J. Organomet. Chem.* **1998**, *550*, 423–429.

[59] Teixidor, F.; Barberà, G.; Viñas, C.; Sillanpää, R.; Kivekäs, R. Synthesis of boron-iodinated o-carborane derivatives. Water stability of the periodinated monoprotic salt. *Inorg. Chem.* **2006**, *45*, 3496–3498.

[60] Barth, R.; Coderre, J.; Vicente, M.; Blue, T. Boron Neutron Capture Therapy of Cancer: Current Status and Future Prospects. *Clin. Cancer Res.* **2005**, *11*, 3987.

[61] Hao, E.; Vicente, M. Expeditious synthesis of porphyrin–cobaltacarborane conjugates. *Chem. Commun.* **2005**, 1306–1308.

[62] Hawthorne, M.; Maderna, A. Applications of radiolabeled boron clusters to the diagnosis and treatment of cancer. *Chem. Rev* **1999**, *99*, 3421–3434.

[63] Gottumukkala, V.; Ongayi, O.; Baker, D.; Lomax, L.; Vicente, M. Synthesis, cellular uptake and animal toxicity of a tetra (carboranylphenyl)-tetrabenzoporphyrin. *Bioorganic & medicinal chemistry* **2006**, *14*, 1871–1879.

[64] Bregadze, V.; Sivaev, I.; Glazun, S. Polyhedral Boron Compounds as Potential Diagnostic and Therapeutic Antitumor Agents. *Anti Cancer Agents in Medicinal Chemistry* **2006**, *6*, 75–110.

[65] Wang, J.; Ren, C.; Weng, L.; Jin, G. Porphyrin-carborane organometallic assemblies based on 1, 2-dicarba-closo-dodecaborane (12) ligands. *Chem. Commun.* **2006**, *2006*, 162–164.

[66] Hao, E.; Sibrian-Vazquez, M.; Serem, W.; Garno, J.; Fronczek, F.; Vicente, M. Synthesis, Aggregation and Cellular Investigations of Porphyrin-Cobaltacarborane Conjugates. *Chem. Eur. J.* **2007**, *13*, 9035–9042.

[67] Li, H.; Fronczek, F.; Vicente, M. Synthesis and properties of cobaltacarborane-functionalized Zn (II)-phthalocyanines. *Tetrahedron Lett.* **2008**, *49*, 4828–4830.

[68] (a) DuBay, W.; Grieco, P.; Todd, L. Lithium Cobaltbisdicarbollide: A Novel Lewis Acid Catalyst for the Conjugate Addition of Silyl Ketene Acetals to Hindered Unsaturated Carbonyl Compounds. *J. Org. Chem.* **1994**, *59*, 6898–6899; (b) Grieco, P.; DuBay, W.; Todd, L. Lithium Cobaltbisdicarbollide catalyzed substitution reactions of allylic acetates. *Tetrahedron Lett.* **1996**, *37*, 8707–8710.

[69] Tomalia, D. Birth of a new macromolecular architecture: dendrimers as quantized building blocks for nanoscale synthetic polymer chemistry. *Prog. Polym. Sci.* **2005**, *30*, 294–324.

[70] Buhleier, E.; Wehner, W.; Vögtle, F. Cascade and Nonskid-Chain-like Synthesis of Molecular Cavity Topologies. *Synthesis* **1978**, *2*, 155.

[71] R. G. Denkewalter, J. F. Kolc and W. J. Lukasavage, U.S. Patent 4,289,872 (1981).

[72] El término *dendrímero* deriva del griego *dendra* (árbol) y de *meros* (parte). También se ha denominado a estas moléculas *arboroles* (Latín: arbor = árbol), *coliflores*, *starbust polymers* por su semejanza con los ejemplos que la naturaleza construye de forma *fractal*.

[73] Tomalia, D.; Baker, H.; Dewald, J.; Hall, M.; Kallos, G.; Martin, S.; Roeck, J.; Ryder, J.; Smith, P. A New Class of Polymers: Starburst-Dendritic Macromolecules. *Polym. J.* **1985**, *17*, 117–132.

[74] Newkome, G.; Yao, Z.; Baker, G.; Gupta, V. Micelles. Part 1. Cascade molecules: a new approach to micelles. A [27]-arborol. *J. Org. Chem.* **1985**, *50*, 2003–2004.

[75] Tomalia, D.; Fréchet, J. M. J. Discovery of dendrimers and dendritic polymers: A brief historical perspective. *J. Polym. Sci., Part A: Polym. Chem.* **2002**, *40*, 2719–2728.

[76] Newkome, G.; Moorefield, C.; Vögtle, F.; Wiley, J. Dendrimers and Dendrons: Concepts, Syntheses, Applications; Wiley-VCH, 2001.

[77] Tomalia, D.; Fréchet, J. Dendrimers and Other Dendritic Polymers; Wiley Series in Polymer Science, Wiley Chichester, UK, 2001.

[78] Fréchet, J. M. J. Dendrimers and Other Dendritic Macromolecules: From Building Blocks to Functional Assemblies in Nanoscience and Nanotechnology. *J. Polym. Sci. Part A: Polym. Chem.* **2003**, *41*, 3713–3725.

[79] (a) Majoros, I. J.; Williams, C. R.; Baker, J. R. Current dendrimer applications in cancer diagnosis and therapy. *Curr. Top. Med. Chem.* **2008**, *8*, 1165–1179; (b) Gao, Y.; Gao, G.; He, Y.; Liu, T.; Qi, R. Recent advances of dendrimers in delivery of genes and drugs. *Mini-Rev. Med. Chem.* **2008**, *8*, 889 – 900; (c) Singh, I.; Rehni, A. K.; Kalra, R.; Joshi, G.; Kumar, M. Dendrimers and their pharmaceutical applications - a review. *Pharmazie* **2008**, *63*, 491–496; (d) Agarwal, A.; Asthana, A.; Gupta, U.; Jain, N. K. Tumour and dendrimers: a review on drug delivery aspects. *J. Pharm. Pharmacol.* **2008**, *60*, 671 – 688; (e) Cheng, Y.; Xu, T. The effect of dendrimers on the pharmacodynamic and pharmacokinetic behaviors of non-covalently or covalently attached drugs. *Eur. J. Med. Chem.* **2008**, *43*, 2291 – 2297; (f) Najlah, M.; D'Emanuele, A. Synthesis of dendrimers and drug-dendrimer conjugates for drug delivery. *Curr. Opin. Drug Discovery Dev.* **2007**, *10*, 756–767; (g) Parekh, H. S. The advance of dendrimers - A versatile targeting platform for gene/drug delivery. *Curr. Pharm. Des.* **2007**, *13*, 2837–2850; (h) Cheng, Y.; Gao, Y.; Rao, T.; Li, Y.; Xu, T. Dendrimer based prodrugs: design, synthesis, screening and biological evaluation. *Comb. Chem. High Throughput Screen* **2007**, *10*, 336 – 349; (i) Yang, H.; Kao, W. Y. J. Dendrimers for pharmaceutical and biomedical applications. *J. Biomater. Sci., Polym. Ed.* **2006**, *17*, 3–19.

[80] Andrés, R.; de Jesús, E.; Flores, J. C. Catalysts based on palladium dendrimers. *New J. Chem.* **2007**, *31*, 1161 – 1191.

[81] de Jesus, E.; Flores, J. C. Dendrimers Solutions For Catalyst Separation and Recycling-A Review. *Ind. Eng. Chem. Res.* **2008**, *47*, 7968–7981.

[82] (a) Astruc, D.; Ornelas, C.; Aranzaes, J. R. Ferrocenyl terminated dendrimers: Design for applications in molecular electronics, molecular recognition and catalysis. *J. Inorg. Organomet. Polym. Mater.* **2008**, *18*, 4–17; (b) Caminade, A.-M.; Servin, P.; Laurent, R.; Majoral, J.-P. Dendrimeric phosphines in asymmetric catalysis. *Chem. Soc. Rev.* **2008**, *37*, 56 – 67; (c) Javor, S.; Delort, E.; Darbre, T.; Reymond, J. A Peptide Dendrimer Enzyme Model with a Single Catalytic Site at the Core. *J. Am. Chem. Soc.* **2007**, *129*, 13238–13246; (d) Helms, B.; Fréchet, J. M. J. The dendrimer effect in homogeneous catalysis. *Adv. Synth. Catal.* **2006**, *348*, 1125–1148; (e) Reek, J. N. H.; Arevalo, S.; Van Heerbeek, R.; Kamer, P. C. J.; Van Leeuwen, P. W. N. M. Dendrimers in catalysis. *Adv. Catal.* **2006**, *49*, 71–151.

[83] (a) Andraud, C.; Fortrie, R.; Barsu, C.; Stephan, O.; Chermette, H.; Baldeck, P. L. Excitonically Coupled Oligomers and Dendrimers for Two-Photon Absorption. *Adv. Polym. Sci.* **2008**, *214*, 149 – 203; (b) DAmbruoso, G. D.; McGrath, D. V. Energy Harvesting in Synthetic Dendrimer Materials. *Adv. Polym. Sci.* **2008**, *214*, 87 – 147; (c) Puntoriero, F.; Nastasi, F.; Cavazzini, M.; Quici, S.; Campagna, S. Coupling synthetic antenna and electron donor species: A tetranuclear mixed-metal Os(II)-Ru(II) dendrimer containing six phenothiazine donor subunits at the periphery. *Coord. Chem. Rev.* **2007**, *251*, 536–545; (d) Nishiyama, N.; Jang, W. D.; Kataoka, K. Supramolecular nanocarriers integrated with dendrimers encapsulating photosensitizers for effective photodynamic therapy and photochemical gene delivery. *New J. Chem.* **2007**, *31*, 1074–1082; (e) Lo, S. C.; Burn, P. L. Development of dendrimers: Macromolecules for use in organic light-emitting diodes and solar cells. *Chem. Rev.* **2007**, *107*, 1097–1116; (f) Burn, P. L.; Lo, S. C.; Samuel, I. D. W. The development of light-emitting dendrimers for displays. *Adv. Mater.* **2007**, *19*, 1675 – 1688; (g) Peng, Z. H.; Melinger, J. S.; Kleiman, V. Light harvesting unsymmetrical conjugated dendrimders as photosynthetic mimics. *Photosynth. Res.* **2006**, *87*, 115–131; (h) Nantalaksakul, A.; Reddy, D. R.; Bardeen, C. J.; Thayumanavan, S. Light harvesting dendrimers. *Photosynth. Res.* **2006**, *87*, 133–150.

[84] de Gennes, P.; Hervet, H. Statistics of Starburst polymers. *Phys. Lett.* **1983**, *44*, 351–360.

[85] (a) Hawker, C. J.; Fréchet, J. M. J. A new convergent approach to monodisperse dendritic macromolecules. *Chem. Commun.* **1990**, 1010–1013; (b) Hawker, C. J.; Fréchet, J. M. J. Preparation of polymers with controlled molecular architecture. A new convergent approach to dendritic macromolecules. *J. Am. Chem. Soc.* **1990**, *112*, 7638–7647.

[86] (a) Majoral, J.; Caminade, A. Dendrimers containing heteroatoms (Si, P, B, Ge, or Bi). *Chem. Rev.* **1999**, *99*, 845–880; (b) Frey, H.; Lach, C.; Lorenz, K. Heteroatom-Based Dendrimers. *Adv. Mater.* **1998**, *10*, 279–293.

[87] (a) Van der Made, A. W.; Van Leeuwen, P.; De Wilde, J. C.; Brandes, R. A. C. Dendrimeric silanes. *Adv. Mater.* **1993**, *5*, 466–468; (b) Van der Made, A.; Van Leeuwen, P. Silane dendrimers. *Chem. Commun.* **1992**, 1400–1401; (c) Roovers, J.; Zhou, L.; Toporowski, P.; van der Zwan, M.; Iatrou, H.; Hadjichristidis, N. Regular star polymers with 64 and 128 arms. Models for polymeric micelles. *Macromolecules* **1993**, *26*, 4324–4331.

[88] Schlenk, C.; Frey, H. Carbosilane Dendrimers - Synthesis, funcionalization, application. *Monatsh. Chem.* **1999**, *130*, 3–14.

[89] Frey, H.; Schlenk, C. Silicon-Based Dendrimers. *Dendrimers II* **2000**, *210*, 69–130.

[90] (a) Knapen, J.; van der Made, A.; de Wilde, J.; van Leeuwen, P.; Wijkens, P.; Grove, D.; van Koten, G. Homogeneous catalysts based on silane dendrimers functionalized with arylnickel (II) complexes. *Nature* **1994**, *372*, 659–663; (b) Alonso, B.; Cuadrado, I.; Morán, M.; Losada, J. Organometallic Silicon Dendrimers. *Chem. Commun.* **1994**, 2575 – 2576.

[91] (a) Krska, S.; Seyferth, D. Synthesis of Water-Soluble Carbosilane Dendrimers. *J. Am. Chem. Soc.* **1998**, *120*, 3604–3612; (b) Seyferth, D.; Kugita, T.; Rheingold, A.; Yap, G. Preparation of carbosilane dendrimers with peripheral acetylene-dicobalt hexacarbonyl substituents. *Organometallics* **1995**, *14*, 5362–5366.

[92] Kim, C.; Park, E.; Kang, E. Synthesis and Characterization of A Carbosilane Dendrimer Containing Allylic End Groups. *Bull. Korean Chem. Soc.* **1996**, *17*, 592–594.

[93] (a) Grayson, S. M.; Fréchet, J. M. J. Convergent Dendrons and Dendrimers: from Synthesis to Applications. *Chem. Rev.* **2001**, *101*, 3819; (b) Hecht, S.; Fréchet, J. M. J. Dendritic Encapsulation of Function: Applying Nature's Site Isolation Principle from Biomimetics to Materials Science. *Angew. Chem. Int. Ed.* **2001**, *40*, 74.

[94] Newkome, G. R.; Moorefield, C. N.; Keith, J. M.; Baker, G. R.; Escamilla, G. H. Chemistry within a unimolecular micelle precursor: boron superclusters by site- and depth-specific transformations of dendrimers. *Angew. Chem. Int. Ed.* **1994**, *33*, 666–668.

[95] Thomas, J.; Hawthorne, M. F. Dodeca-carboranyl substituted closomers: toward unimolecular nanoparticles as delivery vehicles for BNCT. *Chem. Commun.* **2001**, 1884–1885.

[96] (a) Parrott, M.; Marchington, E.; Valliant, J.; Adronov, A. Synthesis and properties of carborane-functionalized aliphatic polyester dendrimers. *J. Am. Chem. Soc.* **2005**, *127*, 12081–12089; (b) Parrott, M.; Marchington, E.; Valliant, J.; Adronov, A. Preparation of synthons for carborane containing macromolecules. *Macromol. Symp.* **2003**, *196*, 201–211.

[97] (a) González-Campo, A.; Juárez-Pérez, E.; Viñas, C.; Boury, B.; Sillanpää, R.; Kivekäs, R.; Núñez, R. Carboranyl Substituted Siloxanes and Octasilsesquioxanes: Synthesis, Characterization and Reactivity. *Macromolecules* **2008**, *41*, 8458–8466; (b) González-Campo, A.; Viñas, C.; Teixidor, F.; Núñez, R.; Sillanpää, R.; Kivekäs, R. Modular Construction Of Neutral And Anionic Carboranyl-Containing Carbosilane-Based Dendrimers. *Macromolecules* **2007**, *40*, 5644–5652.

[98] Lerouge, F.; Viñas, C.; Teixidor, F.; Núñez, R.; Abreu, A.; Xochitiotzi, E.; Santillan, R.; Farfán, N. High boron content carboranyl-functionalized aryl ether derivatives displaying photoluminescent properties. *Dalton Trans.* **2007**, 1898–1903.

[99] Yao, H.; Grimes, R. N.; Corsini, M.; Zanello, P. Polynuclear Metallacarborane - Hydrocarbon Assemblies: Metallacarborane Dendrimers. *Organometallics* **2003**, *22*, 4381.

[100] Serroni, S.; Denti, G.; Campagna, S.; Juris, A.; Ciano, M.; Balzani, V. Arborols Based on Luminescent and Redox-Active Transition Metal Complexes. *Angew. Chem. Int. Ed.* **1992**, *31*, 1493.

[101] Newkome, G.; He, E.; Moorefield, C. Suprasupermolecules with Novel Properties: Metallodendrimers. *Chem. Rev.* **1999**, *99*, 1689–1746.

[102] Gorman, C. Metallodendrimers Structural Diversity and Functional Behavior. *Adv. Mater.* **1998**, *10*, 295.

[103] Cuadrado, I.; Moran, M.; Casado, C. M.; Alonso, B.; Losada, J. Organometallic dendrimers with transition metals. *Coord. Chem. Rev.* **1999**, *193*, 395.

[104] Caminade, A.; Majoral, J. Phosphorus dendrimers possessing metallic groups in their internal structure (core or branches): Syntheses and properties. *Coordination Chemistry Reviews* **2005**, *249*, 1917–1926.

[105] Jin, R.; Aida, T.; Inoue, S. Caged porphyrin: the first dendritic molecule having a core photochemical functionality. *Chem. Commun.* **1993**, 1260–1262.

[106] Newkome, G.; Cardullo, F.; Constable, E.; Moorefield, C.; Thompson, A. Metallomicellanols incorporation of ruthenium (II)-2, 2': 6', 2-terpyridine triads into cascade polymers. *Chem. Commun.* **1993**, 925–927.

[107] Marx, H.-W.; Moulines, F.; Wagner, T.; Astruc, D. Hexakis (but- 3-ynyl)Benzene. *Angew. Chem. Int. Ed.* **1996**, *35*, 1701 – 1704.

[108] (a) Astruc, D. Organometallic chemistry at the nanoscale. Dendrimers for redox processes and catalysis. *Pure Appl. Chem* **2003**, *75*, 461–481; (b) Méry, D.; Astruc, D. Dendritic catalysis: Major concepts and recent progress. *Coord. Chem. Rev.* **2006**, *250*, 1965–1979; (c) Hwang, S. H.; Shreiner, C. D.; Moorefield, C. N.; Newkome, G. R. Recent progress and applications for metallodendrimers. *New J. Chem.* **2007**, *31*, 1192–1217; (d) Astruc, D.; Ornelas, C.; Ruiz, J. Metallocenyl dendrimers and their applications in molecular electronics, sensing, and catalysis. *Acc. Chem. Res.* **2008**, *41*, 841–856; (e) Oosterom, G.; Reek, J.; Kamer, P.; van Leeuwen, P. Transition metal catalysis using functionalized dendrimers. *Angew. Chem. Int. Ed* **2001**, *40*, 1828.

[109] Zimmerman, S. C.; Lawless, L. J. Supramolecular chemistry of dendrimers. *Dendrimers IV* **2001**, *217*, 95–120.

[110] Donnio, B.; Buathong, S.; Bury, I.; Guillon, D. Liquid crystalline dendrimers. *Chem. Soc. Rev.* **2007**, *36*, 1495–1513.

[111] Marcos, M.; Martín-Rapún, R.; Omenat, A.; Serrano, J. Highly congested liquid crystal structures: dendrimers, dendrons, dendronized and hyperbranched polymers. *Chem. Soc. Rev.* **2007**, *36*, 1889–1901.

[112] Ponomarenko, S.; Boiko, N.; Shibaev, V.; Richardson, R.; Whitehouse, I.; Rebrov, E.; Muzafarov, A. Carbosilane Liquid Crystalline Dendrimers: From Molecular Architecture to Supramolecular Nanostructures. *Macromolecules* **2000**, *33*, 5549–5558.

[113] Stoddart, J. F.; Welton, T. Metal containing dendritic polymers. *Polyhedron* **1999**, *18*, 3575–3591.

[114] Svenson, S. Dendrimers as versatile platform in drug delivery applications. *Eur. J. Pharm. Biopharm.* **2009**, *71*, 445–462.

[115] Florence, A. T. Dendrimers A Versatile Targeting Platform. *Adv. Drug Delivery Rev.* **2005**, *57*, 2104.

[116] (a) Ornelas, C.; Boisselier, E.; Martinez, V.; Pianet, I.; Aranzaes, J.; Astruc, D. New water-soluble polyanionic dendrimers and binding to acetylcholine in water by means of contact ion-pairing interactions. *Chem. Commun.* **2007**, 5093–5095; (b) Boisselier, E.; Ornelas, C.; Pianet, I.; Aranzaes, J. R.; Astruc, D. Four generations of water-soluble dendrimers with 9 to 243 benzoate tethers: Synthesis and dendritic effects on their ion pairing with acetylcholine, benzyltriethylammonium, and dopamine in water. *Chem. Eur. J.* **2008**, *14*, 5577–5587.

[117] Stiriba, S.; Frey, H.; Haag, R. Dendritic Polymers in Biomedical Applications: From Potential to Clinical Use in Diagnostics and Therapy. *Angew. Chem. Int. Ed* **2002**, *41*, 1329–1334.

[118] Krause, W.; Hackmann-Schlichter, N.; Maier, F.; Müller, R. Dendrimers in Diagnostics. *Dendrimers II* **2000**, *210*, 261–308.

[119] Wu, G.; Barth, R. F.; Yang, W.; Chatterjee, M.; Tjarks, W.; Ciesielski, M. J.; Fenstermaker, R. A. Site specific conjugation of boron-containing dendrimers to anti-EGF receptor monoclonal antibody cetuximab (IMC-C225) and its evaluation as a potential delivery agent for neutron capture therapy. *Bioconjugate Chem.* **2004**, *15*, 185 – 194.

[120] Barth, R. F.; Adams, D. M.; Soloway, A. H.; Alam, F.; Darby, M. V. Boronated starburst dendrimer-monoclonal antibody immunoconjugates: Evaluation as a potential delivery system for neutron capture therapy. *Bioconjugate Chem.* **1994**, *5*, 58–66.

[121] Ulman, A. Formation and structure of self-assembled monolayers. *Chem. Rev.* **1996**, *96*, 1533–1554.

[122] Guerrero, G.; Mutin, P. H.; Vioux, A. Anchoring of phosphonate and phosphinate coupling molecules on titania particles. *Chem. Mater.* **2001**, *13*, 4367–4373.

[123] Mutin, P. H.; Guerrero, G.; Vioux, A. Hybrid materials from organophosphorus coupling molecules. *J. Mater. Chem.* **2005**, *15*, 3761–3768.

[124] Caro, J.; Noack, M.; Kolsch, P. Chemically modified ceramic membranes. *Microporous Mesoporous Mater.* **1998**, *22*, 321.

[125] Villemin, D.; Jaffres, P.-A.; Nechab, B.; Courivaud, F. Palladium complexes supported on hybrid organic-inorganic zirconium phosphite: selectivity in the Heck reaction. *Tetrahedron Lett.* **1997**, *38*, 6581.

[126] Grätzel, M. Solar Energy Conversion by Dye-Sensitized Photovoltaic Cells. *Inorg. Chem.* **2005**, *44*, 6841–6851.

[127] Gawalt, E. S.; Avaltroni, M. J.; Danahy, M. P.; Silverman, B. M.; Hanson, E. L.; Midwood, K. S.; Schwarzbauer, J. E.; Schwartz, J. Bonding Organics to Ti Alloys: Facilitating Human Osteoblast Attachment and Spreading on Surgical Implant Materials. *Langmuir* **2003**, *19*, 200.

[128] (a) Buriak, J. M. Organometallic Chemistry on Silicon and Germanium Surfaces. *Chem. Rev.* **2002**, *102*, 1271 – 1308; (b) Onclin, S.; Ravoo, B. J.; Reinhoudt, D. N. Engineering Silicon Oxide Surfaces Using Self-Assembled Monolayers. *Angew. Chem. Int. Ed.* **2005**, *44*, 6282 – 6304.

[129] Wang, R.; Baran, G.; Wunder, S. Packing and Thermal Stability of Polyoctadecylsiloxane Compared with Octadecylsilane Monolayers. *Langmuir* **2000**, *16*, 6298–6305.

[130] Nam, H.; Granier, M.; Boury, B.; Park, S. Functional Organotrimethoxysilane Derivative with Strong Intermolecular-Interaction: One-Pot Grafting Reaction on Oxidized Silicon Substrates. *Langmuir* **2006**, *22*, 7132–7134.

[131] van der Veen, N. J.; Flink, S.; Deij, M. A.; Egberink, R. M. J.; van Veggel, F. C. J. M.; Reinhout, D. N. Monolayer of a Na^+ Selective Fluoroionophore on Glass: Connecting the Fields of Monolayers and Optical Detection of Metal Ions. *J. Am. Chem. Soc.* **2000**, *122*, 6112.

[132] Wilson, D. S.; Nock, S. Recent Developments in Protein Microarray Technology. *Angew. Chem. Int. Ed.* **2003**, *42*, 494.

[133] Perzyna, A.; Dal Zotto, C.; Durand, J.; Granier, M.; Smietana, M.; Melnyk, O.; Stará, I.; Starý, I.; Klepetárová, B.; Saman, D. Reaction of Isocyanate-Functionalised Silicon Wafers with Complex Amino Compounds. *Eur. J. Org. Chem.* **2007**, 4032.

[134] Hong, L.; Sugimura, H.; Furukawa, T.; Takai, O. Photoreactivity of Alkylsilane Self-Assembled Monolayers on Silicon Surfaces and Its Application to Preparing Micropatterned Ternary Monolayers. *Langmuir* **2003**, *19*, 1966.

[135] Wu, A.; Kakimoto, M. A. LEDs Based on Poly(p-phenylenevinylene) and Polyimide LB Films. *Adv. Mater.* **1995**, *7*, 812.

[136] Halik, M.; Klauk, H.; Zschieschang, U.; Schmid, G.; Dehm, C.; Schutz, M.; Maisch, S.; Effenberger, F.; Brunnbauer, M.; Stellacci, F. Low-voltage organic transistors with an amorphous molecular gate dielectric. *Nature* **2004**, *431*, 963 – 966.

[137] Facchetti, A.; Abbotto, A.; Beverina, L.; van der Boom, M. E.; Dutta, P.; Evmenenko, G.; Marks, T. J.; Pagani, G. A. Azinium (pi-Bridge)-Pyrrole NLO-Phores: Influence of Heterocycle Acceptors on Chromophoric and Self-Assembled Thin-Film Properties. *Chem. Mater.* **2002**, *14*, 4996.

[138] Kawanishi, T.; Tamaki, T.; Sakuragi, M.; Seki, T.; Suzuki, Y.; Ichimura, K. Photochemical induction and modulation of nematic homogeneous alignment by the polarization photochromism of surface azobenzenes. *Langmuir* **1992**, *8*, 2601.

[139] Collum, D. Is Tetramethylethylenediamine a Good Ligand for Lithium? *Acc. Chem. Res.* **1992**, *25*, 448–454.

[140] Venable, T.; Hutton, W.; Grimes, R. Two-dimensional boron-11-boron-11 nuclear magnetic resonance spectroscopy as a probe of polyhedral structure: application to boron hydrides, carboranes, metallaboranes, and metallacarboranes. *J. Am. Chem. Soc.* **1984**, *106*, 29–37.

[141] Rojo, I.; Teixidor, F.; Viñas, C.; Kivekäs, R.; Sillanpää, R. Relevance of the electronegativity of boron in apto-5 coordinating ligands: Regioselective monoalkylation and monoarylation in cobaltabisdicarbollide clusters. *Chem. Eur. J.* **2003**, *9*, 4311–4323.

[142] Horakova, H.; Vespalec, R. Optical spectra of anionic boron cluster compounds and their utilization for photometric detection. *Spectrochim. Acta, Part A* **2006**, *65*, 378–386.

[143] Parr, R.; Yang, W. Density-Functional Theory of Atoms and Molecules; Oxford University Press, USA, 1989.

[144] (a) Becke, A. D. Density-functional exchange-energy approximation with correct asymptotic behavior. *Phys. Rev. A* **1988**, *38*, 3098–3100; (b) Lee, C.; Yang, W.; Parr, R. G. Development of the Colle-Salvetti correlation-energy formula into a functional of the electron density. *Phys. Rev. B* **1988**, *37*, 785.

[145] (a) Hawthorne, M.; Zink, J.; Skelton, J.; Bayer, M.; Liu, C.; Livshits, E.; Baer, R.; Neuhauser, D. Electrical or Photocontrol of the Rotary Motion of a Metallacarborane. *Science* **2004**, *303*, 1849–1851; (b) Núñez, R.; Tutusaus, O.; Teixidor, F.; Viñas, C.; Sillanpää, R.; Kivekäs, R. Highly Stable Neutral And Positively Charged Dicarbollide Sandwich Complexes. *Chem. Eur. J.* **2005**, *11*, 5637–5647; (c) Llop, J.; Viñas, C.; Teixidor, F.; Victori, L.; Kivekäs, R.; Sillanpää, R. Frozen-out rotamers of mixed cobaltacarborane complexes. *Organometallics* **2002**, *21*, 355–361.

[146] Bühl, M.; Hnyk, D.; Macháček, J. Computational Study of Structures and Properties of Metallaboranes: Cobalt Bis (dicarbollide). *Chem. Eur. J.* **2005**, *11*, 4109.

[147] Juárez-Pérez, E.; Viñas, C.; Teixidor, F.; Núñez, R. First example of the formation of a Si-C bond from an intramolecular Si-H...H-C diyhydrogen interaction in a metallacarborane: A theoretical study. *J. Organomet. Chem.* **2009**, *694*, 1764–1770.

[148] (a) Alkorta, I.; Elguero, J. Non-conventional hydrogen bonds. *Chem. Soc. Rev.* **1998**, *27*, 163–170; (b) Desiraju, G. R. Hydrogen bonds and other intermolecular interactions in organometallic crystals. *Dalton Trans.* **2000**, 3745–3751; (c) Custelcean, R.; Jackson, J. Dihydrogen bonding: structures, energetics, and dynamics. *Chem. Rev.* **2001**, *101*, 1963–80; (d) Epstein, L.; Shubina, E. New types of hydrogen bonding in organometallic chemistry. *Coord. Chem. Rev.* **2002**, *231*, 165–181.

[149] (a) Bader, R. Atoms in Molecules: A Quantum Theory; Clarendon Press Oxford, UK, 1994; (b) Popelier, P. Characterization of a Dihydrogen Bond on the Basis of the Electron Density. *J. Phys. Chem. A* **1998**, *102*, 1873–1878; (c) Alkorta, I.; Elguero, J.; Grabowski, S. How To Determine Whether Intramolecular H... H Interactions Can Be Classified as Dihydrogen Bonds. *J. Phys. Chem. A* **2008**, *112*, 2721–2727.

[150] Tsirelson, V.; Stash, A. Analyzing experimental electron density with the localized-orbital locator. *Acta Crys. B* **2002**, *58*, 780–785.

[151] Perdew, J. P. Density-functional approximation for the correlation energy of the inhomogeneous electron gas. *Physical review. B, Condensed matter* **1986**, *33*, 8822–8824.

[152] ADF2007.01, SCM, Theoretical Chemistry, Vrije Universiteit, Amsterdam, The Netherlands.

[153] Richardson, T.; de Gala, S.; Crabtree, R.; Siegbahn, P. Unconventional Hydrogen Bonds: Intermolecular BH...HN Interactions. *J. Am. Chem. Soc* **1995**, *117*, 12875–12876.

[154] Espinosa, E.; Molins, E.; Lecomte, C. Hydrogen bond strengths revealed by topological analyses of experimentally observed electron densities. *Chem. Phys. Lett.* **1998**, *285*, 170–173.

[155] Juárez-Pérez, E. J.; Viñas, C.; Teixidor, F.; Núñez, R. Polyanionic Carbosilane And Carbosiloxane Metallodendrimers Based On Cobaltabisdicarbollide Derivatives. *Organometallics* **2009**, submitted.

[156] Comunicación privada de S. Gómez-Ruiz.

[157] (a) Antiñolo, A.; Fajardo, M.; Gómez-Ruiz, S.; López-Solera, I.; Otero, A.; Prashar, S. Hydrosilylation in the Design and Functionalization of ansa-Metallocene Complexes. *Organometallics* **2004**, *23*, 4062–4069; (b) Gómez-Ruiz, S.; Prashar, S.; Fajardo, M.; Antiñolo, A.; Otero, A.; Maestro, M.; Volkis, V.; Eisen, M.; Pastor, C. Synthesis, hydrosilylation reactivity and catalytic properties of group 4 ansa-metallocene complexes. *Polyhedron* **2005**, *24*, 1298–1313.

[158] Domanska, U.; Bogel-Lukasik, E.; Bogel-Lukasik, R. Octanol-Water Partition Coefficients of 1-Alkyl-3-methylimidazolium Chloride. *Chem. Eur. J.* **2003**, *9*, 3033 – 3041.

[159] Justus, E.; Rischka, K.; Wishart, J.; Werner, K.; Gabel, D. Trialkylammoniododecaborates Anions for Ionic Liquids with Potassium, Lithium and Protons as Cations. *Chem. Eur. J.* **2008**, *14*, 1918–1923.

[160] Ornelas, C.; Ruiz, J.; Astruc, D. Giant Cobalticinium Dendrimers. *Organometallics* **2009**, DOI: 10.1021/om900079y.

[161] Kim, C.; Jung, I. Preparation of ethynylsilane dendrimers. *J. Organomet. Chem.* **2000**, *599*, 208–215.

[162] Buggins, T.; Dickinson, P.; Taylor, G. The effects of pharmaceutical excipients on drug disposition. *Adv. Drug Delivery Rev.* **2007**, *59*, 1482–1503.

[163] Juárez-Pérez, E. J.; Viñas, C.; Teixidor, F.; Santillan, R.; Farfan, N.; Abreu, A.; Yepez, R.; Núñez, R. Polyanionic Aryl-Ether Metallodendrimers Based On Cobaltabisdicarbollide Derivatives. Photoluminescent Properties. *Macromolecules* **2009**, in preparation.

[164] Sambasivarao, K.; Dhurke, K.; Kakali, L.; Raghavan, S. B. Synthesis of C3-Symmetric Nano-Sized Polyaromatic Compounds by Trimerization and Suzuki-Miyaura Cross-Coupling Reactions. *Eur. J. Org. Chem.* **2004**, *19*, 4003.

[165] Khotina, I. A.; Lepnev, L. S.; Burenkova, N. S.; Valetsky, P. M.; Vitukhnovsky, A. G. Phenylene dendrimers and novel hyperbranched polyphenylenes as light emissive materials for blue OLEDs. *J. Luminiscence* **2004**, *110*, 232.

[166] Allen, M.; Tildesley, D. Computer simulation of liquids; Oxford University Press, USA, 1989.

[167] Arturo Abreu, Elba Xochitiotzi y Rosa Santillan del Centro de Investigación y Estudios Avanzados del Instituto Politécnico Nacional de México.

[168] Adronov, A.; Fréchet, J. M. J. Novel Two-Photon Absorbing Dendritic Structures. *Chem. Mater.* **2000**, *12*, 2838.

[169] Núñez, R.; Juárez-Pérez, E. J.; Teixidor, F.; Santillan, R.; Farfan, N.; Abreu, A.; Yepez, R.; Viñas, C. Decorating Poly(Alkyl Aryl-Ether) Dendrimers With Metallacarboranes. *Inorg. Chem.* **2009**, in preparation.

[170] Brook, M. A. Silicon in Organic, Organometallic, and Polymer Chemistry; J. Wiley and Sons and Inc: New York, 2000; p 256.

[171] Juárez-Pérez, E. J.; Mutin, H.; Granier, M.; Teixidor, F.; Núñez, R. Anchoring Phosphorous-containing Cobaltabisdicarbollide Derivatives on Titania Particles. *Chem. Mater.* **2009**, in preparation.

[172] Plešek, J.; Grüner, B.; Císařová, I.; Báča, J.; Selucký, P.; Rais, J. Functionalized cobalt bis(dicarbollide) ions as selective extraction reagents for removal of M^{2+} and M^{3+} cations from nuclear waste. *J. Organomet. Chem.* **2002**, *657*, 59–70.

[173] Tiritiris, I.; Schleid, T.; Müller, K. Solid-State NMR Studies on Ionic closo-Dodecaborates. *Applied Magnetic Resonance* **2007**, *32*, 459–481.

[174] Juárez-Pérez, E. J.; Granier, M.; Mutin, H.; Viñas, C.; Núñez, R. Approaches For Anchoring Cobaltabisdicarbollide Anions Onto Oxidized Silicon Wafers. *Langmuir* **2009**, in preparation.

[175] Ardes-Guisot, N.; Durand, J.; Granier, M.; Perzyna, A.; Coffinier, Y.; Grandidier, B.; Wallart, X.; Stievenard, D. Trichlorosilane isocyanate as coupling agent for mild conditions functionalization of silica-coated surfaces. *Langmuir* **2005**, *21*, 9406–9408.

Anexo I

Artículos posteriores a la Comisión de Doctorado de Abril de 2009.

Artículos manuscritos enviados o pendientes de publicación posteriores a la Comisión de Doctorado de la UAB en Abril de 2009:

a) Polyanionic Carbosilane And Carbosiloxane Metallodendrimers Based On Cobaltabisdicarbollide Derivatives. Emilio José Juárez-Pérez, Clara Viñas, Francesc Teixidor, Rosario Núñez. *Organometallics* **2009**, *submitted*.

b) Polyanionic Aryl-Ether Metallodendrimers Based On Cobaltabisdicarbollide Derivatives. Photoluminescent Properties. Emilio José Juárez-Pérez, Clara Viñas, Francesc Teixidor, Rosa Santillan, Norberto Farfán, Arturo Abreu, Rebeca Yépez, Rosario Núñez. *In preparation*.

c) Decorating Poly(Alkyl Aryl-Ether) Dendrimers With Metallacarboranes. Rosario Núñez, Emilio José Juárez-Pérez, Francesc Teixidor, Rosa Santillan, Norberto Farfán, Arturo Abreu, Rebeca Yépez, Clara Viñas. *In preparation*.

d) Anchoring Phosphorous-containing Cobaltabisdicarbollide Derivatives on Titania Particles. Emilio José Juárez-Pérez, Hubert Mutin, Michel Granier, Francesc Teixidor, Rosario Núñez. *In preparation*.

e) Approaches For Anchoring Cobaltabisdicarbollide Anions Onto Oxidized Silicon Wafers. Emilio José Juárez-Pérez, Michel Granier, Hubert Mutin, Clara Viñas, Rosario Núñez. *In preparation*.

f) Thumb Rules to Establish the Rotamer Configuration in Metallacarborane Sandwiches. The relevance of the $C_C{-}H\cdots H{-}B$ Self Interactions. Emilio J. Juárez-Pérez, Rosario Núñez, Clara Viñas, Reijo Sillanpää, Francesc Teixidor. *Inorg. Chem.* **2009**, *submitted*.

a) Polyanionic Carbosilane And Carbosiloxane Metallodendrimers Based On Cobaltabisdicarbollide Derivatives.

Polyanionic carbosilane and carbosiloxane metallodendrimers based on cobaltabisdicarbollide derivatives.

Emilio José Juárez-Pérez,[a#] *Clara Viñas,*[a] *Francesc Teixidor,*[a] *Rosario Núñez*[a*]

[a] Institut de Ciència de Materials, CSIC, Campus U.A.B., 08193 Bellaterra, Spain

Email address: rosario@icmab.es

RECEIVED DATE (to be automatically inserted after your manuscript is accepted if required according to the journal that you are submitting your paper to)

Corresponding Author: Dr. Rosario Núñez, Institut de Ciència de Materials, CSIC, Campus U.A.B., 08193 Bellaterra, Barcelona, Spain. Tel.: +34 93 580 1853. Fax: +34 93 580 5729. rosario@icmab.es

[#] Enrolled in the UAB PhD program.

ABSTRACT. Carbosilane and carbosiloxane metallodendrimers, that contain one, four and eight peripheral cobaltabisdicarbollide derivatives have been synthesized using regiospecific hydrosilylation with the anionic cobaltabisdicarbollide derivative [1,1'-μ-SiMeH-3,3'-Co(1,2-$C_2B_9H_{10})_2$]$^-$, **(1)**$^-$, of vinyl terminated dendrimers. A methodology to synthesize a trifunctional molecule containing one cobaltabisdicarbollide and three vinylsilane moieties, **(2)**$^-$, has been developed starting with tetravinylsilane. Different generations of anionic metallacarborane-containing metallodendrimers were constructed via hydrosilylation of the first and second generation of carbosilane dendrimers containing four or eight peripheral vinyl functions with **(1)**$^-$ as the hydrosilylation agent to give metallodendrimers **(3)**$^{4-}$, **(4)**$^{8-}$ and **(5)**$^{8-}$, respectively. Furthermore, it has been possible to apply this methodology to commercial vinyl terminated cyclocarbosiloxanes and a first generation obtained from this, to yield metallodendrimers, **(6)**$^{4-}$, **(7)**$^{4-}$ and **(8)**$^{8-}$ with four, and eight cobaltabisdicarbollide moieties in the periphery of the dendrimer, respectively. Products are fully characterized by FTIR, NMR and UV-Vis spectroscopies. For metallodendrimers with high molecular weights, the UV-Vis absorptions were used for corroborating the full functionalization with cobaltabisdicarbollide moieties attached to the periphery and consequently the unified character of dendrimers. In addition, UV-Vis spectroscopic measurements have also allowed to study the solubility and behaviour in water/DMSO solutions of these metallodendrimers.

KEYWORDS. Macromolecules, dendrimer, carborane, cluster compound, sandwich complexes, carbosilane, boron clusters.

Introduction

Dendrimers are known for their well-defined globular hyperbranched structures, and low polydispersity, that combined with the high number of functional groups and metal fragments, that can be localized at the core or at the periphery, provides a wide range of macromolecules with interesting catalytic, redox, magnetic, photo-optical and biomedical properties.[1,2] In the last years, carbosilane dendrimers[3] have been used as inert scaffolds for attaching functional groups on the periphery according to the required application.[4,5] More recently, examples of cationic carbosilane dendrimers have been described in order to be used as potential carriers for phosphorothioate oligodeoxynucleotide (ODN),[6] or for other biocompatible applications.[7] However, to our knowledge, few reports exist on anionic silyl-containing dendrimers designed to have a surface of negative charges, which could be capable of specific binding to a number of different cationic species.[3i,8] In the course of our research on high boron-content molecules,[9] we recently developed different synthetic strategies for the preparation of anionic carboranyl-terminated dendrimeric systems, by using carbosilane dendrimers as scaffold in which anionic *nido*-carborane clusters were placed at the periphery.[10] Following our studies on developing boron-rich anionic dendrimers, we considered appropriate to use the monoanionic cobaltabisdicarbollide, $[(3,3'\text{-Co-}(1,2\text{-}C_2B_9H_{11})_2]^-$, **(1)**$^-$,[11] to be peripherally attached to dendrimers. This metallacarborane is an electron-deficient sandwich with 18 boron atoms, that is characterized by its extraordinary chemical and thermal stability.[11b] This compound is hydrophobic,[12] a weakly coordinating and low nucleophilic anion,[13,14] that has made it suitable for a wide range of applications,[15] such as the extraction of radionuclides,[16] in conducting organic polymers,[17] in ion selective PVC membrane electrodes for tuberculosis drug analysis,[18] or for its use in medicine.[19] For this purpose, bio-active functionalized metallacarboranes have been characterized,[20] and cobaltabisdicarbollide derivatives have been attached to different organic groups and biomolecules.[21,22] Up to today, the usual via to attach this metallacarborane to the different groups has been through the boron atom in position 8', by the reaction of the dioxane-metallacarborane derivative, $[8\text{-}O(CH_2CH_2)_2O\text{-}3,3'\text{-Co}(1,2\text{-}C_2B_9\text{-}H_{10})(1',2'\text{-}C_2B_9H_{11})]$[23] with the corresponding nucleophiles.[20-22,24] Here, we report the preparation of boron-rich polyanionic macromolecules by using a new approach to bind metallacarboranes to carbosilane and carbosiloxane dendrimers via hydrosilylation reactions[25] of vinyl-terminated dendrimers with the recently reported C_c-silyl-substituted cobaltabisdicarbollide derivative, $[1,1'\text{-}\mu\text{-SiMeH-}3,3'\text{-Co}(1,2\text{-}C_2B_9H_{10})_2]^-$, **(1)**$^-$.[26] In addition, a solubility test of the dendrimers in DMSO/water has been carried out using the UV-visible spectroscopy.

Results and Discussion

Synthesis of carbosilane and carbosiloxane metallodendrimers. With the objective to design and prepare polyanionic carbosilane and carbosiloxane dendrimers decorated with metallacarboranes on their periphery, suitable dendritic molecules containing terminal C=C functionalities were prepared according to the literature.[3] 1,3,5,7-tetramethylvinylcyclotetrasiloxane (TMViCTS), as core molecules (generation 0); the carbosilane dendrimers: 1G-Vi_4, 1G-Vi_8, 2G-Vi_8 and the cyclosiloxane dendrimers 1G-TMViCTS$(SiVi)_4$ and 1G-TMViCTS$(SiVi)_8$, that are shown in Schemes 1-3, were prepared using a divergent methodology by successive alkenylation and hydrosilylation steps with Karstedt catalyst, according to well known literature procedures.[3a,e,m]

All these starting materials can be hydrosilylated with the recently reported C_c-substituted cobaltabis(dicarbollides) functionalized with the Si-H group, $[1,1'\text{-}\mu\text{-SiMeH-}3,3'\text{-Co}(1,2\text{-}C_2B_9H_{10})_2]^-$, **(1)**$^-$.[26] The hydrosilylation reaction of one equivalent of **(1)**$^-$ with one equivalent of tetravinylsilane, in the presence of catalytic amounts of Karstedt catalyst in THF at 50 ºC, afforded the monoanion **(2)**$^-$ that was isolated as caesium salt in 77% yield (Scheme 1). Thus, applying a 1:1 ratio of reagents, only one vinyl group from the tetravinylsilane was hydrosilylated. However, when a 4:1 ratio **(1)**$^-$/tetravinylsilane was used under the same conditions, a complex mixture of di- and tri-hydrosilylated products was obtained, but never the tetra-functionalized compound, according to the ^{1}H NMR where residual vinyl protons were always observed (Scheme 1). Attempts to achieve the tetrafuntionalization of tetravinylsilane by changing the temperature, the solvent (i.e. toluene), catalyst, longer reaction times, etc. were also carried out, but unsuccessful results were obtained. To our knowledge, the same problem was already observed by A. Otero and co-workers for the hydrosilylation of tetravinylsilane with a silyl-containing *ansa*-metallocene, and even using extreme stoichiometries only the monofunctionalization was achieved.[27] To our opinion, most probably, the steric bulk of the cobaltabisdicarbollide causes the incomplete hydrosilylation and restricts the number of metallacarboranes that can be introduced in the core molecule. Conversely, when the reaction of **(1)**$^-$ with the first generation of a vinyl-terminated carbosilane dendrimer (1G-Vi_4) was carried out in a 4:1 ratio, using the Karstedt catalyst in THF at 50 ºC, the corresponding polyanionic metallodendrimer peripherally functionalized with cobaltabisdicarbollide anions, **(3)**$^{4-}$, was obtained and isolated as the caesium salt in 51% yield (Scheme 2). Thus, it was possible the hydrosilylation of all vinyl functions and bind the four cobaltabisdicarbollide complexes to the molecule. In the same way, **(1)**$^-$ reacted with 1G-Vi_8 and 2G-Vi_8 to give dendrimers **(4)**$^{8-}$ and **(5)**$^{8-}$, respectively, in which eight cobaltabisdicarbollide anions are placed on their periphery (Schemes 2). These dendrimers were isolated as caesium salts by precipitation with hexane in 41 and 62 % yield, respectively. In this case, the reactions were carried out using longer reaction times than those used for conventional organosilanes. In addition, carbosiloxane dendrimers **(6)**$^{4-}$, **(7)**$^{4-}$and **(8)**$^{8-}$ were obtained in 47, 55 and 54 % yield, respectively, by the

reaction of **(1)**$^-$ with TMViCTS, 1G-TMViVTS(SiVi)$_4$ and 1G-TMViVTS(SiVi)$_8$, in a 4:1 or 8:1 ratio, using similar conditions that those used for the previous carbosilane dendrimers (Scheme 3). In all cases, the binding of the cobaltacarborane **(1)**$^-$ to the vinyl-terminated dendrimers was mainly monitored by ^{1}H NMR spectroscopy, following the disappearance of the vinyl protons. In addition, the resonances corresponding to C$_c$-H and Cc-Si-CH$_3$ were shifted respected to the starting **(1)**$^-$.

By using Monte Carlo Simulations, the steric hindrance caused by peripheral groups located in the starting carbosilane dendrimers has been estimated (See Supplementary Material).

Characterization of carbosilane and carbosiloxane metallodendrimers. The novel trifunctional molecule **(2)**$^-$ and dendrimeric structures**, (3)**$^{4-}$, **(4)**$^{8-}$, **(5)**$^{8-}$, **(6)**$^{4-}$, **(7)**$^{4-}$ and **(8)**$^{8-}$, were characterized on the basis of FT-IR, UV-Vis, ^{1}H, ^{11}B, ^{13}C and ^{29}Si NMR spectroscopies and mass spectrometry in some cases, that confirmed the proposed structures. The IR spectra present typical υ(B–H) strong bands for *closo* clusters around 2550 cm^{-1}, and intense bands near 1257 cm^{-1} corresponding to the δ(Si–CH$_3$). In addition, for **(6)**$^{4-}$, **(7)**$^{4-}$ and **(8)**$^{8-}$ intense bands near 1090 cm^{-1} corresponding to the δ(Si–O) are observed. In all compounds the characteristic band at 2110 cm^{-1} due to the υ(Si–H) is not present, indicating total hydrosilylation. The ^{1}H{^{11}B} NMR spectrum of the monoinionic species **(2)**$^-$ shows two resonances centred at δ 6.12 and 5.82 ppm attributed to the vinyl protons. In all compounds broad resonances around 4.50 ppm corresponding to the C$_c$-H protons of the cobaltabisdicarbollide are observed. The ^{1}H{^{11}B} and ^{13}C{^{1}H} NMR spectra exhibit resonances at low frequencies for Si–CH$_3$ group (Table S2 in Supplementary Material), –CH$_2$– proton resonances appear in the range 0.49 to 0.84 ppm, whereas the -CH$_2$- carbons are displayed from 2.44 to 8.98 ppm. The –CH$_2$– protons has not been assigned due to the complexity of the signals. The ^{13}C{^{1}H} NMR spectra for all dendrimers show resonances at 56.16 and 40.99 ppm attributed to the *C$_c$-H* and *C$_c$*-Si atoms, respectively (Table S2). In addition, for the anion **(2)**$^-$ the presence of vinyl functions was confirmed by resonances at 134.51 and 134.22 ppm in the ^{13}C{^{1}H} NMR. The ^{11}B{^{1}H} NMR for compounds **(2)**$^-$**-(8)**$^{8-}$ display very similar spectra with bands in a typical range, from +8.3 to -22.0 ppm, indicative of cobaltabisdicarbollide derivatives,[28] with the general pattern 2:2:4:4:2:2:2 (Figure 1). Due to the similarity of these ^{11}B{^{1}H} NMR spectra with that of the recently reported [1,1'-μ-SiMe$_2$-3,3'-Co(1,2-C$_2$B$_9$H$_{10}$)$_2$], **(9)**$^-$,[26] we have been able to assign each specific resonance to the corresponding boron atom. Figure 1 shows the ^{11}B{^{1}H}NMR spectra of **(1)**$^-$, **(2)**$^-$, **(3)**$^{4-}$, **(5)**$^{8-}$ and **(9)**$^-$. Noticeably, starting **(1)**$^-$ presents a higher asymmetry, that is reflected on the higher number of signals in the spectrum. Nevertheless, upon hydrosilylation for **(3)**$^{4-}$ and **(5)**$^{8-}$ some of the resonances are overlapped to only one as it is observed. In the ^{29}Si{^{1}H} NMR all resonances were assigned on the basis of the chemical shifts and the peak intensities. For **(2)**$^-$ and the first generation of the cyclosiloxane dendrimer **(6)**$^{4-}$, the ^{29}Si{^{1}H} NMR spectra exhibit two signals, whereas three resonances are observed for the rest of dendrimers (See Supplementary Material, Table S3). The resonances due to Si-C$_{cluster}$ appear between 11.15 and 12.15 ppm, shifted around 8.5 ppm to downfield respect to the starting compound **(1)**$^-$ (δ_{Si} = 2.94 ppm). In fact, these resonances have been easily assigned by comparison with their homologous **(9)**$^-$ (δ_{Si} = 13.98 ppm).[26] The Si$_{core}$ atoms appear in the region 5.88 to 11.80 ppm for **(2)**$^-$**-(5)**$^{4-}$, and at higher field, around -20 ppm, for ciclosiloxanes **(6)**$^{4-}$**-(8)**$^{8-}$ in which the Si$_{core}$ are bonded to oxygen atom. The spectra of **(3)**$^{4-}$, **(4)**$^{8-}$, **-(5)**$^{4-}$, **(7)**$^{4-}$and **(8)**$^{8-}$ exhibit additional peaks, in the range 6.65-9.78 ppm, that correspond to the Si atoms of the dendrimer branches.

The UV-vis spectra of these dendrimers were measured in acetonitrile and look very similar to that of **(1)**$^-$. The maximum absorbance around 310 nm can be attributed to the presence of the silyl bridge (μ-SiR$_2$) between ligands, such as was already reported for **(1)**$^-$,[26] that is different to the one observed at 270 nm for unsubstituted [Co(1,2-C$_2$B$_9$H$_{11}$)$_2$]$^-$.[29] A second absorbance at 462 nm is due to the d-d transition in the Co metal of the C$_c$-substituted cobaltabisdicarbollide **(1)**$^-$, which shows a bathocromic shift respect to the signal at 445 nm exhibited for the unsubstituted [Co(1,2-C$_2$B$_9$H$_{11}$)$_2$]$^-$[29]

Two different mass spectrometry techniques have been used for the characterization of compounds: MALDI-TOF and electrospray (ESI). The formula of **(2)**$^-$ was well established by using the MALDI-TOF mass spectrometry in the negative-ion mode without matrix, in which the molecular ion peak appears at *m/z* = 502.2, with a perfect concordance with the calculated pattern (see Supplementary Material, Figure S3.) The ESI mass spectrum of dendrimer **(3)**$^{4-}$ was recorded in CHCl$_3$/CH$_3$OH and shows a signal at m/z = 2490.2 corresponding to [(M-H)+H$_2$O]$^-$. Nevertheless, MALDI-TOF determinations for the higher molecular weight polyanionic dendrimers have been of difficult interpretation, due to the fragmentation of compounds by breaking the molecule into smaller parts. The technique then supports,[30] although does not confirm, the formation of dendrimeric species. Therefore, we have tried to assign the peaks, that in more cases are fragments in high percentage, for example the peak at 324.2 is due to [Co(1,2-C$_2$B$_9$H$_{11}$)$_2$]$^-$ and the peak at 393.4 is assigned to the fragment [Co(1,2-C$_2$B$_9$H$_{11}$)Si(CH$_3$)(CH$_2$)]. Furthermore, it has been observed the presence of trapped solvent molecules.

Elemental analyses (EA) were performed for polyanionic metallodendrimers, however, in some cases, it was difficult to obtain reliable results, probably due to the presence of a high boron content. Nevertheless, the problem to obtain reproducible results for EA in boron-containing anions have been observed by others before.[31]

Indirect identification method, based on UV-Vis spectroscopic measurements, to corroborate the full functionalization with cobaltacarboranes.

As mentioned before, only for the monoanionic **(2)**$^-$ and the dendrimer **(3)**$^{4-}$ it was possible to obtain the molecular weight using mass spectrometry. The rest of compounds only showed fragments, and in no cases the corresponding molecular ion peak was observed. For

such purpose, we have used an alternative method developed by Kim *et al*. for ethynylsilane dendrimers.[32] This method consists on the measurement of the UV absorption of a solution containing the functionalized dendrimers and study the trend of the molar absorptivity, taking into account that for our particular case the molar absorptivities (ε_{max}) of the cobaltabisdicarbollides-containing dendrimers must be proportional to the number of metallacarboranes attached to the periphery. The UV-Vis spectroscopic measurements were carried out in two different solvents, DMSO and acetonitrile. In the Supplementary Material, Table S3 collects the molar absorptivities values (ε) for all dendrimers in both solvents and the relation between them and the number of metallacarboranes (X). Figure 2 shows the UV-Vis spectra in acetonitrile for **(2)**$^{-}$, **(5)**$^{8-}$ and **(7)**$^{4-}$, which contain one, eight and four cobaltabisdicarbollide moieties respectively, with a λ_{max} around 310 nm. In Figure 3 the graphics represent the molar absorptivity (ε) measured at 462 nm, in acetonitrile and DMSO for the reported compounds, versus the number of metallacarboranes (X) attached to different dendrimers. In our case, it has been more adequate to use the wavelength at 462 nm, that correspond to the d-d transition of the C_c-silyl-substituted cobaltabisdicarbollide, instead of the band at 310 nm because for dendrimers containing a very high number of cobaltacarboranes, this band is very intense and requires to work with very low concentrations (around 10^{-8} M), however, the band at 462 nm allowed us to work at more realistic concentrations (10^{-3} to 10^{-5} M), as it is specified in the Experimental Part. Using these concentrations the band at 462 nm is adequate for measuring the absorption bands and permits to calculate the absorptivity with accuracy. It is important to notice that for both solvents the graphic slope is quite similar, for DMSO solutions is 326.7 $M^{-1}cm^{-1}$ whereas for acetonitrile solutions is 354.8 $M^{-1}cm^{-1}$. Consequently, the molar absorptivity increases as a consequence of the higher degree of functionalization on the dendrimeric surface. So we can concluded that this method is suitable to corroborate the full functionalization and the unified character of the different metallocarboranes-containing dendrimers such as can be observed in the graphics. This has been only an additional method used for us to confirm the previous spectroscopic data, due to the difficulty to obtain reliable elemental analyses and mass spectra.

Solubility of caesium salts of cobaltabisdicarbollide-containing metallodendrimers.

With the potential applications in biomedicine previously mentioned for these anionic dendrimers in mind, it is important to know the behaviour of these salts and their solubility in different solvents, especially in water. It has been reported that a challenge in the development of boron delivery agents for BNCT is to achieve boron concentrations around 20 $\mu g \cdot g^{-1}$ tumor to deliver therapeutic doses of radiation to the tumor.[19c] The caesium salts of the cobaltabisdicarbollide anion and their derivatives present good solubilities in organic polar solvents,[33] but a poor solubility in pure water. The solubility of $Cs[Co(1,2\text{-}C_2B_9H_{11})_2]$ measured by UV-Vis in water at 22 ºC is $9.75 \cdot 10^{-4}$ M,[33] the hexabromo derivative $Cs[Co(1,2\text{-}C_2B_9H_8Br_3)_2]$ is $3 \cdot 10^{-4}$ M,[34] whereas for C*c*-substituted Cs[1,1'-μ-SiMeH-3,3'-$Co(1,2\text{-}C_2B_9H_{10})_2$], **Cs(1)**, and Cs[1,1'-μ-$SiMe_2$-3,3'-$Co(1,2\text{-}C_2B_9H_{10})_2$], **Cs(9)**, the water solubilities measured in this work are $8.5 \cdot 10^{-4}$ M and $1.9 \cdot 10^{-3}$ M, respectively. On the other hand, salts of the cobaltabisdicarbollide with potassium, sodium or lithium have a higher solubility in water.[35] In this respect, there exist two possibilities for enhancing the solubility of these anionic metallodendrimers in aqueous solutions; the first is to exchange the caesium by another cation, such as sodium or potassium, using ion-exchange resins,[22] however, in our case the resulting salts are difficult to isolate; the second way is to prepare a concentrated metallodendrimer solution in an organic solvent such as DMSO,[22b] a pharmaceutical excipient commonly used,[36] followed by dilution with a buffer or water. The second way is more convenient when the possible drug to be delivered is in cationic form, because the solvent mixtures can be tailored for each anion-cation system. Thus, for testing the solubility and behaviour of these caesium salts of metallodendrimers, compound **(9)**$^{-}$ has been used as reference compound to construct a calibration curve, by measuring the absortions at 462 nm in pure DMSO for different concentrations (see Experimental Data and Figure 4). Then, different DMSO/water solutions for the caesium salts of the anions **(4)**$^{8-}$, **(7)**$^{4-}$ and **(2)**$^{-}$ were prepared and their absorption values at 462 nm are represented in Figure 4. It can be there observed that these metallodendrimers present good solubility at different concentration ranges, depending on the degree of functionalization. Therefore, it should be possible to extrapolate this DMSO-water solubility study to other systems formed by this kind of anionic metallodendrimers combined with more complex cations, which present biological activity or targeting functionalities.

Conclusions.

The cobaltacarboranyltrivinylsilane **(2)**$^{-}$ and two families of polyanionic cobaltabisdicarbollide-containing carbosilane and carbosiloxane metallodendrimers, **(3)**$^{4-}$ **– (5)**$^{8-}$ and **(6)**$^{4-}$ – **(8)**$^{8-}$, respectively, have been prepared by hydrosilylation of the suitable dendritic molecules containing terminal C=C functionalities, with the anion [1,1'-μ-SiMeH-3,3'-$Co(1,2\text{-}C_2B_9H_{10})_2$]$^{-}$, **(1)**$^{-}$**,** in the presence of Karstedt catalyst and optimized reaction conditions. The synthetic methodology described here has allowed to produce in one pot reaction polyanionic metallodendrimers with four and eight negative charges localized on the periphery. Concerning the characterization of these compounds, it was not possible for the dendrimers with the highest molecular weights to obtain the mass spectra, therefore the UV-Vis spectroscopy was used as an undirected method to corroborate the full functionalization of dendrimers with cobaltabisdicarbollide moieties, and subsequently confirm the unified character of the dendritic macromolecules. In addition, the UV-Vis has also been a good tool for the study of the metallodendrimers solubility in water/DMSO solutions, by measuring the absorptivities of different metallodendrimers concentrations.

Experimental Section

Instrumentation. IR spectra were recorded with KBr pellets or NaCl on a Shimadzu FTIR-8300 spectrophotometer. UV-visible spectroscopy was carried out with a Shimadzu UV-Vis 1700 spectrophotometer, at 22 ºC temperature, using 1 cm quartz cuvettes. The Electrospray-Ionization mass spectra (ESI-MS) were recorded on a Bruker Esquire 3000 spectrometer using a source of ionization and a ions trap analyzer. MALDI-TOF-MS mass spectra were recorded in the negative ion mode using a Bruker Biflex MALDI-TOF [N_2 laser; λ_{exc} 337 nm (0.5 ns pulses); voltage ion source 20.00 kV (Uis1) and 17.50 kV (Uis2)] and dithranol as matrix. The ^{1}H, ^{1}H{^{11}B} NMR (300.13 MHz), ^{11}B, ^{11}B{^{1}H} NMR (96.29 MHz), ^{13}C{^{1}H} NMR (75.47 MHz) and ^{29}Si{^{1}H} NMR (59.62 MHz) spectra were recorded on a Bruker ARX 300 spectrometer equipped with the appropriate decoupling accessories at room temperature in acetone-d_6 solutions. Chemical shift values for ^{11}B NMR and ^{11}B{^{1}H} spectra were referenced to external $BF_3{\cdot}OEt_2$, and those for ^{1}H, ^{1}H{^{11}B}, ^{13}C{^{1}H}NMR and ^{29}Si{^{1}H} NMR spectra were referenced to $SiMe_4$. Chemical shifts are reported in units of parts per million downfield from reference, and all coupling constants are reported in Hertz.

Materials. All manipulations were carried out under a dinitrogen atmosphere using standard Schlenck techniques. Solvents were reagent grade and were purified by distillation from appropriate drying agents before use. $[Si(CH{=}CH_2)(CH_3)O]_4$, $(CH_3)_2HSiCl$, $(CH_3)HSiCl_2$ and Karstedt's catalyst (platinum divinyltetramethyldisiloxane complex, 2.1-2.4% platinum in vinyl terminated polydimethylsiloxane) were purchased from ABCR and used as received. The $[Si(CH{=}CH_2)_4]$ was purchased from Across. The *n*-BuLi solution (1.6 M in hexanes) was purchased from Lancaster or Aldrich and $CH_2{=}CHMgCl$ 1.6 M in THF from Aldrich. Compound Cs[1,1'-μ-SiMeH-3,3'-Co(1,2-$C_2B_9H_{10})_2$], **Cs(1)** and Cs[1,1'-μ-$SiMe_2$-3,3'-Co(1,2-$C_2B_9H_{10})_2$], **Cs[9];**[26] and dendrimers 1G-Vi_4, 1G-Vi_8, 2G-Vi_8, 1G-TMViCTS($SiVi)_4$ and 1G-TMViCTS($SiVi)_8$ were prepared according to the literature procedures.[3]

Synthesis of Cs[1,1'-μ-Si(CH_3){(CH_2)$_2$-Si($CHCH_2$)$_3$}-3,3'-Co($C_2B_9H_{10})_2$], Cs[2]. In a Schlenk flask, $Si(CH{=}CH_2)_4$ (72.2 mg, 0.53 mmol), 10 μL of Karstedt catalyst and 2 mL of THF were stirred for 10 min at room temperature. To the solution Cs[1,1'-μ-Si(CH_3)H-3,3'-Co(1,2-$C_2B_9H_{10})_2$] 264.3 mg (0.53 mmol) were added and the mixture was stirred overnight at 50 ºC. After, the addition of hexane to the mixture give **Cs(2)** as an orange solid. Yield: 259.1 mg, 77 %. Anal. calcd. for $C_{13}H_{36}B_{18}CoCsSi_2$: C, 24.59; H, 5.71. Found: C, 23.24; H, 5.67. ^{1}H NMR: δ 6.12 (m, 3H, -C*H*=CH_2), 5.83-5.81 (m, 6H, -CH=CH_2), 4.49 (br s, 2H, C_c-*H*), 0.81-0.76 (m, 4H, -Si-CH_2-CH_2-Si), 0.32 (s, 3H, Si-CH_3). ^{1}H{^{11}B} NMR: δ 6.12 (m, 3H, -C*H*=CH_2), 5.83-5.81 (m, 6H, -CH=CH_2), 4.49 (br s, 2H, C_c-*H*), 3.39 (br s, 2H, B-*H*), 3.28 (br s, 2H, B-*H*), 3.08 (br s, 2H, B-*H*), 2.33 (br s, 2H, B-*H*), 2.20 (br s, 2H, B-*H*), 1.92 (br s, 2H, B-*H*), 1.66 (br s, 6H, B-*H*), 0.81-0.76 (m, 4H, -Si-CH_2-CH_2-Si), 0.32 (s, 3H, Si-CH_3). ^{11}B NMR: δ 8.32 (d, ^{1}J(B,H) = 126 Hz, 2B), 2.98 (d, ^{1}J(B,H) = 135 Hz, 2B), -1.60 (d, ^{1}J(B,H) = 141 Hz, 4B), -3.60 (d, ^{1}J(B,H) = 144 Hz, 2B), -4.53 (d, ^{1}J(B,H) = 128 Hz, 2B), -14.19 (d, ^{1}J(B,H) = 155 Hz, 2B), -16.32 (d, ^{1}J(B,H) = 185 Hz, 2B), -21.84 (d, ^{1}J(B,H) =137 Hz, 2B). ^{13}C{^{1}H} NMR: δ 134.51 (*C*H_2=*C*H-), 134.22 (*C*H_2=*C*H-), 55.30 (C_c-H), 40.99 (C_c-Si), 4.14 (-*C*H_2-), 3.35 (-CH_2-), -7.72 (Si-*C*H_3). ^{29}Si{^{1}H} MR: δ 12.15- (μ-Si-$C_{cluster}$), 11.80 (Si_{core}). FTIR (KBr), cm^{-1}: 3051 (υ(C_c-H)), 3008 (υ($C_{alkenyl}$-H)), 2943 (υ(C_{alkyl}-H)), 2885 (υ(C_{alkyl}-H)), 2550 (ν (B-H)), 1257 (δ (Si-CH_3)). MALDI-TOF-MS *m/z*: 324.2 ([Co(1,2-$C_2B_9H_{11})]^-$, 17 %), 393.2 ([Co(1,2-$C_2B_9H_{10}$)Si(CH_3)(CH_2)], 2 %), 502.2 (M - Cs, 100 %).

Synthesis of [Cs]$_4${2G-[1,1'-μ-Si(CH_3)(CH_2CH_2)-3,3'-Co($C_2B_9H_{10})_2]_4$}, Cs_4[3]. In a Schlenk flask, 1G-Vi_4 (56.0 mg, 0.12 mmol), 10 μL of Karstedt catalyst and 2 mL of THF were stirred for 10 min. at room temperature. To the solution of Cs[1,1'-μ-Si(CH_3)H-3,3'-Co(1,2-$C_2B_9H_{10})_2$], 239.4 mg (0.48 mmol) were added and the mixture was stirred overnight at 50 ºC. After, the addition of a solution of hexane to the mixture give **Cs_4(3)** as an orange solid. Yield: 150.7 mg, 51 %. Anal. calcd. for $C_{44}H_{148}B_{72}Co_4Cs_4Si_9$: C, 21.34; H, 6.02. Found: C, 22.38; H 6.16. ^{1}H NMR: δ 4.51 (br s, 8H, C_c-*H*), 0.49 (m, 32H, -Si-CH_2-CH_2-Si), 0.32 (s, 12H, Si-CH_3), 0.01 (s, 24H, Si-CH_3). ^{1}H{^{11}B} NMR: δ 4.51 (br s, 8H, C_c-*H*), 0.49 (m, 32H, -Si-CH_2-CH_2-Si), 0.32 (s, 12H, Si-CH_3), 3.39-1.59 (br, 80 H, B-*H*), 0.01(s, 24H, Si-CH_3). ^{11}B NMR: δ 8.15 (d, ^{1}J(B,H) = 110 Hz, 2B), 2.93 (d, ^{1}J(B,H) = 132 Hz, 2B), -1.54 (d, ^{1}J(B,H) = 145 Hz, 4B), -4.54 (d, ^{1}J(B,H) = 113 Hz, 4B), -14.61 (d, ^{1}J(B,H) = 185 Hz, 2B), -16.54 (d, ^{1}J(B,H) = 178 Hz, 2B), -21.81 (d, ^{1}J(B,H) =153 Hz, 2B). ^{13}C{^{1}H} NMR: δ 55.55 (C_c-H), 41.33 (C_c-Si), 6.49 (-*C*H_2-), 5.05 (Si-*C*H_2), 4.07 (Si-CH_2), 2.44 (Si-*C*H_2), -5.11 (Si-*C*H_3), -7.72 (Si-*C*H_3). ^{29}Si{^{1}H} NMR: δ 11.98 (μ-Si-$C_{cluster}$), 6.65 (Si_{branch}), 5.88 (Si_{core}). FTIR (KBr), cm^{-1}: 3062 (υ(C_c-H)), 2950 (υ(C_{alkyl}-H)), 2905 (υ(C_{alkyl}-H)), 2550 (ν (B-H)), 1257 (δ (Si-CH_3)). ESI-MS *m/z*: 2490.2 (M + H_2O, 2 %).

Synthesis of Cs_8{2G-[1,1'-μ-Si(CH_3)(CH_2CH_2)-3,3'-Co($C_2B_9H_{10})_2]_8$}, Cs_8[4].
In a Schlenk flask, 1G-Vi_8 (32.7 mg, 0.062 mmol), 10 μL of Karstedt catalyst and 2 mL of THF were stirred for 10 min. at room temperature. To the solution, Cs[1,1'-μ-Si(CH_3)H-3,3'-Co(1,2-$C_2B_9H_{10})_2$] 246.6mg (0.496 mmol) were added and the mixture was stirred for 40 h. at 50 ºC. After, 10 ml of CH_2Cl_2 were added to produce two solvent phases. The halogenated solvent was discarded by decantation. To the other oily dark orange phase, 10 ml of hexane was added to give **Cs_8(4)** as an orange solid. Yield: 114.5 mg, 41 %. Anal. calcd. for $C_{68}H_{244}B_{144}Co_8Cs_8Si_{13}$: C, 18.07; H, 5.44. Found: C, 20.25; H 5.88. ^{1}H NMR: δ 4.50 (br s, 16H, C_c-*H*), 0.52 (m, 48H, -Si-CH_2-CH_2-Si), 0.32 (s, 24H, Si-CH_3), 0.09 (s, 12H, Si-CH_3). ^{1}H{^{11}B} NMR: 4.50 (br s, 16H, C_c-*H*), 3.39 (br s, 16H, B-*H*), 3.28 (br s, 16H, B-*H*), 3.08 (br s, 16H, B-*H*), 2.33 (br s, 16H, B-*H*), 2.20 (br s, 16H, B-*H*), 1.92 (br s, 16H, B-*H*), 1.66 (br s, 48H, B-*H*), 0.52 (m, 48H, -Si-CH_2-CH_2-Si), 0.32 (s, 24H, Si-CH_3), 0.09 (s, 12H, Si-CH_3).^{11}B NMR: δ 6.96 (d, ^{1}J(B,H) = 119 Hz, 2B), 1.89 (d, ^{1}J(B,H) =129 Hz, 2B), -2.65 (d, ^{1}J(B,H) =110 Hz, 4B), -5.60 (d, ^{1}J(B,H) = 156 Hz, 2B), -16.13 (d, ^{1}J(B,H) =166 Hz, 2B), -17.56 (d, ^{1}J(B,H)

=175 Hz, 2B), -22.95 (d, 1J(B,H) =147 Hz, 2B). $^{13}C\{^1H\}$ NMR: δ 55.32 ($C_{cluster}$-H), 41.24 ($C_{cluster}$-Si), 8.49, 7.18, 4.13, 3.50 (-CH_2-), -1.09 (Si-CH_3), -7.63 ($C_{cluster}$-Si-CH_3). $^{29}Si\{^1H\}$ NMR: δ 11.73 (μ-Si-$C_{cluster}$), 9.78 (Si_{branch}), 8.28 (Si_{core}). FTIR (KBr), cm^{-1}: 3051 (υ($C_{cluster}$-H)), 2958 (υ(C_{alkyl}-H)), 2905 (υ(C_{alkyl}-H)), 2557 (ν (B-H)), 1257 (δ (Si-CH_3)). MALDI-TOF-MS *m/z*: 324.2 ($[Co(1,2\text{-}C_2B_9H_{11})]^-$, 100 %), 393.2 ($[Co(1,2\text{-}C_2B_9H_{10})Si(CH_3)(CH_2)]$, 18 %), 435.7 ((M + MeOH)/8, 16 %).

Synthesis of Cs_8{3G-[1,1'-μ-Si(CH_3)-3,3'-Co($C_2B_9H_{10}$)$_2$]$_8$}, Cs_8[5].

This compound was prepared using the same procedure as for **Cs_8[4]**, by using 2G-Vi_8 (39.0 mg, 0.032 mmol), 10 μL of Karstedt catalyst, and Cs[1,1'-μ-Si(CH_3)H-3,3'-Co(1,2-$C_2B_9H_{10}$)$_2$] 127.7 mg (0.256 mmol) in 2 mL of THF. The mixture was stirred for 36 h. at 50 ºC. After work up, **Cs_8(5)** was obtained as an orange solid. Yield: 103.4 mg, 62 %. Anal. Calcd. for $C_{100}H_{324}B_{144}Co_8Cs_8Si_{21}$: C, 23.06; H, 6.27. Found: C, 24.67; H 6.65. ^1H NMR: δ 4.50 (br s, 16H, C_c-*H*), 0.52 (m, 80H, -Si-C*H*$_2$-C*H*$_2$-Si), 0.31 (s, 24H, Si-C*H*$_3$), 0.10 (br s, 36H, Si-C*H*$_3$). $^1H\{^{11}B\}$ NMR: 4.50 (br s, 16H, C_c-*H*), 3.39 (br s, 16H, B-*H*), 3.28 (br s, 16H, B-*H*), 3.08 (br s, 16H, B-*H*), 2.33 (br s, 16H, B-*H*), 2.20 (br s, 16H, B-*H*), 1.92 (br s, 16H, B-*H*), 1.66 (br s, 48H, B-*H*), 0.52 (m, 80H, -Si-C*H*$_2$-C*H*$_2$-Si), 0.31 (s, 24H, Si-C*H*$_3$), 0.10 (br s, 24H, Si-C*H*$_3$). ^{11}B NMR: δ 7.58 (d, ^1J(B,H) = 131 Hz, 2B), 2.06 (d, ^1J(B,H) = 150 Hz, 2B), -2.42 (d, ^1J(B,H) = 150 Hz, 4B), -5.02 (d, ^1J(B,H) = 131 Hz, 2B), -15.00 (d, ^1J(B,H) = 169 Hz, 2B), -17.27 (d, ^1J(B,H) = 188 Hz, 2B), -22.80 (d, ^1J(B,H) =169 Hz, 2B). $^{13}C\{^1H\}$ NMR: δ 55.30 ($C_{cluster}$-H), 41.08 ($C_{cluster}$-Si), 8.52, 6.60, 4.34, 4.10, 3.55, 3.11 (-*C*H$_2$-), -1.13 (Si-*C*H$_3$), -5.02 (Si-*C*H$_3$), -7.77 ($C_{cluster}$-Si-*C*H$_3$). $^{29}Si\{^1H\}$ NMR: δ 11.52 (μ-Si-$C_{cluster}$), 8.03, 6.32 (Si_{branch}). FTIR (KBr), cm^{-1}: 3067 (υ($C_{cluster}$-H)), 2955 (υ(C_{alkyl}-H)), 2905 (υ(C_{alkyl}-H)), 2550 (ν (B-H)), 1257 (δ (Si-CH_3)). MALDI-TOF-MS *m/z*: 324.1 ($[Co(1,2\text{-}C_2B_9H_{11})]^-$, 100 %), 393.2 ($[Co(1,2\text{-}C_2B_9H_{10})Si(CH_3)(CH_2)]$, 16 %),599.7 ((M + 2dithranol+ 6MeOH)/8, 53 %), 633.7 [(M + 4(dithranol)+ H_2O)/8, 42 %].

Synthesis of cyclosiloxane dendrimer Cs_4{1G-[1,1'-μ-Si(CH_3)-3,3'-Co($C_2B_9H_{10}$)$_2$]$_4$}, Cs_4[6].

This compound was prepared using the same procedure as for **Cs_8[4]**, by using 1,3,5,7-tetramethylvinylcyclotetrasiloxane (19.4 mg, 0.056 mmol), 10 μL of Karstedt catalyst and Cs[1,1'-μ-Si(CH_3)H-3,3'-Co(1,2-$C_2B_9H_{10}$)$_2$] (111.7 mg, 0.224 mmol) in 2 mL of THF. After work up, **Cs_4(6)** was obtained as un orange solid. Yield: 61.6 mg, 47 %. ^1H NMR: δ 4.51 (br s, 8H, C_c-*H*), 0.57 (m, 16H, -Si-CH$_2$-C*H*$_2$-Si), 0.34 (s, 12H, Si-C*H*$_3$), 0.16 (s, 12H, Si-C*H*$_3$). $^1H\{^{11}B\}$ NMR: 4.51 (br s, 16H, C_c-*H*), 3.39 (br s, 16H, B-*H*), 3.28 (br s, 16H, B-*H*), 3.08 (br s, 16H, B-*H*), 2.33 (br s, 16H, B-*H*), 2.20 (br s, 16H, B-*H*), 1.92 (br s, 16H, B-*H*), 1.66 (br s, 48H, B-*H*), 0.57 (m, 16H, -Si-CH$_2$-C*H*$_2$-Si), 0.34 (s, 12H, Si-C*H*$_3$), 0.16 (s, 12H, Si-C*H*$_3$). ^{11}B NMR: δ 7.55 (d, ^1J(B,H) =136 Hz, 2B), 2.02 (d, ^1J(B,H) =169 Hz, 2B), -2.75 (d, ^1J(B,H) =141 Hz, 4B), -5.43 (d, ^1J(B,H) =144 Hz, 2B), -15.79 (d, ^1J(B,H) =155 Hz, 2B), -17.08 (d, ^1J(B,H) =150 Hz, 2B), -23.10 (d, ^1J(B,H) =131 Hz, 2B). $^{13}C\{^1H\}$ NMR: δ 56.16 ($C_{cluster}$-H), 41.93 ($C_{cluster}$-Si), 8.44 (-*C*H$_2$-), 4.21 (-*C*H$_2$-), -1.04, (O-Si-*C*H$_3$), -6.70 ($C_{cluster}$-Si-*C*H$_3$). $^{29}Si\{^1H\}$ NMR: δ 11.85 (μ-Si-$C_{cluster}$), -20.53 (O-Si). FTIR (KBr), cm^{-1}: 3059 (υ($C_{cluster}$-H)), 2955 (υ(C_{alkyl}-H)), 2905 (υ(C_{alkyl}-H)), 2550 (ν (B-H)), 1257 (δ (Si-CH_3)), 1095 (δ (Si-O)). MALDI-TOF-MS *m/z*: 324.2 ($[Co(1,2\text{-}C_2B_9H_{11})]^-$, 51 %), 393.2 ($[Co(1,2\text{-}C_2B_9H_{10})Si(CH_3)(CH_2)]$, 100 %), 494.4 ((M + Cs + 2H_2O)/4, 21 %).

Synthesis of cyclosiloxane dendrimer Cs_4{2G-[1,1'-μ-Si(CH_3)-3,3'-Co($C_2B_9H_{10}$)$_2$]$_4$}, Cs_4[7].

This compound was prepared using the same procedure as for **Cs_8[4]**, by using 1G-tetravinylcyclotetrasiloxanes (60.5 mg, 0.096 mmol), 10 μL of Karstedt and Cs[1,1'-μ-Si(CH_3)H-3,3'-Co(1,2-$C_2B_9H_{10}$)$_2$] (191.6 mg, 0.384 mmol) in 2 mL of THF. The mixture was stirred overnight at 50 ºC. After addition and vigorous stirring of 20 ml of CH_2Cl_2, **Cs_4[7]** was precipitated, filtered and dried in vacuo. Yield: 138.3 mg, 55 %. Anal. Calcd. for $C_{48}H_{160}B_{72}Co_4Cs_4O_4Si_{12}$: C, 21.47; H, 6.01. Found: C, 20.55 ; H 6.01. ^1H NMR: δ 4.50 (br s, 8H, C_c-*H*), 0.50 (m, 32H, -Si-C*H*$_2$-CH$_2$-Si), 0.30 (s, 12H, Si-C*H*$_3$), 0.08 (s, 12H, Si-C*H*$_3$), 0.00 (s, 24H, -Si-C*H*$_3$). $^1H\{^{11}B\}$ NMR: 4.50 (br s, 16H, C_c-*H*), 3.40 (br s, 16H, B-*H*), 3.26 (br s, 16H, B-*H*), 3.05 (br s, 16H, B-*H*), 2.33 (br s, 16H, B-*H*), 2.21 (br s, 16H, B-*H*), 1.92 (br s, 16H, B-*H*), 1.66 (br s, 48H, B-*H*), 0.50 (m, 32H, -Si-C*H*$_2$-CH$_2$-Si), 0.30 (s, 12H, Si-C*H*$_3$), 0.08 (s, 12H, Si-C*H*$_3$), 0.00 (s, 24H, Si-C*H*$_3$). ^{11}B NMR: δ 7.24 (d, ^1J(B,H) = 126 Hz, 2B), 1.81 (d, ^1J(B,H) = 135 Hz, 2B), -2.92 (d, ^1J(B,H) = 141 Hz, 4B), -5.70(d, ^1J(B,H) = 144 Hz, 2B), -15.73 (d, ^1J(B,H) = 155 Hz, 2B), -17.50 (d, ^1J(B,H) = 185 Hz, 2B), -23.20 (d, ^1J(B,H) =137Hz, 2B). $^{13}C\{^1H\}$ NMR: δ 55.29 ($C_{cluster}$-H), 41.16 ($C_{cluster}$-Si), 8.98, 5.65, 5.05, 4.04 (-*C*H$_2$-), -1.05, (O-Si-*C*H$_3$), -5.15 (Si-*C*H$_3$), -7.75 ($C_{cluster}$-Si-*C*H$_3$). $^{29}Si\{^1H\}$ NMR: δ 11.85 (μ-Si-$C_{cluster}$), -20.53 (O-Si). FTIR (KBr), cm^{-1}: 3063 (υ($C_{cluster}$-H)), 2955 (υ(C_{alkyl}-H)), 2908 (υ(C_{alkyl}-H)), 2554 (ν (B-H)), 1257 (δ (Si-CH_3)), 1080 (δ (Si-O)). MALDI-TOF-MS *m/z*: 324.2 ($[Co(1,2\text{-}C_2B_9H_{11})]^-$, 100 %), 393.2 ($[Co(1,2\text{-}C_2B_9H_{10})Si(CH_3)(CH_2)]$, 48 %).

Synthesis of cyclosiloxane dendrimer Cs_8{2G-[1,1'-μ-Si(CH_3)-3,3'-Co($C_2B_9H_{10}$)$_2$]$_8$}, Cs_8[8].

This compound was prepared using the same procedure as for **Cs_4[7]**, by using 1G-octavinylcyclotetrasiloxanes (18.0 mg, 0.024 mmol), 10 μL of Karstedt catalyst and Cs[1,1'-μ-Si(CH_3)H-3,3'-Co(1,2-$C_2B_9H_{10}$)$_2$] (97.5 mg, 0.195 mmol) in 3 mL of THF. The mixture was stirred for 48 h at 50 ºC. After work up, **Cs_8[8]** was obtained as an orange solid. Yield: 62 mg, 54 % ^1H NMR: δ 4.51 (br s, 16H, C_c-*H*), 0.55 (m, 48H, -Si-C*H*$_2$-C*H*$_2$-Si), 0.32 (s, 24H, Si-C*H*$_3$), 0.12 (s, 24H, Si-C*H*$_3$). $^1H\{^{11}B\}$ NMR: δ 4.51 (br s, 16H, C_c-*H*), 3.38 (br s, 16H, B-*H*), 3.25 (br s, 16H, B-*H*), 3.07 (br s, 16H, B-*H*), 2.30 (br s, 16H, B-*H*), 2.21 (br s, 16H, B-*H*), 1.95 (br s, 16H, B-*H*), 1.67 (br s, 48H, B-*H*), 0.55 (m, 48H, -Si-C*H*$_2$-C*H*$_2$-Si), 0.32 (s, 24H, Si-C*H*$_3$), 0.12 (s, 24H, Si-C*H*$_3$). ^{11}B NMR: δ 7.60 (d, ^1J(B,H) = 132 Hz, 2B), 2.24 (d, ^1J(B,H) = 115 Hz, 2B), -2.54 (d, ^1J(B,H) = 131 Hz, 4B), -5.52 (d, ^1J(B,H) = 130 Hz, 2B), -15.12 (d, ^1J(B,H) = 132 Hz, 2B), -17.46 (d, ^1J(B,H) = 151 Hz, 2B), -22.98 (d, ^1J(B,H) =124 Hz, 2B). $^{13}C\{^1H\}$ NMR: δ 50.95 ($C_{cluster}$-H), 43.83 ($C_{cluster}$-Si), 8.57, 7.68, 5.62, 4.40 (-*C*H$_2$-), -0.65, -1.82 (Si-*C*H$_3$), -7.73 ($C_{cluster}$-Si-*C*H$_3$). $^{29}Si\{^1H\}$

NMR: δ 11.74 (μ-Si-$C_{cluster}$), 8.88 (Si_{branch}), -19.94 (O-Si). FTIR (KBr), cm^{-1}: 3061 (υ($C_{cluster}$-H)), 2958 (υ(C_{alkyl}-H)), 2916 (υ(C_{alkyl}-H)), 2552 (ν (B-H)), 1259 (δ (Si-CH_3)), 1084 (δ (Si-O)). MALDI-TOF-MS *m/z*: 324.2 ($[Co(1,2\text{-}C_2B_9H_{11})]^-$, 2 %), 393.2 ($[Co(1,2\text{-}C_2B_9H_{10})Si(CH_3)(CH_2)]$, 14 %), 454.7 ((M – CH_3O)/8, 49 %).

Indirect identification method, based on UV-Vis spectroscopic measurements, to corroborate the full functionalization with cobaltacarboranes.

UV-Vis spectra have been measured using the following procedure: stock solutions of compounds were obtained by preparing solutions of several milligrams, in the range of 1-10 mg, of the solids compound in 4 ml of DMSO or acetonitrile. The molar concentration for the solutions of **Cs[2]**, **Cs_4[3]**, **Cs_8[4]**, **Cs_8[5]**, **Cs_4[6]**, **Cs_4[7]** and **Cs_8[8]** in DMSO are $3.21\cdot10^{-3}$ M, $7.27\cdot10^{-5}$ M, $2.08\cdot10^{-4}$ M, $1.04\cdot10^{-4}$ M, $2.05\cdot10^{-4}$ M, $3.87\cdot10^{-4}$ M, $3.27\cdot10^{-5}$ M, and in acetonitrile are $1.35\cdot10^{-3}$ M, $2.42\cdot10^{-5}$ M, $1.24\cdot10^{-4}$ M, $5.76\cdot10^{-5}$ M, $1.28\cdot10^{-4}$ M, $9.65\cdot10^{-5}$ M, $6.80\cdot10^{-5}$ M, respectively. The UV-Vis absorption at 462 nm was measured and the molar absorptivity (ε) was obtained according to the relationship $\varepsilon = A_{462}/M$, where M is the molar concentration of the solution (See Table S4 Supplementary Material). For each sample the A_{462} was measured three times.

Test of solubility in water/DMSO for caesium salts of metallodendrimers.

*Calibration Curve of **Cs[9]** in DMSO (Figure 5).*

The UV-Vis absorptions for DMSO solutions of **Cs[9]** at 10^{-2} M, $5\cdot10^{-3}$ M, $2.5\cdot10^{-3}$ M, $1.25\cdot10^{-3}$ M, $6.25\cdot10^{-4}$ M, $3.13\cdot10^{-4}$ M, $1.56\cdot10^{-4}$ M, $7.8\cdot10^{-5}$ M, $3.9\cdot10^{-5}$ M, $1.95\cdot10^{-5}$ M were measured at 462 nm in order to construct the calibration curve. The Lambert-Beer law is applied and the relationship between the absorptions and concentrations has been calculated as $A_{462}=368.8\cdot$**[Cs[9]]** (R^2 = 0.9997); where A_{462} is the absorption of the solution at 462 nm, 368.8 is the molar absorptivity ε ($mol\cdot L^{-1}cm^{-1}$) at 462 nm and **[Cs[9]]** is the molar concentration ($mol\cdot L^{-1}$) for **Cs[9]** in DMSO.

Solubility Tests (Table S5 in Supplementary Material).

Entry 1 in Table S5: 11.3 mg of **Cs[2]** were dissolved in 13 mL of DMSO to give a solution $1.37\cdot10^{-3}$M. This solution was further diluted to $4.6\cdot10^{-4}$ M by addition of 25 ml of H_2O. To 1 mL of this solution were added 2 mL of pure water to give a final concentration of $1.5\cdot10^{-4}$M, with 87.9 % of water (w/w).

Entry 2 in Table S5: A solution $7.5\cdot10^{-5}$M, with 93.9 % of water (w/w), was prepared by addition of 2 mL of water to 2 mL of the previous solution $1.5\cdot10^{-4}$M of **Cs[2]**.

Entry 3 in Table S5: 12.5 mg de **Cs_8[4]** were dissolved in 0.25 mL of DMSO to give a concentration of $1.1\cdot10^{-2}$M. This solution was further diluted to $1.1\cdot10^{-4}$M (98.9 % of water) by addition of 25 ml of H_2O.

Entry 4 in Table S5: A solution of concentration $5.5\cdot10^{-5}$M, with 99.5 % of water (w/w), was prepared by addition of 2 mL of H_2O to 2 mL of the previous solution $1.1\cdot10^{-4}$M of **Cs_8[4].**

Entry 5 in Table S5: A solution of concentration $2.8\cdot10^{-5}$M, with 99.7 % of water (w/w), was prepared from by addition of 2 mL of H_2O to 2 mL of the previous solution $5.5\cdot10^{-5}$M of **Cs_8[4]**.

Entry 6 in Table S5: 24 mg of **Cs_4[7]** were dissolved in 2 mL of DMSO to give a concentration of $4.5\cdot10^{-3}$M. This solution was further diluted to $1.2\cdot10^{-4}$M (97.4 % of water) by addition of 75 ml of H_2O.

Entry 7 in Table S5: A solution $6.0\cdot10^{-5}$M, with 98.7 % of water (w/w) was prepared by addition of of H_2O (2 mL) to 2 mL of the previous solution $1.2\cdot10^{-4}$M of **Cs_4[7].**

Entry 8 in Table S5: A solution $3.0\cdot10^{-5}$M, with 99.4 % of water, was prepared by addition of H_2O (2 mL) to 2 mL of the solution $6.0\cdot10^{-5}$M of **Cs_4[7]**.

Acknowledgements: This work has been supported by the CICYT (MAT2006-05339) and the Generalitat de Catalunya, 2005/SGR/00709. E.J.J.P. thanks to the Ministerio de Educación y Ciencia for a FPU grant.

Scheme 1. Preparation of compound **(2)**$^-$ by hydrosilylation of tetravinylsilane with metallacarborane **(1)**$^-$.

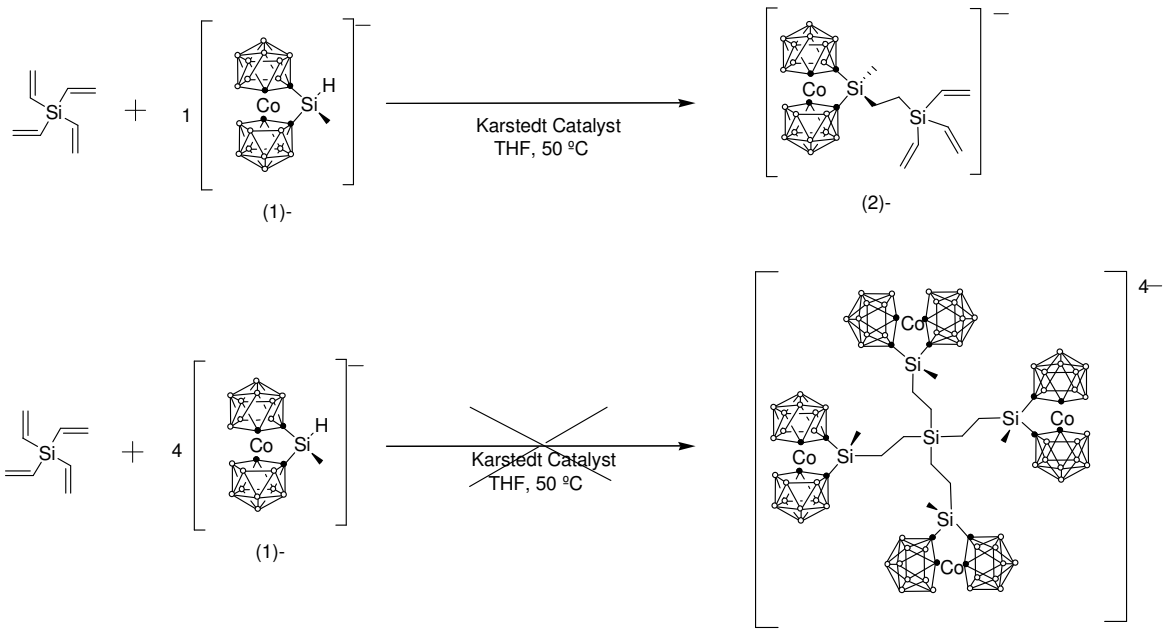

Scheme 2. Preparation of carbosilane dendrimers **(3)**$^{4-}$ and **(4)**$^{8-}$ and **(5)**$^{8-}$.

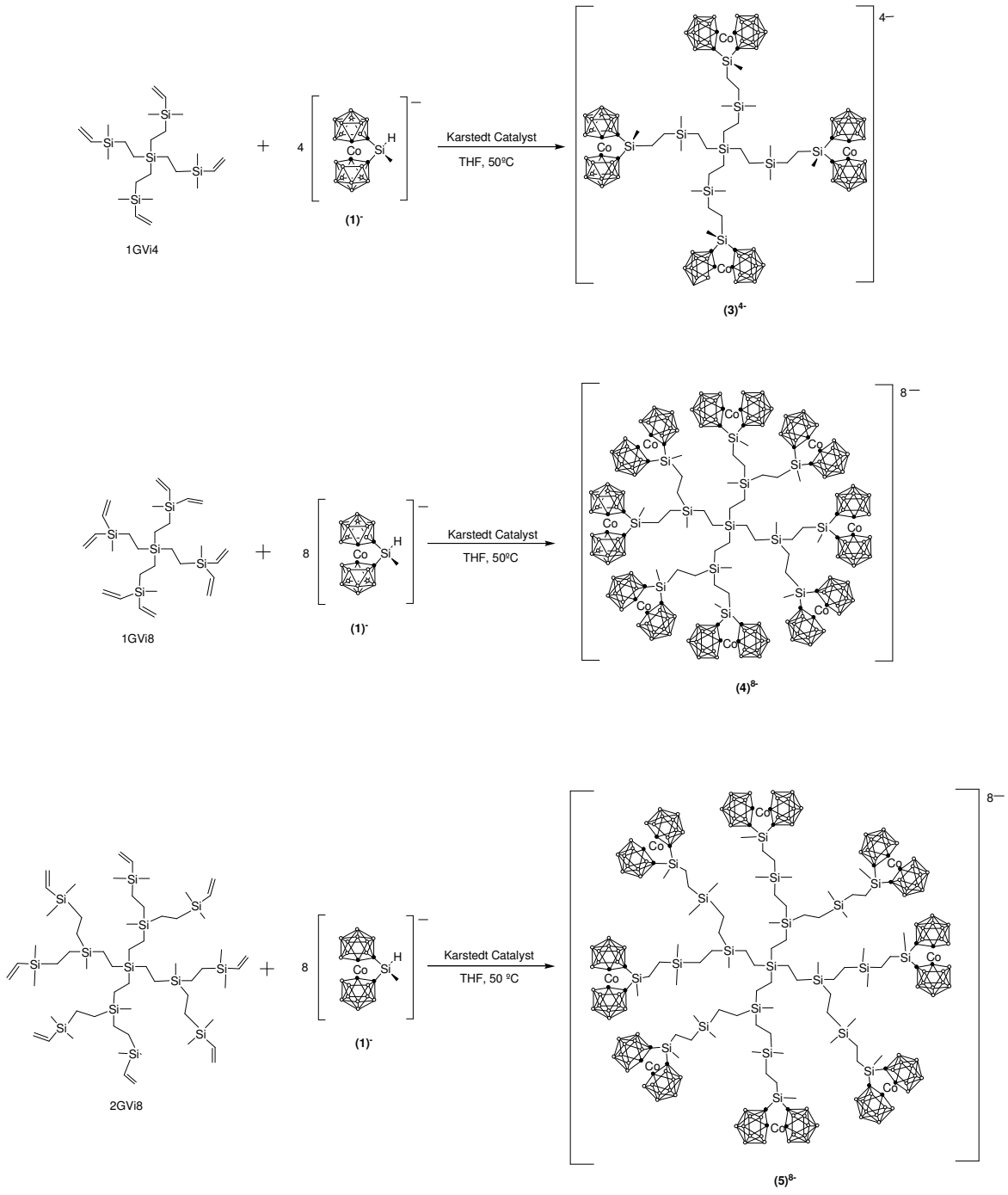

Scheme 3. Preparation of carbosiloxane dendrimers **(6)$^{4-}$**, **(7)$^{4-}$** and **(8)$^{8-}$**.

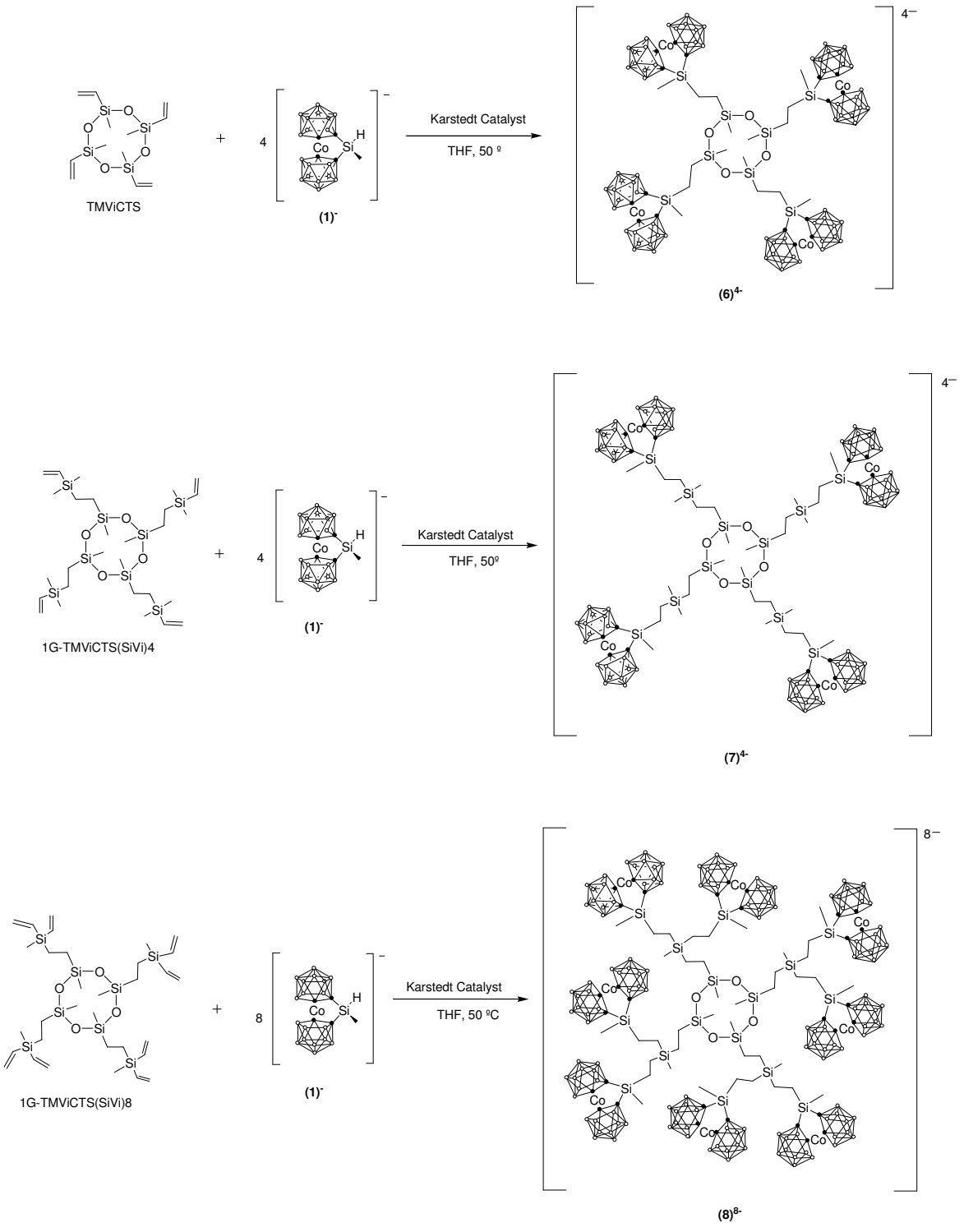

Figure 1. $^{11}B\{^{1}H\}$ NMR spectra for compounds **(1)**$^{-}$, **(2)**$^{-}$, **(3)**$^{4-}$, **(5)**$^{8-}$ and **(9)**$^{-}$.

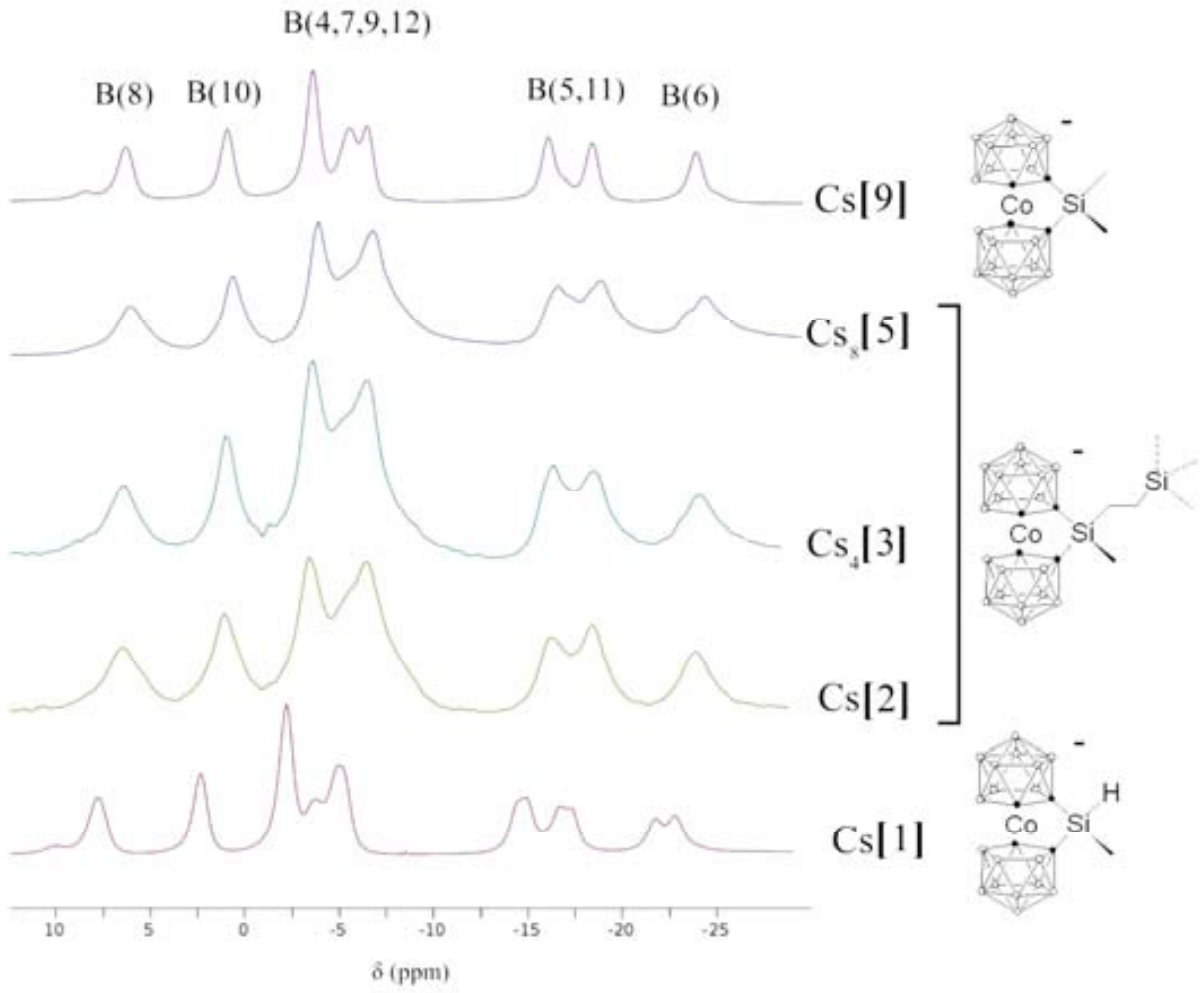

Figure 2. UV-Vis spectra in acetonitrile for compounds **Cs(2)**, **Cs_8(5)** and **Cs_4(7)**.

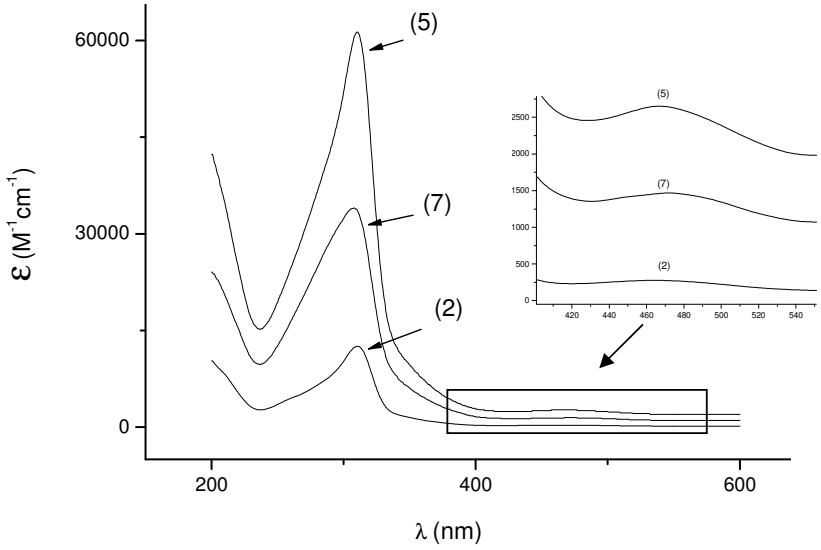

Figure 3. UV molar absorptivity (ε) at λ = 462 nm versus number of cobaltabisdicarbollide moieties (X) attached to the periphery of the dendrimers in a) DMSO, b) acetonitrile.

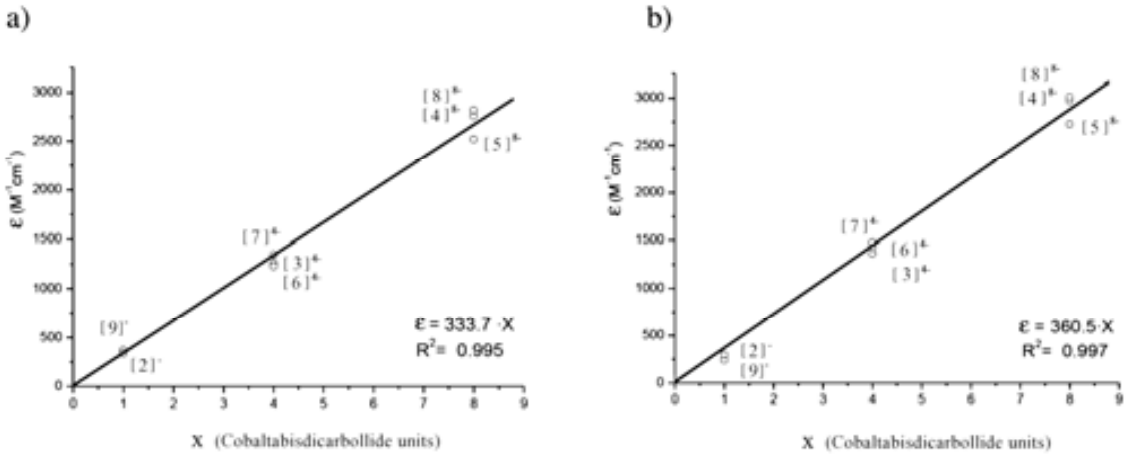

Figure 4. Calibration curve of **(9)**$^{-}$ in DMSO and absorption values (A) towards molar concentrations (M) of **Cs(2)**, **Cs_8(4)** and **Cs_4(7)** in water/DMSO solutions.

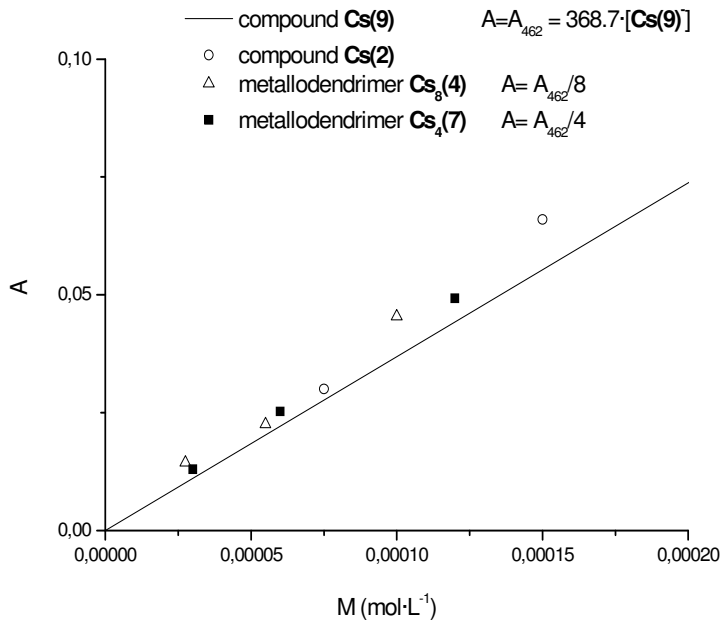

References

(1) (a) *Dendrimers and other dendritic polymers* Fréchet, J. M.; Tomalia, D. A. Eds.; Wiley Series in Polymer Science, John Wiley & sons, Ltd., UK, 2001. (b) Astruc, D.; Chardac, F. *Chem. Rev.* **2001**, *101*, 2991. (c) Crooks, R.M.; Zhao, M.; Sun, L.; Chechik, V.; Yeung, L. K. *Acc. Chem. Res.* **2001**, *34*, 181. (d) Newkome, G. R.; Moorefield, C. N.; Vötgle, F. *Dendrimers and Dendrons: Concepts, Synthesis, Applications*; Wiley: New York, 2002. (e) Boas, U.; Heegarard, P. M.H. *Chem. Soc. Rev.* **2004**, *33*, 43. (f) Caminade, A. M.; Majoral, J. P.; *Acc. Chem. Res.* **2004**, *37*, 341. (g) Liang, C.; Fréchet, J. M. *Prog. Polym. Sci.* **2005**, *30*, 385. (h) Jiang, D. L.; Aida, T. *Prog. Polym. Sci.* **2005**, *30*, 403. (i) Astruc, D.; Ornelas, C.; Ruiz, J. *Acc. Chem. Res.* **2008**, *41*, 841. (j) Caminade, A. M.; Servin, P.; Laurent, R.; Majoral, J. P.; *Chem. Soc. Rev.* **2008**, *37*, 56.

(2) (a) Qualmann, B.; Kessels, M. M.; Mussiol, H.-J; Sierralta, W. D.; Jungblut, P. W.; Moroder, L. *Angew. Chem.* **1996**, *108*, 970; *Angew. Chem. Int. Ed. Engl.* **1996**, *35*, 909. (b) Yamamoto, K.; Higuchi, M.; Shiki, S.; Tsuruta, M.; Chiba, H. *Nature* **2002**, *415*, 509. (c) Frey, H.; Haag, R. *Rev. Mol. Biotechnol*. **2002**, *90*, 257. (d) van Heerbeeck, R.; Kamer, P. C.J.; van Leeuwen, P. W. N. M.; Reek, J. N. H. *Chem. Rev.* **2002**, *102*, 3717. (e) Gillies E. R.; Fréchet, J. M. J. *Drug. Discor. Today*, **2005**, *10*, 35. (f) Méry, D.; Astruc, D. *Coord. Chem. Rev.* **2006**, *250*, 1965. (g) Cheng, Y; Wang, J; Rao, T; He, X; Xu, T. *Frontiers in Bioscience* **2008**, *13*, 1447. (h) Cheng, Y.; Xu, Z.; Ma, M.; Xu, T. *J. Pharm. Sci.* **2008**, *97*, 123. (i) Agarwal, A.; Saraf, S.; Asthana, A.; Gupta, U.; Gajbhiye, V.; Jain, N.K. *Int. J. Pharm.*, **2008**, *350* , 3. (j) Caminade, A. M.; Turrin, C. O.; Majoral, J. P. *Chem. Eur. J.*, **2008**, *14*, 7422. (k) Jang, W. D.; Selim, K. M. K.; Lee, C. H.; Kang, I. K. *Prog. Polym. Sci.* **2009**, 34, 1, and references therein.

(3) (a) van der Made, A. W.; van Leeuwen, P. W. N. M. *J. Chem. Soc., Chem. Commun*. **1992**, 1400. (b) Seyferth, D.; Son, D. Y.; Rheingold, A. L.; Ostrader, R. L. *Organometallics* **1994**, *13*, 2682. (c) Alonso, B.; Cuadrado, I.; Morán, M.; Losada, J. *J. Chem. Soc., Chem. Commun.* **1994**, 2575. (d) van der Made, A. W.; van Leewen, P. W. N. M., de Wilde, J. C.; Brances, R. A. C. *Adv. Mater*. **1993**, *5*, 466. (e) Zhan, L.-L.; Roovers, J. *Macromolecules* **1993**, *26*, 963. (f) Seyferth, D.; Kugita, T.; Rheingold, A. L.; Yap, G. P. A. *Organometallics* **1995**, *14*, 5362. (g) Krsda, S. W.; Seyferth, D. *J. Am. Chem. Soc.* **1998**, *120*, 3604. (h) Lühmann, B.; Lang, H.; Bröning, K. *Phosphorus Sulfur Silicon Relat. Elem.* **2001**, *65*, 133. (i) Casado, M. A.; Hack, V.; Camerano, J. A.; Ciriano, M. A.; Tejel, C.; Oro, L. A. *Inorg. Chem.* **2005**, *44*, 9122. (j) Donnio, B.; Buathong, S.; Bury, I.; Guillon, D.; *Chem. Soc. Rev.* **2007**, *36*, 1945. (k) Zamora, M.; Alonso, B.; Pastor, C.; Cuadrado, I. *Organometallics*, **2007**, *26*, 5153. (l) Andrés, R.; de Jesús, E.; Flores, J. C. *New J. Chem.* **2007**, *31*, 1161. (m) Kim, C.; An, K. *J. Organomet. Chem.* **1997**, *547*, 55. (n) Kim, C.; An, K.; *Bull. Korean Chem. Soc.* **1997**, *18*, 164. (o) Kim, C.; Park, E.; Kang, E.; *Korean Chem. Soc.* **1996**, *40*, 347.

(4) (a) Cuadrado, I.; Morán, M.; Casado, C. M.; Alonso, B.; Losada, J. *Coord. Chem. Rev.* **1999**, *193-195*, 395. (b) Gudat, D. *Angew. Chem., Int. Ed. Engl.* **1997**, *36*, 1951. (c) Frey, H.; Schlenk, C. *Top. Curr. Chem*. **2000**, *210*, 69. (d) Kreiter, R.; Kleij, A. W.; Gebbink, R. J. M. K.; van Koten G. *Top. Curr. Chem.* **2001**, *217*, 163.

(5) (a) Kleij, A. W.; Gossage, R. A.; Gebbink, R. J. M. K.; Brinkmann, N.; Reijerse, E. J.; Kragl, U.; Lutz, M.; Spek, A. L.; van Koten, G. *J. Am. Chem. Soc.* **2000**, *122*, 12112. (b) Rossell, O.; Seco, M.; Angurell, I. *C. R. Chimie*., **2003**, *6*, 803. (c) Angurell, I.; Rossell, O.; Seco, M.; Ruiz, E. *Organometallics*, **2005**, *24*, 6365. (d) Rodríguez, L.I.; Rossell, O.; Seco, M.; Grabulosa, A.; Muller, G.; Rocamora, M. *Organometallics*, **2006**, *25*, 1368. (e) *Silicon-Containing Dendritic Polymers (Advance in Silicon Science)* Dvornic, P.; Owen, M. J., Eds. Springer, 2009,Vol. 2.

(6) (a) Ortega, P.; Bermejo, J. F.; Chonco, L.; de Jesús, E.; de la Mata, F. J.; Fernández, G.; Flores, J. C.; Gómez, R.; Serramía, M. J.; Muñoz-Fernández, M. A. *Eur. J. Inorg. Chem.* **2006**, *7*, 1388. (b) Bermejo, J. F.; Ortega, P.; Chonco, L.; Eritja, R.; Samaniego, R.; Müller, M.; de Jesús, E.; de la Mata, F. J.; Flores, J. C.; Gómez, R.; Muñoz-Fernández, M. A. *Chem.-Eur. J.* **2007**, *13*, 483. (c) Chonco, L.; Bermejo-Martín, J. F.; Ortega, P.; Shcharbin, D.; Pedziwiatr, E.; Klajnert, B.; M.; de la Mata, F. J.; Gómez, R.; Bryszewska, M.; Muñoz-Fernández, M. A. *Org. Biomol. Chem.* **2007**, *5*, 1886. (d) Gras, R.; Almonacid, L.s; Ortega, P.; Serramia, M. J; Gómez, R.; de la Mata, F. J.; López-Fernández, L. A.; Munoz-Fernández, M. A. *Pharm Res.*, **2009**, *26*, 577.

(7) (a) Kleij, A. W.; van de Coevering, R.; Klein-Gebbink, R. J. M.; Nordman, A.-M.; Spek, A. L.; van Koten, G. *Chem. Eur. J.* **2001**, *7*, 181. (b) Weber, N.; Ortega, P.; Clemente, M. I.; Shcharbin, D.; Bryszewska, M.; de la Mata, F. J.; Gómez, R.; Muñoz-Fernández, M. A., *J. Control. Release.* **2008**, *132*, 2008.

(8) (a) Ornelas, C.; Boisselier, E.; Martinez, V.; Pianet, I.; Ruiz-Arenzaes, J.; Astruc, *Chem. Commun*. **2007**, 5093. (b) Boisselier, E.; Ornelans, C.; Pianet, I.; Ruiz-Arenzaes, J.; Astruc, D. *Chem. Eur. J.* **2008**, *14*, 5577. c) Malik, N.; Wiwattanapatapee, R.; Klopsch, R.; Lorenz, K.; Frey, H.; Weener, JW; Meijer, EW; Paulus, W.; Duncan, R. *J. Control. Release* **2000**, *65*, 133.

(9) (a) Núñez, R.; González, A.; Viñas, C.; Teixidor, F.; Sillanpää, R.; Kivekäs, R. *Org. Letters* **2005**, *7*, 231. (b) Núñez, R.; González-Campo, A.; Viñas, C.; Teixidor, F.; Sillanpää, R.; Kivekäs, R. *Organometallics,* **2005**, *24*, 6351. (c) Núñez, R.; González-Campo, A.; Laromaine, A.; Teixidor, F. Sillanpää, R.; Kivekäs, R.; Viñas, C. *Org. Letters* **2006**, *8*, 4549. (d) Lerouge, F.; Vicas, C.; Teixidor, F.; Núñez, R.; Abreu, A.; Xochitiotzi, E.; Santillan, R.; Farfán, N. *Dalton Trans.* **2007**, 1898.

(10) (a) González-Campo, A.; Viñas, C.; Teixidor, F.; Nuñez, R.; Kivekäs, R.; Sillanpää, R. *Macromolecules* **2007**, *40*, 5644. (b) González-Campo, A.; Juárez-Pérez, E. J.; Viñas, C.; Boury, B.; Kivekäs, R.; Sillanpää, R.; Núñez, R. *Macromolecules* **2008**, *41*, 8458.

(11) (a) Hawthorne, M. F.; Andrews, T. D. *J. Chem. Soc., Chem. Commun.* **1965**, 443. (b) Sivaev, I. B.; Bregadze, V. I. *Collect. Czech. Chem. Commun*. **1999**, *64*, 783.

(12) (a) Ma, L.; Hamdi, J.; Hawthorne, M. F. *Inorg. Chem.* **2005**, *44*, 7249. (b) Matejicek, P.; Cigler, P.; Procházka, K.; Kral, V. *Langmui*r, **2006**, *22*, 575. (c) Chevrot, G.; Schurhammer, R.; Wipff, G. *J. Phys. Chem. B* **2006**, *110*, 9488.
(13) (a) Strauss, S. H. *Chem. Rev.* **1993**, *93*, 927. (b) Reed, C. A. *Acc. Chem. Res.* **1998**, *31*, 133.
(14) Masalles, C.; Llop, J.; Viñas, C.; Teixidor, F. *Adv. Mater.* **2002**, *14*, 826.
(15) Plesek, J. *Chem. Rev.* **1992**, *92*, 269.
(16) (a) Viñas, C.; Gómez, S.; Bertran, J.; Teixidor, F.; Dozol, J.-F.; Rouquette, H. *Chem. Commun.* **1998**, 191. (b) Viñas, C.; Gómez, S.; Bertran, J.; Teixidor, F.; Dozol, J.-F.; Rouquette, H. *Inorg. Chem. 1998*, *37*, 3640. (c) Grüner, B.; Plesek, J.; Baca, J.;Cisarova, I.; Dozol, J.-F; Rouquette, H.; Viñas, C.; Selucky, P.; Rais, J. *New J. Chem.* **2002**, *26*, 1519. (d) Mikulásek, L; Grüner, B.; Crenguta, D.; Rudzevich, V.; Böhmer,V.; Haddaoui, J.; Hubscher-Bruder, V.; Arnaud-Nue, F.; Caslavsky, J.; Selucky, P. *Eur. J. Org. Chem.* **2007**, 4772.
(17) (a) Masalles, C.; Borrós, S.; Viñas, C.; Teixidor, F., *Adv. Mater.* **2000**, *12*, 1199. (b) Borrós, S.; Llop, J.; Viñas, C.; Teixidor, F. Adv. Mater. **2002**, *14*, 449. (c) Gentil, S., Crespo, E., Rojo, I.; Friang, A.; Viñas, C., Teixidor, F.; Grüner, B.; Gabel, D. *Polymer* **2005**, *46*, 12218. (d) Crespo, E.; Gentil, S.; Viñas, C.; Teixidor, F. *J. Phys. Chem. C* **2007**, *111*, 18381. (e) Errachid, A.; Caballero, D.; Crespo, E.; Bessueille, F.; Pla-Roca, M.; Mills, C.; Christopher, A.; Teixidor, F; Samitier, J. *Nanotechnology* **2007**, *18*, 485301. (f) Stoica, A. I. ; Viñas C. ; Teixidor, F. *Chem. Commun.* **2008**, 6492.
(18) Stoica, A. I.; Viñas C. ; Teixidor, F *Chem. Commun.* **2008**, 48, 6492**.**
(19) (a) Hawthorne, M. F.; Maderna, A. *Chem. Rev.* **1999**, *99*, 3421. (b) Hao, E.; Vicente, M. G. H. *Chem. Commun.* **2005**, 1306. (c) Barth, R. F.; Coderre, J. A.; Vicente, M. G. H.; Blue, T. E. *Clin. Cancer Res.* **2005**, *11*, 3987. (d) Gottumukkala, V., Ongayi, O.; Baker, D. G.; Lomax, L. G.; Vicente, M. G. H. *Bioorg. Med. Chem.* **2006**, *14*, 1871. (e) Wang, J.-Q.; Ren, C.-X.; Weng, L.-H.; Jin, G.-X. *Chem. Commun*. **2006**, 162. (f) Bregadze, V. I.; Sivaev, I. B.; Glazun, S. A. *Anti-Cancer Agents Med. Chem.*, **2006**, *6*, 75. (f) Cígler, P.; Kozisek, M.; Rezacova, P.; Brynda, J.; Otwinowski, Z.; Pokorná, J.; Plesek, J.; Grüner, B.; Dolecková-Maresová, L.; Masa, M.; Sedlácek, J.; Bodem, J.; Kräusslich, H.-G.; Král, V.; Konvalinka, J. *Proc. Natl. Acad. Sci. U.S.A*. **2005***, 102*, 15394. (g) Crossley, E. L.; Ziolkowski, E. J.; Coderre, J. A.; Rendina, L. M. *Mini-Rev. Med. Chem.* **2007**, *7*, 3003.
(20) Valliant, J. F.; Guenther, K. J.; King, A. S.; Morel, P.; Schaffer, O. O., Sogbein, K. A.; stephenson, K. A. *Coord. Chem. Rev.* **2002**, *232*, 173.
(21) (a) Olejniczak, A. B.; Plesek, J.; Kriz, O.; Lesnikowski, Z. J. *Angew. Chem. Int. Ed.* **2003**, *42*, 5720. (b) Lesnikowski, Z.; Paradowska, E.; Olejniczak, A. B.; Studzinska, M.; Seekamp, P.; Schüβler, U.; Gabel, D.; Schinazi, R. F.; Plesek, J.; *Bioorg. Med. Chem.* **2005**, *13*, 4168. (c) Olejniczak, A. B.; Plesek, J.; Lesnikowski, Z. J. *Chem. Eur. J.* **2007**, *13*, 311.
(22) (a) Sibrian-Vazquez, M.; Hao, E.; Jenssen, T. J.; Vicente, M.G. H. *Biocong. Chem.* **2006**, 17, 928. (b) Hao, E.; Sibrian-Vazquez, M.; Serem, W.; Garno, J. C.; Fronczek F. R.; Vicente, M. G. H. *Chem. Eur. J.* **2007**, *13*, 9035. (c) Li, F.; Fronczek, F. R.; Vicente, M. G. H. *Tetrah. Lett.*, **2008**, *49*, 4828.
(23) Plesek, J.; Hermanek, S.; Franken, A.; Cisarova, I.; Nachtigal, *Ch. Collect. Czech. Chem. Commun.* **1997**, *62*, 47.
(24) Llop, J.; Masalles, C.;Viñas, C.; Teixidor, F.; Sillanpää R.; Kivekäs, R. *Dalton Trans.* **2003**, 556.
(25) Marciniec, B. *Hydrosilylation: A Comprehensive Review on Recent Advances* In Advances in Silicon Science,. Matisons, J. Ed; Springer Netherlands, 2009. Vol. 1.
(26) (a) Juárez-Pérez, E. J.; Viñas, C.; González-Campo, A.; Teixidor, F.; Kivekäs, R.; Sillanpää R.; Núñez, R. *Chem. Eur. J*. **2008**, *14*, 4924. (b) Juárez-Pérez, E. J.; Teixidor, F.; Viñas, C.; Núñez, R.; *J. Organomet. Chem.* **2009**, 694, 1764.
(27) (a) Antiñolo, A.; Fajardo, M.; Gómez-Ruiz, S.; López-Solera, I.; Otero, A.; Prashar, S. *Organometallics* **2004**, *23*, 4062. (b) Gómez-Ruiz, S.; Prashar, S.; Fajardo, M.; Antiñolo, A.; Otero, A.; Maestro, M.; Volkis, V.; Eisen, M.; Pastor, c. *Polyhedron* **2005**, *24*, 1298.
(28) (a) Tood, L. J. *Progress in NMR Spectroscopy*, Ed. Pergamon Press Ltd. **1979**, 13, 87. (b) Rojo, I.; Teixidor, F.; Viñas, C.; Kivekäs, R.; Sillanpää, R. *Chem. Eur. J.* **2004**, *10*, 5376.
(29) Rojo, I.; Teixidor, F.; Viñas, C.; Kivekäs, R.; Sillanpää, R. *Chem. Eur. J.* **2003**, *9*, 4311
(30) (a) Teixidor, F.; Pedrajas, J.; Rojo, I.; Viñas, C.; Kivekas, R.; Sillanpaa, R.; Sivaev, I.; Bregadze, V.; Sjoberg, S. *Organometallics* **2003**, *22*, 3414-3423. (b) Farràs, P.; Teixidor, F.; Kivekäs, R.; Sillanpää, R.; Viñas, C.; Grüner, B.; Cisarova I.; *Inorg. Chem.*, **2008**, *47*, 9497.
(31) Justus, E.; Rischka, K.; Wishart, J.; Werner, K.; Gabel, D. *Chem. Eur. J.* **2008**, *14*, 1918.
(32) Kim, C.; Jung, I. *J. Organomet. Chem.* **2000**, 599, 208.
(33) Rais, J.; Selucky, P.; Kyrs, M. *J. Inorg. Nucl. Chem.* **1976**, *38*, 1376.
(34) Plesek, J.; Base, K.; Mares, F.; Hanousek, F.; Stirr, B.; Hermanek, S. *Collect. Czech. Chem. Commun.*, **1984**, *49*, 2776.
(35) Fanning, J.C. *Coord. Chem. Rev.* **1995**, *140*, 27.
(36) (a) Buggins, Talia R.; Dickinson, Paul A.; Taylor, Glyn *Adv. Drug Delivery Rev.* **2007**, *59*, 1482. (b) Himmel, Herbert M. *J. Pharmacol. Toxicol. Methods* **2007**, *56*, 145.

Polyanionic carbosilane and carbosiloxane metallodendrimers based on cobaltabisdicarbollide derivatives.

Emilio José Juárez-Pérez,[a#] Clara Viñas,[a] Francesc Teixidor,[a] Rosario Núñez[a*]

Supplementary Material

Steric Hindrance quantification by Monte Carlo Method.[1]

The Monte Carlo method has been applied in this work for the stochastic generation of stable configurations in the dendrimers studied at 300 K. Solvation is not incorporated into the model and the bulky [1,1'-μ-Si(CH_3)CH_2-3,3'-Co(1,2-$C_2B_9H_{11}$)$_2$]$^-$ fragment has been substituted by a -Si(CH_3)$_3$ moiety. The aim of these calculations is to obtain a parameter that quantify the steric hindrance in the periphery of any carbosilane dendrimer. It could be achieved taken in account the most external Si atoms in the branches and recording the average distance between them. This average distance for all configurations simulated by Monte Carlo method may provide a representative value to compare between dendrimeric structures about the steric hindrance in the periphery. We define this parameter as η (Å), equation 1.

$$\eta = \frac{1}{M \cdot N} \sum_{j=1}^{M} \sum_{i=1}^{N} d_i \qquad (1)$$

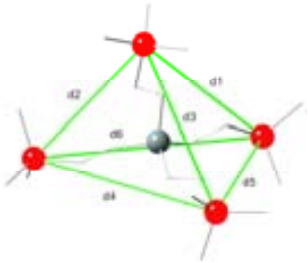

Figure S1. Tetravinylsilane four times hydrosilylated with HSi(CH_3)$_3$ showing the six distances measured.

Where M means the number of simulated configurations, usually 100, and N takes the value of 1 for disubtituted, 3 for trisubtituted, 6 for tetrasubstituted and 36 for eight-substituted branches of the dendrimers in the periphery. For example, the case of the tetravinylsilane (**TViSi)** hydrosilylated with four HSi(CH_3)$_3$, **TViS0s4**, the six recorded distances are represented in Figure S1.

This six distances in the 100 simulated configurations for **TViS0s4** applying equation 1 gives η = 7.0 Å. The data for the other dendrimeric structures is represented graphically in Figure S2 and the Table S1 show the values of η.

Low values of this parameter η can be seen as high steric hindrance and high values as low steric hindrance. Then, it can be seen that the tetrasubtituted (**TViS0s4**) has the lowest value of η. Also, the trisubstituted (**TViS1s3**) dendrimer η is lower than disubstituted (**TViS2s2**). The first generation of a tetrafunctionalized dendrimer, the **1G-Vi0s4**, has a higher value than **TViS0s4.** Also, **1G-Vi0s8** has higher value than **TViS0s4**. However, the **1G-Vi0s4**, has a higher value than **1G-Vi0s8** because **1G-Vi0s4** is less overcrowded. The comparison between **1G-Vi0s8** and **2G-Vi0s8** is very interesting, if these dendrimers are drawn on a plane they seem to be as overcrowded as **TViS0s4**, however the η parameter is very different between them, being the crowdedness less when the dendrimer generation is higher. Then, this method permits to know, *a priori*, and as an indirect way, which vinyl terminated dendrimers can be fully hydrosilylated with the [1,1'-μ-Si(CH_3)-3,3'-Co(1,2-$C_2B_9H_{11}$)$_2$]$^-$ fragment. The experimental findings permit to draw a frontier line for the [1,1'-μ-Si(CH_3)-3,3'-Co(1,2-$C_2B_9H_{11}$)$_2$]$^-$ case, that we have placed around 8.5 Å.

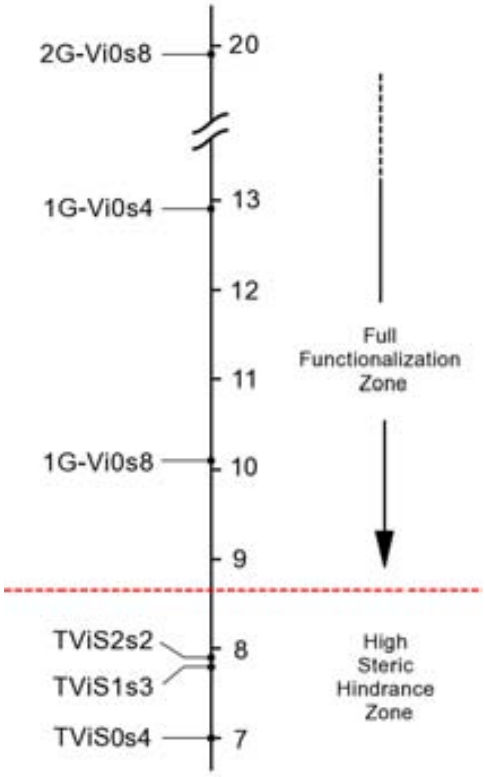

Figure S2. Values of η (Å) for the calculated structures at 300 K. The two zones frontier line is established according to experimental results for the case of the cobaltabisdicarbollide.

dendrimer	η(Å)
TViS0s4	7,0
TViS1s3	7,8
TViS2s2	7,9
1G-Vi0s8	10,1
1G-Vi0s4	12,9
2G-Vi0s8	19,9

Table S1. Values of η for the calculated structures at 300 K.

Experimental Method

Averages computed from a properly equilibrated Monte Carlo simulation correspond to thermodynamic ensemble averages at 300 K. A geometry optimization of the initial structure configuration at semiempirical level PM6[1b] is the starting point for the Monte Carlo simulations.[1c]

Figure S3. MALDI-TOF spectrum for compound **(2)**$^{-}$.

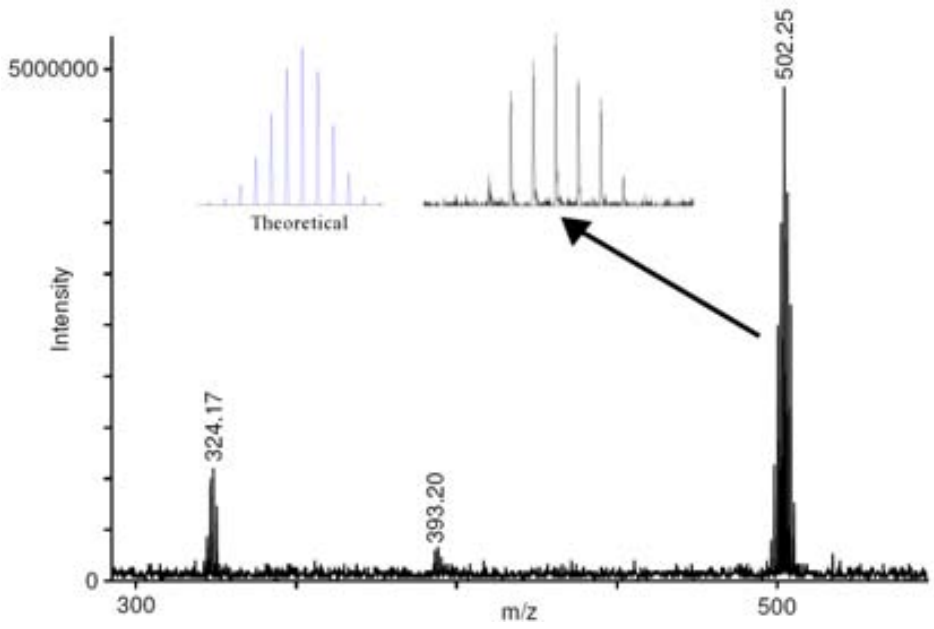

Table S2. Chemical shift values [ppm] of the carbon nuclei in the $^{13}C\{^{1}H\}$ NMR spectrum of dendrimers functionalizated with cobaltabisdicarbollides.

			δ $^{13}C\{^{1}H\}$			
Metallodendrimer	***C*$_c$-H**	**Si-*C*$_c$**	**-*C*H$_2$-**	***C*H$_3$-Si-O**	**Si-*C*H$_3$**	**C$_c$-Si-*C*H$_3$**
(2)$^{-}$	55.30	40.99	4.14, 3.35	–		-7.72
(3)$^{4-}$	55.55	41.33	6.49, 5.05 4.07, 2.44	–	-5.11	-7.72
(4)$^{8-}$	55.32	41.24	8.49, 7.18 4.13, 3.50	–	-1.09	-7.63
(5)$^{8-}$	55.30	41.08	8.52, 6.60 4.34, 4.10 3.55, 3.11	–	-1.13, -5.02	-7.77
(6)$^{4-}$	56.16	41.93	8.44, 4.21	-1.04	–	-6.70
(7)$^{4-}$	55.29	41.16	8.98, 5.65, 5.05, 4.04	-1.05	-5.15	-7.75
(8)$^{8-}$	50.95	43.83	8.57, 7.68, 5.62, 4.40	-0.65	-1.82	-7.73

Table S3. Chemical shift values [ppm] of the silicon nuclei in the $^{29}Si\{^{1}H\}$ NMR spectrum of dendrimers functionalizated with cobaltabisdicarbollides.

	δ $^{29}Si\{^{1}H\}$		
Metallodendrimer	**Si_{core}**	**Si_{branch}**	**Si-C_c**
$(2)^{-}$	11.80	–	12.15
$(3)^{4-}$	5.88	6.65	11.98
$(4)^{8-}$	8.28	9.78	11.73
$(5)^{8-}$		6.32, 8.03	11.52
$(6)^{4-}$	-20.53	–	11.85
$(7)^{4-}$	-19.88	7.63	11.15
$(8)^{8-}$	-19.94	8.88	11.74

Table S4. UV molar absorptivities (ε) in DMSO and CH_3CN for the metallodendrimers. X represents the number of cobaltabisdicarbollide moieties attached to the dendrimer periphery.

	ε (M^{-1})	**ε (M^{-1})**			
Compound	**DMSO**	**CH_3CN**	**X**	**ε/X (DMSO)**	**ε/X (CH_3CN)**
Cs(9)	369	239	1	369	239
Cs(2)	335	294	1	335	294
Cs_4(3)	1259	1362	4	315	340
Cs_8(4)	2755	2970	8	344	371
Cs_8(5)	2518	2726	8	315	341
Cs_4(6)	1228	1427	4	307	357
Cs_4(7)	1345	1476	4	336	369
Cs_8(8)	2818	3011	8	352	376

Table S5. Absorption values (A) towards different molar concentration (M) of **Cs(2)**, **Cs_8(4)** and **Cs_4(7)** in water/DMSO solutions.

Entry	Compound	M (mol·L^{-1})	Abs.	% (w/w) water
1	**Cs(2)**	$1.5 \cdot 10^{-4}$	0.066	87.9
2	**Cs(2)**	$7.5 \cdot 10^{-5}$	0.030	93.9
3	**Cs_4(8)**	$1.1 \cdot 10^{-4}$	0.045	98.9
4	**Cs_4(8**	$5.5 \cdot 10^{-5}$	0.022	99.5
5	**Cs_4(8)**	$2.8 \cdot 10^{-5}$	0.014	99.7
6	**Cs_4(7)**	$1.2\ 10^{-4}$	0.049	97.4
7	**Cs_4(7)**	$6.0 \cdot 10^{-5}$	0.025	98.7
8	**Cs_4(7)**	$3.0 \cdot 10^{-5}$	0.013	99.4

(1) (a) Allen, M.; Tildesley, P. D. J. *Computer Simulation of Liquids*, Oxford University Press, USA, **1989**. (b) MOPAC2007 Version 8.205L, Stewart, J. J. P.; Stewart Computational Chemistry, **2007**. (c) Hyperchem 7.5., Hypercube, **2002**.

b) Polyanionic Aryl-Ether Metallodendrimers Based On Cobaltabisdicarbollide Derivatives. Photoluminescent Properties.

Polyanionic Aryl-Ether Metallodendrimers Based On Cobaltabisdicarbollide Derivatives. Photoluminescent Properties.

Emilio José Juárez-Pérez,[a#] *Clara Viñas,*[a] *Francesc Teixidor,*[a] *Rosa Santillan,*[b] *Norberto Farfán,*[c] *Arturo Abreu,*[d] *Rebeca Yépez,*[b] *Rosario Núñez*[a *]

[a] Institut de Ciència de Materials, CSIC, Campus U.A.B., 08193 Bellaterra, Spain
[b] Departamento de Química, Centro de Investigación y de Estudios Avanzados del IPN, 07000, Apdo. Postal 14-740, México D.F., México
[c] Facultad de Química, Departamento de Química Orgánica, Universidad Nacional Autónoma de México, México D.F. 04510, México
[d]Universidad Politécnica de Pachuca, Carretera Pachuca Cd. Sahagún, Km 20, Zempoala, Hidalgo México.
Email address: rosario@icmab.es

Corresponding Author: Dr. Rosario Núñez, Institut de Ciència de Materials, CSIC, Campus U.A.B., 08193 Bellaterra, Barcelona, Spain. Tel.: +34 93 580 1853. Fax: +34 93 580 5729. rosario@icmab.es

[#] Enrolled in the UAB PhD program.

Introduction

1,3,5-triaryl(benzenes) (TPB) are a class of C3-symmetry compounds important in electrodes and electro luminescent devices. Branched functionalized benzenoid compounds are versatile organic molecules for the synthesis of C60, pharmaceuticals, sensitizers for photographic processes as well as conjugated star polyaromatics. Dendrimers prepared from triphenylbenzene have attracted considerable attention in the last years,[1] among them, the Fréchet type-poly(aryl ether) dendrimers are of current interest because of their properties and multiple applications.

In the last years, the incorporation of boron clusters in the interior or on the periphery of hydrocarbon,[2] poly(lysine)[3] and aliphatic polyester dendrimers,[4] as well as other macromolecules and dendrimeric systems[5] has become an area of great interest. Recently, in our group we have become interested on the use of different types of dendrons and dendrimers as platforms for the incorporation of boron-based molecules.[6] With the aim of preparing boron-rich anionic dendrimers, we have developed different synthetic strategies for the preparation of anionic carboranyl-terminated carbosilane dendrimeric systems, in which *nido*-carborane clusters are placed at the periphery.[7] We have previously reported the efficient preparation of polyanionic macromolecules by using a new approach to bind metallacarboranes to carbosilane and carbosiloxane dendrimers via hydrosilylation reactions of vinyl-terminated dendrimers with the C_c-silyl-substituted cobaltabisdicarbollide derivatives, Cs[1,1'-μ-SiMeH-3,3'-Co(1,2-$C_2B_9H_{10})_2$], **Cs(1)**.[8] The reason to choose the monoanionic cobaltabisdicarbollide, [(3,3'-Co-(1,2-$C_2B_9H_{11})_2]^-$,[9] is due to their boron-rich nature, extraordinary chemical and thermal stability, hydrophobicity,[10] weakly coordinating character[11] and low nucleophilicity.[12] These features make anionic dicarbollides suitable for the stabilization of transient complex cation particles in catalysis, as strong non-oxidizing acids,[13] solid electrolytes,[13] extractant of radionuclides,[14] and doping agent in conducting polymers.[15] Our group has reported the use of the cobaltabisdicarbollide in ion selective PVC membrane electrodes for tuberculosis drug analysis.[16] Cobaltabisdicarbollide derivatives have also been considered promising agents as boron rich carriers for cancer treatment and diagnosis in Boron Neutron Capture Therapy (BNCT).[17] These boron compounds

can be delivered into tumor cells using different strategies for tumor targeting or can be used as building blocks for the synthesis of boron-containing biomolecules. For that reason, this metallacarborane has been attached to different organic groups and biomolecules, such as nucleosides[18] and porphyrins.[19] The recent emergence of applications of carboranes as materials for nanotechnology and pharmacophores in drug design has expanded the potential use of boron clusters in practice.[20] For this purpose, bio-active functionalized metallacarboranes have been characterized,[21] In our continuing investigation of structure/properties relationship in metallacarborane-containing dendrimers, we now report the synthesis and characterization of a new family of star-shaped and dendrimers, that consist of 1,3,5-triphenylbenzene units as fluorescent cores, Fréchet-type poly(aryl ether) fragments as connecting groups and three, six and twelve cobaltabisdicarbollide anions as end moieties. which contain a core and at the periphery. In addition, comparison between the photoluminescent properties of the compounds, before and after functionalization has been carried out.

Results and Discussion

1. Synthesis of polyphenyl aryl ether star shape dendrimers with fluorescent cores. The synthesis of 1,3,5-triarylbenzene can be carried out using Suzuki cross coupling or cyclocondensation reactions from substituted acetophenones.[22] The cyclocondensation allows the synthesis of many chemical species, such as multimetallic pincer,[23] star-shaped thiophenes[24] and organic-inorganic hybrid mesoporous materials,[25] which can be carried out with triflic acid,[24] sulfuric acid-sodium pirosulfate,[25] perfluorinated resins[26] and tetrachlorosilane in ethanol.[23]

In this work we have prepared dendrimers with 1,3,5-triarylbenzene as core and three, six, nine and twelve terminal allyl groups to be used as precursors to attach metallacarborane derivatives at the periphery. The sequence of reactions used for the preparation of 1,3,5-tris(4-allyloxyphenyl)benzene **2** is shown in Scheme 1. 4-allyloxyacetophenone, **1**, was first synthesized in quantitative yields from 4-hydroxyacetophenone and allyl bromide in the presence of potassium carbonate under reflux of acetone, the spectroscopic data of **1** were compared with those reported in the literature.[27a] Triple condensation of **1** in absolute ethanol using tetrachlorosilane led to **2** in 80 % yield. For the synthesis of 1,3,5-(4-(3,5-bisallyloxy)-benzyloxyphenyl)benzene, **5a**, and 1,3,5-(4-(3,4,5-trisallyloxy)-benzyloxyphenyl)benzene, **5b**, in a first step the allyl groups of compound **2** were removed with $Pd(OAc)_2$ in the presence of the previously[28] to give (3,5-dihydroxy)benzyl alcohol, **3**[29], Scheme 1. and the spectral data of **4a** was compared with the literature.[28] The reaction of benzyl chloride derivatives **4a** and **4b**, prepared using procedures described in the literature[30,31,32], with the core **3** at reflux of acetonitrile in the presence of K_2CO_3 and catalytic amounts of 18-crown-6 ether[33] gave **5a** and **5b** as amber oils in 95% and 92% yield, respectively, see Scheme 2. Finally, the reaction of **3** with 3,5-(bisallyloxy)benzylchloride gave 3,5-bis(3,5-bis-allyloxy)benzyl alcohol which was reacted with $SOCl_2$ and Et_3N in CH_2Cl_2 to give **6**. Subsequent reaction of **6** with **3** under reflux of acetone in the presence of K_2CO_3 and catalytic amounts of Bu_4NF [33] gave **7** as amber oil in 53% yield (Scheme 3).

2. General procedure for peripheral functionalization with cobaltabisdicarbollides. To decorate the periphery of fluorescent cores and dendrimers **2**, **5a-b** and **7** with cobaltabisdicarbollide, hydrosilylation reactions of the allyl-terminated groups with Cs[1,1'-μ-SiMeH-3,3'-Co(1,2-$C_2B_9H_{10})_2$], **Cs(8)**,[8] in the presence of Karstedt catalyst in THF at 50 ºC were carried out. The reaction of three equivalents of **Cs(8)** with one equivalent of **2** afforded the cesium salt of the three-functionalized star-shape compound **Cs_3(10)**, in 54% yield (Scheme 4). When the reaction of **Cs(8)** with **5a** and **7** a 6:1 ratio **Cs(8)**/**5a** and 12:1 **Cs(8)**/**7** were used, under the same conditions, a complete hydrosilylation of dendrimers was observed to obtain **Cs_6(11)** and **Cs_{12}(12)**, respectively (Scheme 5). However, all attempts for full hydrosilylation of compound **5b**, which contains nine terminal allyl functions, were unsuccessful (Scheme 6). This was already observed in a previous work, when we tried the hydrosilylation of tetravinylsilane with **Cs(8)**, it was not possible the complete hydrosilylation of the four vynil groups. Most probably, the steric bulk of the cobaltabisdicarbollide causes the incomplete hydrosilylation and restricts the number of metallacarboranes that can be introduced at the periphery. Supplementary material contains a brief Montecarlo simulation study about the steric hindrance in these dendrimers. In all cases, the binding of the cobaltacarborane anion **8** to the allyl-terminated dendrimers was monitored by IR and ^{1}H NMR spectroscopy, following the disappearance of the Si-H signal in both spectra and the allyl protons in the ^{1}H NMR.

Characterization of star-shape and dendrimers before and after functionalization. The starting compounds **1-7** were characterized on the basis of FT-IR, ^{1}H, ^{13}C NMR, UV-Vis and mass spectrometry, whereas compounds **Cs_3(10)**, **Cs_6(11)** and **Cs_{12}(12)** were also characterized by ^{11}B and ^{29}Si NMR. All compounds show resonances between 7.80 and 7.00 ppm attributed to the aromatic protons at 2,4 and 6 positions of the central phenyl ring of the 1,3,5-triphenylbenzene core in the ^{1}H NMR spectra. Compounds **2**, **5a**, **5b** and **7** show resonances in the range δ 6.20 and 5.20 ppm attributed to the allyl protons, that have been assigned according to the area and coupling constants. These signals disappear after hydrosilylation reaction**,** indicating the addition of the cobaltacarboranes to the double bonds and formation of **10**, **11** and **12** with complete functionalization. In the

latter compounds, the presence of -CH_2- proton resonances around 4.00 ppm (-OCH_2-), 1.85 (-CH_2) and 1.00 ppm (-SiCH_2-) corroborates their formation. Broad resonances around 4.50 ppm corresponding to the C_c-H protons of the cobaltabisdicarbollide are also observed in functionalized dendrimers. The ^{1}H NMR spectra also exhibit resonances at low frequencies, around 0.30 ppm, for C_c-Si-CH_3 protons. The $^{13}C\{^1H\}$ NMR spectra show aromatic carbons in the range from +160.5 to + 100.5 ppm for all compounds. Different numbers of resonances attributed to the carbon atoms of the ether groups (O-CH_2-) are observed around 70 ppm for **10**, **11** and **12**. After functionalization with cobaltabisdicarbollide, dendrimers **10-12** show resonances around 55.25 and 40.50 ppm attributed to the C_c-*H* and C_c-Si atoms, respectively. The resonances for the Si-CH_3 units bonded to the C_c appear between -6.03 and -7.09 ppm. Finally, the -CH_2- carbons are displayed from 22.3 to 8.41 ppm.

The ^{11}B NMR spectra of anions **10-12** exhibit an identical 2:2:4:2:2:2:2:2 pattern in the range from +8.40 to -22.30 ppm, typical of cobaltabisdicarbollide derivatives.[34] Due to the similarity of these $^{11}B\{^1H\}$ NMR spectra with that of Cs[1,1'-μ-$SiMe_2$-3,3'-Co(1,2-$C_2B_9H_{10})_2$],[8] **Cs(9)**, it has been possible to assign each specific resonance to the corresponding boron atom. Figure 1 shows the $^{11}B\{^1H\}$NMR spectra of anion **10**. The boron resonance with a relative intensity of 4 is due to a coincidental overlap of two resonances with a 2:2 relative intensity. All the three cobaltabisdicarbollide-functionalized compounds **10**, **11** and **12** show only one peak just about 12.0 ppm in the ^{29}Si NMR spectra, corresponding to the Si-$C_{cluster}$ and shifted around 8.5 ppm to downfield respect to the starting compound **8** (δ_{Si} = 2.94 ppm).[8] Different mass spectrometry techniques have been used for the characterization of compounds: High Resolution mass spectrommetry (HMRS), ESI-MS and MALDI-TOF-MS. The formula of the star-shape compound **10** was well established by using ESI-MS mass spectrometry, in which the molecular ion peak appears at *m/z* = 1837.1 (M-Cs), in concordance with the calculated pattern (Figure 1.) The MALDI-TOF mass spectra of dendrimers **11** and **12** were recorded in the ion mode without matrix, where a big fragmentation was observed. The IR spectra present typical υ(B-H) strong bands for *closo* clusters around 2550 cm^{-1}, and intense bands near 1257 cm^{-1} corresponding to the δ(Si-CH_3).

Absortion and Emission Measurements. The UV/vis absorption measurements for compounds **2**, **5a-b**, **7**, **10**, **11** and **12** were performed in acetonitrile. Table 2 lists the spectroscopic and photophysical properties measured for these compounds. Starting dendrimers **2, 5a-b** and **7** display a significant solvatochromic shift and exhibit bands of absorption maxima in the region 269-272 nm, that correspond to the π to π* transitions in the aromatic core similar to the maximum at 254 nm previously observed for 1,3,5-triphenylsubstituted benzene compounds.[1c] (Figure 2). Metallacarborane-functionalized dendrimers show two maxima absorption bands, one is in the region 271-276 nm due to the core, and the second band between 307-310 nm, which corresponds to the [1,1'-μ-$CH_2Si(CH_3)$1,2-$Co(C_2B_9H_{11})_2]^-$ fragment (Figure 3).

For dendrimers **10-12** it can be appreciated a direct correlation between the number of cobaltabisdicarbollide moieties located at the periphery and the molar absorptivity (ε_{max}). This method was previously used by us to measure the number of cobaltacarboranes in the dendrimer, and consists on the measurement of the UV absorption of a solution containing the functionalized dendrimers and study the trend of the molar absorptivity. Figure 4 shows the molar absorptivities (ε) measured at λ = 309 nm in acetonitrile versus the number of metallacarboranes (n) attached to the different dendrimers, **10-12**, which contain three, six and twelve cobaltabisdicarbollide moieties, respectively. In addition the molar absorptivity for the reference compound [1,1'-μ-$Si(CH_3)_2$-1,2-$Co(C_2B_9H_{11})_2]^-$, (point 1, 12687 in the graph) is also exhibited.[8] It can be appreciate that ε increases with functionalization degree of the dendrimes surface.

It is worth noting that compounds **2**, **5a-b** and **7** exhibit blue emission with λ_{max} around 364 nm after excitation at 270 nm in acetonitrile. Nevertheless, dendrimers **10**, **11** and **12** do not show appreciable fluorescence emission. Tabla 1 collects the data and Figure 5 shows the PL normalized spectra for compounds **2**, **5a**, **5b** and **7**.

The lifetime of **2**, **5a**, **5b**, and **7** was measured giving values around 9.4 ns and their decay is described by a single exponential. The fluorescence quantum yield, Φ, is defined as the ratio of the total number of photons emitted within the total number of absorbed photons. The four samples have a quantum yield around 20 %. However emission of **10**, **11**, **12** is almost negligible indicative of quenching of the core dendrimer emission by the cobaltabisdicarbollide moiety. As a control experiment, the fluorescence of a mixture of compound **2** and 3 eq. of [1,1'-μ-$Si(CH_3)_2$-$(C_2B_9H_{11})_2]^-$ was measured and the result is that quantum yield of this mixture is Φ = 14 %. This fact indicates that the quenching by the cobaltabisdicarbollide moiety is more effective when it is chemically bonded to the fluorescent core. Furthermore, this fact confirms that the intermolecular effects are not significant, and then two possible mechanisms, exchange and dipole–dipole, can be invoked to account for the aromatic core dendrimer to cobaltabisdicarbollide energy transfer. Electron exchange can be discarded because saturated units connecting the respective parts behave like insulators towards electronic communication because the HOMO–LUMO energy separation is large. On this basis, we propose that the occurrence of energy transfer is due possibly to the dipole–dipole mechanism.

The starting dendrimers exhibit photoluminescence properties at room temperature under ultraviolet

irradiation, due to the core molecule, however, after functionalization with C-substituted cobaltabisdicarbollide, the fluorescence properties are quenched. By using steady-state and time-resolved luminescence measurements, we show that for these metallodendrimers, a mechanism different to photon emission could be available to go from excited singlet state to the ground electronic state, due mainly to peripheral functionalization.

Simulation of UV-Vis and Fluorescence spectra. Excited states of **2** were calculated using a semiempirical method PM6 implemented in MOPAC[35] to simulate their absorption spectra with the effect of a solvent model (COSMO) surrounding the molecule.[36] If the excited state has a sufficiently long lifetime then the system returns to the ground state by emission of a photon, the energy of the emitted photon will be less than that of the exciting photon. In order for fluorescence to occur, the photoemission probability must be quite large, so only transitions of the same spin are allowed. For example, in this case the ground state is S_0, then the fluorescing state would be S_1. The PM6 semiempirical method permits geometry optimization of the excited states, therefore the ground-state S_0 and the first singlet excited-state S_1 have been optimized thus enabling a direct comparison of calculated results with experimental data for the fluorescence spectrum of this molecule. The computed absorption and fluorescence wavelength in acetonitrile for **2** is represented in Figure 6.

The calculated wavelengths and general trends are in very good agreement with experiment, with a theoretical error on the Stokes shift around 16 %. The computed fluorescence wavelength (355 nm) is in very good agreement with the measurement (363 nm). Furthermore, the calculated relative energy difference between S_1 y S_0 is 4.29 eV and the calculated Stokes shift is 1.34 eV that would represent about 30% of quantum yield. If we use the experimental Stokes shifts this percentage of quantum yield reaches 26 % which is very close to the experimental value of 20 %. In summary, the experimental and calculated results present a high degree of accuracy. However, the semiempirical optimization for compounds like cobaltabisdicarbollide is not available and then a deep insight in the quenching mechanism of the fluorescence cannot be envisaged. Probably, when this moieties are attached to the dendrimer surface, the Jablowsky diagram changes from an emissive system A to another non emissive system B. (Figure 7).

Experimental Section

Instrumentation

The melting point of **2** was recorded on an Electrothermal 9200 apparatus and is uncorrected. Microanalyses were performed in the analytical laboratory using a Carlo Erba EA1108 microanalyser. IR spectra were recorded with KBr pellets or NaCl on a Shimadzu FTIR-8300 spectrophotometer. UV/visible spectroscopy was carried out with a Shimadzu UV-Vis 1700 spectrophotometer, at 23 ºC temperature, using 1 cm quartz cuvettes. Fluorescence spectra were measured on Cary Eclipse fluorescence spectrophotometer. The Electrospray-Ionization mass spectra (ESI-MS) were recorded on a Bruker Esquire 3000 spectrometer using a source of ionization and a ions trap analyzer. MALDI-TOF-MS mass spectra were recorded in the negative ion mode using a Bruker Biflex MALDI-TOF [N_2 laser; λ_{exc} 337 nm (0.5 ns pulses); voltage ion source 20.00 kV (Uis1) and 17.50 kV (Uis2)]. Mass spectra were recorded on a Hewlett–Packard 5989A spectrometer using Electron Ionization HRMS (High Resolution Mass Spectroscopy) spectra were obtained on an Agilent Technologies G1969A, and APCI(atmospheric pressure chemical ionization)-ionization time-of-flight spectrometer, coupled to a HPLC model 1100. The ^{1}H, $^{1}H\{^{11}B\}$ NMR (300.13 MHz), ^{11}B, $^{11}B\{^{1}H\}$ NMR (96.29 MHz), $^{13}C\{^{1}H\}$ NMR (75.47 MHz) and $^{29}Si\{^{1}H\}$ NMR (59.62 MHz) spectra were recorded on a Bruker ARX 300 spectrometer equipped with the appropriate decoupling accessories at room temperature in deuterated chloroform or acetone-d_6 solutions. Chemical shift values for ^{11}B NMR and $^{11}B\{^{1}H\}$ spectra were referenced to external $BF_3{\cdot}OEt_2$, and those for ^{1}H, $^{1}H\{^{11}B\}$, $^{13}C\{^{1}H\}$NMR and $^{29}Si\{^{1}H\}$ NMR spectra were referenced to $SiMe_4$. Chemical shifts are reported in units of parts per million downfield from reference, and all coupling constants are reported in Hertz.

Materials. All manipulations were carried out under a dinitrogen atmosphere using standard Schlenck techniques. Solvents were reagent grade and were purified by distillation from appropriate drying agents before use. 3,5-dihydroxybenzyl alcohol, 4-hydroxyacetophenone, palladium (II) acetate and tetrabutylammoniun fluoride hydrate were purchased from Aldrich except the Karstedt's catalyst (platinum divinyltetramethyldisiloxane complex, 2.1-2.4% platinum in vinyl terminated polydimethylsiloxane) from ABCR and used as received. Compounds **1**,[27a] **3**,**¡Error! Marcador no definido.** **4a**,[28] **6**,[37] **Cs(8)** and **Cs(9)**[8] were prepared according to the literature procedures.

1,3,5-tris(4-allyloxy-phenyl)benzene, 2.

Compound **2** was prepared from of **1** (4.80 g, 27.27 mmol) and tetrachlorosilane (12.5 ml, 109.08 mmol) in absolute ethanol at room temperature for 24 h. The precipitate was filtered and washed with methanol to give **2** a**s** a white powder, m. p. 83-85 ^{0}C, Yield: 80 % (3.44 g, 7.26 mmol). ^{1}H NMR (300 MHz; $CDCl_3$), δ (ppm): 7.68 (3H, s, H-1), 7.64 (6H, d, J^3(H,H) = 8.7, H-4), 7.04 (6H, d, J^3(H,H) = 8.7, H-5), 6.11 (3H, ddt, J_{trans} = 17.2, J_{cis} = 10.4, $J^3_{allylic}$ = 5.3 H-8), 5.48 (3H, dd, J_{trans} = 17.2, J^2(H,H)= 1.3, H-9a), 5.34 (3H, dd, J_{cis} = 10.4, J^2(H,H) = 1.3, H-9b), 4.62 (6H, d, $J_{allylic}$ = 5.3, H-7); ^{13}C NMR (75.46 MHz; $CDCl_3$), δ (ppm); 158.5 (C-6), 142.0 (C-2), 134.2 (C-3), 133.4 (C-8), 128.5 (C-4), 124.1 (C-1), 118.0 (C-9), 115.2 (C-5), 69.1 (C-7); MS [m/z], 475 ($[M+H]^+$, 35), 474 (M^+, 100), 434 (27), 433

(81), 292 (42), 351 (21). IR (cm^{-1}) 3130, 1642, 1608, 1511, 1400, 1325, 1234, 1180, 996, 833, 777. HRMS $C_{13}H_{31}O_3$ $[M+H]^+$, calculated 475.2268, found 475.2266, with an error of 0.361 ppm.

(3,4,5-trisallyloxy)benzyl chloride, 4b.
To a solution of 3,4,5-trisallyloxy(benzyloxy)benzene (0.91 g, 3.29 mmol) in dry CH_2Cl_2 were added 5 ml (3.62 mmol) of Et_3N under nitrogen atmosphere. The solution was cooled to 0^o C and $SOCl_2$ (0.262 mmol) was added slowly. The reaction mixture was stirred for 24h at RT, after water was added, and the organic phase extracted with CH_2Cl_2, dried and evaporated under vacuum to give **4b** as an amber oil. Yield: 95% (0.92 g). ^{1}H NMR (270 MHz; $CDCl_3$), 6.60 (2H, s, *H*-3), 6.18-5.98 (3H, m, H-7,H-7'), 5.44 (2H, dd, J_{trans} = 17.2, J_{gem}=1.5 Hz, H-8), 5.35 (1H, dd, J_{trans} = 17.2, J_{gem}=1.5 Hz, H-8'), 5.27 (2H, dd J_{cis} = 10.4, J=1.5 Hz, H-8), 5.19 (IH, d, Jcis= 10.4, J=1.5 Hz, H-8'),)4.55 (6H, d, J=5.4 H-6), 4.47 (2H, s, H-1); ^{13}C NMR (75.46 MHz; $CDCl_3$-d_6), δ (ppm); 152.8 (C-4), 138.1 (C-5), 134.6 (C-7'), 133.3 (C-7), 132.7 (C-2), 117.4 (8'), 117.2 (8), 107.6 (C-3), 73.9 (C-6'), 69.6 (C-6), 46.6 (C-1); IR (NaCl, cm^{-1}) 3080, 1825, 2868, 1590, 1502, 1440, 1422, 1332, 1234, 1128, 1111, 989, 926, 708. MS [m/z], 296 (M^++2, 8), 294 (M^+, 22), 255 (16), 253 (46), 81 (29), 41 (100). HRMS $C_{16}H_{20}O_3Cl$ 295.1095 error 0.1055 ppm

Synthesis of 5a.
Compound **5a** was synthesized from of 1,3,5 tris-(4-hydroxyphenyl)benzene (**3**) (0.625 g, 1.76 mmol) and 3,5-(bisallyloxy)benzyl chloride **(4a)** (1.50 g, 5.30 mmol) under reflux of acetone for 48 h in the presence of K_2CO_3 and catalytic amounts of 18-crown-6 ether. The solid residue was removed by filtration, the solvent evaporated under vacuum to give **5a** as an amber The crude oil product was percolated on silica get eluting with hexane/EtOAc (8:2). Yield: 95% (1.61g, 1.67 mmol). ^{1}H NMR (300 MHz; $CDCl_3$), δ (ppm): 7.67 (3H, s, H-2), 7.61 (6H, d, Jo = 8.8, H-4), 7.08 (6H, d, Jo = 8.8, H-5), 6.68 (6H, d, Jm = 2.2, H-9), 6.48 (3H, t, Jm = 2.2, H-11), 6.14-6.00 (6H, m, H-13), 5.46 (6H, dd, J_{trans} = 17.3, J = 1.5, H-14a) 5.31 (6H, dd, Jcis = 10.5, J =1. 5 Hz, H-14b), 5.08 (6H, s, H7) 4.56 (12H, dt J(HH) = 5.3, J(HH) = 1.4, H-12), 5.07 (6H, s H-7); ^{13}C NMR (75.46 MHz; $CDCl_3$-d_6), δ (ppm); 160.2 (C-10), 158.6 (C-6), 142.0 (C-2), 139.5 (C-8), 134.3 (C-3), 133.3 (C-13), 128.6 (C-4), 124.1 (C-1), 118.0 (C-14), 115.4 (C-5), 106.3 (C-9), 101.5 (C-11), 70.2 (C-7), 69.1 (C-12). IR (NaCl, cm^{-1}) 3128, 2924, 1643, 1601, 1510, 1400, 1324, 1168, 1016, 828. HRMS $C_{63}H_{61}O_9$ $[M+H]^+$, calculated 961.4310, found 961.4331, with an error of 2.173 ppm.

Synthesis of 5b.
The procedure was the same as for **5a** using 1,3,5 tris(4-hidroxyphenyl)benzene (**3**) (0.70 g, 1.97 mmol) and of 3,4,5-trisallyloxy)benzyl chloride (**4b**) (1.90 g, 5.58 mmol) to give an amber oil. 90 % yield, (2.05 g, 1.81 mmol); ^{1}H NMR (400 MHz; $CDCl_3$), δ (ppm): 7.67 (3H, s, H-2), 7.63 (6H, d, Jo = 8.6, H-4), 7.07 (6H, d, J_O = 8.6, H-5), 6.69 (6H, s, H-9), 6.12 - 6.04 (9H, m, H-13, H-13'), 5.43 (6H, dd, J_{trans}=17.2, J=3.3 m, H-14a), 5.33 (3H, dd, J_{trans}=17.2, J=3.3 m, H-14a'), 5.28 (6H, d, J_{ciss}=12.0,, H-14b), 5.21 (3H, d, cis_s=12, H-14b'), 4.64–4.59 (18H, m, H-12, H-12'), 4.99 (6H, s, H-7); ^{13}C NMR (75.46 MHz; $CDCl_3$), δ (ppm); 158.9 (C-6), 153.2 (C-10), 142.2 (C-2), 137.9 (C-11), 135.1 (C-3), 134.5 (C-13'), 133.8 (C-13), 132.7 (C-8), 128.8 (C-4), 124.3 (C-1), 118.0 (C-14'), 117.9 (C-14), 115.7 (C-5), 107.2 (C-9), 74.6 (C-12'), 70.7 (C-7), 70.4 (C-12); IR (NaCl, cm^{-1}) 3126, 2926, 2838, 1643, 1594, 1509, 1439, 1329, 1232, 1112, 992, 926, 828.

Synthesis of 7
Compound **7** was synthesized from **3** (0.78 g, 0.28 mmol) and **3,5- bis[(3,5-bisallyloxy-benzyloxy)benzyl chloride** (**6a**) (0.50 g, 0.88 mmol) under reflux of acetone for 56 hours in the presence of K_2CO_3 and catalytic amounts of Bu_4NF hydrate. The solid residue was removed by filtration, the organic phase was washed with H_2O, dried with Na_2SO_4 and evaporated under vacuum to give **7.** The crude product was percolated over silica get eluting with hexane/EtOAc (7:3) and washed with pentane to give an amber oil in 53 % yield (0.350 g, 1.67 mmol). ^{1}H NMR (400 MHz; $CDCl_3$), δ (ppm): 7.68 (3H, s, H-1), 7.63 (6H, d, Jo = 8.9, H-4), 7.07 (6H, d, J_O = 8.9, H-5), 6.72 (6H, d, J=1.8 H-9), 6.62 (12H, d, J=1.8, H-14) 6.58 (3H, t, J=1.5 Hz H-11), 6.48 (6H, t, J=1.5, H-16), 6.10-6.00 (12H, m, H-18), 5.42 (12H, dd, J_{trans}=17.4, J=1.5, H-19), 5.27 (12H, dd, $Jcis_s$=11.9, J=1.5, H-19), 5.06 (6H, s, H-7), 4.99 (12H, s, H-12), 4.53 (32H, d, J=5.4 Hz, H-17): ^{13}C NMR (75.46 MHz; $CDCl_3$), δ (ppm); 160.2 (C-10), 160.0 (C-15), 158.5 (C-6), 141.8 (C-2), 139.5 (C-8), 139.3 (C-13), 134.2 (C-3), 133.2 (C-18), 128.4 (C-4), 123.9 (C-1), 117.8 (C-19), 115.3 (C-5), 106.5 (C-9), 106.3 (C-14), 101.8 (C-11), 101.5 (C-16), 70.1 (C-12, 7), 69.0 (C-17); IR (NaCl, cm^{-1}) 3135, 1642, 1597, 1400, 1324, 1167, 1052, 830.

Synthesis of Cs_3[10].
In a Schlenk flask, **2** (63.1 mg, 0.133 mmol), 10 µL of Karstedt catalyst and 2 mL of THF were stirred for 10 min at room temperature. To the solution Cs[1,1'-µ-$Si(CH_3)$H-3,3'-Co(1,2-$C_2B_9H_{10})_2$], **Cs[8]** (200.0 mg, 0.401 mmol) were added and the mixture was stirred overnight at 50 ºC. After, 10 ml of Et_2O were added to produce two phases. The Et_2O phase was discarded by decantation. To the other oily dark orange phase, 10 ml of hexane were added to give **Cs_3[10]** as un orange solid. Yield:, 54 % (142.1 mg). ^{1}H NMR (300 MHz, Acetone-d_6) δ(ppm): 7.77 (m, 9H, C_{aryl}), 7.06 (d, 6H, ^{3}J(HH) = 8.5, H- C_6H_5), 4.56 (brs, 6H, C_c-*H*), 4.07 (t, 6H, ^{3}J(HH) = 6.4, -O-CH_2-CH_2-), 1.92 (m, 6H, -CH_2-CH_2-CH_2), 1.07 (m, 6H, -CH_2-CH_2-Si), 0.38 (s, 9H, Si-CH_3). ^{1}H{^{11}B}-RMN (300 MHz, Acetone-d_6) δ(ppm): 7.77 (m, 9H, H_{aryl}), 7.06 (d, 6H, ^{3}J(HH) = 8.5, H_{aryl}),

4.56 (brs, 6H, C_c-*H*), 4.07 (t, 6H, ^{3}J(HH) = 6.4, -O-C*H*$_2$-CH$_2$-), 3.43 (brs, 2H, B-*H*), 3.30 (brs, 2H, B-*H*), 3.10 (brs, 2H, B-*H*), 2.38 (brs, 2*H*, B-H), 2.22 (brs, 2H, B-*H*), 1.94 (brs, 2H, B-*H*), 1.92 (m, 6H, -CH$_2$-C*H*$_2$-CH$_2$), 1.69 (brs, 6H, B-*H*), 1.07 (m, 6H, -CH$_2$-C*H*$_2$-Si), 0.38 (s, 9H, Si-C*H*$_3$). ^{11}B-RMN (96 MHz, Acetone-d$_6$) δ(ppm): 8.26 (d, 2B, ^{1}J(B,H) = 118), 2.84 (d, 2B, ^{1}J(B,H) = 136), -1.68 (d, 4B, ^{1}J(B,H) = 140), -3.47 (2B), -4.68 (d, 2B, ^{1}J(B,H) = 130), -14.34 (d, 2B, ^{1}J(B,H) = 180), -16.62 (d, 2B, ^{1}J(B,H) = 148), -22.10 (d, 2B, ^{1}J(B,H)=147). ^{13}C{^{1}H}-RMN (75 MHz, Acetone-d$_6$) δ(ppm): 157.2-114.6 (*C$_{aryl}$*), 69.50 (O-*C*H$_2$), 55.31 (*C$_c$*-H), 41.29 (*C$_c$*-Si), 22.3 (-*C*H$_2$-), 12.01 (Si-*C*H$_2$), -6.03 (Si-*C*H$_3$). ^{29}Si-RMN (59.6 MHz, Acetone-d$_6$) δ(ppm): 11.96. IR (KBr) υ (cm-1): 3059 (pI, υ(C$_c$-H), 3030 (pI, υ(C-H)$_{aryl}$), 2874 (pI, υ(C-H)$_{alkyl}$), 2546 (mI, υ(B-H)), 1257 (I, δ(Si-CH$_3$)), 1234 (I, υas(C$_{aryl}$-O-C)), 1041 (I, υs(C$_{aryl}$-O-C)), 829 (I, γ(Si-CH$_3$)). ESI-MS: (*m/z*) exp. 1837.1 (M-Cs), calc. 1837.8

Synthesis of Cs$_6$[11].
In a Schlenk flask, **5a** (68.0 mg, 0.071 mmol), 10 µL of Karstedt catalyst and 2 mL of THF were stirred for 10 min at room temperature. To the solution Cs[1,1'-µ-Si(CH$_3$)H-3,3'-Co(1,2-C$_2$B$_9$H$_{10}$)$_2$], **Cs[8]**, (211.7 mg, 0.424 mmol) were added and the mixture was stirred overnight at 50 ºC. After, 10 ml of Et$_2$O were added to produce two phases. The Et$_2$O was discarded by decantation. To the other oily dark orange phase, 10 ml of hexane were added to give **Cs$_6$[11]** as un orange solid. Yield: 63% (176.2 mg). ^{1}H NMR (300 MHz, Acetone-d$_6$) δ(ppm): 7.77 (m, 9H, *H$_{aryl}$*), 7.15 (d, 6H, ^{3}J(HH) =12.0, C$_6$H$_5$), 6.69 (s, 6H, C$_6$*H*$_5$), 6.50 (s, 3H, C$_6$*H*$_5$), 5.12 (s, 6H, O-C*H*$_2$-Ph), 4.56 (brs, 12H, C$_c$-*H*), 4.00 (t, 12H, ^{3}J(HH) = 6.4, -O-C*H*$_2$-CH$_2$-), 1.87 (m, 12H, -CH$_2$-C*H*$_2$-CH$_2$), 1.04 (m, 12H, -CH$_2$-C*H*$_2$-Si), 0.37 (s, 18H, Si-CH$_3$). ^{1}H{^{11}B}-RMN (300 MHz, Acetone-d$_6$) δ(ppm): 7.77 (m, 9H, H$_{aryl}$), 7.15 (d, 6H, ^{3}J(HH) = 12.0, C$_6$H$_5$), 6.69 (s, 6H, C$_6$*H*$_5$), 6.50 (s, 3H, C$_6$*H*$_5$), 5.12 (s, 6H, O-C*H*$_2$-Ph), 4.56 (brs, 12H, C$_c$-*H*), 4.00 (t, 12H, ^{3}J(HH) = 6.4, -O-C*H*$_2$-CH$_2$-), 3.40 (brs, 12H, B-*H*), 3.29 (brs, 12H, B-*H*), 3.09 (brs, 12H, B-*H*), 2.38 (brs, 12H, B-*H*), 2.20 (brs, 12H, B-*H*), 1.88 (brs, 12H, B-*H*), 1.87 (m, 12H, -CH$_2$-C*H*$_2$-CH$_2$), 1.66 (brs, 72H, B-*H*), 1.04 (m, 12H, -CH$_2$-C*H*$_2$-Si), 0.37 (s, 18H, Si-CH$_3$). ^{11}B-RMN (96 MHz, Acetone-d$_6$) δ(ppm): 8.35 (d, 2B, ^{1}J(B,H) = 120), 2.86 (d, 2B, ^{1}J(B,H) = 135), -1.72 (d, 4B, ^{1}J(B,H) = 146), -3.50 (2B), -4.76 (d, 2B, ^{1}J(B,H) = 130), -14.59 (d, 2B, ^{1}J(B,H) = 189), -16.79 (d, 2B, ^{1}J(B,H) = 140), -22.30 (d, 2B, ^{1}J(B,H) = 166). ^{13}C{^{1}H}-RMN (75 MHz, Acetone-d$_6$) δ(ppm): 160.4-100.3(*C$_{aryl}$*), 69.70 (O-*C*H$_2$), 55.21 (*C$_c$*-H), 40.7 (*C$_c$*-Si), 22.3 (-*C*H$_2$-), 8.03 (Si-*C*H$_2$), -7.09 (Si-*C*H$_3$). ^{29}Si-RMN (59.6 MHz, Acetone-d$_6$) δ(ppm): 12.04. IR (KBr) υ (cm-1): 3061 (pI, υ(C$_c$-H), 2976 (pI, υ(C-H)$_{aryl}$), 2874 (pI, υ(C-H)$_{alkyl}$), 2554 (mI, υ(B-H)), 1257 (I, δ(Si-CH$_3$)), 1233 (I, υas(C$_{aryl}$-O-C)), 1053 (I, υs(C$_{aryl}$-O-C)), 828 (I, γ(Si-CH$_3$)). MALDI-TOF-MS: (m/z) 530.5 ((M+H$_2$O)/6, 37 %), 1051.6 (M/2, 3 %).

Synthesis of Cs$_{12}$[12].
In a Schlenk flask, (41.2 mg, 0.021 mmol) of **7**, 10 µL of Karstedt catalyst and 2 mL of THF were stirred for 10 min at room temperature. To the solution Cs[1,1'-µ-Si(CH$_3$)H-3,3'-Co(1,2-C$_2$B$_9$H$_{10}$)$_2$], **Cs[8]**, (127.5 mg, 0.255 mmol) were added and the mixture was stirred overnight at 50 ºC. After, 10 ml of Et$_2$O were added to produce two solvent phases. The Et$_2$O was discarded by decantation. To the other oily dark orange phase, 10 ml of hexane was added to give **Cs$_{12}$[12]** as un orange solid. Yield: 86.0 mg, 51 %. ^{1}H NMR (300 MHz, Acetone-d$_6$) δ(ppm): 7.77 (m, 6H, *H$_{aryl}$*), 7.12 (m, 6H, *H$_{aryl}$*), 6.78 (s, 6H, C$_6$*H*$_5$), 6.69 (s, 12H, C$_6$*H*$_5$), 6.54 (s, 6H, C$_6$*H*$_5$), 6.45 (s, 6H, C$_6$*H*$_5$), 6.37 (s, 3H, C$_6$*H*$_5$), 5.11 (s, 6H, O-C*H*$_2$-Ph), 5.06 (s, 12H, O-C*H*$_2$-Ph), 4.50 (brs, 24H, C$_c$-*H*), 3.99 (s, 24H, -O-C*H*$_2$-CH$_2$-), 1.85 (m, 24H, -CH$_2$-C*H*$_2$-CH$_2$), 1.01 (m, 24H, -CH$_2$-C*H*$_2$-Si), 0.32 (s, 36H, Si-CH$_3$). ^{11}B-RMN (96 MHz, Acetone-d$_6$) δ(ppm): 8.40 (d, 2B, ^{1}J(B,H) = 121), 3.03 (d, 2B, ^{1}J(B,H) = 130), -1.59 (d, 4B, ^{1}J(B,H) = 140), -3.38 (2B), -4.54 (d, 2B, ^{1}J(B,H) = 120), -14.22 (d, 2B, ^{1}J(B,H) = 170), -16.46 (d, 2B, ^{1}J(B,H) = 141), -21.90 (d, 2B, ^{1}J(B,H) = 160). ^{13}C{^{1}H}-RMN (75 MHz, Acetone-d$_6$) δ(ppm): 160.6-106.3(*C$_{aryl}$*), 78.36 (O-*C*H$_2$), 69.60 (O-*C*H$_2$), 65.11 (O-*C*H$_2$), 55.24 (*C$_c$*-H), 40.6 (*C$_c$*-Si), 22.3 (-*C*H$_2$-), 14.9, 8.41(Si-*C*H$_2$), 3.70, -1.01, -7.04 (Si-*C*H$_3$). ^{29}Si-RMN (59.6 MHz, Acetone-d$_6$) δ(ppm): 12.40. IR (KBr) υ (cm-1): 3056 (pI, υ(C$_c$-H), 2963 (pI, υ(C-H)$_{aryl}$), 2872 (pI, υ(C-H)$_{alkyl}$), 2535 (mI, υ(B-H)), 1258 (I, δ(Si-CH$_3$)), 1226 (I, υas(C$_{aryl}$-O-C)), 1040 (I, υs(C$_{aryl}$-O-C)), 834 (I, γ(Si-CH$_3$)). MALDI-TOF-MS: (m/z) 530.4 ((M/12 +H$_2$O, 19 %), 1273.3 (M/5 + 3 H$_2$O, 2 %).

UV-Vis and Fluorescence Measurements
UV-Vis, stationary state fluorescent spectra and fluorescent lifetime measurements have been done at room temperature using the following procedure: stock solutions of compounds were obtained by preparing solutions of several milligrams, in the range of 1-10 mg, of the compounds **2**, **5a-b**, **7**, and **10-12** and the quantum yield reference tryptophan[38] in acetonitrile. From stock solutions, three differents concentrantions ranging between $1.92\cdot10^{-5}$ and $1.95\cdot10^{-7}$ M for each compound are prepared. Fluorescent measurements are developed in two situations, with degassed solutions with N_2 and with ambient oxygen atempered and no significance difference in wave number has been noted.

Computational Methods
All calculations have been carried out with PM6 implemented in MOPAC.[35] The bulk solvent effects on the geometries are evaluated by means of the Conductor-like Screening Model (COSMO) continuum approach using as EPS 37.5 for acetonitrile.[36]

Acknowledgements: This work has been supported by the CICYT (MAT2006-05339), the Generalitat de Catalunya, 2005/SGR/00709 and CONACYT-México. E.J.J.P. thanks to Ministerio de Educación y Ciencia for a FPU grant .

Scheme 1.

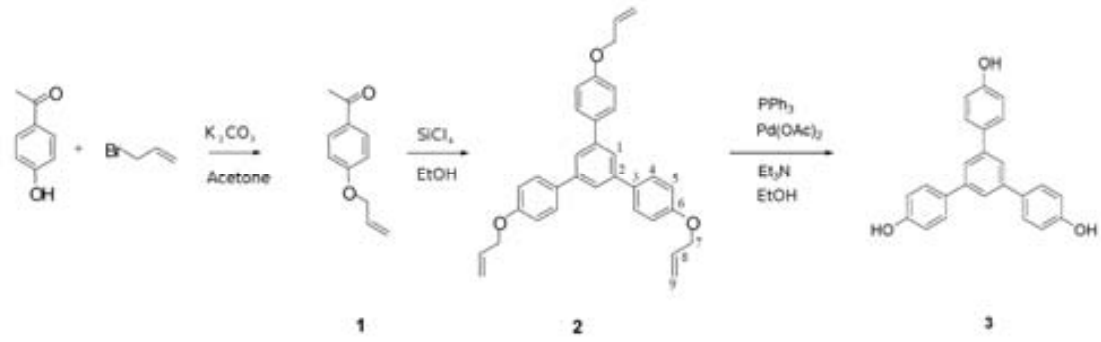

Scheme 2.

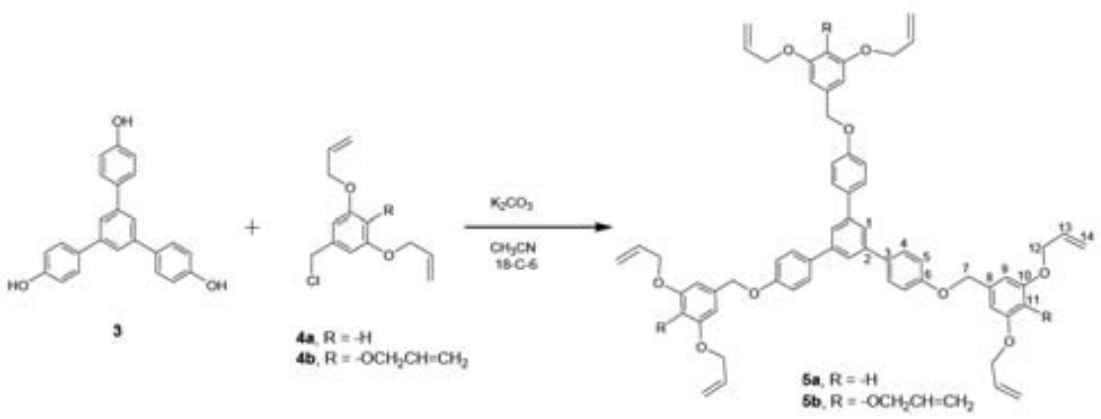

Scheme 3.

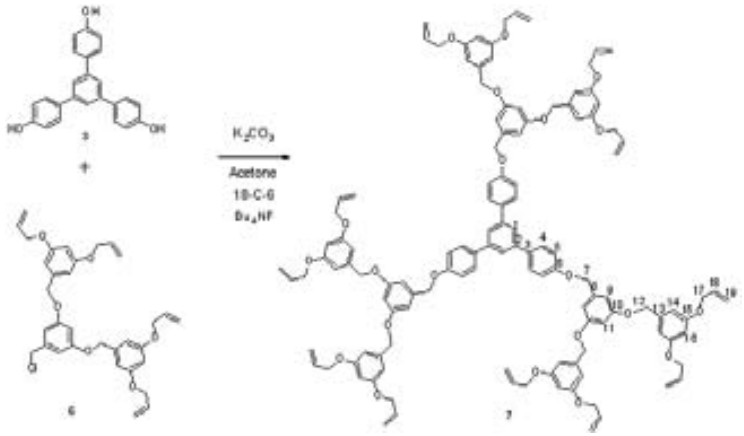

Scheme 4.

Scheme 5.

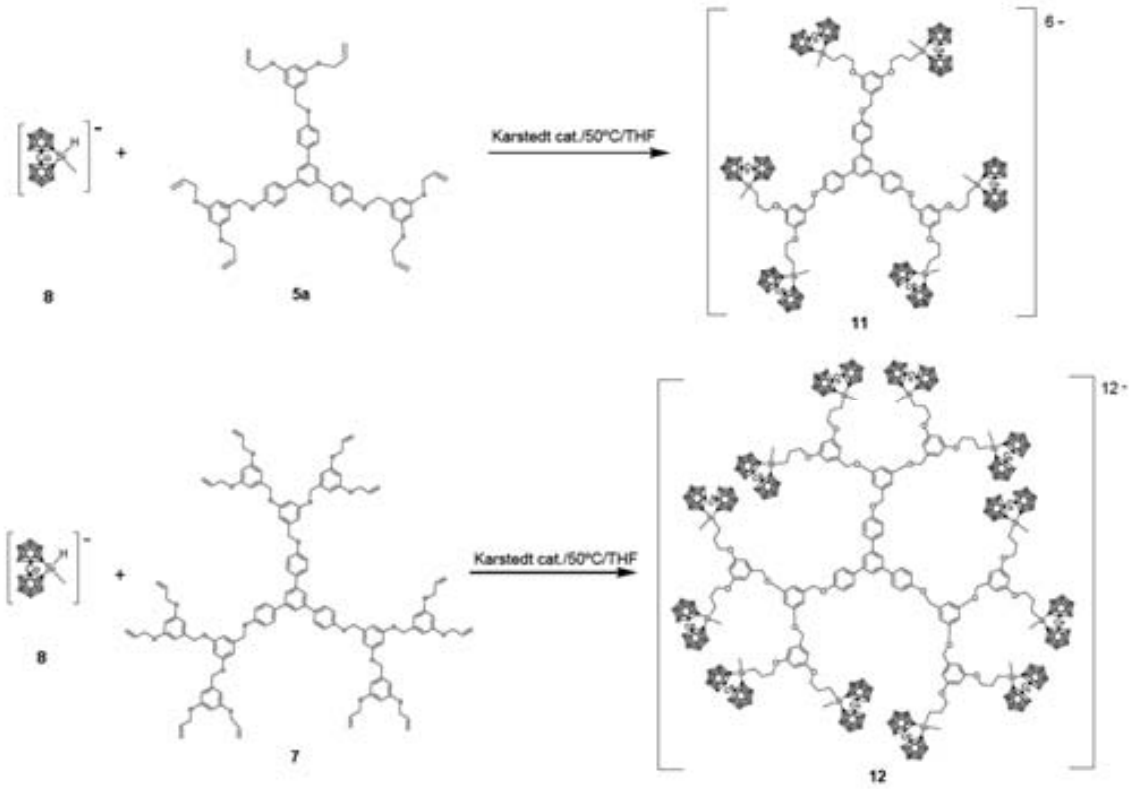

Scheme 6.

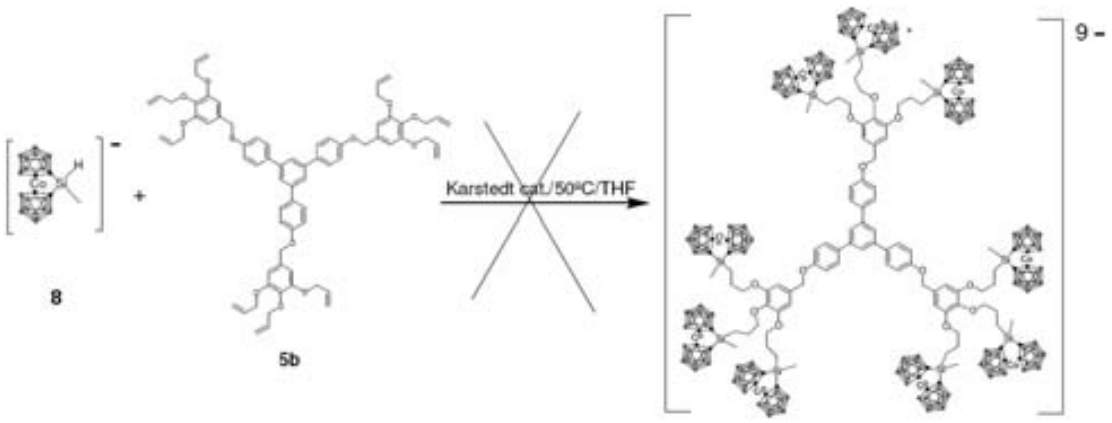

Figure 1.

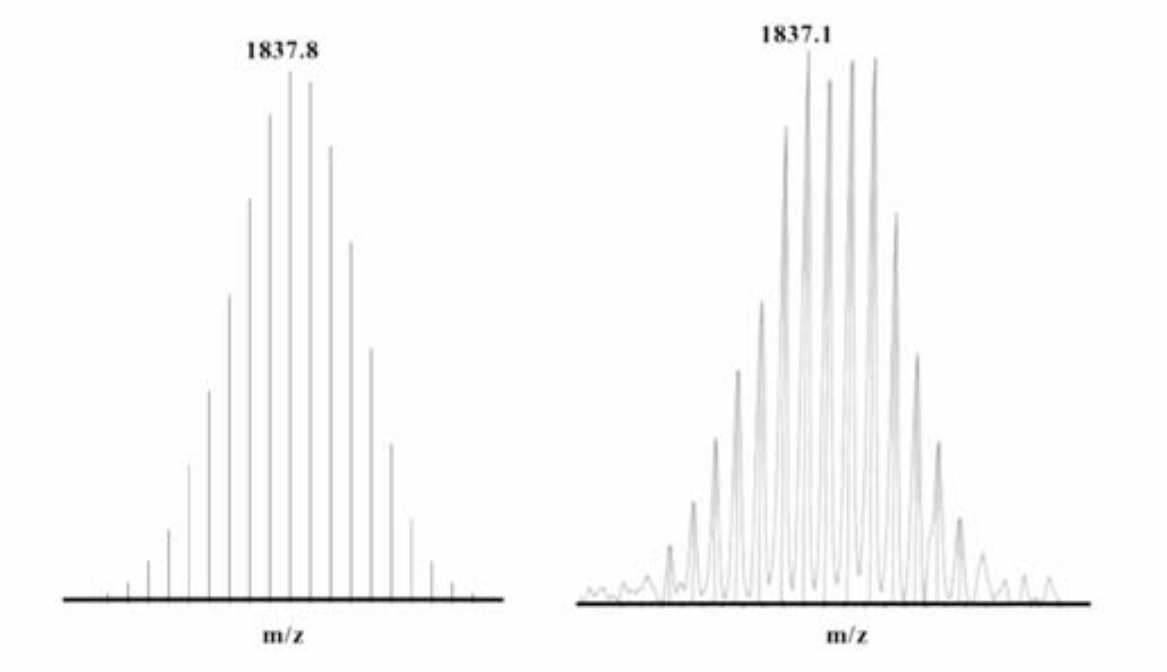

Figure 2. UV-Vis spectra for starting dendrimers **2**, **5a-b** and **7**.

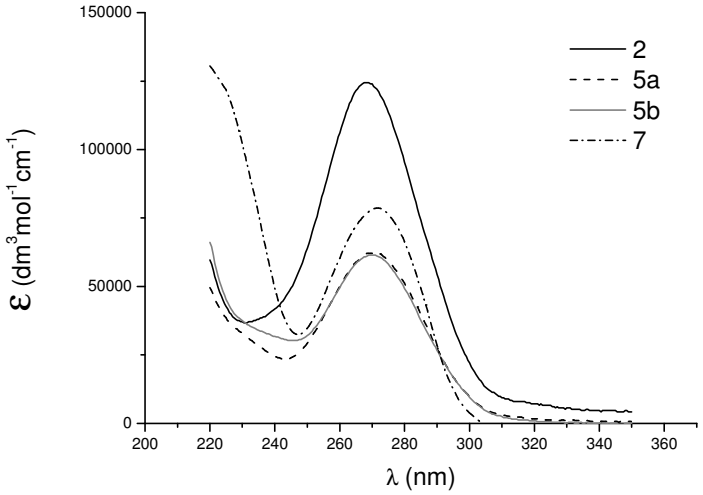

Figure 3. UV-Vis spectra for metallacarborane-containing poly(aryl-ether) dendrimers.

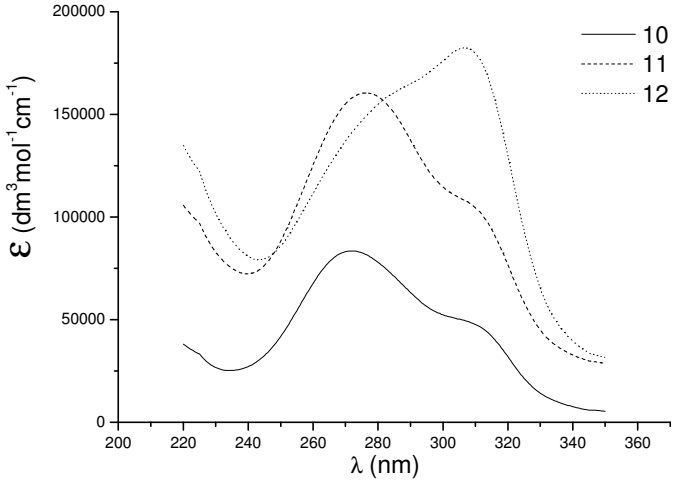

Figure 4. Linear correlation between the number of cobaltabisdicarbollides attached to the periphery and the absorptivity at λ = 309 nm.

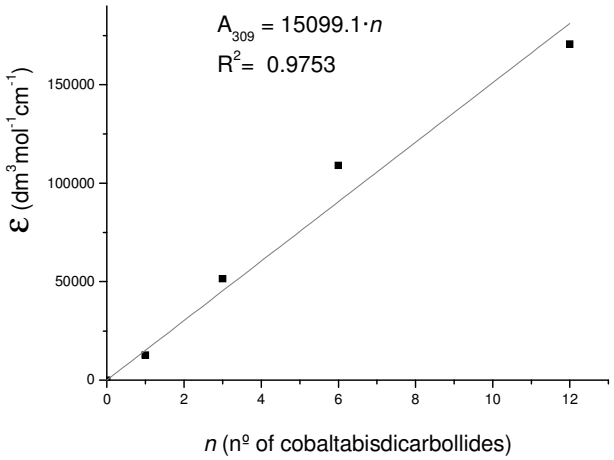

Figure 5. Normalized fluorescence spectra of compounds **2**, **5a-b**, **7** in acetonitrile.

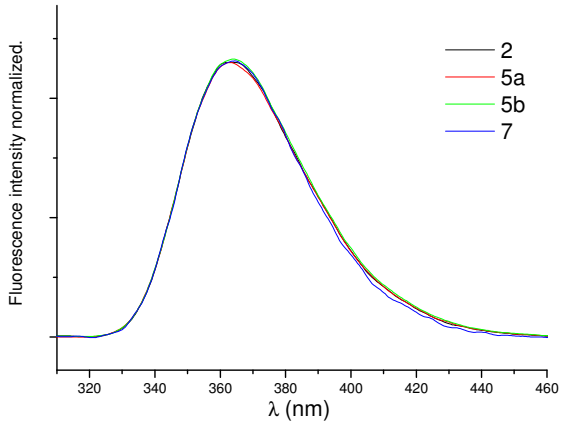

Figure 6.

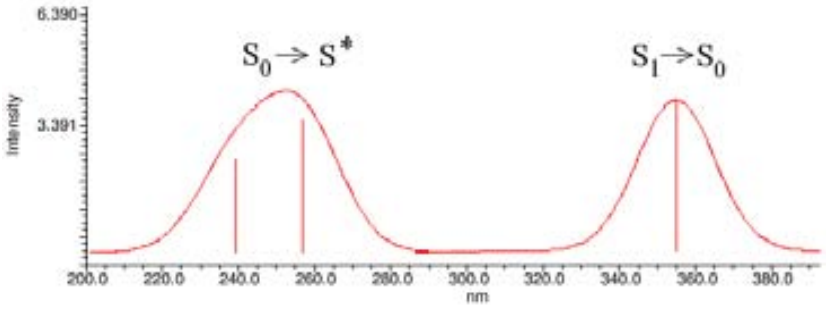

Figure 7. Jabloswky diagram for emissive and no emissive systems.

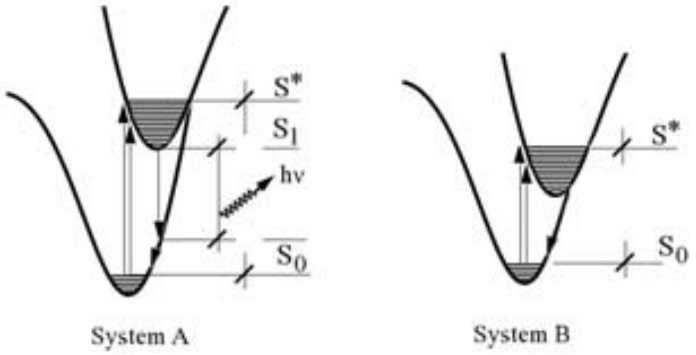

Table 1. Spectroscopic and photophysical data.

	Absorption				Emission		
	λ_{max}(nm)	$\varepsilon(10^{-3}$ dm^3·mol^{-1}·cm^{-1})			λ_{max}(nm)	Φ(%)	μ(ns)
2	269	(127)			364	20	9.3
5a	270	(66)			364	21	9.5
5b	270	(65)			364	21	9.5
7	272	(78)			363	22	9.5
10	271	(86)	310	(52)	-	-	-
11	276	(175)	309	(109)	-	-	-
12	272	(141)	307	(171)	-	-	-

References.

(1) (a) Miller, T. M.; Neeman, T. X.; Zayas, R.; Bair, H. E. *J. Am. Chem. Soc.* **1992**, *114*, 1018. (b) He, Q.; Huang, H.; Yang, J.; Lin, H.; Bai, F. *J. Mater. Chem.* **2003**, *13*, 1085. (c)Hiroyuki, N.; Makoto, M.; Eishun, T. J. Org. Chem. 1998, 63, 7399. (d) Khotina, I. A.; Lepnev, L. S.; Burenkova, N. S.; Valetsky, P. M.; Vitukhnovsky, A. G. *J. Luminiscence*, **2004**, *110*, 232.
(2) (a) Newkome, G. R.; Moorefield, C. N.; Keith, J. M.; Baker, G. R.; Escamilla, G. H. *Angew. Chem., Int. Ed. Engl.* **1994**, *33*, 666.
(3) Qualmann, B.; Kessels, M. M.; Mussiol, H.-J; Sierralta, W. D.; Jungblut, P. W.; Moroder, L. *Angew. Chem.* **1996**, *108*, 970; *Angew. Chem. Int. Ed. Engl.* **1996**, *35*, 909.
(4) (a) Parrott, M. C.; Marchington, E. B.; Valliant, J. F.; Adronov, A.J. *J. Am. Chem. Soc.* **2005**, *127*, 12081. (b) Ma, L.; Hamdi, J.; Wong, F.; Hawthorne, M. F. *Inorg. Chem.* **2006**, *45*, 278. (c) Parrott, M. C.; Valliant, J. F.; Adronov, A. *Langmuir*, **2006**, *22*, 5251. (d) Benhabbour, S. R.; Parrott, M. C.; Gratton, S. E. A.; Adronov, A. *Macromolecules*, **2007**,
(5) (b) Barth, R. F.; Adams, D. M.; Soloway, A. H.; Alam, F.; Darby, M. V.; *Bioconjugate Chem.* **1994**, *5*, 58. (c) (d) Armspach, D.; Cattalini, M.; Constable, E. C.; Housecroft, C. E.; Phillips, D. *Chem. Commun.* **1996**, 1823. (e) Housecroft, C. E. *Angew. Chem. Int. Ed.* **1999**, *38*, 2717. (f) Thomas, J.; Hawthorne, M. F. *Chem. Commun*. **2001**, 1884. (g) Yao, H.; Grimes, R. N.; Corsini, M.; Zanello, P. *Organometallics* **2003**, *22*, 4381. (h) Mollard, A.; Zharov, I. *Inorg. Chem.* **2006**, *45*, 10172. (i) B.P. Dash, R. Satapathy, J.A. Maguire, N.S. Hosmane, *Org. Lett* **2008**, *10*, 2247-2250.
(6) (a) Núñez, R.; González, A.; Viñas, C.; Teixidor, F.; Sillanpää, R.; Kivekäs, R. *Org. Letters* **2005**, *7*, 231. (b) Núñez, R.; González-Campo, A.; Viñas, C.; Teixidor, F.; Sillanpää, R.; Kivekäs, R. *Organometallics,* **2005**, *24*, 6351. (c) Núñez, R.; González-Campo, A.; Laromaine, A.; Teixidor, F. Sillanpää, R.; Kivekäs, R.; Viñas, C. *Org. Letters* **2006**, *8*, 4549. (d) Lerouge, F.; Viñas, C.; Teixidor, F.; Núñez, R.; Abreu, A.; Xochitiotzi, E.; Santillan, R.; Farfán, N. *Dalton Trans.* **2007**, 1898.
(7) (a) González-Campo, A.; Viñas, C.; Teixidor, F.; Nuñez, R.; Kivekäs, R.; Sillanpää, R. *Macromolecules* **2007**, *40*, 5644. (b) González-Campo, A.; Juárez-Pérez, E. J.; Viñas, C.; Boury, B.; Kivekäs, R.; Sillanpää, R.; Núñez, R. *Macromolecules* **2008**, *41*, 8458.
(8) (a) Juárez-Pérez, E. J.; Viñas, C.; González-Campo, A.; Teixidor, F.; Kivekäs, R.; Sillanpää R.; Núñez, R. *Chem. Eur. J.* **2008**, *14*, 4924. (b) Juárez-Pérez, E. J.; Teixidor, F.; Viñas, C.; Núñez, R.; *J. Organomet. Chem.* **2009**, DOI: 10.1016/j.jorganchem.2008.12.022.
(9) (a) Hawthorne, M. F.; Andrews, T. D. *J. Chem. Soc., Chem. Commun.* **1965**, 443. (b) Sivaev, I. B.; Bregadze, V. I. *Collect. Czech. Chem. Commun*. **1999**, *64*, 783.
(10) (a) Ma, L.; Hamdi, J.; Hawthorne, M. F. *Inorg. Chem.* **2005**, *44*, 7249. (b) Matejicek, P.; Cigler, P.; Procházka, K.; Kral, V. *Langmuir*, **2006**, *22*, 575. (c) Chevrot, G.; Schurhammer, R.; Wipff, G. *J. Phys. Chem. B* **2006**, *110*, 9488.
(11) (a) Strauss, S. H. *Chem. Rev.* **1993**, *93*, 927. (b) Reed, C. A. *Acc. Chem. Res.* **1998**, *31*, 133.
(12) Masalles, C.; Llop, J.; Viñas, C.; Teixidor, F. *Adv. Mater.* **2002**, *14*, 826.
(13) Plesek, J. *Chem. Rev.* **1992**, *92*, 269.
(14) (a) Viñas, C.; Gómez, S.; Bertran, J.; Teixidor, F.; Dozol, J.-F.; Rouquette, H. *Chem. Commun.* **1998**, 191. (b) Viñas, C.; Gómez, S.; Bertran, J.; Teixidor, F.; Dozol, J.-F.; Rouquette, H. *Inorg. Chem. 1998*, *37*, 3640. (c) Grüner, B.; Plesek, J.; Baca, J.;Cisarova, I.; Dozol, J.-F; Rouquette, H.; Viñas, C.; Selucky, P.; Rais, J. *New J. Chem.* **2002**, *26*, 1519. (d) Grüner, B.; Mikulásek, L; Báca, J.; Císarová, I.; Böhmer,V.; Danila, C.; Reinoso-García, M.; Verboom, W.; Reinhoudt, D. N.; Casnati, A. Ungaro R. *Eur. J. Org. Chem.* **2005**, 2022.
(15) (a) Masalles, C.; Borrós, S.; Viñas, C.; Teixidor, F., *Adv. Mater.* **2000**, *12*, 1199. (b) Borrós, S.; Llop, J.; Viñas, C.; Teixidor, F. Adv. Mater. **2002**, *14*, 449. (c) Gentil, S., Crespo, E., Rojo, I.; Friang, A.; Viñas, C., Teixidor, F.; Grüner, B.; Gabel, D. *Polymer* **2005**, *46*, 12218. (d) Crespo, E.; Gentil, S.; Viñas, C.; Teixidor, F. *J. Phys. Chem. C* **2007**, *111*, 18381. (e) Errachid, A.; Caballero, D.; Crespo, E.; Bessueille, F.; Pla-Roca, M.; Mills, C.; Christopher, A.; Teixidor, F; Samitier, J. *Nanotechnology* **2007**, *18*, 485301. (f) Stoica, A. I. ; Viñas C. ; Teixidor, F. *Chem. Commun.* **2008**, 6492.
(16) Stoica, A. I.; Viñas C. ; Teixidor, F *Chem. Commun.* **2008**, 48, 6492**.**
(17) (a) Hawthorne, M. F.; Maderna, A. *Chem. Rev.* **1999**, *99*, 3421. (b) Hao, E.; Vicente, M. G. H. *Chem. Commun.* **2005**, 1306. (c) Barth, R. F.; Coderre, J. A.; Vicente, M. G. H.; Blue, T. E. *Clin. Cancer Res.* **2005**, *11*, 3987. (d) Gottumukkala, V., Ongayi, O.; Baker, D. G.; Lomax, L. G.; Vicente, M. G. H. *Bioorg. Med. Chem.* **2006**, *14*, 1871. (e) Wang, J.-Q.; Ren, C.-X.; Weng, L.-H.; Jin, G.-X. *Chem. Commun*. **2006**, 162. (f) Bregadze, V. I.; Sivaev, I. B.; Glazun, S. A. *Anti-Cancer Agents Med. Chem.*, **2006**, *6*, 75.
(18) (a) Olejniczak, A. B.; Plesek, J.; Kriz, O.; Lesnikowski, Z. J. *Angew. Chem. Int. Ed.* **2003**, *42*, 5720. (b) Lesnikowski, Z.; Paradowska, E.; Olejniczak, A. B.; Studzinska, M.; Seekamp, P.; Schüβler, U.; Gabel, D.; Schinazi, R. F.; Plesek, J.; *Bioorg. Med. Chem.* **2005**, *13*, 4168. (c) Olejniczak, A. B.; Plesek, J.; Lesnikowski, Z. J. *Chem. Eur. J.* **2007**, *13*, 311.
(19) (a) Sibrian-Vazquez, M.; Hao, E.; Jenssen, T. J.; Vicente, M.G. H. *Biocong. Chem.* **2006**, 17, 928. (b) Hao, E.; Sibrian-Vazquez, M.; Serem, W.; Garno, J. C.; Fronczek F. R.; Vicente, M. G. H. *Chem. Eur. J.* **2007**, *13*, 9035. (c) Li, F.; Fronczek, F. R.; Vicente, M. G. H. *Tetrahedron Lett.*, **2008**, *49*, 4828.

(20) (a) Endo, Y.; Yoshimi, T.; Miyaura, C. *Pure Appl. Chem.* **2003**, *5*, 1197. (b) Cígler, P.; Kozisek, M.; Rezacova, P.; Brynda, J.; Otwinowski, Z.; Pokorná, J.; Plesek, J.; Grüner, B.; Dolecková-Maresová, L.; Masa, M.; Sedlácek, J.; Bodem, J.; Kräusslich, H.-G.; Král, V.; Konvalinka, J. *Proc. Natl. Acad. Sci. U.S.A.* **2005***, 102*, 15394. (c) Crossley, E. L.; Ziolkowski, E. J.; Coderre, J. A.; Rendina, L. M. *Mini-Rev. Med. Chem.* **2007**, *7*, 3003. (d) Julius, R. L.; Farha, O. K.; Chiang, J.; Perry, L. J.; Hawthorne, M. F. *Proc. Natl. Acad. Sci. U.S.A.* **2007**, *104*, 4808.
(21) Valliant, J. F.; Guenther, K. J.; King, A. S.; Morel, P.; Schaffer, O. O., Sogbein, K. A.; Stephenson, K. A. *Coord. Chem. Rev.* **2002**, *232*, 173.
(22) K. Sambasivarao, K. Dhurke, L. Kakali, S. B. Raghavan, *Eur. J. Org. Chem.* **2004**, *19*, 4003.
(23) H. P. Dijkstra, C. A. Kruithof, N. Ronde, R. van de Coevering, D. J. Ramón, D. Vogt, G.P.M. van Klink, G. van Koten, *J. Org. Chem*. **2003**, 68, 675.
(24) Y. H. Kim, R. Beckerbauer, *Macromolecules.* **1994**, 27, 1968.
(25) V. V. Maxym, N. Ronny, *J. Am. Chem. Soc.* **2004**, 126, 884.
(26) Y. Takehiko, H. Chieko, N. Yoshiaki, T. Masashi. *J. Chem. Res. (S)*. **1996**, 6, 266.
(27) a) W. S. Marshall, T. Goodson, G. J. Cullinan, D. Swanson-Bean, K. D. Haisch, L. E. Rinkema, J. H. Fleisch, *J. Med. Chem*. **1987**, 30, 682. b) S. Paul,; M. Gupta, *Tetrahedron Letters* **2004**, *45* (48), 8825, c) H. Murakami, T. Minami, F. Ozawa, J. Org. Chem. **2004**, *69*, 4482-4486.
(28) a) V. Percec, A. Dulcey, M. Peterca, M. Ilies, Y. Miura, U. Edlund, P.A. Heiney, Aust. J. Chem., 58, 472-482, 2005. b) A. Jutand, S. Négri, Eur. J. Org. Chem. **1998**, 1811.
(29) Y. Yamakawa, M. Ueda, R. Nagahata, K. Takeuchi, M. Asai, *J. Chem. Soc. Perkin Trans 1*, **1998**, 4135.
(30) O. Haba, K. Haga, M. Ueda, *Chem. Mater*, **1999**, 11, 427.
(31) S. L. Elmer, S. Zimmerman, *J. Org. Chem*, **2004**, 69, 7363.
(32) Jutand, S. Négri, *Eur. J. Org. Chem.* **1998,** 1811
(33) K. Chakraborti, L. Sharma, R. Gulhane, Shivani, *Tethrahedron.* **2003**, 59, 7661.
(34) (a) Tood, L. J. *Progress in NMR Spectroscopy*, Ed. Pergamon Press Ltd. **1979**, 13, 87. (b) Rojo, I.; Teixidor, F.; Viñas, C.; Kivekäs, R.; Sillanpää, R. *Chem. Eur. J.* **2004**, *10*, 5376.
(35) MOPAC2007, James J. P. Stewart, Stewart Computational Chemistry, Version 8.205L web: HTTP://OpenMOPAC.net
(36) A. Klamt and G. Schüümann. *J. Chem. Soc. Perkin Transactions 2* **1993,** 799-805.
(37) J. G. Domínguez-Chávez, I. Lijanova, I. Moggio, E. Arias, R. A. Vázquez García, I. Reyes-Valderrama Maa, T. Klimova, M. Gutiérrez-Nava, M. Martínez-García, J. Nanosci. Nanothecnol. **2007**, *7*, 2758-2766)
(38) D.F. Eaton, Pure Appl. Chem **1988**, *60*, 1107-1114.

Polyanionic Aryl-Ether Metallodendrimers Based On Cobaltabisdicarbollide Derivatives. Photoluminescent Properties.

Supplementary Material

Steric Hindrance quantification by Monte Carlo Method.[1]

The Monte Carlo method has been applied in this work for the stochastic generation of stable configurations in the dendrimers studied at 300 K. Solvation is not incorporated into the model and the bulky [1,1'-μ-Si(CH_3)CH_2-3,3'-Co(1,2-$C_2B_9H_{11}$)$_2$]$^-$ fragment has been substituted by a -Si(CH_3)$_3$ moiety. The aim of these calculations is to obtain a parameter that quantify the steric hindrance in the periphery of any carbosilane dendrimer. It could be achieved taken in account the most external Si atoms in the branches and recording the average distance between them. This average distance for all configurations simulated by Monte Carlo method may provide a representative value to compare between dendrimeric structures about the steric hindrance in the periphery. We define this parameter as η (Å), equation 1.

$$\eta = \frac{1}{M \cdot N} \sum_{j=1}^{M} \sum_{i=1}^{N} d_i \qquad (1)$$

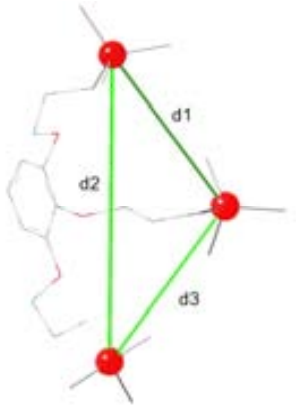

Figure S1. Branch **1TFB0s9** with three terminal -Si(CH_3)$_3$ groups showing the three distances measured.

Where M means the number of simulated configurations, usually 100, and N takes the value of 1 for the disubtituteds **1TFB0s9-x0x**, **1TFB0s9-xx0** and a branch of **1TFB0s6** and 3 for trisubtituted **0TFB0s3**, a branch of **1TFB0s9** and a branch of **1TFB0-ViS0s9** . For example, the case of the branch of **1TFB(allyl)$_9$** hydrosilylated *in silico* with three HSi(CH_3)$_3$, **1TFB0s9**, the three recorded distances are represented in Figure S1.

This three distances in the 100 simulated configurations for **1TFB0s9** applying equation 1 gives η = 7.1 Å. The data for the other dendrimeric structures is representated graphically in Figure S2 and the Table S1 show the values of η.

Low values of this parmeter η can be seen as high steric hindrance and high values as low steric hindrance. Then, it can be seen that the 3-subtituted (**0TFB0s3**) has highest value of η. Also, a branch of the the 6-subtituted (**1TFB0s6**) has a high η value. Also, it can be seen that a branch of the the 9-subtituted with two adjacent vynil groups hydrosililated with HSi(CH_3)$_3$ (**1TFB0s9-xx0**) has lowest value of η. And a branch of the the 9-subtituted (**1TFB0s9**, Figure X1) has a low η value. The comparison between adjacent substituted **1TFB0s9-xx0** and vynil in the middle **1TFB0s9-x0x** shows that the last is less overcrowed. This method permits to know *a priori*,(ref. art. carbosilane) and in an indirect way, which viniyl terminated dendrimers can be fully hydrosililated dendrimers with the [1,1'-μ-Si(CH_3)-3,3'-Co(1,2-$C_2B_9H_{11}$)$_2$]$^-$ fragment. The experimental findings permits to draw a frontier line to the [1,1'-μ-Si(CH_3)-3,3'-Co(1,2-$C_2B_9H_{11}$)$_2$]$^-$ case where we place this line around 8.5 Å. In the case of these dendrimers, the line frontier is located in the same place. It is interesting to note that the increase with a Si-CH2CH2- spaciator (**1TFB0-ViS0s9**) not

increase the η value and then a not full functionalization is waited in this case.

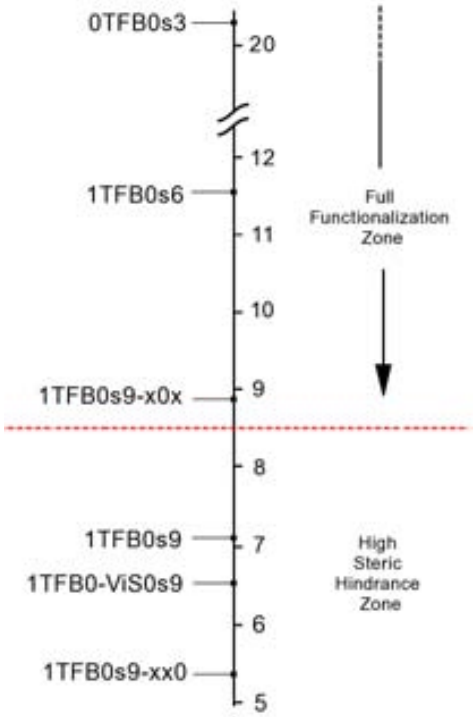

Figure S2. Values of η (Å) for the calculated structures at 300 K. The two zones frontier line is established according to experimental results for the case of the cobaltabisdicarbollide.

dendrimer	η(Å)
0TFB0s3	20.4
1TFB0s6	11.6
1TFB0s9	7.1
1TFB0s9-x0x	8.9
1TFB0s9-xx0	5.4
1TFB0-ViS0s9	6.6

Table S1. Values of η for the calculated structures at 300 K.

Experimental Method

Averages computed from a properly equilibrated Monte Carlo simulation correspond to thermodynamic ensemble averages at 300 K. A geometry optimization of the initial structure configuration at semiempirical level PM6[1b] is the starting point for the Monte Carlo simulations.[1c]

(1) (a) Allen, M.; Tildesley, P. D. J. *Computer Simulation of Liquids*, Oxford University Press, USA, **1989**. (b) MOPAC2007 Version 8.205L, Stewart, J. J. P.; Stewart Computational Chemistry, **2007**. (c) Hyperchem 7.5., Hypercube, **2002**.

c) Decorating Poly(Alkyl Aryl-Ether) Dendrimers With Metallacarboranes.

Decorating Poly(Alkyl Ary-Ether) Dendrimers With Metallacarboranes.

Rosario Núñez,[a] *Emilio José Juárez-Pérez,*[a#] *Francesc Teixidor,*[a] *Rosa Santillan,*[b] *Norberto Farfán,*[c] *Arturo Abreu,*[d] *Rebeca Yépez,*[b] *Clara Viñas*[a*]

[a] Institut de Ciència de Materials, CSIC, Campus U.A.B., 08193 Bellaterra, Spain
[b] Departamento de Química, Centro de Investigación y de Estudios Avanzados del IPN, 07000, Apdo. Postal 14-740, México D.F., México
[c] Facultad de Química, Departamento de Química Orgánica, Universidad Nacional Autónoma de México, México D.F. 04510, México
[d]Universidad Politécnica de Pachuca, Carretera Pachuca Cd. Sahagún, Km 20, Zempoala, Hidalgo México.
Email address: clara@icmab.es

RECEIVED DATE (to be automatically inserted after your manuscript is accepted if required according to the journal that you are submitting your paper to)

Corresponding Author: Prof. Clara Viñas, Institut de Ciència de Materials, CSIC, Campus U.A.B., 08193 Bellaterra, Barcelona, Spain. Tel.: +34 93 580 1853. Fax: +34 93 580 5729. clara@icmab.es

[#] Enrolled in the UAB PhD program.

Introduction

The derivative chemistry of the most intensively studied anionic borate cluster, the cobaltabisdicarbollide $[3,3'\text{-}Co(1,2\text{-}C_2B_9H_{11})]^-$, remains very much unexplored.[1] The fundamental reason is the synthetic strategy leading to these derivatives. Two basic substitutions may occur on $[3,3'\text{-}Co(1,2\text{-}C_2B_9H_{11})]^-$, either on carbon or on boron. With few exceptions,[2] substitutions on carbon have been achieved only at an early stage of the synthetic process, that is, on the starting o-carborane,[3] but not by direct reaction at the $[3,3'\text{-}Co(1,2\text{-}C_2B_9H_{11})]^-$, cage. Substitution at boron has been achieved under Friedel- Crafts conditions[4] or with strong alkylating agents.[5] Consequently, regioselective substitutions were not possible, and specific derivatives could be obtained only after careful separations of complex mixtures. The high yield synthesis and easy preparation of the zwitterionic 8-dioxanate $[3,3'\text{-}Co(8\text{-}C_4H_8O_2\text{-}1,2\text{-}C_2B_9H_{10})(1',2'\text{-}C_2B_9H_{11})]$, **3**, derivative has been reported.[6,7] Compound **3** has been proven to be susceptible to nucleophilic attack on the positively charged oxygen atom, for example, by pyrrolyl,[8] imide, cyanide or amines,[9] phenolate, dialkyl or diarylphosphite,[10] N-alkylcarbamoyldiphenylphosphine oxides,[3d] alkoxides,[7,11] and nucleosides,[12] resulting in one anionic species formed by the opening of the dioxane ring. A recent review[13] covers the known scope of reactions of different oxonium derivatives of polyhedral boron hydrides. Cobaltabisdicarbollide, $[3,3'\text{-}Co(1,2\text{-}C_2B_9H_{11})]^-$, has been proposed in a wide range of applications, such as the extraction of radionuclides,[3b-d 14] in conducting organic polymers,[15] or a use in medicine.[16] Recently, the construction of high-boron-content molecules has received considerable interest.[17] At the same time, the introduction of carboranes into different types of dendrimeric structures, at the inner region or at the surface of the molecules, is also being explored.[18] The design of watersoluble boron-rich dendritic or macromolecular systems is of interest for boron neutron capture therapy (BNCT) or for drug delivery systems. The closo-carboranes have been tested for boron delivery into tumors; however, their extreme lipophilicity often produces water-insoluble

structures with limited bioavailability, precluding thus effective application of such compounds in BNCT. One solution to the problem of the water solubility of BNCT agents could be to replace a neutral carborane with an anionic metallacarborane. Following our studies on metallacarboranes direct substitution, we report herein on the high-yield synthesis of polyanionic species as novel high-boron-content molecules. The synthetic ways were based on the use of alkoxide functions as nucleophiles in the ring-opening reaction of cyclic oxonium [3,3'-Co(8-$C_4H_8O_2$-1,2-$C_2B_9H_{10}$)(1',2'-$C_2B_9H_{11}$)], **3**.

Results

Synthesis and characterization

Tetrabromobenzyl derivatives of **1a** and **1b** were prepared as described previously, and reacted with 4 equivalents of 5-hydroisophtalic ethyl ester to give the corresponding octaesters in 85% and 90 % yields (Scheme 2). Evidence for the formation of the compounds was obtained from ^{1}H NMR which showed the A_2X_3 system for the ethyl ester at 4.38(quarted) y 1.39(triplet) ppm, respectivamente. Also the benzylic methylene is shifted to high frequency (5.11 ppm) with respect to the starting materials. The ^{13}C NMR spectra of **2a** and **2b** show the signals for the ester at 165.7 (CO), 61.5 (CH_2) and 14.4 (CH_3) ppm, and new signals at 70.5 (OCH_2, meta) and 70.1 (OCH_2, para) ppm.

Reduction of the octaesters with $LiAlH_4$ to gave the corresponding alcohols **2a** and **2b** in 69 and 94% yields. Formation of the alcohols was confirmed by NMR, IR and MS. The ^{1}H NMR spectra showed disappearence of the signals corresponding to the ester and a new benzylic methylene signal at 4.45 ppm.

Experimental Section

Instrumentation. Elemental analyses of compound **4a-b**, **5a-b** were not performed because of the problems to obtain reliable results in boron rich high molecular weight compounds.[19] Thus, the purity of this metallodendrimers was assessed by NMR spectroscopy, UV, MALDI-TOF and HPLC. IR spectra were recorded from KBr pellets on a Shimadzu FTIR-8300 spectrophotometer. The ^{1}H NMR (300.13 MHz), ^{11}B{^{1}H} NMR (96.29 MHz) and ^{13}C{1H} NMR (75.47 MHz) spectra were recorded on a Bruker ARX 300 spectrometer. All NMR spectra were recorded in $CDCl_3$ or CD_3COCD_3 solutions at 25 ºC. Chemical shift values for ^{11}B{^{1}H} NMR spectra were referenced to external $BF_3{\cdot}OEt_2$, and those for ^{1}H and ^{13}C{1H} NMR were referenced to $SiMe_4$. Chemical shifts are reported in units of parts per million downfield from reference, and all coupling constants are reported in Hz. UV-vis spectra were recorded using a Shimadzu UV-1700 Pharmaspec spectrophotometer, using 1 cm cuvettes, and the concentration of the compounds was $1.6{\cdot}10^{-5}$ mol·L^{-1} in EtOH. The mass spectra were recorded in the negative ion mode using a Bruker Biflex MALDI-TOF-MS (N_2 laser; λ_{exc} 337 nm, 0.5 ns pulses; voltage ion source 20.00 kV (Uis1) and 17.50 kV (Uis2)). Elution times were measured on HPLC.

Materials. All reactions were performed under an atmosphere of dinitrogen employing standard Schlenk techniques. Dioxane and DMSO were purchased from Merck and distilled from standard methods prior to use. Compounds Cs[3,3'-Co(1,2-$C_2B_9H_{11}$)$_2$] were supplied by Katchem Ltd. (Prague) and used as received. [3,3'-Co(8-$C_4H_8O_2$-1,2-$C_2B_9H_{11}$)(1',2'-$C_2B_9H_{11}$)], **3**, was synthesized according to the literature.[6,7] Compounds **1a** and **1b** were synthesized according to the literature.[20] Starting materials: sulfuric acid, α,α'-dibromo-p-xylene; α,α'-dibromo-m-xylene; 3,5-dihydroxybenzoic acid; triphenylphosphine; carbon tetrabromide; potassium carbonate; lithium hydride; potassium tert-butoxide, Et_2O, CH_2Cl_2 and acetonitrile were commercially available from Aldrich and used as received.

Preparation of precursors 2a .

Compound α,α'-bis[3,5-bis-[[3,5-bis(carboethoxy)phenoxy]methylen]phenoxy]- p-xylene was prepared from 2.00 g (3.02 mmol) of α,α'-bis[3,5-bis(bromomethyl)phenoxy]-p-xylene and 5-hydroxyisophtalic ethyl ester (2.876 g, 12.08 mmol) in the presence of 1.667 g (12.08 mmol) of K_2CO_3 under reflux of acetonitrile for 36 hours. The salts were filtered off and the filtrate concentrated to give **2a** (3.51 g, 2.72 mmol) as a white solid in 90 %. Mp 136-138 ºC. MS (m/z= (%) [M^+, 1290 (3)], 1053 (3), 283 (100), 253 (7), 223 (8), 183 (3), 104 (3), 150 (6), 104 (10), 59 (6). ^{1}H NMR (270 MHz, $CDCl_3$) δ: 8.28 (4H, s), 7.81 (8H, d, Jm = 1.5 Hz), 7.45 (1H, s,), 7.05 (4H, s), 7.12 (2H, s), 5.11 (8H, s), 5.10 (4H, s), 4.38 (16H, q, J = 7.1 Hz), 1.39 (24H, t, J = 7.1 Hz) ppm. ^{13}C NMR (75.47 MHz, $CDCl_3$) δ: 165.7, 159.4, 158.6, 138.3, 136.6, 132.2, 127.9, 123.3, 120.1, 119.0, 113.7, 70.1, 69.9, 61.5, 14.4 ppm. Compound α,α'-bis[3,5-bis-[[3,5-bis(carboethoxy)phenoxy]methylen]phenoxy]- p-xylene (3.00 g, 2.32 mmol) was added in small portions to a stirred suspension of $LiAlH_4$ (0.707 g, 18.6 mmol) in anhydrous THF. The reaction mixture was refluxed 48 hrs, followed by addition of a saturated solution of NH_4Cl, filtered and washed with

CH_2Cl_2, acetone, metanol and water. The filtrate was evaporated under vacuum and the alcohol precipitated in the aqueous phase to give a white solid (2.08 g, 2.18 mmol, 94.0 %). Mp 137-140 °C. IR *v* (KBr), 3367, 2869, 1710, 1597, 1456, 1296, 1154, 1020, 846 cm^{-1}. MS-FAB, m/z (%) [M^+, 955 (1)], 460 (7), 393 (33), 366 (100), 349 (40), 322 (47), 307 (43), 279 (35), 209 (22). ^{1}H NMR (399.78 MHz, DMSO-d_6) δ: 7.45 (4H, s), 7.11 (2H, s), 7.06 (4H, s), 6.86 (2H, s), 6.83 (4H, s), 5.12 (8H, s), 5.05 (4H, s), 4.45 (16H, s) ppm. ^{13}C NMR (100.52 MHz, DMSO-d_6) δ: 159.4, 158.6, 144.5, 139.6, 137.1, 128.4, 119.4, 117.5, 113.7, 111.5, 70.1, 69.9, 63.5 ppm.

Preparation of precursors 2b

Compound α,α'-bis[3,5-bis-[[3,5-bis(carbaethoxy)phenoxy]methylen]penoxy]- m-xylene was prepared from 2.00 g (3.02 mmol) of α,α'-bis[3,5-bis(bromomethyl)phenoxy]-m-xylene and 4 equivalents of 5-hydroxyisophtalic ethyl ester (2.876 g, 12.08 mmol) in the presence of 1.667 g (12.08 mmol) of K_2CO_3 under reflux of acetonitrile for 36 hours. The salts were filtered off and the filtrate concentrated to give **2b** (3.31 g, 2.56 mmol) as a white solid in 85.0 %. Mp 100-106 °C. MS (m/z) (%) [M^+, 1290 (3)], 1053 (3), 283 (100), 253 (57), 223 (78), 183 (168), 104 (39). ^{1}H NMR (270 MHz, $CDCl_3$) δ: 8.30 (4H, t, Jm = 1.3 Hz), 7.83 (8H, d, Jm = 1.3 Hz), 7.55 (1H, s,), 7.43 (2H, s), 7.43 (3H, m), 7.16 (2H, s), 7.08 (4H, s), 5.14 (12H, s), 4.40 (16H, c, J = 7.1 Hz), 1.41 (24H, t, J = 7.1 Hz) ppm. ^{13}C NMR (75.47 MHz, $CDCl_3$) δ: 165.7, 159.5, 158.7, 138.4, 137.2, 132.3, 129.1, 127.4, 126.7, 123.3, 120.1, 119.0, 113.7, 70.5, 70.2, 61.6, 14.4 ppm.

Compound α,α'-bis[3,5-bis-[[3,5-bis(carbaethoxy)phenoxy]methylen]penoxy]- m-xylene (3.0 g, 2.32 mmol) was added in small portions to a stirred suspension of $LiAlH_4$ (0.707 g, 18.6 mmol) in anhydrous THF. The reaction mixture was refluxed 48 hrs, followed by addition of a saturated solution of NH_4Cl, filtered and washed with CH_2Cl_2, acetone, metanol and water. The filtrate was evaporated under vacuum and the alcohol precipitated in the aquous phase to give a white solid (1.53 g, 1.18 mmol, 69.0 %). Mp 94-97 °C. IR *v* (KBr), 3290, 2873, 1698, 1597, 1454, 1296, 1150, 1020, 843, 702 cm^{-1}. MS-FAB, m/z (%) [M^+, 954 (5)], 824 (3), 545 (6), 460 (10), 393 (12), 327 (57), 307 (100), 289 (58), 219 (37). ^{1}H NMR (399.78 MHz, DMSO-d_6) δ: 7.56 (1H, s), 7.43 (2H, s), 7.37 (1H, s), 7.12 (2H, s), 7.07 (4H, s), 6.85 (2H, s), 6.83 (8H, s), 5.13 (4H, s), 5.05 (8H, s), 4.44 (16H, s) ppm. ^{13}C NMR (100.52 MHz, DMSO-d_6) δ: 159.1, 158.8, 144.5, 139.6, 137.7, 129.2, 127.9, 127.6, 119.3, 117.4, 113.6, 111.4, 69.8, 69.4, 63.3 ppm.

Preparation of 4a. To a solution of **1a** (12.8 mg, 0.0312 mmol) in 4 mL of dry DMSO at room temperature, *t*-BuOK (16.2 mg, 0.145 mmol) was added. The suspension was stirred for 30 min at room temperature. After, compound **3** (51.3 mg, 0.125 mmol) was added and stirred for 24 h. The reaction was quenched by the addition of 1 mL of water and one drop of HCl (1 M). Organic solvents were then evaporated in vacuo to give an orange oily residue, that was dissolved in the minimum volume of ethanol (~ 1 mL), and 10 mL of an aqueous solution containing an exces of CsCl was added, resulting in the formation of a fine orange suspension. The suspension was taken up with 10 mL of diethyl ether and the mixture was then transferred to a separatory funnel. The layers were separated and the organic phase was extracted with additional diethyl ether (2 x10 mL). Combined diethyl ether fractions were dried over anhydrous $MgSO_4$ and evaporated. The resulted solid was dissolved in CH_2Cl_2-CH_3CN (1:1) and injected on bottom of a silica gel plate (25 x 25 cm), and chromatographed in the same solvent mixture to give Cs_4(**4a**) as an orange powder. Yield: 41 mg, 51 %. IR (KBr, cm^{-1}): 3042 ν(C_c–H), 2971, 2922, 2873 ν(C_{alkyl}–H), 2561 ν(B–H). ^{1}H NMR ($(CD_3)_2CO$): 7.53 (s, 4H, C_6H_4), 6.97 (s, 4H, C_6H_3), 6.94 (s, 2H, C_6H_3), 5.14 (s, 4H, OCH_2), 4.56 (s, 8H, OCH_2), 4.23 (bs, 16H, C_c-H), 3.64 (m, 24H, OCH_2), 3.56 (t, 8H, ^{3}J(H,H)=6Hz, OCH_2). ^{1}H {^{11}B}NMR ($(CD_3)_2CO$): 7.53 (s, 4H, C_6H_4), 6.97 (s, 4H, C_6H_3), 6.94 (s, 2H, C_6H_3), 5.14 (s, 4H, OCH_2), 4.56 (s, 8H, OCH_2), 4.23 (bs, 16H, C_c-H), 3.64 (m, 24H, OCH_2), 3.56 (t, 8H, ^{3}J(H,H)=6Hz, OCH_2), 2.89 (s, 16H, B-H), 2.75 (s, 8H, B-H), 2.70 (s, 4H, B-H), 2.07 (s, 4H, B-H), 2.02 (s, 8H, B-H), 1.82 (s, 8H, B-H), 1.65 (s, 8H, B-H), 1.55 (s, 8H, B-H), 1.47 (s, 4H, B-H).^{13}C{^{1}H} NMR ($(CD_3)_2CO$): 158.9 (C-1'), 140.7 (C-1), 140.1 (C-3'), 127.9 (C-2), 119.0 (C-4'), 112.7 (C-2'), 72.6 (OCH_2), 71.6 (OCH_2), 69.9 (OCH_2), 69.5 (OCH_2), 69.0 (OCH_2), 68.23 (OCH_2), 53.7 (C_c-H), 46.2 (C_c-H).^{11}B{^{1}H} NMR ($(CD_3)_2CO$): 24.7 (s, 4B, B(8)), 5.9 (d, ^{1}J(B,H)=121, 4B), 1.88 (d, ^{1}J(B,H)=133, 4B), -1.0 (d, ^{1}J(B,H)=139, 4B), -2.9 (d, ^{1}J(B,H)=162, 8B), -5.9 (d, 8B), -6.5 (d, 16B), -15.9 (d, ^{1}J(B,H)=153, 8B), -18.9 (d, ^{1}J(B,H)=154, 8B), -20.4 (d, 4B), -27.0 (d, ^{1}J(B,H)=113, 4B). MALDI-TOF-MS: (m/z) 1024.8 ((M-4Cs+2H)/2).

Preparation of 4b. The procedure was the same as for **4a**, using **1b** (38.4 mg, 0.093 mmol) in 4 mL of DMSO, *t*-BuOK (42 mg, 0.375 mmol) and **3** (156.1 mg, 0.380 mmol). Compound Cs_4(**4b**) was isolated as an orange solid. Yield: 149 mg, 62%. IR (KBr, cm^{-1}): 3041 ν(C_c–H), 2957, 2919, 2870 ν(C_{alkyl}–H), 2561

ν(B–H). ^{1}H NMR ($(CD_3)_2CO$): 7.62 (s, 1H, C_6H_4), 7.45 (s, 3H, C_6H_4), 6.98 (s, 4H, C_6H_3), 6.93 (s, 2H, C_6H_3), 5.15 (s, 4H, OCH_2), 4.55 (s, 8H, OCH_2), 4.17 (bs, 16H, C_c-H), 3.64 (m, 24H, OCH_2), 3.54 (t, 8H, ^{3}J(H,H)=6Hz, OCH_2). ^{1}H {^{11}B}NMR ($(CD_3)_2CO$): 7.53 (s, 4H, C_6H_4), 6.97 (s, 4H, C_6H_3), 6.94 (s, 2H, C_6H_3), 5.14 (s, 4H, OCH_2), 4.56 (s, 8H, OCH_2), 4.23 (bs, 16H, C_c-H), 3.64 (m, 24H, OCH_2), 3.56 (t, 8H, ^{3}J(H,H)=6Hz, OCH_2), 2.91 (s, 16H, B-H), 2.74 (s, 8H, B-H), 2.70 (s, 4H, B-H), 2.02 (s, 8H, B-H), 1.83 (s, 8H, B-H), 1.69 (s, 4H, B-H), 1.63 (s, 8H, B-H), 1.54 (s, 8H, B-H), 1.44 (s, 4H, B-H).^{13}C{^{1}H} NMR ($(CD_3)_2CO$): 159.0 (C-1'), 140.2 (C-3'), 137.9, 128.6, 126.82, 124.7, 119.4, 113.0 (C-2'), 72.2 (OCH_2), 71.8 (OCH_2), 69.8 (OCH_2), 69.5 (OCH_2), 69.2 (OCH_2), 68.2 (OCH_2), 53.3 (C_c-H), 46.2 (C_c-H).^{11}B{^{1}H} NMR ($(CD_3)_2CO$): 24.5 (s, 4B, B(8)), 5.9 (d, ^{1}J(B,H)=125, 4B), 1.3 (d, ^{1}J(B,H)=134, 4B), -1.6 (d, ^{1}J(B,H)=139, 4B), -3.6(d, ^{1}J(B,H)=173, 8B), -6.3, (d, 8B), -6.5 (d, 16B), -16.4 (d, ^{1}J(B,H)=152, 8B), -19.6 (d, ^{1}J(B,H)=156, 8B), -20.8 (d, 4B), -27.6 (d, ^{1}J(B,H)=124, 4B). MALDI-TOF-MS: (m/z) 547.4 ((M-4Cs+2DMSO)/4).

Preparation of 5a. The procedure was the same as for **4a**, using **2a** (12.7 mg, 0.013 mmol) in 6 mL of DMSO, *t*-BuOK (13.51 mg, 0.120 mmol) and **3** (53.7 mg, 0.131 mmol). Compound Cs_8(**5a**) was isolated as an orange solid. Yield: 28 mg, 41%. IR (KBr, cm¯1): 3040 ν(C_c–H), 2959, 2920, 2862 ν(C_{alkyl}–H), 2558 ν(B–H). ^{1}H NMR ($(CD_3)_2CO$): 7.55 (s, 4H, C_6H_4), 7.22 (s, 2H, C6H$_3$), 7.16 (s, 4H, C_6H_3), 7.02 (s, 4H, C_6H_3), 6.99 (s, 8H, C_6H_3), 5.18 (s, 4H, OCH_2), 5.13 (s, 8H, OCH_2), 4.55 (s, 16H, OCH_2), 4.15 (bs, 32H, C_c-H), 3.64 (m, 48H, OCH_2), 3.54 (t, 16H, ^{3}J(H,H)=6Hz, OCH_2).^{1}H{^{11}B} NMR ($(CD_3)_2CO$): 7.55 (s, 4H, C_6H_4), 7.22 (s, 2H, C6H$_3$), 7.16 (s, 4H, C_6H_3), 7.02 (s, 4H, C_6H_3), 6.99 (s, 8H, C_6H_3), 5.18 (s, 4H, OCH_2), 5.13 (s, 8H, OCH_2), 4.55 (s, 16H, OCH_2), 4.15 (bs, 32H, C_c-H), 3.64 (m, 48H, OCH_2), 3.54 (t, 16H, ^{3}J(H,H)=6Hz, OCH_2), 2.88 (s, 32H, B-H), 2.74 (s, 16H, B-H), 2.70 (s, 8H, B-H), 2.03 (s, 16H, B-H), 1.84 (s, 16H, B-H), 1.68 (s, 8H, B-H), 1.63 (s, 16H, B-H), 1.54 (s, 16H, B-H), 1.44 (s, 8H, B-H).^{13}C{^{1}H} NMR ($(CD_3)_2CO$): 159.7 (C-1'), 159.1 (C-1''), 140.3 (C-3''), 135.0, 129.5, 127.81, 119.7, 113.3 (C-2''), 72.5 (OCH_2), 72.2 (OCH_2), 71.9 (OCH_2), 70.0 (OCH_2), 69.7 (OCH_2), 69.4 (OCH_2), 68.4 (OCH_2), 53.2 (C_c-H), 46.5 (C_c-H).^{11}B{^{1}H} NMR ($(CD_3)_2CO$): 24.6 (s, 4B, B(8)), 6.5 (d, ^{1}J(B,H)=120, 4B), 1.9 (d, ^{1}J(B,H)=135, 4B), -1.6 (d, ^{1}J(B,H)=130, 4B), -2.6(d, ^{1}J(B,H)=180, 8B), -6.3, (8B), -6.8 (d, 16B), -16.4 (d, ^{1}J(B,H)=150, 8B), -19.7 (d, ^{1}J(B,H)=151, 8B), -20.8 (d, 4B), -27.6 (d, ^{1}J(B,H)=120, 4B). MALDI-TOF-MS: (m/z) 533.4 ((M-8Cs)/8).

Preparation of 5b. The procedure was the same as for **4a**, using **2b** (29.0 mg, 0.030 mmol) in 6 mL of DMSO, *t*-BuOK (34.2 mg, 0.264 mmol) and **3** (108 mg, 0.263 mmol). Compound Cs_8(**5b**) was isolated as an orange solid. Yield: 75 mg, 47%. IR (KBr, cm¯1): 3043 ν(C_c–H), 2952, 2921, 2869 ν(C_{alkyl}–H), 2562 ν(B–H). ^{1}H NMR ($(CD_3)_2CO$): 7.62 (s, 1H, C_6H_4), 7.45 (s, 3H, C_6H_4), 7.22 (s, 2H, C6H$_3$), 7.15 (s, 4H, C_6H_3), 7.02 (s, 4H, C_6H_3), 6.98 (s, 8H, C_6H_3), 5.19 (s, 4H, OCH_2), 5.13 (s, 8H, OCH_2), 4.55 (s, 16H, OCH_2), 4.13-4.09 (bs, 32H, C_c-H), 3.64 (m, 48H, OCH_2), 3.54 (m, 16H, OCH_2).^{1}H{^{11}B} NMR ($(CD_3)_2CO$): 7.62 (s, 1H, C_6H_4), 7.45 (s, 3H, C_6H_4), 7.22 (s, 2H, C6H$_3$), 7.15 (s, 4H, C_6H_3), 7.02 (s, 4H, C_6H_3), 6.98 (s, 8H, C_6H_3), 5.19 (s, 4H, OCH_2), 5.13 (s, 8H, OCH_2), 4.55 (s, 16H, OCH_2), 4.13-4.09 (bs, 32H, C_c-H), 3.64 (m, 48H, OCH_2), 3.54 (m, 16H, OCH_2), 2.88 (s, 32H, B-H), 2.70 (s, 24H, B-H), 2.03 (s, 16H, B-H), 1.83 (s, 16H, B-H), 1.68 (s, 8H, B-H), 1.62 (s, 16H, B-H), 1.53 (s, 16H, B-H), 1.44 (s, 8H, B-H).^{13}C{^{1}H} NMR ($(CD_3)_2CO$): 159.1 (C-1', C-1''), 140.3 (C-3''), 139.3 (C-3'), 137.6, 128.7, 127.2, 119.8, 119.12, 113.4 (C-2''), 72.8 (OCH_2), 72.5 (OCH_2), 72.0 (OCH_2), 70.0 (OCH_2), 69.7 (OCH_2), 69.4 (OCH_2), 68.4 (OCH_2), 53.1 (C_c-H), 46.6 (C_c-H).^{11}B{^{1}H} NMR ($(CD_3)_2CO$): 24.8 (s, 4B, B(8)), 6.5 (d, ^{1}J(B,H)=125, 4B), 1.5 (d, ^{1}J(B,H)=134, 4B), -1.5 (d, ^{1}J(B,H)=131, 4B), -3.9 (d, ^{1}J(B,H)=160, 8B), -6.1, (24B), -16.2 (d, ^{1}J(B,H)=141, 8B), -19.3 (d, ^{1}J(B,H)=153, 8B), -20.4 (d, 4B), -27.4 (d, ^{1}J(B,H)=111, 4B). MALDI-TOF-MS: (m/z) 3080.1, 3092.8, 3105.5, 31018.8, 618.2 ((M-8Cs+8H)/7).

HPLC

UV-vis Measurements

UV-Vis measurements have been done at room temperature using stock solutions in EtOH of compounds **4a-b**, **5a-b** concentrations of $1.6 \cdot 10^{-5}$ M.

Acknowledgements: This work has been supported by the CICYT (MAT2006-05339), the Generalitat de Catalunya, 2005/SGR/00709 and CONACYT-México. E.J.J.P. thanks to Ministerio de Educación y Ciencia for a FPU grant .

Scheme 1.

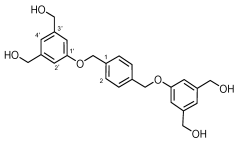

1a

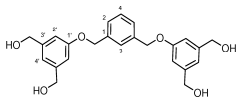

1b

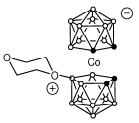

3

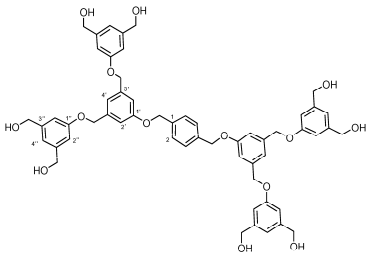

2a

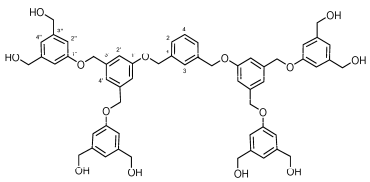

2b

Scheme 2.

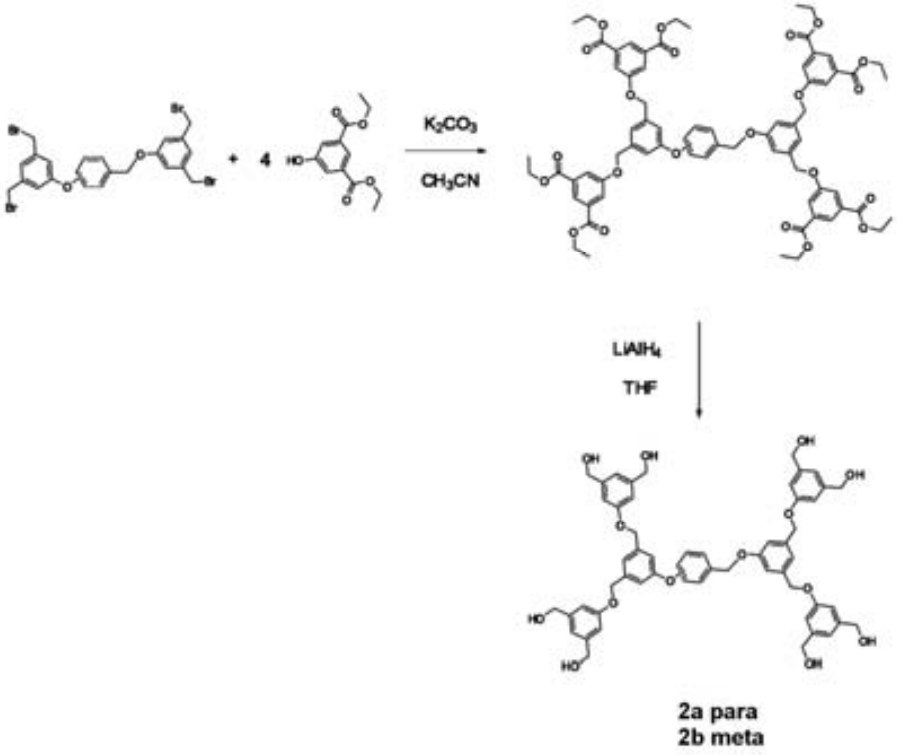

Scheme 4.

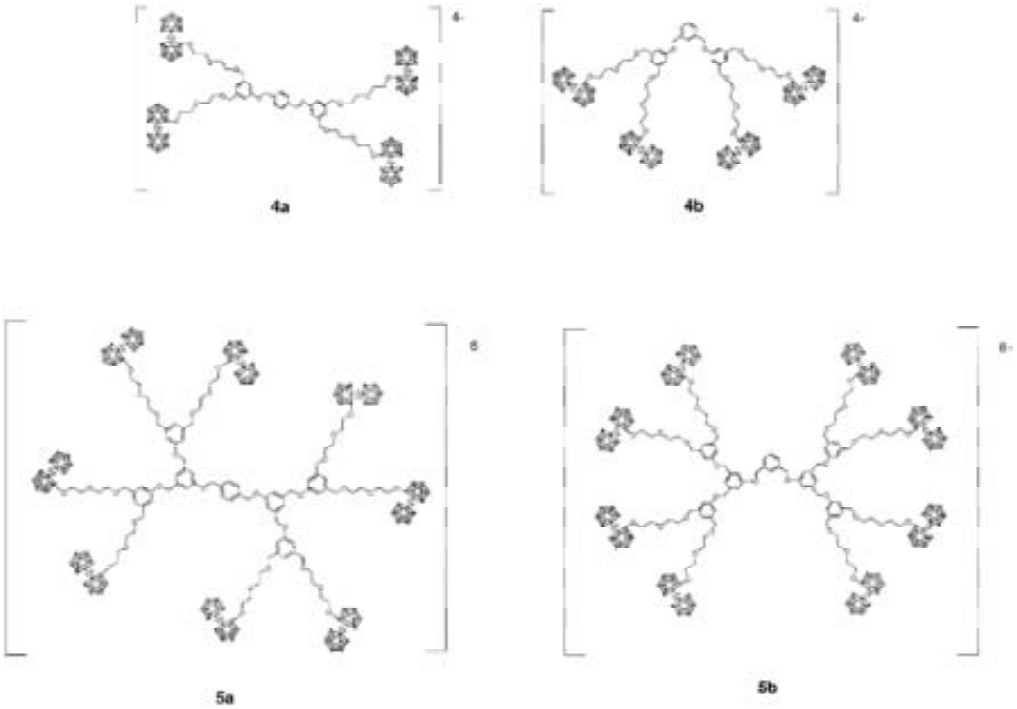

Figure 1. UV-Vis spectra for metallacarborane-containing dendrimers **4a-b** and **5a-b** in EtOH solutions at $1.6 \cdot 10^{-5}$ M.

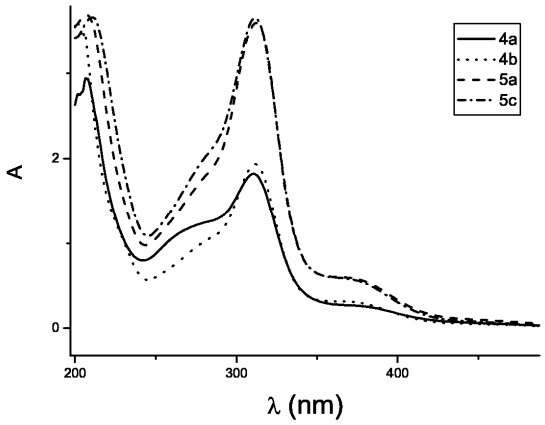

Figure 2. Linear correlation between the number of cobaltabisdicarbollides attached to the periphery and the absorptivity at λ = 310 nm.

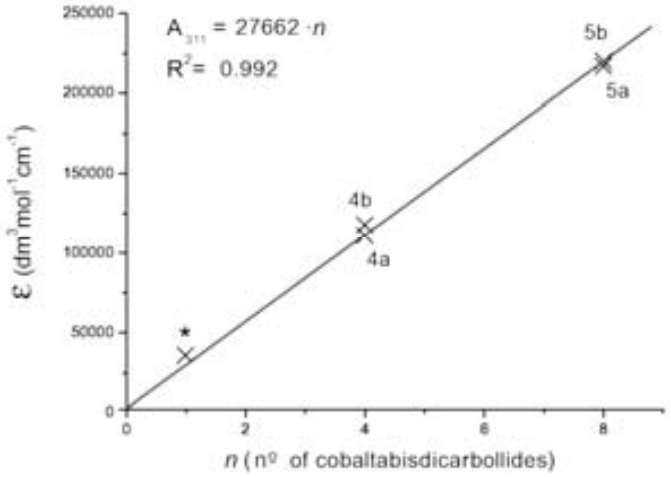

Tables 1

Compound	t(min)
test	1.31
4a	1.38
4b	1.39
5a	1.32
5b	1.31

Table 2.

Compound	lmax (nm)					
4a	268	*69697*	310	*110909*	372	*16364*
4b	273	*56364*	312	*117576*	371	*18788*
5a	274	*99394*	312	*216970*	370	*35758*
5b	273	*109697*	311	*220000*	369	*35152*

.

References

[1] Sivaev, I. B.; Bregadze, V. I. Collect. Czech. Chem. Commun. 1999, 64, 783.
[2] (a) R, M; Chamberlin, B. L.; Scott, M. M; Melo, K. D. A. Inorg. Chem. 1997, 36, 809. (b) Rojo, I.; Teixidor, F.; Viñas, C.; Kivekäs, R.; Sillanpää, R. Chem.sEur. J. 2004, 10, 5376. (c) Juárez-Pérez, E. J.; Viñas, C.; González-Campo, A.; Teixidor, F.; Kivekäs, R.; Sillanpää R.; Núñez, R. *Chem. Eur. J*. 2008, *14*, 4924.
[3] (a) Viñas, C.; Pedrajas, J.; Bertran, J.; Teixidor, F.; Kivekäs, R.;Sillanpää, R. Inorg. Chem. 1997, 36, 2482. (b) Viñas, C.; Gomez, S.;Bertran, J.; Teixidor, F.; Dozol, J. F.; Rouquette, H. Chem. Commun. 1998, 191. (c) Viñas, C.; Gomez, S.; Bertran, J.; Teixidor, F.; Dozol, J. F.; Rouquette, H. Inorg. Chem. 1998, 37, 3640. (d) Viñas, C.;Bertran, J.; Gomez, S; Teixidor, F.; Dozol, J. F.; Rouquette, H.; Kivekäs, R.; Sillanpää, R. J. Chem. Soc., Dalton Trans. 1998, 2849. (e) Viñas, C.; Pedrajas, J.; Teixidor, F.; Kivekäs, R.; Sillanpää, R.; Welch, A. J. Inorg. Chem. 1997, 36, 2988.
[4] Francis, J. N.; Hawthorne, M. F. Inorg. Chem. 1971, 10, 594.
[5] (a) Plesek, J.; HermaÂ´nek, S.; Base, K.; Todd, L. J.; Wright, W. F. Collect. Czech. Chem. Commun. 1976, 41, 3509. (b) Janousek, Z.; Plesek, J.; HermaÂ´nek, S.; Base, K.; Todd, L. J.; Wright, W. F. Collect. Czech. Chem. Commun. 1981, 46, 2818. (c) Rojo, I.; Teixidor, F.; Viñas, C.; Kivekäs, R.; Sillanpää, R. Chem.sEur. J. 2003, 9, 4311.
[6] (a) Plesek, J.; HermaÂ´nek, S.; Franken, A.; Cisarova, I.; Nachtigal, C. Collect. Czech. Chem. Commun. 1997, 62, 47. (b) Selucky, P.; Plesek, J.; Rais, J.; Kyrs, M.; Kadlecova, L. J. Radioanal. Nucl. Chem. 1991, 149, 131.
[7] Teixidor, F.; Pedrajas, J.; Rojo, I.; Viñas, C.; Kivekäs, R.; Sillanpää, R.; Sivaev, I.; Bregadze, V.; SjoÂ¨berg, S. Organometallics 2003, 22, 3414.
[8] Llop, J.; Masalles, C.; Viñas, C.; Teixidor, F.; Sillanpää, R.; Kivekäs, R. Dalton Trans. 2003, 556.
[9] (a) Sivaev, I. B.; Starikova, Z. A.; SjoÂ¨berg, S.; Bregadze, V. I. J. Organomet. Chem. 2002, 649, 1. (b) Sivaev, I. B.; SjoÂ¨bergS.; Bregadze, V. I. International Conference Organometallic Compounds – Materials of the Next Century, Nizhny, Novgorod, Russia, May 29-June 2, 2000.
[10] PlesˇekˇJ.; GruÂ¨ner, B.; HerˇmaÂ´nek, S.; BaÂ´cˇa, J.; MarecˇekˇV.; JaÂ¨nchenova Â´, J.; LhotskyÂ´, A.; Holub, K.; SeluckyÂ´, P.; Rais, J.; CıÂ´sarˇovaÂ´, I.; Cˇ aÂ´slavskyÂ´, J. Polyhedron 2002, 21, 975.
[11] (a) GruÂ¨ner, B.; MikulsˇekˇL.; BacˇaˇJ.; CisarˇovaˇI.; BoÂ¨hmer, V.; Danila, C.; Reinoso-Garcia, M. M.; Verboom, W.; Reinhoudt, D. N.; Casnati, A.; Ungaro, R. Eur. J. Org. Chem. 2005, 2022. (b) MikulasˇekˇL.; GruÂ¨ner, B.; Danila, C.; BoÂ¨hmer, V.;Cˇ aslavsky, J.; Selucky, P. Chem. Commun. 2006, 4001.
[12] (a) Olejniczak, A. B.; Pleek, J.; Krˇizˇ, O.; Lesnikowski, Z. J. Angew. Chem., Int. Ed. 2003, 42, 5740. (b) Lesnikowski, Z. J.; Paradowska, E.; Olejniczak, A. B.; Studzinska, M.; Seekamp, P.; SchuÂ¨ ler, U.; Gabel, D.; Schinazi, R. F.; PlesˇekˇJ. Bioorg. Med. Chem. 2005, 13, 4168. (c) Olejniczak, A. B.; PlesˇekˇJ.; Lesnikowski, Z. J. Chem. Eur. J. 2007, 13, 311.
[13] Semioshkin, A. A.; Sivaev, I. B.; Bregadze, V. I. Dalton Trans. 2008, 977.
[14] (a) GruÂ¨ner, B.; PlesˇekˇJ.; BaÂ´cˇa, J.; CıÂ´sarˇovaÂ´, I.; Dozol, J.-F.; Rouquette, H.; VinˇasˇC.; SeluckyÂ´, P.; Rais, J. New J. Chem. 2002, 26, 1519. (b) Rais, J.; GruÂ¨ner, B. In Ion Exchange and SolVent Extraction; Marcus, Y., Sengupra, A. K.; CRC Press: Boston, 2004; Vol. 17, p 243. (c) Mikulasek, L.; GruÂ¨ner, B.; Crenguta, D.; Rudzevich, V.; Boehmer, V.; Haddaoui, J.; Hubscher-Bruder, V.; Arnaud-Nue, F.; Caslavsky, J.; SeluckyÂ´, P. Eur. J. Org. Chem. 2007, 4772.
[15] (a) Masalles, C.; Borros, S.; Viñas, C.; Teixidor, F. AdV. Mater. 2000, 12, 1199. (b) Masalles, C.; Llop, J.; Viñas, C.; Teixidor, F. AdV. Mater. 2002, 14, 826. (c) Masalles, C.; BorroÂ´s, S.; Viñas, C.; Teixidor, F. AdV. Mater. 2002, 14, 449. (d) Svorcik, V.; Gardasova, R.; Rybka, V.; Hnatowicz, V.; Cervena, J.; PlesˇekˇJ. J. Appl. Polym. Sci. 2004, 91, 40.
[16] (a) Hao, E.; Vicente, M. G. H. Chem. Commun. 2005, 1306. (b) Barth, R. F.; Coderre, J. A.; Vicente, M. G. H.; Blue, T. E. Clin. Cancer Res. 2005, 11, 3987. (c) Gottumukkala, V.; Ongayi, O.; Baker, D. G.; Lomax, L. G.; Vicente, M. G. H. Bioorg. Med. Chem. 2006, 14, 1871. (d) Wang, J.-Q.; Ren, C.-X.; Weng, L.-H.; Jin, G.-X. Chem. Commun. 2006, 162. (e) Bregadze, V. I.; Sivaev, I. B.; Glazun, S. A. Anti-Cancer

Agents Med. Chem. 2006, 6, 75. (f) Cigler, P.; Kozˇisˇek, M.;Rˇ ezacˇova, P.; Brynda, J.; Otwinowski, Z.; Pokorna, J.; Plesˇek, J.; Gruner, B.; Dolecˇkova-Maresˇova, L.; Masˇa, M.; Sedlacˇek, J.; Bodem, J.; KraÂ¨usslich, H.; Kral, V.; Konvalinka, J. PNAS 2005, 102, 15394.

[17] (a) Thomas, J.; Hawthorne, M. F. Chem Commun. 2001, 1884. (b) Azev, Y.; Slepukhina, I.; Gabel, D. Appl. Radiat. Isot. 2004, 61, 1107. (c) Ma, L.; Hamdi, J.; Wong, F.; Hawthorne, M. F. Inorg. Chem. 2006, 45, 278. (d) Genady, A. R.; El-Zaria, M. E.; Gabel, D. J. Organomet. Chem. 2004, 689, 3242. (e) Luguya, R.; Fronczek, F. R.; Smith, K. M.; Vicente, M. G. H. Appl. Radiat. Isot. 2004, 61, 1117. (f) Clark, J. C.; Fronczek, F. R.; Vicente, M. G. H. Tetrahedron Lett. 2005, 46, 2365.

[18] (a) Newkome, G. R.; Moorefield, C. N.; Keith, J. M.; Baker, G. R.; Escamilla, G. H. Angew. Chem., Int. Ed. Engl. 1994, 33, 666. (b) Barth, R. F.; Adamns, D. M.; Solovay, A. H.; Alam, F.; Darby, M. V. Bioconjugate Chem. 1994, 5, 58. (c) Armspach, D.; Cattalini, M.; Constable, E. C.; Housecroft, C. E.; Phillips, D. Chem. Commun. 1996, 1823. (d) Qualman, B.; Kessels, M. M.; Musiol, H.-J.; Sierralta, W. D.; Jungblut, P. W.; Moroder, L. Angew. Chem., Int. Ed. Engl. 1996, 35, 909. (e) Parrott, M. C.; Marchington, E. B.; Valliant, J. F.; Adronov, A. J. Am. Chem. Soc. 2005, 127, 12081. (f) Nun˜ez, R.; GonzaÂ´lez, A.; Viñas, C.; Teixidor, F.; Sillanpää, R.; Kivekäs, R. Org. Lett. 2005, 7, 231. (g) Nun˜ez, R.; GonzaÂ´lez, A.; Viñas, C.; Teixidor, F.; Sillanpää, R.; Kivekäs, R. Organometallics 2005, 24, 6351.

[19] E. Justus, K. Rischka, J. Wishart, K. Werner, D. Gabel, *Chem. Eur. J.* **2008**, *14*, 1918-1923.

[20] (a) T. K. Vinod, H. Hart, *J. Org. Chem.* **1991**, *56*, 5630. (b) P. Rajakumar, M. Dhanasekaran, S. Selvanayagam, V. Rajakannan, D. Velmurugan, K. Ravikumar, *Tetrahedron Lett.* **2005**, *46*, 995.

d) Anchoring Phosphorous-containing Cobaltabisdicarbollide Derivatives on Titania Particles.

Anchoring of Phosphorous-containing Cobaltabisdicarbollide Derivatives on Titania Particles.

Emilio José Juárez-Pérez,[a#] Hubert Mutin,[b] Michel Granier,[b] Francesc Teixidor[a] and Rosario Núñez[a]*

[a]*Institut de Ciència de Materials de Barcelona CSIC, Campus UAB, E-08193 Bellaterra, Spain. E-mail: rosario@icmab.es*

[b]*Institut Charles Gerhardt Montpellier, UMR5253 CNRS-UM2-ENSCM-UM1, Université de Montpellier 2, Place Eugène Bataillon, F-34095 Montpellier Cedex 5, France.*

Received Date (inserted by publisher)
Revised Received Date (inserted by publisher)

The cobaltabisdicarbollide anion, $[3,3\text{-}Co(1,2\text{-}C_2B_9H_{11})_2]^-$, is a sandwich complex characterized by an outstanding chemical and thermal stability.[1] Two different substitutions can be carried out on the cobaltabisdicarbollide, either on carbon or on boron. Few examples have been reported concerning the direct substitutions on carbon atoms (C_c).[2] Conversely, numerous cobaltabisdicarbollide derivatives have been prepared by substitution at boron atoms.[3] Cobaltabisdicarbollide has been shown to be an hydrophobic, weakly coordinating anion with a low nucleophilicity.[4] This anion has been proposed in a wide range of applications such as doping agent in conducting polymers[5] or extractant of radionuclides[6]. Recently, our group has reported the use of cobastabisdicarbollide in ion selective PVC membrane electrodes for tuberculosis drug analysis.[7]

In this paper, we report on the anchoring of cobaltabisdicarbollide derivatives at the surface of TiO_2 particles. Organophosphorus compounds (phosphates, phosphonates and phosphinates) have been shown to be attractive coupling molecules for the modification of titanium dioxide surfaces,[8,9] offering a valuable alternative to the employ of organosilanes, carboxylic acids or organotitanates.[10] Bonding of organophosphorus acids to the surface results from the formation of Ti-O-P bridges by condensation of P-O-H groups with surface hydroxyl groups and coordination of the phosphoryl groups to surface Lewis acidic sites.[11]

Accordingly, two different cobaltabisdicarbollide-phosphorylated derivatives $[1,1'\text{-}\mu\text{-}(HO)(O)P\text{-}3,3'\text{-}Co(1,2\text{-}C_2B_9H_{10})_2]^-$, (**1**), and $[8,8'\text{-}\mu\text{-}(OH)(O)\text{-}P(O)_2\text{<}(1,2\text{-}C_2B_9H_{10})_2\text{-}3,3'\text{-}Co]^-$, (**2**), were prepared with the aim to anchor them to the surface of TiO_2 particles (Figure 1).

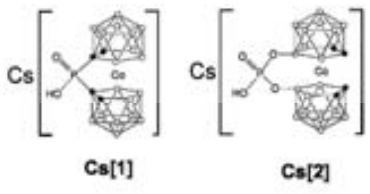

Figure 1. Phosphinate Cs(**1**) and phosphate Cs(**2**) derivatives of cobaltabisdicarbollide.

The anionic phosphinate derivative **1** has been prepared, for the first time, by metallation of $[3,3\text{-}Co\text{-}(1,2\text{-}C_2B_9H_{10})_2]^-$ with *n*-BuLi followed by simple reaction with $Cl_3P(O)$ in 1,2-dimethoxyethane (DME) at room temperature. After treatment with a solution of NaOH and corresponding work-up, compound Cs[**1**] was isolated as a red solid in 82% yield.[12] A similar procedure for attaching

(1) (a) Hawthorne, M. F.; Andrews, T. D. *J. Chem. Soc., Chem. Commun.* **1965**, 443. (b) Sivaev, I. B.; Bregadze, V. I. *Collect. Czech. Chem. Commun.* **1999**, *64*, 783.

(2) (a) Chamberlin, R. M.; Scott, B. L.; Melo, M. M.; K. Abney, D. *Inorg. Chem.* **1997**, *36*, 809. (b) Rojo, I.; Teixidor, F.; Viñas, C.; Kivekäs, R.; Sillanpää, R. *Chem. Eur. J.* **2004**, *10*, 5376. (c) Juárez-Pérez, E. J.; Viñas, C.; González-Campo, A.; Teixidor, F.; Kivekäs, R.; Sillanpää R.; Núñez, R. *Chem. Eur. J.* **2008**, *14*, 4924. (d) Juárez-Pérez, E. J.; Teixidor, F.; Viñas, C.; Núñez R.; *J. Organomet. Chem.* **2009**, DOI: 10.1016/j.jorganchem.2008.12.022.

(3) (a) Janousek, Z.; Plesek, J.; Hermanek, S.; Base, K.; Todd, L.; Wright, W. F. *Collect. Czech. Chem. Commun.* **1981**, *46*, 2818. (b) Plesek, J.; Hermanek, S.; Franken, A.; Cisarova, I.; Nachtigal, *C. Collect. Czech. Chem. Commun.* **1997**, *62*, 47. (c) Rojo, I.; Teixidor, F.; Viñas, C.; Kivekäs, R.; Sillanpää, R. *Chem. Eur. J.* **2003**, *9*, 4311. (d) F. Teixidor, J. Pedrajas, I. Rojo, C. Vinas, R. Kivekas, R. Sillanpaa, I. Sivaev, V. Bregadze, S. Sjoberg, *Organometallics* **2003**, *22*, 3414-3423.

(4) (a) Ma, L.; Hamdi, J.; Hawthorne, M. F. *Inorg. Chem.* **2005**, *44*, 7249. (b) Matejicek, P.; Cigler, P.; Procházka, K.; Kral, V. *Langmuir*, **2006**, *22*, 575. (c) Chevrot, G.; Schurhammer, R.; Wipff, G. *J. Phys. Chem. B* **2006**, *110*, 9488. (d) Strauss, S. H. *Chem. Rev.* **1993**, *93*, 927. (e) Reed, C. A. *Acc. Chem. Res.* **1998**, *31*, 133.(f) Masalles, C.; Llop, J.; Viñas, C.; Teixidor, F. *Adv. Mater.* **2002**, *14*, 826.

(5) (a) Borrós, S.; Llop, J.; Viñas, C.; Teixidor, F. *Adv. Mater.* **2002**, *14*, 449. (b) Crespo, E.; Gentil, S.; Viñas, C.; Teixidor, F. *J. Phys. Chem. C* **2007**, 111, 18381. (c) Errachid, A.; Caballero, D.; Crespo, E.; Bessueille, F.; Pla-Roca, M.; Mills, C.; Christopher, A.; Teixidor, F; Samitier, J. *Nanotechnology* **2007**, *18*, 485301.

(6) (a) Grüner, B.; Plesek, J.; Baca, J.;Cisarova, I.; Dozol, J.-F; Rouquette, H.; Viñas, C.; Selucky, P.; Rais, J. *New J. Chem.* **2002**, *26*, 1519. (b) Rais, J.; Grüner, B. in Ion Exchange and Solvent Extraction, eds. Y. Marcus and A. K. Sengupra, CRC Press, Boston, 2004, vol. 17, 243. (c) Mikulasek, L.; Grüner, B.; Crenguta, D.; Rudzevich, V.; Boehmer, V.; Haddaoui, J.; Hubscher-Bruder, V.; Arnaud-Nue, F.; Caslavsky, J.; Selucký, P. *Eur. J. Org. Chem.* **2007**, 4772.

(7) Stoica, A. I.; Viñas, C.; Teixidor, F. *Chem. Commun.* **2008**, *48*, 6492.

(8) (a) Hofer, R.; Textor, M.; Spencer, N. D. *Langmuir* **2001**, *17*, 4014. (b) Randon, J.; Blanc, P.; Paterson, R. *J. Membrane Sci.* **1995**, *98*, 119. (c) Pechy, P.; Rotzinger, F. P.; Nazeeruddin, M. K.; Kohle, O.; Zakeeruddin, S. M.; Humphrybaker, R.; Gratzel, M. *Chem. Commun.* **1995**, 65. (d) Gao, W.; Dickinson, L.; Grozinger, C.; Morin, F. G.; Reven, L. *Langmuir* **1996**, *12*, 6429.

(9) Guerrero, G.; Mutin, P.; Vioux, A. *Chem. Mater.* **2001**, *13*, 4367.

(10) Plueddemann, E. P. *Silane Coupling Agents*; Plenum Press: New York, 1991.

(11) (a) Mutin, P.H.; Guerrero, G.; Vioux, A. *J. Mater. Chem.* **2005**, *15*, 3761. (b) Brodard-Severac, F.; Guerrero, G.; Maquet, J.; Florian, P.; Gervais, C.; Mutin, P. H. *Chem. Mater.* **2008**, 20, 5191.

.

(12) *Synthesis of [1,1'-μ-(HO)(O)P(1,2-$C_2B_9H_{10}$)$_2$-3,3'-Co]Cs, Cs[**1**].* *n*BuLi (0.49 mL, 0.79 mmol) was added dropwise to a Schlenk flask containing a stirred solution of $[3,3'\text{-}Co(1,2\text{-}C_2B_9H_{11})_2]Cs$ (180 mg, 0.39 mmol) in DME (12mL) at -78 C. The low-temperature bath was removed and the purple suspension was stirred for 45 min. The suspension was then

chlorodiphenylphosphines directly to the $C_{cluster}$ (C_c) atoms was previously reported by our group.[2b] The anionic phosphate **2** was prepared according to literature procedures.[13] The ^{11}B, ^{1}H and ^{31}P NMR spectra of **1** agree well with the proposed structure shown in Figure 1. The ^{11}B NMR spectrum of **1** a 1:1:1:1:1:1:1:2 pattern (see Figure 2) in the range in the range +8.0 to -17.0 ppm indicative of a *closo* species with all boron atoms in non-equivalent vertexes. This could seem surprising, since both dicarbollide ligands are bonded to a phosphinic group through the C_c atoms suggesting a *cisoide* conformation with the presence of a symmetry plane. However, as it was previously reported by our group, the crystal structure of a cobaltabisdicarbollide with a phenylphosphine oxide group, showed that both C_2B_3 faces are eclipsed and rotated 72º between them.(REf. Isabel) On the contrary, the ^{11}B NMR of **2** displays a different 1:1:2:2:2:1 pattern in the range +23.5 to -28.0 ppm.[13] The boron resonances with a relative intensity of 2 are due to a coincidental overlap of two resonances, and the low field peak at +23.5 ppm is assigned to the boron atoms B(8) bonded to oxygen. The ^{31}P NMR spectra show only one resonance at +47.48 ppm for **1** and at -5.29 ppm for **2**. Finally, the ^{1}H NMR for **1** displays a broad singulet at 4.17 ppm atributed to the C_c-H protons and a peak at 3.36 ppm due to the P(OH) group.

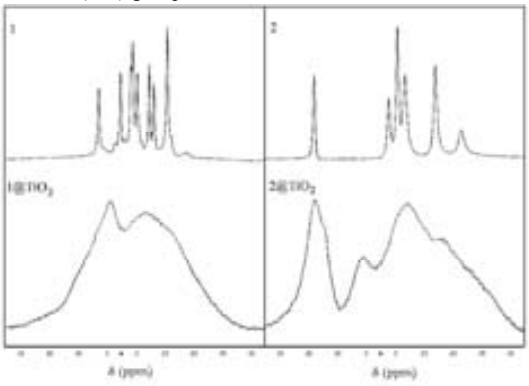

Figure 2. Solution ^{11}B NMR spectra for coupling molecules **1** and **2** (up) and ^{11}B MAS NMR solid spectra for modified titania particles **1@TiO₂** and **2@TiO₂** (down).

cooled to - 78 ºC and $Cl_3P(O)$ (0.05 mL, 0.40 mmol) was added dropwise. The suspension was stirred at room temperature for 3 h to give a red solution and a white solid. The solid was filtered off and the solution concentrated in vacuum. The residue was dissolved in a solution of NaOH in water (10ml, 0.1 M) and the mixture was stirred over a period of 2 h at room temperature, transferred to a separatory funnel, and extracted with Et_2O, concentrated in vacuum and an aqueous solution of CsCl (135 mg, 7 mL) was added dropwise to give an red solid. The solid was washed with H_2O (2 x 15 mL) and hexane (2 x 15 mL). (yield: 178 mg, 82%). ^{1}H {^{11}B} NMR: δ 4.17 (br s, 2H; C_c-H), 3.36 (br s, 1H; P-OH); ^{13}C{^{1}H} NMR: δ 50.94 (Cc-H); ^{11}B NMR: δ 7.67 (d, ^{1}J(H, B) = 149, 2B), 0.07 (d, ^{1}J(H, B) = 147, 2B), -3.58 (d, ^{1}J(H, B) = 158, 2B), -4.13 (d, ^{1}J(H,B) = 153, 2B), -5.72 (d, ^{1}J(H, B) = 178, 2B), -9.90 (d, ^{1}J(H, B)= 153, 2B), -11.54 (d, ^{1}J(H, B) = 188, 2B), -16.21 (d, ^{1}J(H, B) = 162, 2B); ^{31}P{^{1}H} NMR: δ 47.48 ppm; IR: υ=3042 (C_c H), 2538 (B H), 1597, 995, 870, 736.

(13) J. Plesek, B. Gruner, I. Cisarova, J. Baca, P. Selucky, J. Rais, *J. Organomet. Chem.* **2002**, *657*, 59.

Phosphorus-containing anions **1** and **2** have been used to modify the surface of titanium dioxide particle, following an experimental procedure previously described.[9] The TiO_2 particles were reacted with a solution of the phosphate or phosphinate coupling molecules in a 5-fold excess relative to the amount needed for a full surface coverage on the particles (assuming an area of 160 $Å^2$ per molecule).[14] After anchoring **1** an **2** on the TiO_2 surface, materials **1@TiO₂** and **2@TiO₂** were obtained (Figure 3) and studied by infrared, ^{31}P and ^{11}B NMR spectroscopies.

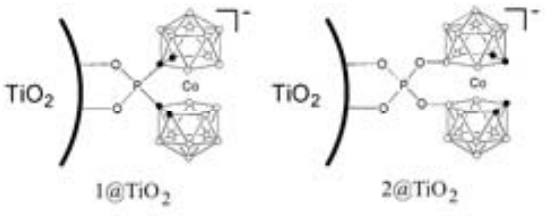

Figure 3. Modified titania particles with cobaltabisdicarbollide derivatives.

The IR spectra in the 2400-3100 cm^{-1} Where are these spectra? and 800-1400 cm^{-1} regions of the modified titania particles and those of the starting coupling molecules are given in Figure 4.

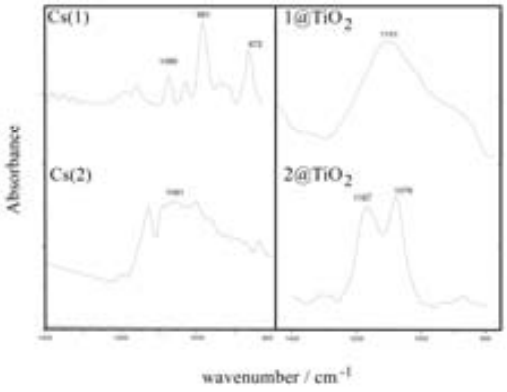

Figure 4. IR spectra of the coupling molecules **1** and **2** (left) and modified titania particles **1@TiO₂** and **2@TiO₂** (right).

A broad stretching band characteristic of the υ(B-H) is observed at 2540 cm^{-1} in **1** and the respective modified **1@TiO₂**, whereas this band appears around 2560 cm^{-1} in **2** and **2@TiO₂**. The presence of these bands clearly indicates that cobaltabisdicarbollide derivatives have been attached to the TiO_2 surface. The spectra in the P-O stretching region appear quite different after anchoring on titania. The coupling molecule **1** shows intense bands at 872 and

(14)*Preparation of the sample*. **1** or **2** (0.233 mmol) was dissolved in a flask with 375 mL of ethanol and 125 mL of water, and a suspension of 1 g of TiO_2 in 100 mL of water was added. The resulting suspension was stirred at room temperature for 5 days. After modification, the anchored TiO_2 particles were filtered off, washed successively with EtOH, acetone, and Et_2O to remove unreacted or physisorbed coupling molecules, and dried under vacuum (110 °C, 5 h, 10^{-2} mbar).

991cm^{-1} ascribed to P-OH stretching, whereas the modified particle presents a very broad P-O stretching band between 900 and 1200 cm^{-1}. The disappearance of the P=O band near 1200-1250 cm^{-1} suggests the coordination of the phosphoryl oxygen functions to surface Lewis acid sites, leading to bidentate phosphinate units.

^{11}B NMR spectroscopy has proven to be a powerful tool for the study of boron-containing compounds both in the liquid and in the solid state. In solid, this technique has been applied to borosilicate glasses, boron halides and organoboron compounds, but there are very few examples in the literature for boron hydrides.[15] The ^{11}B MAS NMR spectra of modified TiO_2 particles are given in Figure 2. The ^{11}B MAS NMR spectra for **1@TiO$_2$** and **2@TiO$_2$** show very broad resonances typical of amorphous compounds However, the ^{11}B resonances appear in the same region as for the starting anions, which confirms the presence of cobaltabisdicarbollide units anchored to the TiO_2 surface. In the ^{11}B MAS NMR spectrum of **2@TiO$_2$** the resonance at at 25 ppm, corresponding to B(8) boron atoms bonded to O atoms is clearly distinguished, indicating that molecule **2** has been efficiently attached to the TiO_2 surface.

The ^{31}P MAS NMR spectrum (Figure 5) of the modified particle **1@TiO$_2$** shows a major resonance around 21 ppm and could be attributed to $(C_c)_2P(OTi)_2$, that was upfield shifted compared to the starting compound **1** (47.48 ppm). A minor peak around 5 ppm was also observed, that could result from the photodegradation of the phosphinate group, as previously reported for $Ph_2P(O)(OH)$ anchored to TiO_2.[11] The ^{31}P MAS NMR of **2@TiO$_2$** displayed a resonance centered at -11.5 ppm, upfield shifted compared to the starting compound **2** (-5.29 ppm).

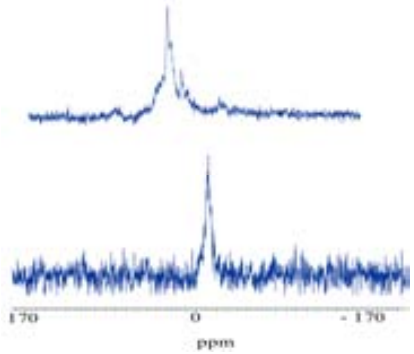

Figure 5. ^{31}P MAS NMR spectra of **1@TiO$_2$** (up) and **2@TiO$_2$** (down).

This work has been supported by the CICYT (MAT2006-05339) and the Generalitat de Catalunya, 2005/SGR/00709. E.J.J.P. thanks to Ministerio de Educación y Ciencia for a FPU grant.

(15) Tiritris, I.; Schleid, T.; Müller, K. *Appl. Magn. Reson.* **2007**, *32*, 459.

e) Approaches For Anchoring Cobaltabisdicarbollide Anions Onto Oxidized Silicon Wafers.

Approaches For Anchoring Cobaltabisdicarbollide Anions Onto Oxidized Silicon Wafers.

Emilio José Juárez-Pérez,[a#] *Michel Granier,*[b] *Hubert Mutin,*[b] *Clara Viñas,*[a] *Rosario Núñez*[a*]

[a] Institut de Ciència de Materials, CSIC, Campus U.A.B., 08193 Bellaterra, Spain

Email address: rosario@icmab.es

RECEIVED DATE (to be automatically inserted after your manuscript is accepted if required according to the journal that you are submitting your paper to)

Corresponding Author: Dr. Rosario Núñez, Institut de Ciència de Materials, CSIC, Campus U.A.B., 08193 Bellaterra, Barcelona, Spain. Tel.: +34 93 580 1853. Fax: +34 93 580 5729. rosario@icmab.es

[#] Enrolled in the UAB PhD program.

Introduction

The recent emergence on applications of carboranes as materials for nanotechnology and pharmacophores in drug design has expanded the potential use of boron clusters in practice.[1] The cobaltabisdicarbollide [3,3-Co(1,2-$C_2B_9H_{11})_2]^-$,**(1)**$^-$, is a sandwich complex characterized by its extraordinary chemical and thermal stability. Two different substitutions can be carried out on the cobaltabisdicarbollide, either on carbon or on boron. Few examples have been reported concerning the direct substitutions on carbon atoms,[2] however, a large number of cobaltabisdicarbollide derivatives have been prepared by substitution at boron.[3,4] The zwitterionic dioxane-metallacarborane derivative, [8-$O(CH_2CH_2)_2$O-3,3'-Co(1,2-C_2B_9-H_{10})(1',2'-$C_2B_9H_{11}$)], **(2)**, has been easily prepared with very good yield,[5] and has been proven to be susceptible to nucleophilic attack on the oxygen atom, by different nucleophiles causing the opening of the dioxane ring.[6] As a consequence, compound **(2)** has been attached to different organic groups and biomolecules, such as nucleosides,[7] porphirines[8] and calixarenes.[9] Cobaltabisdicarbollide **(1)** has shown to be hydrophobic,[10] a weakly coordinating[11] and low nucleophilic anion,[12] that makes it suitable for stabilisation of transient complex cation particles in catalysis and for using as strong non-oxidizing acids,[13] or solid electrolytes. It has been proposed in a wide range of applications such as doping agents in conducting polymers[14] extractants of radionuclides,[15] or to be used in medicine.[16] Derivatives of this polyhedral metallacarborane have been recognized as potent and specific inhibitors of HIV protease.[17] Recently, Teixidor *et al.* has reported the use of cobastabisdicarbollide in ion selective PVC membrane electrodes for tuberculosis drug analysis.[18] Great expectations have risen from these promising pharmaceutical tectons, and works about their type of binding in solid state, or association in solution, are been developed in order to understand the behaviour of this borane compounds facing biological mechanisms.[19].

In this paper, we report on grafting **(2)** to different types of SiO_2 surfaces (silica gel, quartz and wafers) by using dioxane ring-opening reaction based on the use amines and cyanide, covalently attached to the surface, as nucleophiles.

Experimental Part

Materials

All manipulations were carried out under a dinitrogen atmosphere using standard Schlenck techniques at room temperature otherwise it is mentioned. Solvents were reagent grade and were purified by distillation from appropriate drying agents before using. Cs[3-Co-1,2-($C_2B_9H_{11})_2$] was supplied by Katchem Ltd. (Prague) and used as received. (11-aminooxy)undecyltrimethoxysilane was purchased from Sigma and used as received. 10-Isocyanatodecyltrichlorosilane,[20] [3,3'-Co(8-$C_4H_8O_2$-1,2-$C_2B_9H_{10}$)(1',2'-$C_2B_9H_{11}$)],[3] (**1**), and [8-NH_2-$C_4H_8O_2$-3,3-Co(1,2-$C_2B_9H_{10}$)(1,2-$C_2B_9H_{11}$)]H, (**2**),[6a] were prepared according to the literature procedures. Silica gel with pore size of 60 Å and particle size of 40-63 μm (230-400 mesh) purchased from SDS (Chromagel)

Grafting of cobaltabisdicarbollide on Silica gel particles using *In situ* Dioxane ring opening for surface functionalization.

Silica gel was activated by refluxing in a mixture of concentrated HCl and distilled water (1:1) for 5 h, and then washed thoroughly with distilled water and dried at 110 °C for 2 h under vacuum. The activated silica (0.25 g) was added to a solution of (11-aminooxy)undecyltrimethoxysilane in dry trichloroethylene (10 ml, 0.12 M) and stirred for 24 h at room temperature. After, a solution of (**1)** (575 mg**,** 1.4 mmol) in trichloroethylene (5 ml) was added and stirred for 6 h. at room temperature. The functionalized silica was filtered off, washed with THF, EtOH, CH_3Cl, H_2O and Et_2O following this order, and dried in vacuum at room temperature for 5 h to give a light orange silica.

Grafting of cobaltabisdicarbollide on Si(100) and quartz surfaces using *In situ* Dioxane ring opening for surface functionalization .

(a) Preparation of Oxidized Silicon Si(100) and quartz Surfaces. The native oxide layer was removed from the Si(100) by immersion in aqueous HF solution (40%) until total dewetting of the surface (about 10 s). The substrates were cleaned by rinsing with HPLC water. The substrates were then exposed to a homebuilt UV-ozone chamber. This technique is well-known to eliminate all organic impurities from a surface but was also used to oxidize silicon and obtain a hydrated flat silica surface free from organic pollution. The wafers were placed at a maximum distance of 5 mm from a two-wavelength low-pressure mercury lamp (λ = 185 and 254 nm) under an O_2 stream. The quartz wafer follows a similar process without HF solution treatment. After 30 min. of exposition, a hydrophilic silica surface (contact angle θ 10°) was obtained. The thickness, measured by ellipsometry, was about 1.8–2.0 nm and the roughness, measured by tapping mode atomic force microscopy, was about 0.15 nm.

(b) Grafting of (**1**) on the oxidized silicon surface and quartz. The oxidized silicon wafer (or quartz wafer) was placed into a Schlenk tube under a nitrogen atmosphere. The grafting solution containing (11-aminooxy)undecyltrimethoxysilane (10^{-2} M) in 10 mL trichloroethylene and one drop of diisopropylethylamine solution (1M). The wafer was treated with the solution at 0 °C for 24 h. under a nitrogen atmosphere without stirring. Then, the solution was removed and a solution containing (**1**) (205 mg, 0.5 mmol) in trichloroethylene (5 ml) was added. After 48 h. the wafer was washed with trichloroethylene, THF, again trichloroethylene and chloroform under sonication.

Grafting of cobaltabisdicarbollide on Si(100) surfaces using compound 2. Pre-opening of Dioxane ring and functionalization forming group -NH-C=O-NH- .

(a) The preparation of Oxidized Silicon Si(100) Surface follows identical procedure as above.

(b) Grafting of 10-Isocyanatodecyltrichlorosilane on the Oxidised Silicon Surface. The oxidised silicon wafer was placed into a Schlenk under a nitrogen atmosphere. The grafting solution containing 10-isocyanatodecyltrichlorosilane (10^{-2}M) in 10 mL of TCE and diisopropylethylamine (2 x 10^{-1} M) in trichloroethylene (5 ml) was introduced into the tube. The wafer was treated with the solution at 0 °C for 45 min under a nitrogen atmosphere without stirring. Then, the solution was removed, and the wafer was washed with trichloroethylene, THF and trichloroethylene again.

(c) Reaction of the Immobilised Isocyanate with **2**.

After washing the wafer surface in the Schlenk tube, a solution containing **2** (64mg, 10^{-2}M) in trichloroethylene (15 mL) was introduced. The wafer was treated with the solution at 0 °C for 2 h under a nitrogen atmosphere. Then, the solution was removed, and the wafer was rinsed with methanol (5 min), THF (5 min), trichloroethylene (5 min) and dried in a stream of nitrogen.

---

(1) (a) Endo, Y.; Yoshimi, T.; Miyaura, C. *Pure Appl. Chem.* **2003**, *5*, 1197. (b) Crossley, E. L.; Ziolkowski, E. J.; Coderre, J. A.; Rendina, L. M. *Mini-Rev. Med. Chem.* **2007**, *7*, 3003. (c) Julius, R. L.; Farha, O. K.; Chiang, J.; Perry, L. J.; Hawthorne, M. F. *Proc. Natl. Acad. Sci. U.S.A.* **2007**, *104*, 4808.

(2) (a) Chamberlin, R. M.; Scott, B. L.; Melo, M. M.; K. Abney, D. *Inorg. Chem.* **1997**, *36*, 809. (b) Rojo, I.; Teixidor, F.; Viñas, C.; Kivekäs, R.; Sillanpää, R. *Chem. Eur. J.* **2004**, *10*, 5376. (c) Juárez-Pérez, E. J.; Viñas, C.; González-Campo, A.; Teixidor, F.; Kivekäs, R.; Sillanpää R.; Núñez, R. *Chem. Eur. J.* **2008**, *14*, 4924. (d) Juárez-Pérez, E. J.; Teixidor, F.; Viñas, C.; Núñez R.; *J. Organomet. Chem.* **2009**, DOI: 10.1016/j.jorganchem.2008.12.022.

(3) Francis, J. N.; Hawthorne, M. F. *Inorg. Chem.* **1971**, *10*, 594.

(4) (a) Plesek, J.; Hermanek, S.; Base, K.; Todd, L. J.; Wright, W. F. *Collect. Czech. Chem. Commun.* **1976**, *41*, 3509. (b) Janousek, Z.; Plesek, J.; Hermanek, S.; Base, K.; Todd, L.; Wright, W. F. *Collect. Czech. Chem. Commun.* **1981**, *46*, 2818. (c) Rojo, I.; Teixidor, F.; Viñas, C.; Kivekäs, R.; Sillanpää, R. *Chem. Eur. J.* **2003**, *9*, 4311.

(5) (a) Selucky, P.; Plesek, J.; Rais, J.; Kyrs, M.; Kadlecova, L. *J. Radioanal. Nucl. Chem.* **1991**, *149*, 131. (b) Plesek, J.; Hermanek, S.; Franken, A.; Cisarova, I.; Nachtigal, C. *Collect. Czech. Chem. Commun.* **1997**, *62*, 47. (c) F. Teixidor, J. Pedrajas, I. Rojo, C. Vinas, R. Kivekas, R. Sillanpaa, I. Sivaev, V. Bregadze, S. Sjoberg, *Organometallics* **2003**, *22*, 3414-3423.

(6) (a) Sivaev, I. B.; Starikova, Z. A.; Sjöberg S.; Bregadze, V. I. *J. Organomet. Chem.* **2002**, *649*, 1. (b) Sivaev, I. B.; Sjöberg S.; Bregadze, V. I., International Conference Organometallic Compounds - Materials of the Next Century, Nizhny Novgorod, Russia, May 29-June 2, **2000**. (c) Plešek, J.; Grüner, B.; Heřmánek, S.; Báča, J.; Mareček, V.; Jänchenová, J.; Lhotský, A.; Holub, K.; Selucký, P.; Rais, J.; Císařová I.; Čáslavský, J. *Polyhedron* **2002**, *21*, 975. (d) Llop, J.; Masalles, C.;Viñas, C.; Teixidor, F.; Sillanpää R.; Kivekäs, R. *Dalton Trans.* **2003**, 556. (e) Grüner, B.; Mikulašek, L.; Bača, J.; Cisařova, I.; Böhmer, V.; Danila, C.; Reinoso-Garcia, M. M.; Verboom, W.; Reinhoudt, D. N.;

Casnati, A.; Ungaro, R. *Eur. J. Org. Chem.* **2005**, 2022. (f) Mikulášek, L.; Grüner, B.; Danila, C.; Böhmer, V.; Časlavsky, J.; Selucky, P. *Chem. Commun.* **2006**, 4001. (g) Farràs, P.; Teixidor, F.; Kivekäs, R.; Sillanpää, R.; Viñas, C.; Grüner, B.; Cisarova I.; *Inorg. Chem.*, **2008**, *47*, 9497. (h) Šícha, V.; Farràs, Pau.; Štíbr, B.; Teixidor, F.; Grüner, B.; Viñas C. *J. Organomet. Chem.*, **2009**, DOI: 10.1016/j.jorganchem.2008.10.059.

(7) (a) Olejniczak, A. B.; Plesek, J.; Kriz, O.; Lesnikowski, Z. J. *Angew. Chem. Int. Ed.* **2003**, *42*, 5720. (b) Lesnikowski, Z.; Paradowska, E.; Olejniczak, A. B.; Studzinska, M.; Seekamp, P.; Schüβler, U.; Gabel, D.; Schinazi, R. F.; Plesek, J.; *Bioorg. Med. Chem.* **2005**, *13*, 4168. (c) Olejniczak, A. B.; Plesek, J.; Lesnikowski, Z. J. *Chem. Eur. J.* **2007**, *13*, 311.

(8) (a) Sibrian-Vazquez, M.; Hao, E.; Jenssen, T. J.; Vicente, M.G. H. *Biocong. Chem.* **2006**, 17, 928. (b) Hao, E.; Sibrian-Vazquez, M.; Serem, W.; Garno, J. C.; Fronczek F. R.; Vicente, M. G. H. *Chem. Eur. J.* **2007**, *13*, 9035. (c) Li, F.; Fronczek, F. R.; Vicente, M. G. H. *Tetrah. Lett.*, **2008**, *49*, 4828.

(9) Grüner, B.; Mikulásek, L; Báca, J.; Císarová, I.; Böhmer,V.; Danila, C.; Reinoso-García, M.; Verboom, W.; Reinhoudt, D. N.; Casnati, A. Ungaro R. *Eur. J. Org. Chem.* **2005**, 2022.

(10) (a) Ma, L.; Hamdi, J.; Hawthorne, M. F. *Inorg. Chem.* **2005**, *44*, 7249. (b) Matejicek, P.; Cigler, P.; Procházka, K.; Kral, V. *Langmuir*, **2006**, *22*, 575. (c) Chevrot, G.; Schurhammer, R.; Wipff, G. *J. Phys. Chem. B* **2006**, *110*, 9488.

(11) (a) Strauss, S. H. *Chem. Rev.* **1993**, *93*, 927. (b) Reed, C. A. *Acc. Chem. Res.* **1998**, *31*, 133.

(12) Masalles, C.; Llop, J.; Viñas, C.; Teixidor, F. Adv. Mater. **2002**, *14*, 826.

(13) Plesek, J. *Chem. Rev.* **1992**, *92*, 269.

(14) (a) Masalles, C.; Borrós, S.; Viñas, C.; Teixidor, F., *Adv. Mater.* **2000**, *12*, 1199. (b) Borrós, S.; Llop, J.; Viñas, C.; Teixidor, F. Adv. Mater. **2002**, *14*, 449. (c) Gentil, S., Crespo, E., Rojo, I.; Friang, A.; Viñas, C., Teixidor, F.; Grüner, B.; Gabel, D. *Polymer* **2005**, *46*, 12218. (d) Crespo, E.; Gentil, S.; Viñas, C.; Teixidor, F. *J. Phys. Chem. C* **2007**, *111*, 18381. (e) Errachid, A.; Caballero, D.; Crespo, E.; Bessueille, F.; Pla-Roca, M.; Mills, C.; Christopher, A.; Teixidor, F; Samitier, J. *Nanotechnology* **2007**, *18*, 485301.

(15) (a) Grüner, B.; Plesek, J.; Baca, J.;Cisarova, I.; Dozol, J.-F; Rouquette, H.; Viñas, C.; Selucky, P.; Rais, J. *New J. Chem.* **2002**, *26*, 1519. (b) Rais, J.; Grüner, B. in *Ion Exchange and Solvent Extraction*, eds. Y. Marcus and A. K. Sengupra, CRC Press, Boston, **2004**, vol. *17*, 243. (c) Mikulasek, L.; Grüner, B.; Crenguta, D.; Rudzevich, V.; Boehmer, V.; Haddaoui, J.; Hubscher-Bruder, V.; Arnaud-Nue, F.; Caslavsky, J.; Selucký, P. *Eur. J. Org. Chem.* **2007**, 4772.

(16) a) Hao, E.; Vicente, M. G. H. *Chem. Commun.* **2005**, 1306. b) Barth, R. F.; Coderre, J. A.; Vicente, M. G. H.; Blue, T. E. *Clin. Cancer Res.* **2005**, *11*, 3987. c) Gottumukkala, V., Ongayi, O.; Baker, D. G.; Lomax, L. G.; Vicente, M. G. H. *Bioorg. Med. Chem.* **2006**, *14*, 1871. d) Wang, J.-Q.; Ren, C.-X.; Weng, L.-H.; Jin, G.-X. *Chem. Commun*. **2006**, 162. e) Bregadze, V. I.; Sivaev, I. B.; Glazun, S. A. *Anti-Cancer Agents Med. Chem.*, **2006**, *6*, 75.

[17] Cígler, P.; Kozisek, M.; Rezacova, P.; Brynda, J.; Otwinowski, Z.; Pokorná, J.; Plesek, J.; Grüner, B.; Dolecková-Maresová, L.; Masa, M.; Sedlácek, J.; Bodem, J.; Kräusslich, H.-G.; Král, V.; Konvalinka, J. *Proc. Natl. Acad. Sci. U.S.A.* **2005**, *102*, 15394.

[18] Stoica, A. I.; Viñas, C. ; Teixidor, F. *Chem. Commun.* **2008**, 48, 6492**.**

[19] a) Fanfrlík, J.; Lepsik, M.; Horinek, D.; Havlas, Z.; Hobza, P. *ChemPhysChem* 2006, *7*, 1100. b) Fanfrlík, J.; Hnyk, D.; Lepsik, M.; Hobza, P. *Phys. Chem. Chem. Phys.,* **2007**, *9*, 2085. c) Fanfrlík, J; Brynda, J.; Rezac, P.; Hozba, M.; Lepsik, M. *J. Phys. Chem. B.* **2008**, *112*, 15094.

(20) (a) N. Ardes-Guisot, J. Durand, M. Granier, A. Perzyna, Y. Coffinier, B. Grandidier, X. Wallart, D. Stievenard, *Langmuir* **2005**, *21*, 9406-9408. (b) Perzyna, A.; Zotto, C.; Durand J.O.; Granier, M.; Smietana, M.; MeInyk, O.; Stara, I.G.; Stary, I.; Klepetarova, B.; Saman, D.; *Eur. J. Org. Chem.* **2007**, *24*, 4032.

Scheme 1.

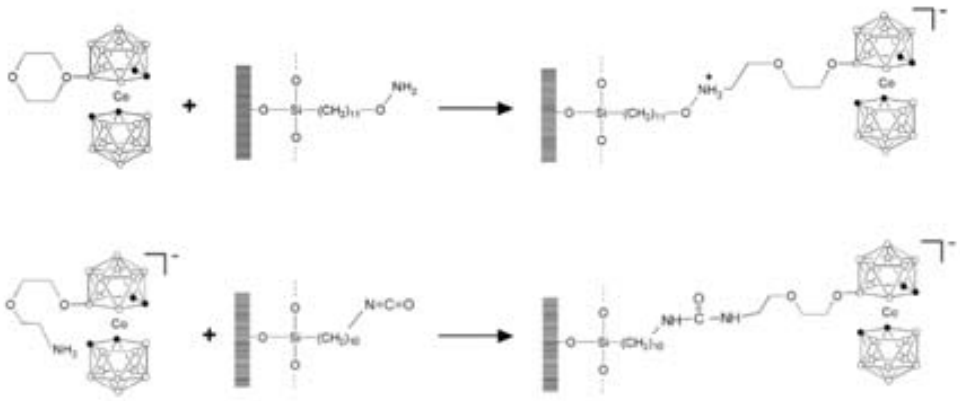

Figure 1. ATR-FTIR measurements for the anchoring process of **1**@wafer.

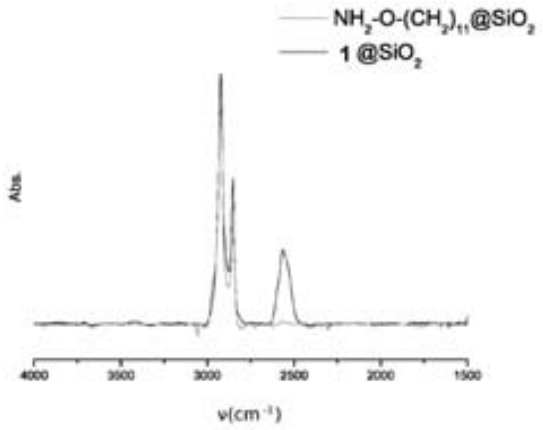

Figure 2. ATR-FTIR measurements for the anchoring process of **2**@wafer.

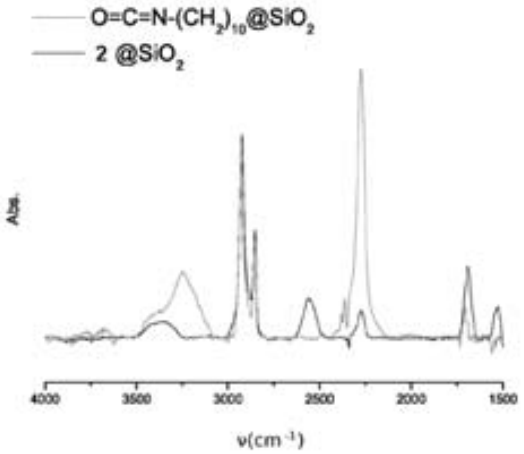

Figure 3. UV measurements of **1**@quarz

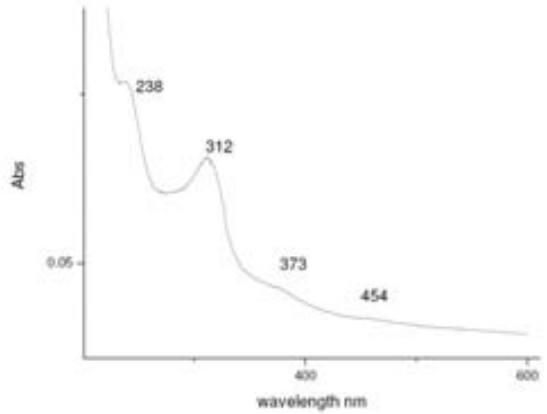

Figure 4. AFM measurements.

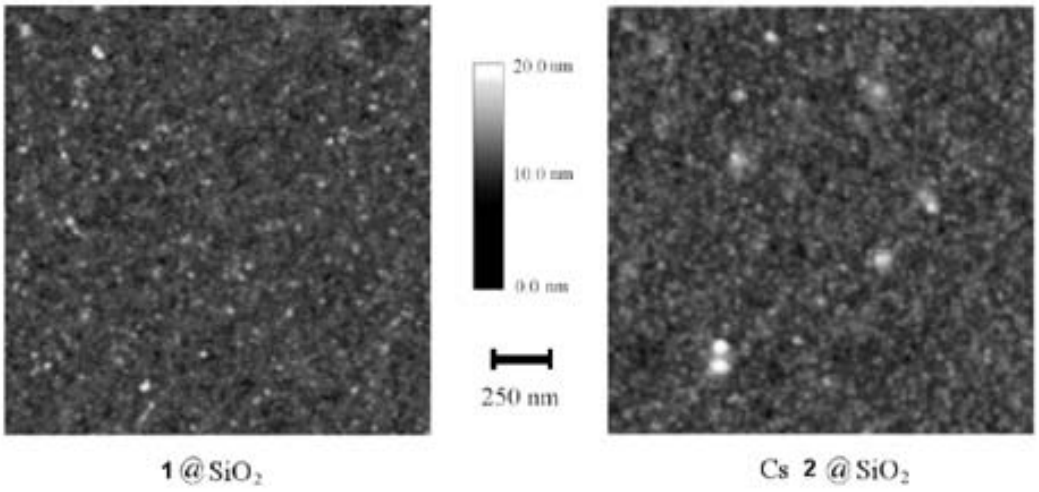

Table 1. Contact Angle and IR measurements.

compound	contact angle (degrees)	ν(B-H) (cm-1)
1@silica	-	2551
1@SiO_2wafer	81.8 ± 2.3	2565
2@SiO_2wafer	75.2 ± 2.0	2563

f) Thumb Rules to Establish the Rotamer Configuration in Metallacarborane Sandwiches. The relevance of the Cc-H···H-B Self Interactions.

Thumb Rules to Establish the Rotamer Configuration in Metallacarborane Sandwiches. The relevance of the Cc-H···H-B Self Interactions.

*Emilio J. Juárez-Pérez,[a]# Rosario Núñez,[a] Clara Viñas,[a] Reijo Sillanpää,[b] and Francesc Teixidor[a]**

[a] Institut de Ciència de Materials de Barcelona, CSIC, Campus U.A.B., 08193 Bellaterra, Spain.

[b] Department of Chemistry, University of Jyväskylä, FIN-40351, Jyväskylä, Finland.

[#] Enrolled in the UAB PhD program.

RECEIVED DATE (to be automatically inserted after your manuscript is accepted if required according to the journal that you are submitting your paper to)

Author to whom correspondence should be addressed. E-mail: teixidor@icmab.es

Abstract

The aim of this work is to explore the self-interaction capability of the anion $[3,3'\text{-}Co(1,2\text{-}C_2B_9H_{11})_2]^-$ through C_c-H···H-B dihydrogen bonds. The quaternary ammonium $[NMe_4]^+$ has been chosen as an expectedly innocent cation. A set of theoretical and empirical data aiming to establish the main rules that account for the binding mode between the negatively charged borane framework made by $[3,3'\text{-}Co(1,2\text{-}C_2B_9H_{11})_2]^-$ and the $[NMe_4]^+$ ions have been compiled. The interaction between cation and anion is mainly electrostatic but the covalent contribution is also proven and quantified. The existing intermolecular H···H short contacts have been studied and are compared with available data from the Cambridge Structural Database. The results show that the electronic configuration of the transition metal atom in the sandwich complex is not enough to define the preferred $[3,3'\text{-}Co(1,2\text{-}C_2B_9H_{11})_2]^-$ rotamer due to the influence of the anion environment and the H···H interaction present in the solid state.

KEYWORDS

boron clusters, carboranes, sandwich complexes, DFT calculations, QTAIM, short contacts bond.

Introduction

In the last 50 years a large knowledge about the cobaltabisdicarbollide anion, [3,3'-Co(1,2-$C_2B_9H_{11})_2$]$^-$, **1**, and its derivatives has been accumulated.[1] Until now, the anion **1** and its C_c and B substituted derivatives are the most ubiquitous sandwich metallacarborane compounds. This metallacarborane shows extraordinary chemical and thermal stability, hydrophobicity, weakly coordinating character and low nucleophilicity. [2,3] These properties make it suitable for a large number of applications, such as strong non-oxidizing acids, [4] electrolytes,[4] as electroactive species in sensors, doping agent in conducting polymers,[5] in the extraction of radionuclides, [6] but also medicine. [7,8] Recently, derivatives of this polyhedral metallacarborane have been recognized as potent and specific inhibitors of HIV protease.[9] Great expectations have risen from these anions, and theoretical works about their type of binding in solid state, or association in solution, have been developed in order to understand the behaviour of this family of borane cluster.[10] Neverthless, in the literature there exist much more types of full-sandwich metallacarboranes, in which the metal atom is coordinated η^5 to the pentagonal C_2B_3 face of the dicarbollide ligands.[11] The main reports are concerning to their crystal structures and redox properties due to the similarity of metallacarboranes to metallocenes. In fact, it has been published that in the case of redox couples, the electron transfer process will influence the metallacarborane structure,[11] changing the distance C_2B_3-M and providing a conformation rotation. Besides, it has been noted that such rotation could be exploited as a molecular motor,[12] but in some cases the rotation appears to be partial, based on the solid state molecular structures.[13] Furthermore, it is known that the adopted conformation plays an important role to define physical properties in the material.[14] To our knowledge the C-H···H-B and other X···H-B dihydrogen bonds (DHBs) have never been used before to interpret the higher stability of one rotamer *vs.* another in solid state, although they have been studied in metallacarboranes,[15] carborane[16] or borane derivatives.[10,17] This will be one of the main goal of this work.

In this paper we report details that explain the preferred *cisoid* conformation in solid state for anion **1** when the more stable conformation in gas phase would be *transoid*. The relevance of hydrogen and dihydrogen bonds to account for this fact is paramount. To reach this goal, the crystal structure of **[NMe_4][3,3'-Co(1,2-$C_2B_9H_{11})_2$], [NMe_4][1]**, has been resolved and compare with their homologous with Ni and Fe. The self-association of **1** in solid state is studied using a procedure to calculate the energy of the interactions between **1** and $[NMe_4]^+$. In addition, the Quantum Theory of Atoms in Molecules and inspection of the electrostatic surface potential has been used.

Experimental Section

General considerations. MALDI-TOF-MS mass spectra were recorded in the negative and positive ion mode using a Bruker Biflex MALDI-TOF [N_2 laser; lexc 337 nm (0.5 ns pulses); voltage ion source 20.00 kV (Uis1) and 17.50 kV (Uis2)]. All manipulations were carried out under a normal atmosphere. Reagent grade solvents were purchased from Aldrich and used as supplied. Cs[3,3'-Co(1,2-$C_2B_9H_{11})_2$] was commercially obtained from KATCHEM and the chemicals [NMe_4]Cl, NaOH and HCl (*aq.* 33%) from Aldrich.

Preparation of [NMe_4][3,3'-Co(1,2-$C_2B_9H_{11})_2$], [NMe_4][1]. [NMe_4][1] was prepared in 99% yield from the corresponding sodium salt Na[3,3'-Co(1,2-$C_2B_9H_{11})_2$], that was previously prepared from Cs[3,3'-Co(1,2-$C_2B_9H_{11})_2$] (91.3 mg, 0.2 mmol), following the literature procedures.[18] **[NMe_4][1]** crystallized from an acetone solution of at room temperature. The NMR and IR spectra of the product are similar to those earlier reported in the literature.[19] MALDI-TOF-MS: negative mode, m/z calcd. for **1** 324.38, found 324.20, positive mode, m/z calcd. for $[NMe_4]^+$ 74.10 found 74.05.

Theoretical Methods

Optimized geometries of the ground states of rotamers for the anion **1** and the **[NMe_4][1]** salt were performed using Density Functional Methods[20] of the Amsterdam Density Functional Package[21] (ADF-2007). The generalized gradient approximation (GGA non-local) method was used, by means of Vosko, Wilk and Nusair's local exchange correlation[22] with nonlocal exchange corrections by Becke[23] and non-local correlation corrections by Perdew.[24] The basis set employed in our calculations are all-electron double-ζ Slater type orbital in the core and triple-ζ in the valence shell with two polarization functions for C, B and H atoms (TZ2P) and TZ2P+ basis set for the cobalt atom. This TZ2P+ basis set is nearly identical to TZ2P except for a better description introducing 4 d-functions instead of 3. We label in this paper this basis set combination for the molecular ion as TZ2P(+). All calculations were no frozen core. Atomic charges and population analyses were computed within Voronoi Deformation Density Method as implemented in ADF.[25] Topological Bader analysis[26] was performed using Xaim[27] software on the BP86/TZ2P(+) total electron densities. Magnetic shieldings were computed for the geometry optimized rotamers at BP86/TZ2P(+) level employing DFT-GIAO[28] method with a "Statistical Average of Orbital dependent model Potential" (SAOP) implemented in ADF[29,30] using TZ2P(+) basis set. ^{11}B-NMR chemical shifts were calculated relative to B_2H_6 and converted to the usual $BF_3{\cdot}OEt_2$ scale by using the experimental value of B_2H_6 of 16.6 ppm.[31]

Search Parameters for Cambridge Structural Database

Search procedures in Cambridge Structural Database (CSD) were done using ConQuest.[32] The CSD (version 5.30, February 2009) was examined using the following criteria: 3D coordinates determined, not disordered, and without errors. The R factor is below 5% or as specified in the text.

X-ray crystallography

Single-crystal data collection for **[NMe$_4$][1]** was performed at –100 ºC with an Enraf Nonius KappaCCD diffractometer using graphite monochromatized Mo K_α radiation. The structures were solved by direct methods and refined on F^2 by the SHELXL97 program.[33] The non-hydrogen atoms were refined with anisotropic displacement parameters. The hydrogen atoms were treated as riding atoms using the SHELXL97 default parameters. **[NMe$_4$][1]** crystallizes in a non-centrosymmetric space group, and its absolute configuration was determined by refinement of Flack *x* parameter.(Ref) Crystallographic parameters, summary of the structure refinement parameters for **[NMe$_4$][1]** are gathered in Table 1.

Results and Discussion

1. Rotamers discrepancy for the cobaltabisdicarbollide anion and explanation from a Kohn-Sham-DFT geometry optimization. Slow evaporation of an acetone solution of **[NMe$_4$][1]** at room temperature gave orange crystals suitable for their structural determination by X-ray diffraction, that revealed a *cisoid* conformation for **1** (Figure 1). Selected bonding parameters are shown in Table 2. In the Cambridge Structural Database (CSD), there are 18 crystal structures that contain at least one anion **1** in a *cisoid* conformation, with R-factor below 5% (see Experimental part). The average value of the θ dihedral angles formed by B8', Co3, B10, B8 atoms in *cisoid* rotamers is 38.3±1.7º, which includes our profile of 39.3±0.3º.[34,35] The average angle between the C_2B_3 planes for *cisoid* rotamers of **1** in CSD is 3.1±0.7 degrees.

In a CSD search for **1** (without any restriction), 56 crystal structures have been found, from which it is noticed that the *cisoid* conformation is preferred for **1**, whereas only a 10% of [3,3'-Co(1,2-$C_2B_9H_{11}$)$_2$]$^-$ fragments present *transoid* conformation. Figure 2 shows a graphical representation of the different rotamers deposited in the CSD.[36] In 1967 the XRD crystal structure of Cs[**1**] was determined for the first time, however, the carbon atoms were ambiguously located and it was not possible to distinguish if the anion presented *transoid*, *gauche* or *cisoid* disposition.[37] Thirty years later, it was reported the first *transoid* conformation for the dianion [3,3'-Co(1,2-$C_2B_9H_{11}$)$_2$]$^{2-}$, with the cobalt atom as a formal d^7 Co(II).[38] Afterward, other crystal structures in which the anion **1** posses a *transoid* disposition, with a formal d^6 Co(III), have also been reported in the CSD.[14,39,40,41,42,43] In this respect, all crystal structures containing the *transoid* rotamer/s present some distinct characteristics: a) they present more than one type of rotamer in the asymmetric unit and b) the salt formulation could be consistent with a cobaltabisdicarbollide either as Co(II) or Co(III) oxidation states, due to the ambivalent nature of the cation[14,39] **¡Error! Marcador no definido.** From the later consideration it could be deduced that the oxidation state of Co should be capital to define the rotamer, however, in many of the *transoid* examples the oxidation state of Co is unambiguously Co(III). In addition, there are some structural parameters that clearly point out the non-equivalence between the *transoid* examples noted with Co(III) and that with Co(II),[38] so that the centroid distance between C_2B_3 and Co(III) is significantly shorter (1.469-1.477 Å) than between C_2B_3 and Co(II) (1.561 Å), which could be attributed to the distinct ionic radii for a Co atom with d^6 or d^7 electronic configuration, being higher for the last one. From the unique data available on a d^7 Co(II), [3,3'-Co(1,2-$C_2B_9H_{11}$)$_2$]$^{2-}$, and the crystal structure of the anion [3,3-Ni(1,2-$C_2B_9H_{11}$)$_2$]$^-$ in *transoid* conformation, with a d^7 Ni(III),[12, 44] it could be tentatively deduced that d^7 electronic configuration favours *transoid* rotamers whereas Co(III) with d^6 tends to produce *cisoid* rotamers, as will be discuss later. Nevertheless, due to the Co(III) *transoid* rotamers found in the CSD (10%) and the examples with *gauche* conformation, it is important to note that the anionic environment shall be taken into account to define the rotamer.

A DFT study on the isolated anion **1** in gas phase has been carried out in order to compare the rotamer energies without the external influence of the cation. The Kohn-Sham DFT method for geometry optimization was employed for this purpose.[45] In a previous theoretical work,[34] the Gaussian Type Orbitals (GTO) were used for the geometry optimization of the rotamers, whereas the Slater Type Orbitals (STO) have been applied here. Both theoretical studies have shown parallel results, where the more stable conformation is the *transoid* and showing similar difference of energy (11 kJ/mol) between the *transoid* and *cisoid* rotamers (Figure 3). However, the theoretical results are the opposite of those found in the CSD research, where the preferred conformation for the solid state is the *cisoid*. From the DFT calculations an estimation of the dipole moment of the anion for each rotamer in gas phase has been obtained. The *transoid* rotamer has C_{2h} symmetry and presents a null dipole moment. On the contrary, *gauche* and *cisoid* rotamers present C_s symmetry and the calculated profile of the dipole moment increases from 3.1 to 5.4 D, respectively. Thus, the increase in energy of the different rotamers parallels the dipole moment, and this is reflected on the abundance of the observed rotamers in the CSD.

2. Energy stabilization of the *cisoid* rotamer of the cobaltabisdicarbollide anion via ionic bonding and intermolecular Cc-H···H-B solid state interactions.

The low energetic gap of 11 kJ/mol between the three rotamers implies that, in solution, all three coexist. Thus, why is the *cisoid* rotamer more abundant in solid

state?. With the aim to quantify the energy of the interaction between the innocent $[NMe_4]^+$ cation and **1**, and of the latter with a like anion, an energy decomposition calculation with the Amsterdam Density Functional package (ADF[21]) has been carried out. The optimized geometry for the *cisoid* at BP/TZ2P(+) level of theory shows the best agreement with the experimental atom positions in the crystal structure (Tables with selected geometric parameters calculated for the three rotamers and experimental values are in the Supporting Information). In addition, theoretical ^{11}B-NMR chemical shifts for the rotamers of **1** have also been calculated using the previously optimized geometries showing a well agreement with the experimental data. (Table S5 and Figure S1 including calculated chemical shifts are deposited in the Supported Information). The geometrical parameters found in the asymmetric unit to locate the non-hydrogen atoms have been taken. The hydrogen atoms positions have been optimized at the BP86/TZ2P(+) level. This approach minimizes the computing time and allows us to obtain an accurate value for the bonding energy. The calculated interaction energy from ADF is presented as a Morokuma–Ziegler energy decomposition scheme with corrected basis set superposition error (BSSE).[46] The calculated cation/anion and anion/anion interaction energy (ΔE_{int}) can be split into three main components: $\Delta E_{int} = \Delta E_{elst} + \Delta E_{Pauli} + \Delta E_{oi}$; where ΔE_{elst} is the electrostatic interaction between the ions, ΔE_{Pauli} are the repulsive interactions and ΔE_{oi} is the stabilizing orbital interaction term that accounts for electron pair bonding, charge transfer and orbital mixing on one fragment due to the presence of a second fragment. Table 3 shows the results for the individual energy term and total energies for these anion/anion and cation/anion interactions. As expected, ΔE_{elst} is the largest energy term, although ΔE_{oi}, is not negligible. In fact, the ΔE_{oi} value is remarkable for the anion/anion interaction, and even though ΔE_{int} is positive, thus repulsive, the ΔE_{oi} value, that accounts mostly for the H···H intermolecular interaction is negative, -24.1 kJ/mol, thus attractive. All this shows the relevance of these non-bonding interactions to define the crystal packing, and so that the nature of the rotamer. The ΔE_{oi} value is larger than the energy difference between the *transoid* and *cisoid* rotamers (11 kJ/mol), so that it could be the clue to explain why the *cisoid* isomer is in general preferred in the solid state, as will be discuss bellow.

In the crystal structure of **$[NMe_4][1]$**, two types of intermolecular H···H short contacts have been observed: a) those involving the B-H and C_c-H hydrogens from the clusters, and b) those involving B-H hydrogens with hydrogen atoms of a methyl moiety in the $[NMe_4]^+$ cation (C_{Me}-H). This short contacts could be considered as dihydrogen bonds [47] (DHB) and/or H-H bonding interactions.[48] Figure 4 shows a motif from the crystal structure where a central cobaltabisdicarbollide anion, with the dicarbollide clusters named α and β, is surrounded by three $[NMe_4]^+$ cations (A, B, C) and four anions (1, 2, 3, 4), that establish thirteen H···H short contacts below the cut-off of 2.4 Å. These H···H short contacts are hydrogen interactions between the acidic C_c-H hydrogens from the central anion and hydrides B10-H, B5-H and B11-H from the four surrounding anions. In addition, H···H short contacts from the central anion via B7-H, B11'-H and B12'-H to C_{Me}-H units from the three neighbouring $[NMe_4]^+$ are also observed (Table 4).

The Quantum Theory of Atoms In Molecules of Bader (QTAIM)[26] has been applied to the study of the above mentioned H···H short contacts. Bond critical points (BCP) have been observed for all of them and the topological criteria for existence of DHB given by Koch and Popelier[49] are mainly matched. The calculated energy density (H) and $\nabla^2\rho$ values at the BCP suggest closed shell interactions of weak-medium strength (Table 5).[50,51] Additionally, the H···H bond energy (E_{HB}) from the energy parameters in AIM has been estimated (Table 5) according to the empirical relationship of Espinosa *et. al.* ($E_{HB} = 0.5 \cdot V$).[52] The values are in the range -4.24 to -5.94 kJ/mol. Combining these values with the ΔE_{oi} for the anion/anion interaction given above (-24.1 kJ/mol), it results that a maximum of four H···H would be for each pair of interacting anions. In Figure 4 the central ion has eight interactions with four neighbouring anions involving two interaction per each pair The fact that the number of interactions is lower than the maximum of four is consistent with the fact that ΔE_{oi} includes other energy terms besides the H···H interactions and that in Figure 4 only those with a cut-off distance of 2.4 Å are shown. The Voronoi Deformation Density (VDD) method implemented in ADF has been preferred to calculate the charge populations in these hydrogen atoms involved in H···H interactions.[25] Table 6 shows the distances between hydrogen atoms found in the crystal structure (*d'*), and the calculated distances after optimization at BP86/TZ2P(+), (*d*). The VDD* charge represents the hydrogen charge for the non-interacting ionic fragment whereas the VDD charge is the hydrogen charge after interaction. The VDD are less positive for the protic hydrogens and less negative for the hydride hydrogens than VDD*, which indicates a redistribution of charges. This charge redistribution explains the different nature of the C_{Me}-H···H-B and C_c-H···H-B interactions, so that the different charge sign in the hydrogen atoms for C_{Me}-H···H-B is representative of DHB; while the same charges in C_c-H···H-B suggests H-H bonding interactions.[48] These results are supported by the important ΔE_{oi} energy term of -24.1 kJ/mol.

Once the relevance of the H···H interactions have been established, a study to understand the benefits of a *cisoid vs.* a *transoid* rotamer in the crystal was necessary. For this, the C*isoid-1* conformation for the central cobaltabisdicarbollide anion depicted in Figure 4 was taken as energetically benchmark by means of the above established short contact interactions, C_{Me}-H···H-B and C_c-H···H-B. A counterclockwise rotation of the α ligand was performed to reach *gauche-1*, *transoid*, *gauche-2* and *cisoid-2* conformations, and for each step the possible repulsive interactions for C_{Me}-H··/·H-C_c or B-H··/·H-B and attractive interactions C_{Me}-H···H-B and C_c-H···H-B were computed, found that the *cisoid-1* conformation was the most energetically stable (Figure 5). One possible explanation is that the *cisoid* conformation provides a better synthon to generate a higher number of

energetically favourable H···H non-bonding contacts than the *trans* conformation. Although this method is highly qualitative, and differences of energy have to be taken with caution, the calculated energy paths give an idea of the importance of the C_c-H···H-B interactions that seem to be capital to decide the crystal packing, instead of the $[NMe_4]^+$, that acts as a spectator cation . In this respect, when the cation is weakly interacting thus innocent, the adopted conformer results from the anion/anion interaction, whereas if the cation is an interacting one, a balance of the cation/anion and anion/anion interaction energies shall determine the more appropriate conformation. If the non-innocent cation has better hydrogen acceptors than B-H to bind the C_c-H proton donors of the dicarbollide ligand it certainly will influence on the anion's conformation. All CSD reported *transoid* conformations incorporate a π system in the cation and CH/π interactions between these cations and C_c-H .[53]

Figure 4 shows the motif of the non-bonding interactions between a central anion **1** and four neighboring like anions and three cations, according to the crystal structure of **[NMe$_4$][1]**. Interestingly, a very similar motif was found in the crystal structure of **[NEt$_3$H][1]**,[54] that is graphically shown in Figure 6. In this structure similar H···H short contacts can be observed between the central anion **1** and three surrounding cations via C_{Et}-H···BH, in addition to C_c-H···H-B motifs between **1** and two like anions, that govern the crystal packing.

Even in the absence of cation-anion interactions, the cation has a preferential site to bind the anion, for $[3,3'\text{-}Co(1,2\text{-}C_2B_9H_{11})_2]^-$ the cation is located is in the vicinity of the negatively charged B-H framework. A qualitative and effective method to learn where the cation would be localized is by simple inspection of the potential electrostatic surfaces (PES) on the anion. The more negative zones with the highest electrostatic potentials will be the prevalent localizations of the cation. In Figure 7 it can be seen that these negative zones match the B-H dominating sites of **1**. This method has also been employed to localize preferential binding zones for cations in aromatic systems.[55]

3. Hydrogen interactions between $[NMe_4]^+$ cation, the Cc-H donor and the cluster B-H framework in other metallacarboranes. There are two further examples of metallabisdicarbollides containing $[NMe_4]^+$ as counterion**:** **[NMe$_4$][3,3'-Ni(1,2-C$_2$B$_9$H$_{11}$)$_2$]**,[44] and **[NMe$_4$]$_2$[3,3'-Fe(1,2-C$_2$B$_9$H$_{11}$)$_2$],** [56] in which the metallacarborane display the *transoid* conformation (Figure 8). The **[3,3'-Ni(1,2-C$_2$B$_9$H$_{11}$)$_2$]$^-$** anion establish four C_{Me}-H···H-B short contacts, whereas in the dianion **[3,3'-Fe(1,2-C$_2$B$_9$H$_{11}$)$_2$]$^{2-}$,** fourteen C_{Me}-H···H-B short contacts are established between the central anion and eight cations, but none of the type C_c-H···H-B between like anions. Why do these crystal structures present *transoid* conformation? The **[3,3'-Ni(1,2-C$_2$B$_9$H$_{11}$)$_2$]$^-$** anion contains a Ni(III)(d^7) atom, whereas the **[3,3'-Fe(1,2-C$_2$B$_9$H$_{11}$)$_2$]$^{2-}$** dianion has a Fe(II)(d^6). The electronic configuration for Co in the crystal structure of **[NMe$_4$][3,3'-Co(1,2-C$_2$B$_9$H$_{11}$)$_2$]** is Co(III)(d^6). Comparing the Ni and Co complexes, both are in the same oxidation state, however, the Ni has one more electron in the valence shell. On the other hand, both Fe and Co are d^6, but the Fe atom is in a lower oxidation state. Thus, the Ni and Fe transition metals form more negatively charged sandwich anions than the Co atom. The consequence is more electron-rich C_c-H hydrogen atoms as shown by a VDD charge determination, which reveals that for **[3,3'-Ni(1,2-C$_2$B$_9$H$_{11}$)$_2$]$^-$**, **[3,3'-Fe(1,2-C$_2$B$_9$H$_{11}$)$_2$]$^{2-}$** and **[3,3'-Co(1,2-C$_2$B$_9$H$_{11}$)$_2$]$^-$** the charge in the C_c-H proton is 0.097, 0.109, 0.125 au, respectively. Thus, these additional examples with $[NMe_4]^+$ show that the acidity of the proton atom in the C_c-H moiety determines the B-H···H-Cc interaction strength, and may explain the preferential *cisoid* conformation observed in **[3,3'-Co(1,2-C$_2$B$_9$H$_{11}$)$_2$]$^-$** crystal structures, and the innocence of the $[NMe_4]^+$ cation. In the first part of the manuscript, we have already considered the characteristics of the crystal structures for the dianion **[3,3'-Co(1,2-C$_2$B$_9$H$_{11}$)$_2$]$^{2-}$** with d^7 Co(II).[38] The VDD charge calculated for C_c-H in this complex is 0.118 au, less acid than for monoanion **[3,3'-Co(1,2-C$_2$B$_9$H$_{11}$)$_2$]$^-$.** Subsequently, and according to the previous discussion, lower C_c-H···H-B interactions are expected, and a *transoid* configuration should be the more stable in the presence of an innocent cation. Effectively, the crystal structure show a *transoid* rotamer in which no short contacts C_c-H···H-B was observed. Concerning the preferred *cisoid* configuration for d^6 complexes, and *transoid* configuration for d^7 complexes, it was already discussed by Chamberlain *et al.*, however in this case a different explanation was provided.[38]

Nevertheless, even when the oxidation state and the electronic configuration are capital to provide Cc-H···H-B interactions and determine the conformation of the anion, the other important factor is the cation. A non-innocent counterion can play a fundamental role to definitively establish the conformation of the anion, such as is the case for the tetrathiafulvalenium (TTF) in salts of **[3,3'-Fe(1,2-C$_2$B$_9$H$_{11}$)$_2$]$^-$**,[13a] **[3,3'-Co(1,2-C$_2$B$_9$H$_{11}$)$_2$]$^-$**[14] and **[3,3'-Ni(1,2-C$_2$B$_9$H$_{11}$)$_2$]$^-$**. [13a] In these three cases, there are abundant similarities: the oxidation state for the three central atoms is +3; the space group is P21/n, the sandwich conformation is *cisoid* and there are hydrogen interactions between the aromatic C-H of the cation and the B-H framework of the dicarbollide ligands for the three crystal structures. The differences between the three crystal structures are mainly two: a) the first is related to the electronic configuration of the transition metal, d^5, d^6 and d^7 respectively, that influences to the centroid distance C_2B_3-M(III), being 1.528, 1.471 1.541 Å, respectively. Consequently, the density of the crystal structure is 1.426, 1.446 and 1.437 g/cm^3; b) the most important difference is that the Fe(III) anion does not form any Cc-H···H-B interaction, the Co(III) anion forms two interactions being the shortest H···H distance 2.261 Å, and the Ni(III) forms only one interaction just in the limit of 2.398 Å. This fact prove that the acidity of the Cc-H for each sandwich remains even that conformation is changed.

Conclusion

A CSD research on the $[3,3'\text{-}Co(1,2\text{-}C_2B_9H_{11})_2]^-$ anion determines that the preferred conformation in solid state is the *cisoid* rotamer, just the opposite to that shown by gas phase theoretical calculations. Several factors seems to determine the conformation for anion **1** and their homologous with other metals: a) the electronic configuration, the experimental distance between C_2B_3 and the metal depends on this factor, giving higher values for d^5 and d^6 (around 1.54 Å) than for d^6 (1.47 Å), subsequently providing more freedom rotation; b) the oxidation state of the metallic center is crucial since affords the acidity of the C_c-H protons, higher acidity gives the larger number of C_c-H···H-B interactions, only observed in *cisoid* conformations; c) the cation is the third factor to determine the rotamer conformation and the crystal packing. We have found that innocent or non-innocent cations influence in the adopted conformation in the following manner: the former drives to adopted conformers where the anion/anion interaction play the main rule in the crystal packing, however, if the cation is an interacting one, a balance of the cation/anion and anion/anion interaction energies shall determine the more appropriate conformation. In other words, if a non-innocent cation has better hydrogen acceptors than B-H to bind the C_c-H proton donors of the dicarbollide ligand it certainly will influence on the anion's conformation. In general these anionic carborane derivatives structures are capable to form specific intermolecular interactions.

Acknowledgments

This work has been supported by the CICYT (MAT2006-05339) and the Generalitat de Catalunya, 2005/SGR/00709. E.J.J.P. thanks to Ministerio de Educación y Ciencia for a FPU grant. This research have been achieved in part by CESCA and CTI from CSIC.

Figure 1. Structure of $[NMe4][3,3'\text{-}Co(1,2\text{-}C_2B_9H_{11})_2]$ showing the labeling system. Displacement ellipsoids are drawn at 30% probability level.

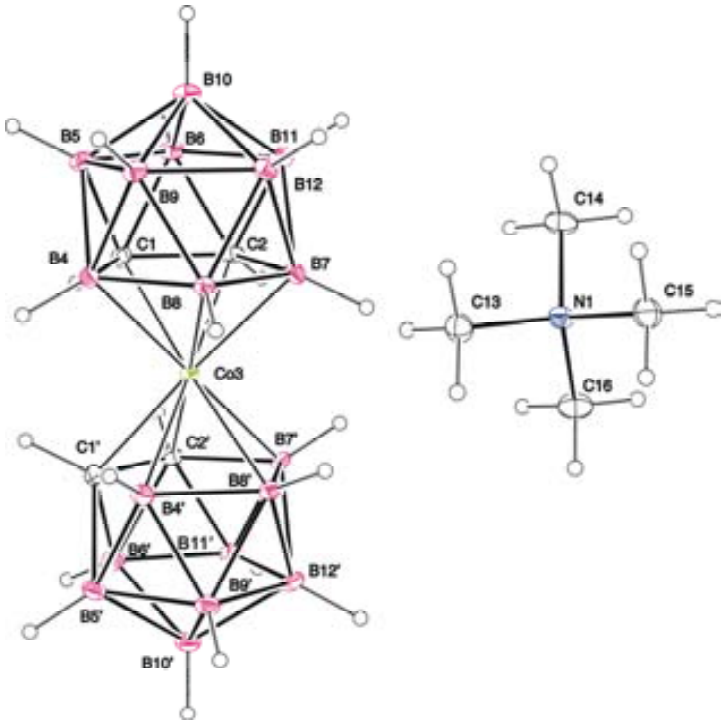

Figure 2. a) θ dihedral angle formed by B8'-Co-B10-B8 in crystal structures reported in CSD containing **[3,3'-Co(1,2-$C_2B_9H_{11}$)$_2$]$^-$**. b) Time evolution of the reported crystal structures containing **[3,3'-Co(1,2-$C_2B_9H_{11}$)$_2$]$^-$**. See search details in CSD in the text.

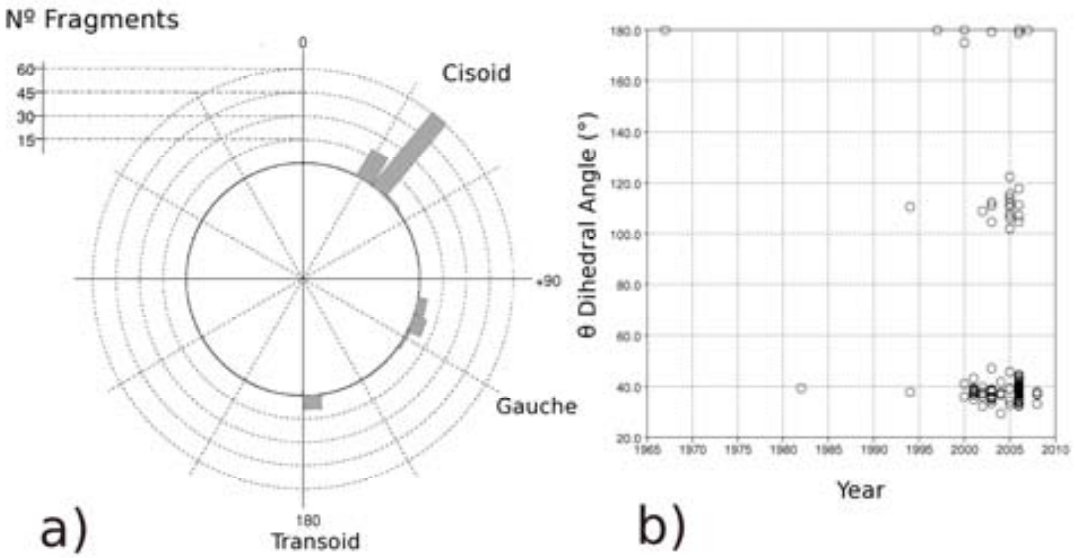

Figure 3. Relative energies (kJ/mol) for each optimized geometries of the rotamers of the **[3,3'-Co(1,2-$C_2B_9H_{11}$)$_2$]$^-$** anion obtained at BP86/TZ2P(+) (this work) and at BP86/AE level of theory(ref. 34).

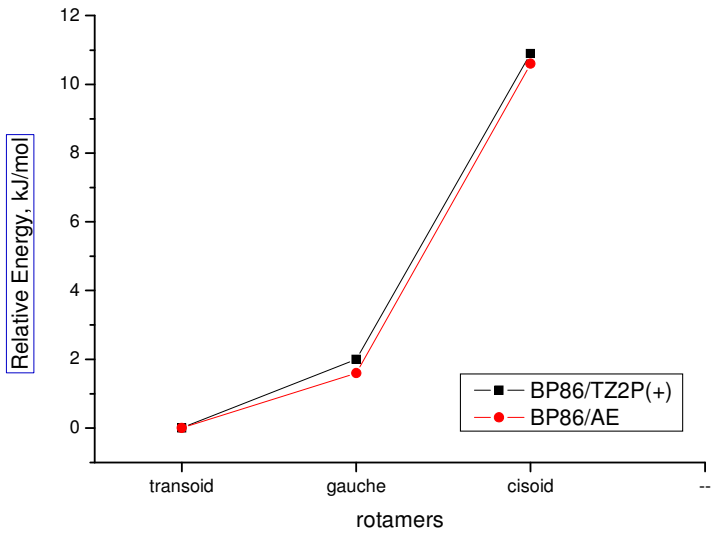

Figure 4. Central cobaltabisdicarbollide anion surrounded for other four anions and three cations. The C_c of the dicarbollide ligands are represented in ellipsoidal form.

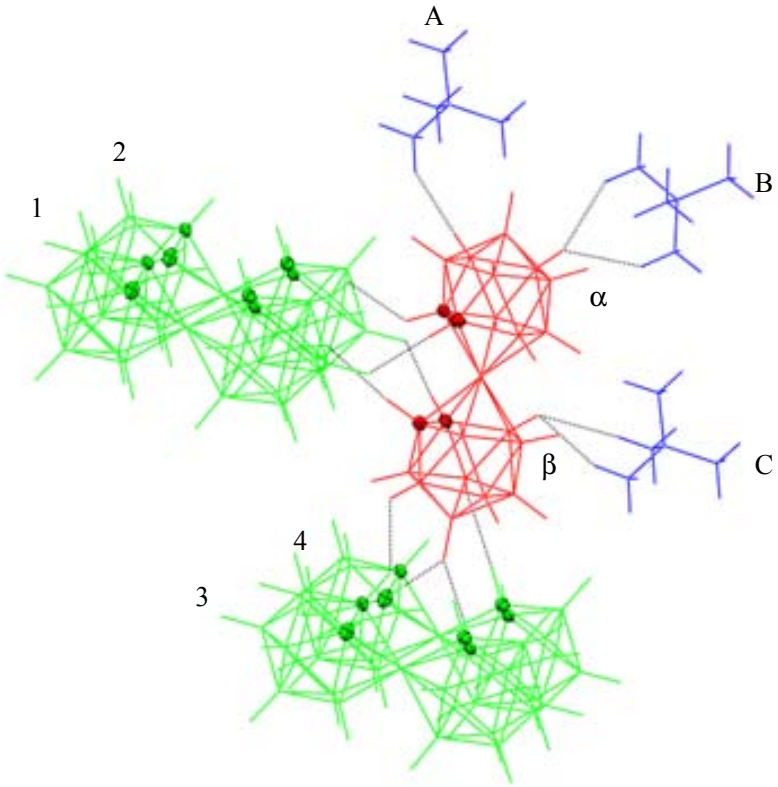

Figure 5. Relative energy stabilization of a central cobaltabisdicarbollide depending of the conformation.

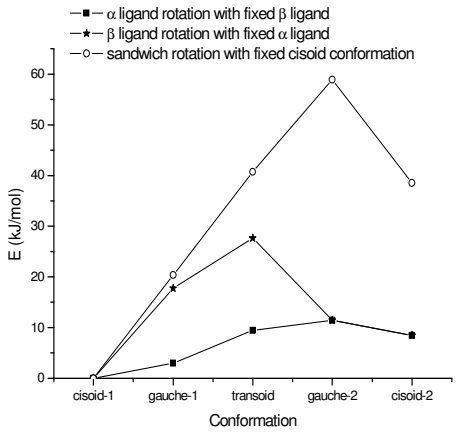

Figure 6. **[3,3'-Co(1,2-$C_2B_9H_{11}$)$_2$]$^-$** anion establishing H···H short contacts (VdW cutoff: 2.4 Å) with three **[NEt_3H]$^+$** cations and two **[3,3'-Co(1,2-$C_2B_9H_{11}$)$_2$]$^-$** anions.

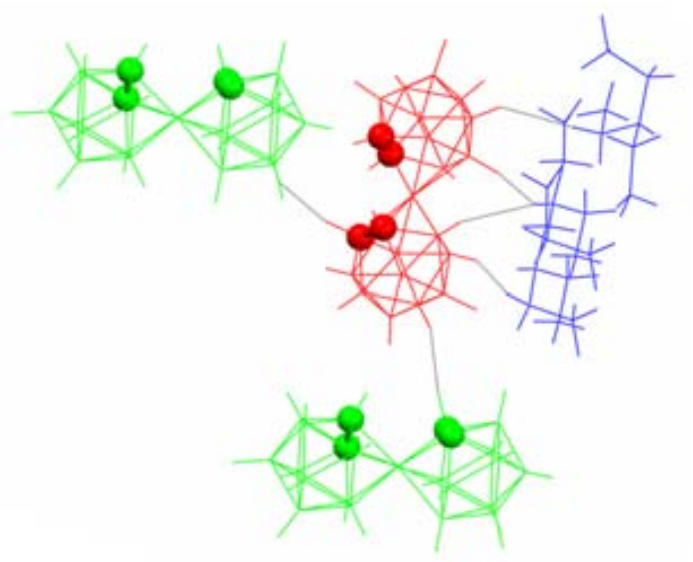

Figure 7. Potential electric surface for a *cisoid* rotamer of **[3,3'-Co(1,2-$C_2B_9H_{11}$)$_2$]$^-$** anion.

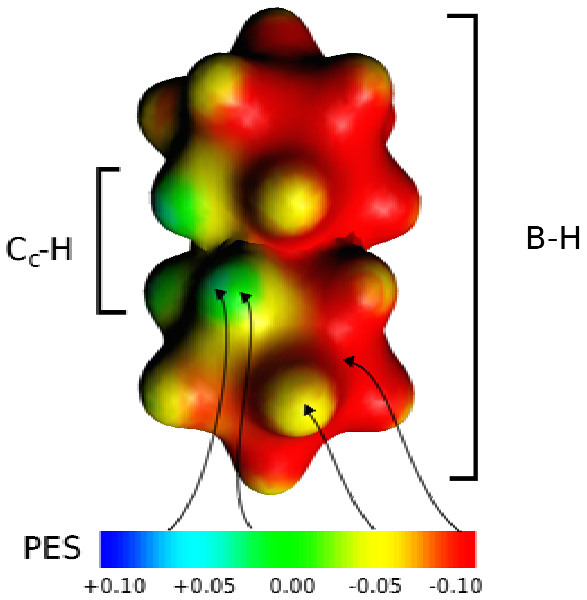

Figure 8. Central anion and short contact interactions established for $[NMe_4][3,3'\text{-}Ni(1,2\text{-}C_2B_{10}H_{12})_2]$ (left) and $[NMe_4][3,3'Fe(1,2\text{-}C_2B_{10}H_{12})_2]$ (right).

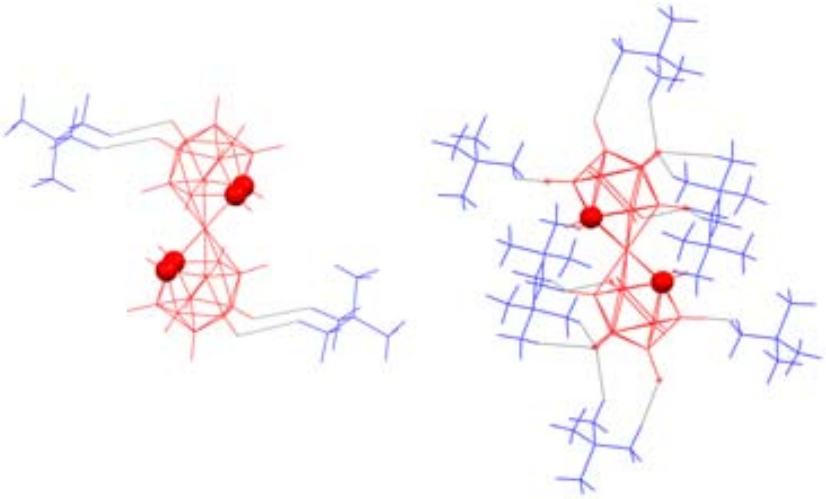

Table 1 Crystallographic data and structure refinement parameters for **[NMe_4][3,3'-Co(1,2-$C_2B_9H_{11}$)$_2$]**

Formula	$C_8H_{34}B_{18}CoN$
M_r	358.77
Crystal system	Monoclinic
Crystal habit, color	plate, yellow
Space group	*Cc* (no. 9)
a/Å	6.9009(2)
b/Å	28.7402(9)
c/Å	10.7259(4)
α/°	90
β/°	91.129(2)
γ/°	90
V/Å^3	2126.89(12)
Z	4
T/ºC	-100
λ/Å	0.71073
ρ_{calcd}/g cm^{-3})	1.243
μ/mm^{-1}	0.802
Data/restraints/parameters	4280/2/257
goodness-of-fit[a] on F^2	1.042
R[b] [$I > 2\sigma(I)$]	0.0399
R_w[c] [$I > 2\sigma(I)$]	0.0789
Flack's parameter x	0.033(17)

[a] $S = [\Sigma(w(F_o^2 - F_c^2)^2]/(n-p)^{1/2}$, [b] $R = \Sigma||F_o| - |F_c||/\Sigma|F_o|$, [c] $R_w = [\Sigma w(|F_o^2| - |F_c^2|)^2/\Sigma w|F_o^2|^2]^{1/2}$.

Table 2 Relevant bond lengths (Å), bond angles and dihedral angles (degrees) in the crystal structure of **[NMe_4][3,3'-Co(1,2-$C_2B_9H_{11}$)$_2$]**.

Lenghts	
Co3-C1	2.046(3)
Co3-C1'	2.034(3)
Co3-C2	2.042(3)
Co3-C2'	2.037(5)
Co3-B4	2.097(3)
Co3-B4'	2.087(4)
Co3-B7	2.084(4)
Co3-B7'	2.093(3)
Co3-B8	2.108(5)
Co3-B8'	2.115(3)
C1-C2	1.618(5)
C1'-C2'	1.606(6)
Angles	
B4-B8-B7	106.4(3)
B4'-B8'-B7'	107.0(3)
B10-Co3-B10'	177.9(1)
Dihedrals	
B8-Co3-B10'-B8'	38.9(3)
B8'-Co3-B10-B8	39.6(3)

Table 3. Energy Decomposition for the cation/anion and anion/anion interaction. Energies in kJ/mol. Positive value indicates repulsion.

	$[NMe_4]^+$/[3,3'-Co(1,2-$C_2B_9H_{11}$)$_2$]$^-$	[3,3'-Co(1,2-$C_2B_9H_{11}$)$_2$]$^-$/[3,3'-Co(1,2-$C_2B_9H_{11}$)$_2$]$^-$
ΔE_{elst}	-252.21	127.93
ΔE_{Pauli}	33.69	31.53
ΔE_{oi}	-46.19	-24.1
BSSE	3.21	2.45
ΔE_{int}	**-261.50**	**137.81**

Table 4. H···H short contacts for the system depicted in Figure 4.

Interaction Type	Anion/Cation tag	C_x-*H*	B-*H*	Distance (Å)
C_cH···H-B	1	H1	H11	2.141
C_cH···H-B	1	H1'	H10	2.206
C_cH···H-B	2	H2	H10	2.195
C_cH···H-B	2	H2'	H5	2.058
C_cH···H-B	3	H2	H10	2.195
C_cH···H-B	3	H2'	H5	2.058
C_cH···H-B	4	H1	H11	2.141
C_cH···H-B	4	H1'	H10	2.206
C_{Me}-H···H-B	A	H14	H11'	2.306
C_{Me}-H···H-B	B	H15	H12'	2.269
C_{Me}-H···H-B	B	H16	H12'	2.318
C_{Me}-H···H-B	C	H13	H7	2.380
C_{Me}-H···H-B	C	H14	H7	2.395

Table 5. Topological Parameters (au) of the Bond Critical Point at the H...H short contacts.

Interaction	Cx-*H*{anion/cation}	B-*H*	ρ(au)	$\nabla^2\rho$(au)	G(au)	V(au)	H(au)	E_{HB}(kJ/mol)
C_{Me}-H···H-B	H13{C}	H7	0.00830	0.02368	0.00479	-0.00366	0.00113	-4.81
C_{Me}-H···H-B	H14{C}	H7	0.00710	0.02249	0.00444	-0.00326	0.00118	-4.28
C_cH···H-B	H1{4}	H11	0.00943	0.02872	0.00585	-0.00453	0.00133	-5.94
C_cH···H-B	H1'{4}	H10	0.00720	0.02251	0.00443	-0.00323	0.00120	-4.24

Table 6. VDD Atomic Charges of hydrogen atoms involuctraded in the H···H short contacts. The d and d' distances in Å.

Interaction	Cx-*H*{anion/cation}	B-*H*	*d'*	*d*	VDD* (C-**H**···**H**-B)	VDD (C-**H**···**H**-B)
C_{Me}-H···H-B	H13{C}	H7	2.395	2.208	0.086/-0.034	0.015/-0.030
C_{Me}-H···H-B	H14{C}	H7	2.380	2.401	0.086/-0.034	0.020/-0.030
C_cH···H-B	H1{4}	H11	2.141	2.145	0.125/-0.033	0.020/0.009
C_cH···H-B	H1'{4}	H10	2.206	2.240	0.125/-0.030	0.021/0.015

References

[1] a) Hawthorne, M. F.; Andrews, T. D. *J. Chem. Soc., Chem. Commun.* **1965**, 443. b) Sivaev, I. B.; Bregadze, V. I. *Collect. Czech. Chem. Commun*. **1999**, *64*, 783.
[2] a) Ma, L.; Hamdi, J.; Hawthorne, M. F. *Inorg. Chem.* **2005**, *44*, 7249; b) Matejicek, P.; Cigler, P.; Procházka, K.; Kral, V. *Langmui*r, **2006**, *22*, 575; c) Chevrot, G.; Schurhammer, R.; Wipff, G. *J. Phys. Chem. B* **2006**, *110*, 9488.
[3] a) Strauss, S. H. *Chem. Rev.* **1993**, *93*, 927; b) Reed, C. A. *Acc. Chem. Res.* **1998**, *31*, 133.
[4] Plesek, J. *Chem. Rev.* **1992**, *92*, 269.
[5] a) Stoica, A. I. ; Viñas C. ; Teixidor, F. *Chem. Commun.* **2008**, 48, 6492. b) Crespo, E.; Gentil, S.; Viñas, C.; Teixidor, F. *J. Phys. Chem. C.* **2007**, *111*, 18381. c) Masalles, C.; Borros, S.; Viñas, C.; Teixidor, F. *Adv. Mater.* **2000**, 12, 1199. d) Masalles, C.; Llop, J.; Viñas, C.; Teixidor, F. *Adv. Mater.* **2002**, *14*, 826.
[6] a) Viñas, C.; Gómez, S.; Bertrán, J.; Teixidor, F.; Dozol, J. F.; Rouquette, H. *Chem. Commun.* **1998**, 191. b) Viñas, C.; Gómez, S.; Bertrán, J.; Teixidor, F.; Dozol, J. F.; Rouquette, H. *Inorg. Chem.* **1998**, *37*, 3640. c) Grüner, B.; Plesek, J.; Baca, J.; Cisarova, I.; Dozol, J.-F; Rouquette, H.; Viñas, C.; Selucky, P.; Rais, J. *New J. Chem.* **2002**, *26*, 1519. d) Rais, J.; Grüner, B. in *Solvent Extraction*, eds. Marcus, I. & SenGupta, A. K. Dekker, New York, 2005, pp. 243. e) Grüner, B.; Mikulásek, L; Báca, J.; Císarová, I.; Böhmer,V.; Danila, C.; Reinoso-García, Marta M.; Verboom, W.; Reinhoudt, D. N.; Casnati, A. Ungaro R. *Eur. J. Org. Chem.* **2005**, 2022.
[7] a) Hawthorne, M. F.; Maderna, A.; *Chem. Rev.* **1999**, *99*, 3421. b) Soloway, A. H.; Tjarks, W.; Barnum, B. A.; Rong, T. D.; Barth, R. F.; Codogni, I. M.; Wilson, J. G. *Chem. Rev.* **1998**, *98*, 1515.
[8] a) Hao, E.; Vicente, M.G. H. *Chem. Commun.* **2005**, 1306. a) Sibrian-Vazquez, M.; Hao, E.; Jenssen, T. J.; Vicente, M.G. H. *Biocong. Chem.* **2006**, 17, 928. c) Hao, E.; Sibrian-Vazquez, M.; Serem, W.; Garno, J. C.; Fronczek F. R.; Vicente, M. G. H. *Chem. Eur. J.* **2007**, *13*, 9035. d) Li, F.; Fronczek, F. R.; Vicente, M. G. H. *Tetrah. Lett.*, **2008**, *49*, 4828.
[9] Cígler, P.; Kozisek, M.; Rezacova, P.; Brynda, J.; Otwinowski, Z.; Pokorná, J.; Plesek, J.; Grüner, B.; Dolecková-Maresová, L.; Masa, M.; Sedlácek, J.; Bodem, J.; Kräusslich, H.-G.; Král, V.; Konvalinka, J. *Proc. Natl. Acad. Sci. U.S.A.* **2005***, 102*, 15394.
[10] a) Fanfrlík, J.; Lepsik, M.; Horinek, D.; Havlas, Z.; Hobza, P. *ChemPhysChem* **2006**, *7*, 1100. b) Fanfrlík, J.; Hnyk, D.; Lepsik, M.; Hobza, P. *Phys. Chem. Chem. Phys.,* **2007**, *9*, 2085. c) Fanfrlík, J; Brynda, J.; Rezac, P.; Hozba, M.; Lepsik, M. *J. Phys. Chem. B.* **2008**, *112*, 15094.
[11] Corsini, M.; Fabrizia, F.; Zanello, P. *Coord. Chem. Rev.* **2006**, *250*, 1351 and references therein.

[12] Hawthorne, M. F.; Zink, J. I.; Skelton, J. M.; Bayer, M. J.; Liu, C.; Livshits, E.; Baer, R.; Neuhauser, D. *Science* **2004**, *303*, 1849.
[13] a) Forward, J. M.; Mingos, D. M. P.; Muller, T. E.; Williams, D. J.; Yan, Y. K. *J. Organomet. Chem.* **1994**, *467*, 207-216. b) Mickinney, J. D.; McQuillan, F. S.; Chen, H.; HAmor, T. A.; Jones, M.; Slaski, M.; Cross, G. H.; Harding, C. J. *J. Organomet. Chem.* **1997**, *547*, 253. c) Chetcui, P. A.; Hofherr, W.; Liégard, A.; Rihs, G.; Rist, G.; Keller, H.; Zech, D.; *Organometallics*, **1995**, *14*, 666.

[14] HENREY: Kazheva, O. N.; Chekhlov, A. N.; Alexandrov, G. G.; Buravov, L. I.; Kravchenko, A. V.; Starodub, V. A.; Sivaev, I. B.; Bregadze, V. I.; Dyachenko, O. A. *J. Organomet. Chem.* **2006**, *691*, 4225.
[15] Planas, J G.; Viñas, C.; Teixidor, F.; Comas-Vives, A.; Ujaque, G.; Lledós, A.; Light, M. E.; Hursthouse, M.B. *J. Am. Chem. Soc.* **2005**, 127, 15976.
[16] a) Barberà, G.; Viñas, C.; Teixidor, F.; Rosair, G. M.; Welch, A.J. *J. Chem. Soc., Dalton Trans*., **2002**, 3647. b) Teixidor, F.; Barberà, G.; Viñas, C.; Sillanpää, R.; Kivekäs, R. *Dalton Trans*., **2007**, 1668**.** c) Alekseyeva, E. S.; Batsanov, A. S.; Boyd, L. A.; Fox, M. A.; Hibbert, T. G. ; Howard,J. A. K.; MacBride, J. A. H.; Mackinnon, A.; Wade, K. *Dalton Trans.*, **2003**, 475. d) Batsanov,A. S.; Fox, M. A.; Hibbert, T. G.; Howard, J. A. K.; Kivekäs, R.; Laromaine, A. Sillanpää, R.; Viñas, C.; Wade, K. *Dalton Trans*., **2004**, 3822.
[17] a) Shubina, E. S.; Bakhmutova, E. V.; Filin, A. M.; Sivaev, I. B.; Teplitskaya, L. N.; Chistyakov, A. L.; Stankevich, I. V.; Bakhmutov, V. I.; Bregadze, V. I.; Epstein, L. M. *J. Organomet. Chem.* **2002**, *657*, 155. b) Glukhov, I. V.; Lyssenko, K. A.; Korlyukov, A. A.; Antipin, M. Y. *Faraday Discuss.* **2007**, *135*, 203.
[18] Hawthorne, M. F.; Andrews, T. D.; Garret, P. M.; Olsen, F. P.; Reintjes, M.; Tebbe, F. N.; Warren, L. F.; Wegner, P. A.; Young, D. C.; Alexander, R. P.; Blundon, R. W.; Schroeder, H. A.; Heying, T. L. *Inorg. Synth.* **1967**, 91.
[19] a) Hawthorne, M. F.; Young, D. C.; Andrews, T. D.; Howe, D. V.; Pilling, R. L.; Pitts, A. D.; Reintjes, M.; Warren Jr, L. F.; Wegner, P. A. *J. Am. Chem. Soc.* **1968**, *90*, 879. b) Siedle, A. R.; Bodner, G. M.; Todd, L. J. *J. Organomet. Chem.* **1971**, *33*, 137.
[20] Parr, R.G.; Yang, W. *Density-Functional Theory of Atoms and Molecules*, Oxford University Press, New York, 1989.
[21] a) ADF-2007.01, SCM, Theoretical Chemistry, Vrije Universiteit, Amsterdam, The Netherlands, http://www.scm.com. b) te Velde, G.; Bickelhaupt, F. M.; Baerends, E. J.; Guerra, C. F; van Gisbergen, S. J. A.; Snijders, J. G.; Ziegler, T. *J. Comput. Chem.* **2001**, *22*, 931. c) Guerra, C. F.; Snijders, J. G.; te Velde, G.; Baerends, E. J. *Theor. Chem. Acc.* **1998**, *99*, 391.
[22] Vosko, S. H.; Wilk, L.; Nusair M. *Can. J. Phys*. **1980**, *58*, 1200.

[23] Becke, A. D. *Phys. Rev. A* **1988**, *38*, 3098.
[24] Perdew, J.P. *Phys. Rev. B* **1986**, *33*, 8822.
[25] Guerra, C. F.; Handgraaf, J. W.; Baerends, E. J.; Bickelhaupt, F. M. *J. Comput. Chem.* **2004**, *25*, 189.
[26] Bader, R. F. W. *Atoms in Molecules: a Quantum Theory*, Clarendon Press, Oxford; New York, 1990.
[27] Xaim 1.0. Ortiz, J. C.; Bo, C. Universitat Rovira i Virgili. Tarragona. Spain. 1998. http://www.quimica.urv.es/XAIM
[28] Friedrich, K.; Seifert, G.; Grossmann G. Z. *Phys. D* **1990**, *17*, 45.
[29] Poater, J.; van Lenthe, E.; Baerends, E. J. *J. Chem. Phys.* **2003**, *118*, 8584.
[30] Schreckenbach, G.; Ziegler, T. *J. Phys. Chem.* **1995**, *99*, 606.
[31] Onak, T. P.; Landesman, H. L.; Williams, R. E.; Shapiro, I. *J. Phys. Chem.* **1959**, *63*, 1533.
[32] a) Allen, F. H. *Acta Crys. B* **2002**, *58*, 380. b) Bruno, I. J.; Cole, J. C.; Edgington, P. R.; Kessler, M.; Macrae, C. F.; McCabe, P.; Pearson, J.; Taylor, R. *Acta Crys. B* **2002**, *58*, 389.
[33] Sheldrick, G. M. *Acta Cryst*. **2008**, *A64*, 112.
[34] Bühl, M.; Hnyk, D.; Machacek, J. *Chem. Eur. J.* **2005**, *11*, 4109.
[35] The θ dihedral angle B8'-Co-B10-B8 defines the conformation of the rotamers. The ideal θ dihedral angle vary from 36º for ideal *cisoid* conformation, 108º for ideal *gauche* conformation and 180º for ideal *transoid* conformation. In this paper, the average dihedral angle in the crystal structure is for B8'-Co-B10-B8 and B8-Co-B10'-B8'.
[36] In this search the R parameter is not restricted and the range is found between 2.56 and 14.14 %, for other search parameters (see Experimental Section). The 56 reported crystal structures contain 109 observations for **1:** 83 in *cisoid*, 17 in *gauche* and 9 in *transoid* configuration.
[37] CSCBCO: Zalkin, A; Hopkins T. E.; Templeton, D. H. *Inorg. Chem.* **1967**, *6*, 1911.
[38] RINMIK: Chamberlin, R. M.; Scott, B. L.; Melo, M. M.; Abney, K. D. *Inorg. Chem.* **1997**, *36*, 809.
[39] LUHKAA: Nadolinny, V. A.; Polyanskaya, T. M.; Volkov, V. V.; Drozdova, M. K. *Khim. Interesakh Ustoich. Razvit.(Russ)* **2000**, *8*, 229.
[40] QAJNAQ: Hardie, M. J.; Raston, C. L. *Angew. Chem. Int. Ed.* **2000**, *39*, 3835.
[41] MEFNER: Cunha-Silva, L.; Westcott, A.; Whitford, N.; Hardie, M. J. *Cryst. Growth Des.* **2006**, *6*, 726.
[42] HADWIT: Plesek, J.; Backovsky, J.; Cisarova, I. *Private Communication to CSD* **2003**. HADWIT has one *cisoid* and another *transoid* rotamer fragment of **[3,3'-Co(1,2-$C_2B_9H_{11}$)$_2$]$^-$**, the angle measurement is referred to the *cisoid* fragment.
[43] LINDIW, LINDOC: Kazheva, O. N., Alexandrov, G. G., Kravchenko, A. V., Starodub, V. A., Sivaev, I. B., Lobanova, I. A., Bregadze, V. I., Buravov, L. I., Dyachenko, O. A., *J. Organomet. Chem.* **2007**, *692*, 5033.

[44] UCNBOR: Hansen, F. V.; Hazell, R. G.; Hyatt, C. Stucky, G. D. *Acta Chem. Scand.* **1973**, *27*, 1210.
[45] Bickelhaupt, F. M.; Baerends, E. J., Kohn-Sham density functional theory: predicting and understanding Chemistry. Reviews of Computational Chemistry. Boyd, D. B.; Lipkowitz, K. B. Eds., Wiley-VCH: New York, **2000**.
[46] Boys, S. F.; Bernardi, F. *Mol Phys* **1970**, *19*, 553.
[47] a) Alkorta, I.; Elguero, J.; Grabowski, S. J. *J. Phys. Chem. A* **2008**, *112*, 2721. b) Grabowski, S. J.; Sokalski, W. A.; Leszczynski, J. *Chem. Phys.* **2007**, *337*, 68. c) Grabowski, S. J.; Sokalski, W. A.; Leszczynski, J. *J. Phys. Chem. A* **2005**, *109*, 4331.
[48] Matta, C. F.; Hernandez-Trujillo, J.; Tang, T. H.; Bader, R. F. W. *Chem. Eur. J.* **2003**, *9*, 1940.
[49] Popelier, P.L.A. *J. Phys. Chem. A* **1998**, *102*, 1873.
[50] Rozas, I.; Alkorta, I.; Elguero, J. *J. Am. Chem. Soc.* **2000**, *122*, 11154.
[51] Grabowski, S. J.; Sokalski, W. A.; Leszczynski, J. *Chem. Phys.* **2007**, *337*, 68.
[52] Espinosa, E.; Molins, E.; Lecomte, C. *Chem. Phys. Lett.* **1998**, *285*, 170.
[53] Nishio, M; Hirota, M.; Umezawa, Y. The CH-[pi] Interaction: Evidence, Nature, and Consequences, Wiley-VCH, 1998.
[54] Borodinsky, L., Sinn, E., Grimes, R. N., *Inorg. Chem.* **1982**, 21, 1686.

[55] Ma, J. C.; Dougherty, D. A. *Chem. Rev* **1997**, *97*, 1303.
[56] KIWJOP: Kang, H. C.; Lee, S. S.; Knobler, C. B.; Hawthorne M. F. *Inorg. Chem.* **1991**, *30*, 2024.